A GEO-THERMOCHRONOLOGICAL STUDY OFFSHORE WEST OF IRELAND:

the timing of exhumation and magmatic activity and the nature of the basement on the Irish Atlantic Margin

PhD Thesis

2021

Rémi Rateau

Trinity College Dublin
Coláiste na Tríonóide, Baile Átha Cliath
The University of Dublin

Declaration

I declare that this thesis has not been submitted as an exercise for a degree at this or any other university and it is entirely my own work.

I agree to deposit this thesis in the University's open access institutional repository or allow the Library to do so on my behalf, subject to Irish Copyright Legislation and Trinity College Library conditions of use and acknowledgement.

I consent to the examiner retaining a copy of the thesis beyond the examining period, should they so wish (EU GDPR May 2018).

Summary

In recent years, the use of multiple low-temperature thermochronometers combined with inverse thermal history modelling of multiple samples on vertical profiles has been shown capable of detecting low magnitude exhumation events that characterise many passive margins. Such approaches have shed new insights on the Mesozoic and Cenozoic exhumation history of onshore Ireland and Britain. A similar approach has been used in this study to investigate the exhumation history of the Irish Atlantic Margin (IAM), the southern segment of the North-East Atlantic Margin, which until now has been primarily studied by apatite fission track dating in isolation.

More than 40 new samples (from PAD and Ifremer) were acquired from borehole cuttings and cores and seabed dredge samples all along the IAM (from the Donegal and NE Rockall basins to the north to the southern tip of the Porcupine High and the Goban Spur to the south). After compiling all the low-temperature thermochronological data from Ireland and the UK, a set of legacy AFT and AHe samples was also selected to complement the new samples, as half of the samples collected in this study did not yield enough apatite. Zircon and apatite U/Pb dating and apatite trace element determinations were undertaken to constrain the thermal history model and derive new insights on the timing of magmatism and nature of the basement offshore west of Ireland.

The thermal histories derived from the thermochronological data show that the investigated segments of the IAM are dominated by Late Jurassic and Early Cretaceous cooling associated with the main phases of rifting and hyperextension in the Porcupine and Rockall basins and between the Celtic margin and its conjugate margins (North Iberia and Canada). North to south diachronous Mesozoic cooling and exhumation has been observed in thermal histories employing vertical profiles on earlier studies on the western Ireland onshore. This study shows that such a trend is not observed on the IAM. Instead, the AFT age spatial pattern complied from the new data and legacy data from Ireland and Britain points towards differential exhumation of the IAM on either side of the Anton-Dorhn Transfer Zone and its extension onto the onshore, with more exhumation observed up to the end of the Early Cretaceous on the SW, ocean-side of the lineament; while shorter-wavelength rift-shoulder uplift would explain some of the younger ages observed north of the lineament. The regional Caledonian faults were also a likely major influence. Tectonic blocks/terranes bounded by these faults seem to respond differently to the Mesozoic exhumation as observed on an AFT age map of Northern Scotland. This observation could also explain some of the dispersion seen in the exhumation trends of spatially close samples in the North Porcupine High. A regional Late Paleocene-Early Eocene exhumation event was not detected in the northern part of the IAM despite the inferred presence of a thick body of underplated igneous rock, but has been detected on the North Porcupine High as was predicted by

earlier subsidence modelling studies in the North Porcupine Basin. A km-scale Miocene exhumation event was confirmed in the northern part of the study area but was found to be absent south of the Slyne Basin.

The new geochronological dataset has led to the discovery of Dalradian metasedimentary rocks on Finnian's Spur, on the eastern edge of the North Porcupine High. These metasedimentary rocks were affected by a Caledonian tectonothermal event. A 1.7 Ga basement unit on the NW flank of the North Porcupine High has also been detected, while earlier interpretations of a granite at the bottom of a borehole on the eastern margin of the North Porcupine Basin have been reappraised as a Caledonian metaconglomerate sourced from the Grampian Belt. The age of Late Variscan granitoids that crop out on the southern tip of the Goban Spur (4000 m water depth) have been confirmed by the new apatite and zircon dating. The apatite trace element data suggests an I-type granite affinity, unlike the S-type Late Variscan granites of the Cornubian Batholith located to the NE on the same Caledonian lineament. A Cadomian granulite likely represents the local basement to these granites, while an Archean metamorphic rock with Middle Eocene AFT and AHe ages recovered from the Goban Spur is believed to represent an ice-rafted clast derived from the Archean basement of Scotland or Greenland. Similarly, a gneiss from the southern tip of the Porcupine High yielded a Mesoarchean crystallisation age and Permian AFT age and is believed to be an ice-rafted clast. In the same area, a Mesoproterozoic metagabbro and a Late Caledonian granite both yield Triassic AFT ages. They may represent *in-situ* basement but additional dating of samples from this area would be required to be confirm this.

This study also presents new geochronology data from previously undated igneous rocks from the IAM. An undated gabbro in a borehole located offshore NW Donegal (13/03-1) was dated at 297 Ma and is interpreted as a tilted gabbroic dyke that may represent the westernmost extension of the latest Carboniferous-earliest Permian tholeiitic Scottish dyke swarm. A sandstone from the eastern margin of the North Porcupine Basin (26/30-1) was revealed to be of tuffaceous origin and yielded Oxfordian volcanic apatite, while an undated dolerite from the Slyne Basin (18/25-2) was dated as Late Jurassic to Early Cretaceous. A sill of probably Paleogene age and previously interpreted as a sandstone was discovered in a borehole on the eastern margin of the North Porcupine High (34/05-1). The Late Oligocene age of three sills in a borehole from the Porcupine Basin (35/13-1) has been revised to Danian-Selandian, while the sills and lava flows from a nearby borehole (35/15-1) revealed a probable Danian age for the mafic magmatism but also Selandian zircons that are interpreted as sourced from a tuffaceous microconglomerate just above the basalts.

Acknowledgements

I would like to first thank my supervisor Prof. DAVID CHEW for his support throughout the 4.5 years of this thesis both academically but also personally. I would also like to thank him for his amazingly quick replies to any email or reviews I sent him, speeds that never failed to surprise me.

I would like to express my gratitude to ICRAG and its operational team for providing a studentship (through a grant from Science Foundation Ireland (SFI) co-funded under the European Regional Development Fund and by PIPCO RSG) and operational and training support throughout the duration of the project. I would like to sincerely thank OONAGH O'LOUGHLIN from the Department of Communications, Climate Action and Environment (DCCAE, ex-PAD) for handling my numerous sampling and data requests, EWAN PELLETER and THIERRY DALLE MULLE from Ifremer for allowing and organising a sampling trip at their core store in Brest and KERRY GALLAGHER from the University of Rennes for providing access to QTQt and kindly replying to questions I had.

I would like to also thank my office team mates through the years, in particular CLAIRE A., KERSTIN D., ISADORA H., CESCO and VINCENT M. with which I really enjoyed chatting and working with for the last couple of years, and before that CHRIS M., REJANE, DANIEL G. and NATHAN C. Also a big thank to FRANK, CORA, MAURA, NOEL, LEONA, COLLIN, FOTEINI and PAUL for their great help and support for sample preparation and lab work. Thank you also to MARIA JUDGE from the GSI for her time and help regarding finding some seabed temperature data, BRYONY STEWART at Schlumberger for proving free academic Petrel licences, ALICE MITCHINSON and MARTIN DAVIES from PIP for providing free PIP reports, ROB RAINE from the GNSI for providing some AFT reports from Northern Ireland, BEN KING from the PESGB for giving free Atlantic Margin structural maps, KARA ENGLISH from PAD for tips, MARGARET ROONEY at TCD for helping me find textbooks and past theses, JACKIE JAMES from the UK Environment Agency for giving me some background information about some mysterious cuttings in the TCD archives, MUDASAR SAQAB at UCD for providing some merged seismic surveys, DAMIEN GAGNEVIN at UCD for providing some VR data, and BERNHARD FÜGENSCHUH and BERNHARD NIKOLAUS from the University of Bonn for their help identifying their Goban Spur sample from their paper.

Finally a big thank to my partner SHARON for supporting me the last couple of years and in particular in the final few months for being patient despite spending quite a few weekends and late nights on the thesis.

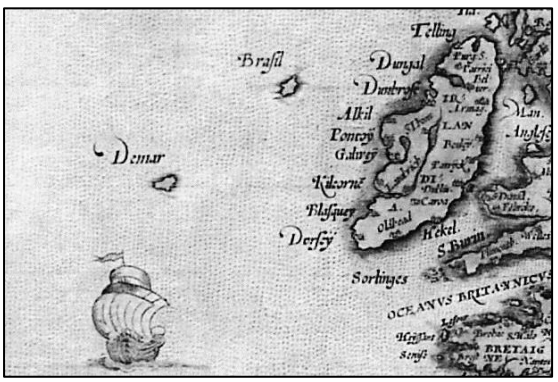

The Irish Atlantic Margin as represented in a 16th-century map of Europe (Ortelius, 1572)

Table of figures

Table of tables

1 Introduction

1.1 Uplift of the NW European Continental Margin

The NW European Continental Margin (NWECM), which extends from the Armorican shelf in the south to the Western Barents Sea Margin in the north, resulted from the break-up of Pangea during the Early Cretaceous (separation of the Armorican/Celtic margin from the Iberian and NE Canadian margins at 125-83 Ma) and Paleogene (separation of the NE Atlantic margin from the Greenland margin at 54-25 Ma) (Ziegler (1988); Doré et al. (1999); Ellis and Stoker (2014)). Prior to break-up, aborted rifting resulted in the creation of many sedimentary basins throughout the entire NWECM, with depocenters that tend to become younger towards the present-day continent-ocean boundary (Doré et al., 1999) (FIGURE 1).

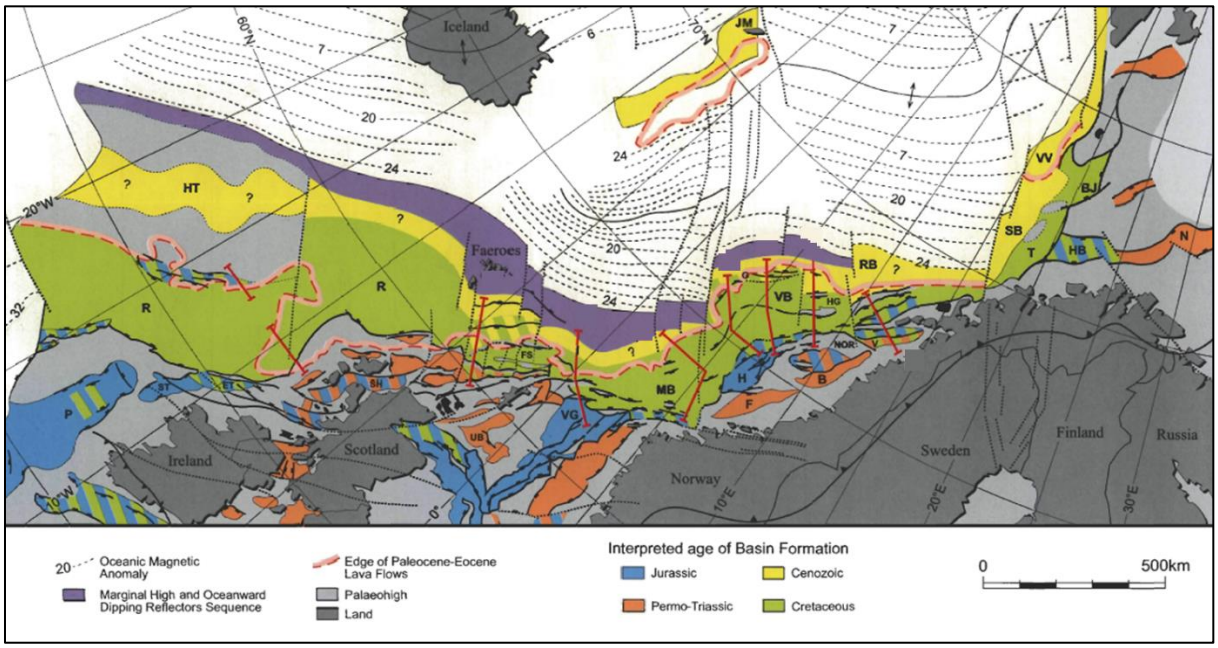

Figure 1: Geological map of the NW European Continental Margin (modified after Doré et al. (1999))

The NWECM is a typical 'passive' margin, as opposed to margins with tectonic activity caused by subduction, oceanic accretion, or transfer fault movements. As such the primary geodynamical process affecting the margin after break-up is post-rift thermal subsidence. However, during the past few decades, several Cenozoic episodes of uplift or subsidence not predicted by post-rift thermal subsidence models (McKenzie (1978); Jarvis and McKenzie (1980)), and therefore often described as 'anomalous', have been identified throughout the margin (see reviews in Japsen and Chalmers (2000); Doré et al. (2002); Praeg et al. (2005); Stoker et al. (2005); Holford et al. (2009); Anell et al. (2009)).

Three main episodes of regional Cenozoic uplifts have been identified as affecting the entire NWECM: 1) break-up: Paleocene-Early Eocene (c. 60-50 Ma); 2) post-break-up: Mid-Cenozoic (40-25 Ma) and 3) Late Cenozoic (c. 20-0 Ma) (FIGURE 2).

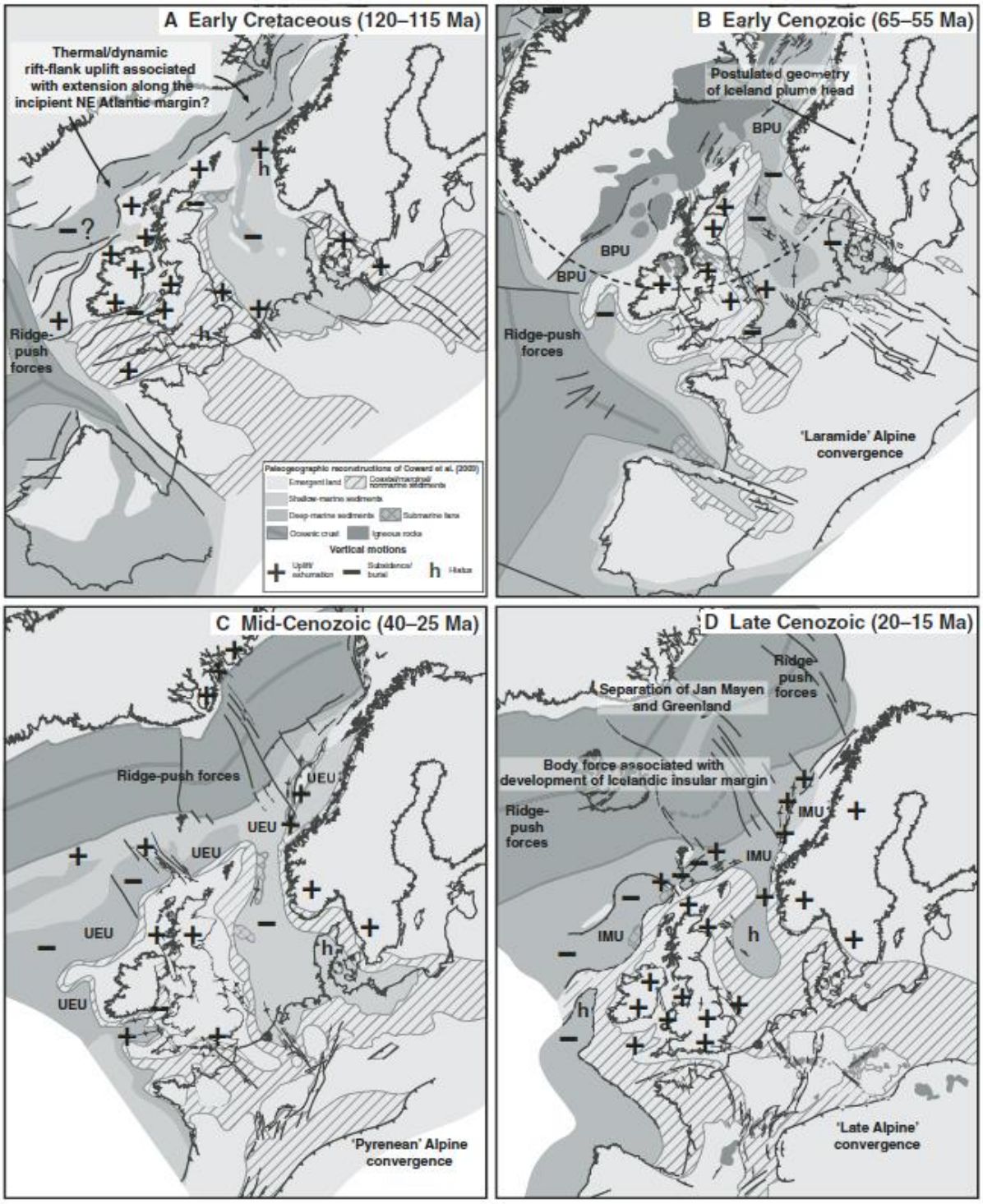

Figure 2: Paleogeographic maps of NW Europe with main patterns of uplift and subsidence during the a) Early Cretaceous, b) Early Cenozoic, c) Mid-Cenozoic and d) Late Cenoeozic (Holford et al., 2009)

There is on-going debate about the cause of these exhumation events which hinges on the role played by the proto-Icelandic Plume. Many mechanisms have been invoked and they can be categorized as plume-related or non-plume-related.

The plume-related mechanisms are 1) dynamic uplift above the plume head and advection of mantle plume material, which creates transient uplift followed by renewed subsidence and has been invoked to explain episodes of Paleocene to Early Eocene uplift all around the NE Atlantic (White and McKenzie (1989); Knox (1996); Underhill (2001); Jones et al. (2001b); Smallwood and Gill (2002); Maclennan and Jones (2006); Champion et al. (2008a); Rudge et al. (2008); Hartley et al. (2011); Barnett-Moore et al. (2017)); 2) *idem* but leading to permanent ponding of plume materials (Bott and Bott (2004); Arrowsmith et al. (2005)); 3) mafic igneous underplating leading to permanent uplift (Cox et al. (1993), Brodie and White (1994); Brodie and White (1995); Clift and Turner (1998); Rowley and White (1998); White and Lovell (1997); Maclennan and Lovell (2002); Jones et al. (2002); Al-Kindi et al. (2003); Tiley et al. (2004); Mackay et al. (2005); Tomlinson et al. (2006); Davis et al. (2012); Cogné et al. (2016); Łuszczak et al. (2018)); and 4) partial lithospheric delamination caused by the arrival of the plume at the base of the lithosphere (Nielsen et al., 2002).

However, the existence of the proto-Icelandic plume during the Paleogene has been questioned (Ellis and Stoker, 2014), leading to alternative non-plume-related explanations for Paleogene uplift such as 1) rift flank uplift in areas close to active Paleogene rifting (Ellis and Stoker (2014); Mudge (2015)); 2) syn-rift compressional deformation, again, only in areas affected by Paleogene rifting such as the Farore-Shetland Basin (Stoker et al., 2018) and 3) the interaction of mantle flow-derived dynamic topography with overlying moving plates (Hoggard et al., 2016).

For the post-break-up uplift, several additional mechanisms have been invoked, such as 1) plate-boundary deformation, *i.e.* the far-field transmission of compressional forces generated at the plate boundary, such as the Pyrenean and Late Alpine phases of the Alpine Orogenies in the SE, continuous ridge push effects from the Atlantic Mid-oceanic Ridge in the NW and SW (Cloetingh et al., 1990; Hillis et al., 2008; Holford et al., 2009; Holford et al., 2008) and singular localized events that impact the stress field such as the formation of the Iceland Plateau in the Mid-Miocene to the present-day (Doré et al. (2008); Stoker et al. (2010)); 2) ridge depleted mantle flow under the continental crust (Carminati et al., 2009); 3) an astenospheric diapir model (Rayleigh-Taylor instability caused by hot buoyant asthenosphere below a cold lithosphere) (Rohrman and van der Beek, 1996) and 4) post-glaciation isostatic rebound, which explains part of the Late Neogene uplift observed on the margin.

The debate about the origin and nature of these anomalous uplift events is highly dependent on constraining their spatial extension, timing, duration, and magnitude. The qualitative and quantitative,

spatial and temporal, characterisation of these events has been provided by a large suite of techniques including backstripping and tectonic subsidence modelling, compaction studies (sonic or seismic velocities), mass balance studies, vitrinite reflectance studies, geomorphological analyses, seismic stratigraphy and structural reconstruction and low-temperature thermochronology (see reviews of techniques in Corcoran and Doré (2005) and Anell et al. (2009)). Among all these techniques, low-temperature thermochronology has the advantages of providing absolute time constraints on uplift events and a minimum estimate on the amount of exhumation, and does not rely on the preservation of post-erosion sediments.

1.2 A brief history of low-temperature thermochronology in the British Isles

1.2.1 Introduction

There is a long history of apatite thermochronological studies in Britain and Ireland. A compilation of 29 peer-reviewed papers yielded 632 AFT ages and 109 AHe ages, while 27 Geotrack industry reports from Ireland (Geotrack reports from the UK have not been requested for this study), two TCD PhD theses and an unpublished TCD dataset yielded another 225 AFT ages and 21 AHe ages (FIGURE 3 AND FIGURE 4).

The first published studies were by Hurford in the late 1970s (Hurford, 1977a; Hurford, 1977b). These early studies were aimed at developing the still new technique of fission track analysis and assess if they would give meaningful age information. Using Scottish granites, he found both Mesosoic and Paleogene AFT ages which became the premises for two dominant topics of research in the following decades: 1) the exhumation of Scotland, and the Britain and Ireland in general, during the Mesozoic rifting; and 2) the origin of anomalously young AFT ages around the Irish Sea. From a methodological point of view, these early studies used a variety of apatite fission track dating techniques (external detector method or EDM, population method and same grain method) reflecting the period of pre-standardization of the EDM and zeta approach that would come to dominate from the 1980s until now (FIGURE 3).

1.2.2 Exhumation of the British Isles

Numerous studies focused on the exhumation of Scotland (Hurford (1977b); Lewis et al. (1992a); Carter et al. (1995); Thomson et al. (1999) ; Jolivet (2007) ; Persano et al. (2007); Holford et al. (2010) and Fame et al. (2018)) while fewer studies have targeted the exhumation of the rest of Great Britain. Such studies have been undertaken in the East Midlands (Green, 1989), in Wales (Carter, 1990) and in Cornwall (Chen et al., 1996).

Reference	Location	Methods		Samples	Etching protocol	Age eq.		Lengths		Kin.	Modelling
		AFT	AHe			Grains	Type	MTL	Proj.		FMorIM
Hurford, 1997a	Scotland - Highlands	POP EDM SAME	-	24	5M 10-30s@20°C	Aliquot	Abs.	-	-	-	-
Hurford 1977b	Scotland - Lowlands	POP	-	5	5M 20s@room T.	Aliquot	Abs.	-	-	-	-
Duddy et al 1983	Ireland - Rockall Plateau	EDM	-	5	5M 20s@20°C	Single	Abs.+Zeta	Yes	-	-	-
Green 1986	England - North	EDM	-	23	5M 20s@room T.	Single	Zeta	Yes	-	-	-
Green 1989	England - East Midlands	EDM	-	62	?	?	Zeta	Yes	-	-	-
Carter 1990	Wales - North	EDM	-	5	5M 15s@20°C	?	Zeta	-	-	-	-
Hurford 1990	England - Northwest	EDM	-	2	?	?	Zeta	-	-	-	-
Lewis et al 1992a	Scotland - Islands	EDM	-	39	?	?	Zeta	Yes	-	-	AFTAMOD
Lewis et al 1992b	England - Northwest	EDM	-	45	?	?	Zeta	Yes	-	-	AFTAMOD
Keeley et al 1993	Ireland - Southeast	EDM	-	10	?	Single	Zeta	Yes	-	-	AFTAMOD
McCulloch 1993	Ireland - All onshore & offshore W Ireland	EDM	-	64	5M 20s@room T.	Single	Zeta	Yes	-	-	Yes
McCulloch 1994	Ireland - Northeast	EDM	-	16	5M 20s@room T.	Single	Zeta	Yes	-	-	?
Carter et al 1995	Scotland - Highlands	EDM	-	2	?	Single	Zeta	Yes	-	-	-
Chen et al 1996	England - Southwest	EDM	-	4	?	Single	Zeta	Yes	-	-	Yes
Thomson et al 1999	Scotland - Highlands	EDM	-	31	?	Single	Zeta	Yes	-	Cl(?)	Yes
Green et al 2000	Ireland - All onshore	EDM	-	32	?	Single	Zeta	Yes	-	?	?
Allen et al 2002	Ireland - All onshore	EDM	-	71	5M HNO3 20s@20±1°C	Single	Zeta	Yes	-	-	Yes
Green 2002	England - Northwest	EDM	-	6	?	Single	Zeta	Yes	-	?	?
Fugenshuh et al 2003	Ireland - Goban Spur	EDM	-	1 (6)	6.5% HNO3 40s@20°C	Single	Zeta	Yes	-	-	-
Jolivet 2007	Scotland - Highlands	EDM	-	17	6.5% HNO3 45s@20°C	Single	Zeta	Yes	-	Dpar	AFTSolve
Persano et al 2007	Scotland - Islands & Highlands	EDM	AHe	7/12	n/a	Aliquot	Zeta	Yes	-	Dpar	AFTSolve
Holford et al 2010	Scotland - Islands & Highlands	EDM	-	78	?	Single	Zeta	Yes	-	-	*in-house*
Cogné et al 2014	Ireland - West	LAFT	AHe	23	5.5M 20s@21°C	Single	L-Zeta	Yes	Yes	Dpar/Cl	QTQt
Cogné et al 2016	Ireland & UK - Peri-Irish Sea	LAFT	AHe	42	5.5M 20s@21°C	Single	L-Zeta	Yes	Yes	Dpar/Cl	QTQt
Doepke 2017	Ireland & Scotland	LAFT	AHe	18	5.5M 20s@21°C	Single	L-Zeta	Yes	Yes	Dpar/Cl	QTQt
Łuszczak et al 2017	Northwest England & Scottish Lowlands	EDM	-	22	5.5M 20s@20°C	Single	Zeta	Yes	Yes	Dpar	QTQt
Fame et al 2018	Scotland - Islands & Highlands	-	AHe	15	n/a	Single	N/A	n/a	n/a	n/a	QTQt
Łuszczak et al 2018	Northwest England & Scottish Lowlands	-	AHe	20	n/a	Single	N/A	n/a	n/a	n/a	QTQt
This study	**Ireland - Offshore W Ireland**	**LAFT**	**AHe**		**5.5M 20s@21°C**	Single	**L-Zeta**	Yes	Yes	**Dpar/Cl**	**QTQt**
Geotrack, 1991	27/13-1	EDM	-	3	5M HNO3 20s@20°C	Single	Zeta	Yes	-	Cl	*in-house*
Geotrack, 1992	27/13-1	EDM	-	6	5M HNO3 20s@20°C	Single	Zeta	Yes	-	Cl	*in-house*
Geotrack, 1993a	42/12-1, 48/19-1, 49/9-1, 50/3-1, 57/9-1	EDM	-	9	5M HNO3 20s@20°C	Single	Zeta	Yes	-	Cl	*in-house*
Geotrack, 1993b	12/13-1	EDM	-	6	5M HNO3 20s@20°C	Single	Zeta	Yes	-	Cl	*in-house*
Geotrack, 1994	56/14-1	EDM	-	7	5M HNO3 20s@20°C	Single	Zeta	Yes	-	Cl	*in-house*
Geotrack, 1995a	42/12-1, 42/17-1	EDM	-	6	5M HNO3 20s@20°C	Single	Zeta	Yes	-	Cl	*in-house*
Geotrack, 1995b	33/17-1, 33/21-1, 33/22-1,	EDM	-	14	5M HNO3 20s@20°C	Single	Zeta	Yes	-	Cl	*in-house*
Geotrack, 1996	27/05-1	EDM	-	7	5M HNO3 20s@20°C	Single	Zeta	Yes	-	Cl	*in-house*
Geotrack, 1997a	18/20-1	EDM	-	10	5M HNO3 20s@20°C	Single	Zeta	Yes	-	Cl	*in-house*
Geotrack, 1997b	19/05-1	EDM	-	6	5M HNO3 20s@20°C	Single	Zeta	Yes	-	Cl	*in-house*
Geotrack, 1997c	18/20-1, 27/05-1, 27/13-1	EDM	-	26	5M HNO3 20s@20°C	Single	Zeta	Yes	-	Cl	*in-house*
Geotrack, 1999	42/16-1, 42/21-1	EDM	-	8	5M HNO3 20s@20°C	Single	Zeta	Yes	-	Cl	*in-house*
Geotrack, 2001a	16/28-sb01, 83/20-sb01, 24-sb01, 02	EDM	-	12	5M HNO3 20s@20°C	Single	Zeta	Yes	-	Cl	*in-house*
Geotrack, 2001b	05/22-1	EDM	-	7	5M HNO3 20s@20°C	Single	Z				
Geotrack, 2002	26/28-1, 35/08-2	EDM	-	6	5M HNO3 20s@20°C	Single	Z				
Geotrack, 2003	12/02-1	EDM	-	6	5M HNO3 20s@20°C	Single	Z				
Geotrack, 2004a	43/13-1	EDM	-	5	5M HNO3 20s@20°C	Single	Z				
Geotrack, 2004b	19/11-1A	EDM	-	4	5M HNO3 20s@20°C	Single	Z				
Geotrack, 2004c	18/20-1, 18/25-1, 18/25-2, 19/05-1, 11-1A	EDM	-	40	5M HNO3 20s@20°C	Single	Z				
Geotrack, 2005a	48/30-1, 49/26-1A	EDM	-	11	5M HNO3 20s@20°C	Single	Z				
Geotrack, 2005b	42/21-1	EDM	-	9	5M HNO3 20s@20°C	Single	Z				
Geotrack, 2008	19/08-1	EDM	-	7	5M HNO3 20s@20°C	Single	Z				

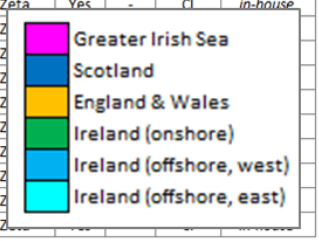

Figure 3: Summary of all published AFT and AHe data/- for the Britain and Ireland (top) and the offshore Ireland Geotrack industry reports (bottom).*

The first Irish study was actually an apatite and titanite FT study undertaken on a very remote part of the Irish Atlantic margin, the Hatton Bank, as part of the DSDP Leg 81 campaign (Duddy et al., 1983) (FIGURE 4). In the mid-1990s, the first AFT data were obtained for onshore Ireland and some boreholes in the Donegal and Porcupine Basin offshore west of Ireland (Keeley et al. (1993); McCulloch (1993); McCulloch (1994)).

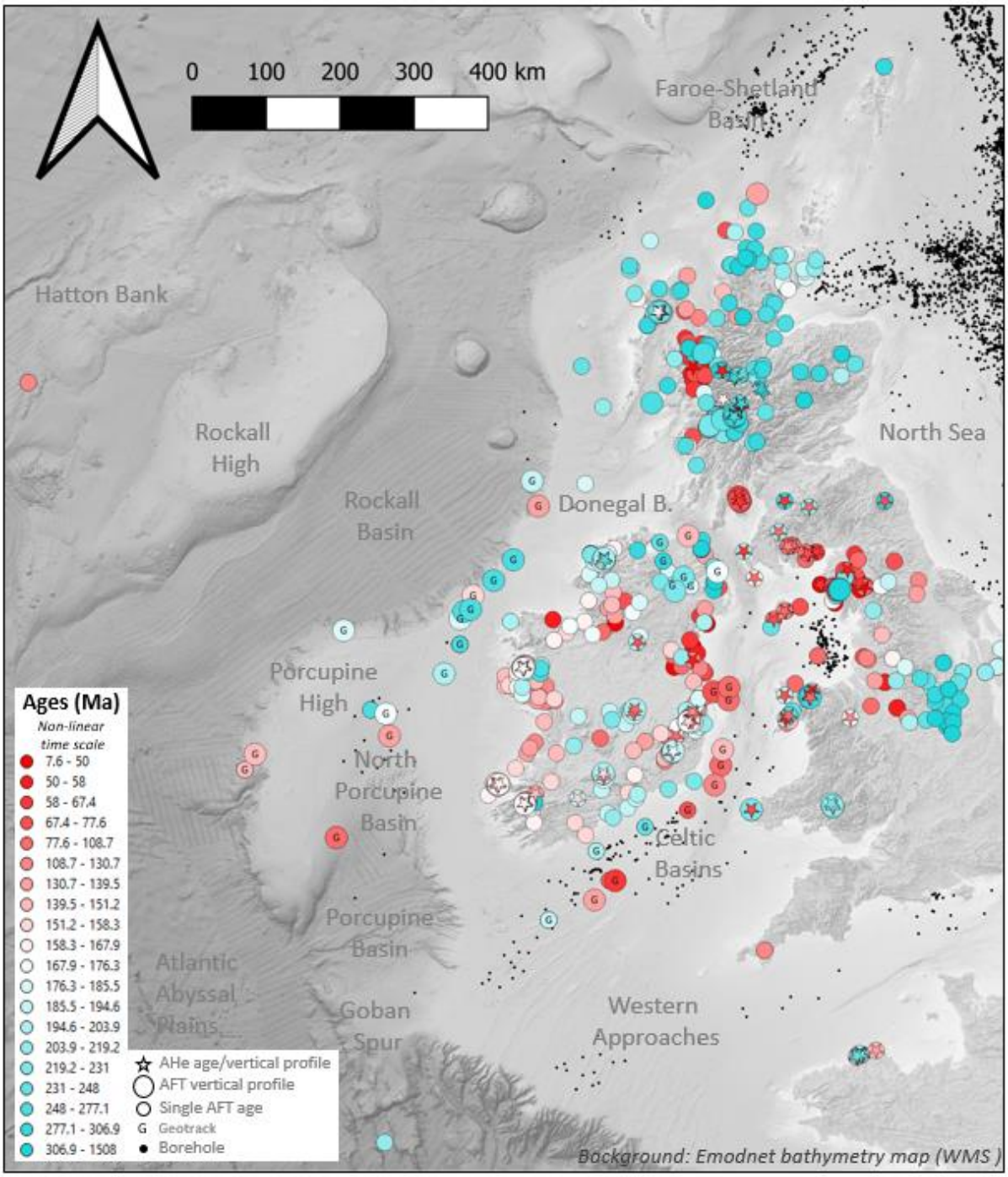

Figure 4: Map of legacy low-temperature thermochronological studies in the British-Irish Isles

These local studies were expanded in the early 2000s by two large-scale, all-Ireland, onshore studies that indicated post-Triassic denudation in the range of 2-4 km but with a large spatial and temporal variation (Green et al. (2000); Allen et al. (2002)) (FIGURE 4). Overall, these studies demonstrated cumulative exhumation of <4 km on the western cost and on the eastern coast between Dublin and Co. Down, and <2km in the Midlands and NE of Ireland; of which 1-2 km occurring during the Cenozoic. After these large-scale regional studies, the first fission track data from the offshore Goban Spur area were published (Fügenschuh et al., 2003), while more recently, a team at TCD used LA-ICP-MS AFT-

U/Pb dual-dating and AHe dating of samples on vertical profiles throughout Ireland to better constrain small-scale exhumation events (Cogné et al. (2014), Cogné et al. (2016), Döpke (2017)). They concluded that c. 2.5 km of exhumation occurent during the Late Jurassic-Early Cretaceous on the western coast of Ireland, probably due to rift-shoulder uplift, followed by another major phase of 1-2 km exhumation during the late Neogene, although the post-rift thermal history might have been more complex and with additional exhumation events such as during the Paleogene (Cogné et al., 2014). They also noted that the timing of exhumation becomes younger towards the south, starting at c. 180 Ma in NW Ireland and as young as c. 125 Ma in the SW of Ireland (Cogné et al., 2014). A similar trend can be observed on the scale of Britain and Ireland using the surface AFT central ages with the oldest ages in Scotland and NE Ireland and younger ages for the rest of Ireland (FIGURE 4). Cogné et al. (2014) proposed that rift-shoulder uplift, associated with a southwards-propagating mid-Mesozoic rifting activity offshore west of Ireland, might be a possible mechanism to explain the age pattern. This hypothesis could be further tested by analysing the Mesozoic exhumation history of the highs offshore Ireland (Slyne-Erris, Porcupine Highs) as they were spatially closer to the locus of rifting in the Porcupine and Rockall Basins (FIGURE 4). The combination of both AFT and AHe thermochornometers and a vertical profile approach allowed the detection of c. 1 to 2 km of exhumation in the east of Ireland and the Central Irish Sea during the Early Cenozoic (Cogné et al., 2016), part of what is termed here the 'Greater Irish Sea anomaly' (see discussion in next section).

1.2.3 The Greater Irish Sea anomaly

One of the topics that has attracted the attention of most studies since the 1980s is the anomalously young fission track ages found in Cumbria (UK), the central Irish Sea and parts of the east coast of Ireland, and here termed the 'Greater Irish Sea anomaly' (FIGURE 5). After anomalous young AFT ages were found in southern Scotland (Hurford, 1977a), the first study was initiated by Green (due to a childhood school trip, see review in Oldroyd (2002)) in NW England (Green, 1986). Subsequent studies then provided new constraints on the spatial extent of the anomaly (Hurford (1990a), Lewis et al. (1992c), Green et al. (1993), McCulloch (1994), Green et al. (1997), Green et al. (2002), Green (2002)). The last study was the first vertical profile study in the British Isles and concluded that the anomaly was caused by elevated heat flows and paleogeothermal gradient (c. 60°.km^{-1}) during the early Cenozoic combined with c. 700 m of exhumation (Green, 2002), contrary to previous studies that invoked a much larger exhumation (e.g. 3 km, Lewis et al. (1992c)). A detailed review of the exhumation studies of NW England and the associated debates, from the early 20th century until 2000, can be found in Oldroyd (2002).

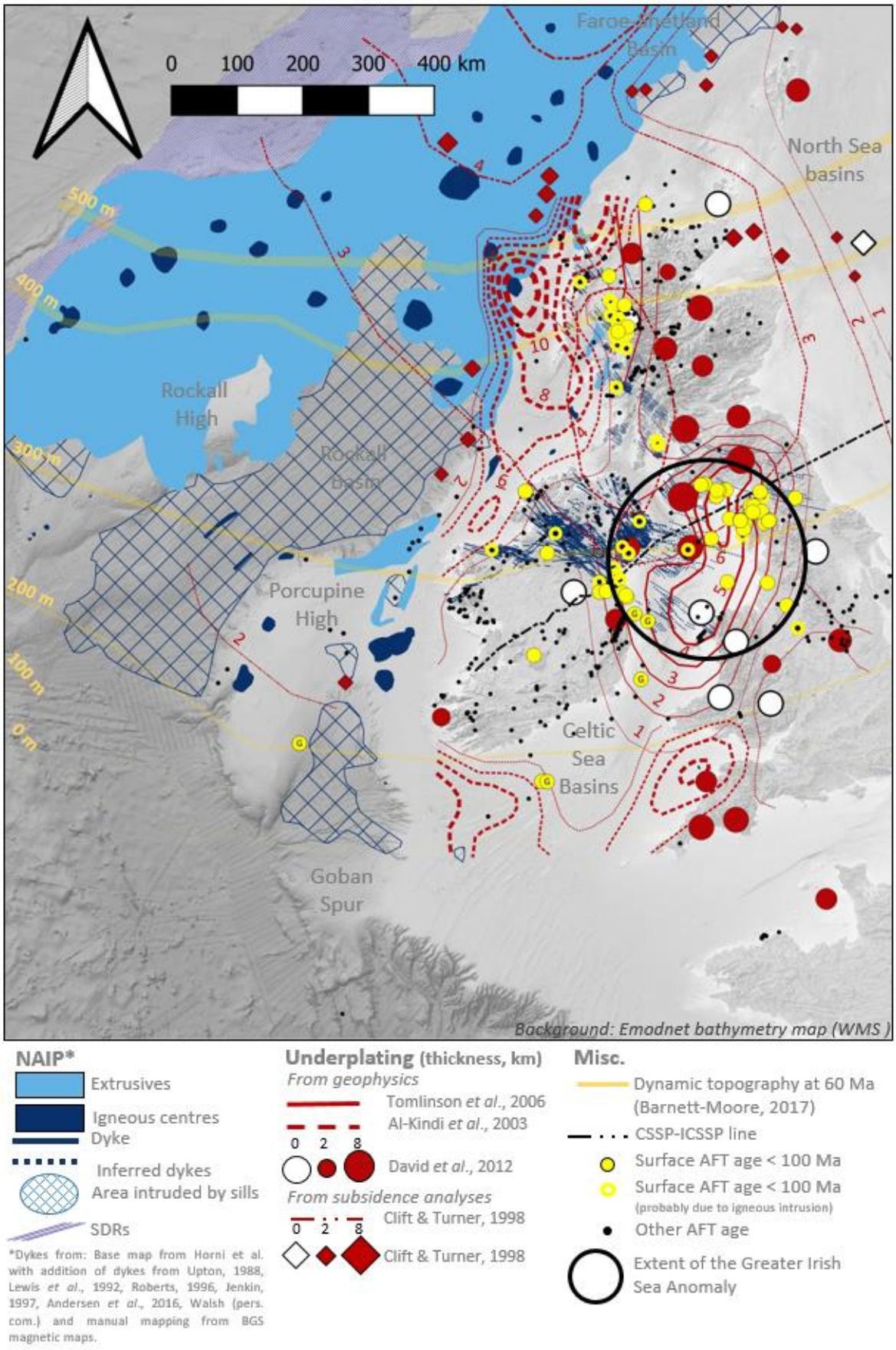

Figure 5: Summary of estimates of thickness of igneous underplating under the British-Irish Isles and surrounding offshore area, NAIP magmatism and extent of the Greater Irish Sea Anomaly.

The topic was recently re-visited with the use of modern AFT techniques (such as projected track lengths, compositional proxies), the AHe and ZHe thermochronometers and thermal history inverse modelling (QTQt, Pecube) (FIGURE 3) to shed a new light on the origin of the anomaly (Cogné et al. (2016), Döpke (2017), Łuszczak et al. (2017) and Łuszczak et al. (2018)).

Combining all these recent studies, it is likely that the Paleogene AFT and AHe ages of the Greater Irish Sea anomaly were caused by a series of uplift and erosion event between 70-40 Ma with a peak at c. 60-56 Ma (just before continental breakup and oceanization of the Northeast Atlantic). These exhumation events were probably caused by a combination of 1) a localized permanent uplift centered on the eastern part of the Irish Sea induced by mafic magmatic underplating and 2) a transient regional uplift affecting the entire NEAM and caused by the Iceland mantle plume swell (Łuszczak et al., 2018). In total, 1-2.4 km of rocks were eroded during the Early Cenozoic in this area (Łuszczak et al., 2018) while the paleogeothermal gradient is estimated to vary between 40-100°C.km^{-1} in the now eroded sediments above the high heat-generating granitic batholiths (thermal blanket effect; Holliday (1993), Łuszczak et al. (2017)).

If the exhumation associated with the Greater Irish Sea anomaly is indeed primarily driven by magmatic underplating originating from the proto-Icelandic plume, then a continuous exhumation trail should be expected to extend from the plume to the Irish Sea, such as has been mapped by Clift and Turner (1998) using backstripping and tectonic subsidence modeling in boreholes (FIGURE 5). The presence of a high-velocity body at the base of the crust below the Irish Sea and NW England has been confirmed and constrained by numerous geophysical studies (CSSP-ICSSP line: Al-Kindi et al. (2003) and Tiley et al. (2004); single seismometers spread across Scotland-NW England: Tomlinson et al. (2006) and Davis et al. (2012)). However, the datasets and studies do not agree on the distribution and geometry of these high-velocity bodies in other parts of the British-Irish Isles. For example, Davis et al. (2012) identify a thick body below Scotland but no such body in the Hebrides, while on the contrary Tomlinson et al. (2006) identify a thick body below the Hebrides but none below the central part of Scotland (FIGURE 5). Also, the linear belt of igneous centres and dyke swarms extending from the Faroes to NE Ireland and Scotland (FIGURE 5) has been interpreted as representing the surface footprint of underlying magmatic underplating (Rowley and White, 1998). But the area that has been the most affected by Late Paleocene-Early Eocene exhumation (with AFT ages <100 Ma), *i.e.* NW England and the eastern part of the Central Irish Sea, does not contain many intrusions, contrary to NE Ireland and the Hebrides and west of Scotland which did not experience this major Paleogene exhumation (FIGURE 5). Finally, the correlation between thermal history-based exhumation and underplating in Scotland in Cogné et al. (2016) is mostly dependent on the Isle of Arran samples, which are from a Paleocene granite. Although the nature and texture of the Arran granite implies at least 2 km of exhumation post-

emplacement, this exhumation might have partly occurred during the Neogene and therefore the 2 km exhumation constraint is not a reliable data point as suggested in their map.

Consequently, while the Greater Irish Sea anomaly is most probably related to the high-velocity body at the base of the crust that can be observed in the geophysical dataset; its nature, origin, extent in NW Scotland and in the offshore parts of NW Ireland and Scotland, and any possible associated Paleogene exhumation, remain much more uncertain and shed some doubts on its Icelandic provenance.

The geophysical datasets do not extend to the Porcupine and Rockall basins, only to the offshore Donegal platform (FIGURE 5). Offshore NW Donegal, a small 6 km-thick body seems to be the southern extension of a 12 km-thick body centered on St Kilda, NW of the Outer Hebrides (Al-Kindi et al., 2003) (FIGURE 5). Constraining the Late Paleocene-Early Eocene at this location might help better understand the nature and origin of these bodies and their relantionship with the exhumation of onshore Britain and Ireland and their offshore platforms, while the pattern of exhumation in the rest of the IAM, where no suitable geophysical data is available, might help predicts the location of the these bodies

1.3 Geology and exhumation of the offshore Irish Atlantic margin

1.3.1 Geological history of the Irish Atlantic Margin

The Irish Atlantic Margin (IAM) is the southern and widest segment of the NWECM (FIGURE 1). The IAM comprises a series of inboard (elongated, shallow waters) basins (Donegal-Malin, Slyne, Erris and Northern Porcupine basins), outboard deep-water basins (Goban Spur, Porcupine, Rockall and Hatton Basins) separated by basement highs (Erris Ridge, Porcupine High, Rockall High, Hatton High) and by the Irish Mainland Platform which extends between onshore Ireland and the offshore basins (Naylor and Shannon, 2005) (FIGURE 6).

Like the rest of the NWECM, the offshore basement geology is poorly constrained by only a few boreholes and dredges and relies mostly on the projected offshore extension of the onshore terranes and Caledonian faults (FIGURE 7). Broadly, the Donegal, Slyne, Erris, North Porcupine basins and most of the Porcupine High are underlain by Paleoproterozoic to Ordovician-Silurian basement associated with the Laurentian margin while the southern part of the Porcupine High and Basin and the Goban Spur are underlain by Avalonian basement; while remnants of Devonian and Carboniferous basins are found dispersed throughout the margin (Tate and Dobson (1989); Roberts et al. (1999); Štolfová and Shannon (2009)).

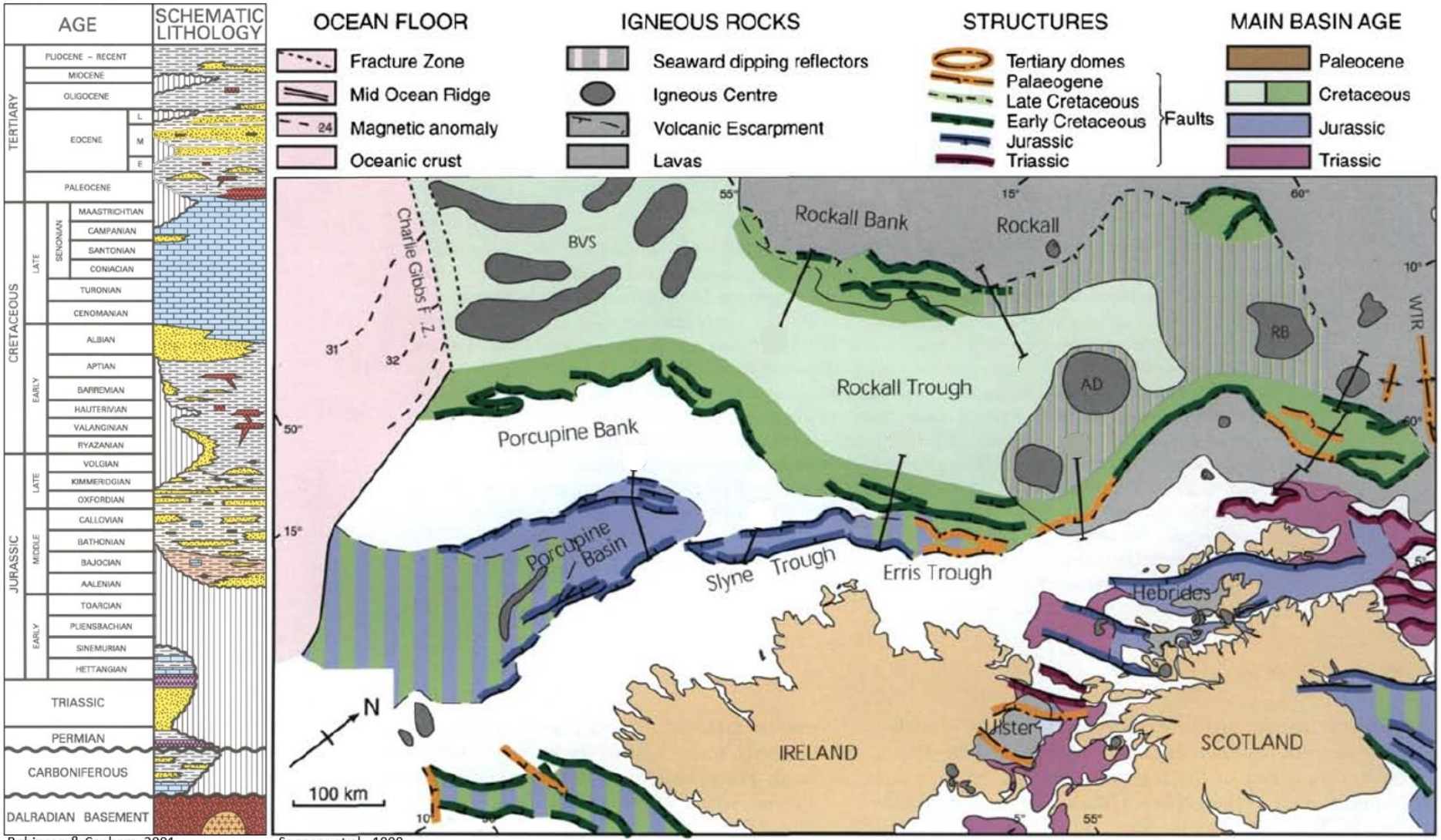

Figure 6: Geological map of the Irish Atlantic Margin and a representative lithostratigraphic column from the Porcupine Basin (after Robinson and Canham (2001) and Spencer et al. (1999)).

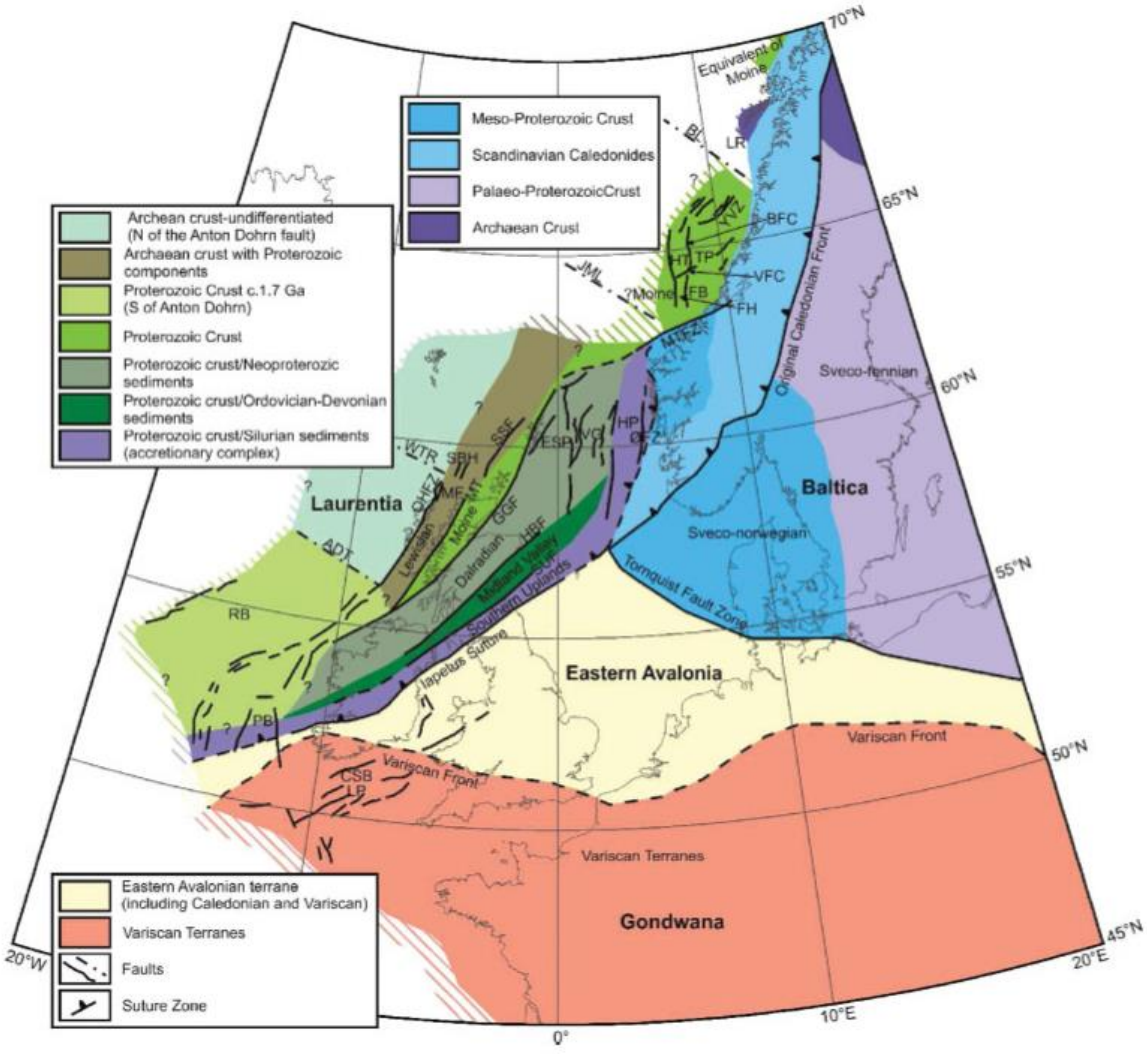

Figure 7: Structural and terrane map of the North-West European Atlantic Margin (Štolfová and Shannon, 2009). ADT, Anton Dohrn Transfer; BFC, Bremstein Fault Complex; BL, Bivrost Lineament; CSB, Celtic Sea Basins; ESP, East Shetland Platform; FB, Froan Basin; FH, Frøya High; GGF, Great Glen Fault; HBF, Highland Boundary Fault; JML, Jan Mayen Lineament; HP, Horda Platform; HT, Halten Terrace; LP, Labadie Bank-Pembrokeshire Ridge; LR, Lofoten Ridge; MF, Minch Fault; MTFZ, Møre-Trøndelag Fault Zone; MT, Moine Thrust; ØFZ, Oygarden Fault Zone; OHFZ, Outer Hebrides Fault Zone; PB, Porcupine Basin; RB, Rockall Basin; SBH, Solan Bank High; SSF, Shetland Spine Fault; SUF, Southern Upland Fault; TP, Trøndelag Platform; VFC, Vingleia Fault Complex; VG, Viking Graben; WTR,Wyville-Thompson Ridge; YVZ, Ylvingen Fault Zone. Dashed areas represent uncertain terrane occurrence or boundary

During the Permian and Triassic, the collapse of the Variscan Orogen led to the creation of multiple, narrow, fault-bounded basins, either due to rifting or simply due to post-orogenic sagging. Rifting associated with the opening of the Atlantic started in the Middle Jurassic (notably in the Slyne Basin) but the main phase of rifting occurred during the Late Jurassic in the Porcupine and Rockall Basins (Johnston et al. (2001), Naylor and Shannon (2005)).

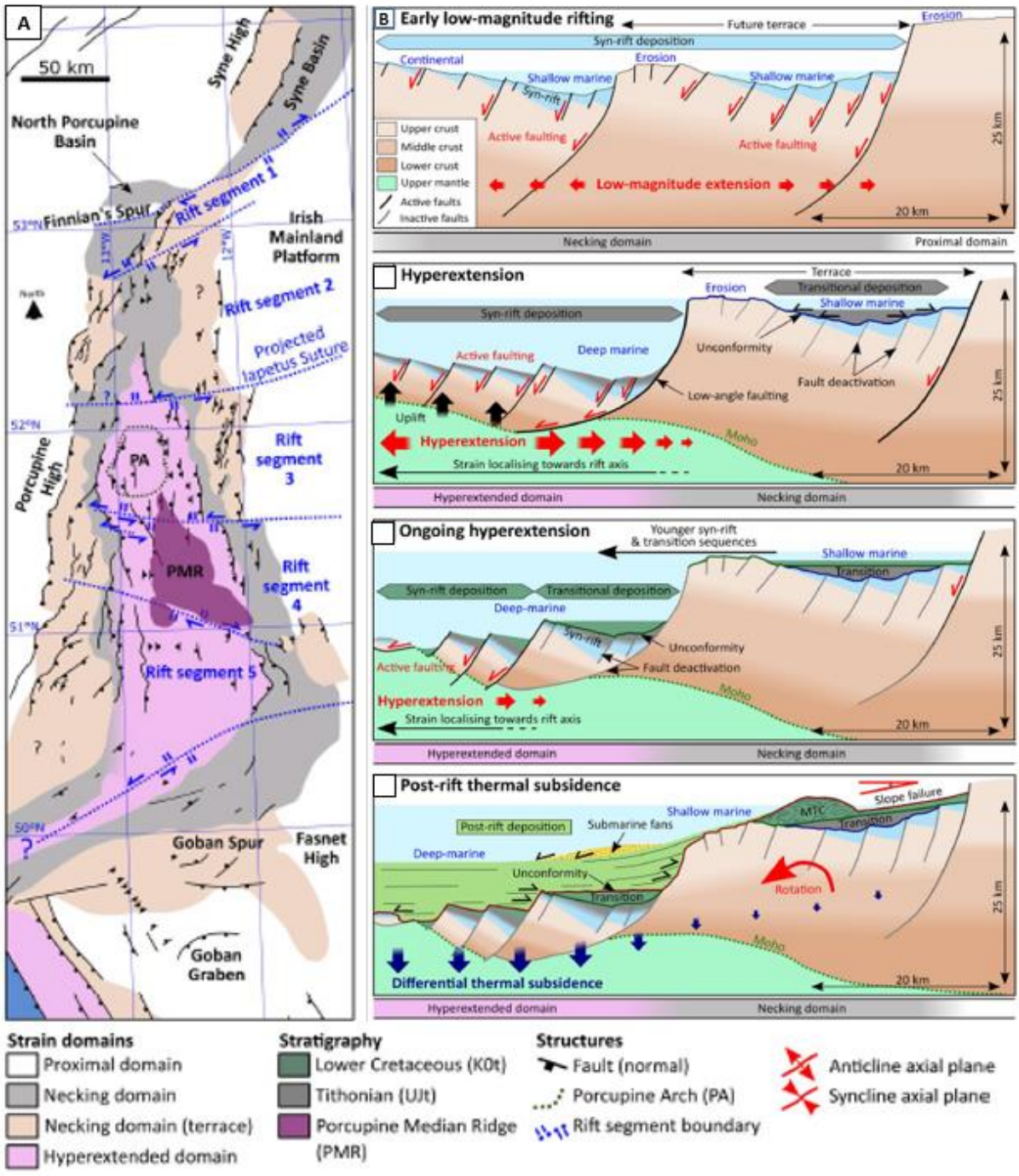

Figure 8: A) Crustal architecture of the hyperextended Porcupine Basin; and B) conceptual sedimentary filling of hyperextended basins during the syn-rift, transitional/hyperextenion and post-rift phases (Whiting et al., 2020).

During the Late Jurassic, the Rockall and Porcupine Basins experienced hyperextension and possibly localized mantle exhumation (Lundin and Doré (2011); Whiting et al. (2020)) (FIGURE 8). A margin-wide erosional unconformity (the Base Cretaceous Unconformity, BCU) separates the Late Jurassic sediments from the Early Cretaceous sediments in the inboard basins of the IAM and marks the end of the Late Jurassic phase of rifting and extension dominated by brittle faulting (Naylor and Shannon, 2009). The uplift and erosion is poorly understood but believed to have been caused by a major plate reorganisation combined with an eustatic sea-level lowstand (Doré et al., 1999).

Hyperextension might have continued in the south Porcupine Basin and Rockall Basin during the Berriasian-Hauterivian but had mostly stopped by then in the North Porcupine Basin (Johnston et al., 2001), which experienced the onset of post-rift thermal subsidence. A major phase of plate re-organization occurred during Barremian-Albian times, with sea-floor spreading starting between Iberia and NE Canada at 118 Ma and in Early Albian times in the Bay of Biscay and between the IAM and NE Canada (Nirrengarten et al., 2018), leading to regional uplift and minor magmatism, except for the south Porcupine Basin that recorded subsidence, possibly due to depth-dependent extension (Baxter et al., 2001).

During the Late Cretaceous to Paleocene, post-rift subsidence dominated over sedimentation, which combined with coeval sea-level highstands, created deep-water conditions in the Porcupine and Rockall basins. The Late Cretaceous-Danian succession is dominated by limestones and chalks that probably covered the entire margin as well as what is presently onshore Ireland (Naylor and Shannon, 2005). Subsidence was interrupted by several episodes of regional uplift during Paleocene to Middle Eocene, creating several erosional unconformities across the area (the Base Paleogene Unconformity, BPU and the Lower Eocene Unconformity, LEU, Praeg et al. (2005)) (FIGURE 9) and a succession of shallow marine and deltaic sediments in the northern part of the Porcupine Basin (Moore and Shannon, 1992) and linked submarine sandy fans in the south of the basin (Shannon, 1992). Based on seismic mapping, the north Porcupine deltaic and turbiditic sands were probably sourced from the Porcupine High to the west and from the Slyne Ridge to the north (McDonnell and Shannon, 2001). This period of uplift was coeval with widespread intrusive and extrusive magmatism on the Rockall Plateau but more sporadic magmatism further east in the Rockall-Porcupine area (Tate and Dobson (1988); Horni et al. (2017)) (FIGURE 5).

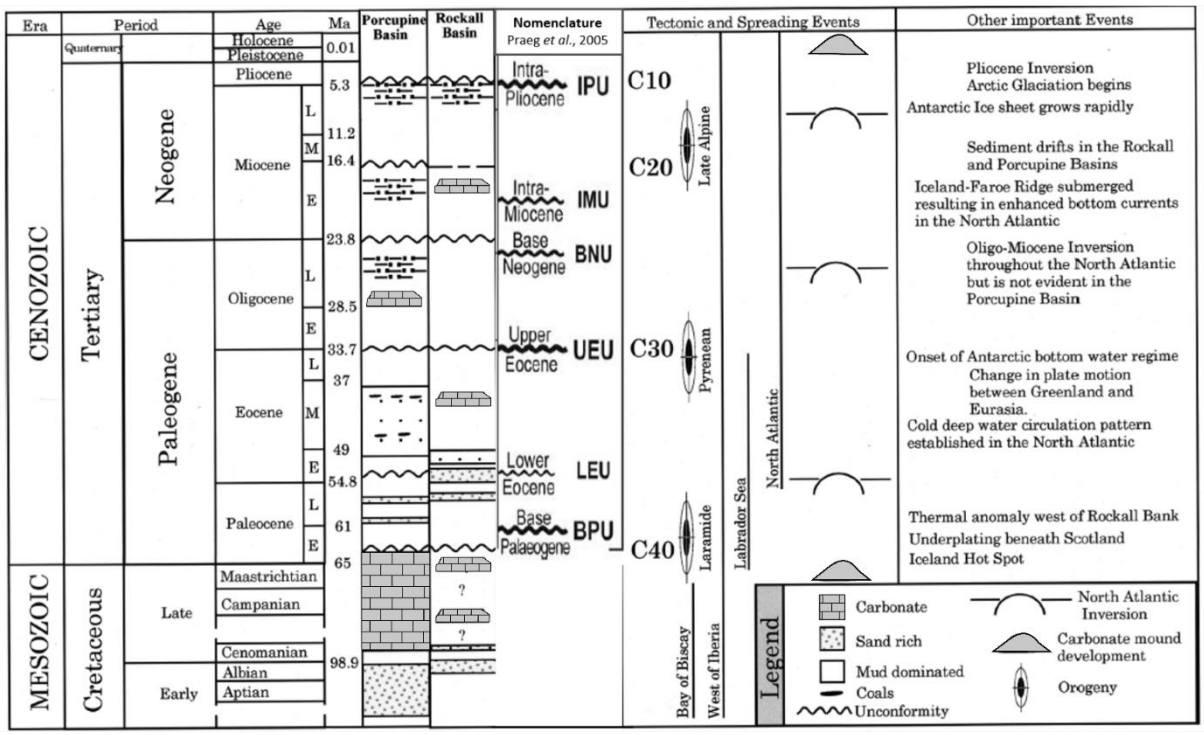

Figure 9: Cretaceous and Cenozoic lithostratigraphic framework of Porcupine nd Rockall basins (modified after McDonnell and Shannon (2001) and Praeg et al. (2005)).

Deep water conditions returned during the Middle and Late Eocene. A regional unconformity (UEU, Praeg et al. (2005)) (FIGURE 9) separating the Eocene and Oligocene sediments is associated with a major change in depositional environments from a restricted environment to the onset of regional deep-water bottom current activity (Stoker, 1997) that led to the deposition of silty contourites in both the Rockall and Porcupine basins (McDonnell and Shannon, 2001). The depositional environment remained dominantly open and deep until the present-day. A latest Early Miocene unconformity (IMU) is coeval with a global sea-level fall that probably changed the bottom water currents and resulted in submarine erosion in parts of the basin. Finally, an Early Pliocene unconformity (IPU) is interpreted as caused by an episode of margin-wide exhumation Japsen and Chalmers (2000) (FIGURE 9).

Despite more than 50 years of research and a vast amount of published studies, one conclusion of Stoker et al. (2016) is that the "evolution of the NE Atlantic rift systems remains enigmatic". This is particularly true for the IAM which has a much lower density of seismic surveys and deep boreholes than most of the rest of the NEAM.

1.3.2 Exhumation of the IAM

The exhumation history of the IAM has been constrained with the use of tectono-stratigraphic studies (Hall and White (1994); Clift and Turner (1998); Jones et al. (2001b)), vitrinite reflectance studies (Robeson et al., 1988), thermal modelling studies (Geotrack industry reports 1991-2008; McCulloch (1993)), seismic inversion (Mackay and White (2006); Biancotto et al. (2009), (Biancotto, 2012)) and

integrated thermal/stratigraphic/compaction studies (Scotchman and Thomas (1995); Chapman et al. (1999); Corcoran and Mecklenburgh (2005)) (FIGURE 10).

Study	Type	Area	Thermal					Compaction			Struc	Stratigraphic		*Integ.*
			AFT	AHe	VR	FI	Bio	Son	Poro	Seis	Subs	Proj	Mass	
This project (aims at)	*PhD thesis*	IAM												
Biancotto, 2012	PhD thesis	Slyne								2/3D		!		!
Hardy *et al.*, 2008a,b, 2010	Paper	Slyne								2/3D				
Green, 2008	Report	Slyne												
Mackay & White, 2006	Paper	IMP								2D				
Corcoran, 2006	PhD thesis	Irish offshore												
Corcoran & Doré, 2005	Paper	Irish offshore												
Corcoran & Mecklenburgh, 2005	Paper	Slyne												!
Ceramicola et al., 2005	Paper	Rockall												
Green, 2004b; 2004c	Report	Slyne-Erris	!											
Green, 2004a	Report	Porcupine S												
Green, 2003	Report	Rockall												
Green, 2002	Report	Porcupine												
Jones *et al.*, 2002	Paper	Porc. & Rock.											!	
Jones *et al.*, 2001, 2003	Paper	Porcupine												
Green, 2001a	Report	Porc. High												
Green, 2001b	Report	Rockall												
Corcoran & Clayton, 2001	Paper	IAM			!									
Chapman et al., 1999	Paper	Erris												
Clift & Turner, 1998	Paper	Erris, Porc.												
Green, 1997a,b & c	Report	Slyne	!											
Green, 1996	Report	Slyne												
Scotchman & Thomas, 1995	Paper	Slyne												!
McCulloch, 1993	Paper	Porc., Donegal												
Green, 1993a	Report	Erris												
Green, 1991; 1992; 1993b	Report	Slyne 27/13-1												
Robeson *et al.*, 1988	Paper	Erris			!									
Duddy *et al.*, 1983	Paper	Hatton												

Legend: AFT = apatite fission track study; AHe = (U-Th)/He on apatite study; Bio = biomarkers maturation study; FI = fluid inclusion study; Integ = integrated study; Mass = mass alance study; Por = porosity logs; Proj = structural-straigraphic projections of eroded sections; Seis = seismic velocities; Son = sonic logs; Subs = subsidence study; VR = vitrinite reflectance study; ! = key studies for their category

Figure 10: Exhumation studies, offshore west of Ireland.

Apart from the few published studies mentioned in SECTION 1.2.2 (Duddy et al. (1983), McCulloch (1993), Fügenschuh et al. (2003)), the main source of legacy thermochronological data (and exhumation studies) for the Irish Atlantic Margin is a set of oil and gas industry reports carried out by Geotrack between 1991 and 2008 on 18 boreholes (FIGURE 3) from the Rockall, Donegal, Erris, Slyne, Porcupine and Macdara basins (FIGURE 4). These reports can be accessed with permission from the DCCAE. The reports contain raw AFT data (ages, track lengths, chlorine content), often associated with VR data and an interpretation based on Geotrack in-house methodology. However, the track length annealing model used to derive the thermal history models and interpretations is not disclosed and therefore has never been compared to the widely used published models (Laslett et al. (1987), Ketcham et al. (1999), Ketcham et al. (2007)). The results of these studies has been compiled in FIGURE 11 (together with the thermal histories from the vertical profiles onshore west of Ireland (Cogné et al. (2014), top of figure).

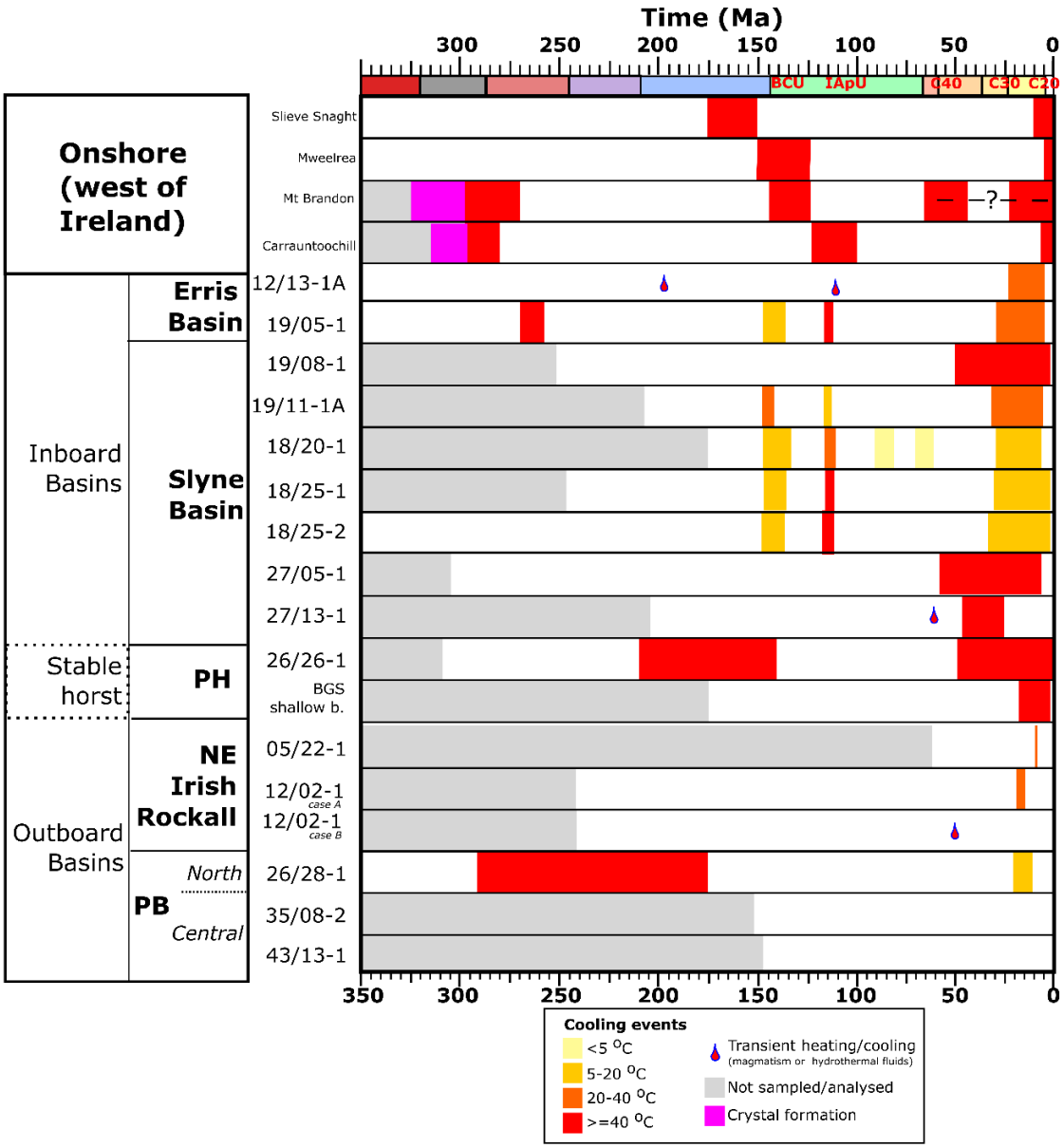

Figure 11: Summary of legacy models, west of onshore Ireland and offshore west of Ireland.

The first observation that can be made is that an important late Neogene cooling and exhumation event is visible in all the boreholes from the Erris and Slyne Basins and Porcupine High, similar to the one observed on the vertical profiles from onshore west of Ireland (Cogné et al., 2014). However, this event is almost nonexistent in the boreholes from the Mesozoic Porcupine and Rockall Basins. This suggests differential Neogene exhumation between the high and the basins. Paleocene-Early Eocene uplift events are rarely identified, which could imply that this part of the IAM has not been significantly affected by this uplift event. Finally, both the Base Cretaceous and Aptian uplift events are modelled in the boreholes of the Slyne Basin but appear as two distinct events due to external constraints on the models rather than due to the thermochronological information contained in the AFT data. Also

noticeable is the identification of several transient thermal events caused by hydrothermal fluids or magmatism (FIGURE 11).

1.4 Aims and methods of the study

As reviewed in section 1.1 to 1.3, the exhumation of the IAM has been dominantly constrained by AFT data from Geotrack industry reports. However, this dataset is representative of the time at which it was acquired and has a number of limitations:

1) No (U-Th)/He ages: Although known since 1987 (Zeitler et al., 1987), this geochronometer became widely used only after the development of predictive helium diffusion models in the late 2000s (e.g. Flowers et al. (2009)). Moreover, the Geotrack analysts now do not consider it as a reliable thermochronometer (Green and Duddy, 2018).
2) Unknown modelling methodology and result accuracy: The forward/inverse modelling algorithm used by Geotrack has not been made public, nor the track annealing model used and the reports do not shows any plots or indicators of the model accuracy (Gallagher, 2021).
3) No projected track lengths: The projected track length correction was developed and implemented in QTQt and HeFTy only in the late 2000s (Ketcham et al., 2007) and have not been used in the Geotrack reports.
4) No compositional proxies (some reports only): Some of the older studies do not report Cl contents.

This study will aim at better constraining the Cenozoic and Mesozoic exhumation of the IAM by acquiring new low-temperature thermochronological data using modern best practices and methodologies which has been successful to resolve small-scale exhumation events onshore Ireland and Britain (Cogné et al. (2014); Cogné et al. (2016); Łuszczak et al. (2018)): notably, LA-ICP-MS-based AFT-UPb dual-dating (Chew and Donelick (2012); Danišík (2019) ; Cogné et al. (2020)), AHe dating (Zeitler et al., 1987), multi-sample vertical profiles (Gallagher et al. (2005), Lisker et al. (2009)), projected fission track lengths (Ketcham et al., 2007), the use of Dpar/Cl compositional proxies and thermal history inverse modelling (Gallagher, 2012) using known track annealing and helium diffusion models (e.g. Ketcham et al. (2007); Flowers et al. (2009)). In particular the study will aim at addressing the following primary research questions:

1) What is the magnitude, timing and spatial distribution of the Paleocene-Early Eocene exhumation offshore west of Ireland and is it consistent with a phase of magmatic underplating (FIGURE 12)? If not, and if exhumation is detected, can we identify its main drivers? Does the magnitude of exhumation match the uplift estimation of Jones et al. (2001b) for the North Porcupine High?
2) What is the magnitude and timing of the Neogene exhumation offshore west of Ireland and how does it fit within the regional pattern of Neogene exhumation?

3) What is the magnitude and timing of the Late Jurassic-Early Creatceous exhumation offshore west of Ireland and is there a north-south exhumation age trend as hypothesized for Ireland by Cogné et al. (2014)?

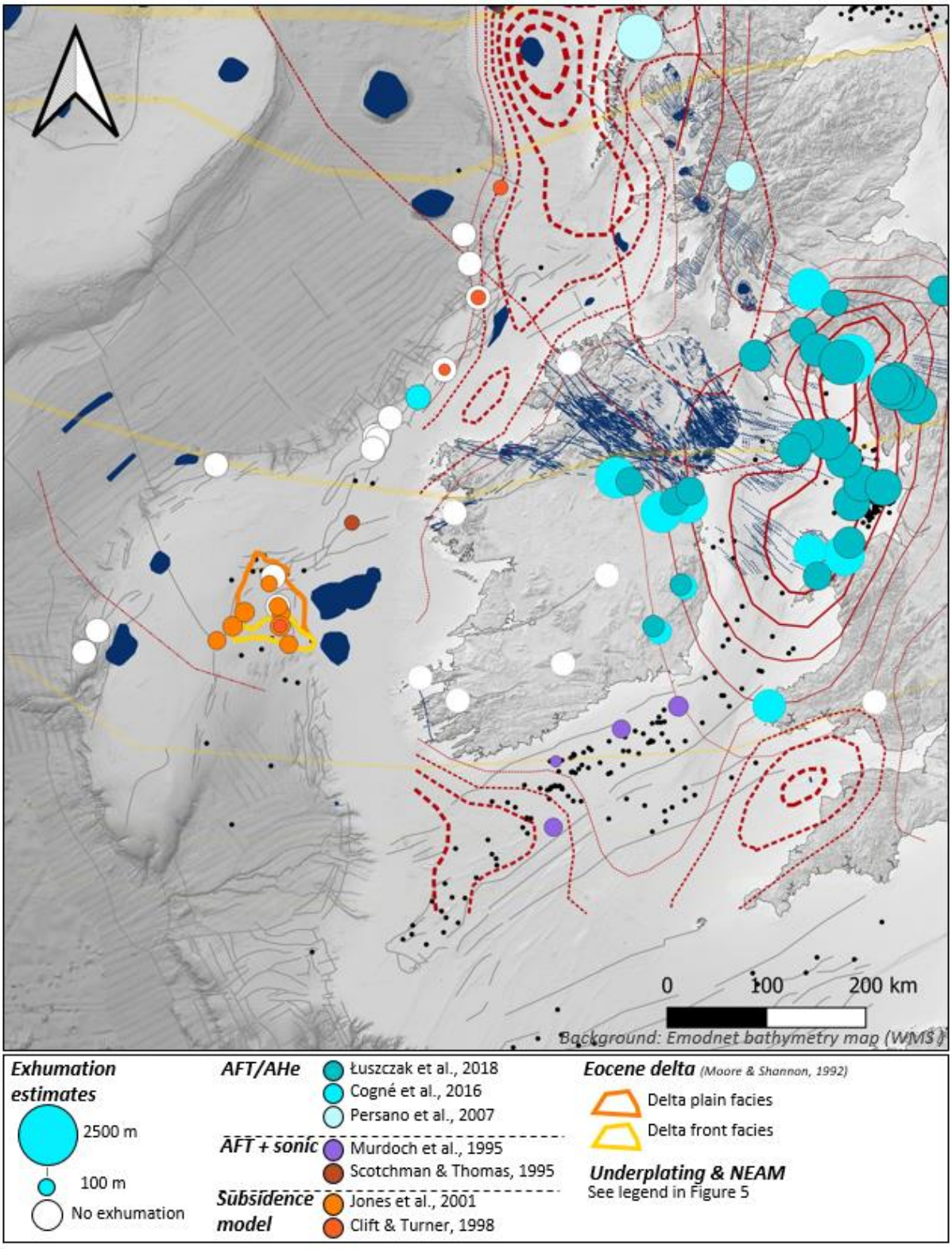

Figure 12: Map of legacy Paleocene-Eocene exhumation estimates.

In addition to the low temperature theromochronolgy constraints produced by this study, the apatite dual-dating method yields apatite U/Pb ages along with FT ages. Combining the apatite U/Pb ages with zircon LA-ICP-MS U/Pb dating generates a new dataset of high and medium-temperature geochronological constraints for the west of Ireland offshore. Apart from a series of recent basement geochronological studies on seabed dregdes led by teams at NUIG, TCD and UCD (Tyrrell (2013); Cogné and Chew (2017); Barry et al. (2017); Chew et al. (2019)), studies that constrain the timing of crystallization of igneous and basement rocks offshore Ireland are rare and often based on older less reliable dating techniques (e.g. K-Ar for igneous rocks, Seemann (1984)). Therefore, a set of secondary research questions for this study, based on this new dataset, are:

4) Can we better constrain the age of magmatism offshore west of Ireland?
5) Can we better characterize the age and nature of the basement offshore west of Ireland and therefore the offshore extension of the main structural lineaments onshore?

The detailed methodology used for this study is given in the next section (CHAPTER 2) while the results are presented in CHAPTER 3. The results are discussed in three chapters corresponding to three geographical zones: the Northern Zone (CHAPTERS 4), the Central Zone (CHAPTER 5) and the Southern Zone (CHAPTER 6). The division in zones from north to south is based on 1) the hypothesized north-south exhumation trend discussed above, 2) their unique geodynamical and structural characteristics (the southern zone was directly affected by mantle exhumation, breakup and oceanic crust accretion on its SW margin; the Central Zone is a structural boundary between the Porcupine Basin and High and the Slyne/Erris/Donegal Basins to the north which is the Northern Zone) and 3) to create manageable amount of sample to be analysed and interpreted. Finally, a synthesis is given in CHAPTER 7.

2 Methodology

2.1 Sampling

2.1.1 Sampling strategy

The sampling targeted apatite-bearing lithologies at depths where the temperature would be colder than 120°C (otherwise both the AFT and AHe ages are reset and cannot constrain the thermal history). In boreholes, cores were favoured over cuttings (less risk of contamination) and in dredges and dives, clasts believed to be *in-situ* were favoured over clasts with a more uncertain origin. The best apatite-yielding lithologies are coarse-grained felsic igneous and metamorphic rocks (Chew et al., 2020), however these lithologies were rarely targeted in hydrocarbon boreholes from offshore Ireland and were only found in a few boreholes that have reached the basement and in some Ifremer dredges in the Porcupine High and Goban Spur area. Therefore, the bulk of the sampling was done on mafic igneous rocks (gabbro, doletite, basalt) and clastic sedimentary rocks (conglomerate, sandstone). Some tuffaceous horizons were also targeted (SEE RESULTS IN SECTION 3).

2.1.2 Sample nomenclature, coordinates, depths and depostional age

In the text, figures, tables and annexes, legacy samples have the names from the original report or paper with an added prefix “L-” (for legacy). A set of samples analysed at TCD in the last few years by Nathan Cogné but not published have the prefix “C-” (for Cogné). All the new samples analysed in this study have the prefix “R-” (for Rateau).

Depths quoted from the well reports or composite logs are given in the same unit as the reports (feet or meters) and as ‘measured depth’ (MD), *i.e.* with the KB/RT as datum. For the samples, depths are reported as average depth between the top and bottom depths of the sampling interval, and converted to true vertical depths in meters below seabed (m TVD BSB), which allows for a better estimation of the amount of overburden above the sample (by removing the effect of well path deviation, seawater column and KB/RT height).

For the detrital samples, the depositional age was obtained using the age provided in the composite log, well report or campaign report (usually derived from a biostratigraphic study) and converted to a quantitative age using version 2020/01 of the International Chronostratigraphic Chart (ICC) from the International Commission on Stratigraphy (Cohen et al., 2013 updated 2020). For Carboniferous samples and intervals, ages are often reported using stage names from the Western European regional stratigraphic scale (Namurian, Westphalian A-D, Stephanian A-C, Autunian). The ICC does not provide correlations between the subdivisions of their timescale and the Western European scale. Therefore,

absolute ages for the Western European Carboniferous stages were derived from the correlations in Davydov et al. (2012) (TABLE 1).

Table 1: Absolute ages of the Carboniferous stage boundaries used in this study (Davydov et al., 2012)

	Top	Base
Autunian (Permian)	297.5*	298.9
Autunian (Carb)	298.9	302.5*
Stephanian C	302.5*	303.7
Stephanian B	303.7	304.5*
Stephanian A + Cantabrian	304.5*	307.5*
Westphalian D	307.5*	310*
Westphalian C	310*	315.2
Westphalian B	315.2	318*
Westphalian A	318*	319*
Namurian	319*	329*
Visean	329*	346.7
Tournaisian	346.7	358.9

** approximate age from visual inspection*

For the igneous and metamorphic samples, any information about the assumed age of the rock or radiometric ages derived from whole-rock or mineral dating has been compiled, but usually only the apatite U/Pb age acquired in this study (a medium temperature thermochronometer) is useful for constraining the low-temperature thermal history modelling.

2.1.3 Sample temperature

The present-day sample temperature (before collection during drilling or dredging) is a key constraint for thermal history modelling and can be derived from the seabed temperature and geothermal gradient.

2.1.3.1 Seabed temperature

The temperature at the seabed for the study area has been derived from 4063 bottom water temperatures from a GSI and Marine Institute dataset that cover the entire study area. Bottom water temperatures are assumed to be a good proxy for seabed temperatures. Sea-bottom temperatures decreases with water depths and are constrained within a narrow temperature range, except for water depths below 100-150 m where a much larger temperature dispersion is observed (FIGURE 13). The correlation between water depths and temperatures can be described in three segments:

- For water depths <500 m: the seabed temperature averages 10 ± 1°C.

- Between 500-2500 m: the temperature decrease with depth according to a 4th-order polynomial (see formula in FIGURE 13). An error of ±1°C covers most of the temperature dispersion.
- For water depths >2500 m: the seabed temperature averages 3 ± 1°C.

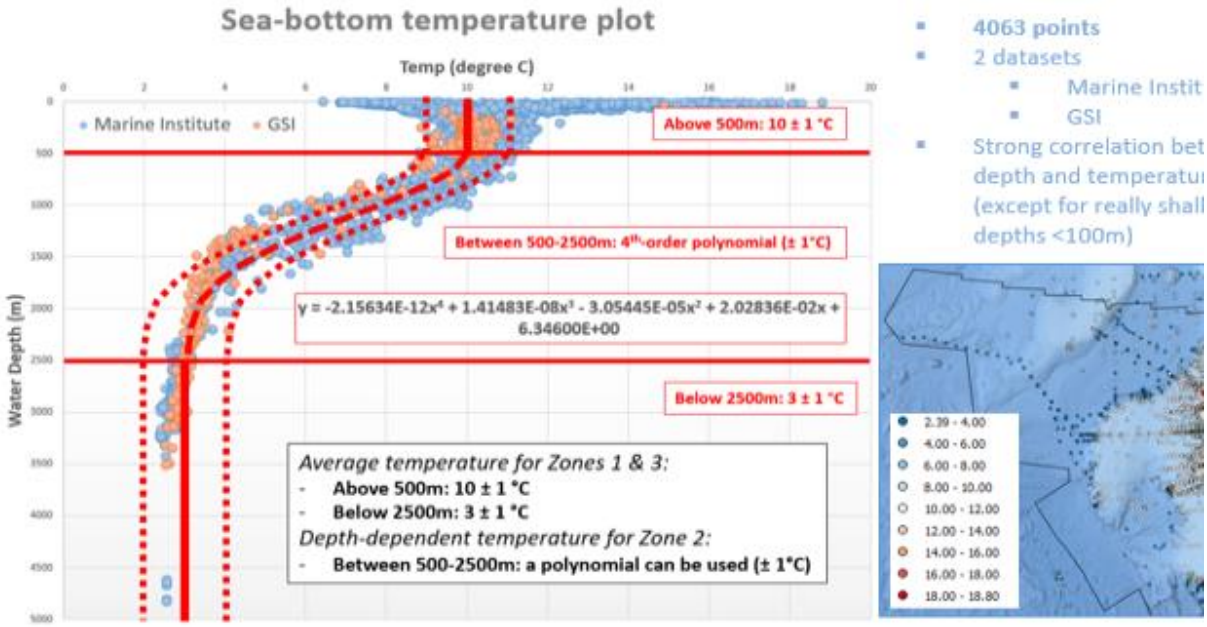

Figure 13: Determination of seabed tempertures based on depths.

This seabed depth-temperature relationship has been used to estimate the seabed temperature at the sample locations (SEE RESULTS IN SECTION 3).

2.1.3.2 Geothermal gradient

For samples in boreholes, the present-day geothermal gradient in the borehole has to be estimated using the seabed temperature and bottom-hole temperatures (BHTs). BHTs are measured during logging. However, the temperature of the mud is always colder than the temperature of the formations. Therefore, BHTs would often underestimate the true formation temperatures. When several measures are taken at different points of time at the same depths, and if the mud did not circulate in between each measurement, the measured temperatures would usually increase with time passing, reflecting the heating of the mud to reach an equilibrium with background formation temperature (Rider, 2002). If several measures are available, and if the time since circulation stopped is known, then this phenomenon can be used to calculate the true formation temperature. This technique is known as a Horner correction. If only some of this information is known, cruder corrections can be made. If no information is know expect a BHTs, then a simple addition of 18 ± 9°C can be made to correct the BHTs (ZetaWare, 2003). Even in the best case, Horner corrected BHTs, and therefore the derived geothermal gradients, have large uncertainties.

For each borehole, all relevant temperature information has been compiled and the appropriate Horner correction applied when necessary. For boreholes without any BHTs, the geothermal gradient has been estimated based on the closest borehole(s) with BHT (TABLE 2).

Table 2: Geothermal gradients for boreholes used in this study.

Well	Total depth	Seabed temp.	# of BHT	Gradient °C/km			Data quality	Comment
	m MD	°C		Min.	Best	Max.		
12/02-1	4146	5	2	35.0	**40.2**	40.7	Poor	Already Horner corrected by operator. Operator estimated 35°C/km above 3850m. Contradictory dataset.
12/13-1A	2869	10	3	20.2	**27.3**	31.1	Poor	Last resort correction used for best estimate
13/03-1	1366	10	3	n/a	**28.0**	40.0	Poor	Not corrected (last resort correction yields high GG, used as max.)
16/28-sb01	148.25	5	0	n/a	**28.3**	n/a	Absent	Used closest well 26/26-1
18/25-1	3770	10	0	n/a	**30.0**	n/a	Good	From Geotrack (30.2°C) & Corcoran & Mecklenburgh, 2005 (30.5°C, 30.9°C), Corrib field
18/25-2	2966	10	2	n/a	**28.2**	n/a	Good	BHTs not found in well reports but found in Geotrack report. No correction applied.
19/11-1A	4685	10	5	n/a	**33.7**	n/a	Average	Used a simple 'time since circulation' correction. Operator ahd 33.5°C/km.
26/26-1	1256	10	2	n/a	**28.3**	n/a	Good	Already Horner corrected by operator. Operator had 28°C/km.
26/28-1	3315	10	3	n/a	**38.5**	n/a	Good	Already Horner corrected by operator.
26/30-1	1722	10	0	28.0	**33.0**	38.0	Absent	Used 26/26-1 as min, 26/28-1 as max and the average of two as best estimate.
27/05-1	1910	10	2	23.5	**31.0**	n/a	Average	Horner correction by op. Operator had 23.5 (used as min) and 28°C/km as estimates.
34/05-1	1488	10	0	n/a	**28.3**	n/a	Absent	Used closest well 26/26-1
35/13-1A	4405	10	5	n/a	**29.2**	n/a	Good	Already Horner corrected by operator. Operator had 29°C/km.
35/15-1	3688	10	1	n/a	**35.7**	n/a	Poor	Already Horner corrected by operator but 1 BHT only.
36/16-1	2745	10	0	n/a	**35.7**	n/a	Absent	Used closest well 35/15-1
				Min.	*27.3*			
				Average:	*31.8*	*(borehole without BHT excluded)*		
				Max	*40.2*			

Sample temperatures were then calculated using the seabed temperature and geothermal gradients (SEE RESULTS IN SECTION 3).

2.2 Sample preparation

2.2.1 Mineral separation

For this project, the rock samples consisted of borehole cuttings (washed and dried or unwashed wet-cut), pieces of borehole cores and seabed rock fragments from dredges and dives. Wet cuttings were dried up in an oven at 40°C for 24-48 hours. A couple of samples were also very clay-rich and were hand panned beforehand to remove most of the clay. Using a jaw crusher and stainless-steel mesh sieves, the rocks and cuttings were crushed to obtain particles <350 µm. The crushed rocks were then washed using either a Wilfley table or hand panning to remove the clays and very fine particles. The washed fraction was dried in an oven at 40-50°C for 24-72 hours.

Ferromagnetic and paramagnetic minerals were separated from the non-magnetic minerals using a magnetic separator (Frantz Model LB-1) with a side slope of 25° and a forward slope of 15° (magnetite was first removed using a Nd-Fe alloy hand magnet). The grains from the non-magnetic fraction were then separated using a standard two-step heavy liquid separation procedure with a liquid specific gravity of 2.9 (mixture of methyil iodide, MI, and acetone) and then 3.32 (pure MI).

2.2.2 Picking

2.2.2.1 Picking grains for AFT and AHe studies

Separates containing the apatite grains were investigated under a Nikon SMZ1500 binocular microscope. For AHe studies, good quality euhedral apatites without any visible inclusions or defects (Farley, 2002) were placed on a glass slide with tape for further investigation using a Zeiss AxioImager Z1m with a maximum magnification of 1000x (100X Epiplan Neofluar DIC lens, 10X eyepiece magnification) to look for inclusions. If three to ten suitable grains could be found within one sample, the grains were then quantitatively and qualitatively characterized (length, diameter and shape) and photographed.

Additional apatite grains were picked and placed in lines on a layer of double-sided tape on another glass slide. Some grains from the apatite separate were spread around the picked grains in case there was not enough of them to obtain a suitable amount of AFT ages (>40). Zircons from the heavy mineral separate (SG >3.25) were also picked (> 100 if possible) and deposited in lines on a layer of double-sided tape on a thick glass slide. These samples were then mounted in epoxy (Section 2.2.4).

Apatite grain characterization for AHe studies

In order to calculate precise alpha-ejection correction factors (F_T), the program Qt_Ft was used (Gautheron and Tassan-Got (2010); Ketcham et al. (2011); Gautheron et al. (2012b)). It allows to better replicate the true geometry of the grains (e.g. hexagonal prism with pyramidal or flat terminations, ellipsoid) than the default shapes provided by UCL in their results spreadsheet (sphere, cylinder, prolate spheroid). The photos of each selected AHe grain were used to select a geometry that best resembled the true geometry of the grain. The hexagonal prism or ellipsoid geometries were both used. Three lengths are needed for the calculation of the volume in Qt_Ft: W, L and H. W is the long diameter (opposite vertices) and L is the small diameter (opposite sides) of the hexagonal section, while H is the longitudinal length of the grain from termination to termination. Both W and L have been calculated as the average of the 6 long diameters and 6 small diameters (FIGURE 14A).

For the hexagonal prism, several terminations are possible: broken, flat or pyramidal (one option for each side). For the calculation of the volume, the flat and broken options yield the same results. The two flat terminations have been chosen for grains with no pyramids or very small ones, or for grains with clean broken ends. The one pyramidal and one flat termination have been chosen for 1) grains with a one pyramidal termination and one flat termination; and for 2) grains with two pyramidal terminations but the pyramids have low angles (<45°). Rather than using two flats or two pyramids, this option is believed to better represent the volume of the grain. The two pyramid terminations have been chosen for grains with two pyramids with angles close to 45° (FIGURE 14A).

a) Apatite grain characterization

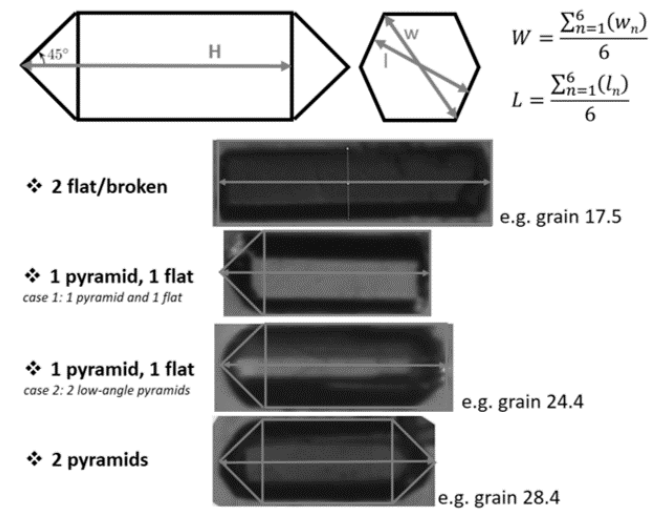

b) Apatite density estimates

Source		Min	Mean	Max
UCL result spreadsheet		n/a	3.16	n/a
Mindat.org	Apatite	3.1	n/a	3.25
	Fluorapatite	3.1	n/a	3.25
	Chlorapatite	3.17	n/a	3.18
	Hydroxy-apatite	3.1	n/a	3.21
Webmineral.com		3.16	3.19	3.22
Glozbach et al., 2019		n/a	3.2	n/a
Ketcham et al., 2011		n/a	3.2	n/a
Reiners & Nicolescu, 2006		n/a	3.1	n/a
This study		3.1	3.2	3.3

Figure 14: Selection of apatite grain shape, terminations and calculation of the length parameters L, W and H for the AHe study.

Grain mass and [U], [Th], [Sm]

In order to compare the concentration of U, Th and Sm of the AHe and AFT dating, the concentration of the AHe study given in nmol have to be converted based on the mass of the grain. The mass of an apatite grain can be calculate using its density and volume. The result spreadsheet provided by UCL uses the following method to derive the mass of the apatite grains. The default density for apatite is set at 3.16 $g.cm^{-3}$. The volume is calculated using one of three shapes characterized with two measurements, the length or diameter of the long axis (L) and the length or diameter of the small axis, or width (W): 1) Volume of a sphere (L = W); 2) Volume of a cylinder (L > W); 3) Volume of a prolate spheroid (L > W). While providing a reasonable approximation of the mass of each apatite grain, another approach has been used in this study to obtain a more accurate estimation of the weight.

In this study, the volume is calculated in Qt_Ft using the three length parameters (see section above). In the literature and online databases, several values are proposed for the minimum, maximum and average density of apatite (FIGURE 14B). Based on this compilation of estimates, the apatite density is defined as 3.2 ± 0.1 $g.cm^{-3}$ for this study. The use of a mean density of 3.2 $g.cm^{-3}$ is predominant in recent publications and very close to webmineral.com value (3.19). The average density is used to calculate the concentration of [U], [Th] and [Sm], while the minimum and maximum density estimate are used to estimate the error on the concentration.

2.2.3 Packing for AHe studies

1-mm high platinum tubes were cleaned by placing them in a clean capped glass crucible and heated in an oven at 500°C for one hour (excluding warming-up and cooling-down periods). Each grain was

then inserted in a tube which were closed on both side with a tweezer and placed in a tagged plastic box. The samples were sent to the UCL Geochronology Lab in London.

2.2.4 Mount preparation for the AFT/UPb analyses

Epoxy-only mounts (fission track: 1.6 mm thick, 1.6 cm wide, and U/Pb zircon: 2.5 cm wide) were made using an Epoxy resin (Struers Epofix) mixed with a hardener and then polished using a three-step process (Struers Diapro, 6 µm and 1 µm) to expose the surface of the grains. The apatite mounts were then etched in a 5.5M nitric acid bath for 20 seconds at 21°C (one of the most common etching protocols, Carlson et al. (1999), Donelick et al. (2005)) and then dipped into a large amount of deionized water to immediately stop the etching reaction. Three copper markers (SEM target grids) were then glued on the rim of each mount in order to locate and spatially reference the counted grains under the fission track microscope and later on under the camera of the laser ablation system. The zircon pucks were carbon coated and cathodoluminescence (CL) greyscale maps were created for some of the samples using the Tescan MIRA XMU field emission microscope (FE-SEM) or the Tescan TIGER MIRA3 Variable Pressure Field Emission Scanning Electron Microscope (VP-FE-SEM), both equipped with a Tescan CL detectror and located at the iCRAG@TCD/CMA Lab, in order to identify suitable zircon grains for dating both core and rim.

2.3 Geochemical analyses methodology

2.3.1 LA-ICP-MS AFT – U/Pb dual-dating and trace element analysis (LAFT-U/Pb-TE)

2.3.1.1 Fundamentals of LAFT-U/Pb-TE

The apatite fission track (AFT) dating system (Price and Walker, 1963) relies on the spontaneous fission of ^{238}U in minerals into two heavy nucleii that travel in a random (but opposite directions) to each other, creating a trail of amorphous material of c. 5-9 nm in diameter and 16-21 µm in length (Li et al., 2010), called a fission track. The track can become visible under an optical microscope when etched by an acid, such as diluted NHO_3, for a few tens of seconds. Etched tracks can be counted on an internal surface of a grain (revealed by polishing) and, together with a measurement of the uranium concentration, an age can be calculated using a standard radiometric age equation. However, tracks heal themselves when subjected to temperatures greater than c. 60°C for periods >1 Ma. This temperature-dependent healing process is called annealing and results in the shortening of tracks until complete disappearance when exposed to temperatures greater than c. 120°C. The temperature window corresponding to the onset of annealing but without the complete disappearance of a track is called the partial annealing zone (PAZ). It is the combination of track accumulation (dependent on time and [^{238}U]) and annealing (dependent on time and temperature) that allows the derivation of thermal

histories and makes AFT a low-temperature thermochronometer (see reviews in Donelick et al. (2005); Lisker et al. (2009); Malusa and Fitzgerald (2019)).

The most commonly-used method to calculate the concentration in ^{238}U in apatite grains is the external detector method (EDM) (Gleadow (1981); Hurford and Green (1983); Hurford (1990b)). The EDM relies on the artificial and controlled fission of ^{235}U in the natural apatite into a U-free mica (the external detector) placed in intimate contact with the apatite mount surface (or a dosimeter glass) by neutron irradiation in a research nuclear reactor. The induced fission of ^{235}U leaves 'induced' tracks in both the apatite and mica that can be counted and, when combined with the known concentration of ^{235}U in the mica and the natural constant ratio of $^{238}U/^{235}U$, the unknown [^{238}U] in the apatite unknown can be derived.

However, the several downsides of the EDM (long waiting time between counting tracks and ^{238}U measurements, the need for a licence to handle irradiated materials, difficulty in accessing nuclear research reactors) led to the development of alternative methods. The possibility of measuring [^{238}U] using laser-ablation induction-coupled-plasma mass spectrometry (LA-ICP-MS) was envisaged in the early 2000s (Cox et al., 2000). Several protocols have been published starting with absolute dating (Hasebe et al., 2004) and then various versions using zeta equivalent calibrations with a primary age standard (Hasebe et al. (2004); Donelick et al. (2005); Chew and Donelick (2012); Hasebe et al. (2013); Soares et al. (2014); Cogné et al. (2020)). The technique has been shown not to be affected by the effects of chemical etching (Hasebe et al., 2009), allows for the measurement of [Cl] (Chew et al., 2014a) which is used as kinetic proxy for thermal history modelling (Green et al. (1986); Ketcham et al. (1999)) and can be combined with U/Pb dating within the same session (dual-dating apatite FT-U/Pb, Chew and Donelick (2012)). For this study, the protocol of Cogné et al. (2020) has been used.

2.3.1.2 Track counting and characterization

Using the Trackworks software developed by Melbourne University and Autoscan Systems (Gleadow (2010); Gleadow et al. (2019)), 40 grains were selected per sample whenever possible. For each grain, the c-axis is defined and a circle slightly larger than the laser spot size (36 µm) is used as the counted area to derive the areal track density. After counting the tracks intersecting the exposed surface of the grain, several track pit lengths (Dpar) were measured to obtain an average Dpar value for each grain; and all visible confined track lengths were measured and their angles to the c-axis calculated. Both confined track lengths originating from other tracks (TINTs) and from cleavages (TINCLEs) were measured but only TINTs were used for density plots analysis and thermal history modelling as TINCLEs have been proven to misrepresent the true confined track length distribution (Barbarand et al., 2003).

2.3.1.3 LA-ICP-MS apatite spot analysis

2.3.1.4 Equipment

The analyses were done on a Photon Machines Analyte Excite 193 µm ArF Excimer laser with a Helex two-volume cell coupled to an Agilent 7900 ICP-MS at Trinity College Dublin, Ireland (iCRAG Lab@TCD).

2.3.1.5 Primary Zeta session

For the LAFT technique, each analyst has to calculate their primary zeta factor (ζ_{ICP}) (Cogné et al., 2020). The zeta factor was calculated based on the counting of 3788 tracks from 69 shards of a crushed Durango apatite crystal. The background and drift-corrected $^{238}U/^{43}Ca$ ratio of each shard was measured by LA-ICP-MS in three successive sessions using a square spot of 35 µm, 240 shots at 15 Hz, an analysis time of 16 s and a washout time of 8 s, and the NIST-612 trace element standard (FIGURE 15). Using a reference Durango age of 31.44 ± 0.09 Ma (1σ) (McDowell et al., 2005), a zeta factor of 9.72 ± 0.16 (1σ) was derived. This factor is used in all subsequent AFT age calculation for the unknowns (Cogné et al., 2020).

2.3.1.6 Analyses for apatite FT-U/Pb dual-dating and trace elements

The samples were analysed over ten sessions spanning two years and each session was run using a 36 µm circle spot with 300 shots at a repetition rate of 13-15 Hz and a laser fluence of 2.25-2.5 J/cm^2 (FIGURE 15). The matrix-matched sample-standard bracketing method was used (Cogné et al., 2020) with 1) the Durango (DUR) grains used for the zeta calculation as the LAFT primary age standard (Cogné et al., 2020), 2) the Madagascar apatite (MAD) as the primary U/Pb age standard (473.5 ± 0.7 Ma, Cochrane et al. (2014), Thomson et al. (2012)), 3) the McClure Mountain (MM) and Durango apatites as secondary U/Pb age standards (respectively 523.51 ± 1.47 Ma, Schoene and Bowring (2006), Thomson et al. (2012); and 31.44 ± 0.18 Ma, McDowell et al. (2005)), 4) the Bamble (BAM) apatite as the primary standard for chlorine (^{35}Cl) concentration (6.54 ± 0.14 wt%, Chew et al. (2014a); but MM with [Cl] = 0.0056 wt% and DUR with [Cl] = 0.37 wt% also used as optional constraints, Cogné et al. (2020)) and 5) the NIST-612 glass (NIST612) as the trace element primary standard (NIST (1992); Pearce et al. (1997)). The results of the secondary age standards are presented in section 3.2.2. A series of 30 masses were analysed that are used for AFT dating (^{238}U) and ablation volume normalisation (^{43}Ca), annealing kinetics proxy (^{35}Cl), U/Pb dating ($^{206\text{-}207\text{-}208}Pb$, ^{232}Th, ^{238}U), inclusion detection (zircon, monazite, xenotime etc) (^{31}P, ^{89}Y, ^{90}Zr, ^{139}La), Hg interference from argon gas (^{202}Hg) and trace-element characterisation (REEs, ^{88}Sr, etc) (FIGURE 15).

2.3.1.7 Analyses for zircon U/Pb dating

The samples were analysed over eight sessions spanning two years and each session was run using a 24 µm circular or square spot with 300 shots at a repetition rate of 11-13 Hz and a laser fluence of 2.25-2.5 J/cm^2 (FIGURE 15). The matrix-matched sample-standard bracketing method was used with 1)

the 91500 zircon as primary age standard (1062.4 ± 0.4 Ma, Wiedenbeck et al. (1995) and Wiedenbeck et al. (2004)), and 2) the Plešovice, WRS 1348 and GZ7s zircons as a secondary age standards (respectively 337.13 ± 0.37 Ma, Sláma et al. (2008); 526.26 ± 0.70 Ma, Pointon et al. (2012) ; and 530.26 Ma ± 0.05 Ma, Nasdala et al. (2018)). The results of the secondary age standards are presented in section 3.2.2. A series of 12 masses were analysed including $^{206\text{-}207\text{-}208}$Pb, ^{232}Th, ^{238}U for U/Pb dating and ^{202}Hg for Hg interference from argon gas (FIGURE 15).

Session Information						Laser Photon Machines (now Teledyne) Analyte Excite with a HelEx two-volume cell														ICP-MS	
Session date	Op.*	Phase	Runs	Analysis		Wave-length	Energy setpoint	Fluence	Type	Shape	Size	Rep rate	Shots **Speed	Time			Gas flows			Mixing device	Carrier Ar	Masses & Stds***
				Total	Unknowns only									Analysis time	Washout Total	Washout Inc. laser warm-up	MFC 1	MFC 2	MFC 3			
						nm	mJ	J.cm-2			µm	Hz		s	s	s	L.m-1	L.m-1	L.m-1		L.m-1	
13/11/2017	DC+CA +RR	AP	3	103	70	193	2.5	2.5	spot	square □	35	15	240	16	8	?	0.15	0.25	11	Yes	0.75	3
		AP		103	70	193	2.5	2.5	spot	square □	35	15	240	16	?	?	0.15	0.25	11	Yes	0.75	3
		AP		103	70	193	2.5	2.5	spot	square □	35	15	240	16	?	?	0.15	0.25	11	Yes	0.75	3
03/07/2018	DC+RR	AP	2	206	116	193	3	2.27	spot	circle O	36	15	300	20	6	1	0.3	0.1	7	Yes	0.75	1
		AP		147	57	193	3	2.27	spot	circle O	36	15	300	20	?	1	0.3	0.1	7	Yes	0.75	1
04/12/2018	DC+RR	AP	2	384	219	193	4	2.25	spot	circle O	36	15	300	20	?	2	0.25	0.15	9	Yes	0.6	1
		AP		45	41		4	2.25	lines	square □	12	40	**6	n/a	n/a	n/a	0.25	0.15	9		0.6	1
15/07/2019	GO'S+RR	AP	2	234	122	193	4	2.25	spot	circle O	36	13	300	23.1	?	5	0.25	0.15	8	Yes	0.65	1
		AP		169	89	193	4	2.25	spot	circle O	36	13	300	23.1	?	5	0.25	0.15	8	Yes	0.65	1
16/07/2019	GO'S+RR	AP	2	119	54	193	5	2.25	spot	circle O	36	13	300	23.1	?	5	0.25	0.15	8	Yes	0.65	1
		ZR		204	114	193	5	2.5	spot	circle O	24	13	300	23.1	?	5	0.25	0.15	8	Yes	0.65	2
17/07/2019	GO'S+RR	ZR	1	711	465	193	5	2.5	spot	square □	24	13	300	23.1	?	4	0.25	0.15	7	Yes	0.65	2
23/08/2019	RR	AP	1	171	81	193	4	2.5	spot	circle O	36	15	300	20	12	6	0.275	0.125	8	Yes	0.65	1
30/08/2019	RR	ZR	1	389	228	193	5	2.5	spot	square □	24	12	300	25	15	4	0.275	0.125	8	Yes	0.65	2
03/09/2019	RR	ZR	1	325	186	193	5	2.5	spot	square □	24	12	300	25	15	5	0.275	0.125	8	Yes	0.65	2
23/09/2019	RR	ZR	1	180	100	193	4	2.5	spot	square □	24	12	300	25	?	5	0.2	0.12	8	Yes	0.65	2
03/08/2020	FD+RR	AP	1	409	225	193	4	2.5	spot	circle O	36	15	300	20	?	5	0.25	0.15	12	Yes	0.63	1
04/08/2020	FD+RR	ZR	1	682	492	193	4	2.5	spot	circle O	24	12	300	25	?	5	0.25	0.16	12.5	Yes	0.68	2
05/08/2020	FD+RR	ZR	1	?	?	193	4	?	spot	circle O	24	?	?	?	?	?	0.25	0.16	12	Yes	0.66	2
07/10/2020	FD+RR	AP	1	505	309	193	3	2.5	spot	circle O	36	15	300	20	11	3	0.25	0.15	11	Yes	0.69	1
04/11/2020	FD+RR	ZR	1	250	180	193	3	2.25	spot	circle O	24	11	300	27.3	?	3	?	?	?	Yes	?	2

*** Masses measured

1 (AP): x30 - P31,Cl35,Ca43,V51,Mn55,Sr88,Y89,Zr90,Ba137,La139,Ce140,Pr141,Nd146,Sm147,Eu153,Gd157,Tb159,Dy163,Ho165,Er166,Tm169,Yb172,Lu175,Hg202,Pb204,Pb206,Pb207,Pb208,Th232,U238

2 (ZR): x12 - Ti47,Ti49,Zr91,Lu175,Hf178,Hg202,Pb204,Pb206,Pb207,Pb208,Th232,U238

3 (AP primary zeta): x2 - Ca43 (0.02), 238U (0.02)

*** Standards

1 (AP): NIST SRM 612, MAD, BAM, MM, DUR

2 (ZR): NIST SRM 612, 91500, Plesovice, WRS 1348, GZ7

3 (AP): NIST SRM 612

* Operators

CA = Claire Ansberque

DC = David Chew

GO'S = Gary O'Sullivan

FD = Foteini Drakou

RR = Remi Rateau

Figure 15: LA-ICP-MS session parameter and result summary

2.3.1.8 LAFT-U/Pb-TE data reduction

The LA-ICP-MS analysis output data was processed using Iolite 2.5, a data processing software package for time-resolved mass spectromety data (Hellstrom et al. (2008); Paton et al. (2011)) built on top of the scientific data analysis software Igor Pro 6.37 (WaveMetrics). The data is first imported into the software package and the integration boxes (time windows) for both samples (individual unknowns) and the background (baseline) are defined. The data reduction for trace element determinations is undertaken using Iolite's default Trace Element (TE) data reduction scheme (DRS) (Hellstrom et al., 2008) with an internal element standard (^{43}Ca) as the standardisation method and NIST612 as the reference material and consists of a background correction and internal standard normalization relative to the published NIST612 concentrations. The data reduction for the LAFT data is done using the TE-DRS in semi-quantitative standardisation mode and with an added script that calculates a weighted ^{238}U/^{43}Ca ratio to take in account the fact that the contribution of the uranium to fission tracks on the mount surface decreases with laser spot depth (Cogné et al., 2020). The data reduction

for the U/Pb data is undertaken using the VizualAge_UcomPbine DRS (Chew et al., 2014b) and consists of baseline subtraction followed by downhole fractionation and drift corrections based on the primary age standard (MAD). Before and after reduction, the dataset is inspected (notably the raw, downhole-corrected and final $^{206}Pb/^{238}U$ and $^{207}Pb/^{235}U$ channels and the raw ^{31}P, ^{89}Y, ^{90}Zr, ^{139}La channels for inclusions) and cleaned to remove failed ablated grains, adjust integration boxes and exclude any inclusions. The data is exported as a text file that includes internal (for trace element and AFT data) or internal and propagated errors (for U/Pb data).

2.3.1.9 LAFT-U/Pb-TE age calculation and data plotting

LAFT dating

The LAFT data output from iolite is imported in an in-house Excel spreadsheet to calculate the AFT ages (Cogné et al., 2020). The spreadsheet combines the reduced data from Iolite (SECTION 2.3.1.8) together with the U/Ca data and zeta factor from the primary zeta calibration session (SECTION 2.3.1.5) and the counted track data from Trackworks (SECTION 2.3.1.2) to calculate the LAFT age for each grain together with the age error. The data is quality controlled and grains with implausible geological ages or with very large outlier ages are discarded. The LAFT ages for each sample is plotted in a radial plot (Galbraith and Green, 1990) using the software package RadialPlotter (Vermeesch, 2009).

The confined track lengths measured in Trackworks were exported to an Excel spreadsheet and plotted in a histogram and Kernel Density Estimate (KDE) plots using the DensityPlotter software package (Vermeesch, 2012) and the mean track length (MTL), minimum, maximum and median track length were calculated to quantitatively characterize the track length distribution of each sample.

Apatite U/Pb dating

The apatite U/Pb data output from Iolite is imported in an Excel spreadsheet and the ages and errors are calculated and plotted on Tera-Wasserburg concordia using the Excel plug-in Isoplot 4.15 (Ludwig, 1988). When relevant (mostly for detrital samples), ^{207}Pb-corrected ages were also plotted in a histogram and Kernel Density Estimate (KDE) plots using DensityPlotter.

Trace elements

The apatite trace element data were plotted in $^{88}Sr/^{89}Y$ *vs* light rare-earth elements (LRRE (ppm) = $[^{139}La] + [^{140}Ce] + [^{141}Pr] + [^{146}Nd]$ (ppm)) discriminant biplot (O'Sullivan et al., 2020) in order to determine the likely bedrock source of the apatites. The following abbreviations is used for the eight fields of the biplot: ALK = alkali-rich igneous rocks; IM = mafic I-type granitoids and mafic igneous rocks; LM = low- and medium-grade metamorphic and metasomatic; HM = partial-melts/leucosomes/high-grade metamorphic; S = S-type granitoids and high aluminium saturation index (ASI) 'felsic' I-types; UM = ultramafic rocks including carbonatites, lherzolites and pyroxenites (O'Sullivan et al., 2020).

2.3.2 (U-Th-Sm)/He dating (AHe)

2.3.2.1 Fundamentals of AHe dating

Introduction

The apatite (U-Th-Sm)/He thermochronometer (AHe for short) is a radiometric technique based on the accumulation of ^{4}He from the radioactive decay of the ^{238}U, ^{235}U, ^{232}Th and ^{147}Sm nuclides, and its loss from the sample via temperature-dependent volume diffusion. Its use as thermochronometer in apatites was pioneered by both Zeitler et al. (1987), based on their experience with AFT dating, and by a group at Heidelberg University in Germany (published PhD of Boschmann Käthler (1986) and Lippolt et al. (1989), Lippolt et al. (1989)). Helium is lost by diffusion between c. 40-80°C, which is known as the partial He retention zone (PHeRZ) (Wolf et al. (1998), Farley (2000)).

Parent and daughter isotope measurements

Early AHe studies measured ^{4}He using a resistance-heating furnace which allows for isothermal and step-heating experiments (Zeitler et al. (1987), Lippolt and Weigel (1988), Wolf et al. (1996), Farley (2000)), but this technique is time-consuming, has high blanks and hence cannot be used for single-grain studies. An alternative extraction method using a laser beam was developed at the turn of the century (Stuart and Persano (1999), Reiners and Farley (1999), House et al. (2000)) and has now become the main extraction technique as it allows for single-grain analyses, a quicker sample throughput and lower blanks (Vermeesch et al., 2012). Once extracted, the helium, together with a spike, is measured by gas source mass spectrometry.

In the 1980s and 1990s, a wide range of methods have been used to measure the concentrations of the parent isotopes ^{238}U, ^{235}U, ^{232}Th and ^{147}Sm, such as isotope-dilution alpha-spectrometry (Zeitler et al., 1987), isotope-dilution thermal ionization mass spectrometry (TIMS) (Wolf et al., 1996), mixed alpha-spectrometry and TIMS (Lippolt and Weigel, 1988) and inductively coupled plasma mass spectrometry (ICP-MS) (Warnock et al., 1997). However, since the early 2000s, isotope-dilution ICP-MS is the most-commonly used technique. All the above techniques start with the complete dissolution of the apatites in an acid (e.g. 7M HNO3, Evans et al. (2005)) and the addition of spikes of suitable isotopes (absent or in negligible quantity in natural samples) of the parent elements (e.g. ^{235}U and ^{230}Th, Evans et al. (2005)).

Limitations

The AHe dating method has several limitations that have to be addressed to derive meaningful ages. The long stopping distance of ^{4}He leads to its loss on the rims of grains. Several methods have been proposed to correct for this phenomenon such as analysing only large grains (Lippolt et al., 1994), various versions of an age correction (F_T) based on the surface-to-volume ratio of the grain (Farley et

al. (1996), Farley (2002)) or a correction based on Monte-Carlo simulations of various typical apatite grain shapes (Ketcham et al., 2011). The Monte-Carlo-derived factor can be calculated (together with a sphere-equivalent radius for analytical modelling) using a suite of software packages: *Alpha Ft-ejection Factor* (Gautheron et al., 2012b) and *S/V Computation* (Gautheron and Tassan-Got, 2012) based on the results from Gautheron and Tassan-Got (2010), Ketcham et al. (2011) and Gautheron et al. (2012a). The correction factor can be used to correct the age (Farley et al., 1996), the measured He (Min et al., 2003) or the measured parent elements (Ketcham et al., 2011) but for Phanerozoic ages, all three methods yield similar results.

One fundamental assumption of the AHe technique is that the apatite grain is inclusion-free. If U-Th-Sm-rich inclusions (mineral or fluid) are present in a crystal, they will also produce ^{4}He through time that will be ejected or diffuse into the apatite crystal lattice. In apatites, the most common inclusions are monazite and zircons, followed by quartz, then feldspars, xenotime and sulphides (Farley and Stockli, 2002). Hence the two most common mineral inclusions in apatite are U-Th-Sm-rich. As zircons are not dissolved by the acid used to dissolve the apatite grain, the main way to avoid inclusions in the grains is to screen for them during grain selection (Farley, 2002).

Parent isotope zonation has three main effects on AHe dating, if undetected: 1) it affects the accuracy of the F_T correction factor; 2) it alters the diffusion behaviour due to a change in the He concentration profile; and 3) it creates an heterogenous radiation damage pattern that also affects the diffusion behaviour (Farley et al., 2011). However, Ault and Flowers (2012) concluded that parent nuclide (^{238}U, ^{232}Th) zonation has very limited impact on AHe ages and therefore on the age dispersion of grains within a sample. This observation was confirmed by Johnstone et al. (2013).

Many studies have focused on characterizing the diffusion of ^{4}He in apatite (e.g. Farley (2000), Shuster et al. (2006), Shuster and Farley (2009), Gautheron and Tassan-Got (2010), Zeitler et al. (2017)). One of the main factors controlling diffusion is the amount of radiation damage caused by alpha ejection in the grain and several quantitative models have been developed to predict diffusion based on the initial parent element concentration, grain size and a proxy for radiation damage (the effective uranium content $eU = {}^{238}U + 0.234 * {}^{232}Th + 0.00463 * {}^{147}Sm$) (Flowers et al. (2009), Gautheron et al. (2009)).

These limitations often lead to high age dispersion within samples, which often remains unexplained even after considering the above mentioned possible causes. This has led some researchers to question the reliability of the AHe thermochronometer for geological interpretations (Green and Duddy, 2018).

2.3.2.2 Methodology

The analyses were undertaken at the London Geochronology Centre (LGC) of University College London (under the supervision of Prof. Andy Carter).

Helium measurement

The Pt tubes are placed in holes drilled in a copper planchet which is then inserted in the sample chamber of the laser. A laser beam (Laservall fibered 25W diode laser) is directed at the sample to heat the Pt tube for 120 seconds (reaching temperatures >1000°C). The tube distributes the heat homogenously across the sample and enables the diffusion of all the He outside of the grain into the sample chamber. A spike of pure ^{3}He (0.2258 ± 0.0012 cc) is injected in the line before the He from the sample is released. The released gas (^{4}He but also argon, possibly hydrocarbons etc.) mixes with the background gases and ^{3}He spike in the chamber, expands throughout the entire system (equilibration) and is purified by cold and hot getters that trap non-He gases (for a duration of 168 s, with an overlap of 53 s with the laser heating). Once purified, the gas is sent through another getter to an electron ionization quadrupole mass spectrometer (EI-Q-MS, Pfeiffer Prisma 100, operated with the Baltzer Quadstar 422 software) for a recording period of 200 s. Once the analysis is finished, an ion pump is activated to remove all the gas from the system (for 363 s) before the next sample is analysed.

Blanks are analysed at the start, middle and end of the session. At the start and end of each session/day a ^{3}He-spiked ^{4}He standard is measured, which combined with the ^{4}He/^{3}He ratio of each spiked sample allow the derivation of [4He] in the samples using the following formula:

Equation 1: Concentration of ^{4}He in a sample.

$$4\text{He Sample} = \frac{4\text{He}/3\text{He}_{\text{Spiked Sample}}}{4\text{He}/3\text{He}_{\text{Spiked Qstandard}}}$$

For each planchet, at least three external standards of (Durango apatite are also analysed.

U, Th, Sm concentration: solution ICP-MS

After degassing, each Pt tube is opened with a tweezer and dropped in a plastic tube to which is added a solution of HNO_3 spiked with known amounts of ^{230}Th, ^{235}U and ^{149}Sm (isotopes absent or in negligible amount in natural minerals) and known ratios of ^{230}Th/^{232}Th and ^{235}U/^{238}U. The apatite is dissolved overnight by the acid and the solution is then analysed by solution ICP-MS with an Agilent 7700x. The ratios of non-natural and natural isotopes are then converted to concentrations of natural parent isotopes.

Age equation

The AHe age for each grain is calculated using the non-iterative solution of Meesters and Dunai (2005).

2.3.2.3 Data processing

The raw data from the parent and daughter isotope measurements were processed in a spreadsheet provided by UCL which calculates the AHe age for each grain. The error on the age has been estimated to be ± 15% based on the results from the secondary standards (SECTION 3.2.2.2). The results for the samples and Durango secondary standards are presented in section 3.2.

2.4 Sample quality scoring and selection for thermal history modelling

Inverse modelling of thermochronological data uses input data of various quality and reliability. Therefore, it can be assumed that the reliability of the thermal history is (at least partially) dependent on the reliability of the input data.

A scoring system is proposed in order to assess the quality of the input data for thermal history modelling purposes. This score can be used to both select suitable samples for modelling and also each thermal history can be then presented with its associated score that allows a quick evaluation of the quality of the input data. Comparing models with such scores might improve how these models are used and interpreted.

The scoring system assumes that there are three main types of low-temperature thermochronological data: fission track ages (central age and error), track lengths (MTL and distribution) and (U-Th)/He ages. A score from 0 (less reliable) to 3 (most reliable) is assigned for each category and then all three scores are added to obtain a final score between 0 and 9. When comparing two thermal histories, if one has a score of 9 and the other one a score of 2, more weight should be put on the thermal history with the higher score.

The quality of the fission track central age is mostly dependent on the number of grains analysed, therefore the score is based on the number of grains (TABLE 3). Thermal histories are highly sensitive to the track length distribution which can only be properly estimated with a sufficient number of tracks, therefore the number of tracks is used as the quality criterion (TABLE 3). The quality of helium data is mostly based on the repeatability of the ages. A sample with low dispersion will be much more reliable than a sample with high age dispersion, therefore the quality score is based on an estimation of age dispersion (TABLE 3).

The score for each category and the total score for each sample is displayed in TABLE 3. As a general rule, a total score of 2 with a minimum FTA score of 1 is the threshold for a sample to be considered suitable for thermal history modelling in this study. The average score for all samples in the thermal history models presented in this study is displayed on each model as a reminder of the data quality on

which models are based. The scoring system is simple and could be improved upon (e.g. a different scoring system for detrital *vs* igneous samples, additional inputs such as VR etc).

Table 3: Scoring system for quality of input data for THM.

QIDS	0	1	2	3
FTA	<10 ages	10-19 ages	20-29 ages	>30 ages
CTL	<25 TINTS	25-50 TINTS	50-100 TINTS	>100 TINTs
AHe	No ages	No cluster	Cluster <50% of grains	Cluster >50% of grains

2.5 Thermal history modelling

2.5.1 Introduction

The aim of thermal history modelling is to find a set of thermal histories for a sample, or a suite of samples in a borehole/vertical profile, that can reasonably explain their thermochronological data. For this study, the thermal history modelling was undertaken using QTQt v.5.7 (Gallagher, 2012), a software package particularly suited for multi-sample datasets.

2.5.2 QTQt modelling method

QTQt defines a random set of K time (t_i)-temperature (T_i) points (tT) for the shallowest sample and a random offset (O_i) between the shallowest and deepest sample at each tT point. The deeper samples all share the same number of K tT points and the same t_i as the top samples. Their temperature is calculated by linear interpolation of the temperature of the shallowest sample (T_i) and the deepest sample ($T_i + O_i$) based on their relative depths (e.g. a sample located at mid-depth between the top and bottom samples would have a temperature of $(2T_i + O_i)/2$). The selection of the initial set of points is random but constrained by the ranges of the prior information, such as the general prior time-temperature box and the prior offset. At each iteration of the modelling, the current thermal history is perturbed by either moving a time point, moving a temperature point, moving an offset value, removing a tT point (death), adding one (birth), moving the kinetic parameter of a single sample or moving an observed value for a single sample. The perturbed model is called the proposed model and it is either rejected or accepted and then becomes the current model for the next iteration. The rejection or acceptance of the proposed model is based on an acceptance function that compares the likelihood of predicting the observed data of the two models and rejects proposed models that do not come close to or improve upon the current model. The total number of iterations is split between an initial phase of model space exploration (called 'burn-in') and a second phase (called 'post-burn-in').

The burn-in phase is used to narrow down the range of realistic values for each parameter (notably the number of tT points K) and once completed is discarded. The post-burn-in phase, which benefits from the findings of the burn-in phase, is run to obtain the final posterior distribution for the model parameters, including the thermal histories (Gallagher, 2012).

2.5.3 Modelling strategy

2.5.3.1 Introduction

The following section describes the strategy used for this study. The strategy aims at finding a balance between consistency between samples to facilitate comparison of inverse model results, and some measure of flexibility and sample-specific choices to extract as much information as possible from each sample. Unless stated otherwise in the text, all models have been built utilizing this procedure.

2.5.3.2 Sample specific parameters

AFT ages

For the new samples, the Ns, LAFT age and error and Dpar were imported in QTQt. Geotrack legacy data was also directly imported in QTQt with Cl (when available) as the annealing compositional parameter. The legacy data from papers do not contain AFT data for each grain, therefore the QTQt 'Resample age/count data' method was used. This method requires only a the central age, error and Ns/Ni values and number of grains (n) to derive a population of n synthetic grains that yield similar results and can be employed in modelling (Gallagher, 2017).

AFT lengths

For the samples measured in this study, the confined track lengths were imported to QTQt when 15 or more lengths were available (minimum threshold), together with their c-axis angle for QTQt to calculate the projected track lengths (Ketcham et al., 2007) and the Dpar average value of the host grain for grain-specific annealing. For the Geotrack legacy data, the lengths do not have c-axis angle data associated with them so projected lengths could not be used. The legacy data from papers/reports also do not contain individual track length data, therefore a synthetic track length distribution has been recreated based on length histogram plots (using QTQt 'Manual entry' option); or, when no length histogram was available, from the mean track length and associated standard deviation and standard error. The etchant was 5.5M for the samples from this study and 5M for the legacy data.

AHe ages

By default, all non-outlier AHe ages have been imported in QTQt. The imported data correspond to the uncorrected AHe age, age error, uranium/thorium/samarium concentrations (in ppm) and the sphere-

equivalent radius derived from the Monte-Carlo modelling as a proxy for the size (sphere selected as the modelled shape).

Annealing and diffusion models

For the fission track data, the annealing model used is from Ketcham et al. (2007) with the initial track length calculated for each grain based on its compositional information (Dpar or Cl); while for the AHe data, the radiation damage-based diffusion model of both Gautheron et al. (2009) and Flowers et al. (2009) were typically used.

Final temperature

The present-day temperature constraint of the samples can be defined as a constraint in the sample file. The temperature and associated error calculated for each sample in function of the water depths and geothermal gradient in the borehole (SECTION 2.1.3) have been used for this constraint.

Initial time-temperature

For detrital samples (and some metasedimentary samples), the initial age was defined as the depositional age based on the composite log and geological report (SECTION 2.1.2). The initial temperature is defined as the present-day seabed temperature average (10 ± 10°C) for shallow water as it represents a realistic range of temperatures for a large range of depositional environments for the Phanerozoic (the present-day seabed temperature calculated in section 2.1.3.1 is more accurate and precise but cannot be used for past surface conditions). For detrital samples, the option of allowing for a pre-depositional thermal history has been selected (to mimic some amount of fission track accumulation and annealing in the apatite prior to deposition).

For crystalline rock samples with a homogenous apatite age population (igneous and some metamorphic samples), the apatite U/Pb age was used as the initial age. The closure temperature for the apatite U/Pb system is c. 375-600°C (Kirkland et al., 2018) but for the sake of simplification and to reduce the size of the prior time-temperature domain of the models, the temperature at the time of crystallisation is set at 140°C (*i.e*. high enough for complete annealing of any fission tracks).

2.5.3.3 Prior information constraints

The general prior (the time-temperature box that can be samples by the modelling process) was defined by the default value selected by QTQt, based on the oldest AFT age and 70 ± 70°C. The geothermal gradient calculated by QTQt was verified against the expected geothermal gradient to ensure integrity of the imported depths and temperatures. By default, the gradient was not allowed to change between tT points and/or between iterations. The maximum rate of temperature change allowed to be used by the modelling is 1000°C.Ma^{-1} (default value), except when models were generating heating spikes and modelling results without such spikes were desired.

2.5.3.4 Intermeditate time-temperature constraints

In boreholes, the biostratigraphic information can be used to place additional time-temperature constraints in the models. For each separate stratigraphic unit, an assumption is made that the midpoint (at depth X, in m MD) of each unit was at that time a paleoseabed. A sample located below this midpoint (at depth Y, in mMD, with Y > X) was therefore located at a paleodepth of Z = Y - X at the time that X was at the surface (as a seabed) (compaction effects are ignored for the sake of simplification).A constraint can then be placed with the x-axis corresponding to the time interval of that stratigraphic unit (using the time scale described above) and the y-axis corresponding to the assumed temperature of the sample using the paleodepth Z and the present-day geothermal gradient.

2.5.3.5 Run parameters

Unless stated otherwise, the modelling was based on 200,000 iterations, divided equally between burn-in and post-burn-in, with a thinning factor of 1. The default models were run using the 'Reject more complex that do not improve data fit' option which creates models with only a few time-temperature points (c. 2-10 points, called 'simple' models thereafter). Some models were also run without this option, leading to thermal histories with c. 10-50 points (called 'complex' models thereafter).

2.5.4 Reporting of modelling results

2.5.4.1 Stability of the log likelihood and log posterior chains

The log likelihood and log posterior chains are presented for each model to show the chain convergence. Convergence is a sign that enough iterations of the modelling have been run and that, based on the given input data, further exploration of the time-temperature space would probably not lead to significant improvements of the model fit. The plots are also presented in ANNEX 2.

2.5.4.2 Terminology

The simple 'maximum posterior model', 'expected model', 'maximum likelihood model' and the complex 'expected model' will be referred to respectively as the 'posterior model', 'expected model', 'likelihood model' and 'complex model'.

2.5.4.3 Results

The choice of input data, model constraints and a discussion of the results with a selection of relevant thermal history plots are presented for each borehole in the discussion chapters (SECTIONS 4, 4 AND 6). However, the results of all models, together with the measures of the prediction accuracy, can be consulted in ANNEX 2.

3 Results

3.1 Sampling results

Two sampling trips to the Petroleum Affair Directorate (PAD) core store (Dublin, on 10-11/05/2017 and 10/05/2018) and one to the Ifremer core store (Brest, France, on 26/03/2018) yielded 43 new samples from 14 boreholes and eight seabed dredges/dives. A sub-set of 30 legacy samples has also been selected to be integrated with the new samples (FIGURE 16 AND TABLE 4).

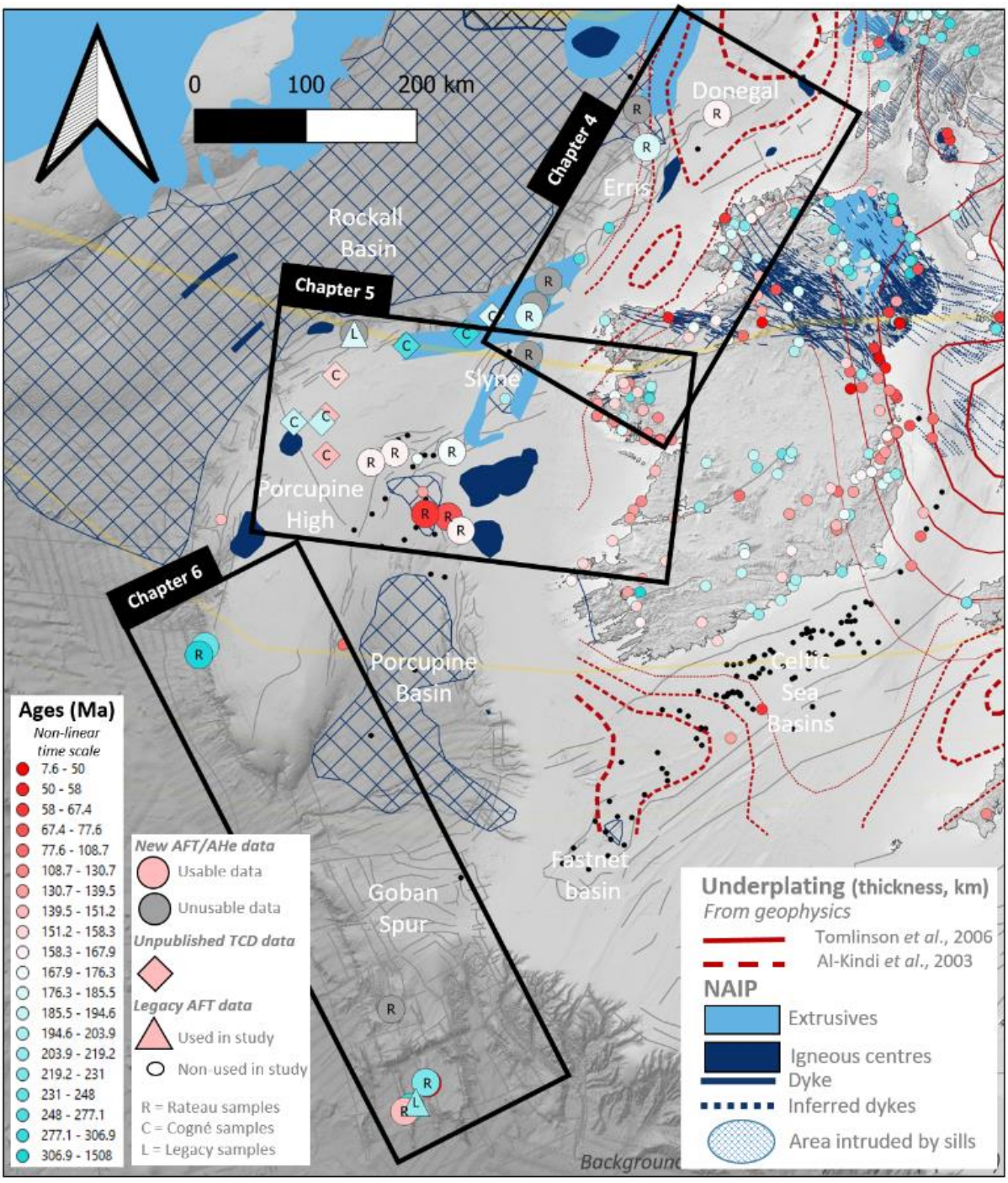

Figure 16: Location of the new samples and legacy samples used in this study, colour-coded by AFT central age.

Table 4: Summary of new and legacy samples used in the study.

Well Dredge	Sample	Coordinates		Depths		Seabed	Temperature		Source	Type	Weight	Lithology	Age		
		Lat	Long	Report unit	Average		Seabed	Samples				Targeted/Sampled	Stratigraphic age or Apatite age		
		(deg)	*(deg)*	*MD*	*m BSB*	*m MSL*	*°C*	*°C*			*g*			*Ma*	±
12/02-1Z	R-33	55.9224	-9.6524	3962.25-.5 m	2456	1476	5	101	This study	core	n/a	Basalt	Early Permian?	n/a	n/a
	R-34	55.9224	-9.6524	3963.25 m	2457	1476	5	101	This study	core	n/a	Sandstone	Middle Jurassic	168.8	5.3
12/13-1A	R-37	55.6177	-9.5106	7300-7450 ft	1756	480	10	62	This study	cuttings	n/a	Dolerite?	not dated		
13/03-1	R-1	55.8885	-8.5023	1420-1540 ft	294	131	10	18	This study	cuttings	1080	Tuffaceous sand	Steph. B-Westph. D	307.3	3.8
	R-2	55.8885	-8.5023	4473-4483 ft	1208	131	10	44	This study	core	585	Quartz dolerite	Ea. Permian?		
	L-D1	55.8885	-8.5023	4473-4483 ft	1208	131	10	44	McCulloch	core	n/a	Quartz dolerite	Ea. Permian?		
16/28-sb01	L-GC777-1	54.0222	-13.5143	41-41 mBSB	41	1465	5	6	Geotrack	core	n/a	Sandstone	Middle Eocene	42.8	5.0
	L-GC777-9	54.0222	-13.5143	41-80 mBSB	61	1465	5	7	Geotrack	core	n/a	Sandstone	Middle Eocene	42.8	5.0
	R-3	54.0222	-13.5143	80-98 mBSB	89	1462	5	7	This study	core	230	Sandstone	Early-Middle Eocene	51.9	14.1
	R-4	54.0222	-13.5143	127-146 mBSB	137	1462	5	9	This study	core	400	Sandstone	Early Eocene	61.0	5.0
	R-5	54.0222	-13.5143	146-148 mBSB	147	1462	5	9	This study	core	180	Sandstone	Late Cretaceous	83.3	17.3
	L-GC777-2	54.0222	-13.5143	147-147 mBSB	147	1465	5	9	Geotrack	core	n/a	Sandstone	Late Cretaceous	83.3	17.3
18/25-1	R-41	54.3201	-11.0469	2208-2232 m	1546	336	10	56	This study	cuttings	400	Dolerite	not dated		
	R-42	54.3201	-11.0469	2346-2370 m	1858	336	10	66	This study	cuttings	500	Dolerite	not dated		
18/25-2	R-44	54.2300	-11.1192	2085-2148 m	1791	299	10	60	This study	cuttings	1100	Dolerite	not dated		
19/11-1A	R-6	54.5158	-10.8637	1190-1200 m	772	397	10	36	This study	cuttings	340	Dolerite	not dated		
25/27-sb(MeBo)2	C-MeBo2	53.0260	-13.7833	N/A-N/A m	0	192	10	10	Cogné	core	n/a	Gneiss	Apatite: Late Caledonian	383.9	5.8
25/7-sb(MeBo)3	C-MeBo	53.6782	-13.7287	N/A-N/A m	0	254	10	10	Cogné	core	n/a	Orthogneiss	Apatite: post-Grenville cooling	880.0	n/a
26/26-1	R-7	53.0791	-12.8660	593-692 m	268	363	10	18	This study	cuttings	1410	Sandstone	Early -Middle Eocene	46.9	9.1
	L-PB1	53.0791	-12.8660	644-657 m	276	363	10	18	McCulloch	cuttings	n/a	Sandstone	Early -Middle Eocene	46.9	9.1
	L-PB2	53.0791	-12.8660	780-793 m	412	363	10	22	McCulloch	cuttings	n/a	Sandstone	Hauterivian	131.0	1.6
	L-PB3	53.0791	-12.8660	1096-1120 m	733	363	10	31	McCulloch	cuttings	n/a	Sandstone	Tournaisian-Visean	344.9	14.0
	L-PB4	53.0791	-12.8660	1138-1168 m	778	363	10	32	McCulloch	cuttings	n/a	Metasediments	Dalradian?	655.0	145.0
	R-8	53.0791	-12.8660	1129-1256 m	818	363	10	33	This study	cuttings	1950	Metasediments	Dalradian?	655.0	145.0
	L-PB5	53.0791	-12.8660	1227-1255 m	866	363	10	35	McCulloch	cuttings	n/a	Metasediments	Dalradian?	655.0	145.0
26/30-1	R-68	53.1093	-12.1002	4184-4880 ft	1108	249	10	47	This study	cuttings	?	Sandstone	Oxfordian-Bathonian	162.8	5.5
	R-50	53.1093	-12.1002	5430-5550 ft	1400	249	10	56	This study	cuttings	50	Granite wash	Westphalian C	313.1	1.9
	R-51	53.1093	-12.1002	5560-5640 ft	1434	249	10	57	This study	cuttings	50	Granite	not dated		
27/05-1	R-9	53.9194	-11.1077	1690-1705 m	1471	201	10	56	This study	cuttings	560	Dolerite	not dated		
34/05-1	R-10	52.9910	-13.1792	680-710 m	381	289	10	21	This study	cuttings	180	Sandstone	Paleocene-Eocene	50.0	16.1
	R-11	52.9910	-13.1792	710-738 m	410	289	10	22	This study	cuttings	190	Sandstone	Albian?	106.8	6.3
	R-12	52.9910	-13.1792	870-980 m	611	289	10	27	This study	cuttings	680	Sandstone	Westphalian C-D	311.0	4.0
	R12-14	52.9910	-13.1792	870-1230 m	736	289	10	31	This study	cuttings	n/a	Sandstone	Westphalian C-D	311.0	4.0
	R-13	52.9910	-13.1792	1010-1100 m	741	289	10	31	This study	cuttings	1070	Sandstone	Westphalian C	313.1	1.9
	R-14	52.9910	-13.1792	1100-1230 m	851	289	10	34	This study	cuttings	1620	Sandstone	Westphalian C	313.1	1.9
	R-15	52.9910	-13.1792	1425-1490 m	1144	289	10	42	This study	cuttings	1200	Sandstone	Westphalian B	316.1	1.1

Table 5 (continued on next page): Apatite U/Pb, AFT and AHe results for new (green) and selected legacy samples (white) and suitability for thermal history modelling. Sample information is in Table 4. Colour code explained in section 2.4.

Well Dredge	Sample	Temp.		Lithology	Age		U/Pb		FTA					CTL				Kinetic			AHe						Inverse Modeling							
		SB	Spl.	Targeted/Sampled	Age	±	n	Age Youngest*	n	Ns	$P(\chi^2)$	Central Age		Tracks	MTL	SD	SE	Cl	Dpar	U	n	Mean eU	Age cluster?	Raw	F_T-corrected	Score				QTQt file	Model		
		°C	°C				-	*Ma+2σ*	-	-	-	*Ma*	*±1σ Ma*	-	*μm*	*μm*	*μm*	*wg%*	*μm*	*ppm*	-	*ppm*	-	*Min-Mean-Max*	*Min-Mean-Max*	*F*	*C*	*A*	*Total*		*Model?*	*Inputs*
12/02-1Z	R-33	5	101	Basalt	?	?	n/a	n/a	<4	-	-	-	-	-	-	-	-	n/a	n/a	n/a	0	n/a	n/a	n/a	n/a	0	0	0	0	No	No	No
	R-34	5	101	Sandstone	168.8	5.3	n/a	n/a	0	-	-	-	-	-	-	-	-	n/a	n/a	n/a	0	n/a	n/a	n/a	n/a	0	0	0	0	No	No	No
12/13-1A	R-37	10	62	Volcanoclastics	250.1	48.8	64	284.1*	24	229	<1	**185**	19	64	**10.33**	2.27	0.28	0.12	1.61	26	0	n/a	n/a	n/a	n/a	2	2	0	4	No	No	No
13/03-1	R-1	10	18	Tuffaceous sand	307.3	3.8	73	n/a	72	3075	<1	**163.3**	7.2	194	**11.19**	2.44	0.17	0.16	1.72	27	10/10	50	4/10	7-**47**-105	9-**69**-160	3	3	2	8	Yes	Yes	A+T+H
	R-2	10	44	Quartz dolerite	n/a	n/a	123	297 ± 9	123	400	100	**166.3**	8.4	1	**12.03**	-	-	0.21	1.76	1.7	4/4	10	3/4	9-**15**-16	13-**21**-23	3	0	3	6	Yes	Yes	A+H
	L-D1	10	44	Quartz dolerite	n/a	n/a	n/a	n/a	29	167	70	**183.1**	19.2	0	-	-	-	n/a	n/a	n/a	n/a	n/a	n/a	n/a	n/a	2	0	0	2	Yes	Yes	A
16/28-sb01	L-GC777-1	5	6	Sandstone	42.8	5.0	n/a	n/a	2	4	0.14	**57.3**	33.1	2	**12.16**	0.16	0.11	0.40	n/a	4	n/a	n/a	n/a	n/a	n/a	0	0	0	0	No	No	No
	L-GC777-9	5	7	Sandstone	42.8	5.0	n/a	n/a	20	366	<0.01	**180.6**	21.1	82	**13.68**	1.06	0.16	0.03	n/a	22	n/a	n/a	n/a	n/a	n/a	2	2	0	4	Yes	Yes	A+T
	R-3	5	7	Sandstone	51.9	14.1	1	n/a	1	8	-	**126.8**	45.26	1	**6.70**	0.00	0.00	0.09	1.23	9	0	n/a	n/a	n/a	n/a	0	0	0	0	No	No	No
	R-4	5	9	Sandstone	61.0	5.0	0	n/a	0	-	-	-	-	-	-	-	-	n/a	n/a	n/a	0	n/a	n/a	n/a	n/a	0	0	0	0	No	No	No
	R-5	5	9	Sandstone	83.3	17.3	1	n/a	1	43	-	**104.5**	16.7	1	**12.90**	0.00	0.00	0.08	1.62	32	0	n/a	n/a	n/a	n/a	0	0	0	0	No	No	No
	L-GC777-2	5	9	Sandstone	83.3	17.3	n/a	n/a	17	445	0.51	**161.7**	11.3	43	**13.31**	1.51	0.17	0.11	n/a	13	n/a	n/a	n/a	n/a	n/a	1	1	0	2	Yes	Yes	A+T
18/25-1	R-41	10	56	Dolerite	n/a	n/a	n/a	n/a	0	-	-	-	-	-	-	-	-	n/a	n/a	n/a	0	n/a	n/a	n/a	n/a	0	0	0	0	No	No	No
	R-42	10	66	Dolerite	n/a	n/a	n/a	n/a	0	-	-	-	-	-	-	-	-	n/a	n/a	n/a	0	n/a	n/a	n/a	n/a	0	0	0	0	No	No	No
18/25-2	R-44	10	60	Dolerite	n/a	n/a	55	126 ± 20	34	74.0	0.99	**177.0**	**21.0**	1.0	12.3	-	-	0.97	2.45	1.7	0	n/a	n/a	n/a	n/a	3	0	0	3	No	No	No
19/11-1A	R-6	10	36	Dolerite	122.8	22.3	3	n/a	3	115	<0.01	**174.0**	81	14	**10.88**	1.46	0.39	0.17	1.65	41	0	n/a	n/a	n/a	n/a	0	0	0	0	No	No	No
25/27-sb(MeBo)2	C-MeBo2	10	10	Gneiss	n/a	n/a	n/a	383.9 ± 5.8	28	377	0.42	**144.1**	7.5	101	10.29	2.45	0.24	0.27	1.44	n/a	4	31	3/4	25-**34**-71	34-**47**-107	2	3	3	8	Yes	Yes	A+T+H
25/7-sb(MeBo)3	C-MeBo	10	10	Orthogneiss	n/a	n/a	n/a	1038 ± 12	15	459	0.00	**157**	27	102	13.03	1.21	0.12	0.05	1.36	n/a	3	21	3/3	144-**148**-151	186-**192**-197	1	3	3	7	Yes	Yes	A+T+H
26/26-1	R-7	10	18	Sandstone	46.9	9.1	0	n/a	0	-	-	-	-	-	-	-	-	n/a	n/a	n/a	0	n/a	n/a	n/a	n/a	0	0	0	0	No	No	No
	L-PB1	10	18	Sandstone	46.9	9.1	n/a	n/a	4	54	0.40	**255**	50.5	0	-	-	-	n/a	n/a	n/a	n/a	n/a	n/a	n/a	n/a	0	0	0	0	No	No	No
	L-PB2	10	22	Sandstone	131.0	1.6	n/a	n/a	13	128	0.50	**241**	31	25	**11.24**	2.39	0.49	n/a	n/a	n/a	n/a	n/a	n/a	n/a	n/a	1	1	0	2	Yes	Yes	A+T
	L-PB3	10	31	Sandstone	344.9	14.0	n/a	n/a	5	91	<0.05	**171**	30	14	**11.36**	2.04	0.55	n/a	n/a	n/a	n/a	n/a	n/a	n/a	n/a	0	0	0	0	No	No	No
	L-PB4	10	32	Metasediments	Dalradian?		n/a	n/a	16	279	0.55	**162.2**	13	56	**11.72**	1.54	0.21	n/a	n/a	n/a	n/a	n/a	n/a	n/a	n/a	1	2	0	3	Yes	Yes	A+T
	R-8	10	33	Metasediments	Dalradian?		56	390.8±6.3	64	1483	<0.01	**159**	8	65	**11.20**	2.20	0.27	0.03	1.63	14	5/5	14	No	58-**86**-101	77-**107**-127	3	2	1	6	Yes	Yes	A+T+H
	L-PB5	10	35	Metasediments	Dalradian?		n/a	n/a	20	578	0.65	**164.3**	9.3	84	**11.81**	1.87	0.20	n/a	n/a	n/a	n/a	n/a	n/a	n/a	n/a	2	2	0	4	Yes	Yes	A+T
26/30-1	R-68	10	47	Sandstone	162.8	5.5	131	159.8±3.1*	43	895	<0.01	**172**	10	28	10.63	2.89	0.55	0.23	1.68	17	n/a	n/a	n/a	n/a	n/a	3	1	0	4	Yes	Yes	A+T
	R-50	10	56	Granite wash	313.1	1.9	17	296.3*	2	27	0.7	**75.0**	**15.0**	0	-	-	-	0.13	n/a	54	n/a	n/a	n/a	n/a	n/a	0	0	0	0	No	No	No
	R-51	10	57	Granite	313.1	1.9	33	399.8*	15	210	<0.01	**151**	**23**	11	11.28	1.64	0.49	0.10	1.94	14	n/a	n/a	n/a	n/a	n/a	1	0	0	1	No	No	No
27/05-1	R-9	10	56	Dolerite	n/a	n/a	7	197.9	8	294	0.18	**228**	14	21	**10.77**	1.99	0.43	0.19	1.84	18	4/4	25	No	29-**60**-87	40-**85**-121	0	0	1	1	No	No	No
34/05-1	R-10	10	21	Sandstone	50.0	16.1	2/2	n/a	2	70	0.02	**130**	27	3	**13.18**	1.36	0.79	0.04	1.87	19	0	n/a	n/a	n/a	n/a	0	0	0	0	No	No	No
	R-11	10	22	Sandstone	106.8	6.3	0	n/a	0	-	-	-	-	-	-	-	-	n/a	n/a	n/a	0	n/a	n/a	n/a	n/a	0	0	0	0	No	No	No
	R-12	10	27	Sandstone	311.0	4.0	2/2	n/a	2	105	0.04	**164**	24	19	**11.86**	1.82	0.42	0.11	1.86	33	3/5	92	No	33-**47**-60	59-**79**-101	0	0	1	1	No	No	No
	R12-14	10	31	Sandstone	311.0	4.0	29/31	n/a	30	1107	<0.01	**166**	8	77	**11.63**	1.90	0.22	0.16	1.80	30	3/5	92	No	33-**47**-60	59-**79**-101	3	2	1	6	Yes	Yes	A+T+H
	R-13	10	31	Sandstone	313.1	1.9	19/21	n/a	20	729	<0.01	**165**	11	39	**11.50**	2.16	0.35	0.15	1.75	30	0	n/a	n/a	n/a	n/a	2	1	0	3	No	No	A+T
	R-14	10	34	Sandstone	313.1	1.9	8/8	n/a	8	272	0.03	**167**	16	19	**11.66**	1.29	0.30	0.19	1.91	28	0	n/a	n/a	n/a	n/a	0	0	0	0	No	No	No
	R-15	10	42	Sandstone	316.1	1.1	11/11	n/a	11	277	0.02	**110**	13	10	**11.52**	2.14	0.68	0.14	1.80	44	4/5	45	No	15-**35**-53	25-**55**-81	1	0	1	2	Yes	Yes	A+H

Well Dredge	Sample	Temperature		Lithology	Age		U/Pb		FTA					CTL				Kinetic			AHe						Inverse Modeling						
		Seabed	Sample	Targeted/Sampled	Age	±	n	Age	n	Ns	$P(\chi^2)$	Central Age		Tracks	MTL	SD	SE	Cl	Dpar	U	n	Mean eU	Age cluster?	Raw	F_T-corrected	Score				QTQt file	Model		
		°C	°C				-	*Ma+2σ*	-	-	-	*Ma*	*±1σ Ma*	-	*µm*	*µm*	*µm*	*wg%*	*µm*	*ppm*	-	*ppm*	-	*Min-Mean-Max*	*Min-Mean-Max*	*F*	*C*	*A*	*Total*		*Model?*	*Inputs*
35/13-1A	R-54	10	109	Dolerite	n/a	n/a	99	61.6 ± 5.6	38	61	1.0	66.8	8.6	0	-	-	-	0.6	1.6	1.8	0	n/a	n/a	n/a	n/a	3	0	0	3	No	No	No
	R-55	10	112	Dolerite	n/a	n/a	n/a	n/a	0	-	-	-	-	-	-	-	-	n/a	n/a	n/a	0	n/a	n/a	n/a	n/a	0	0	0	0	No	No	No
35/15-1	R-16	10	68	Basalt	n/a	n/a	4	c. 62 Ma	1	4	n/a	**100.2**	50.3	0	-	-	-	0.15	2.46	3.94	0	n/a	n/a	n/a	n/a	0	0	0	0	No	No	No
	R-17	10	70	Basalt	n/a	n/a	0		0	-	-	-	-	-	-	-	-	n/a	n/a	n/a	5/5	1	4/5	16-**31**-38	24-**43**-52	0	0	3	3	Yes	Yes	H
	R-18	10	72	Basalt	n/a	n/a	10		9	33	0.88	**89**	16	1	**13.33**	-	-	1.46	2.66	3.50	5/5	5	3/5	0-**0**-51	0-**0**-62	1	0	3	4	Yes	Yes	A+H
	R-19	10	77	Microgabbro	n/a	n/a	3		3	11	0.99	**81**	25	0	-	-	-	0.87	2.45	2.61	3/4	9	No	0-**4**-11	0-**6**-17	0	0	1	1	Yes	Yes	H
	R-20	10	104	Tuffaceous sand	n/a	n/a	0	n/a	0	-	-	-	-	-	-	-	-	n/a	n/a	n/a	0	n/a	n/a	n/a	n/a	0	0	0	0	No	No	No
36/16-1	R-58	10	36	Sandstone	51.9	4.1	32	174.5 ± 93.3*	20	581	<0.01	**153**	22	23	**12.51**	2.32	6.83	0.10	1.58	16.7	0	n/a	n/a	n/a	n/a	2	0	0	2	No	No	No
	R-59	10	50	Sandstone	57.6	1.6	0	n/a	0	-	-	-	-	-	-	-	-	n/a	n/a	n/a	0	n/a	n/a	n/a	n/a	0	0	0	0	No	No	No
	R-60	10	43	Sandstone	308.8	1.3	52	300.6 ± 90.2*	15	636	<0.01	**163**	12	28	**11.63**	1.99	0.38	0.13	1.73	37.2	0	n/a	n/a	n/a	n/a	2	2	0	4	No	No	No
CY 32-2	R-21	3	3	Gabbro	n/a	n/a	40	c. 1400	38	884	0.14	**238**	9	18	**12.27**	1.33	0.31	0.24	1.63	10.4	0	n/a	n/a	n/a	n/a	3	0	0	3	No	No	No
CY 34-3	R-22	3	3	Granite	n/a	n/a	40	425.6 ± 7.5	40	1525	<0.01	**222**	11	122	**12.63**	1.42	0.13	0.13	1.66	40.3	4/4	23	No	93-**158**-214	120-**193**-260	3	3	1	7	No	No	No
CY 34-8	R-23	3	3	Gneiss	n/a	n/a	39	c. 2800	40	709	<0.01	**420**	23	18	**11.09**	3.32	0.78	0.35	1.87	4.4	3/4	5	No	104-**122**-138	134-**156**-173	3	0	1	4	No	No	No
DR08 D01	R-24	3	3	Granite	n/a	n/a	40	297.2 ± 1.5	39	2737	<0.01	**192**	9	291	**12.01**	2.81	0.16	0.26	1.95	45.3	5/5	103	3/5	59-**91**-173	87-**134**-136	3	3	3	9	Yes	Yes	A+T+H
DR09 B14	R-25	3	3	Diorite/Metamorphic	n/a	n/a	40	1714 ± 16	40	294	0.58	**42**	3	2	**13.14**	1.38	0.98	0.12	1.52	20.4	5/6	25	4/5	32-**41**-63	39-**49**-75	3	0	3	6	Yes	Yes	A+H
DR10 D05	R-26	3	3	Granite	n/a	n/a	40	296.1 ± 1.5	40	1181	<0.01	**222**	11	66	**12.86**	2.03	0.25	0.11	1.69	18.8	4/6	81	3/4	45-**84**-84	63-**109**-112	3	2	3	8	Yes	Yes	A+T+H
DR12 B21	L-DR12-B21	3	3	Gneiss/Granulite?	n/a	n/a	n/a	n/a	16	1082	0.44	**212**	10	101	**12.98**	1.30	0.13	n/a	n/a	n/a	n/a	n/a	n/a	n/a	n/a	1	3	0	4	Yes	Yes	A+T
	R-27	3	3	Gneiss/Granulite?	n/a	n/a	38	446 ± 11	38	1709	0.01	**284**	9	152	**12.91**	1.78	0.14	0.20	2.02	20.9	0	n/a	n/a	n/a	n/a	3	3	0	6	Yes	Yes	A+T
CH67 DR13	R-28	3	3	Granite	n/a	n/a	40	288.3 ± 1.4	40	1263	<0.01	**143**	6	97	**13.04**	1.67	0.17	0.08	1.74	25.3	5/6	121	4/5	10-**70**-76	14-**95**-101	3	2	3	8	Yes	Yes	A+T
CH67 DR18	R-29	3	3	Sandstone	n/a	n/a	8	433.7 ± 52.9*	8	211	0.20	**126**	10	13	**11.40**	2.18	0.60	0.11	1.66	31.0	0	n/a	n/a	n/a	n/a	0	0	0	0	No	No	No
GSI PH1	C-PH1	10	10	Psammite	c. 671	201	?	Detrital	20	443	0.10	**142**	8	101	**9.69**	3.01	0.3	0.08	1.69	n/a	0	n/a	n/a	n/a	n/a	2	3	0	5	No	No	No
GSI PH4	C-PH4	10	10	Psammite	c. 672	201	?	Detrital	24	322	0.11	**184**	12	118	**9.86**	3.01	0.28	0.13	1.65	n/a	4	23	No	66-**93**-130	98-**132**-172	2	3	1	6	No	No	No
GSI PH5	C-PH5	10	10	Psammite	c. 673	201	?	Detrital	21	390	0.09	**194**	11	114	**9.79**	2.86	0.27	0.06	1.67	n/a	3	9	No	86-**107**-129	115-**135**-162	2	3	1	6	No	No	No
GSI PH10	C-PH10	10	10	Psammite	c. 674	201	?	Detrital	20	436	0.06	**193**	11	121	**9.76**	3.25	0.3	0.08	1.73	n/a	0	n/a	n/a	n/a	n/a	2	3	0	5	No	No	No
GSI PH12	C-PH12	10	10	Psammite	c. 675	201	?	Detrital	16	230	<0.01	**191**	20	92	**9.72**	3.08	0.32	0.06	1.49	n/a	0	n/a	n/a	n/a	n/a	1	2	0	3	No	No	No
GSI PH4-12	*C-PH4-12*	*10*	*10*	Psammite	c. 676	201	?	Detrital	*81*	*1378*	*<0.01*	***190.3***	*6.7*	*524*	***9.71***	*3.09*	*0.14*	*0.09*	n/a	n/a	*7*	*32*	*No*	*66-**99**-129*	*98-**133**-162*	*3*	*3*	*2*	*8*	Yes	Yes	A+T+H
CV14-021 204	C-204-1	10	10	Micaschist	n/a	n/a	?	?	23	505	0.31	**180**	8	100	**12.46**	1.5	0.15	0.02	1.61	n/a	2	4	No	55-**76**-98	78-**101**-123	2	3	1	6	No	No	No
CV14-021 302	C-302-1	10	10	Psammite	n/a	n/a	?	405 ± 27	30	912	0.33	**143**	5	100	**12.61**	1.62	0.16	0.12	1.62	n/a	4	10	No	50-**73**-95	68-**103**-139	3	3	1	7	No	No	No
CV14-021 303	C-303-1	10	10	Amphibolite	n/a	n/a	?	1750 ± 20	25	1214	0.08	**283**	9	100	**12.65**	1.81	0.18	0.11	1.63	n/a	5	25	3/5	239-**351**-358	347-**459**-480	2	3	3	8	No	No	No
CV14-021 402	C-402-1	10	10	Gneiss	n/a	n/a	?	1739 ± 16	30	891	0.10	**425**	16	105	**12.05**	2.09	0.2	0.16	1.7	n/a	4/5	7	4/5	0-**0**-1	0-**1**-2	3	3	3	9	No	No	No
	C-402-3	10	10	Gneiss	n/a	n/a	?	1697 ± 12	27	376	0.09	**289**	16	101	**12.03**	1.89	0.19	0.07	1.61	n/a	0	n/a	n/a	n/a	n/a	2	3	0	5	No	No	No
	C-402-4	10	10	Gneiss	n/a	n/a	?	967 ± 6	29	513	0.51	**216**	10	103	**12.69**	1.45	0.14	0.08	1.69	n/a	0	n/a	n/a	n/a	n/a	2	3	0	5	No	No	No
	C-402-6	10	10	Greenschist	n/a	n/a	?	381 ± 34	19	106	1.00	**190**	19	106	**12.49**	1.49	0.15	0.17	1.7	n/a	5	17	5/5	35-**44**-51	51-**64**-82	1	3	3	7	No	No	No
	C-402-8	10	10	Gneiss	n/a	n/a	?	1774 ± 11	28	1288	0.09	**546**	18	100	**12.2**	1.8	0.18	0.33	1.67	n/a	3	62	3/3	276-**280**-285	351-**368**-379	2	3	3	8	No	No	No
	C-402-9	10	10	Gneiss	n/a	n/a	?	981 ± 7	27	1246	0.07	**198**	7	61	**12.67**	1.83	0.23	0.06	1.55	n/a	5	34	No	246-**293**-343	313-**383**-444	2	2	3	7	No	No	No
	C-402-11	10	10	Metamorphic	n/a	n/a	?	1764 ± 16	29	1218	0.25	**167**	5	300	**12.58**	1.83	0.11	0.34	1.76	n/a	4	19	4/4	63-**72**-80	91-**93**-99	2	3	3	8	No	No	No
	C-402-13	10	10	Amphibolite	n/a	n/a	?	1120 ± 100	23	219	0.24	**261**	18	66	**12.57**	1.71	0.21	0.12	1.71	n/a	2	5	2/2	66-**68**-69	95-**97**-99	2	2	2	6	No	No	No

BSB = True vertical depth below seabed

MD = Measured depths

MSL = Mean sea level

New sample

Fügenschuh = Fügenschuh et al., 2003

Geotrack = Geotrack report (PAD), see Figure 3

Cogné = Unpublished study by Cogné & Chew, TCD
(the samples come from 3 dredging/drilling campaigns, full details are given at section 5.5.1.1,

McCulloch = McCulloch, 1993

*Table 6 (continued on next page): AHe results summary (continued below).*1/2T = 1 or 2 non-broken terminations, 1/2B = 1 or 2 broken terminations, P = pyramidal termination, F = flat termination. Inc.= probability of inclusions. Degassing: green = good, orange = minor He leak, red = major He leak. F_T = alpha ejection correction parameter. R_{eq} = sphere-equivalent radius.*

Sample	Grain	Shape in GFTC			Length	Diameter		S/V	Temp.	$[^{238}U]$	$[^{232}Th]$	$[^{147}Sm]$	eU	Inc	Th/U weight	[He]	Degas. sing	Raw Age	Error	F_T	R_{eq}	Correc. age	Error	Comment
					W	Max	Min																	
		Geometry	*Terminations**	*GFT*	*µm*	*µm*	*µm*		*°C*	*ppm*	*ppm*	*ppm*	*ppm*			*nmol/g*		*Ma*	*Ma*		*µm*	*Ma*	*Ma*	
1	3	Ellipsoid	Unknown	N/A	146	121	93	0.052	19	2	70	311	20	N/A	28.4	0.8		7	1	0.742	57.4	9	1	
	6	Hexagonal prism	2T	1P1F	195	124	105	0.048	19	50	46	350	62	N/A	0.9	4.9		14	2	0.77	62.8	18	3	
	5	Ellipsoid	Unknown	N/A	166	112	81	0.056	19	1	73	182	19	N/A	73.7	1.5		14	2	0.724	53.6	20	3	
	4	Ellipsoid	Unknown	N/A	149	92	87	0.059	19	11	83	178	31	N/A	7.6	8.1		47	7	0.71	50.8	66	10	cluster
	9	Hexagonal prism	2T	1P1F	218	72	61	0.073	19	25	69	334	43	N/A	2.7	10.9		45	7	0.658	40.9	69	10	cluster
	1	Ellipsoid	Unknown	N/A	158	120	81	0.055	19	34	99	433	59	N/A	2.9	16.7		50	8	0.727	54.3	69	10	cluster
	7	Hexagonal prism	2B	2F	151	72	61	0.078	19	37	190	453	83	N/A	5.2	21.4		46	7	0.644	38.6	72	11	cluster
	2	Ellipsoid	Unknown	N/A	158	111	81	0.057	19	33	43	714	46	N/A	1.3	19.5		73	11	0.721	53.1	101	15	
	10	Hexagonal prism	2T	1P1F	125	86	73	0.071	19	33	38	687	45	N/A	1.1	22.9		88	13	0.669	42	132	20	
	8	Hexagonal prism	2T	2P	181	75	64	0.073	19	74	49	508	88	N/A	0.7	51.6		105	16	0.657	41.2	160	24	
2	2	Hexagonal prism	2B	2F	268	83	72	0.063	46	2	12	922	9	N/A	4.9	0.6		9	1	0.704	47.5	13	2	
	3	Hexagonal prism	2B	2F	259	74	65	0.070	46	2	12	915	9	N/A	5.2	0.9		14	2	0.676	43.1	20	3	cluster
	4	Hexagonal prism	2B	2F	206	86	78	0.062	46	3	15	1119	12	N/A	4.8	1.3		15	2	0.708	48	21	3	cluster
	1	Hexagonal prism	2B	2F	277	81	71	0.064	46	2	11	889	9	N/A	4.7	1.1		16	2	0.7	46.9	23	3	cluster
8	3	Hexagonal prism	2P	2P	209	112	109	0.050	33	8	8	210	11	N/A	1.0	3.6		58	9	0.758	59.5	77	12	
	5	Hexagonal prism	2P	2P	250	108	99	0.050	33	17	8	288	21	N/A	0.5	8.8		75	11	0.759	59.8	99	15	
	1	Hexagonal prism	1B	1P1F	324	173	163	0.032	33	7	1	302	9	N/A	0.2	5.0		93	14	0.843	92.6	111	17	cluster
	2	Hexagonal prism	2B	1P1F	340	161	143	0.034	33	5	2	312	7	N/A	0.4	4.6		103	15	0.834	87.1	124	19	cluster
	4	Hexagonal prism	1T1B	1P1F	190	148	132	0.043	33	18	3	462	21	N/A	0.2	12.3		101	15	0.795	70	127	19	cluster
9	2	Ellipsoid	Unknown	N/A	127	100	87	0.059	51	4	20	702	12	N/A	5.5	2.2		29	4	0.708	50.7	40	6	
	3	Hexagonal prism	1T1B	2F	153	106	73	0.061	51	5	38	521	16	N/A	8.2	4.5		47	7	0.717	49.3	66	10	
	5	Hexagonal prism	1T1B	1P1F	127	91	69	0.071	51	32	49	252	44	N/A	1.5	18.7		75	11	0.673	42.5	112	17	
	4	Ellipsoid	N/A	N/A	155	105	83	0.057	51	12	48	867	27	N/A	4.0	14.4		87	13	0.719	52.6	121	18	
12	4	Hexagonal prism	1T1B	1P1F	135	56	48	0.098	27	15	89	1131	41	N/A	6.1	7.9		33	5	0.558	30.7	59	9	
	3	Hexagonal prism	2B	2F	109	65	59	0.089	27	57	470	1993	176	N/A	8.3	47.3		47	7	0.601	33.9	79	12	
	2	Ellipsoid	N/A	N/A	104	72	59	0.082	27	41	71	477	60	N/A	1.7	20.2		60	9	0.6	36.5	101	15	
	1	Hexagonal prism	2T	1P1F	109	57	37	0.110	27	1	11	10	3	N/A	18.9	16.6		898	135	0.507	27.2	1770	266	low parent
	5	Hexagonal prism	2B	2F	98	59	54	0.097	27	1	8	6	2	N/A	11.8	22.8		1556	233	0.568	30.9	2739	411	low parent
15	1	Hexagonal prism	2B	2B	84	69	62	0.090	42	3	46	736	17	N/A	16.5	1.6		15	2	0.598	33.3	25	4	
	4	Hexagonal prism	2B	2F	208	66	58	0.080	42	1	34	337	11	N/A	29.2	2.3		36	5	0.633	37.7	57	9	
	3	Hexagonal prism	2B	2F	117	78	68	0.076	42	3	291	591	74	N/A	91.5	15.4		37	6	0.653	39.5	57	9	
	5	Hexagonal prism	2B	2F	114	80	71	0.075	42	20	242	607	79	N/A	12.1	23.7		53	8	0.658	40	81	12	
	2	Hexagonal prism	2B	2F	124	76	67	0.076	42	0	5	8	1	N/A	44.1	10.7		1320	198	0.651	39.2	2027	304	outlier

17	4	Hexagonal prism	2B	2F	166	87	77	0.065	68	1	3	4	2	N/A	3.2	0.2	Lack of heat	16	2	0.699	46.2	24	4	
	2	Hexagonal prism	2B	2F	235	94	83	0.057	68	0	2	4	1	N/A	3.6	0.1		26	4	0.73	52.2	36	5	cluster
	3	Hexagonal prism	2B	2F	227	84	71	0.064	68	1	3	2	1	N/A	3.7	0.2		27	4	0.699	46.6	38	6	cluster
	1	Hexagonal prism	2B	2F	329	86	75	0.060	68	1	2	2	1	N/A	2.5	0.2	Small leak	33	5	0.718	50.1	47	7	cluster
	5	Hexagonal prism	2B	2F	320	90	78	0.058	68	0	1	1	1	N/A	3.8	0.2		38	6	0.729	52.2	52	8	cluster
18	2	Hexagonal prism	2B	2F	167	96	84	0.060	71	4	7	90	6	N/A	1.7	0.0	Lack of heat	0	0	0.721	50.2	0	0	cluster
	3	Hexagonal prism	1T1B	1P1F	191	78	70	0.069	71	4	4	57	5	N/A	1.1	0.0		0	0	0.679	43.7	0	0	cluster
	4	Hexagonal prism	1T1B	1P1F	157	76	67	0.082	71	4	6	68	6	N/A	1.3	0.0		0.0	0.0	0.664	36.7	0	0	cluster
	5	Hexagonal prism	1T1B	1P1F	192	146	135	0.043	71	4	4	58	5	N/A	1.0	0.3	small leak	11.8	1.8	0.796	70.2	15	2	
	1	Hexagonal prism	2B	2F	219	163	143	0.037	71	2	1	1	2	N/A	0.5	0.6		51	8	0.821	80.2	62	9	
19	3	Hexagonal prism	2B	2F	165	65	57	0.083	75	6	9	134	9	N/A	1.6	0.0		0	0	0.62	36.1	0	0	
	1	Hexagonal prism	1T1B	2F	145	80	70	0.071	75	2	11	914	9	N/A	5.1	0.1		1	0	0.672	42.1	2	0	
	2	Hexagonal prism	2B	2F	209	63	56	0.083	75	2	12	987	10	N/A	5.4	0.8		11	2	0.621	36.4	17	3	
	4	Hexagonal prism	2B	2F	221	63	55	0.082	75	0	0	0	0	N/A	-920.9	0.0		118	18	0.622	36.6	190	29	no parent
22	4	Hexagonal prism	2T	2P	206	133	119	0.046	3	6	2	604	9		0.4	5.6		93	14	0.779	65.2	120	18	
	2	Hexagonal prism	2T	2P	290	129	94	0.045	3	21	3	858	26		0.2	20.3		128	19	0.782	66.5	164	25	
	1	Hexagonal prism	2T	1P1F	313	183	166	0.032	3	27	4	387	30		0.2	34.0		195	29	0.847	94.8	230	35	
	7	Hexagonal prism	2T	2F	231	160	144	0.037	3	24	9	175	27		0.4	32.7		214	32	0.823	80.7	260	39	
23	4	Hexagonal prism	2T	1P1F	210	127	111	0.046	3	3	4	87	4		1.6	2.4		104	16	0.773	64.7	134	20	
	7	Hexagonal prism	2T	1P1F	235	119	105	0.047	3	3	4	85	4		1.4	3.1		125	19	0.774	63.4	161	24	
	2	Hexagonal prism	2T	2F	198	140	130	0.042	3	4	5	85	6		1.2	4.9		138	21	0.799	70.9	173	26	
	1	Hexagonal prism	2T	1P1F	420	212	188	0.026	3	0	0	0	0			6.4		21184	3178	0.871	133.2	24321	3648	no parent
24	4	Hexagonal prism	2T	1P1F	213	75	72	0.069	3	101	255	1263	166		2.5	55.0		59	9	0.677	43.6	87	13	
	2	Hexagonal prism	2T	1P1F	183	76	70	0.071	3	81	55	968	98		0.7	48.3		87	13	0.67	42.4	130	20	cluster
	3	Hexagonal prism	2T	1P1F	189	75	67	0.072	3	65	47	896	80		0.7	41.2		90	14	0.666	42	136	20	cluster
	1	Hexagonal prism	2T	2P	203	84	75	0.064	3	95	61	956	114		0.6	60.6		95	14	0.696	46.8	136	20	cluster
	7	Hexagonal prism	2T	1P1F	316	115	106	0.046	3	43	39	616	55		0.9	54.7		173	26	0.782	65.9	221	33	
25	2	Hexagonal prism	2T	1P1F	270	184	123	0.037	3	30	6	156	32		0.2	5.7		32	5	0.827	83.7	39	6	cluster
	3	Hexagonal prism	2T	1P1F	195	175	113	0.042	3	13	11	476	18		0.8	4.2		40	6	0.801	72	49	7	cluster
	4	Hexagonal prism	2T	1P1F	273	177	159	0.034	3	29	6	139	31		0.2	7.6		44	7	0.837	89	53	8	cluster
	6	Hexagonal prism	2T	1P1F	313	184	173	0.031	3	15	1	48	16		0.1	4.1		47	7	0.845	96	56	8	cluster
	1	Hexagonal prism	2T	1P1F	357	182	134	0.033	3	29	6	66	30		0.2	10.5		63	9	0.842	91.7	75	11	
	5	Hexagonal prism	2T	1P1F	232	142	106	0.435	3	1	2	5	2		1.9	8.5		883	132	0.792	69	1114	167	low parent
26	6	Hexagonal prism	2T	2P	209	85	79	0.063	3	105	155	2267	152		1.5	38.8		45	7	0.703	47.9	63	10	
	2	Hexagonal prism	2T	2P	199	147	129	0.044	3	36	49	834	52		1.4	24.3		82	12	0.786	67.5	104	16	cluster
	5	Hexagonal prism	2T	2P	260	111	106	0.045	3	41	60	876	59		1.5	28.8		85	13	0.768	66.1	111	17	cluster
	4	Hexagonal prism	2T	2P	270	99	90	0.053	3	42	66	899	62		1.6	29.5		84	13	0.747	56.6	112	17	cluster
	1	Hexagonal prism	2T	1P1F	358	171	147	0.033	3	21	26	319	28		1.2	38.5		236	35	0.842	91.6	280	42	outlier
	3	Hexagonal prism	2T	1P1F	224	118	106	0.048	3	36	46	402	49		1.3	77.6		280	42	0.768	62.5	365	55	outlier
28	7	Hexagonal prism	2T	1P1F	181	96	74	0.062	3	103	1158	1841	383		11.2	20.3		10	1	0.706	48.7	14	2	
	1	Hexagonal prism	2T	1P1F	380	161	145	0.034	3	42	44	553	55		1.0	23.5		76	11	0.837	89.3	91	14	cluster
	6	Hexagonal prism	2T	1P1F	185	90	84	0.061	3	62	68	697	81		1.1	30.1		66	10	0.712	48.9	93	14	cluster
	5	Hexagonal prism	2T	1P1F	199	70	65	0.074	3	76	95	1010	102		1.3	36.4		63	9	0.652	40.5	97	14	cluster
	3	Hexagonal prism	2T	1P1F	263	106	90	0.051	3	73	95	1066	100		1.3	43.3		76	11	0.754	58.4	101	15	cluster

3.2 AFT, U/Pb and AHe results

3.2.1 Result summary

A summary of the apatite FT, U/Pb and AHe results is presented in TABLE 5 and TABLE 6. Only 21 out of 43 samples yielded a sufficient amount of datable apatites to be used for thermal history inverse modelling. The poor apatite yield for the other samples is believed to be caused by either unintended sampling of inappropriate lithologies (e.g. claystones instead of sandstone or dolerite) or apatite-poor sandstones (in particular some of the Early Cretaceous and Eocene sandstones). Most of the apatite-poor samples come from the borehole samples (not from the seabed dredge samples). The limited apatite yields hinders modelling of multi-sample profiles in most boreholes, and thus significantly limits the potential of this study as originally intended. All the results per sample are presented in in ANNEX 1 and summarized and interpreted in Section 4, 4 AND 6.

3.2.2 Secondary age standards

3.2.2.1 U/Pb secondary standards results

The results of the U/Pb secondary standards are presented in TABLE 7.

Table 7: Results of the apatite and zircon secondary standards

			Apatite U/Pb standards								Zircon U/Pb standards											
Session			MM				DUR				Plesovice				WRS 1348				GZ7			
#	Phase	Samples	*n*	*Age*	*±*	*Diff.*	*n*	*Age*	*±*	*Diff.*	*n*	*Age*	*±*	*Diff.*	*n*	*Age*	*±*	*Diff.*	*n*	*Age*	*±*	*Diff.*
		Reference age		523.51	1.47			31.44	0.18			337.13	0.37			526.26	0.7			530.26	0.05	
4	AP	R-1 to 10	19	521.0	9.3	-0.5%	15	32.7	1.4	4.0%	n/a											
5	AP	R12 to 19	18	521.4	6.2	-0.4%	14	31.9	1.2	1.5%	n/a											
6	AP	R-1j, 2j, 8j, 13j, 14j	27	543.1	7.7	3.7%	32	31.95	0.95	1.6%	n/a											
8	AP	R-22, 24, 25	17	523.9	6.6	0.1%	20	33.51	0.95	6.6%	n/a											
9	AP	R-27, 28, 29	14	550	21	5.1%	14	31.7	1.1	0.8%	n/a											
10	AP	R-26, 12j to 18j	12	520.2	9.4	-0.6%	13	32.1	1.1	2.1%	n/a											
11	ZI	R-21, 22, 27	n/a								20	345.9	3	2.6%	20	532.9	4.9	1.3%	20	542.8	4.8	2.4%
12	ZI	R-23-26, 28, 29	n/a								53	337.6	3.6	0.1%	53	533.1	2.7	1.3%	53	534.0	3.0	0.7%
13	AP	R-21, 23	not ablated				29	34.81	0.75	10.7%	n/a											
14	ZI	R-6, 8, 9	n/a								32	337.8	1.8	0.2%	31	521.7	3.1	-0.9%	30	531.5	3.0	0.2%
15	ZI	R-16-20	n/a								32	338.6	1.9	0.4%	32	526.0	2.6	0.0%	32	529.3	2.7	-0.2%
16	ZI	R-29bis	n/a								20	340.3	2.4	0.9%	20	520.4	3.4	-1.1%	20	533.2	2.8	0.6%
17	AP	R-41-68a	38/39	569.5	8.7	8.8%	25	32.6	1.1	3.7%	n/a											
18	ZI	R-1,3,7,51,68b	n/a								38	345.8	1.8	2.6%	38	524.5	3.3	-0.3%	38	535.8	2.0	1.0%
19	ZI	R-11-15	n/a								34	343.4	2.1	1.9%	34	529.1	4.6	0.5%	34	534.2	2.4	0.7%
20	AP	R-37, 54, 58, 68b	32	515.6	6.5	-1.5%	28	31.67	0.76	0.7%	n/a											
21	ZI	R-5	n/a								14	340.2	3	0.9%	14	521.5	4.3	-0.9%	14	535.7	3.9	1.0%
					Min	-1.5%			*Min*	0.7%			*Min*	0.1%			*Min*	-1.1%			*Min*	-0.2%
					Max	8.8%			*Max*	10.7%			*Max*	2.6%			*Max*	1.3%			*Max*	2.4%

3.2.2.2 AHe secondary standard results

For the first session (the borehole samples), the three Durango standards yielded ages of 31.9, 32 and 32.2 Ma which corresponds to a 2 RSD uncertainty of +1.5 to +2.5% (true age of 31.44 Ma, McDowell et al. (2005)). For the second session (Goban Spur dredge samples), there were seven Durango samples (three large fragments from TCD, three smaller fragments provided by UCL and one fragment used as a blind test). One grain yielded a very old age (2 Ga) due to very low amount of parent elements

and is believed to have been lost between the steps of He degassing and acid dissolution. Out of the six remaining standards, five of them yielded AHe ages of 30, 30.8, 31.5, 32.3 and 32.5 Ma which corresponds to a 2 RSD age uncertainty of -4.6 to +3.4%. The last standard yielded an age of 24.5 Ma, i.e. a 2 RSD age uncertainty of -22%. Excluding this last age, the standards show that the 2 RSD age uncertainty is at least ±5%.

3.3 Conclusions

The analysed samples provide a wealth of new apatite U/Pb, zircon U/Pb, LAFT, AHe and apatite trace element data from the Irish Atlantic Margin. However, the large amounts of samples that cannot be used as input data for thermal history modelling prevent the modelling of multi-sample profiles that would have better characterized the exhumation episodes targeted in this study.

The following chapters will present the geochronological and thermochronological results with a focus on three areas of the AIM, from north to south: 1) the Northern Zone comprising the Donegal, Erris and Slyne Basin (CHAPTER 4); 2) the Central Zone, comprising the North Porcupine High, Slyne Ridge, North Porcupine Basin and eastern margin of the Porcupine Basin (CHAPTER 5); and 3) the Southern Zone, comprising the Goban Spur and southern tip of the Porcupine High (*i.e.* the Celtic Margin bordering the Atlantic oceanic crust and abysall plains) (CHAPTER 6).

4 Northern Zone: NE Rockall, Erris, Donegal-Malin basins

4.1 Introduction

In this study, the northern zone refers to the shallow platform to the west of NW Ireland which comprises the Carboniferous Donegal-Malin basins, the Permo-Triassic and Jurassic Erris and Slyne basins and their bounding basement highs. New samples were taken from five boreholes in this area, wells 12/02-1Z, 12/13-1A, 13/03-1, 18/25-1 and 18/25-2 (FIGURE 17).

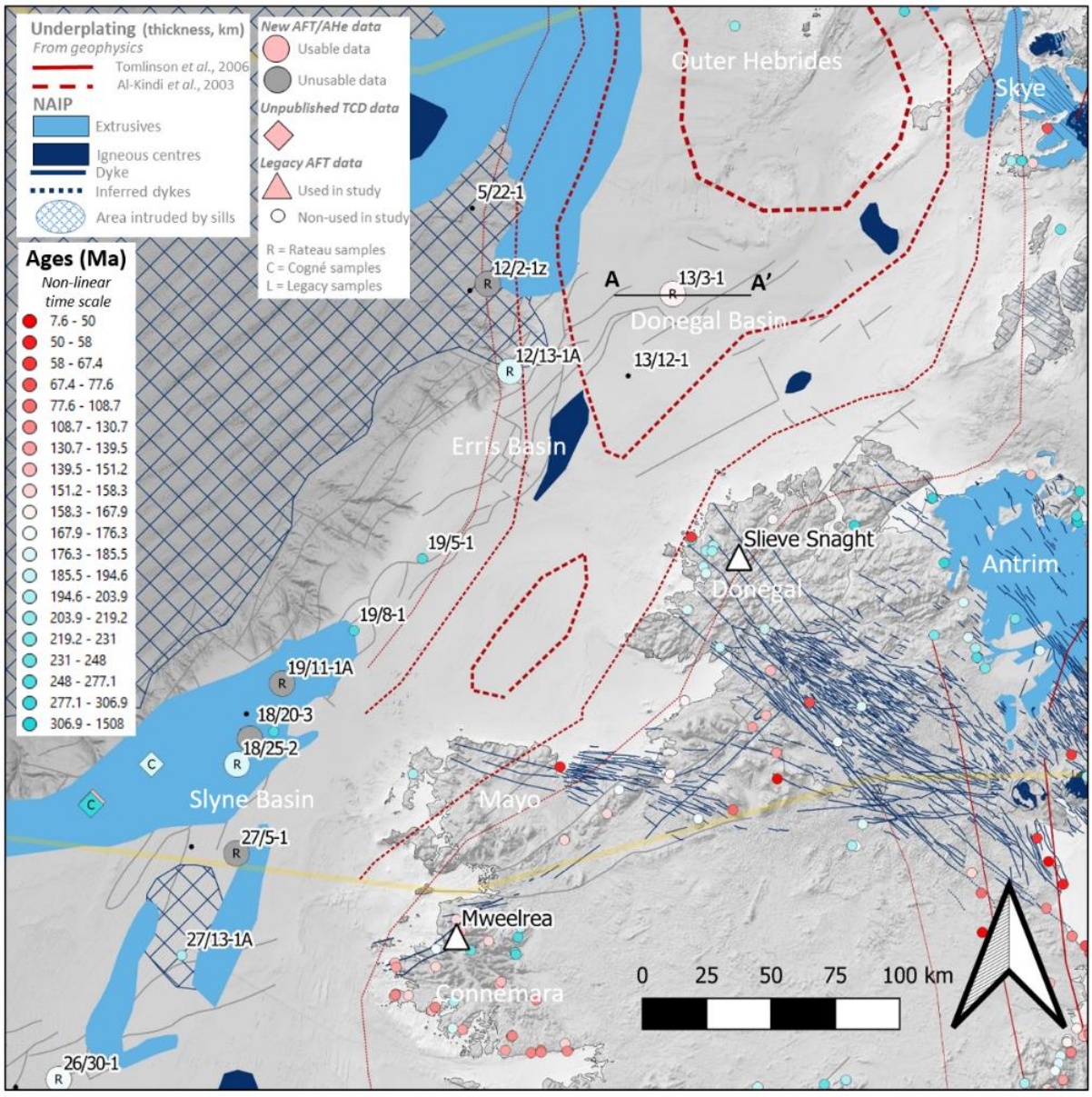

Figure 17: Map of the Northern Zone with the location of boreholes discussed in chapter 4.

4.2 Borehole 12/02-1Z

Deviated borehole 12/02-1Z was drilled by Shell in 2003 on the eastern margin of the NE Irish Rockall Basin (FIGURE 17). Two samples were taken from an extrusive basaltic lava (R-33, core sample,

3962.25-3962.5 mMD) and the sandstone immediately underneath (R-34, core sample, 3963.25 mMD) with the expectation that the apatite AFT/AHe ages in the sand would have been reset by the lava flow emplacement.

The well report states that the basalt is extrusive in nature and possibly has an age of 250 Ma (Malcom Pringle pers. comm. as cited in Mecklenburgh (2003)). However, the extrusive basalt has been placed at the base of an Early Cretaceous package and resting above Middle Jurassic sediments by Serica (Serica, 2014), suggesting a Middle Jurassic to Early Cretaceous age for the magmatism. The regional significance of this basalt is discussed in section 7.2.2.

The basalt yielded only a few apatites and the sandstone yielded no apatites, preventing the absolute dating of the basalt and any thermochronology study. However, a Geotrack study was done on the main borehole 12/02-1 in 2003 on six samples between 2540-4119 mMD (Green, 2003). The interpretation of the AFT data is complicated by the inferred presence of a zone of overpressure at the bottom of the well that resulted in a higher than expected BHT. Geotrack proposes two thermal histories: 1) (least probable) Rapid temperature increase from the Late Cretaceous to present-day due to burial, interrupted by a Late Oligocene-Middle Miocene exhumation event (50°C cooling at the bottom of the well); or 2) a similar rapid temperature increase from Late Cretaceous to present-day, this time interrupted by a heating spike from hot fluid circulation at some time between 60-30 Ma (Green, 2003) (FIGURE 18).

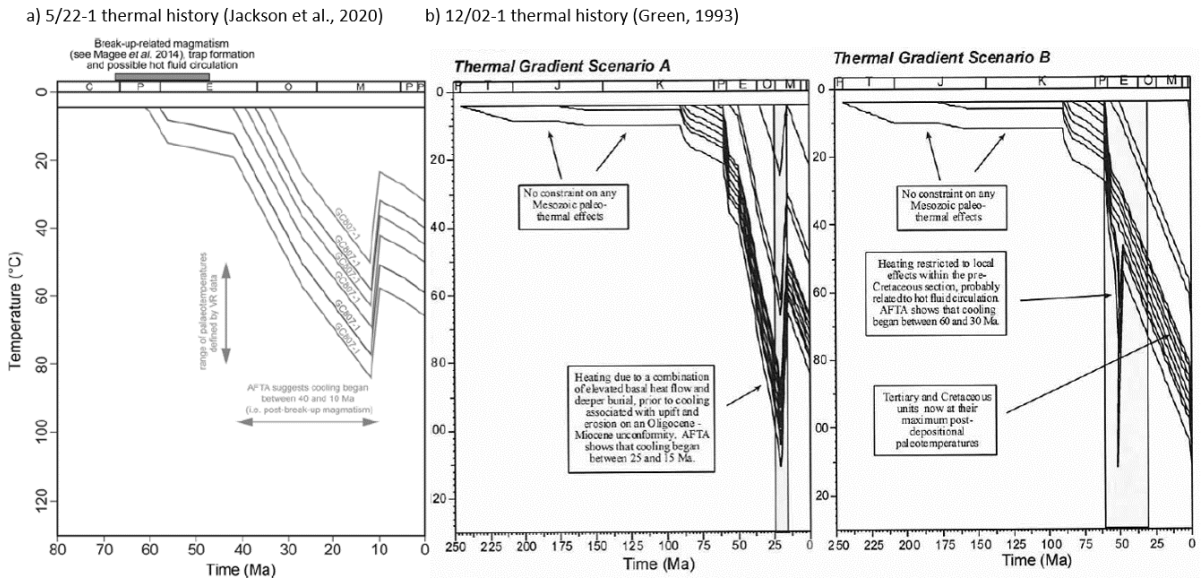

Figure 18: Preferred thermal histories for 5/22-1 and 12/02-1.

The results from the Geotrack study can be compared to another Geotrack study from nearby borehole 5/22-1 (FIGURE 17), which was integrated with a petrophysical and seismic study (Jackson et al., 2020). They found that poor reservoir quality in the Paleocene-Eocene sandstones were probably

partly the result of the circulation of hot fluids (up to c. 120°C based on fluid inclusion data) caused by the emplacement of a sill complex (Magee et al. (2014), Jackson et al. (2020)), supporting the second thermal history hypothesis of Green (2003) for 12/02-1. However, the thermal history proposed by Geotrack for 5/22-1 includes a small exhumation event (c. 20°C cooling) between 40-10 Ma (Late Eocene-Miocene) (Green (2001a), Jackson et al. (2020)), supporting the first thermal history hypothesis for 12/02-1 (FIGURE 18).

4.3 Borehole 12/13-1A

Well 12/13-1A was drilled in 1979 by Amoco in the Erris Basin, 35 km SSE of 12/02-1 (Odell and Walker, 1979) (FIGURE 17). One sample was taken from a Permo-Triassic volcaniclastic sandstone (R-37, 7940-8020 ft MD).

The apatite U/Pb ages (see detailed description in ANNEX 1, SECTION 1.3.1) confirmed the detrital nature of the sample which is dominated by Mesoproterozoic and Paleoproterozoic ages. The three youngest grains yield a discordia age of 291.3 ± 8.4 Ma and their trace elements suggest that they are mafic igneous apatites (FIGURE 19). It is likely that these grains belong to the syn-sedimentary volcanic fraction of this volcaniclastic sandstone. Despite the low number of grains, the discordia age suggests that the sandstone is Early Permian in age, which fits within the lower range of the age estinate provided by the operator (Permian-Triassic). The LAFT data yielded a central age of 185 ± 19 Ma (Early Jurassic) and track lengths with a MTL of 10.3 ± 2.2 µm and a bimodal distribution. If the sandstone is Early Permian in age, then the AFT data suggests complete resetting of the AFT ages after desposition during the Jurassic while the bimodal distribution suggests a complex thermal history with re-heating within the PAZ after the main exhumation event. The apatites found were not suitable for an AHe study.

A legacy study by Geotrack based on six samples yielded a thermal history characterized by a cooling episode of at least 30°C during the Cenozoic, corresponding to erosion of c. 900 m at the seabed (Green, 1993). The AFT central age of the new sample (185 Ma) is significantly younger than the legacy AFT ages (222-242 Ma for the samples above and below this sample R-37). Based on the absence of AHe data and the lack of consistency between legacy and new AFT data, no thermal history inverse modelling was attempted for this borehole.

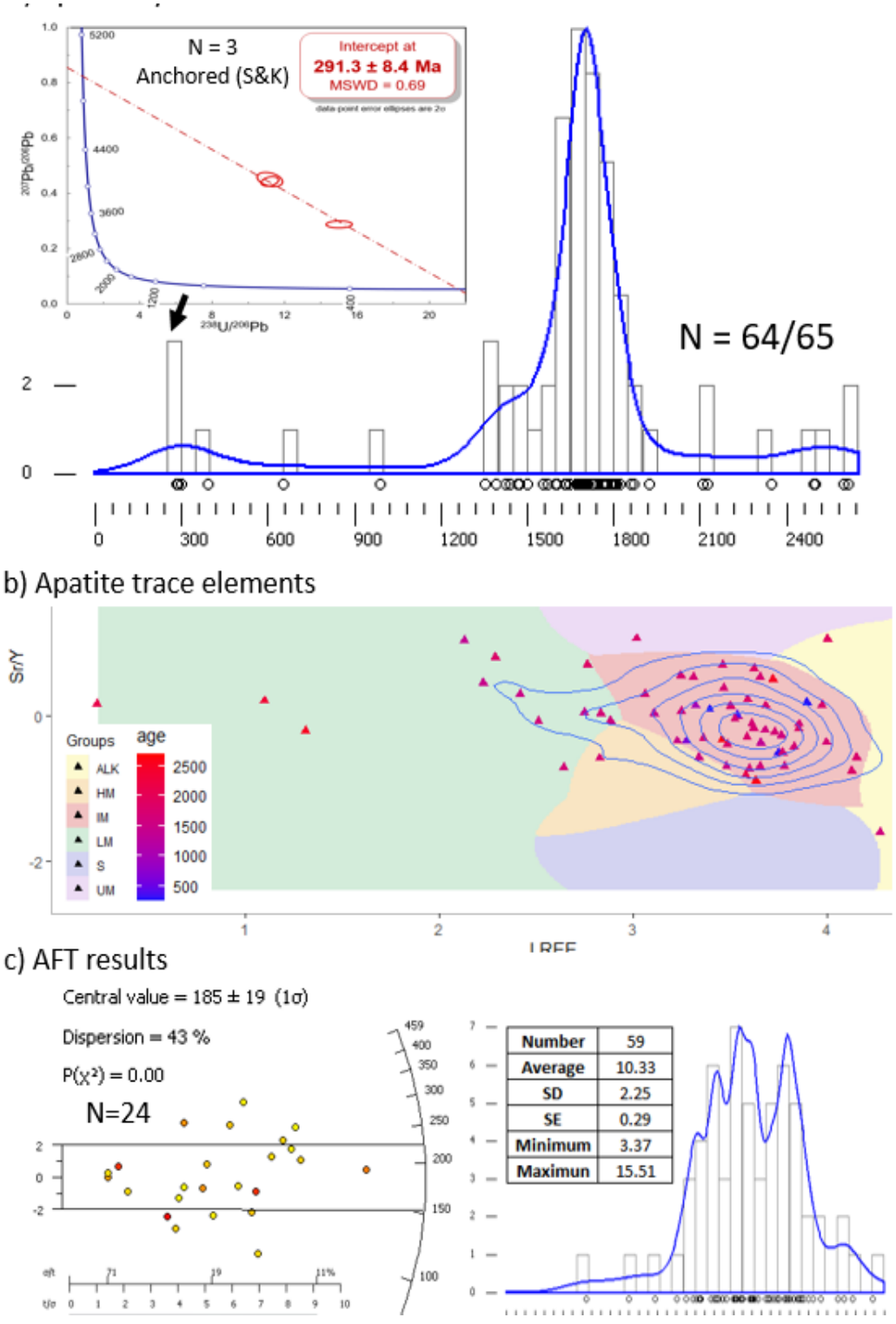

Figure 19: Apatite U/Pb dating (a), trace elements (b) and AFT results (c) for sample R-37 (12/13-1A). Abbreviations for the trace element biplot background colours: ALK = alkali-rich igneous rocks; IM = mafic I-type granitoids and mafic igneous rocks; LM = low- and medium-grade metamorphic and metasomatic; HM = partial-melts/leucosomes/high-grade metamorphic; S = S-type granitoids and high aluminium saturation index (ASI) 'felsic' I-types; UM = ultramafic rocks including carbonatites, lherzolites and pyroxenites (O'Sullivan et al., 2020).

4.4 Borehole 13/03-1

4.4.1 Exploration history

Borehole 13/03-1 is a dry hydrocarbon exploration well drilled in 1978 by Texaco. The well is located in located in the Malin Sea, 80 km north-west of the Donegal coast, NW Ireland (FIGURE 17). The primary reservoirs targeted by the well were Permo-Triassic sandstones in a faulted northwest-southeast trending anticlinal structure (Stuart, 1978a). The well was drilled vertically to a depth of 4483 ft MD.

4.4.2 Geological summary

The borehole was drilled in the offshore Donegal Basin which is bounded by the Outer Hebrides Platform to the north and the Islay-Donegal Platform to the south. The well is located in the footwall of the northeast-southwest trending Skerryvore Fault that separates the main Donegal Basin (in the northwest) from the South Donegal Basin, Skerryvore Trough and Malin Terrace (in the southeast) (FIGURE 20).

The well first encountered 221 m of Quaternary to possibly Pliocene clastics, with a basal 2.1 m layer of shell fragments with silts and loose sands that is tentatively attributed to the Miocene (with a question mark). The Cenozoic sediments unconformably overlie 949 m of Upper Carboniferous detrital and volcaniclastic sediments of Stephanian B/Westphalian D to Westphalian B/C age. The well unexpectedly encountered a mafic intrusion at 4355 ft MD that was drilled for 128 ft (39 m) until TD at 4483 ft (Stuart et al., 1978) (FIGURE 21 AND FIGURE 22). The intrusion was not isotopically dated at the time due to a lack of suitable minerals for geochronology. Based on the presence of numerous NAIP-related intrusive and extrusive igneous rocks of Paleogene age in Scotland, Northern Ireland and in the offshore basins, the operator hypothesized that the intrusion was probably Paleogene in age (Stuart, 1978a). However, Robeson et al. (1988) suggested that it might be Late Carboniferous-Early Permian in age based on the absence of a coke texture in the coals from the overlying Late Carboniferous sediments (suggesting very low vitrinite reflectance values at the time of intrusion, and therefore little burial). The pre-Cenozoic age of the intrusion was confirmed later by the AFT study of McCulloch (1993) and provided a minimum age (an AFT central age) for emplacement of the gabbro of 183.1 ± 19.2 (Middle Jurassic or older), which was used by Chapman et al. (1999) to infer a Permian age for the intrusion.

Dobson & Whittington, 1992

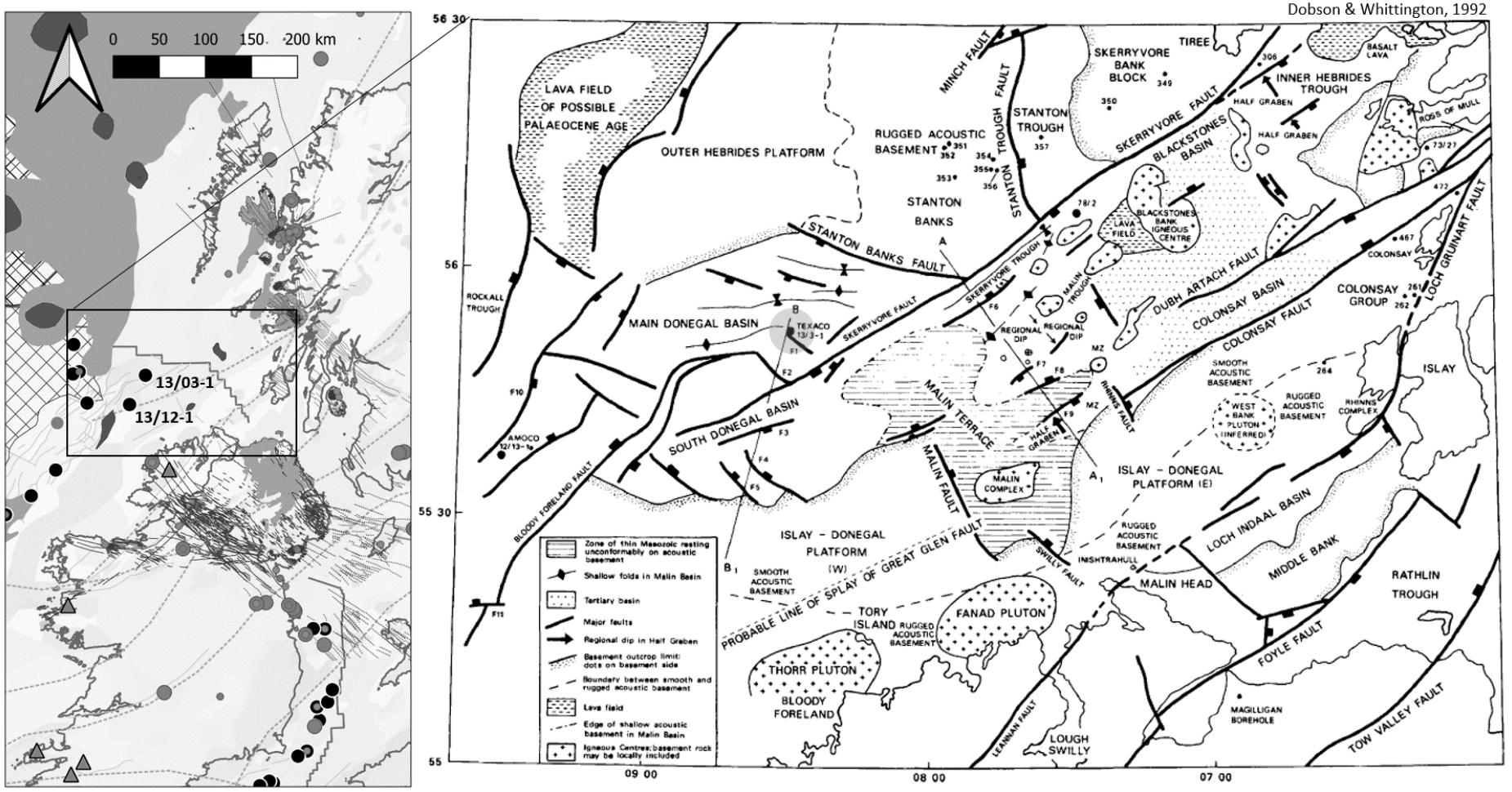

Figure 20: Location of borehole 13/03-1, Donegal Basin, offshore NW Ireland.

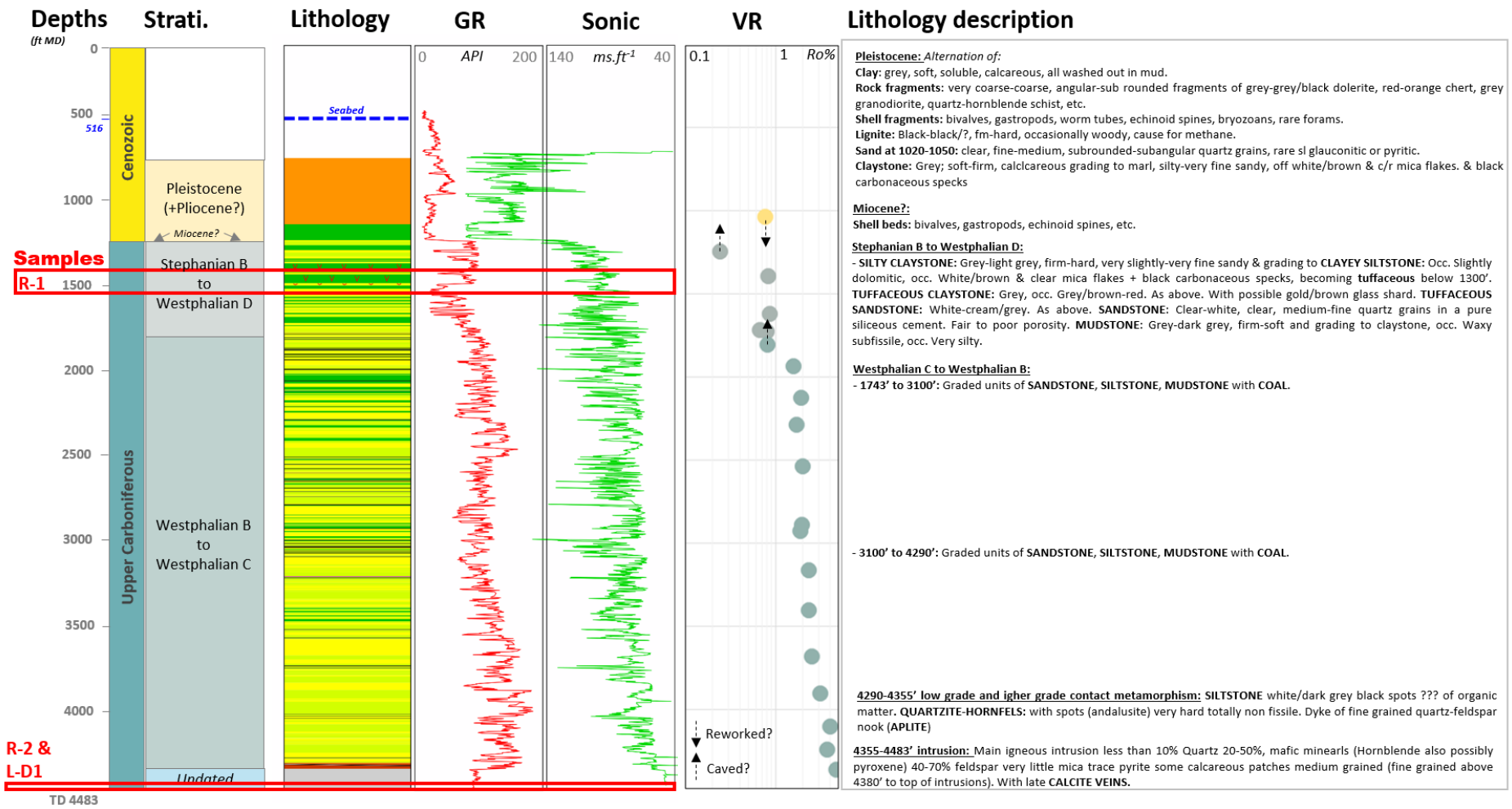

Figure 21: Lithology, stratigraphy and GR/sonic logs for borehole 13/03-1 (log data and lithology description from the composite well log, Stuart et al. (1978); VR data from Cooper et al. (1978)).

;

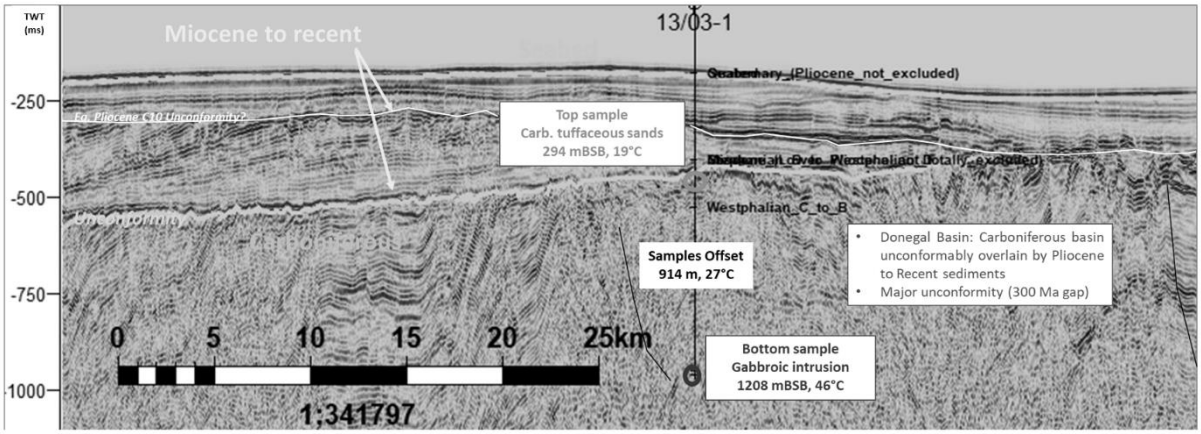

Figure 22: Interpreted seismic section through well 13/03-1 with sample location (location of seismic line in Figure 20).

4.4.3 VR data

A set of 20 VR measurements from the Cenozoic and Late Carboniferous sediments is available (Cooper et al., 1978) (FIGURE 21). The dataset shows a step change between 1810 and 1940 ft MD, with values between 0.65 and 0.85 Ro% above and values increasing from 1.55 to 4.6 Ro% below. Assuming that the sample at 1805 ft MD is a caving from the Stephanian B-Westphalian D sediments, the step change would correspond to a stratigraphic break (FIGURE 21).

High VR values in Carboniferous sediments are common in the southern part of Ireland, probably caused by a combination of burial and northward-directed hydrodynamic flow of fluids heated by the Variscan orogeny to the south and propagating through the major fault zones (Corcoran and Clayton, 2001). However, no such high heat flows are expected so far to the north. The operator interpreted the high VR values of the Westphalia B-C sediments as resulting from contact heating caused by the igneous intrusion rather than by burial. This hypothesis is supported by borehole 13/12-1, drilled 36 km to the south of 13/03-1, which encountered the same unit of Westphalian B-C sediments but with VR values of c. 0.8 Ro% (Boutoutaou, 2006).

It is unlikely that a sill could thermally affect such a thick pile of sediments (c. 740 m). Iyer et al. (2013) modelled the effects of a 100 m thick sill intruded at 1 km depth in a sedimentary basin and predicted the VR values reached by the host sediments after 5000 years of heat diffusion and cooling. For the case of low permeability sediments (which is the case for 13/03-1), only 260 m of sediments above the sill could reach VR values as high as 1.5 Ro%, confirming that a sill could not have affected the 740 m of sediments observed in the borehole (FIGURE 23A).

a) Thermal effects of a sill intrusion (Iyer et al., 2013)

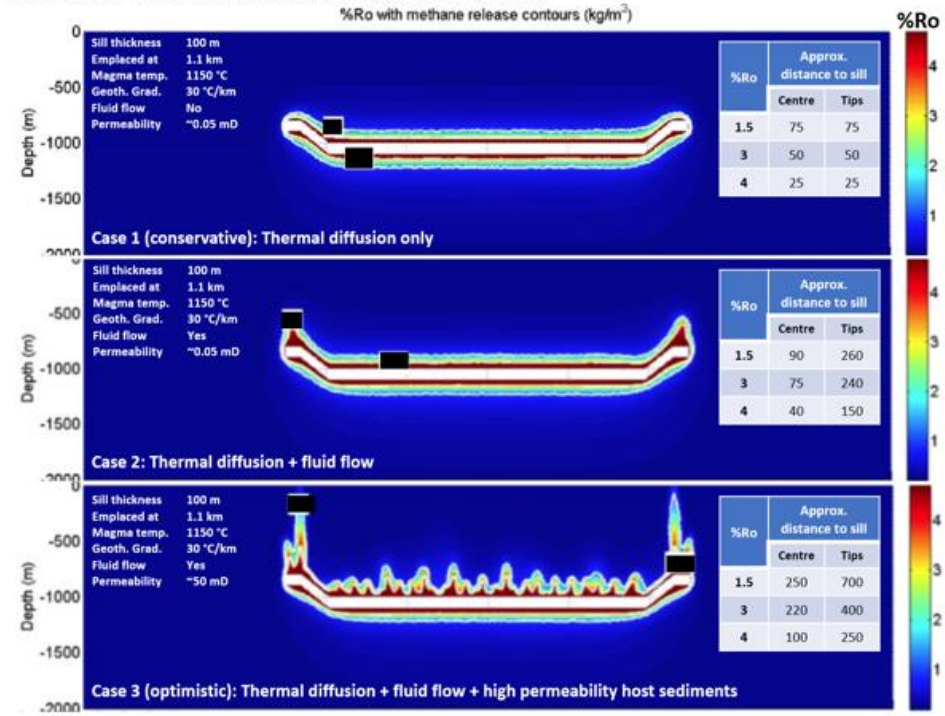

b) 13/03-1 tilted dyke hypothesis

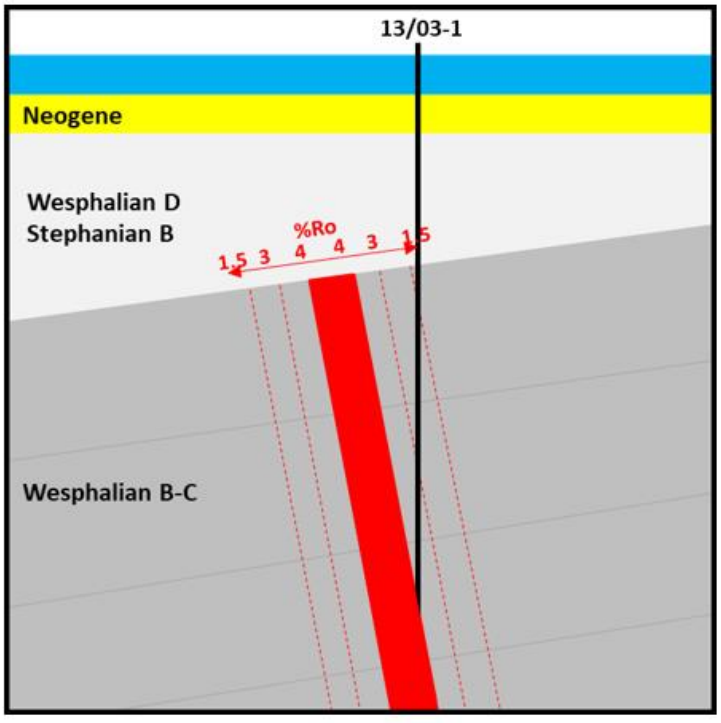

Figure 23: Igneous intrusion effects (a) and geometry hypotheses (b) in well 13/03-1.

It is possible that the intrusion is instead a tilted dyke. The dipmeter indicates a dip of a couple of degrees towards the south-west in the first 200 m of sediments above the intrusion, increasing to 2-15° in the remaining part of the Westphalian B-C unit (Stuart et al., 1978). While not very reliable, the dipmeter seems to indicate that the Carboniferous sediments have been tectonically tilted by at least

a few degrees. If we assume a dip of 2.5°, the dyke would be at a horizontal distance of c. 35 m from the top of the thermally affected pile of sediments. The model of Iyer et al. (2013) predicts that for a case with vertical thermal diffusion only, sediments located c. 75m above the sill would reach 1.5 Ro% (FIGURE 23A). Although thermal diffusion in a horizontal direction (in our hypothesis of a dyke) would be much lower than in the vertical direction (as in the model of Iyer et al. (2013)), it seems plausible that sediments located at a few tens of meters from the dyke might have been heated to temperatures that could have generated the VR values observed in the well. In conclusion, a vertical dyke could have thermally affected the host rock on either side over a few tens of meters and could have subsequently be tectonically tilted, which would have resulted in the present-day VR profile observed in the borehole (FIGURE 23B).

4.4.4 Samples

4.4.4.1 Sampling strategy

This borehole was selected primarily because of the gabbro at the bottom of the well (sample R-2) and also because of the overlying Carboniferous sandstones (sample R-1) that allow for a vertical profile modelling approach (FIGURE 21). The basal gabbro was the subject of an AFT study by McCulloch (1993) with one dated sample (here referred to as L-D1).

4.4.4.2 Apatite and zircon yield

Numerous apatites were found in both sample R-1 (78 dated grains yielding 72 AFT ages; 10 AHe ages) and R-2 (126 dated grains yielding 123 AFT ages; 4 AHe ages). Numerous zircons were found in the Eocene sample R-1 (97 grains) but none were found in the basal gabbro R-2 (as expected for a gabbro).

4.4.5 U/Pb and trace element results

The detailed description of the U/Pb and trace element results is presented in ANNEX 1 (SECTION 1.3.1). Below is a summary and discussion of the results.

4.4.5.1 Sample R-7 (Stephanian B-Westphalian D tuffaceous sandstone)

The sandstone is primarily dominated by a source of Caledonian apatites and zircons (Caledonian plutons crop out 100 km to the south on the west coast of Donegal, O'Connor et al. (1987)). In the apatite U-Pb age spectrum, there are secondary peaks at c. 1.1 and 1.5-1.7 Ga as well as a few Archean grains. They could represent first-cycle detrital grains from the Proterozoic basement that crops out in the area and from the Archean Lewisian basement that crops out in the Outer Hebrides and probably also very close to the north of 13/03-1.

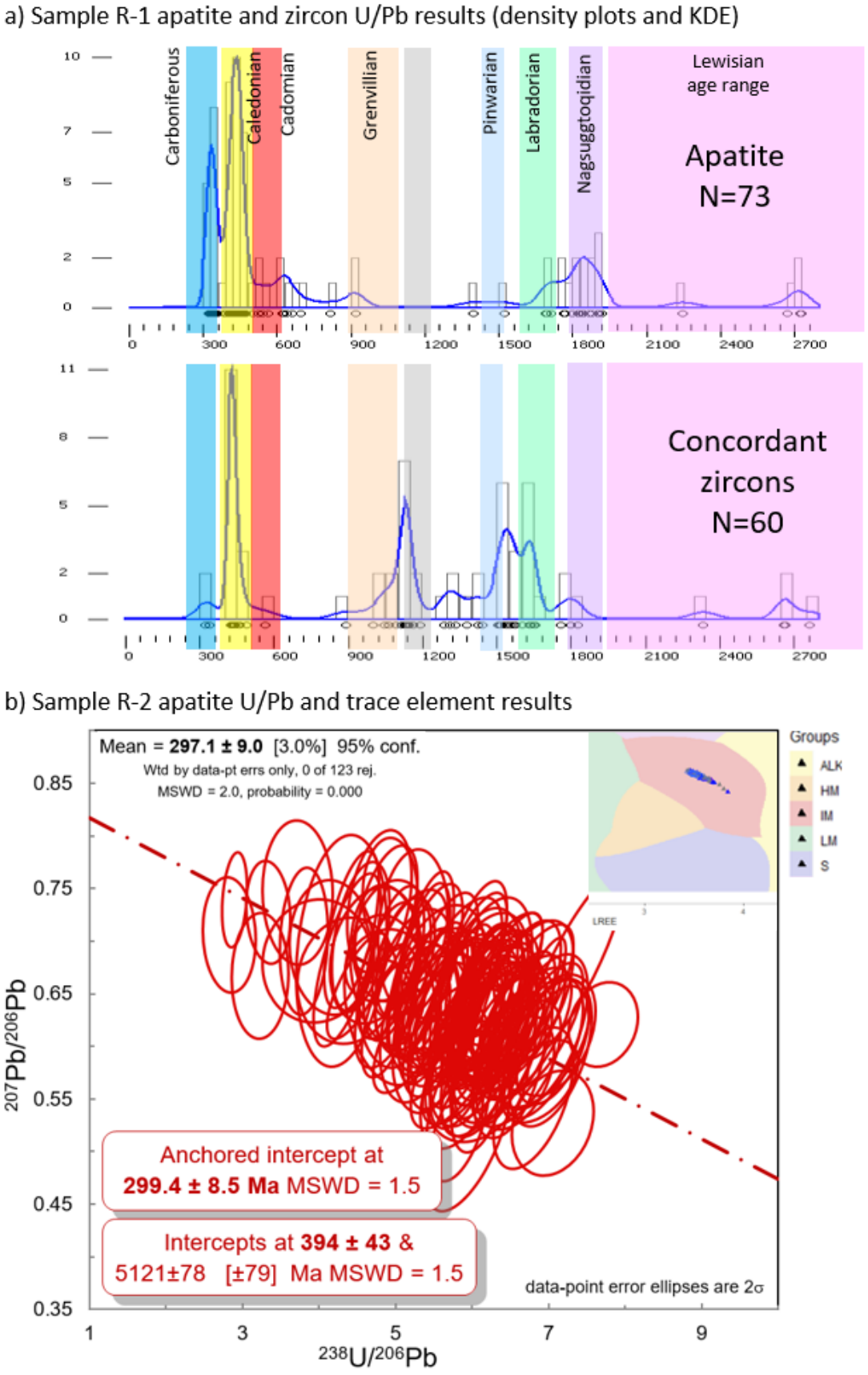

Figure 24: Zircon U/Pb and and apatite U/Pb and trace element results for samples R-1 and R-2.

For the zircons, the older grains form a small peak at c. 1.8-1.85 Ga which might have been sourced from the Rhinns Complex which is interpreted to crop out within the Colonsay-West Islay block and Inishtrahull (Inishtrahull is <100 km to the SE, FIGURE 20) and has been dated at 1.7-1.9 Ga on Inishtrahull and the Rhinns of Islay (Daly et al. (1991), Muir et al. (1994)). The youngest apatite and zircons grains are c. 320-340 Ma in age (Namurian-Visean), which is older than the depositional age (Stephanian B-Westphalian D, *i.e.* 307.3 ± 3.8 Ma). Therefore, the tuffs found in this sandstone might be an older, reworked, Early Carboniferous tuff, rather than a syn-depositional tuff. Consequently, the AFT sample will be modelled as a detrital sample.

4.4.5.2 Sample R-8 (Undated basal gabbro)

As hypothesized by Robeson et al. (1988) and Chapman et al. (1999), the gabbro is indeed Late Carboniferous-Early Permian in age with an apatite U/Pb age of 297.1 ± 9 Ma (Carboniferous-Permian boundary) (FIGURE 24B).

The apatites fall within the IM (mafic) field of the trace element biplot, which is in accordance with the mafic nature of the gabbro. A petrographic study of a 3 m core (Gaida, 1978) concluded that the rock is a subhedral uralized gabbro with labradorite, bytownite and clinopyroxene as the dominant minerals and titanomagnetite, ilmenite, pyrite, sphalerite, leucoxene, biotite, spinel and apatites as accessory and ore minerals, and the presence of intergrown quartz and alkali-feldspars exhibiting graphic texture in the interstices of some plagioclases (Stuart, 1978b). The rock-forming mineral distribution is given by Robeson et al. (1988) as 40-70% plagioclase, 40-60% ferromagnesian minerals, <10% of quartz, which categorized the rock as a quartz-dolerite. The presence of quartz and absence of olivine points towards an intrusion derived from a tholeiitic magma (Yoder and Tilley, 1962).

In conclusion, the quartz-gabbro is a 297 ± 9 Ma intrusion that probably originated from a tholeiitic magma and intruded the Carboniferous sediments as a vertical dyke but was later tectonically tilted by a few degrees. The significance of the age and nature of this intrusion is discussed in SECTION 7.2.1.

4.4.6 AFT and AHe results

The detailed description of the AFT and AHe results of sample R-1, R-2 and legacy sample L-D1 is presented in ANNEX 1 (SECTION 2.3.1). Below is a summary and discussion of the results.

Table 8: AFT and AHe results for samples R-1, R-2 and L-D1 (13/03-1).

Sample information								FTA					CTL				Kinetic			AHe			
Sample	Depths		Temp.		Lithology	Age		n	Ns	$P(\chi^2)$	Central Age		Tracks	MTL	SD	SE	Cl	Dpar	U	n	Mean eU	Age cluster?	F_T-corr. Age
	Seabed	Sample	Seabed	Sample		Age	±																
	m MSL	*m BSB*	*°C*	*°C*				-	-	-	*Ma*	*±1σ Ma*	-	*µm*	*µm*	*µm*	*wg%*	*µm*	*ppm*	-	*ppm*	-	*Min.Avg.Max*
R-1	131	294	10	18.2	Tuff. sand	307.3	3.8	72	3075	<1	**163.3**	7.2	194	**11.19**	2.44	0.17	0.16	1.72	26.89	10/10	50	Yes 4/10	9-**69**-160
R-2	131	1208	10	43.8	Quartz-gabbro	297.0	9.0	123	400	100	**166.3**	8.4	1	**12.03**	-	-	0.21	1.76	1.70	4/4	10	Yes 3/4	13-**21**-23
L-D1	131	1208	10	43.8	Quartz-gabbro	297.0	9.0	29	167	70	**183.1**	19.2	0	-	-	-	n/a			n/a			

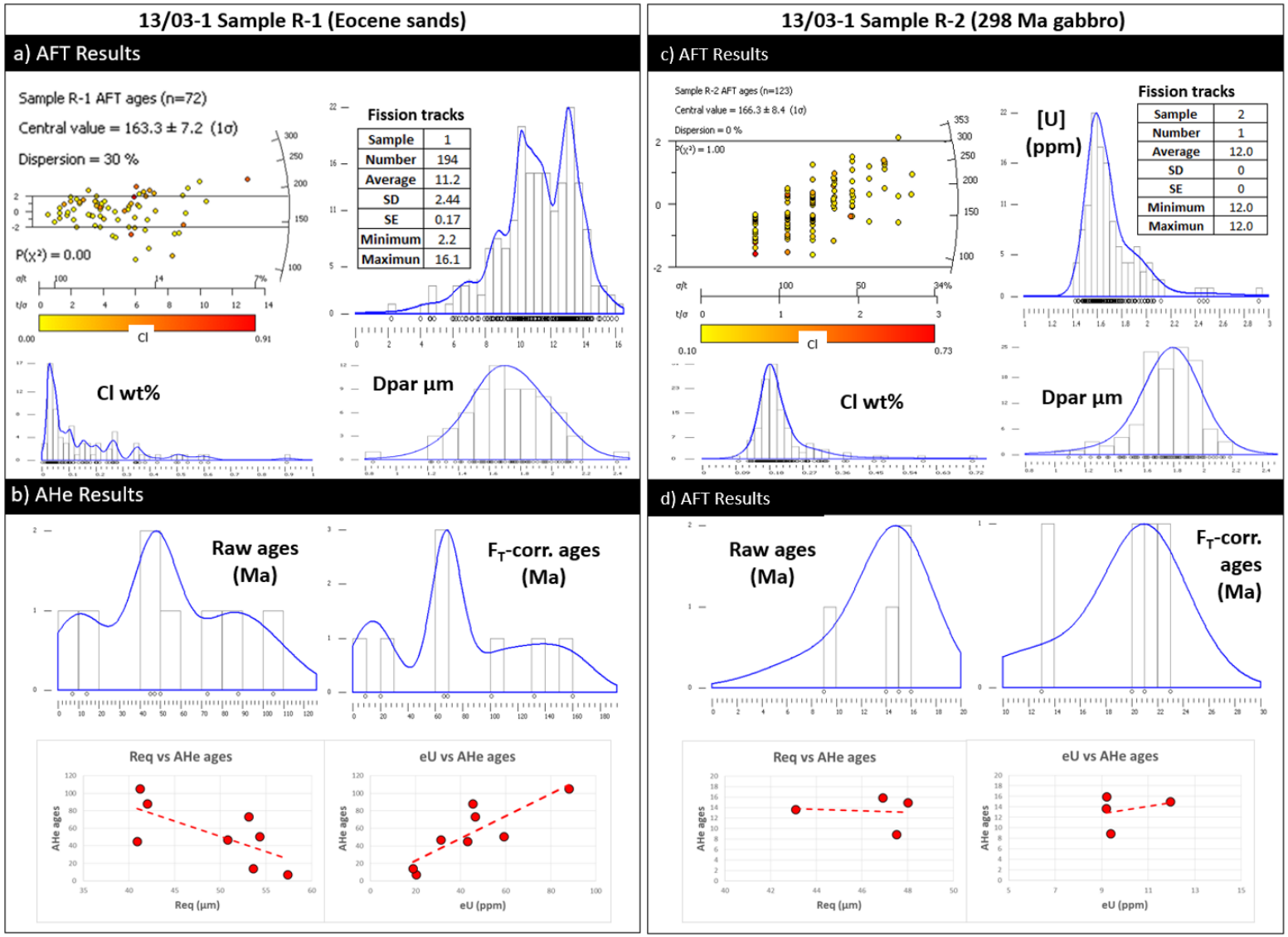

Figure 25: AFT and AHe results for sample R-1 and R-2 (13/03-1).

The gabbro sample R-2 yielded a younger AFT central age (166.3 ± 8.4 Ma) than the legacy result of 183.1 ± 19.2 Ma from McCulloch (1993), although the 1σ age uncertainty overlaps over the range 164-175 Ma (Middle Jurassic). But since the new sample age is based on more grains (123 *vs* 29) it will be used as the reference age (TABLE 8). Both the top (R-1) and bottom (R-2) samples yielded very similar AFT central ages of 163.3 and 166.3 Ma respectively (FIGURE 25 A AND C). It might suggest that they cooled quickly through the PAZ around that time.

The Carboniferous gabbro sample R-1 has track lengths with a bimodal distribution suggesting that the sample might have experienced reheating within the PAZ after a first exhumation event. The presence of numerous small track lengths also suggests that the sample spent a significant amount of time within the PAZ. The absence of measurable confined track lengths in sample R-2 and L-D1 is due to the very low uranium content of the grains (1.7 ppm in average), which is common for mafic igneous rocks (FIGURE 25A).

The eight AHe ages for the detrital Carboniferous sample R-1 show a large F_T-corrected age dispersion from 9 Ma (Late Miocene) to 160 Ma (Late Jurassic), which is partially explained by radiation damage. However, four grains form a cluster with AHe ages of 66-72 Ma (Maastrichtian) (FIGURE 25B). The much younger AHe ages (on average) versus AFT age suggest that the sample spent a significant amount of time within the PAZ and PHeRZ, supporting the observation made above based on track length data. The basal gabbro yielded four homogenous F_T-corrected AHe ages of 13-23 Ma (Early-Middle Miocene), with a cluster of three ages at 20-23 Ma (Aquitanian) (FIGURE 25D). The much younger AHe ages versus AFT age suggest that this sample also spent a significant amount of time within the PAZ and PHeRZ.

4.4.7 Thermal history modelling

4.4.7.1 Input data

AFT and AHe input data

For the thermal history modelling, 72 AFT ages and 10 AHe ages will be used for sample R-1 and 123 AFT ages and 4 AHe ages will be used for sample R-2. One VR sample was also selected to represent the low VR values of the Stephanian B-Westphalian D unit (VR_0 at 1725 ft MD), since the VR data from the Westphalian B-C sediments are most probably affected by the thermal aureole of the intrusion (FIGURE 26).

a) Prior information and MCMC chain parameters

Categories		Values
Prior information	Time Temperature	166.54 ± 166.54 Ma 70 ± 70 °C
	Max dT/dt, Reheating Gradient temp offset, Offset	1000 °C.My, Yes 27.96 ± 27.96, 25.56 °C, Constant
MCMC chain	Burn-in/Post-burn-in/Thinning	100,000 / 100,000/1
Proposed move	Time/Temp/Offset Resample/Reject, Reject complex	30/28/0.001 Resample, Yes

b) Scenario names and characteristics

Scenario	Samples	Const.	Max dt/dT	Gradient	tT points
0a	2 + VR	None	1000	Constant	Low (simple)
1a	2 + VR	None	10	Constant	Low (simple)
2a	2 + VR	3	10	Constant	Low (simple)
3a	2 + VR	3	10	Variable	Low (simple)
4a 4b	2 + VR No top AHe	3	10	Constant	Low (simple) High (complex)

c) Time-temperature constraints

Constraints	Time	Temperature
Initial R-1 Initial R-2	306.85 ± 3.15 Ma 297 ± 9 Ma	10 ± 10 °C 140 °C
1	14.18 ± 8.85	12.07 ± 10
2	1.44 ± 1.26	13.76 ± 10
3	0.06 ± 0.06	16.82 ± 10
Final R-1 Final R-2	0 Ma	18.22 ± 1 °C 43.78 ± 1 °C

d) Model parameters and constraints

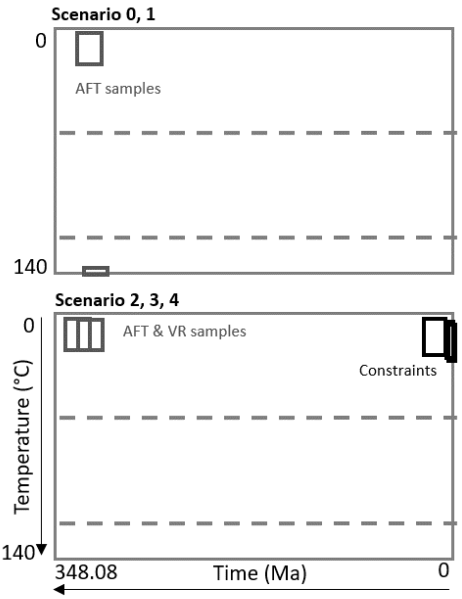

Figure 26: Thermal history modelling parameters and constraints for borehole 13/03-1.

Initial and final time-temperature constraints

Final conditions: Present-day temperature of sample

Three BHT are available for this borehole (Stuart, 1978b), which together with a seabed temperature of 10°C, yield a geothermal gradient of 27.97°C.km^{-1}. Using this gradient, the two samples have present-day temperatures of 18.22°C (R-1) and 43.78°C (R-2) (FIGURE 26).

Initial conditions - Emplacement age and temperatures

Sample R-1 is biostratigraphically dated as Stephanian B-Westphalian D, i.e. 306.85 ± 3.15 Ma (TABLE 1). Being a detrital sample, the temperature at the time of emplacement is defined as 10 ± 10°C. The igneous apatites of sample R-2 are dated at 297 ± 9 Ma (SECTION 4.4.6) while the temperature at the time of crystallisation is set at 140°C (see rational in section 2.5.3.2) (FIGURE 26).

Intermediate constraints

The top (Westphalian D-Stephanian B) sample is overlain by three dated stratigraphic units: 1) Miocene (14.18 ± 8.85 Ma, but with some uncertainty), 2) Older Pleistocene (= Gelasian-Chibanian)-Pliocene (1.44 ± 1.26 Ma) and 3) Pleistocene (glacial) (= Late Pleistocene) to Recent (0.06 ± 0.06 Ma). At the time of deposition of these three units, the top sample was located at a depth of respectively

c. 73.9, 134.3 and 243.7 m, ignoring any compaction effects. Using the present-day geothermal gradient (27.97°C.km^{-1}), these paleodepths correspond to paleo-temperatures of 12.07 ± 10, 13.76 ± 10 and 16.82 ± 10°C (FIGURE 26).

4.4.8 Modelling results

Introduction

All models yielded stable log likelihood and log posterior chains (FIGURE 27A). The detailed results of each model can be consulted in ANNEX 2, while thermal histories are summarized in FIGURE 27B.

Scenario 0: Thermochronological samples only (AFT, AHe), no intermediate constraints

This scenario is run to evaluate the thermal history information contained in the thermochronological data alone, without any intermediate constraints.

The modelling yields a thermal history characterized by heating from surface temperatures to c. 120°C between 300 and 250 Ma (Permian), followed by monotonic cooling to the present-day that is interrupted by a very rapid heating spike (> 100-120°C) at c. 10 Ma (FIGURE 27B). The likelihood, posterior and expected models all yielded similar thermal histories with predicted data that matches the measured data for the AHe ages for both samples and the AFT and track length data of the top sample, but not for the AFT age of the bottom sample whose predicted age (c. 100-110 Ma) is significantly younger than the measured age (c. 150 Ma). The individual AHe ages of the top sample are not all well predicted, suggesting that the age dispersion is not entirely explained by grain size and radiation damage.

The 10 Ma heating spike is probably caused by the AHe ages of the bottom sample. However, it is difficult to reconcile this spike with the known geology of the region as no magmatic event is known to have occurred during the Miocene.

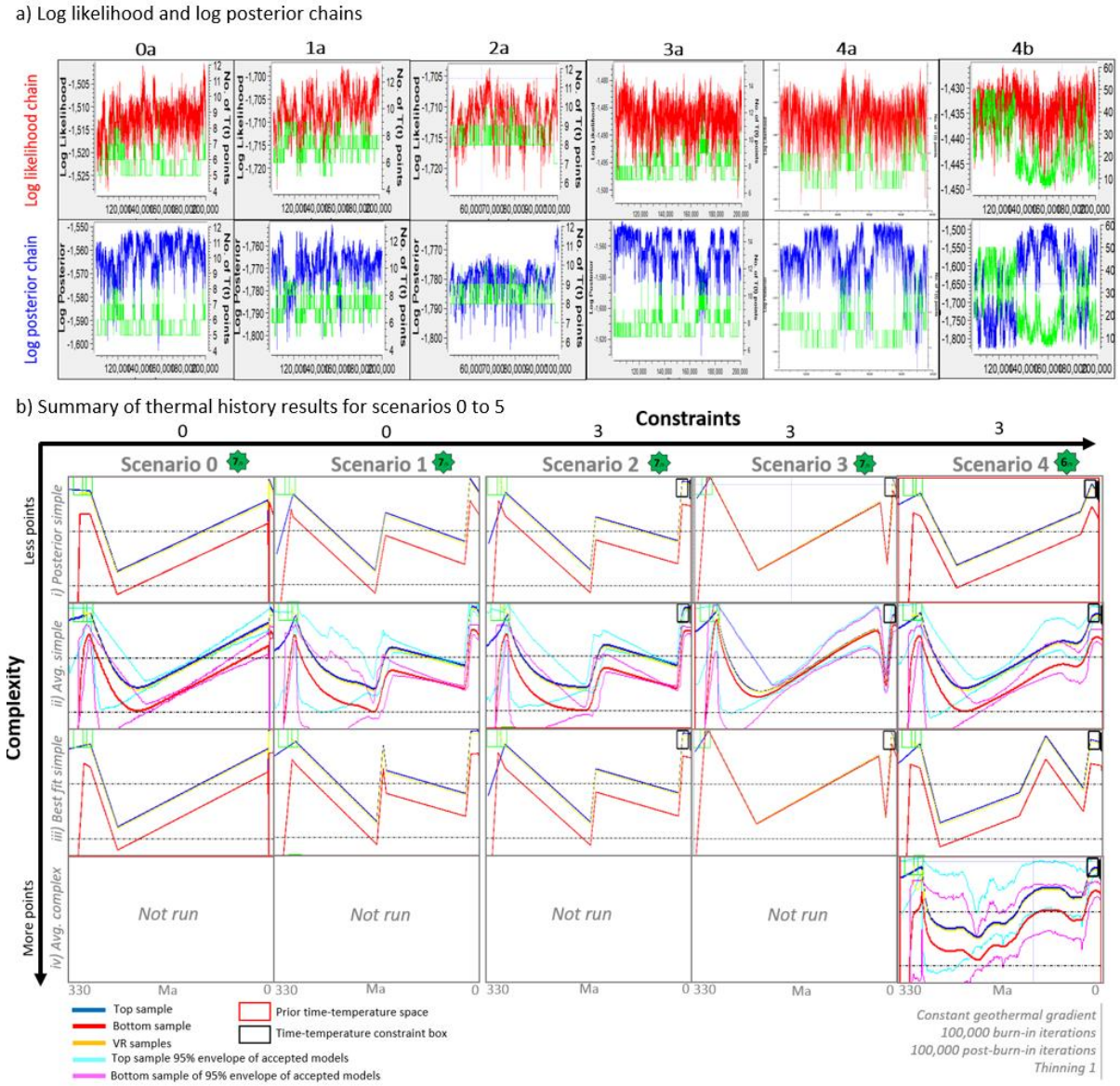

Figure 27: Summary of thermal history modelling for 13/03-1. a) Log likelihood and log posterior chains, b) Thermal histories.

Scenario 1: Same as scenario 0 but with a maximum cooling/heating rate of 10°C.Ma^{-1}

This scenario is run to investigate thermal histories that do not contain the presumably unrealistic 10 Ma heating spike. To prevent the modelling trending towards this solution to match the AHe ages, the maximum heating/cooling rate constraint is reduced from the default value (1000°C.Ma^{-1}) to 10°C.Ma^{-1}.

This scenario yields similar thermal histories for the likelihood, posterior and expected models and characterized by two cooling episodes: 1) c. 60°C (through the PAZ) at c. 165-150 Ma (Late Jurassic); and 2) c. 70°C (from the upper part of the PAZ to surface temperatures) at c. 10-25 Ma (Early-Middle Miocene) (FIGURE 27B). This scenario yielded similar predicted data quality as scenario 0.

This thermal history is more realistic than scenario 0 as the Late Jurassic cooling can be attributed to rift-related exhumation and there is no requirement for the 10 Ma heating spike.

Scenario 2: Same as scenario 1 with intermediate constraints.

This scenario aims at testing the impact of intermediate constraints, based on the Late Cenozoic stratigraphic constraints, on the thermal history derived in scenario 1.

The modelling yields a very similar thermal history to scenario 1 (FIGURE 27B) which could suggest that the shelly sands in the borehole believed to be of Miocene age (with some uncertainty) are indeed of that age and could represent a transgressive sand emplaced during subsidence that followed Early-Miocene exhumation.

However, the poor prediction of the AFT age of the bottom sample needs to be addressed. The modelling suggests that the bottom AFT age should be younger than what is measured. The low [U] of the bottom sample led to large errors on each individual grain age and could be the cause of age inaccuracy. However, the legacy L-D1 (from the same gabbro and depths), yielded an even older AFT age (183 Ma *vs* 166 Ma in this study), suggesting that a younger AFT age is unlikely. Both the top and bottom samples have similar ages (c. 150-160 Ma) suggesting a very rapid exhumation through the PAZ around that time. However, the track length distribution of the top sample suggests protracted cooling through the PAZ (a broad distribution with small track lengths). A possible hypothesis is that the paleogeothermal gradient changed over time which is explored in scenario 3.

Scenario 3: Same as scenario 2 with a variable geothermal gradient

An alternative interpretation for the mismatch between predicted and measured data in scenario 2 is that the geothermal gradient was significantly different in the past. Scenario 3 tests this hypothesis by allowing the geothermal gradient to change through time and at each iteration.

The modelling yields a likelihood, posterior and expected thermal history characterized by an unrealistic fast heating/cooling episode at c. 30-10 Ma, with the two samples being at effectively the same temperature until c. 20-10 Ma and their present-day temperature offset developing only between 20 and 0 Ma (FIGURE 27B). These thermal histories successfully match the predicted and measured data, including the AFT central age of the bottom sample. The fact that the AHe ages of both samples are predicted by the same thermal history implies that the AHe age difference (c. 20 Ma vs 60 Ma) between these two samples is possibly solely due to grain size and radiation damage. If a more realistic thermal history for the top sample is assumed (such as the one from scenario 2 with a cooling event during the Late Jurassic and a slow heating phase until the Miocene), then a similar result (the matching of all AFT and AHe ages) would probably be obtained if the bottom sample was at the same temperature asthe top sample from the Mesozoic exhumation event to c. 20 Ma. This

thermal history was not found by modelling scenario 3 but would most probably be successful as the bottom sample would spend less time within the PAZ and therefore the tracks would not have time to anneal which would thus preserve the Late Jurassic AFT central age.

This thermal history model implies that two samples were probably close (i.e. at similar depths) from c. 200 Ma until 20-10 Ma based on the lack of a significant temperature offset; and at the present-day depth/temperature offset between 20-10 Ma and now. Such a scenario could be explained by the samples having similar depths during the Mesozoic as a result of extensional faulting, and then being affected by reactivation of this fault during Miocene inversion (associated with the cooling and exhumation event). The stratigraphic break between the Westphalian B-C and Westphalian D-Stephanian B sections (FIGURE 21) could represent the location of such a fault. Although the break in VR data has been interpreted as representing the effect of a tilted dyke (SECTION 4.4.3), the operator suggested that it might be due to a fault (Stuart, 1978b). The seismic lines available in the area are of poor quality and do not allow for the detection of faults in the Carboniferous section (FIGURE 22).

Scenario 4: No AHe ages for bottom samples

Although scenario 3 successfully explains the thermochronological data, another hypothesis is that some of the input data is inaccurate. Initially, several models were run by removing one set of input data at a time in order to identify an origin for the (potentially) anomalously young bottom AFT age of the bottom sample. After testing various combinations of input data, both the top and bottom sample AHe data seem to be the cause of this mismatch. Eight models were run (2x 10,000 runs, no intermediate constraints) with only the bottom sample AFT age, the top sample track length data and between one to eight of the oldest AHe ages of the top sample. They yielded a bottom sample predicted AFT age of c. 140, 140, 120, 110, 110, 100, 70 and 50 Ma respectively, indicating that it is the youngest AHe ages in the top sample that forces the model to yield a younger AFT central age than measured for the bottom sample. Similarly, a scenario with both the top and bottom AFT ages but only the bottom sample AHe ages yielded a bottom sample AFT central age of 120 Ma (*i.e.* c. 30 Ma younger than the measured age). The young AHe ages in both the top and bottom samples force the thermal history to reach high temperatures during the Cenozoic that probably shorten the track lengths of the bottom sample and result in a younger AFT age. Since the age dispersion of the AHe ages of the top sample is very large in comparison to the bottom sample, scenario 4 is run to evaluate the thermal histories produced by all the input data and the intermediate constraints, but without the AHe ages of the top sample.

The simple likelihood model shows a thermal history characterized by slow cooling between c. 260 and 130 Ma (Triassic to earliest Cretaceous), followed by rapid cooling to surface temperatures between 130-100 Ma (Barremian-Albian), rapid heating to 60°C (top sample) - 90°C (bottom sample)

between 100-30 Ma (Late Cretaceous-earliest Oligocene), rapid cooling to surface temperatures at 30-20 Ma and finally slow heating to present-day temperatures since 10 Ma. This thermal history is geologically plausible with the slow and rapid Mesozoic cooling corresponding to the protracted and accelerated rifting and hyperextension seen in the nearby Rockall Basin. The magnitude of the Late Cretaceous-Eocene heating is probably too high to have been by burial alone but could also be due to elevated heat flow due to NAIP magmatism (in this case the temperature offset between the two samples would be different which is not the case here as the paleogeothermal gradient is fixed). The predicted AFT age of the bottom sample is 105 Ma which is still far from the measured age but better than for scenario 2. The predicted and expected models display unrealistic thermal histories with protracted cooling throughout the Mesozoic and Cenozoic. The complex model shows that the low temperature thermal history between c. 50-120 Ma is poorly constrained, suggesting that an episode of Paleogene cooling (up to 50°C) might have occurred but is not detectable with the dataset at hand.

4.4.9 Discussions

The AFT and AHe dataset for the new samples in well 13/03-1 has not been fully reproduced by the thermal history modelling. The apparent contradiction between the AFT ages, track length distribution and AHe ages results in the AFT age of the bottom sample having a predicted age that is always younger than measured. Several hypotheses have been tested to explain the apparent mismatch: 1) the samples did not always have the same vertical separation and have experienced normal faulting (during Mesozoic rifting) followed later by reactivation of the fault during Miocene inversion; 2) inaccuracies in the datasets (notably, large AHe age dispersion for the top sample, low [U] for the bottom sample AFT and AHe dataset) resulted in contradictory thermochronological information.

Despite the uncertainties associated with this mismatch, the following conclusions can be drawn:

- There is probably a major cooling event at c. 170-150 Ma (Middle-Late Jurassic, History A) or a protracted cooling between 250-100 Ma (Triassic to Early Cretaceous, History B)
- There is probably another major cooling event at 30-10 Ma (Oligocene-Middle Miocene)
- The dataset does not rule out a Paleogene cooling event of up to 50°C

Using the present-day geothermal gradient, the Miocene cooling of 50-80°C would represent an exhumation event of 1.8-2.8 km.

4.5 Borehole 18/25-1

Well 18/25-1 was drilled by Enterprise Oil in 1999 in the Slyne Basin (FIGURE 17). Two samples were taken from dolerite intrusions (R-41, 2208-2232 m MD; R-42, 2346-2370 m MD) but no apatites were obtained from them.

In 2004, Geotrack undertook a regional study of the Slyne-Erris basins that included well 18/25-1, together with wells 18/20-1, 18/25-2 and 19/05-1 (Green, 2004). Their preferred thermal history for 18/25-1 shows a decrease in geothermal gradient from 45°C.km^{-1} to 30 °C.km^{-1} at c. 135 Ma, cooling of c. 40°C at 115-110 Ma (Aptian-Albian boundary) corresponding to an estimated exhumation pulse of 1400 m) and cooling of c. 15°C at 30-10 Ma (Oligocene-Miocene) (FIGURE 28).

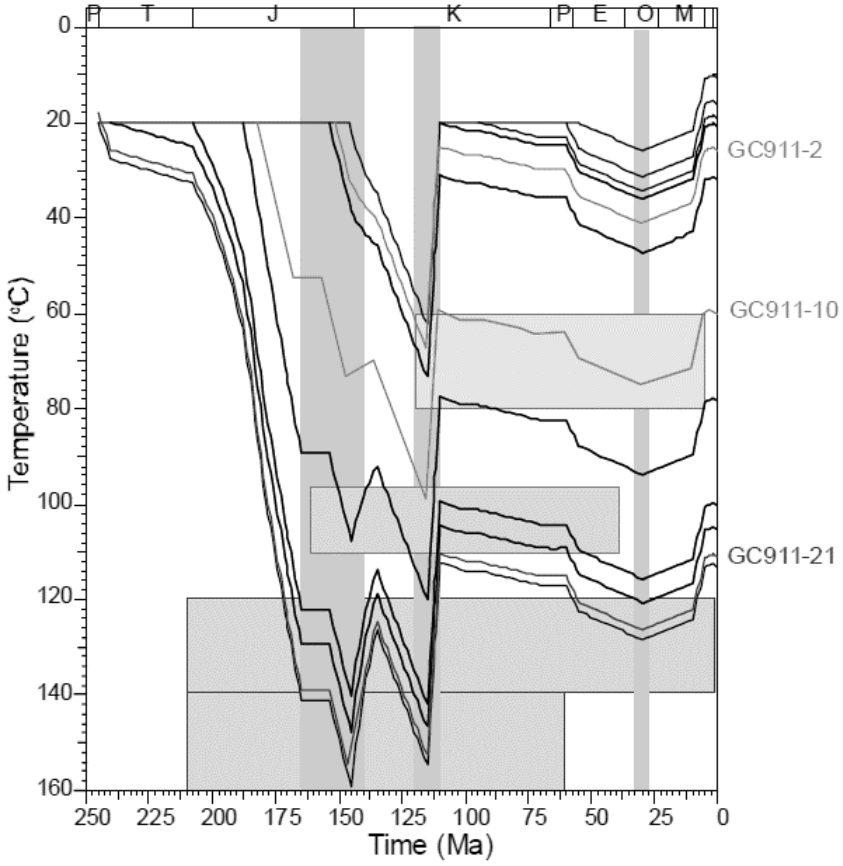

Figure 28: Preferred thermal history for well 18/25-1 from legacy Geotrack AFT study (Green, 2004).

4.6 Borehole 18/25-2

4.6.1 Exploration history and geological summary

18/25-2 is a dry exploration borehole drilled by Enterprise Oil in 1999. The well targeted Triassic sandstones within a tilted fault block in the Slyne Basin (FIGURE 17). It was drilled to a total depth of 2965.5 mMD in 299 m of water. The borehole encountered the following succession: 39 m of uncharacterized Cenozoic sediments, 218 m of chalk, 83 m of Albian sand, 1573 m of Jurassic clastic-dominated sediments, 159 m of Permian evaporites and Early Triassic sands, 411 m of Silurian to possibly Early Carboniferous sands and 157 m of Silurian (Wenlock) clastics. A 71.5 m thick mafic intrusion was also encountered at 2077-.5-2149 mMD within a Lower Jurassic claystone (Pay and Geerlings, 2000).

4.6.2 Samples

4.6.2.1 Sampling strategy and results

The primary sampling target was the mafic intrusion in the Jurassic claystone (sample R-44, 2085-21448 mMD). The sample yielded numerous apatites yielding 40 AFT ages and 59 U/Pb ages but only a few zircons.

4.6.2.2 U/Pb, trace element and AFT results

The detailed description of the U/Pb and trace element results is presented in ANNEX 1 (SECTION 1.3.2 AND SECTION 2.3.2). Below is a summary and discussion of the results.

The grains have a high common Pb content which leads to large uncertainties on U/Pb age of the sample. The non-anchored lower intercept age is 230 ± 45 Ma (Late Triassic). Employing an initial Pb value derived from the Stacey & Kramers (1975) terrestrial Pb model, the weighted average ^{207}Pb corrected age is 129 ± 21 Ma and anchored lower intercept is 126 ± 20 Ma (Early Cretaceous). Therefore, the mafic intrusion is Mesozoic in age and probably Early Cretaceous. The grains yielded an AFT central age of 177 ± 21 Ma (Early Jurassic) which provides a minimum age for the intrusion. The maximum U/Pb age considering the 2σ age uncertainty is c. 140 Ma, while the minimum AFT age is c. 156 Ma at the 1σ level and 135 Ma at the 2σ level. While the two ages only just overlap at the 2σ level, they certainly imply a crystallisation age of latest Jurassic-earliest Cretaceous. The significance of this Mesozoic age is discussed in SECTION 7.2.2.

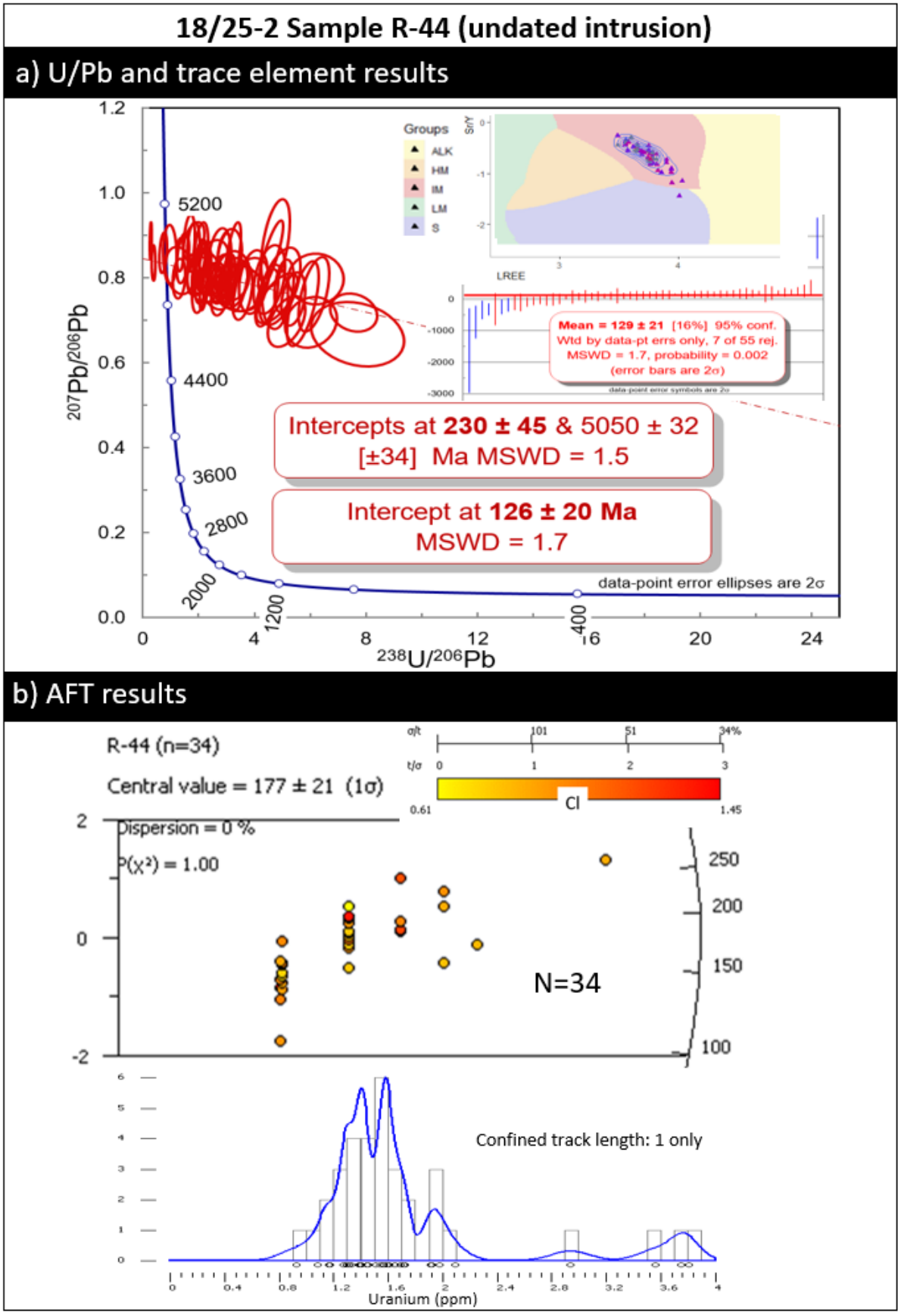

Figure 29: Apatite U/Pb, trace element and AFT results for sample R-44 (18/25-2).

4.7 Discussions: Exhumation of the Northern Zone

4.7.1 Neogene exhumation

Only borehole 13/03-1 yielded enough good quality apatites to undertake multi-sample AFT-AHe thermal history modelling. Despite the contradictory thermal history information contained in the AHe and AFT data, the data points towards a significant 20-10 Ma Miocene exhumation event that might have eroded up to 1.8-2.8 km of sediments. This event correlates well with 1) the 25°C cooling event that is predicted to have occurred at some point between 40 and 10 Ma in well 5/22-1 (Green (2001a), Jackson et al. (2020)), albeit with a lower magnitude of exhumation; and 2) with thermal history A in 12/02-1, that predicts 45°C of cooling between 25 and 15 Ma (Green, 2003) (FIGURE 30 AND FIGURE 31). However, it differs from the Neogene thermal history of onshore NW Ireland that records more recent cooling of c. 50°C between 10 and 0 Ma (Cogné et al., 2014).

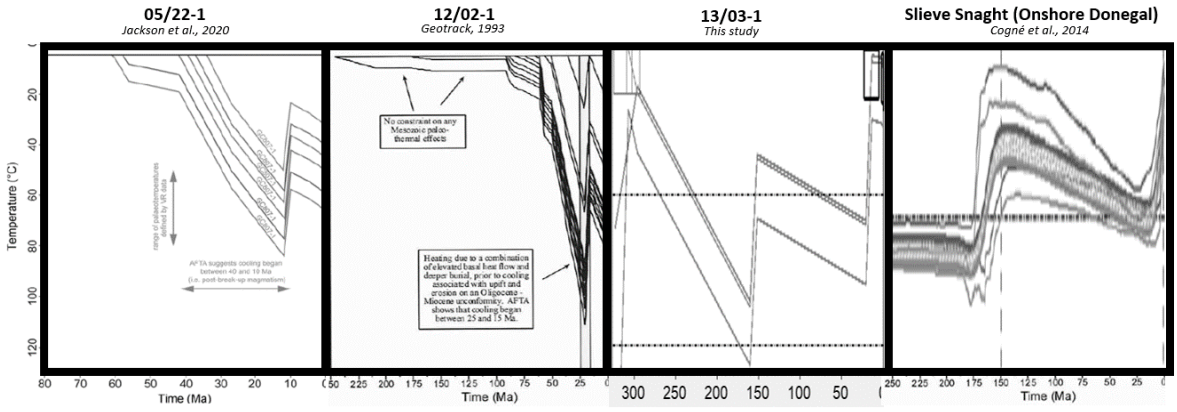

Neogene cooling event

Time	40-10 Ma	25-15 Ma	20-10 Ma	10-0 Ma
Mag.	25°C	45°C	50-80°C	50°C

Figure 30: Neogene cooling events detected by low-temperature thermochronological studies in 5/22-1, 12/02-1, 13/03-1 and onshore NW Ireland.

Based on the well and seismic data further south in the Erris Basin, Chapman et al. (1999) identified c. 800-1000 m of denudation caused by Oligocene-Miocene uplift that they interpreted as basin-wide in scale; similar to findings from a combined AFT, vitrinite reflectance, sonic velocity and seismic stratigraphy study of borehole 27/13-1 that predicted c. 1000 m of exhumation between 30-25 Ma (Scotchman and Thomas, 1995).

Therefore, the new data in 13/03-1 supports the hypothesis of a semi-regional exhumation event (across the entire Northern Zone) that occurred probably at some point in the Early or Middle Miocene (c. 10-20 Ma) and resulted in c. 1 km of uplift and erosion and possibly associated with a higher geothermal gradient prior to uplift.

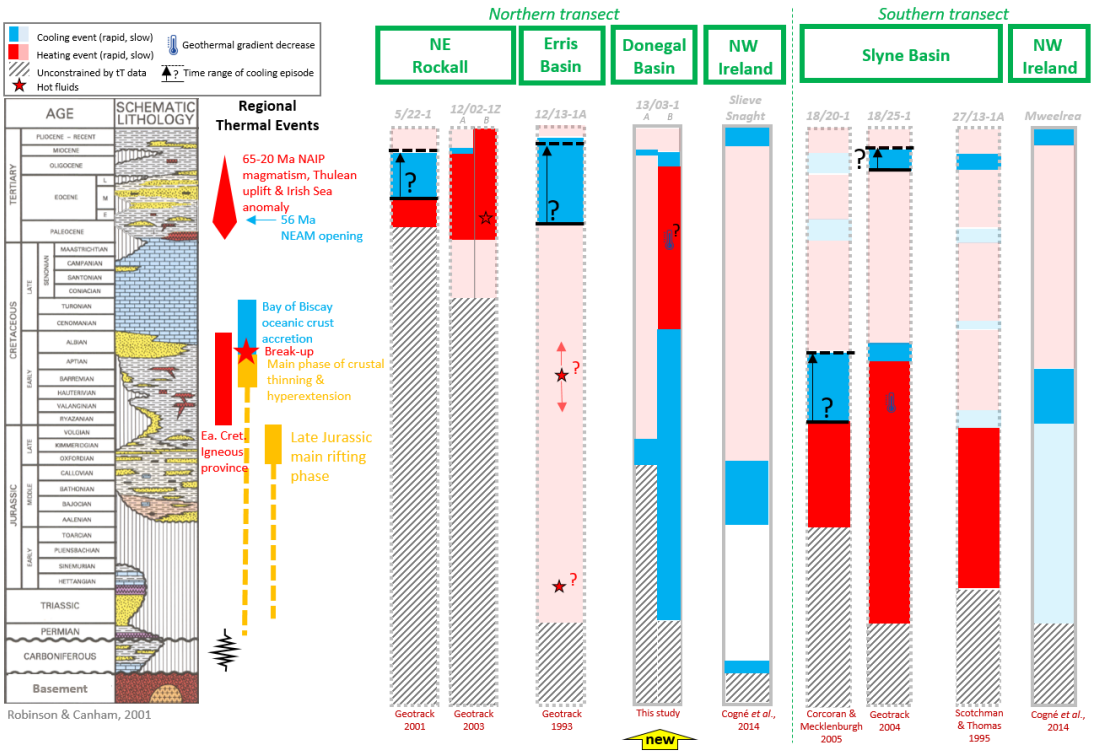

Figure 31: Summary of the new and legacy thermal histories from the Northern Zone.

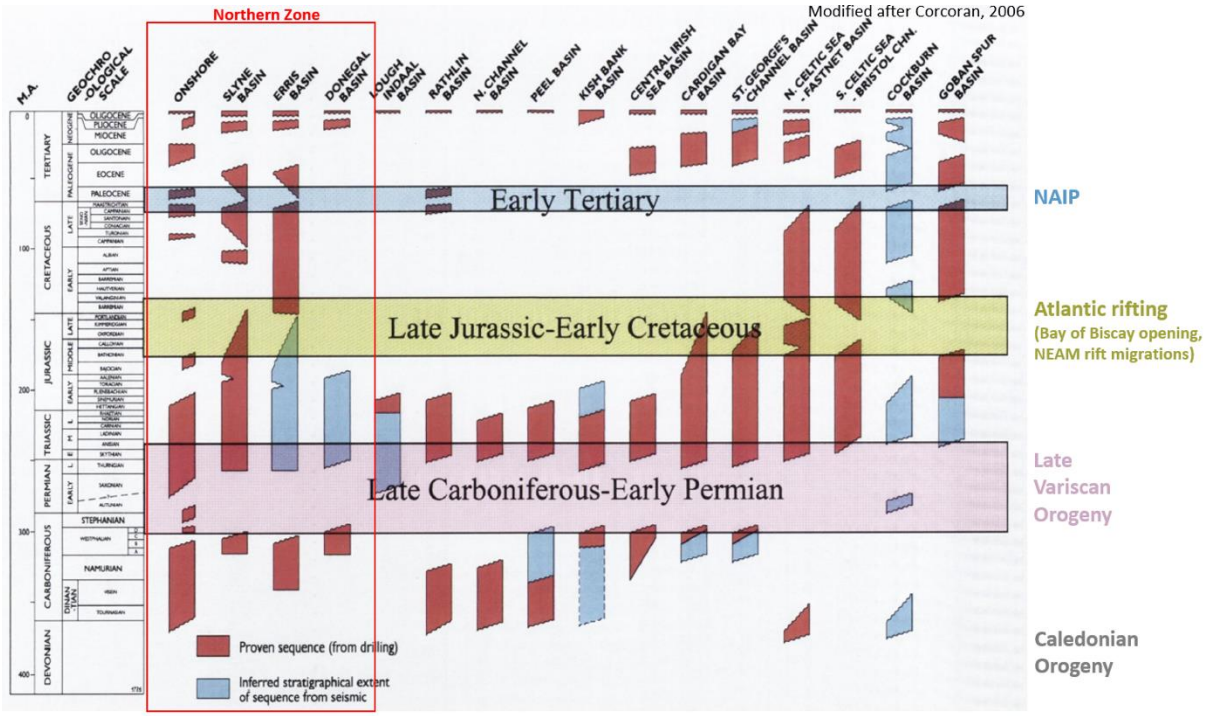

Figure 32: Stratigraphical range chart for the Irish inbound basins. Note the hiatuses associated with the Paleocene-Early Eocene and Oligocene-Miocene exhumation events (modified after Corcoran (2006)).

4.7.2 Paleogene exhumation

Despite borehole 13/03-1 being located above a high-velocity body at the base of the crust that could represent igneous underplating (FIGURE 5), no Paleogene exhumation has been detected by the

thermal history inverse modelling. However, the complex model of scenario 4 suggests that a km-scale exhumation event during the Paleogene might have occurred but not be detected due to the overprinting of the Neogene exhumation. It is also possible that the magnitude of the Neogene cooling might represent the cumulative effect of two smaller magnitude cooling during the Paleogene and Neogene, as has been invoked onshore west of Ireland (Cogné et al., 2014). An episode of Paleocene erosion has been interpreted in wells 18/20-1 and 27/13-1A in the Slyne Basin, based mostly on stratigraphic hiatuses (Scotchman and Thomas (1995), Corcoran and Mecklenburgh (2005)) (FIGURE 32). The lack of clear detection of a Paleocene-early Eocene exhumation event in the thermochronological data in the Northern Zone, combined with the presence of Paleocene-Early Eocene hiatuses suggest that any exhumation at that time (contemporaneous with exhumation in the Irish Sea) was small in magnitude. Since this zone is the part of the IAM that is the closest to the assumed path of igneous underplating (Faroes-Outer Hebrides-western Scotland-Irish Sea) and contains possibly thick high velocity bodies (c. 7km below 13/03-1, FIGURE 5), the lack of detectable exhumation is surprising and shed some doubts on the correlation between high-velocity bodies at the base of the crust and their interpretation as representing igneous underplating and/or the correlation between igneous underplating and exhumation. Based on these observations, it is unlikely that Paleocene-Early Eocene exhumation will be detected in the Central and Southern Zones, which are further away from the main axis of assumed igneous underplating. The absence of any significant Paleogene exhumation in central and western Ireland (Cogné et al., 2016) seems therefore to extend to the platform offshore west of Ireland despite the inferred presence of igneous underplating under the Donegal-Malin basins and suggests that the Greater Irish Sea anomaly is possibly a unique feature within the NEAM.

4.7.3 Mesozoic exhumation

The new data from 13/03-1 yields two end-member scenarios for the Mesozoic exhumation: History A) a rapid exhumation event in the Late Jurassic (unconstrained history before that time), or B) protracted slow exhumation from at least the Triassic to the Hauterivian, followed by rapid exhumation during the Barremian-Aptian (FIGURE 31). Both scenarios are plausible, although the second history is more compatible with the expected rifting history of the nearby Rockall Basin which started with protracted rifting followed by hyperextension, probably during the Early Cretaceous. In both cases, the main episode of exhumation is later than recorded in the NW Donegal vertical profile (Slieve Snaght, Middle Jurassic, (Cogné et al., 2014)). The legacy thermal histories in the Slyne Basin also show a main exhumation episode in the Early Cretaceous (FIGURE 31).

5 Central zone: Greater North Porcupine

5.1 Introduction

In this study, the Central zone refers to the North Porcupine High (NPH), North Porcupine Basin (NPB), the Slyne Ridge to the north of the NPB and the elevated margin to the east of the NPB (FIGURE 33).

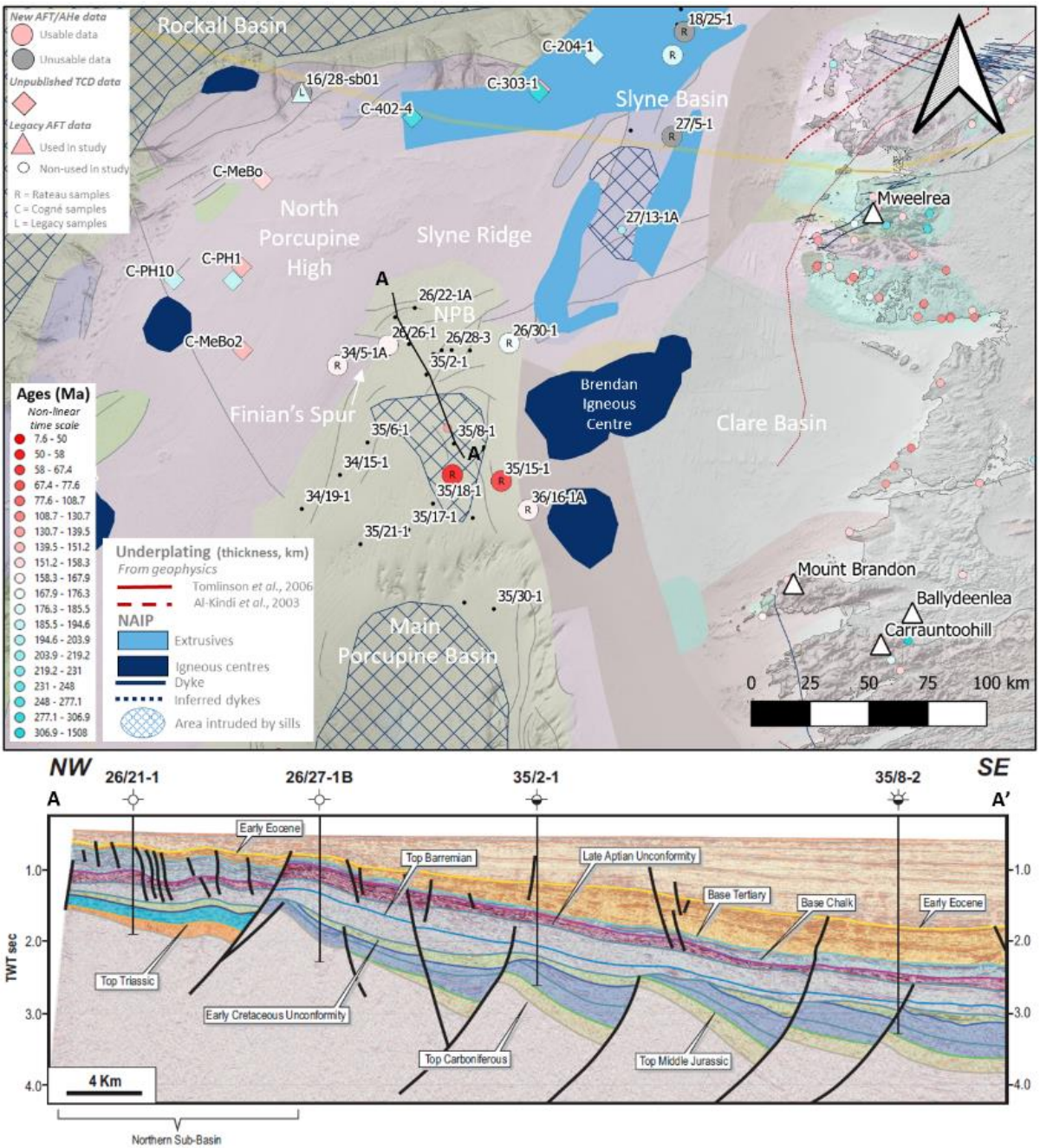

Figure 33: Map of the Central Zone with location of boreholes discussed in chapter 4 and seismic geosection through the northern part of the Porcupine Basin.

The Porcupine High (PH) is a basement high that separates the Rockall Basin to the west from the Porcupine Basin to the east. The continental crust of most of the PH is unstretched and averages c. 28

km in thickness, in contrast to the hyperextended Rockall and Porcupine Basins with crustal thicknesses in the range of 0-20 km and an average of c. 5 km (Kimbell et al., 2010) and sediment thicknesses of up to 10 km (Shannon et al., 1995). However, a series of perched Mesozoic basins occur on the western edge of the PH, notably from south to north: the South and North Bróna Basins, the Cillian Basin, the Macdara Basin and the Colm Basin (Naylor and Shannon, 2005). Early dredges revealed the presence of Late Cretaceous and Late Eocene carbonates on the western edge of the high (Dobson et al., 1976). Shallow boreholes on the perched basins revealed a succession of Jurassic and Early Cretaceous clastics, a thin layer of Late Cretaceous chalk, thick Early Eocene claystones and Middle Eocene sands and a thin layer of Pliocene-Pleistocene sands (Haughton et al., 2005). A description of the geology of the norther part of the Porcupine Basin can be found in Jones and Underhill (2011).

The first section focuses on the North Porcupine High and comprises new data from 16/26-sb01, 26/26-1, 34/05-1 and a set of seabed dredge samples, while the second part focuses on the eastern margin of the norther part of the Porcupine Basin with new data from 26/30-1, 35/13-1A and 35/15-1.

5.2 Borehole 16/28-sb01

5.2.1 Exploration history

Shallow borehole 16/28-sb01 is one of four shallow research boreholes drilled in the summer of 1999 by the 'MV Bucentaur' on the western margin of the Porcupine High (FIGURE 33). The drilling program was initiated by the Rockall Studies Group of the Petroleum Infrastructure Programme. The boreholes aimed to constrain better the Mesozoic and Cenozoic stratigraphic development of the eastern margin of the Rockall Basin.

16/28-sb01 was drilled in the north-east part of the Macdara Basin, a perched Mesozoic sedimentary basin in the northern part of the Porcupine High (FIGURE 33 AND FIGURE 34). It reached a depth of 148.25 m below the seabed (BSB). The entire section was cored but only c. 50% was recovered. The results and geological interpretations of the drilling are summarized in Haughton et al. (2005) based on research mission reports published on the PIP website (e.g. Stoker (1999), Jacovides (2000), Harrington et al. (2000), Green (2001b) and Hetfeld and Clayton (2001)). The reports use the seabed as the datum for all reported depths. Unless stated otherwise, the same datum will be used for this section, *i.e.* all depths are below seabed (BSB).

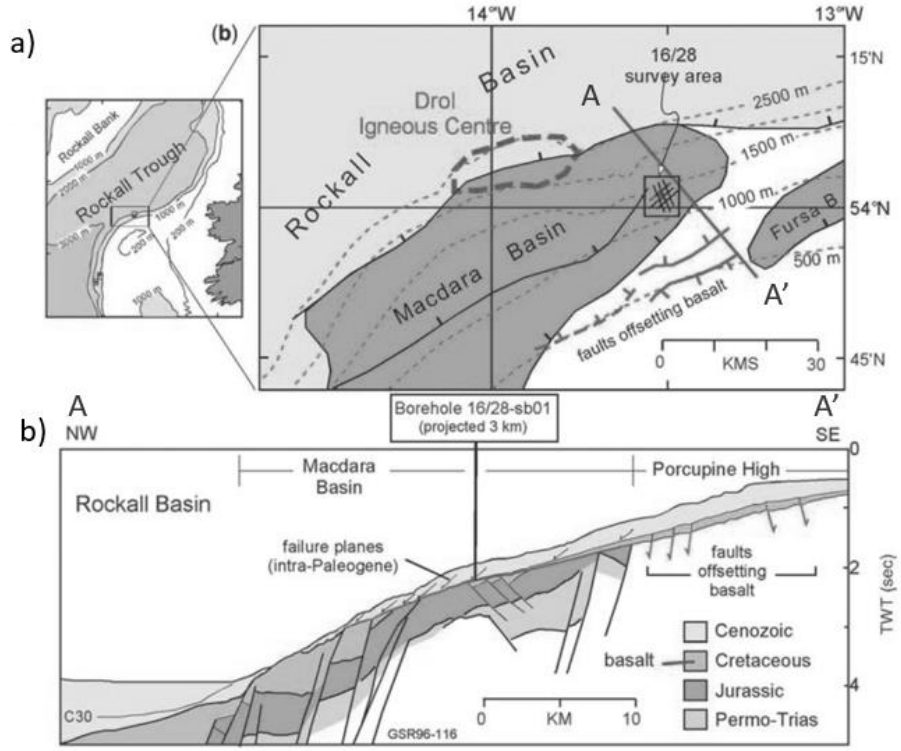

Figure 34: Geosection and seismic section of borehole 16/28-sb01 (Haughton et al., 2005).

5.2.2 Geological summary

The well encountered c. 14.5 m of Late Pliocene-Pleistocene slope clastics and pelagic carbonates, unconformably resting on c. 74 m of Middle Eocene mixed clastic-pelagic carbonates. The Middle Eocene sits conformably above c. 57 m of Lower Eocene outer shelf/slope clay-prone bioturbated hemipelagic deposits, including 2-3 m of basal gravity-remobilized carbonates. The Lower Eocene deposits rest unconformably on top of 2.3 m of Upper Cretaceous high-energy, open marine, mixed clastic-carbonates and 1 m of undated, highly altered fine-grained basalt with a microphyric texture with flow-banded plagioclase laths at the top (FIGURE 34 AND FIGURE 35).

5.2.3 Age of the Upper Cretaceous silty marl and sandstone

The Late Cretaceous age of the basal sediments, given by Haughton et al. (2005) is based on the biostratigrahic study (Harrington et al., 2000). However, the preliminary stratigraphic analysis of Stoker (1999) suggests that the silty marl is Late Maastrichtian in age and the underlying brown sandstone (described as 'brownsands' on the summary log) is possibly Cenomanian in age (with a question mark). Consequently, Stoker (1999) places a stratigraphic unconformity between the marl and the sandstone. The rationale behind the Cenomanian attribution is not explained in the report.

5.2.4 Legacy compaction and thermal data

5.2.4.1 Sonic velocity and VR data

The operator did not acquire sonic velocity data for this shallow borehole. A vitrinite reflectance measurement was attempted in the Upper Cretaceous sandstone at 147.2 m BSB but the sample was barren of organic matter (Hetfeld and Clayton, 2001). No other measurements were attempted and consequently no VR data are available for this borehole.

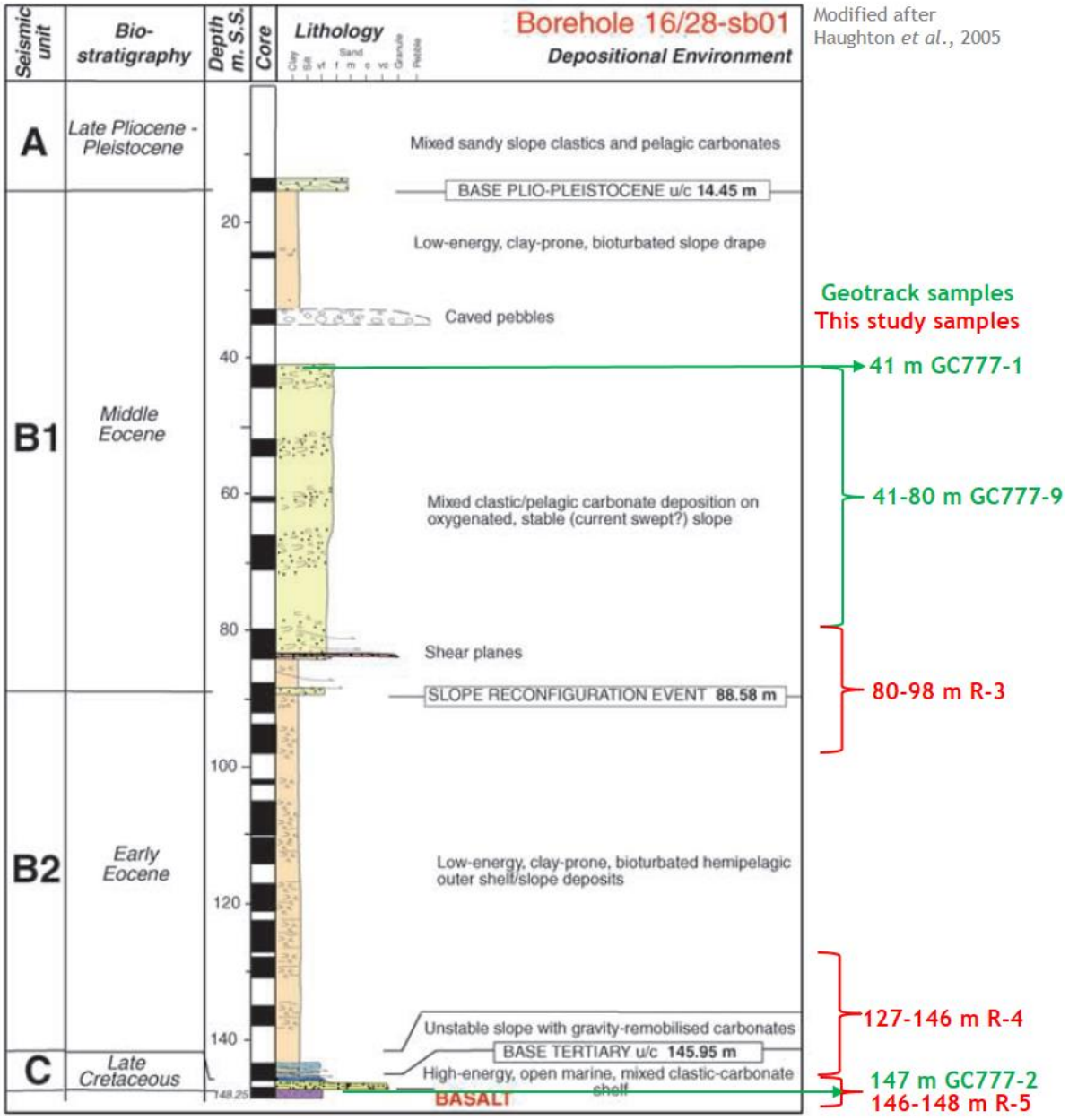

Figure 35: Lithologic and stratigraphic log of borehole 16/28-sb01 with sample names and sampling depths.

5.2.4.2 Fluid inclusion homogenization temperature

Fluid inclusion homogenization temperatures were measured on five samples by Dr John Parnell (Green, 2001b). The selected inclusions are located in calcite cements and quartz trails. Two samples come from the Middle Eocene sandstone and three samples from the Maastrichtian marl (TABLE 9).

The temperatures range from <50°C to c. 200°C. The quartz trail inclusions yielded only high temperatures in the range of c. 90°C to c. 200°C (group 1). The calcite inclusions can be divided into two groups: one with high homogenization temperatures ranging from c. 80°C to c. 100°C (group 2) and one with lower temperatures ranging from <50°C to 67.5°C (group 3) (TABLE 9).

Table 9: Fluid inclusion homogenization temperatures from Green (2001b). Number in brackets is the number of inclusions analysed for each population.

		Quartz					Calcite			
Depth (m)	Stratigraphic age	Cement	Trail 1	Trail 2	Trail 3	Trail 4	Cement	Recryst.	Cement 2	Vein
40.87	Eocene		89.7 (5)	143.9 (4)			101.3 (1)			
41.0	Eocene						98.3 (8)			
147.08	?Maastrichtian				161.3 (11)		80.3 (4)		<50 (6)	
147.18	?Maastrichtian		94 (2)		154.7 (1)	190.2 (5)	104.5 (3)		67.5-<50 (11)	
147.2	?Maastrichtian				163.9 (9)	198.3 (9)	79.3 (7)		<50 (4)	
			Group 1				Group 2		Group 3	

Using quantitative modelling, Green (2001b) concluded that only the temperatures from group 3 matched the temperatures derived from the AFT data and could therefore be derived from burial alone. Green (2001b) hypothesized that the cements from groups 1 and 2 were caused by episodes of transient hot fluid pulses. They empirically demonstrated that for the samples to experience higher temperatures up to 200°C, the duration of heating must have been very short so as to not reset the AFT data. For example, fluids with temperatures of 200°C must have been emplaced in less than 10 years and fluids with temperatures of c. 125°C in less than c. 0.1 Ma.

The timing of these short-lived (<0.1 Ma) hot fluid pulses is poorly constrained. The presence of high fluid inclusion homogenization temperatures in both the Middle Eocene and Maastrichtian samples implies that some hot fluids must have been active after the deposition of the Middle Eocene sandstone, but some older flows might have also been active between the Maastrichtian and the Middle Eocene.

5.2.5 Geo-thermochronology samples

5.2.5.1 Sampling strategy

This borehole was selected because it is located on the Porcupine High, a key source of sediments for both the Porcupine and Rockall Basins (FIGURE 33), as a high is more prone to erosion during uplift events. The borehole also contains sandstones and a basalt, which can both be good sources of apatite (although grain size can be a fertility issue for fine-grained basalts).

Initially, the targeted sampling intervals were the Middle Eocene sandstone (40-88.58 m), the Lower Eocene siltstone (88.58-145.95 m) and the Upper Cretaceous sandstone and basalt (145.9-148.25 m). However, sampling issues led to the sampling of the intervals 80-98 m (R-3, Lower-Middle Eocene clastics), 127-146 m (Lower Eocene siltstones), 146-147.3 m (Upper Cretaceous sandstone) while the basalt was not sampled. Apatite and zircon fission track data were also available from three legacy samples from a Geotrack study (Green, 2001b). The three samples are from the Middle Eocene sandstone, L-GC777-1 (at 41 m BSB) and L-GC777-9 (41-80 m BSB), and from the Upper Cretaceous sandstone, L-GC777-2 (147 m BSB) (FIGURE 35).

5.2.5.2 Apatite and zircon yield

Apatite and zircon yield

Only a few apatites were found in samples R-3 (Lower to Middle siltstone and sandstone) and R-5 (Upper Cretaceous sandstone), resulting in only one AFT grain age for each sample. Sample R-4 (Lower Eocene siltstone) did not yield any apatite at all. Samples R-3, R-4 and R-5 yielded >60, 2 and >250 zircons respectively. The legacy samples yielded only two datable apatites in sample L-GC777-1, at the top of the Middle Eocene sandstone. The paucity of FT data in this sample led Green (2001b) to resample the Middle Eocene sandstone. This new sample, L-GC777-9, yielded at least 20 datable grains and 11 zircons. Finally, sample L-GC777-2 (Upper Cretaceous sandstone) yielded 17 datable apatites and seven datable zircons (Green, 2001b).

Discussion

The Middle Eocene sandstone yielded enough datable apatites for AFT analysis. On the contrary, the Eocene sandstones in nearby wells 26/26-1 and 34/05-1 yielded very few apatites. The difference in yields is probably due to a difference in depositional settings. The apatite-poor sandstone might have experienced an extended period of time in a flood plain during a low stand, where the apatites were exposed to sustained weathering and dissolution; on the contrary, the apatite-rich sandstones might have been deposited directly into a marine setting without an extended period of flood plain residence, possibly during a high stand (Morton et al., 2012). The apparent absence of apatite and rarity of zircons in the Lower Eocene siltstone is probably due to grain size. The Upper Cretaceous

sandstone yielded some apatite and many zircons. The good apatite yields from the Middle Eocene and Upper Cretaceous sandstones in the legacy study were not replicated in the new sampling undertaken for this study, possibly due to a thinner sampling interval of the Middle Eocene sandstone but without apparent explanation for the Upper Cretaceous sandstone.

5.2.5.3 Apatite U/Pb and trace element results

Only one U/Pb age and trace element signature was obtained for both samples R-3 and R-5, which is not statistically significant for U/Pb dating and trace element characterisation. No U/Pb or trace element analyses are available for the legacy samples.

5.2.5.4 Zircon U/Pb results

The detailed analysis of the results are presented in ANNEX 1 SECTION 1.2.1 and discussed in this section.

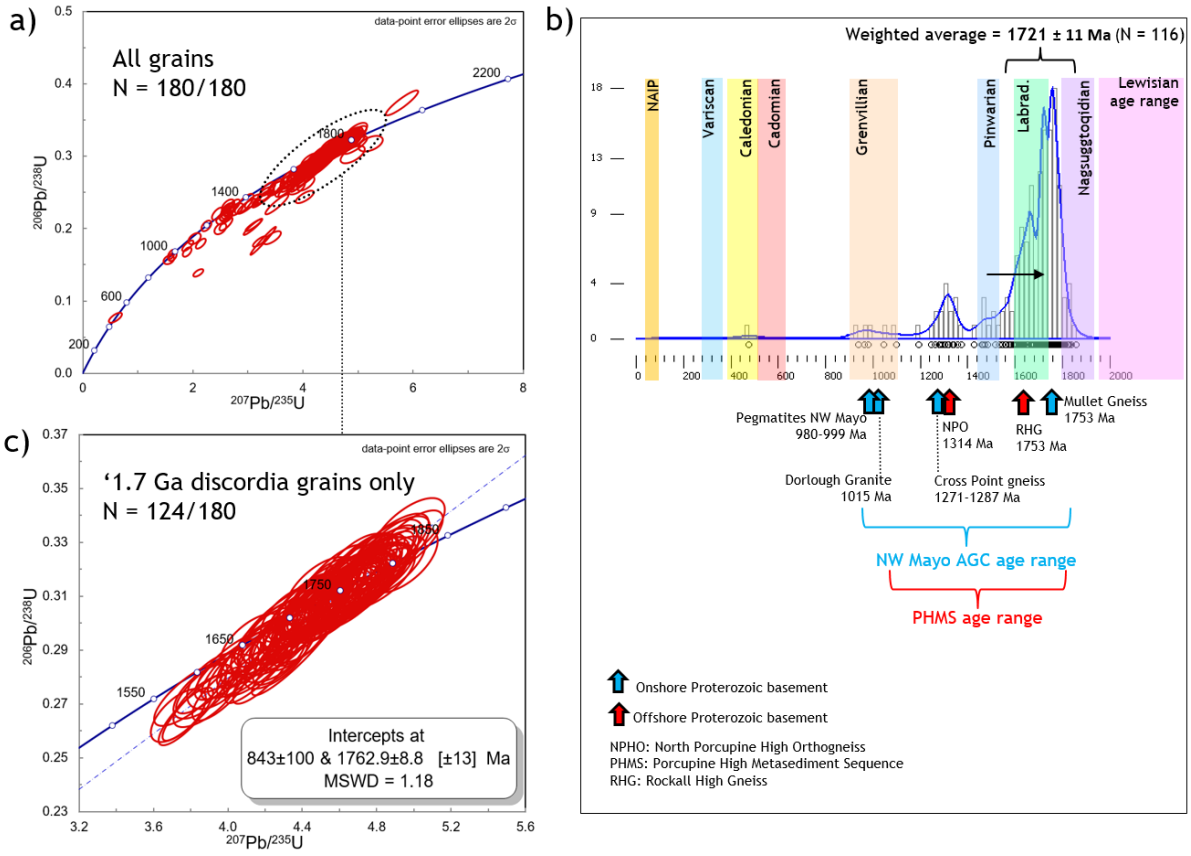

Figure 36: Zircon U/Pb results for sample R-5 (16/28-sb01). a) Wetherill plot, b) Density plot and KDE function for concordant grains only, and ages of the main Precambrian basement units offshore and onshore west of Ireland c) Wetherill plot of all the c. 1.7 Ga grains that align on a discordia and discordia ages.

Provenance of the Upper Cretaceous sandstone (sample R-5)

The zircon age spectrum of the Upper Cretaceous sandstone is dominated by a c. 1.7 Ga source (c. 76%) but also has a contribution from a c. 1.3 Ga source (c. 10%), a 1.5-1.6 Ga source (c. 5%), a

Pinwarian (1.45-1.51 Ga) source (c. 5%), a Grenville source (c. 3%) and a very minor contribution from an Early Caledonian (Grampian) source (1 grain, <1%) (FIGURE 36).

The 1.3 Ga source is probably the North Porcupine High Orthogneiss (NPHO) which crops out only 40 km to the south (up dip, FIGURE 37).

The c. 1.7 Ga source (FIGURE 36) is similar in age to the Mullet Gneiss in onshore NW Co. Mayo (1753 Ma) (FIGURE 37). The Mullet Gneiss belongs to the Annagh Gneiss Complex which also comprises c. 1271-1287 Ma gneisses, a 1015 Ma granite and c. 980-999 Ma pegmatites (Daly, 1996). Gneisses with similar ages (U/Pb zircon ages of 1.5-2.02 Ga) were also found in dredges on the northern edge of the North Porcupine High (Chew et al., 2019) (FIGURE 37). The presence and predominance of these c. 1.7 Ga grains in the sandstone reinforces the hypothesis that such a 1.7 Ga basement unit, equivalent to the Annagh Gneiss Complex (AGC), does indeed crop out on the North Porcupine High. The suspected outcrop of Proterozoic gneisses and granites equivalent in age to the AGC, but probably located on the NW side of the North Porcupine High is here named the 'Porcupine High Gneiss Complex' (PHGC). The PHGC must be located north of the assumed terrane boundary defined by a magnetic anomaly boundary (SEE SECTION 5.5.2.4 BELOW) and NW of the North Porcupine High crest (see dotted orange circle in FIGURE 37).

A Pb isotopic analysis of detrital K-feldspar from the same sample also revealed a basement source of Proterozoic affinity (Tyrrell et al., 2007) which is in accordance with the new zircon U/Pb data described above.

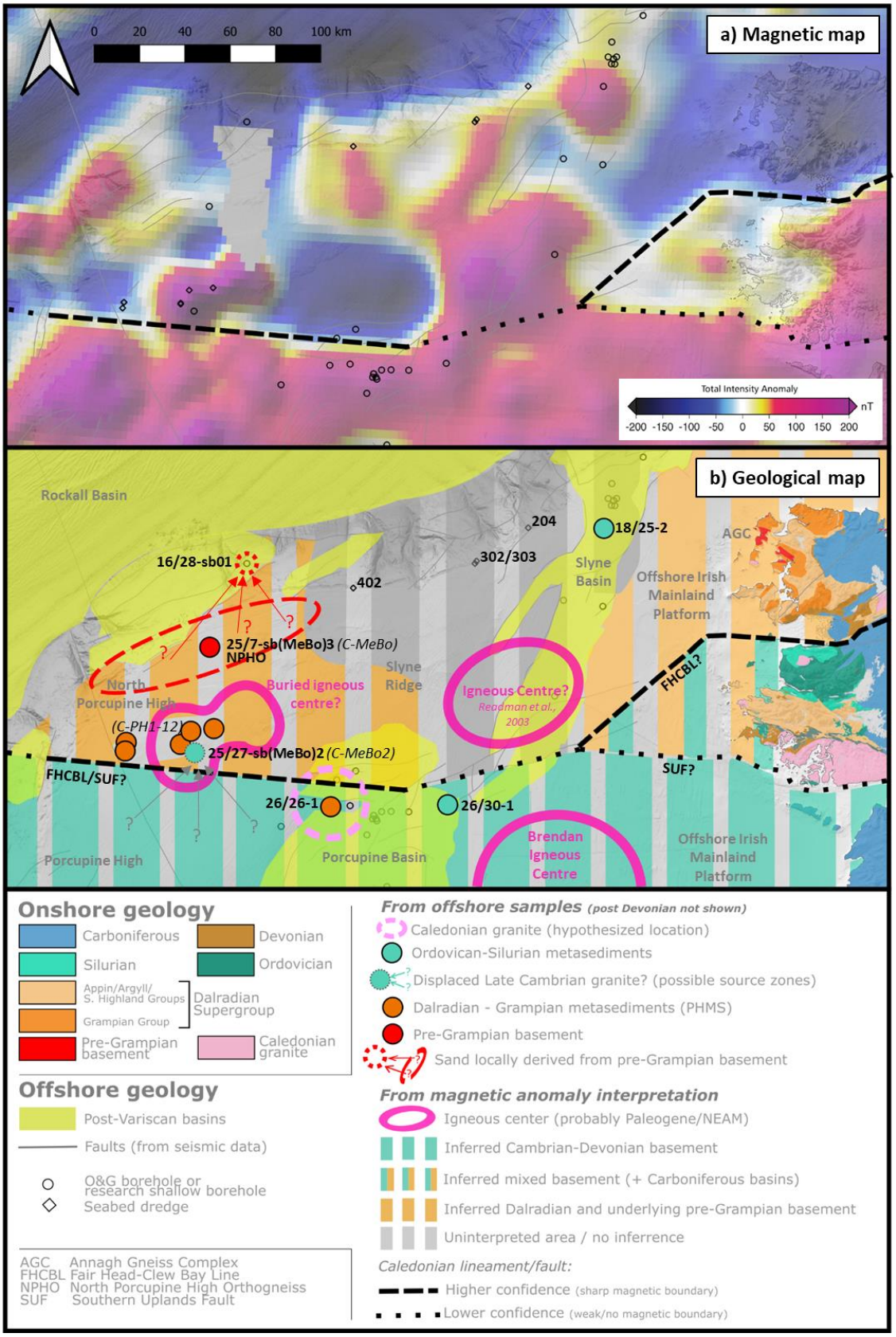

Figure 37: Magnetic and geological basement map of the North Porcupine High-Slyne Ridge area. a) Observed magnetic field over the Irish Continental Shelf (NOAA EMAG2: Earth Magnetic Anomaly Grid - 2-arc-minute resolution) overlain by offshore borehole and dredge locations. Background map: EMODnet (European Marine Observation and Data Network) bathymetry and topographic greyscale map. b) Geological basement map of the area based on the interpretation and correlation of offshore borehole and dredge samples and the magnetic data. Same background map as in a).

The Pinwarian grains (FIGURE 36) are probably sourced from the Porcupine High Metasedimentary Sequence (PHMS) which crop out on the summit of the Porcupine High to the south (FIGURE 37). The PHMS would also have contributed grains of Labradorian and Grenville ages. Based on the relative proportion of Grenville and Labradorian ages in comparison to Pinwarian ages in the PHMS (Tyrrell, 2013), it is likely that all the Grenville grains in R-5 are sourced from the PHMS (as opposed to c. 1 Ga granites and pegmatites in the PHGC) and that c. 10-15 Labradorian grains (out of c. 100+ grains) are also sourced from the PHMS (FIGURE 36).

The Caledonian grain could either be a very minor contribution from a more distant source or else a caving from the Eocene to Recent sands above (FIGURE 38). The absence of Cadomian and Archean grains and rarity of Caledonian grains indicate that the source of this Upper Cretaceous sand was probably local and restricted.

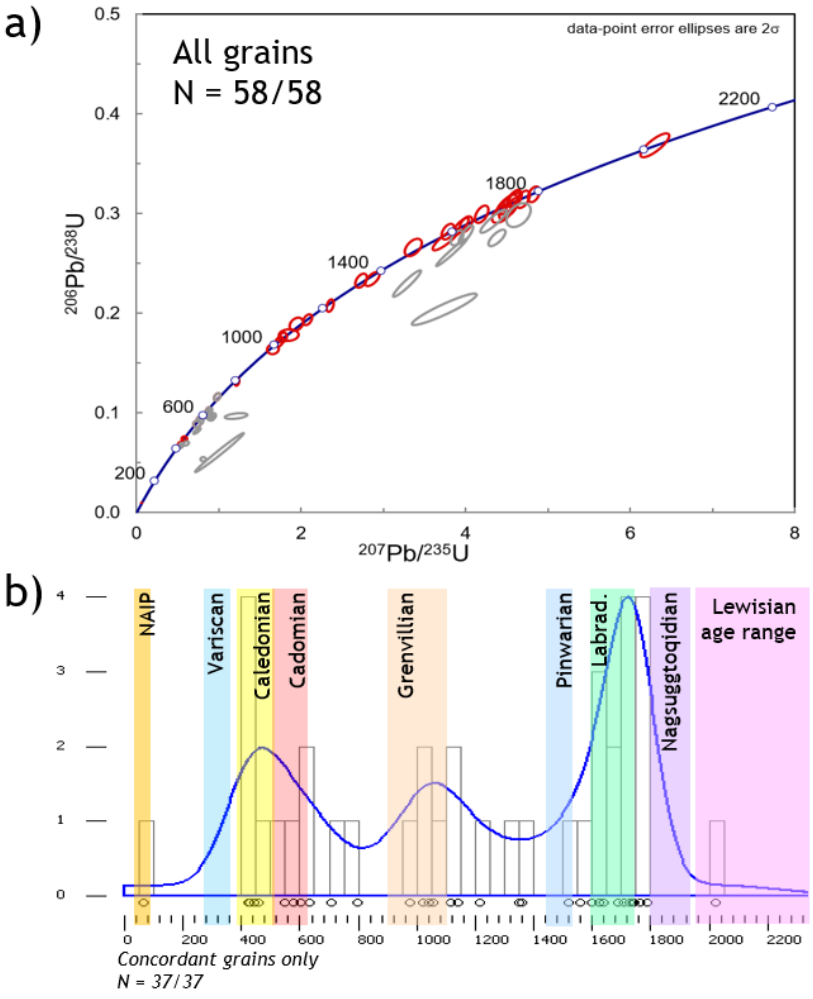

Figure 38: Zircon U/Pb results for sample R-3 a) Wetherill plots, b) Density plots and KDEs

In conclusion, the Upper Cretaceous sandstone is probably sourced from an outcrop of Proterozoic basement which comprises rocks (probably gneisses and granites) with an age of c. 1.7 and 1.3 Ga.

This outcrop is probably located on the NW flank of the NPH (FIGURE 37) where a c. 1.3 Ga gneiss (the NPHO) has previously been identified (Daly et al. (2008c), Chew et al. (2019)) and c. 1.5-2.02 Ga gneiss complex equivalent to the AGC was also suspected (Chew et al., 2019). The dominance of c. 1.7 Ga grains in this locally sourced Upper Cretaceous sandstone confirms that such an AGC equivalent is indeed present on the NW flank of the North Porcupine High. A minor contribution from the PHMS metasediments is also inferred due to the presence of a small amount of Pinwarian grains. The absence of Cadomian, Archean and rarity of Caledonian grains indicate that at the time of deposition the area was likely disconnected from the Irish Offshore Mainland Platform and onshore west of Ireland. Most of the area was probably under water and covered with carbonates which restricted the source of clastic sediments to only some paleo-highs, of which the North Porcupine High must have been one.

Provenance of the Eocene sandstone

The Eocene sandstone has a much more diverse range of zircon U/Pb ages. The main peak is Labradorian in age (similar to the Upper Cretaceous sand) (FIGURE 38). The presence of a small peak of c. 1.3 Ga grains indicates that they probably shared the same local source, the PHGC. The greater abundance of Grenville grains probably indicates a more substantial contribution from the PHMS (the absence of Pinwarian grains could be due to a small population size bias). There is a large contribution of Caledonian and Cadomian grains which probably come from more distant sources, probably reworking from older sands from the offshore basins or from onshore west of Ireland (Nauton-Fourteu et al., 2020). One Paleogene grain indicates syn-depostional NAIP magmatism (or reworking of Paleocene sands with volcanic grains) and confirms the Paleogene age of the sand.

In conclusion, the zircon U/Pb ages of sample R-3 confirm that the sand is Paleogene in age and that it has a much wider range of sources, both local (North Porcupine High) and far travelled, than the Upper Cretaceous sandstone.

5.2.5.5 AFT results (Table 10 and Figure 39)

The legacy and newly acquired AFT data are described in ANNEX 1 SECTION 2.2.1 and a qualitative interpretation is given here. The samples are ordered from shallowest to deepest sampling depths.

Table 10: AFT and ZFT results.

AFT Results

Sample	Depth		n	Ns	Ni	Area	U/Ca	P(χ^2)	Central Age	±1σ	Tracks	MTL	SD	SE	Inverse?	
	m MD	*m BSB*				*cm²*			*Ma*	*Ma*		*µm*	*µm*	*µm*	*FTA*	*FTL*
L-GC777-1	41	41	2	4	16	n/a	n/a	0.14	57.3	33.1	2	12.16	0.16	0.11	No	No
L-GC777-9	60.5	61	20	366	422	n/a	n/a	<0.01	180.6	21.1	82	13.68	1.06	0.16	Yes	Yes
R-3	89	89	1	8	n/a	1.43E-05	4.25E-02	n/a	126.8	45.3	1	6.70	0.00	0.00	No	No
R-4	136.5	136.5	0	-	n/a	-	n/a	n/a	-	-	-	-	-	-	No	No
R-5	147	147	1	43	n/a	2.64E-05	1.50E-01	n/a	104.5	16.7	1	12.9	0	0	No	No
L-GC777-2	147	147	17	445	640	n/a	n/a	0.51	161.7	11.3	43	13.31	1.51	0.17	Yes	Yes

ZFT Results (Green, 2000)

Sample	Grains	Age	±1σ	Age type
		Ma	*Ma*	
L-GC77-9	11	260	23	Pooled age
L-GC77-2	7	245	43	Central age

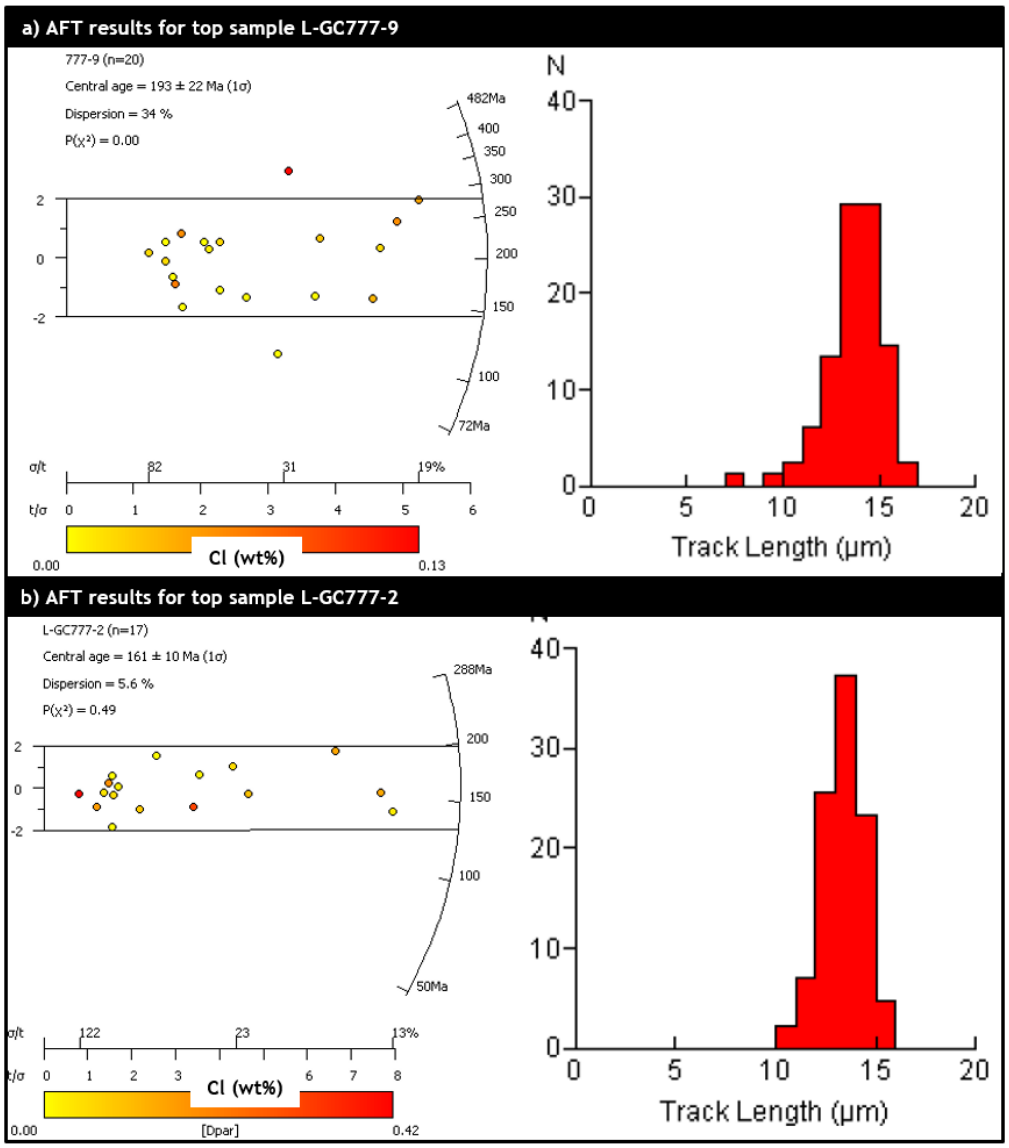

Figure 39: AFT results for legacy samples L-GC777-9 and L-GC777-2, after Green (2001b).

5.2.5.6 Discussions

The new sampling failed to produce new AFT and AHe data. Both legacy apatite and zircon fission track ages are older than the stratigraphic age of the samples. This older age indicates that the samples did not experienced temperatures greater than c. 100°C since at least the Late Cretaceous (FIGURE 39).

5.2.6 Thermal history modelling of the AFT data

5.2.6.1 Input data

The apatites and zircons from the Middle Eocene and Upper Cretaceous sandstones do not necessarily share the same detrital source. Moreover, the old ZFT age cannot be used to unravel the post-Cenomanian thermal history. Therefore, the AFT and ZFT data have been modelled independently of each other.

Only samples L-GC777-9 and L-GC777-2 have enough apatite fission track data to be used for inverse modelling purposes. Both samples meet the minimum requirements for both AFT ages (>= 10 ages) and track lengths (>= 25 lengths). These samples do not have any AHe data and no VR data is available for any section of the borehole.

5.2.6.2 Initial and final time-temperature constraints

Final conditions: Present-day temperature of samples

This shallow borehole does not have any temperature data. The best estimate for the geothermal gradient at this location is from the closest borehole, 26/26-1, which has a geothermal gradient of 28.34 ± 5.3°C.km^{-1}. Using this gradient and a seabed temperature of 5°C, sample L-GC777-9 has a present-day temperature of 6.71 ± 0.32°C, while sample L-GC777-2 has a temperature of 9.17 ± 0.78°C (FIGURE 40A).

Initial conditions - Emplacement age and temperatures

L-GC777-9 and L-GC777-2 are detrital samples therefore the temperature at the time of deposition is defined at 10 ± 10°C. The depositional age of sample L-GC777-9 is 42.8 ± 5 Ma (Middle Eocene) (FIGURE 40A). As discussed in section 5.2.3, the deposition age of sample L-GC777-2 is either Late Cretaceous, *i.e.* 83.25 ± 17.25 Ma (Harrington et al. (2000), Haughton et al. (2005)) or possibly Cenomanian, 97.2 ± 3.3 Ma (Stoker, 1999). The Late Cretaceous age is the most conservative hypothesis and will be the age constraint employed in most models. The Cenomanian age will be tested as an alternative hypothesis in one model (FIGURE 40A).

5.2.6.3 Intermediate constraints

Time-temperature constraint boxes can be added to the model based on stratigraphic or external thermal indicator constraints (e.g. VR-derived Tmax). In QTQt, in the case of modelling a vertical

profile, constraints only apply to the topmost sample (so L-GC777-9 until the Middle Eocene and then L-GC777-2 until Recent).

Burial constraints from stratigraphy

For all models

Sample L-GC777-2 is located at a depth range of 147 mMD. The Lower Eocene claystone is at a depth range of 88.58-145.95 m BSB corresponding to an average depth of 117.3 mMD. Consequently L-GC777-2 was at a depth of 111.5 m at some point during the Early Eocene and at a depth of c. 29.7 m at some point during the Lower Eocene (47.8-56 Ma or 51.9 ± 4.1 Ma). Using the present-day geothermal gradient and a seabed temperature of 10 ± 10°C, this depth of 29.7 m corresponds to a paleotemperature of 10.8 ± 10°C. Therefore a QTQt constraint box can be created with an x-axis of 51.9 ± 4.1 Ma and a y-axis of 10.8 ± 10°C (FIGURE 40A).

Sample L-GC777-9 is located at a depth range of 41-80 mMD, so an average depth of 60.5 mMD. The Late Pliocene-Quaternary clastics are at a depth range of 0-14.45 mMD corresponding to an average depth of 7.2 mMD. Consequently L-GC777-9 was at a depth of 53.3 m at some point during the Late Pliocene-Quaternary (0-3.6 Ma or 1.8 ± 1.8 Ma). Using the present-day geothermal gradient and a seabed temperature of 5 ± 5°C (since the Plio-Pleistocene seabed conditions can be assumed to be similar to present-day conditions), this depth of 53.3 m corresponds to a paleotemperature of 6.5 ± 5°C. Therefore a QTQt constraint box can be created with an x-axis of 1.8 ± 1.8 Ma and a y-axis of 6.5 ± 5°C (FIGURE 40A).

For models with basal sample dated as Cenomanian

For these models, in addition to the two constraints described just above, an additional constraint can be created using the Maastrichtian marls. The Maastrichtian silty marl is located at a depth range of 145.95-146.5 m BSB corresponding to an average depth of 146.5 ± 0.3 m BSB. Consequently, L-GC777-2 was at a depth of c. 0.5 m during the Maastrichtian (69.05 ± 3.05 Ma). At that time, the sample must have been at the seabed temperature, which is estimated at 10 ± 10°C. Therefore for these models, a QTQt constraint box can be created with an x-axis of 69.05 ± 3.05 Ma and a y-axis of 10 ± 10°C (FIGURE 40A).

5.2.6.4 Prior box and run parameters

For all models, the prior box is defined at 193.41 ± 193.41 Ma for the x-axis and 70 ± 70°C for the y-axis. Except when stated otherwise, the geothermal gradient of 28.34°C.km^{-1} is kept constant throughout the thermal history (*i.e.* the temperature gap between the two samples always remains the same between models and does not change with time within a single model) (FIGURE 40B).

a) Scenario constraints

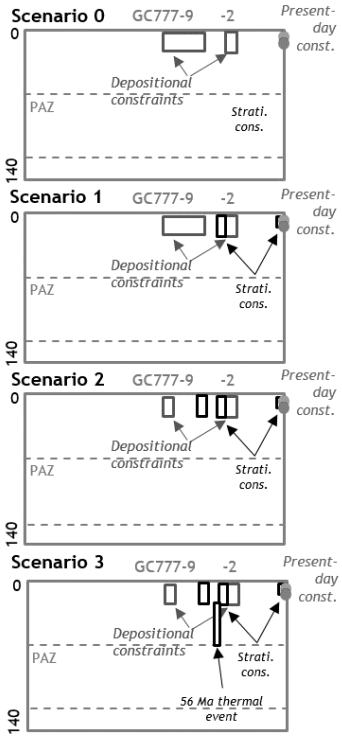

b) Prior information and MCMC chain parameters

Categories		Values
Prior information	Time Temperature	193.41 ± 193.41 Ma 70 ± 70 °C
	Max dT/dt Reheating Temperature offset Offset	1000 °C.My Yes 2.46 °C Constant
MCMC chain	Burn-in Post-burn-in Thinning	100,000 100,000 1
Proposed move	Time Temperature Offset Resample/Reject Reject complex	30 30 0.001 Resample Yes

c) Model names and characteristics

Scenario	Samples	Inputs	Age of bottom sample	Const.	Geoth. Grad.	tT points
0a 0b	Both	Age + lengths	Late Cretaceous	None	Constant	Low (Simple) High (Complex)
1a 1b	Both	Age + lengths	Late Cretaceous	2	Constant	Low (Simple) High (Complex)
2a 2b	Both	Age + lengths	Cenomanian	3	Constant	Low (Simple) High (Complex)
3a 3b	Both	Age + lengths	Cenomanian	4	Constant	Low (Simple) High (Complex)

Figure 40: Parameters and constraints for the thermal history inverse modelling.

5.2.6.5 Modelling scenarios

Several geological scenarios have been run with a variable number of constraints and input data (FIGURE 40A AND FIGURE 40C). This approach allows a better discrimination of which input data (either FT ages, track lengths or time-temperature constraints) control certain aspects of the modelled thermal histories. Summaries of the results of each modelling run with predictions are available in ANNEX 2. Both simple and complex models were run for all scenarios.

5.2.6.6 Modelling results

All the models yielded convergent log likelihood and posterior chains (*i.e.* no trend in post-burn-in models) (FIGURE 41).

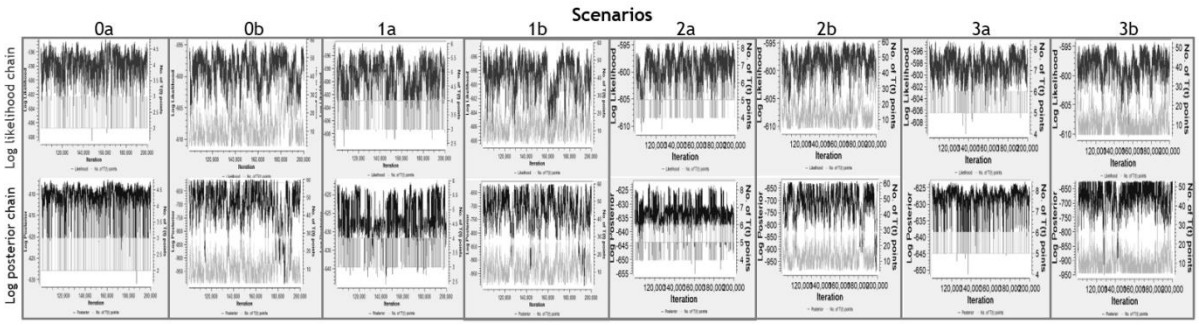

Figure 41: Log likelihood and log posterior chains. All chains are stable.

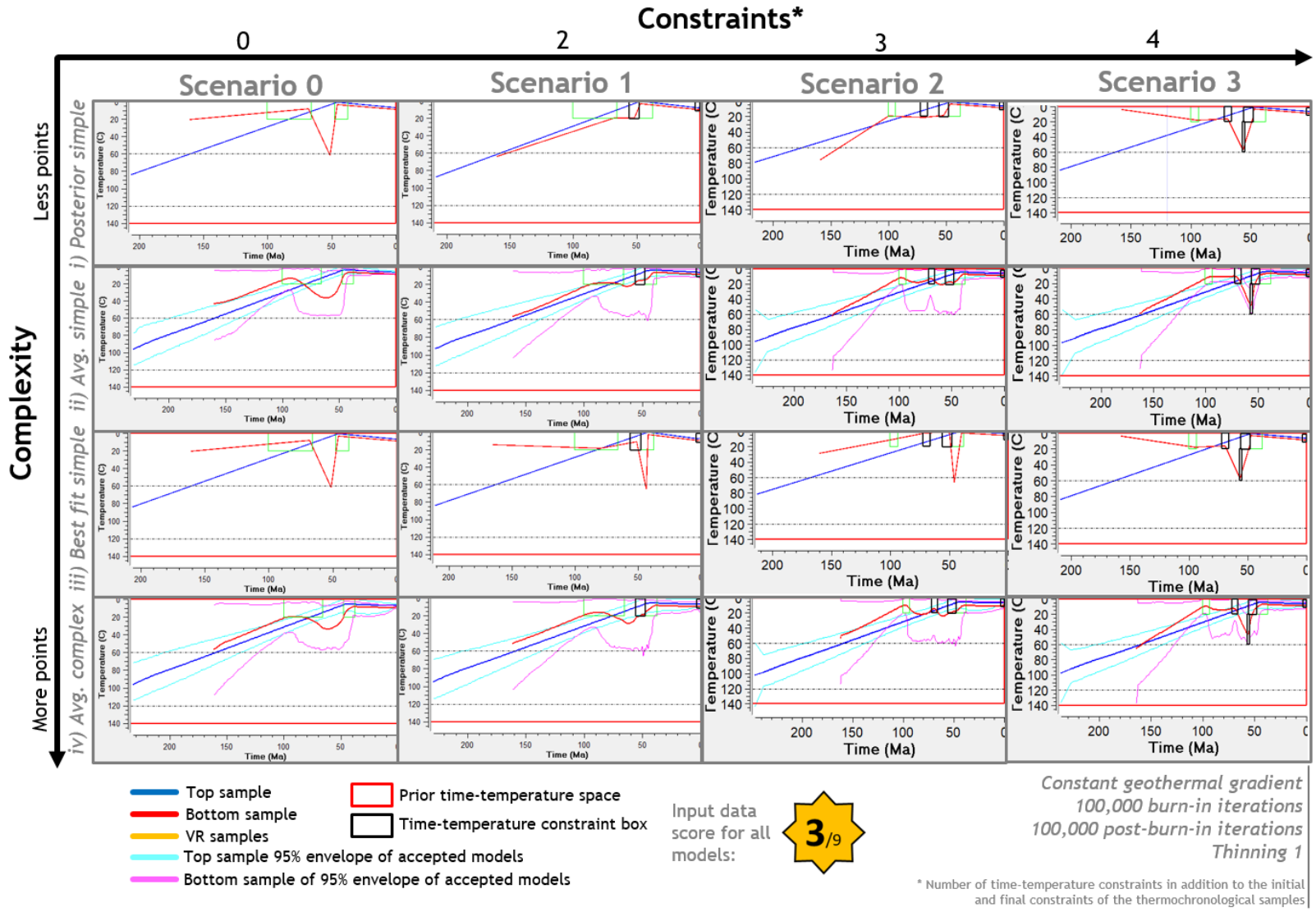

Figure 42: Summary of the various inverse modelling results.

Scenario 0: No intermediate constraint

This scenario is run to evaluate the information contained in the AFT alone, independent of any geological assumptions about the temperature of the sample at any point in time except for the initial and final conditions. Therefore this model does not include any intermediate time-temperature constraint (FIGURE 40A AND FIGURE 40C).

All models show that between the Late Cretaceous and Middle Eocene, the bottom sample must have experienced heating to c. 60°C. After the Middle Eocene, the samples remained close to surface-temperatures with possible monotonic heating (burial) to present-day temperatures (FIGURE 42). The peak to 60°C affecting the basal sample is constrained by the MTL and the track length distribution.

Scenario 1: Two stratigraphy-based constraints

This scenario is like the previous one but with the two intermediary constraints provided by the stratigraphic data (FIGURE 40A AND FIGURE 40C).

The results are almost identical to the previous scenario with most thermal histories having a temperature peak up to c. 60°C. Depending on the scenarios, the peak occurs at any time between the Late Cretaceous and the Maastrichtian, but the highest likelihood model has a peak that occurs between the Early and Middle Eocene (FIGURE 42).

Although most models have such a peak, the thermal history of the posterior model does not show any significant heating between the Late Cretaceous and the Middle Eocene (only up to 20°C). Despite the lack of heating, there is still an acceptable match between the modelled and measured FT ages and track lengths. The modelled MTL for the bottom sample in this scenario is 13.65 µm for a measured MTL of 13.31 µm, while the likelihood scenario, with the heating peak to 60°C, yields a modelled MTL of 13.43 µm (ANNEX 2).

Scenario 2: Cenomanian sandstone

This scenario is identical to scenario 2 but this time the depositional age for the bottom sample is Cenomanian and there is an additional constraint based on the Maastrichtian marl to see the impact of the stratigraphic interpretation of Stoker (1999) on the thermal history (FIGURE 40A AND FIGURE 40C).

The new initial and intermediate constraints do not affect the modelled thermal histories that are almost identical to the previous scenario (FIGURE 42).

5.2.6.7 Discussion

Late Cretaceous-Eocene thermal history

During the Late Cretaceous to Eocene times most models show one episode of heating to a maximum of c. 60°C followed by cooling to surface temperatures. However, a few models that still fit reasonably

well to the observed thermochronological data do not have this peak and the bottom sample remains at near-surface temperatures at all times (FIGURE 42).

The heating and subsequent cooling could be due to either burial and erosion or magmatism-related conductive or advective heating. In the case of the burial and uplift hypothesis, using a minimum and maximum paleo-surface temperature of 0°C and 20°C and the assumed present-day geothermal gradient, this maximum temperature of 60°C translates to a burial under c. 1.4 to 2.1 km of sediments during the Late Cretaceous and Paleocene. Consequently, during this period, the thermochronology data allow for burial followed by uplift and erosion of c. 0-2 km of sediments.

Timing and cause of the heating peak

If the heating occurred between the Early and Middle Eocene, the burial and erosion hypothesis is hard to reconcile with regional geology since at that time no episodes of significant uplift and erosion has been recognized in the North-East Atlantic Margin (NEAM) (e.g. Praeg et al. (2005)). It is more likely that such uplift occurred at the Cretaceous-Paleocene boundary or at the Paleocene-Eocene boundary which are known unconformities in the NEAM (Praeg et al., 2005).

Magmatism-related conductive or advective heating would probably be related to the North Atlantic Igneous Province magmatism (NAIP). This magmatism extended mainly from c. 64 Ma to c. 35 Ma (with possibly a few younger intrusions as young as 20 Ma) but the bulk of magmatism occurred around the time of the break-up of the North-East Atlantic between c. 60 Ma and 50 Ma (Wilkinson, 2016). However, most magmatism in the British Tertiary Igneous Province (BTIP), a sub-province of the NAIP to which offshore Ireland is spatially close, occurred during the pre-break-up phase between c. 64 Ma and 56 Ma. Therefore, while it is possible that magmatism-related heating occurred between the Early and Middle Eocene, it is more likely that such heating occurred between the Paleocene and earliest Eocene.

Therefore, for both the burial and magmatism hypotheses, a pre-Early Eocene timing is more likely. The hypothesis that the thermal event occurred at the Paleocene-Eocene boundary (either due to Paleocene burial and Paleoecene-Eocene boundary uplift or Paleocene-Eocene boundary magmatism) has been tested in a third modelling scenario where an additional time-temperature constraint has been placed at 56 ± 1 Ma with a temperature range of 40 ± 20°C (scenario 3, FIGURE 40).

In this scenario, most thermal histories (including the posterior and likelihood models) show gradual heating up to 60°C between the Maastrichtian and 56 Ma, followed by rapid cooling during the Early Eocene. The rates of heating and cooling in the models point towards burial and erosion rather than thermal pulses caused by magmatism. However, a much more rapid heating and cooling event (< 1

Ma) caused by magmatism could also lead to shorter track lengths as observed in the samples if the temperature is greater than 60°C. Therefore the magmatic hypothesis cannot be discarded.

Timing of the short-lived hot fluid pulses

Despite the higher likelihood for a pre-Eocene uplift or magmatic event, the fluid inclusion homogenization temperatures described in SECTION 5.2.4.2 actually support a scenario of pre- and post-Middle Eocene advective heating.

Indeed, the hot fluids might have been related to the NAIP since the magmatic activity occurred during the Paleocene-early Eocene and possibly extended to the earliest Miocene (Wilkinson, 2016). The presence of inclusions with high homogenization temperatures in the Middle Eocene support the hypothesis that syn- or post-Middle Eocene NAIP magmatism occurred in the area (although such late magmatism in the region is not abundant as discussed above in the previous section). Consequently, NAIP-related hydrothermal fluids could have precipitated the cements in both the Upper Cretaceous and Middle Eocene sandstones.

The 'hot' fluid inclusions in the Middle Eocene sandstone have temperatures that range from c. 90 to 144°C while the fluid inclusions in the Upper Cretaceous sandstone have temperatures that range from c. 80 to 200°C (TABLE 9). It is possible that the lower maximum temperature in the Middle Eocene sandstone compared to the Upper Cretaceous sample is a reflection of the decrease in magmatic activity between the Paleocene and earliest Eocene (highest activity so more likely to reach higher temperatures) and the post-Early Eocene (lower activity so less likely to reach high temperatures).

If these hot fluid pulses were active for period of times greater than 0.1 Ma, they would have partially annealed the apatite fission track lengths. The earlier hypotheses that the thermal event observed in the models could be due to magmatism-related heating with temperatures greater than 60°C is therefore supported by the fluid inclusion homogenization temperatures.

Eocene to present-day thermal history

All models from all scenarios agree that the samples remained at near-surface temperatures since the Eocene (< 20°C). However, the AFT data does not place constraints on thermal histories below c. 60°C so a small amount of heating between 20 and 60°C (*i.e*. burial by up to c. 2 km of sediments) would still be theoretically possible but not detected by the thermochronology data at hand.

5.2.7 Thermal history modelling of the ZFT data

5.2.7.1 Rationale

The ZFT data do not provide thermal history information for the Upper Cretaceous and Eocene sandstones, but rather provide thermal information about the sources of these sands. Only the Upper

Cretaceous sandstones have a well-constrained source which is believed to be a Proterozoic gneiss complex on the NW flank of the North Porcupine High (see SECTION 5.2.5.4). Therefore the ZFT data can be used to characterize the thermal history of the NW flank of the NPH (or a part of it). The ZFT data from the Eocene sample are not modelled because of the large degree of uncertainty on the potential sources for this sample.

5.2.7.2 Input data

Only seven ZFT ages are available for sample L-GC777-2. When modelling AFT data, only samples with more than 10 AFT ages are used because a low number of AFT grains may not be representative. However, an exception is made for this ZFT dataset since it is a valuable opportunity to obtain higher temperature thermal history information for the Porcupine High.

5.2.7.3 Time-temperature constraints

There are no U/Pb age data for the zircons from the ZFT study. Hence the ZFT dataset of sample L-GC777-2 have been modelled using a maximum initial age constraint of 470 Ma which is much older than the ZFT pooled age (c. 260 Ma). This 470 Ma constraint is older than the oldest individual grain ZFT age (c. 440 Ma) and corresponds to a regionally important geodynamic event (the Grampian phase of the Caledonian Orogenic Cycle). An older age could be selected (e.g. 1.7 Ga, the main zircon U/Pb age peak of sample R-5 from the same sandstone unit) but it would increase greatly the x-axis (time) of the prior box without providing any useful thermal history information since all the ZFT ages are all <500 Ma. The initial temperature constraint is defined as 200 ± 200°C. The final temperature constraint is similar to that employed for the AFT modelling (9.17 ± 0.97°C).

5.2.7.4 Model parameters

The modelling was done with 50,000 burn-in iterations and 50,000 post-burn-in iterations with a prior box defined as 235 ± 235 Ma and 200 ± 200°C. Complex models were rejected.

5.2.7.5 Modelling results

The models show that the thermal history is poorly constrained. However, two observations can be made:

- The zircons did not experience temperatures greater than 300°C since 220 Ma
- It is likely that the zircons were at a temperature of c. 275 ± 25°C at 250 ± 50 Ma (Permian-Triassic. This is shown by the higher relative probability of time-temperature paths within that temperature-time window as shown in FIGURE 43.

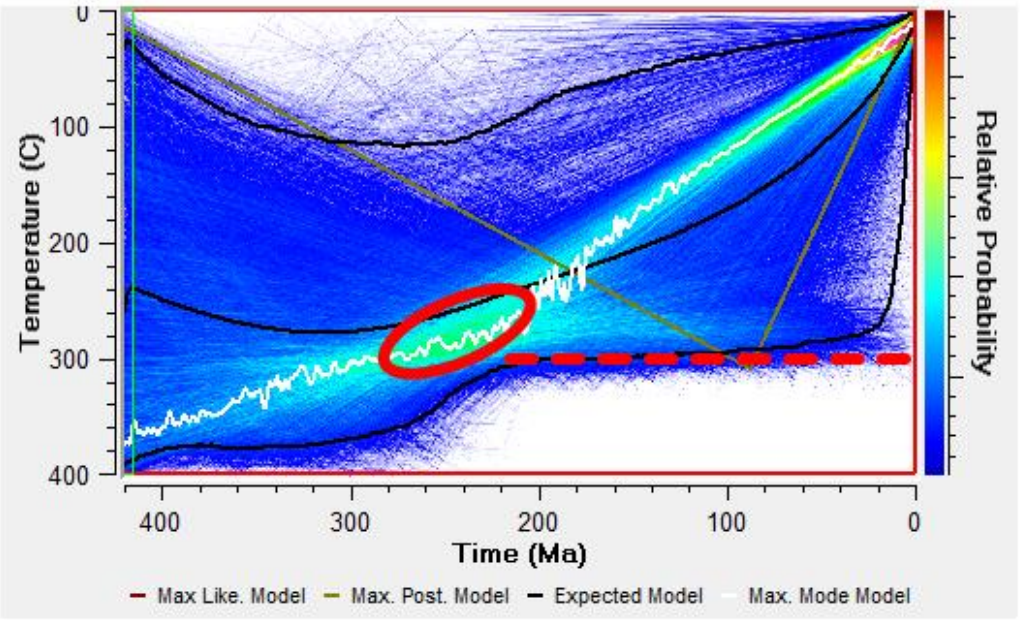

Figure 43: ZFT thermal history modelling of sample L-GC777-2 (Upper Cretaceous sand).

5.2.7.6 Discussion

The modelling indicates that the rocks that crop out on the NW flank of the North Porcupine High that were the source for the Late Cretaceous sandstones in 16.28-sb01 probably experienced temperatures of 250-300°C during the Permian-Triassic but less than 300°C after the Triassic.

The high temperatures during the Permian-Triassic could be due to either:

- Gradual post-Variscan exhumation of the basement (from temperatures higher than 300°C before the Permian to temperatures lower than 300°C after the Triassic); or
- Burial during Permian-Triassic rifting associated with higher paleogeothermal gradients due to Late Variscan magmatism and/or Permian-Triassic rifting).

A multi-proxy provenance study of Triassic sandstones from boreholes in the Slyne Basin suggests that the sands were partly sourced from the North Porcupine High (Franklin et al., 2019), which would supports the first hypothesis (gradual post-Variscan exhumation) rather than the second one (Triassic burial).

Using a paleogeothermal gradient of 30 and 60°C.km^{-1}, these temperatures would corresponds to burial depths of 5 to 10 km. Alternatively, the rocks may have been shallower but heated by hydrothermal fluids or the thermal effects of an intrusion (e.g. Late Variscan magmatism).

5.2.8 Conclusions

5.2.8.1 Thermal history

The modelling of the AFT data combined with legacy fluid inclusion temperature data leads to the following conclusions:

1) The pre-Late Cretaceous thermal history is poorly constrained but a maximum erosion rate of c. 48 $m.My^{-1}$ is allowed for the Mesozoic syn-rift exhumation (assuming monotonic cooling and erosion).
2) Between the Late Cretaceous and Middle Eocene the area was subject to either:
    a. Burial under up to 2 km of sediments and subsequent erosion during uplift events, probably at the Cretaceous-Paleocene boundary and/or at the Paleocene-Eocene boundary, or;
    b. Multiple pulses of hot fluid flows related to the NAIP magmatism that probably occurred mostly during the Paleocene to Early Eocene but at least until the Middle Eocene and up to the earliest Miocene, or;
    c. A combination of the two mechanisms above.
3) During the Middle Eocene to present-day, the models do not show any significant heating but deposition and erosion of a maximum of up to c. 2 km of sediments is theoretically possible.

5.2.8.2 Provenance

1) The newly acquired detrital zircon U/Pb ages for the Upper Cretaceous sandstone indicate that this sandstone was derived from a proximal source of Proterozoic basement, probably located on the NW flank of the Porcupine High.
2) The predominance of c. 1.7 Ga zircons confirms the presence of such a previously suspected Paleoproterozoic basement unit on the North Porcupine High.
3) The Proterozoic basement source is probably similar to the AGC and is named the 'Porcupine High Gneiss Complex' (PHGC).
4) Another minor source was probably the PHMS, located on the summit of the high
5) The North Porcupine High was probably one of the rare topographic high in the region that were still above water during the Late Cretaceous.
6) The Eocene sandstone likely represents a mixture of proximal (North Porcupine High PHGC and PHMS) and far travelled detritus (onshore basement and reworking of offshore and onshore sediments).

5.2.8.3 ZFT data

The identification of the source of the Upper Cretaceous zircons on the NW flank of the North Porcupine High allows for the first time to use the ZFT data acquired by Geotrack to derive thermal history information about this source area.

Although there are no track length data and few ZFT ages, the thermal history modelling indicates that the Proterozoic basement that was cropping out during the Late Cretaceous probably experienced temperatures of 250-300°C at some point during the Permian-Triassic, either through burial at depths of 5-10 km, or through magmatism-related heating at shallower depths. The source area did not experience temperatures greater than 300°C since the Triassic.

5.3 Borehole 26/26-1

5.3.1 Exploration history and geological summary

Borehole 26/26-1 is a dry hydrocarbon exploration well drilled in 1981 by Shell to a depth of 1256 mMD. The well was drilled on Finnian's Spur, a tectonic high from extending the eastern margin of the Porcupine High towards the east and separating the northern part of the main Porcupine Basin from the North Porcupine Basin (FIGURE 33 AND FIGURE 44).

The first lithology encountered in the drilling of the well was c. 300 m of Cenozoic clastics, with a Lower-Middle Eocene sandstone (of terrestrial or coastal facies) at the bottom. This Eocene sandstone rests unconformably on top of c. 100 m Lower Cretaceous (Upper Hauterivian to Middle Barremian) marine limestone and basal marl and claystone. The Lower Cretaceous unit lies unconformably above 330 m of Carboniferous (Upper Tournaisian to Westphalian B-(C)) clastics and carbonates which in turn unconformably overlies c. 120 m of metasediments (biotite schists and feldspar gneisses) attributed to the Dalradian Supergroup (FIGURE 44 AND FIGURE 45). The metasediments have been described as tonalitic orthogneisses and yielded a Sm/Nd model age of 1810 Ma (Paleoproterozoic) (Daly 1990).

5.3.2 Top Carboniferous Unconformity (TCU) exhumation estimates

Using the legacy data, the amount of uplift and erosion associated with the TCU can be estimated using both a compaction-based method (sonic velocities) and a temperature-based method (VR) (Corcoran and Doré, 2005). Both methods yield estimates of the amount of uplift and erosion but no information about the timing of such uplift. The detailed analysis is provided in ANNEX 1 SECTION 3.2.

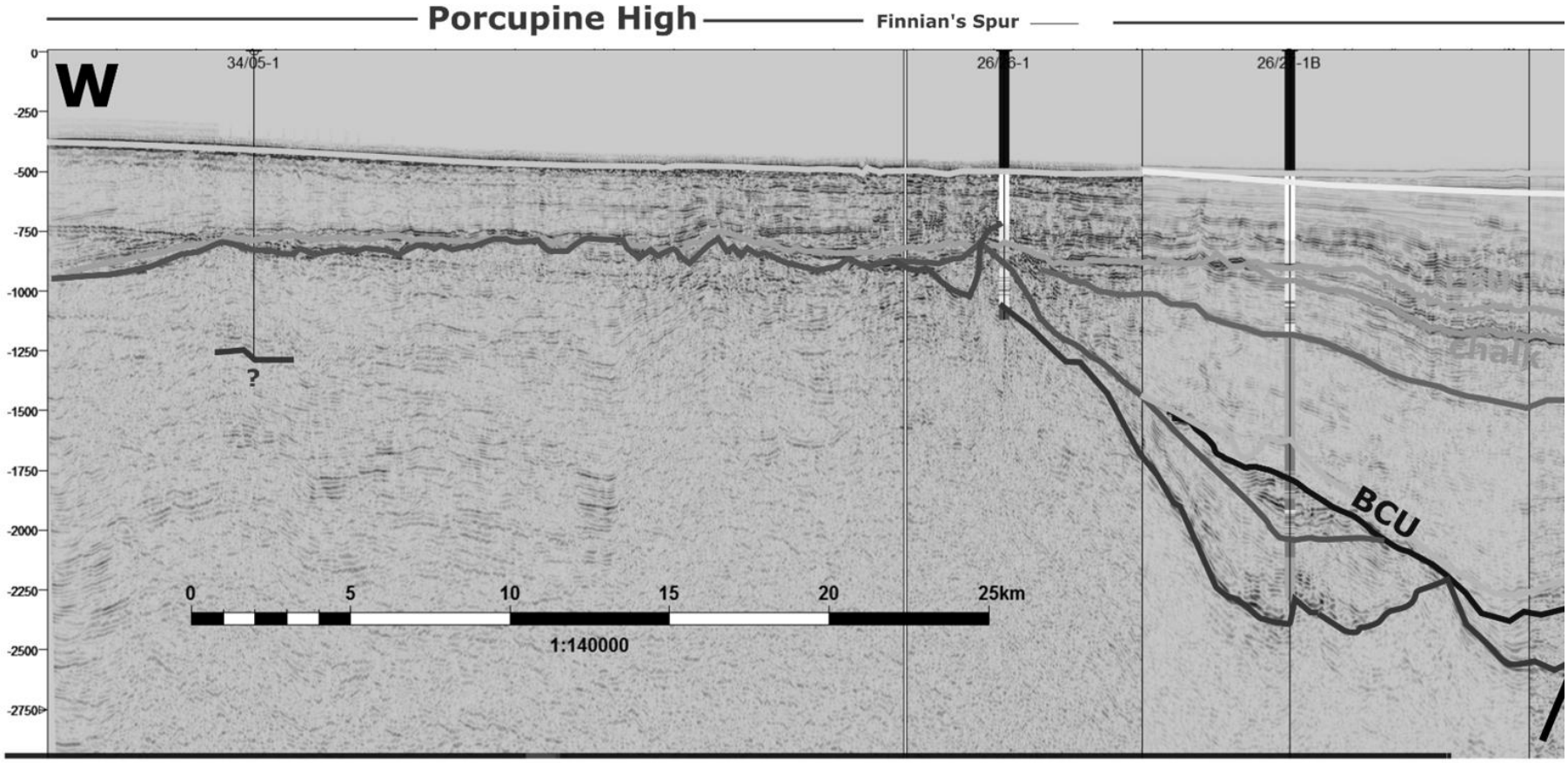

Figure 44: Seismic geosection of the North Porcupine Basin and border highs. BCU: Base Cretaceous Unconformity; LEU: Lower Eocene Unconformity, NeU (yellow): Neogene Unconformity, OMP: Offshore mainland platform.

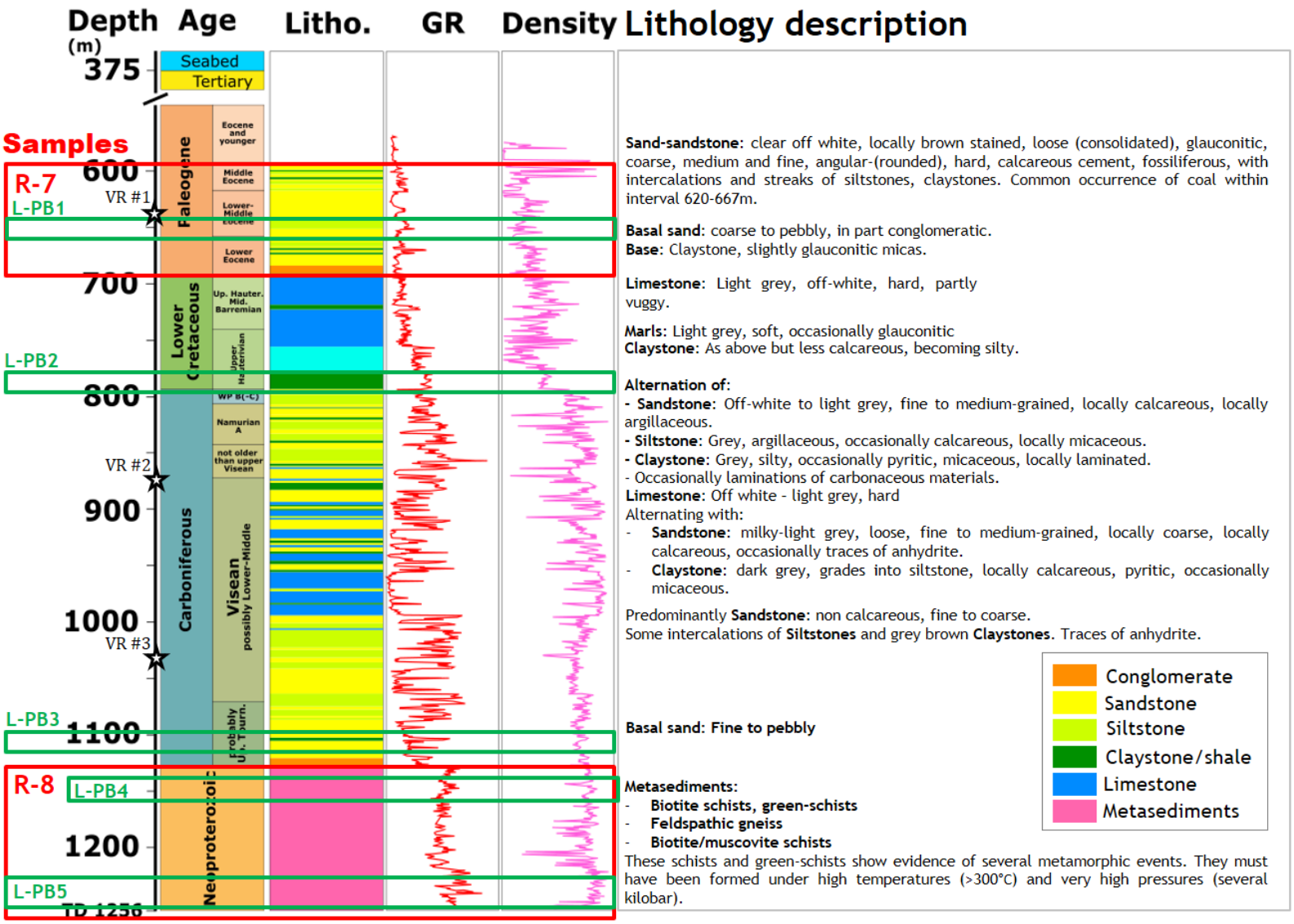

Figure 45: Well 26/26-1 logs, lithology description from composite log and sampling intervals (logs and lithology description from the composite log, Shell (1981)).

The pre-Cretaceous exhumation associated with the TCU is estimated to be c. 2000 ± $^{3000}_{1000}$ m with associated paleogeothermal gradients of c. 60 ± $^{75}_{40}$°C.km^{-1} (FIGURE 46). Two end-member scenarios are envisaged that could explain the data: 1) Peak temperatures were reached during the Late Carboniferous-Permian, associated with high geothermal gradients and lower denudation (1-2 km), or; 2) Peak temperatures reached during the Early Mesozoic rifting, associated with low to medium geothermal gradients and higher amount of pre-rift burial and syn-rift denudation (2-5 km).

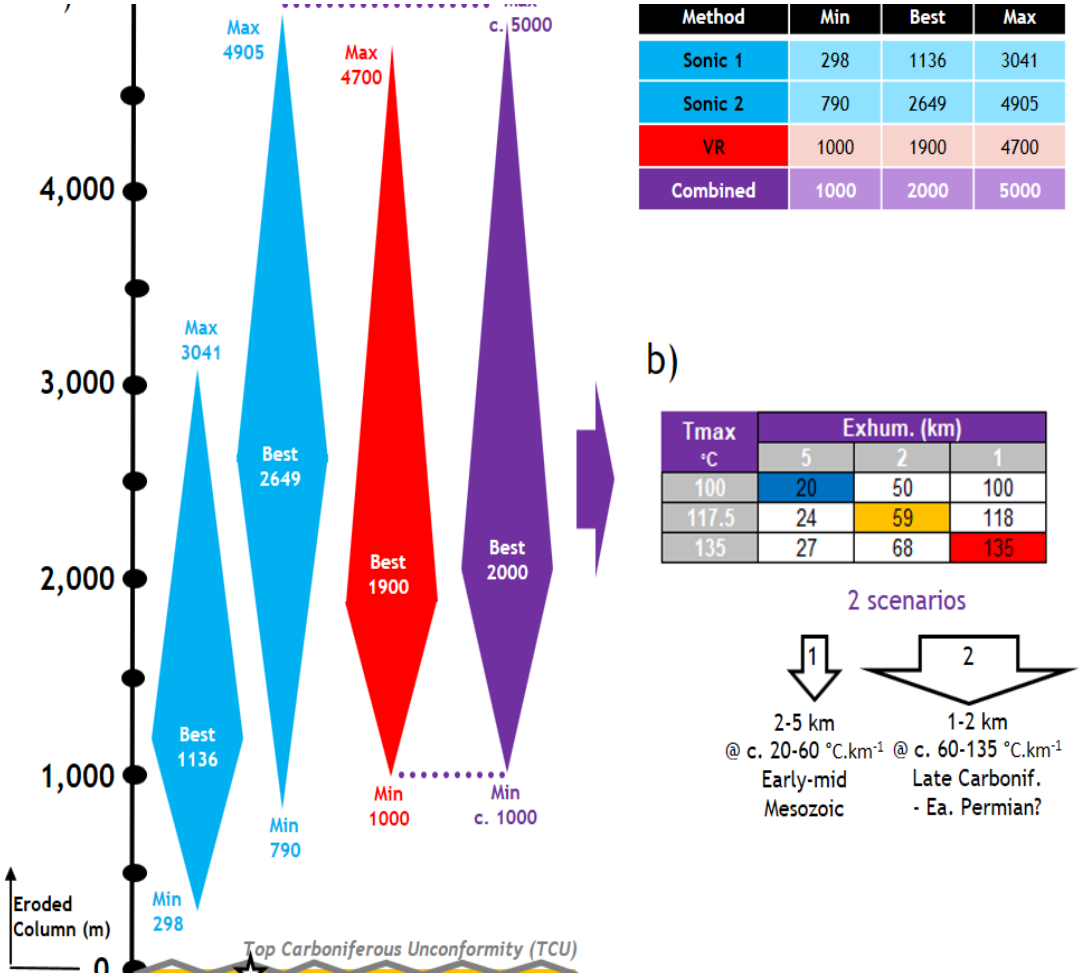

Method	Min	Best	Max
Sonic 1	298	1136	3041
Sonic 2	790	2649	4905
VR	1000	1900	4700
Combined	1000	2000	5000

Tmax °C	Exhum. (km)		
	5	2	1
100	20	50	100
117.5	24	59	118
135	27	68	135

Figure 46: Borehole 26/26-1 exhumation estimates. a) Summary of exhumation estimates at the TCU from sonic velocities and VR data. b) Paleogeothermal gradients required to reach the maximum temperature at 871 mMD depending on the thickness of eroded materials from the combined datasets.

5.3.3 Samples

5.3.3.1 Sampling strategy

This borehole was selected because it is located on a high (which is more prone erosion during uplift events) and has three major stratigraphic unconformities recorded (Base Tertiary Unconformity, Base Cretaceous Unconformity and the Variscan (or Top Carboniferous) Unconformity). The borehole also contains metamorphic rocks, including gneisses, which can be an abundant source of good quality

apatites. Cuttings were sampled from the Eocene sandstone (R-7, 593-692 mMD) and the basal metasediments (R-8, 1129-1256 mMD) (FIGURE 45).

McCulloch (1993) published fission track analysis results from five samples from borehole 26/26-1 (see sample location in FIGURE 45). Based on the FT results, he separated the samples in two groups: 1) The Eocene and Early Cretaceous samples (L-PB1 and L-PB2) yielded a pooled age of respectively 254.8 ± 100.8 Ma and 240.8 ± 62.4 Ma, which are older than the depositional ages; 2) The Early Carboniferous sample (L-PB3) and the two basement samples (L-PB4 and L-PB5) yielded a pooled age of respectively 162.2 ± 26 Ma and 164.3 ± 18.6 Ma, which are younger than the depositional ages.

Zircons were also picked and analysed for U/Pb dating in order to constrain the age and nature of the basal metamorphic unit, but the results for the Eocene sample are also presented here.

5.3.3.2 Apatite and zircon yield

Sample R-7 (Eocene sands)

Only one apatite was identified during picking. Therefore, no AFT/AHe analyses is available for this sample. Eocene sample L-PB1 yielded very few apatites. Both this study and McCulloch (1993) obtained only a few apatites from the Eocene sandstones. The Eocene section of nearby borehole 34/05-1 also yielded very few apatites. The paucity of apatites in Eocene sandstones in this area could be due to prolonged flood plain residence during periods of lowstands (Morton et al., 2012).

Sample R-8 (Basement)

This sample yielded many apatites. The apatites are generally not euhedral. Out of the 71 grains that were counted for fission tracks, 65 were successfully ablated yielding 64 reliable ages and one unreliable age that was discarded. Five grains were selected for AHe analysis. McCulloch (1993) counted 16 and 20 grains for L-PB4 and 5.

Both samples yielded abundant zircons, of which >100 were picked and mounted in a resin puck for U/Pb analysis.

5.3.4 U/Pb and trace element results

The results are presented in ANNEX 1 SECTION 1.2.2 and discussed in this section.

5.3.4.1 Attribution to the Dalradian Supergroup?

Based on the petrography and mineralogy from the cuttings (greenschists, biotite schists, biotite/muscovite schists, feldspathic gneisses), the operator attributed the basal metamorphic unit to an along strike equivalent of the Dalradian Supergroup of onshore Ireland and Scotland. They also concluded that the schists have evidence of several metamorphic events and they must have

experienced high temperatures above 300°C and pressures of several kilobars (Croisile, 1980), *i.e.* low to intermediate-grade metamorphism (FIGURE 45).

The trace element study shows that most apatites belong to the high and low-grade metamorphic rock groups (FIGURE 47), which correspond to the lithologies identified in the cuttings, i.e. feldspathic gneisses and greenschists.

The apatite U/Pb dating shows that most apatites were reset by a thermal event at 391.9 ± 5.9 Ma (Middle Devonian), probably associated with Late Caledonian regional metamorphism or intrusive magmatism (contact/conductive or hydrothermal/advective heating). This suggests the possible presence of a Late Caledonian granitoid pluton in the area. The resetting of the U/Pb geochronometer at 392 Ma indicates that the rocks experienced temperatures greater than 350°C at that time (as an absolute minimum, but probably greater, possibly up to 600°C, Chamberlain and Bowring (2001)). However, the REE signatures of these apatites were probably not reset by this thermal event since REEs in apatite diffuse very slowly, even during high temperature metamorphic events (Antoine et al., 2020).

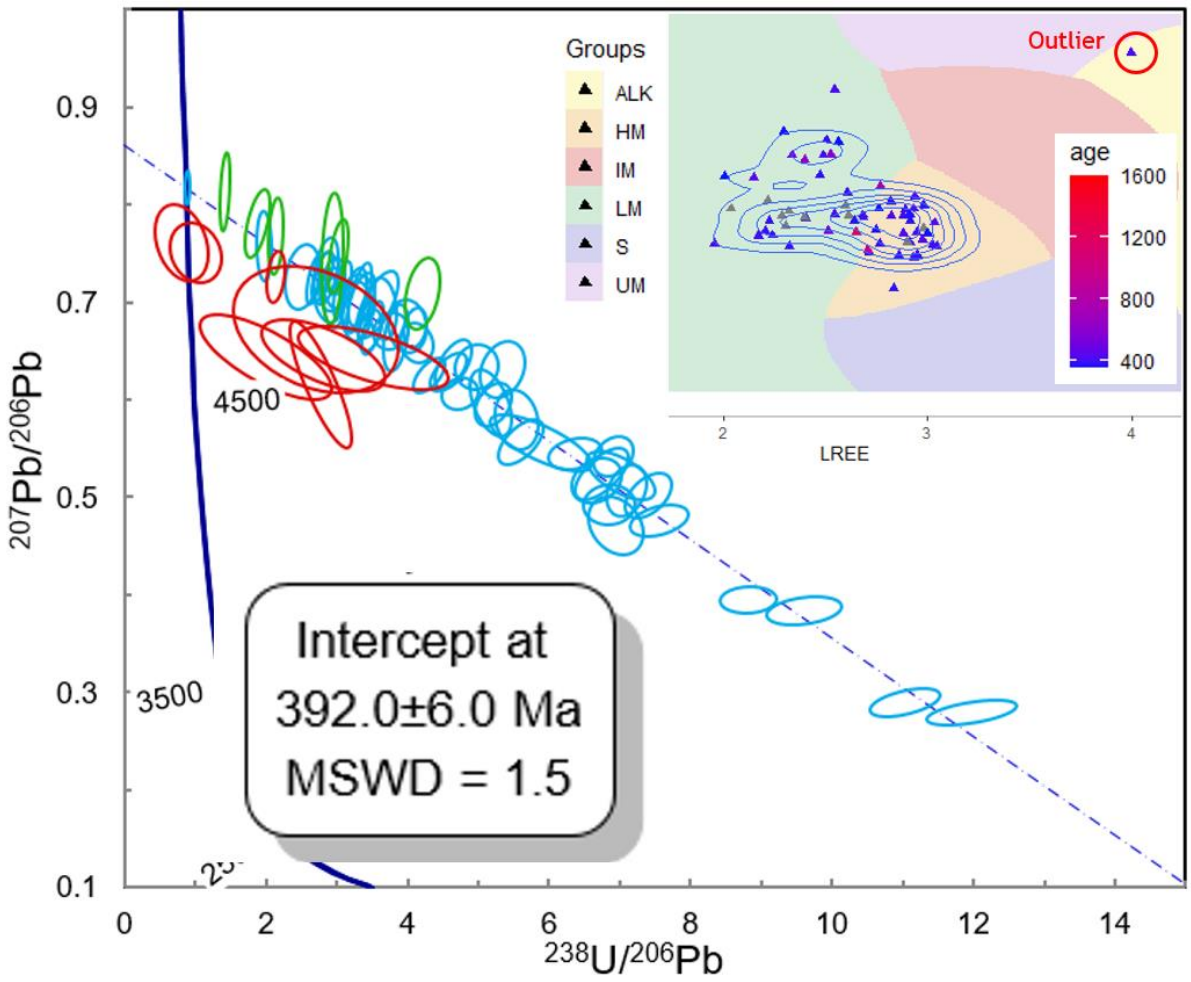

Figure 47: Apatite U/Pb and trace element results for sample R-8 (26/26-1).

The detrital zircon U/Pb age spectrum of the basement rocks is similar to other detrital zircon U/Pb age spectra from the Dalradian Supergroup onshore Ireland and Scotland, and more specifically to the Grampian Group of the Dalradian, which is typically devoid of Archean grains unlike the younger Dalradian groups (Cawood et al. (2003), Cawood et al. (2007), McAteer et al. (2010)). A similar zircon U/Pb signature (*i.e.* extending from c. 850 Ma to 1800 Ma with no, or very few, Archean grains and Grenville, Pinwarian and Labradorian peaks) are found in the Erris Group (equivalent to the Grampian Group) of north Co. Mayo (McAteer et al., 2010) as well as in the recently discovered Porcupine High Metasedimentary Sequence (PHMS) on the Porcupine High, 60 km north-west of 26/26 (Tyrrell, 2013) (FIGURE 48).

Apart from the few Caledonian grains which will be discussed later, the youngest zircon grain has an age of 867 ± 28 Ma, which gives a maximum depositional age for the sediments. The basal Grampian and Appin Groups of the Dalradian are loosely constrained to c. 720-800 Ma (Dempster et al., 2002). The absence of grains younger than 867 Ma is in agreement with a depositional age within the earliest part of the Dalradian sequence (*i.e*. the Grampian Group) and the youngest grain rules out an attribution to the older Moine Supergroup (c. 870-1000 Ma).

5.3.4.2 Caledonian zircons

Six grains have a Caledonian age of c. 424 ± 20 Ma (pink inset in FIGURE 48). If these grains are *in-situ* they must come from a Caledonian igneous rocks present in the Dalradian basement (e.g. a coarse-grained igneous vein from a nearby pluton). In this case this igneous event is likely older and not co-genetic with the thermal event that has reset the apatite U/Pb system.

However, it is more likely that these grains come from the overlying Carboniferous sediments. Sample R-8 comes from cuttings located between the bottom of the well (1256 mMD) and the contact with the Carboniferous sediments (1129 mMD). It is very likely that the first few meters of the basement cuttings might have incorporated grains from the overlying Carboniferous clastics during the ascension of the mud to the platform or because of caving.

5.3.4.3 Eocene sand provenance

The zircon U/Pb age spectrum of the Eocene sands (sample R-7) has only the Grenville and Labradorian peaks in common with the PHMS basement sample. The Pinwarian peak is absent from the Eocene sample which has additional peaks of Caledonian, Cadomian and an early Labradorian age. Therefore it is likely that the PHMS outcropping in the NW of the well contributed only a small amount of clastic materials to the 26/26-1 area (otherwise the three PHMS peaks should be present in the Eocene sands).

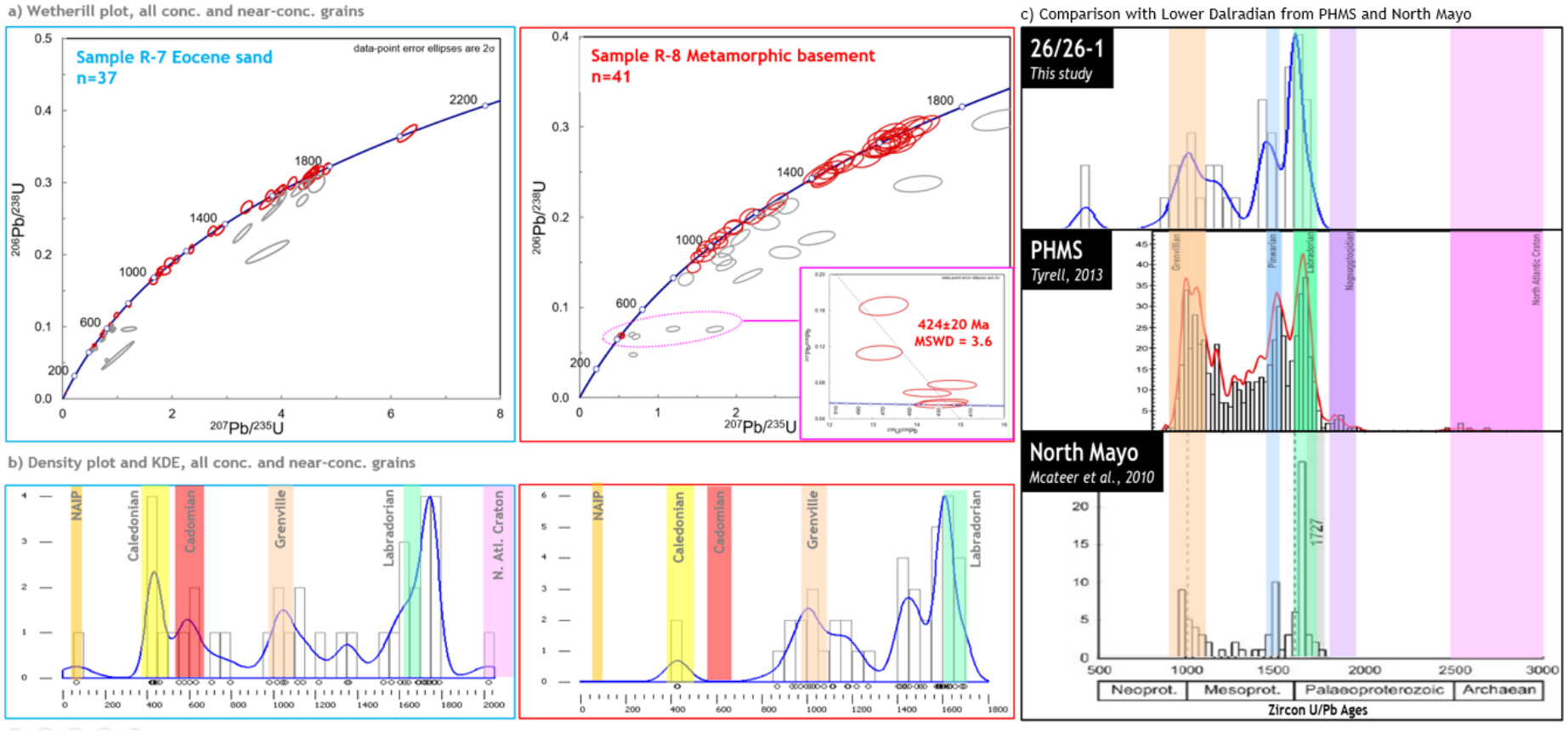

Figure 48: Zircon U/Pb results for samples R-7 and R-8 (26/26-1). a) Wetherill plots, b) Density plots and KDE, c) Zircon U/Pb density plot and KDE of basement sample in 26/26-1, the PHMS dredge samples and the lowermost Dalradian units of Co. Mayo. Note the three peaks of Grenville, Pinwarian and Labradorian ages and the quasi-absence of Archean grains. The two Caledonian grains in 26/26-1 are believed to be contamination from the overlying Carboniferous clastic sediments.

5.3.4.4 *Conclusions*

In conclusion, the basement rocks at the bottom of well 26/26-1 are probably a suite of low to high-grade metamorphic rocks (greenschists, biotite and biotite-muscovite schists and gneisses) that were deposited as sediments during the Tonian (early Neoproterozoic) on the Laurentian continent. They probably belong to the PHMS, which crops out to the NW of borehole 26/26-1, which might be the continuation of the Grampian Group of Scotland and the Erris Group of Ireland (the basal part of the Dalradian Supergroup). They significantly extends the spatial distribution of the PHMS to the SE, up to the margin of the North Porcupine Basin. This therefore creates a new robust spatial constraint for the placement of the Iapetus Suture offshore west of Ireland, which must pass south of borehole 26/26-1.

The basement rocks in well 26/26-1 were subsequently subject to Caledonian metamorphism. In particular, a final Late Caledonian event during the Middle Devonian at c. 392 Ma reset the U/Pb age of most (if not all) basement apatites.

This analysis is one of only two geochronology studies on *in-situ* basement rocks on the Porcupine High (the only other one being shallow borehole 25/7-sb(MeBo)3 reported in Daly et al. (2008) and Tyrrell (2013), since most other ages obtained to date were on dredge or dive samples which cannot be guaranteed to be *in-situ*.

5.3.5 AFT and AHe Results (Table 11 and Table 12)

Both the legacy and newly acquired AFT and AHe data are described in ANNEX 1 SECTION 2.2.2 together with a qualitative interpretation. The samples are ordered from shallowest to deepest sampling depth.

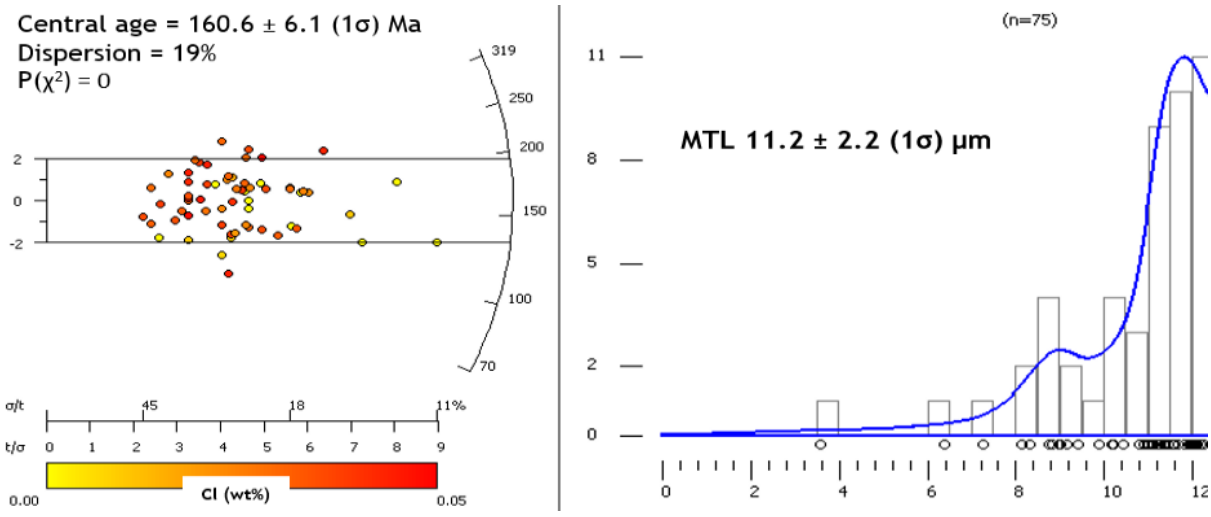

Figure 49: AFT results for basement sample R-8 (26/26-1). Left: Radial plot colour-coded with Cl concentration. Right: confined track length density plot, KDE and MTL.

Table 11: Summary of AFT and AHe results for well 26/26-1.

a) AFT Results

Sample	Depth		n	Ns	Area	U/Ca	$P(\chi^2)$	Central Age	±1σ	Tracks	MTL	SD	SE	Inverse?	
	m MD	*m BSB*			*cm^2*			*Ma*	*Ma*		*µm*	*µm*	*µm*	*FTA*	*FTL*
7	695	381	*0*	-	-	-		-	-	-	-	-	-	-	-
8	724	410	62	1443	1.44E-03	0.062620958	<0.01	160.6	6.1	65	11.20	2.20	0.27	Yes	Yes

b) AHe Results

Sample	Grain	Shape in GFTC		Length	Diameter		S/V	R_{eq}	Weight	Temp.	$[^{238}U]$	$[^{232}Th]$	$[^{147}Sm]$	eU	Th/U weight	[He]	Degassing	Raw Age	Error	F_T	Correc. age	Error
				W	Max	Min																
		Geometry	*GFT**	*µm*	*µm*	*µm*		*µm*	*g*	*°C*	*ppm*	*ppm*	*ppm*	*ppm*		*nmol/g*		*Ma*	*Ma*		*Ma*	*Ma*
R-8	3	Hexagonal prism	2P	209	112	109	0.050	59.5	3.98E-06	33	8	8	210	11	1.0	3.6	Lack of heat	58	9	0.758	77	12
	5	Hexagonal prism	2P	250	108	99	0.050	59.8	4.67E-06	33	17	8	288	21	0.5	8.8	Small leak?	75	11	0.759	99	15
	1	Hexagonal prism	1B	324	173	163	0.032	92.6	1.80E-05	33	7	1	302	9	0.2	5.0	Ok	93	14	0.843	111	17
	2	Hexagonal prism	2B	340	161	143	0.034	87.1	1.60E-05	33	5	2	312	7	0.4	4.6	Small leak?	103	15	0.834	124	19
	4	Hexagonal prism	1T1B	190	148	132	0.043	70	6.80E-06	33	18	3	462	21	0.2	12.3	Ok	101	15	0.795	127	19

Table 12: Comparison of the AFT replicate analysis of the 26/26-1 PHMS basement.

Sample information								Fission track age					Confined track lengths			
Lithology	Sample	Source	Analyst	Sample depth (m MD)		Temperature		n	Ns	$P(\chi^2)$	Central Age		Tracks	MTL	SD	SE
						Seabed	Samples									
				Top	*Base*	*°C*	*°C*	-	-	-	*Ma*	*±1σ Ma*	-	*µm*	*µm*	*µm*
PHMS gneisses & schists	**L-PB4**	*McCulloch et al, 1993*	McCulloch	1138	1168	10	32	16	279	0.55	**162.2**	13	56	**11.72**	1.54	0.21
	R-8	*This study*	Rateau	1129	1256	10	33	64	1483	<0.01	**159**	8	65	**11.20**	2.20	0.27
	L-PB5	*McCulloch et al, 1993*	McCulloch	1227	1255	10	35	20	578	0.65	**164.3**	9.3	84	**11.81**	1.87	0.20
										Average:	*161.8*			*Average:*	*11.6*	

5.3.5.1 Replicate analyses

The FT ages and MTLs of basement samples L-PB4, R-8 and L-PB5 are very similar and indicate a good reproducibility of results for this basement interval despite different samples (three), analysts (McCulloch vs Rateau) and methods (EDM vs LAFT) (TABLE 12). There is a difference in FT age of 5.3 Ma between the younger and the older age, which corresponds to 3% of the average FT age of the three replicates. For the MTL, there is a difference of 0.61 µm between the longest and shortest MTL, which corresponds to 5.3% of the average MTL for the three samples (TABLE 12).

5.3.5.2 Qualitative interpretation

The Eocene and Hauterivian samples contains apatites that have not been reset since their deposition indicating that the area has not experienced significant burial after the Hauterivian. On the contrary the basement and Lower Carboniferous sediments have experienced significant burial after their deposition that led to the complete annealing of apatite fission tracks.

The AHe results indicate that the basement interval did not experience temperatures above c. 100°C after the Lower Cretaceous which is in agreement with the fission track data that shows no significant burial after the Hauterivian. The difference in S/V and eU in R-8.1 and R-8.4 should reduce the number of possible time-temperature paths of the inverse modelling.

5.3.5.3 Samples usable for thermal history inverse modelling

Combining legacy and newly acquired data, thermochronological information are available for four intervals (Eocene, Hauterivian, Carboniferous and Dalradian basement). However, following our internal cut-offs defined in the Methodology chapter, only the Hauterivian and basement samples have enough FT ages and confined track lengths to be used as input data for thermal history inverse modelling.

5.3.6 Thermal history modelling

5.3.6.1 Input data

AFT input data

Only samples L-PB2 and R-8 have enough fission track data to be used for inverse modelling purposes. Both samples meet the minimum requirements for both AFT ages (>= 10 ages) and track lengths (>= 25 lengths).

AHe input data

As discussed in ANNEX 1 SECTION 2.2.2 only grains R-8.1 and R-8.4 from sample R-8 are suitable to be used as input data.

VR data

The only VR sample which is reliable according to the operator (at 871 mMD) has been imported in QTQt. The data is not used to constrain the model but is compared to predicted VR values for the same depth calculated from modelled thermal histories.

5.3.6.2 Initial and final time-temperature constraints

Final conditions: Present-day temperature of sample

Using the estimated geothermal gradient of 28.34 ± 5.3°C.km^{-1}, sample L-PB2 has a present-day temperature of 21.67 ± 2.19°C, while sample R-8 has a temperature of 33.17 ± 4.33°C.

Initial conditions - Emplacement age and temperatures

The emplacement ages of sample L-PB2 and R-8 are respectively 131 ± 1.6 Ma and 391.9 ± 5.9 Ma.

L-PB2 is a detrital sample therefore the temperature at time of emplacement is defined as 10 ± 10°C. On the contrary, sample R-8 is a metamorphic sample and therefore the age represents the time at which the U/Pb system in the apatites was reset. For the sake of simplification and to reduce the size of the prior time-temperature domain, the temperature at that time is set as 140 ± 20°C (*i.e*. high enough for complete annealing of any fission tracks.

5.3.6.3 Intermediate constraints

Time-temperature constraint boxes can be added to the model based on stratigraphy or external thermal indicators (e.g. VR-derived Tmax). In QTQt, in the case of modelling a vertical profile, constraints only apply to the topmost sample (so R-8 until the Hauterivian and then L-PB2 after the Hauterivian).

Burial constraints from stratigraphy

Sample L-PB2 is located at a depth range of 780-793 mMD so an average depth of 786.5 mMD is employed. The Lower Eocene sandstone is at a depth range of 658-692 mMD corresponding to an average depth of 675 mMD while the Middle Eocene sandstone is at a depth range of 593-618 so an average depth of 605.5 mMD us used. Consequently L-PB2 was at a depth of 111.5 m at some point during the Early Eocene and at a depth of 181 m at some point during the Middle Eocene. The x-axes of the two constraint boxes are defined by the age of deposition - 51.9 ± 4.6 Ma for the Early Eocene and 42.8 ± 5 Ma for the Middle Eocene.

Using the present-day geothermal gradient, these depths correspond to paleotemperatures of 13.16 and 15.13°C. The uncertainty of the surface temperature (±10°C) is higher than the uncertainty of the geothermal gradient, therefore it is the former which is propagated to these estimated sample paleo-temperatures. Consequently, the y-axes of the two constraint boxes are respectively 13.16 ± 10°C and 15.13 ± 10°C (FIGURE 50D).

a) Prior information and MCMC chain parameters

Categories		Values
Prior information	Time Temperature	245.5 ± 245.5 Ma 80 ± 80 °C
	Max dT/dt, Reheating Temperature offset, Offset	1000 °C.My, Yes 11.5 °C, Constant
MCMC chain	Burn-in/Post-burn-in Thinning	100,000/100,000 1
Proposed move	Time/Temperature/Offset Resample/Reject Reject complex	30/300.001 Resample Yes

b) Model names and characteristics

Model	Samples	Track lengths	Constraints	Geothermal gradient	tT points
0	Both	Used	None	Constant	Low (Simple)g High (Complex)
1	Both	Used	2 Eocene constraints	Constant	Low (Simple)
2	Both	Used	2 Eocene + VR constraint	Constant	Low (Simple) High (Complex)
3	Both	Not used	2 Eocene + VR constraint	Constant	Low (Simple)

c) Model constraints

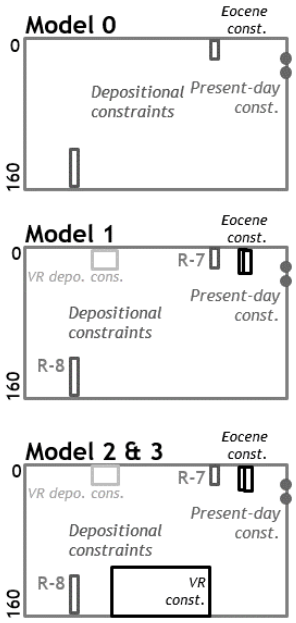

d) Time-temperature constraints

Burial constraint	Depositional age	Depositional Temperature	Present-day temperature	Applies to	Used in scenarios
Mid. Eocene sand	42.8 ± 5	10 ± 10	13.16 ± 10	L-PB2	1,2,3
Ea. Eocene sand	51.9 ± 4.6	10 ± 10	15.13 ± 10	L-PB2	1,2,3
VR #1	53.9 ± 2.7	10 ± 10	17.62	N/A	1,2,3
Tmax constraint	229 ± 90	137 ± 27	N/A	R-8	2,3
Upper Visean-Namurian (VR# 2)	329.9 ± 16.5	10 ± 10	24.35	N/A	1,2,3
Visean clays (VR #3)	343.6 ± 17.2	10 ± 10	28.83	N/A	1,2,3

Figure 50: QTQT modelling parameters for well 26/26-1. a) Prior information and MCMC chain parameters. b) Model names and characteristics. c) Visual retransitions of the different model constraints. d) Intermediate time-temperature constraints.

Burial constraints from VR samples

The three VR samples can be used as input samples for displaying on the thermal histories. As such, temperatures and times of deposition as well as present-day temperatures have to be provided and therefore these VR samples act as intermediate time-temperature constraints for the AFT/AHe samples (independently of their VR values).

The three VR samples at 644, 871 and 1033 mMD have a depositional age of respectively 53.9 ± 2.7 Ma, 329.9 ± 16.5 Ma and 343.6 ± 17.2 Ma, a temperature at time of deposition of 10 ± 10°C and present-day temperatures of 17.6°C, 24.3°C and 28.8 ° C (FIGURE 50D).

Thermal constraint from VR data

The VR analysis discussed in ANNEX 1 SECTION 3.2.1 led to the conclusion that the organic matter at 871 mMD must have experienced temperatures of 100-135°C at some time between the Namurian

and the Hauterivian (but probably before the Early Jurassic), *i.e.* 229 ± 90 Ma. Sample R-8 is 321.5 m below the VR sample so for paleogeothermal gradients ranging from 30 to 90°C.km^{-1}, sample R-8 would have been 10 to 29°C hotter than the VR sample, *i.e.* 110-164°C or 137 ± 27°C. Therefore the constraint box x-axis is 229 ± 90 Ma and the y-axis is 137 ± 27 ° C (FIGURE 50D).

5.3.6.4 Prior box and run parameters

For all models, the prior box is defined by 245.5 ± 245.5 Ma for the x-axis and 80 ± 80°C for the y-axis. Except when stated otherwise, the geothermal gradient of 28.34°C.km^{-1} is kept constant throughout the thermal history (*i.e.* the temperature gap between the two samples always remains the same between models and does not change with time within a single model) (FIGURE 50A).

5.3.6.5 List of scenarios

Several geological scenarios have been run with a variable number of constraints and input data (see summary in FIGURE 50B AND C). This approach allows a better discrimination of which input data (either FT ages, track lengths, AHe ages or time-temperature constraints) control certain aspects of the modelled thermal histories.

5.3.6.6 Modelling results

Summaries of the results of each modelling run are available in ANNEX 2. All the models yielded convergent log likelihood and posterior chains (*i.e.* no trend in post-burn-in models) (FIGURE 51).

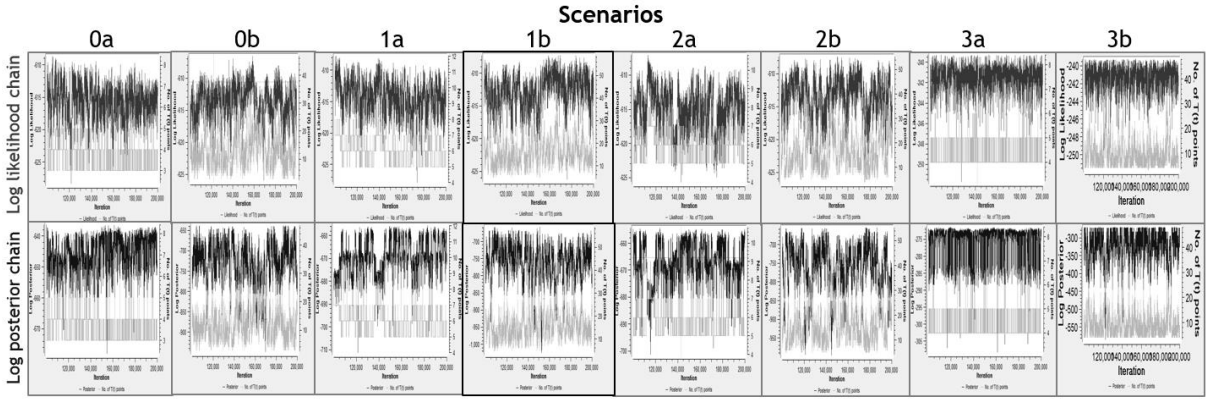

Figure 51: Log likelihood and log posterior chains for 26/26-1 models. All chains are stable.

Scenario 0: No intermediate constraint (FIGURE 52)

This scenario is run to evaluate the information contained in the AFT and AHe data alone, independent of any geological assumptions on the temperature of the sample at any point in time except for the initial and final conditions.

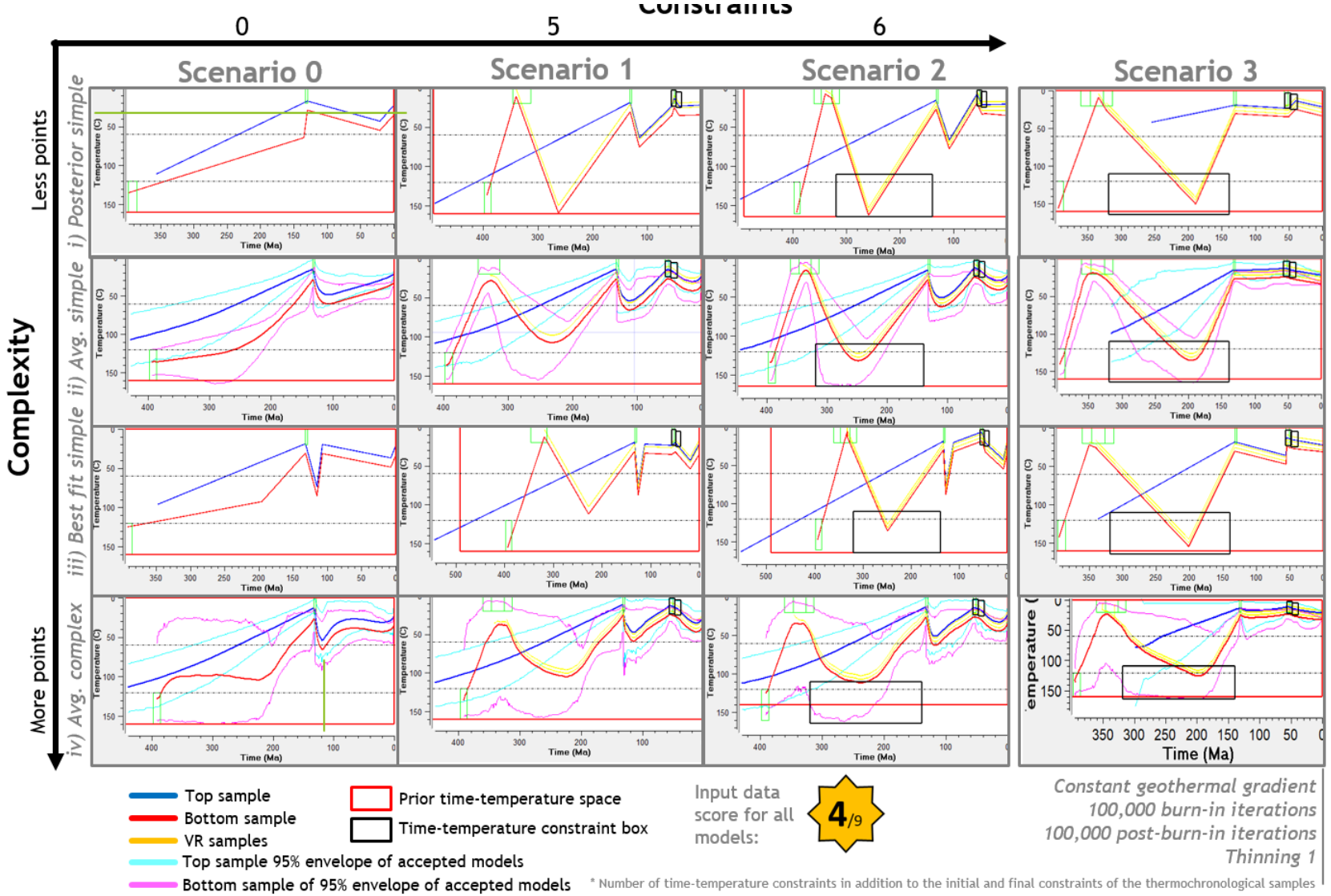

Figure 52: Summary of the various inverse modelling results for borehole 26/26-1.

This least constrained model demonstrates that before 200 Ma the thermal history is not constrained by the thermochronological data. Between 200 Ma and the Hauterivian, the basement sample cooled down from temperatures above 120°C to near-surface temperatures either rapidly during that time or by slow monotonic cooling since before 200 Ma. After the Hauterivian, the model shows that the basement sample (used as the reference, the Hauterivian sample is simply 11.5°C cooler, same in models 1 to 3 below) always remained below 80°C with most models showing a peak heating at c. 120 Ma.

In all models, the AHe ages are always too young by 0-40 Ma. This anomaly probably comes from the fact that the confined track lengths have a low MTL and very few tracks between 13-16 µm, which forces the model to place the samples at relatively high temperatures until recently (for example the heating peak at 120 Ma and subsequent slow cooling through the PHeRZ). These high temperatures then lead to higher He diffusion and younger AHe ages. If the models had lower temperatures during the Cenozoic for example, the observed and modelled AHe ages would probably match much better, but then the confined track distribution would have a poorer fit. This hypothesis is tested by scenario 3 below. Scenario 0 points towards a contradiction between the AHe ages and the confined track length distributions that influences the recent thermal history in opposite directions (cooler for the AHe data, hotter for the confined track lengths).

Scenario 1: Five intermediate constraints in the Carboniferous and the Eocene (FIGURE 52)

This scenario has the same input data as model 0 but with the addition of the three VR samples and the two Eocene stratigraphic constraints described above.

All models (posterior, expected, likelihood and complex) show a rapid cooling of sample R-8 of at least 300°C from the time of metamorphism (c. 392 Ma, Middle Devonian) to the time of deposition of the Carboniferous VR sample (c. 330 Ma, late Visean to Namurian). This cooling is purely constrained by the stratigraphic constraints and not by the thermochronological data.

Between the Namurian and the deposition of the Hauterivian sands (sample L-PB3), all models show an initial heating of the basement sample R-8 from near-surface temperatures to c. 90-110°C at some point between 300 Ma and 200 Ma, followed by a cooling of c. 70°C to c. 30°C from peak heating to the Hauterivian. This peak heating is the highest temperature that the Carboniferous sediments experienced until the present-day and therefore is the time when they acquire their vitrinite reflectance. However, only the expected model, with the largest peak heating at 110°C, creates a good fit with the VR sample as all other models underestimate the VR data.

Between the Hauterivian and early Eocene, all models agree that the basement sample is first heated to average temperatures of c. 65-75°C (maximum 85°C) at some point before c. 100 Ma (so during the

Early Cretaceous rather than during the Late Cretaceous or Paleocene). It is then cooled to temperatures c. 30°C during the Late Cretaceous to Early Eocene.

Between the Middle Eocene and present-day, the posterior model shows almost no variation in temperature. On the contrary, the likelihood model shows that the basement sample is first heated to c. 50°C during the Miocene and then cooled down by c. 15°C to present-day temperature. The expected and complex models show an average of these two end-member scenarios.

All the models yield matching modelled *vs* observed AFT ages and confined track length distributions. However, like in model 0, the modelled AHe ages are younger than the observed ages.

Scenario 2: Idem Model 2 but with one VR-derived constraint (FIGURE 52)

This scenario is identical to scenario 1 but with an additional time-temperature constraint derived from the VR data as discussed above.

Model 2 yields almost the same thermal histories than model 1. Even the maximum heating event during the Permian-Triassic is almost identical, despite model 2 having a VR-derived time-temperature constraint and not model 1. This constraint forces the basement sample to reach a temperature of at least 110°C in model 2 while there is no such constraint in model 1. Since both models show that the basement sample reached a temperature of at least c. 100°C during the Permian-Triassic, it can be deduced that this part of the thermal history is solely constrained by the thermochronological data (mostly the AFT age of the basement sample, as opposed to its AHe ages or track lengths).

Scenario 3: Idem Model 2 but without length data for Eocene sample (FIGURE 52)

This scenario is identical to scenario 2 but without any track length data. This scenario aims at testing the influence of the track length distributions on the thermal history (by comparing the results of this scenario to the previous one that includes track lengths data).

The posterior, expected, likelihood models of both the simple and complex runs show an excellent match of modelled vs measured AHe ages (contrary to scenarios 0, 1 and 2). The thermal histories show that between the Hauterivian and present-day, the basement sample most often remains at c. 30°C and at maximum reaches 50-60°C in some rarer cases (well below the 60-85°C seen in the case of scenarios 0, 1 and 2). As predicted above, when the track length distributions are not part of the inverse model input data, the Early Cretaceous to Recent thermal history is much cooler in order to yield Early Cretaceous AHe ages for the basement sample.

5.3.6.7 Discussion

Timing of maximum temperature

All the models show that the bottom sample experienced its highest temperatures between c. 320-200 Ma (latest Carboniferous to base Jurassic). Regionally, the Carboniferous organic matter is believed to have acquired its highest maturity (and so VR) before the early Jurassic (Robeson et al., 1988) and probably during the Late Paleozoic (Corcoran and Clayton, 2001), which is in accordance with the model for 26/26-1.

Magnitude of pre-Cretaceous exhumation associated with the TCU

The models show that the basement sample cooled down from c. 110°C during the Permian-Triassic to c. 30°C during the Hauterivian. Overburden erosion or a lower geothermal gradient (or a combination of both) are the two main causes that could have led to this 80°C cooling.

As a simplification, only overburden erosion is considered for now. Using the present-day geothermal gradient of 28.34°C.km^{-1} and the average Carboniferous gradient of 60°C (from Corcoran and Clayton (2001)), the cooling corresponds to the erosion of respectively c. 2800 m and 1300 m of sedimentary rocks.

However, more complex scenarios could lead to smaller amounts of denudation. For example, let us assume the basement sample acquired its maximum temperature (c. 110°C) during the late Carboniferous while the geothermal gradient was c. 60°C.km^{-1}. At that time, the basement sample would have then been buried under 1700 m of sedimentary rocks. Subsequent cooling of the gradient to 30°C.km^{-1}, without erosion, would have cooled the temperature of the basement sample by c. 50°C to c. 60°C. To then cool down to c. 30°C as constrained by the models, an exhumation event of c. 700 m would be necessary. Therefore, in this scenario, less than 1 km of uplift and erosion would be necessary, when combined with a cooling of the geothermal gradient at the end of the Carboniferous, to replicate the modelling results. This scenario can be used as a minimum estimate for the magnitude of uplift and erosion that occurred pre-Hauterivian (FIGURE 53).

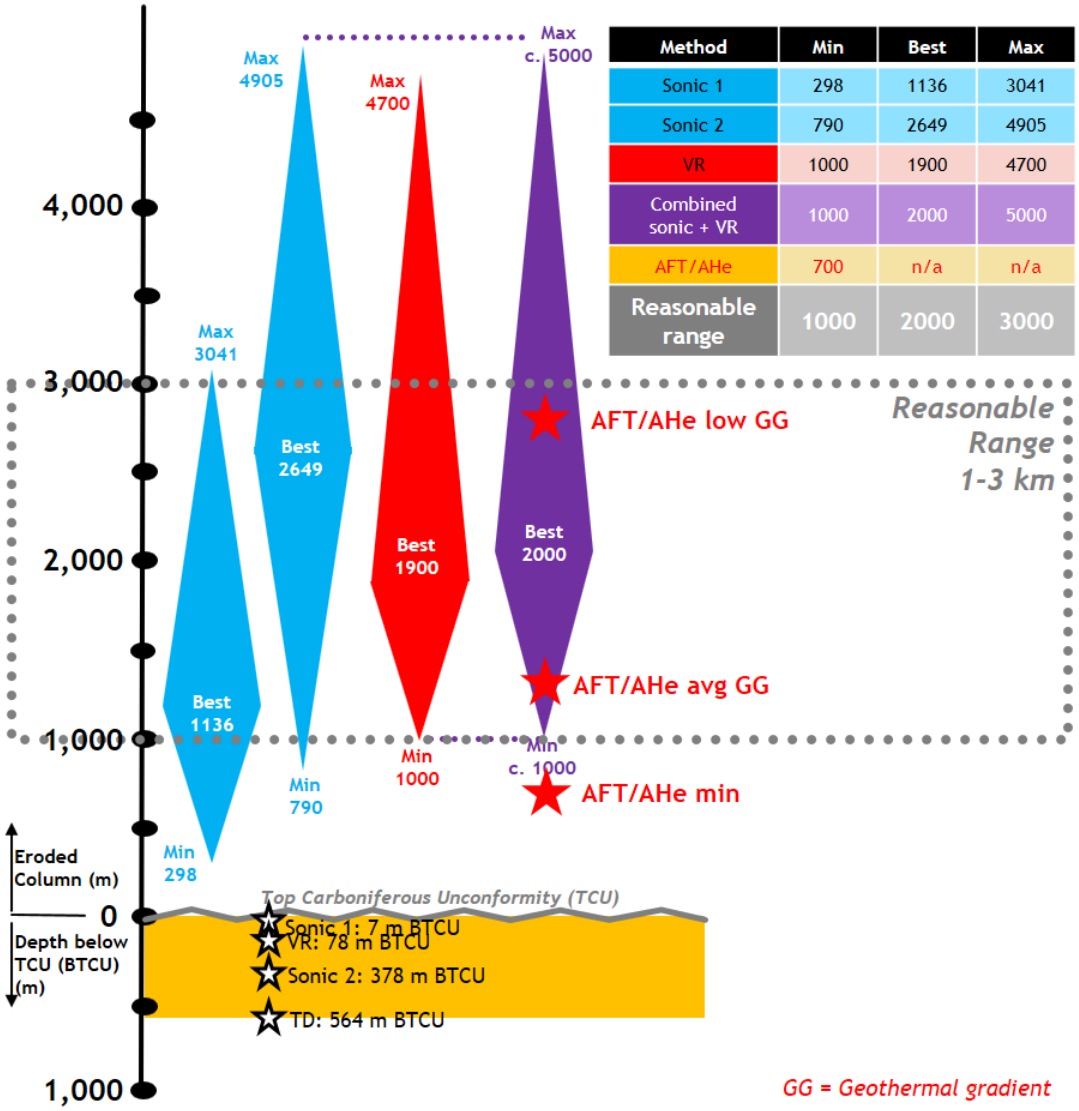

Figure 53: Summary of exhumation estimates for the amaglamed Top Carboniferous Unconformity (TCU) derived from sonic, VR and AFT/AHe data.

When compared to the estimates from the sonic and VR data, the AFT/AHe-derived estimates fall within the same order of magnitude. Thermochronological data cannot provide a maximum estimate since a sample could have experienced much higher temperatures (and therefore much higher subsequent exhumation) before the time of resetting of the FT age (in this case before 200 Ma). The AFT/AHe data constrain a minimum estimate of 700 m which is close to the minimum estimate of the second sonic data point (790 m) and the VR data point (1000 m) (FIGURE 53). The simple erosion models described just above (1300 and 2800 m depending on the paleo geothermal gradients) fall within the range of best-case estimates of the sonic and VR data (1136 to 2649 m) (FIGURE 53).

Overall, when the sonic, VR and AFT/AHe data are taken together, it is possible to define an absolute minimum of 700 m and an absolute maximum of 5000 m of missing sediments between the Carboniferous and Hauterivian in borehole 26/26-1. However, based on the best-case estimates of

each method, it is possible to define a narrower range of more plausible estimates of 2000 ± 1000 m. This range comprises all the best-cases estimates and does not include values outside the range of each method (FIGURE 53).

Regionally, this Late Paleozoic to mid-Mesozoic cooling is probably a combination of late Variscan denudation and geothermal gradient cooling and Triassic-Jurassic rift-related shoulder uplift and erosion.

Cretaceous and Cenozoic thermal history

The Cretaceous and Cenozoic thermal history is largely dependent on the 'weight' placed on either the fission track lengths or the AHe ages.

If the AHe ages are used as the reliable input, then the models from scenario 3 show that the simplest thermal history that can explains the data is that the basement sample remained at near-surface temperatures (20-30°C) throughout the Cretaceous and Cenozoic. However, other models with a good match show that the sample could have been heated to up to c. 50-60°C during the Early Cretaceous in most cases, or, more rarely, just before a cooling event during the Paleocene-Early Eocene. However, these models do not properly reproduce the track length data.

If the track lengths are preferred as the most reliable input data (and not the AHe ages), then most models predict that the basement sample experienced temperatures of 60-85°C during the Aptian followed by rapid cooling during the Albian or more protracted cooling during the rest of the Cretaceous (FIGURE 52). During the Cenozoic, most models point towards an initial heating phase up to 50°C peaking during the Neogene followed by cooling to present-day temperatures. However, these models do not properly reproduce the AHe ages.

The discrepancy could be due to one (or a combination) of three causes:

1) **Inaccuracy of the AHe ages**: AHe dating is known to produce large age dispersion and the source of errors is not yet properly understood (Green and Duddy, 2018).
2) **Inappropriate inverse modelling parameters**: Inverse modelling requires the calculation or definition of an initial track length (at time of fission) and a set of equations that simulate the annealing behaviour of the tracks dependent on temperature and time. An error or inappropriate parameter definition can therefore lead to erroneous results in the final thermal history. In this case, if the initial track length is assumed to be longer that it is in reality, the lack of long track lengths will result in hotter thermal histories to anneal the tracks from the overestimated initial track length to the measured track length peak (Vrolijk et al., 1992a).
3) **Inaccuracy of the track length measurements** (Barbarand et al. (2003), Ketcham et al. (2018)): Creating a dataset of track lengths that is representative of the real track lengths in the

apatites is difficult due to: a) the paucity of confined track lengths in many apatites, b) the under-representation of short track lengths because of the lower chance to be intersected by an etched fission track, c) the over-representation of long track lengths due to optical bias, and other analyst biases, and d) the etching rate variability depending on apatite chemistry.

The third explanation is unlikely in this case since the main bias is towards overestimating the MTL which therefore results in having even shorter track lengths and therefore even more discrepancy between the track lengths and AHe ages. Moreover, the reproducibility of the track lengths measurements between the legacy study and this study points towards the reliability of the measurements (even though the lengths were not calibrated to a length standard).

The first explanation is possible based on the numerous studies that have shown the lack of both accuracy and precision of the AHe method. The only way to validate the accuracy of the ages would be to obtain many more AHe ages for the sample in order to have a statistically meaningful population, which was not possible for this sample.

The second explanation is also very plausible since in this study the initial track length is calculated using the Dpar measurements but without having done an *in-house* calibration and instead relying on the default relationship in QTQt. Moreover, Tamer and Ketcham (2020) highlighted that without a laboratory characterization of each apatite, a lot of uncertainties remains regarding the annealing behaviour of apatites at low temperatures and consequently the length of the unannealed tracks that should be used in the model.

Consequently, based on the well data only, it is not possible to favour the track length data or the AHe ages and consequently to favour the cooler or hotter thermal history for the Barremian to Recent time window. Both scenarios should be seen as plausible end-members until further analyses or data external to the borehole can shed light on the most likely thermal history.

5.3.7 Conclusions

The integration of newly acquired apatite FT and AHe data, apatite and zircon U/Pb ages and apatite trace element data combined with the interpretation of legacy AFT, sonic velocity and VR data allow the following tectonothermal model and conclusions to be derived for borehole 26/26-1:

5.3.7.1 Basement geology

1) A suite of *In-situ* low to high-grade metamorphic basement rocks at the bottom of well 26/26-1 can be attributed with confidence to the Neoproterozoic Grampian Group (the lower part of the Dalradian Supergroup), based on its zircon and apatite U/Pb signature.

2) The suite is probably an extension of the PHMS outcropping on the summit of the Porcupine High, 60 km to the northwest of 26/26-1.
3) This is only the second study undertaking geochronology of *in-situ* basement rocks on the Porcupine High and provides therefore a new robust constraint on the nature and age of the basement rocks in the area and on the location of the Iapetus Suture which must pass south of 26/26-1.
4) The apatite trace element data indicate that most of the apatites are probably sourced from high-grade gneisses.
5) The basement rocks were subjected to Late Caledonian metamorphism or pluton-induced heating to temperatures >350°C that reset the U/Pb age of most the apatites (at 392 Ma).

5.3.7.2 Thermochronology Data

1) Newly acquired AFT and AHe data have been combined with an old fission track study from 1993. Two legacy basement samples and one newly acquired basement sample yielded very similar AFT ages and track lengths statistics, which demonstrated the reproducibility of AFT analysis and the reliability of the results for thermal modelling.
2) The Eocene sands did not yield enough apatites to obtain AFT or AHe data. However, one of the legacy samples (Hauterivian in age), after its data was converted to be QTQt compatible, was used as an additional sample in the modelling in order to create a vertical profile with two samples (Hauterivian and basement), and therefore reducing the number of possible thermal histories that would match the measured input data.
3) The basement sample yielded an AFT age of 161 ± 6 Ma (c. Oxfordian) and a MTL of 11.20 ± 2.20 µm, while the Hauterivian sample yielded an FT age of 241 ± 31 Ma (c. Middle Triassic) and a MTL of 11.24 ± 2.39 µm.
4) Five AHe ages were obtained for the basement sample ranging from 77 ± 12 Ma to 127 ± 19 Ma (F_T-corrected ages). However, only two grains were judged reliable and suitable to be used as input data in the modelling. They have F_T-corrected ages of 111 ± 17 Ma and 127 ± 19 Ma (c. Barremian to Albian).

5.3.7.3 Thermal Histories

1) Between the Middle Devonian and the Early Carboniferous, the basement rocks experienced rapid cooling, most probably due to post-Variscan exhumation, until they were brought to the surface.
2) The basement rocks were buried by 1.5 to 5.5 km of Carboniferous and possibly Permian-Triassic sediments, which combined with a likely higher geothermal gradient, resulted in the highest temperatures that the basement rocks and Carboniferous sediments would

experience until the present day, leading to their acquisition of their present-day vitrinite reflectance values. Peak heating occurred at some time between the latest Carboniferous (*i.e.* Variscan) and late Triassic.

3) One or several periods of uplift and erosion occurred subsequently until the deposition of Hauterivian sediments in the area. The erosion events left only c. 300 m of preserved Carboniferous sediments. By combining sonic velocity, VR data and thermal history modelling of AFT and AHe data, it is estimated that probably 2 ± 1 km of sediments were eroded before deposition of the Hauterivian sediments. This erosion occurred probably during several episodes, including the regionally significant post-Variscan exhumation and Triassic-Jurassic rift-induced exhumation.
4) After the Hauterivian, two thermal histories are envisaged based on conflicting thermochronological data. The first history (the 'hot' history) indicates that the area probably experienced some burial during the Aptian-Albian followed by quick or protracted uplift and erosion during the Late Cretaceous, with some minor burial and exhumation during the Eocene to Recent. The second history (the 'cold' history) indicates a lesser magnitude of burial during the Aptian-Albian, followed by cooling to near-surface temperatures and a relative absence of any significant heating or cooling until the present-day. Both histories record the same Albian-Aptian heating event followed by cooling, the difference being that the 'hot' history has more amplified temperature swings than the 'cold history'.
5) The two scenarios are based on conflicting AHe ages and track length distributions. This apparent conflict cannot be resolved unless new data is acquired (more high-quality AHe ages and more confined tracks normalized to standards) or unless external geological data favour one of the two scenarios.

5.4 Borehole 34/05-1

5.4.1 Exploration history and geological summary

Borehole 34/05-1 is a dry hydrocarbon exploration well drilled in 1980 by Elf Aquitaine (now Total) to a depth of 1488 mMD. The borehole was drilled on the eastern edge of the Porcupine High (FIGURE 33 AND FIGURE 44). The well encountered 386 m of Cenozoic clastics with a basal Eocene-Paleocene sandstone resting unconformably on non-fossiliferous red brick claystones and siltstones of possible Albian age (35 m). This thin Albian unit rests unconformably on a thick succession of Paleozoic sediments of Autuno-Stephanian to Westphalian B age (>750 m). The borehole terminated in a quartzite of indeterminate affinity and age (FIGURE 54).

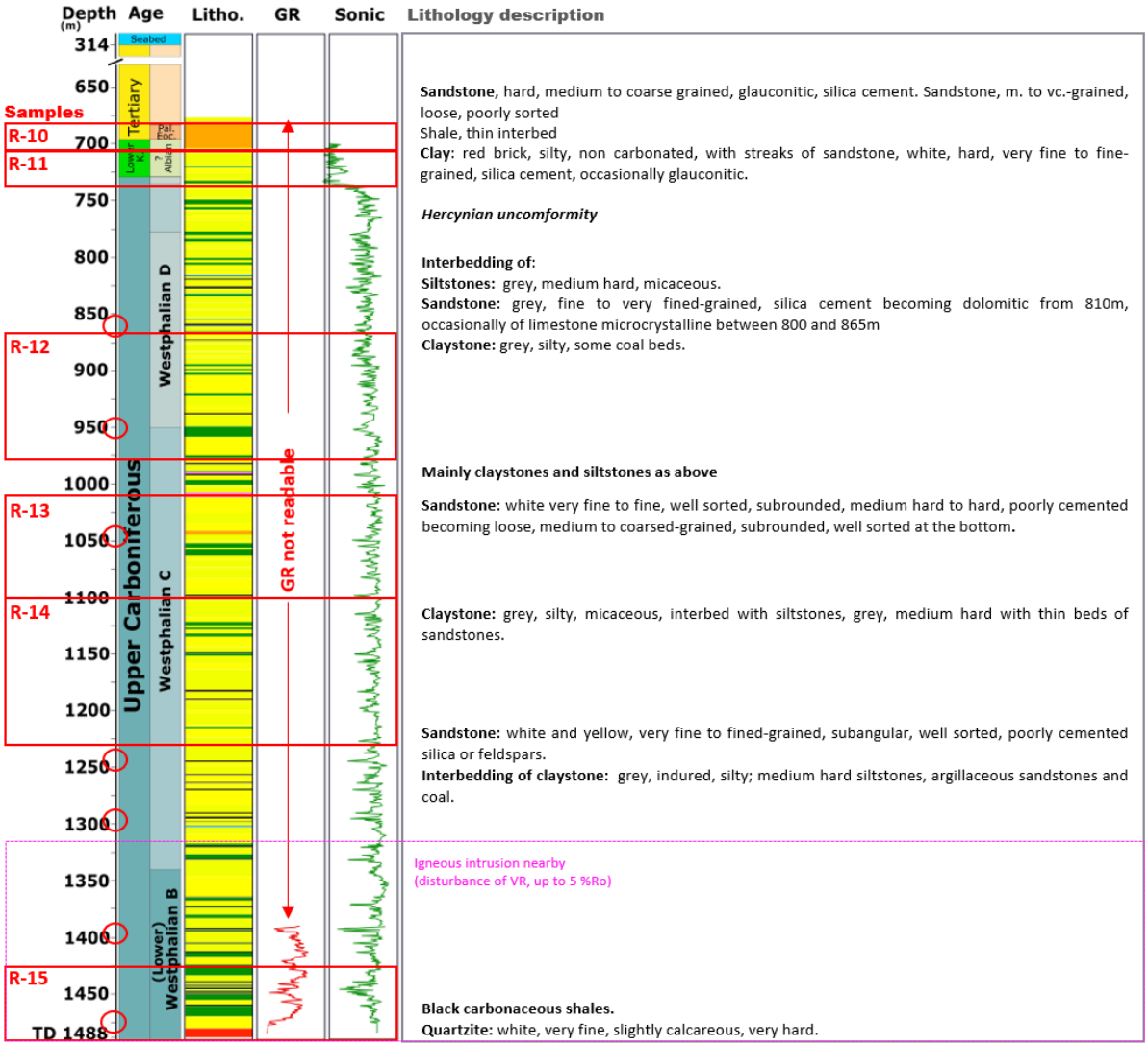

Figure 54: Well 34/05-1 logs, lithology description from composite log and sampling intervals (log data and lithology description from Croisile (1980)).

5.4.2 Igneous intrusion(s) in borehole 34/05-1

A previously unrecognized igneous intrusion has been identified between 1346 and 1364 mMD (previously interpreted as a sand) with a thermal aureole of c. 20 m on either side that explains the thermal indicators anomalies reported in the geochemical report (FIGURE 55). A detailed analyses of the data supporting this interpretation is presented in ANNEX 1 SECTION 5.1. The intrusion is characterized by a blocky and low GR response, high sonic velocities, a zone of spiky low resistivity at the bottom, a grey-green fine-grained lithology (probably dolerite) and the presence of organic matter affected by high temperatures in the vicinity of the intrusion (coke textures in coal, high VR, TAI and T_{max}) (FIGURE 55). Another thin intrusion might be present at 967.5-970 mMD based on the anomalous colour of cuttings and some high VR values a few tens of meters above and possibly just below the base of the borehole.

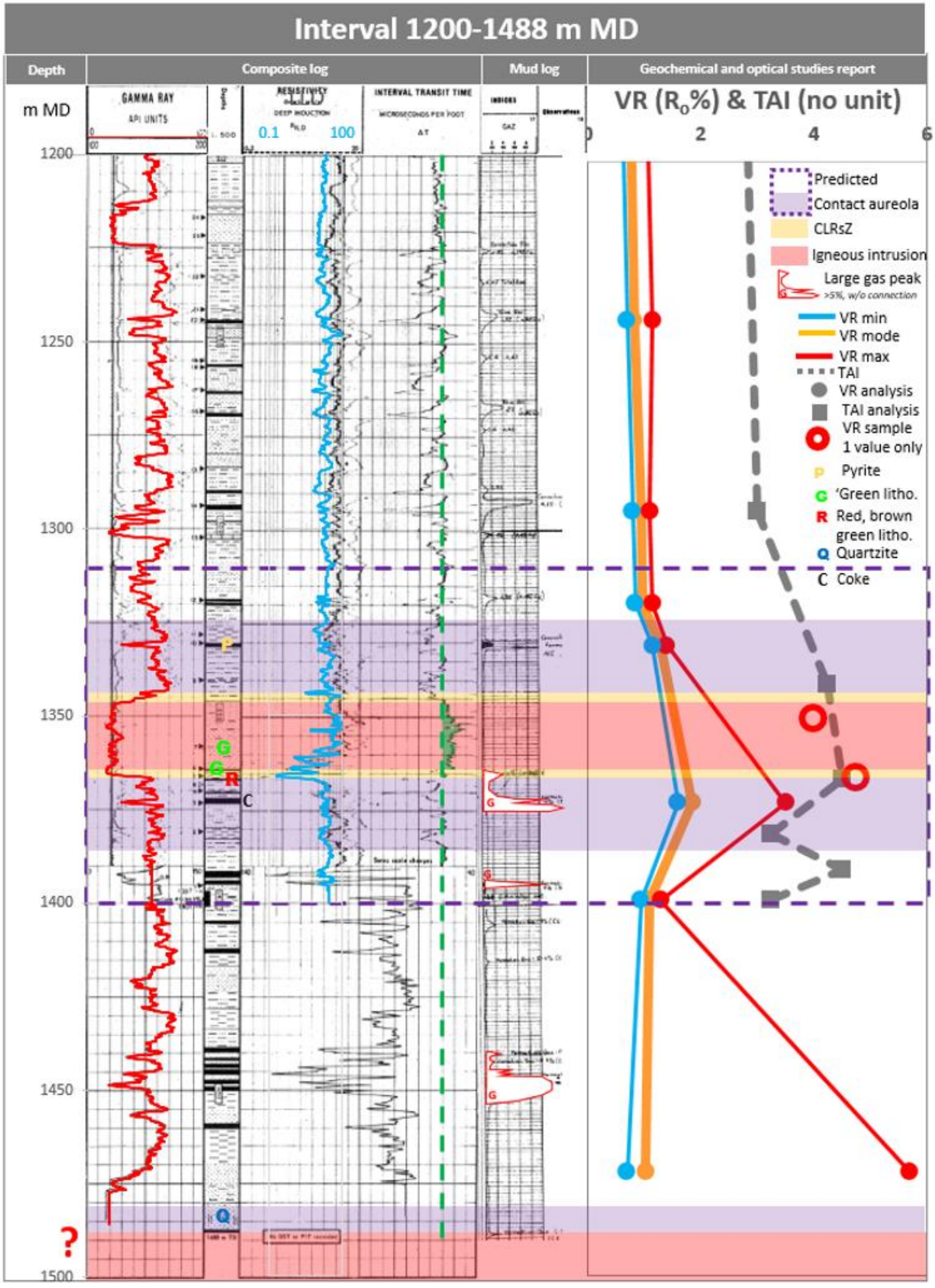

Figure 55: 34/05-1 location of doleritic intrusions between 1200 and 1488 mMD (TD).

5.4.3 Age and significance of the red brick clastic unit

The red clastic unit between the Paleocene-Eocene sandstone and Carboniferous clastics is described as a non-carbonaceous, red-brick silty clay, with streaks of very fine to fine-grained white sandstone, occasionally glauconitic. It is tentatively attributed to the Albian (with a question mark) by the operator (Croisile, 1980) (FIGURE 54). The age of this unit is important because it can yield useful information about the age of its basal unconformity and consequently a better understanding of the timing of uplift and erosion events in the area.

A detailed analysis of the lithological and biostratigraphical data is provided in ANNEX 1 SECTION 6. The borehole data (FIGURE 56) support two main hypotheses for the age of the red unit is:

1) Albian with Paleocene-Eocene cavings (the main hypothesis of the operator)
2) Paleocene-Eocene with Albian reworking

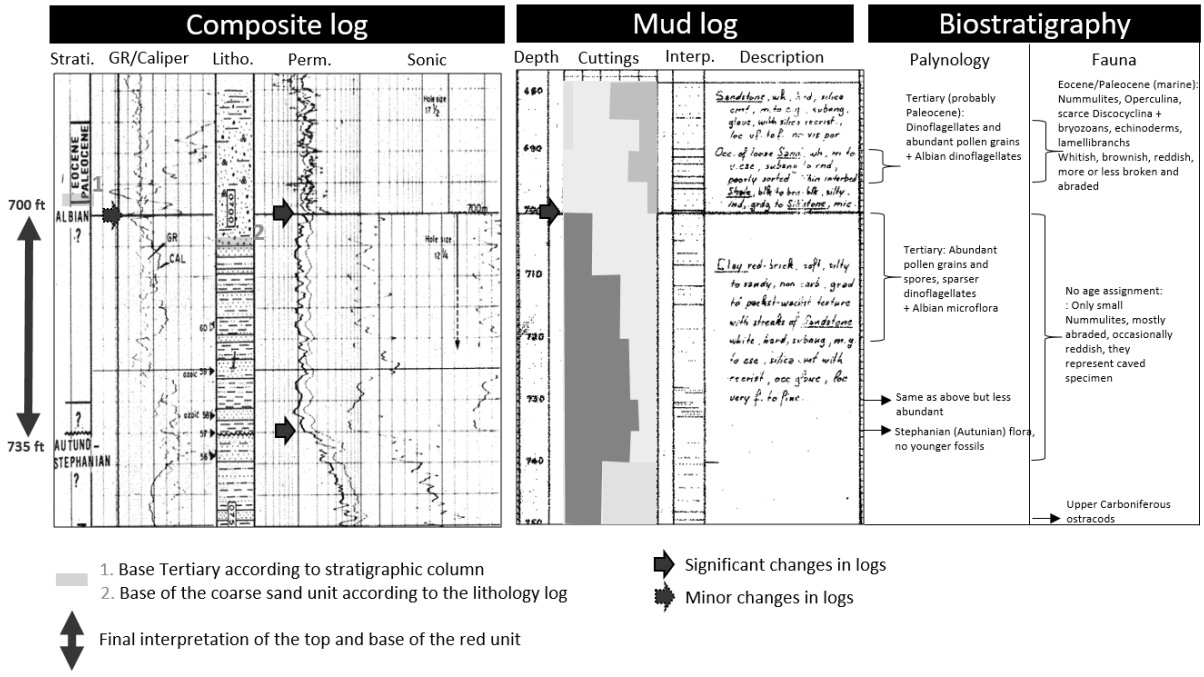

Figure 56: Determination of the top and bottom boundaries of the red unit based on information from the composite log, mud log and biostratigraphical report of borehole 34/05-1.

If the red unit is Paleocene-Eocene in age, the borehole contains only one unconformity at 735 mMD (FIGURE 56), which marks the boundary between the Paleocene-Eocene continental deposits and the Upper Carboniferous sediments. This unconformity is probably an amalgamated unconformity including the regionally widespread Variscan unconformity (VU), the Base Middle Jurassic Unconformity (BMJU), the Base Cretaceous Unconformity (BCU) and the Base Cenozoic Unconformity (BTU). For this study, this unconformity at 735 mMD will be referred as the top Top Carboniferous Unconformity (TCU).

If the red unit is Albian in age as proposed by the operator, the TCU would only include the VU, BMJU and BCU, while the BTU would be located at 700 mMD (FIGURE 56).

5.4.4 TCU exhumation estimates

The same methodology as used for borehole 26/26-1 was used for this borehole. The detailed analysis can be found in ANNEX 1 SECTION 3.2.

Combining the sonic velocity and VR data constrains the amount of uplift and erosion associated to the TCU to 2000 $\pm \frac{2000}{1000}$ m with an associated paleogeothermal gradients of c. 60 $\pm \frac{40}{30}$°C.km^{-1}.

Hypothesis 1: Late Carboniferous-Permian peak temperatures - high geothermal gradient with lower denudation (1-2 km) (FIGURE 57B)

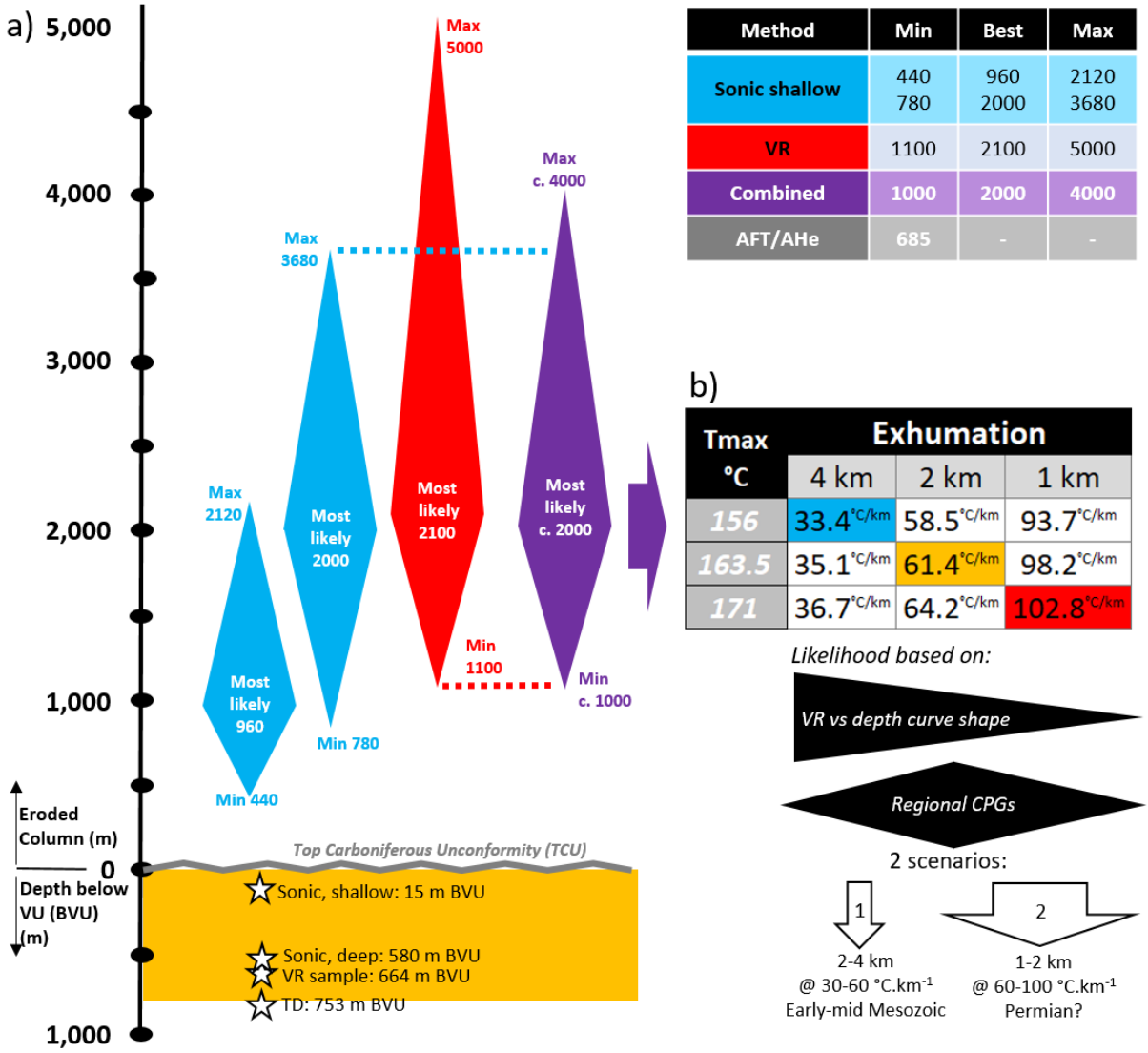

Figure 57: a) Summary of exhumation estimates at the TCU from sonic velocities and VR data (34/05-1). b) Paleogeothermal gradients required to reach the maximum temperature at 1400 mMD depending on the thickness of eroded materials from the combined datasets.

Regionally, the Carboniferous sediments are believed to have acquired their high levels of maturity (VR) during the Carboniferous-Permian as proved by the break in slope and lower VR values of Mesozoic sediments in boreholes containing both Carboniferous and Mesozoic-Cenozoic sediments (Robeson et al., 1988). The average CPG is c. 60°C.km^{-1} as calculated by Corcoran and Clayton (2001), which corresponds to the lower part of the estimated range for 34/05-1.

If the Carboniferous sediments acquired their highest maturity with a high geothermal gradient (60-100°C.km^{-1}) during the Carboniferous-Permian, then a missing section of c. 1000 to 2000 m must be Carboniferous or Early Permian in age. The younger Carboniferous sediments in 34/05-1 are Westphalian D clastics overlain by c. 15 meters of Stephanian (*i.e.* latest Carboniferous) or Autunian (*i.e.* Lower Permian) sediments (from 735 to c. 750 mMD). Therefore the c. 1000-2000 m of eroded section can only be Stephanian or Autunian in age.

In the basins offshore west of Ireland, the borehole with the thickest Stephanian-Autunian section is 34/15-1 (c. 50 km south of 34/05-1) which penetrated 354 m of Autunian sediments and 98 m of Stephanian sediments. The well stopped at 4446 mMD in Stephanian sediments so the Stephanian could be thicker. The Autunian is overlain unconformably by Middle Jurassic sediments so the Autunian could have been thicker as well before being partly eroded. Consequently, it is plausible that one to two kilometers of Stephanian to Autunian sediments was present at the location of borehole 34/05-1 and subsequently eroded. However, the Stephanian sediments in 34/15-1 have VR values of c. 2 R_o% which is significantly higher than in 34/05-1, so it would require a significant higher thickness of Stephanian-Autunian sediments in 34/15-1 or a higher geothermal gradient.

Based on the surrounding wells, it is possible that an additional 1000-2000 m of Stephanian - Autunian sediments were present above the present-day TCU, although no such thickness is preserved presently in any well offshore west of Ireland.

Hypothesis 2: Early Mesozoic peak temperatures - low to medium geothermal gradient with higher denudation (2-4 km) (FIGURE 57B)

Another hypothesis, supported by the shape of the VR *vs* depth curve, is that the Carboniferous organic matter acquired its maximum maturity with a low to medium geothermal gradient of c. 30-60°C.km^{-1}. Such gradient requires a greater thickness of eroded sediments, c. 2000-4000 m, which implies an erosion of Upper Carboniferous to Mesozoic sediments (possibly Upper Carboniferous to Lower Jurassic). The lower geothermal gradients (c. 30-40°C.km^{-1}, similar to present day gradient) at the time the Carboniferous organic matter reaches maximum peak temperature could be explained by average continental crust geothermal gradient, while the higher ones (40-60°C.km^{-1}) could have been caused by rifting in the nearby Porcupine Basin.

5.4.5 Samples

5.4.5.1 Sampling strategy

This borehole was selected because it is located on a high (and is thus more prone to be eroded during uplift events) and has one (possibly two) major unconformities (the Top Carboniferous Unconformity and possibly a Base Cenozoic Unconformity if the red unit is Albian in age).

Six samples were taken from cuttings from the Paleocene-Eocene sandstone (R-10, 680-710mMD), Paleocene-Eocene (or Albian) siltstones (R-11, 710-738 mMD) and Westphalian D (R-12, 870-980 mMD), Westphalian C (R-13, 1010-1100 mMD & R-14, 1100-1230 mMD) and Westphalian B (R-15, 1425-1490 mMD) clastics (FIGURE 54). At the time of sampling, the igneous intrusion discussed above had not yet been recognized and therefore no sampling of this potential igneous rock was undertaken.

To constrain various uplift events, it is important to have thermochronometry data from either side of an unconformity. Consequently, the first two samples are very important since they are the only sample that could be taken above the TCU. Only limited material was available for both of them (180-190 g). This is the first thermochronological study undertaken for this borehole, so no legacy sample is available. Zircon were also picked for all samples with the primary goal of better constraining the age of the red unit (by comparing its zircon age profile to the Eocene and Lower Cretaceous samples) and the secondary goal of providing provenance data.

5.4.5.2 Apatite and zircon yield

Apatite yield

Due to a small amount of materials available the first two samples yielded very few apatites. Only two of them were suitable for AFT ages for sample R-10 and none for R-11. None of the grains were suitable for AHe studies because of their small size and quality.

Samples R-12, R-13, R-14 and R-15 all had a few dozens of apatites. Most of them were of poor quality, either small and/or fractured and/or anhedral. Due to the low amount of good quality apatites in samples R-13-14, these two samples were combined as one sample to select three grains for AHe analysis. Five grains for both samples R-12 and R-15 were also selected for AHe analysis.

Zircon yield

Numerous zircons (>100 grains) were found for all six samples.

5.4.5.3 U/Pb and trace element results

The results are presented in details in ANNEX 1 SECTION 1.2.1 and are discussed below.

Age of the red unit

The red unit (or part of the lower section of the unit) could be either Albian or Eocene in age (SEE SECTION 5.4.3). The presence of apatite or zircon grains younger than Albian in age would have reinforced the Eocene hypothesis, however no such young grains have been found (FIGURE 58 AND FIGURE 59). But since no Paleogene grains have been found in the Eocene sample R-10 either, it is also not proof that the unit is older than Eocene. The presence of a zircon dated at 100.3 ± 3.4 Ma (Albian-Cenomanian boundary) in this unit (sample R-11) could be explained by syn-sedimentary volcanism (e.g. ash fall) if the unit is Albian or by erosion of Albian volcanics if the unit if Eocene in age. Therefore, this grain cannot help to refine the age of the red unit.

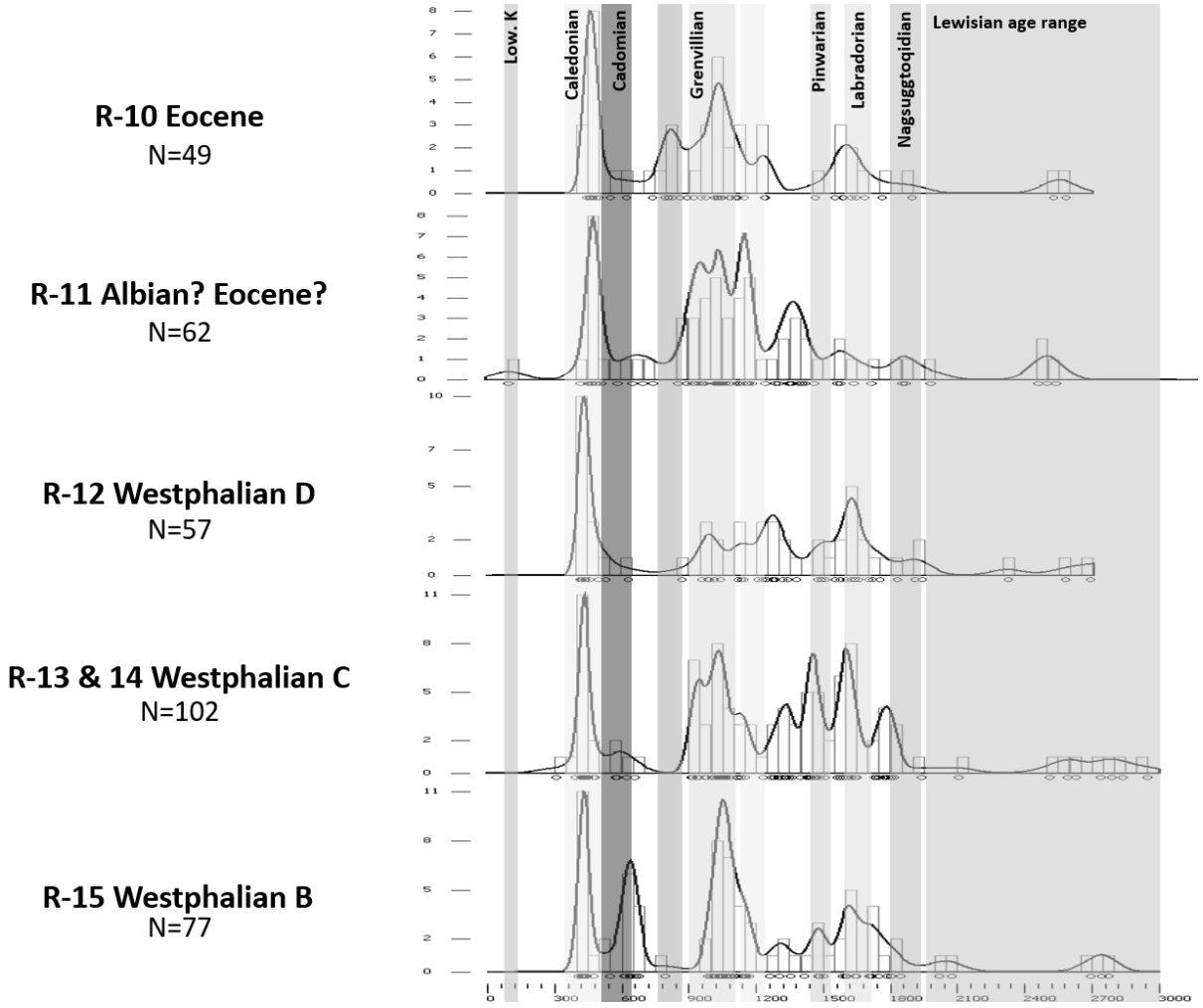

Figure 58: Histograms and KDEs of zircon $^{206}Pb/^{238}U$ ages (concordant grains only) from samples R-10, R-11, R-12, R-13-14 and R-15 (34/05-1).

Clastic sources

From Late Carboniferous to Eocene times, the clastic sediments deposited in the area of 34/05-1 seem to be predominantly sourced from Caledonian outcrops with secondary inputs from Grenvillian and Labradorian terranes and minor input from other Proterozoic and Archean terranes. However, all the

zircons in samples R-10 and R-11 and the older (i.e. pre-Caledonian) zircons in the Carboniferous samples could also have been recycled from older sedimentary rocks (FIGURE 58).

A peak of Cadomian zircons is present in the bottom sample R-15 but absent in the younger samples R-10 to R-13-14. A small peak of post-Grenvillian zircons (c. 812 Ma, Knoydartian Orogeny?) is present in the Eocene sample R-10 but not in the older samples. This could tentatively suggest that Knoydartian igneous rocks could be present on the Porcupine High and were exposed and eroded at the beginning of the Cenozoic (FIGURE 58); the closest identified exposures of Knoydartian igneous rocks are in the Moine Supergroup of NW Scotland.

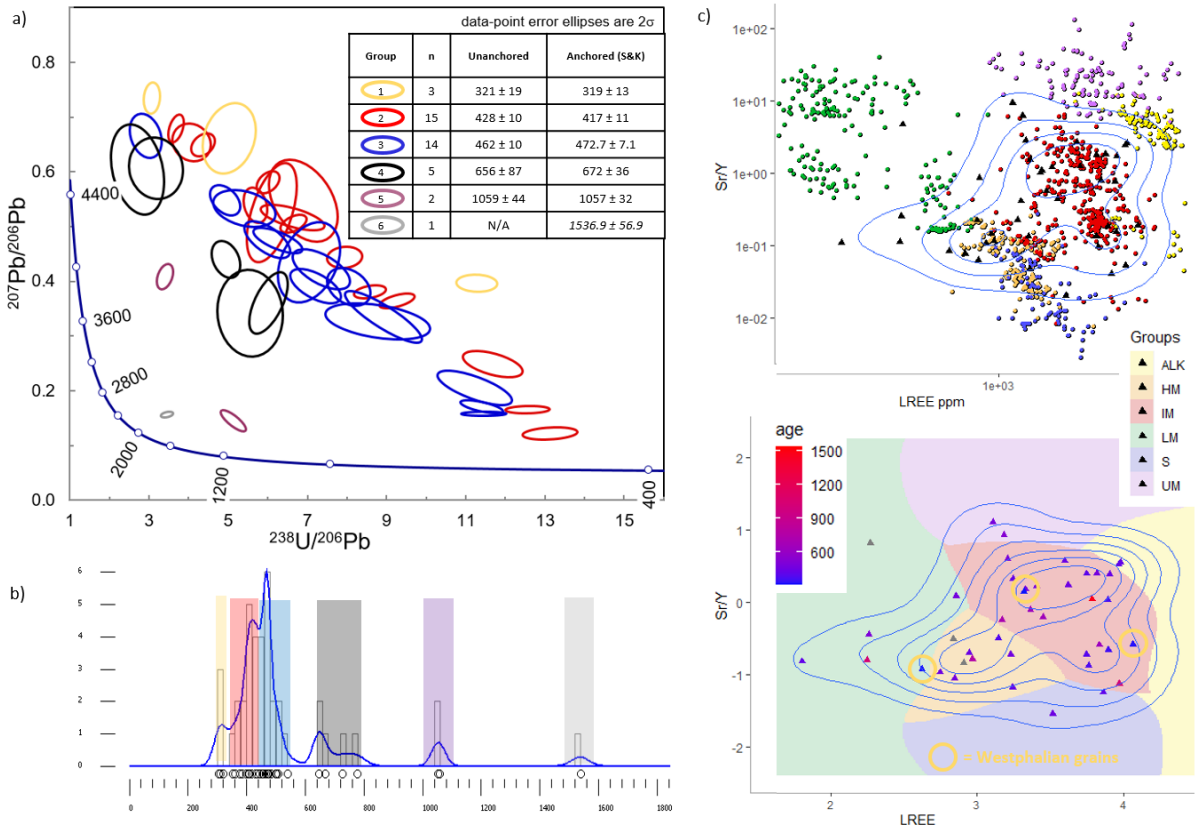

Figure 59: Carboniferous samples R-12-15 (34/05-1) apatite U/Pb results. a) Tera-Wasserburg plot of all 40 grains, colour-coded by age groups. The table shows the discordia lower intercept age for each group (without and with common Pb anchoring). b) Histogram and KDE of the ^{207}Pb-corrected ages, colour-coded by groups (see a)). c) Sr/Y vs LREE biplot for apatite grains from samples R10 and R-12-15.

Contemporary tuffs?

Three apatite grains and one zircon grain have a Late Carboniferous age of respectively 319 ± 13 Ma (Visean to Stephanian A) for the apatites and 305.9 ± 6.9 Ma (^{206}Pb/^{238}U, Westphalian C to Autunian) to 312.7 ± 11.3 Ma (^{207}Pb/^{235}U, Namurian to Autunian) for the zircon. The apatites come from samples R-12, 14 and 15 with a depositional age of Westphalian B, C and D, while the zircon comes from R-13 with a depositional age of Westphalian C.

It is therefore possible that these apatites and zircons are syn-depositional igneous grains deposited from ash falls (tuffs) or transported as eroded materials from Carboniferous extrusive rocks. No tuff is described in the well report or composite log of borehole 34/05-1 (Croisile, 1981). However, significant volcanism is known throughout the Carboniferous in Ireland (e.g. Limerick Volcanic Basin, Shelford (1967)) and particularly in Scotland (Upton et al., 2004). Carboniferous tuffs have been identified in boreholes 13/03-1 in the Donegal Basin and 35/15-1 on the eastern margin of the Porcupine High (Robeson et al., 1988). These apatites and zircons attest to the likely existence of previously unrecognized tuff layers in the Carboniferous section of borehole 34/05-1.

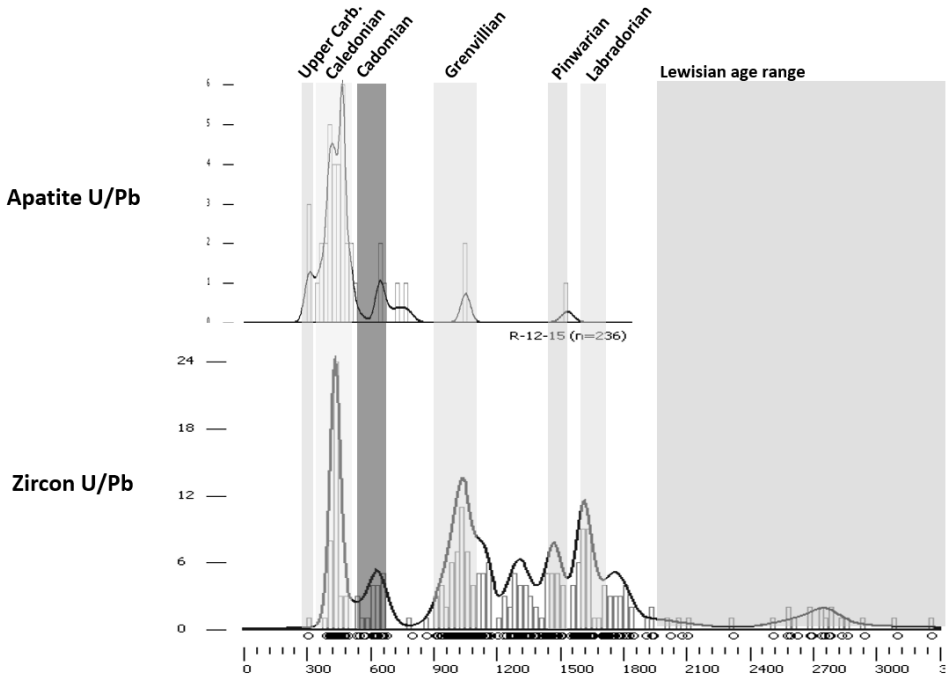

Figure 60: Apatite and zircon U/Pb ages for combined sample R-12-15 (34/05-1).

No Paleogene igneous intrusion at the sampling depths

There are no Paleogene apatites or zircons in any of the samples. This lack of Paleocene grains supports the assumption that the depth intervals corresponding to each sample do not contain any undetected Paleocene igneous intrusions.

5.4.5.4 AFT and AHe results

The detailed presentation of the AFT and AHe results are in ANNEX SECTION 2.2.3, a summary is given in TABLE 13 and FIGURE 61 and discussed in this section.

Table 13: Summary of the AFT and AHe results for samples R-10 to R-15 (well 34/05-1, Porcupine High).

a) AFT Results

Sample	Depth		n	Ns	Area	U/Ca	P(χ^2)	Central Age	±1σ	Tracks	MTL	SD	SE	Inverse?	
	m MD	m BSB			cm^2			Ma	Ma		µm	µm	µm	FTA	FTL
10	695	381	2	70	6.23E-05	0.08872934	0.02	130	27	3	13.18	1.36	0.79	No	No
11	724	410	0	-	-	-	-	-	-	-	-	-	-	No	No
12	925	611	2	105	3.96E-05	0.163171201	0.04	164	24	19	11.86	1.82	0.42	No	No
12-14	1050	734	31	1107	0.000576	0.117338511	<0.01	165.8	8.4	77	11.63	1.90	0.22	No	No
			29	1082	0.000535	0.12	<0.01	168.5	7.7	75	11.59	1.92	0.22	Yes	Yes
13	1055	741	21	730	0.000368	0.121875993	<0.01	166	11	39	11.50	2.16	0.35	No	No
14	1165	851	8	272	0.000169	0.096710739	0.03	167	16	19	11.66	1.29	0.30	No	No
15	1457.5	1144	11	277	0.000246	0.117276108	0.02	110	13	10	11.52	2.14	0.68	Yes	No
			9	103	0.000218	0.034194478	0.90	136	14	9	13.18	-	-	Yes	No

b) AHe Results

Sample	Grain	Shape in GFTC		Length	Diameter		S/V	R_{eq}	Weight	Temp.	$[^{238}U]$	$[^{232}Th]$	$[^{147}Sm]$	eU	Th/U weight	[He]	Degassing	Raw Age	Error	F_T	Correc. age	Error
				W	Max	Min																
		Geometry	GFT*	µm	µm	µm		µm	g	°C	ppm	ppm	ppm	ppm		nmol/g		Ma	Ma		Ma	Ma
12	4	Hexagonal prism	1P1F	135	56	48	0.098	30.7	7.70E-07	27.3	15	89	1131	41	6.1	7.9	Ok	33	5	0.558	59	9
	3	Hexagonal prism	2F	109	65	59	0.089	33.9	9.80E-07	27.3	57	470	1993	176	8.3	47.3	Ok	47	7	0.601	79	12
	2	Ellipsoid	N/A	104	72	59	0.082	36.5	7.40E-07	27.3	41	71	477	60	1.7	20.2	Lack of heat	60	9	0.6	101	15
	1	Hexagonal prism	1P1F	109	57	37	0.110	27.2	5.10E-07	27.3	1	11	10	3	18.9	16.6	Ok	898	135	0.507	1770	266
	5	Hexagonal prism	2F	98	59	54	0.097	30.9	7.40E-07	27.3	1	8	6	2	11.8	22.8	Lack of heat	1556	233	0.568	2739	411
15	1	Hexagonal prism	2B	84	69	62	0.090	33.3	8.50E-07	42.4	3	46	736	17	16.5	1.6	Ok	15	2	0.598	25	4
	4	Hexagonal prism	2F	208	66	58	0.080	37.7	1.88E-06	42.4	1	34	337	11	29.2	2.3	Ok	36	5	0.633	57	9
	3	Hexagonal prism	2F	117	78	68	0.076	39.5	1.50E-06	42.4	3	291	591	74	91.5	15.4	Ok	37	6	0.653	57	9
	5	Hexagonal prism	2F	114	80	71	0.075	40	1.54E-06	42.4	20	242	607	79	12.1	23.7	Ok	53	8	0.658	81	12
	2	Hexagonal prism	2F	124	76	67	0.076	39.2	1.51E-06	42.4	0	5	8	1	44.1	10.7	Ok	1320	198	0.651	2027	304

**GFT = Type of prism terminations used in the Alpha Ft-ejection factor software of Gautheron et al.*

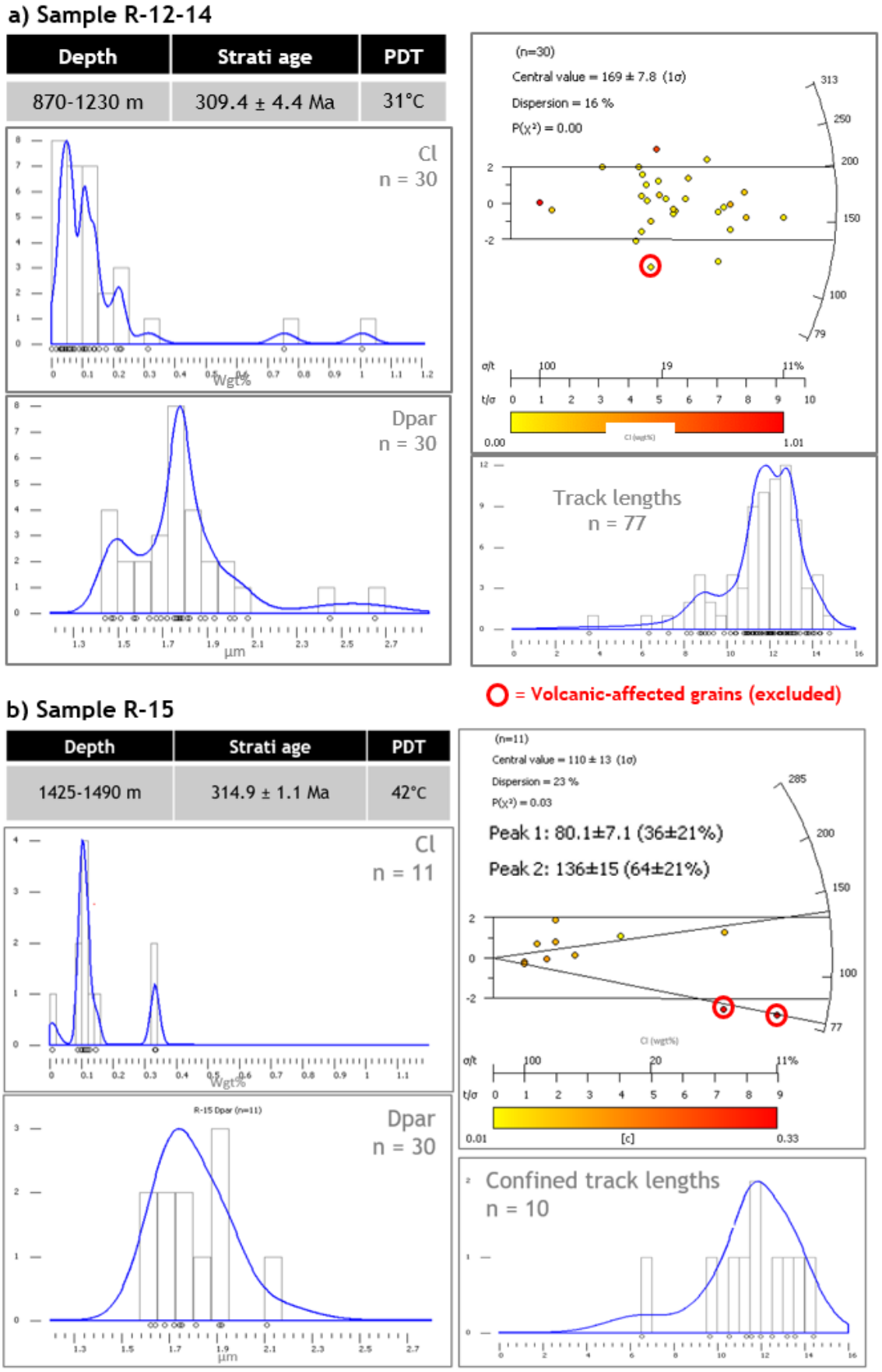

Figure 61: AFT results for borehole 34/05-1. a) AFT results of sample R-12-14. b) AFT results for sample R-15.

Only two samples have yielded enough AFT ages and track length data to be used for thermal history modelling and subsequent geological interpretation (Carboniferous samples R-13 and R-15). The absence of apparent unconformities in the Carboniferous and the close depth range of samples R-12 to R-14 allows them to be combined as one sample with enough AFT ages and confined tracks to be used for inverse modelling (FIGURE 61). However, this merging cannot be done for the first two samples (R-10 and R-11) as they are separated by a major unconformity (and also do not have enough fission track ages and track lengths).

The Eocene sample does not seem to have experienced any significant amount of time in the high temperature portion of the PAZ. On the contrary, the two Carboniferous samples (R-12-14 and R-15) have probably experienced complete annealing after deposition since their AFT age is much younger than their stratigraphic age. Sample R-15 has a younger AFT age than the shallower R-12-14, which is expected since it resided at higher temperatures throughout the burial history. This difference of age with depth will help reduce the range of thermal histories fitting the data using inverse modelling.

Both samples have grains with low chlorine content and a narrow range of Dpar lengths, which suggests that each sample can be modelled without the need to separate the grains into families with different kinetic values.

Both samples R-13 and R-15 contain grains that might have been reset by Paleogene volcanic activity (thermal aureoles of intrusions or hydrothermal fluids). These grains support the hypothesis of the existence of an igneous intrusion a few meters below the TD of the well (1488 mMD) and a thin unrecognized intrusion at c. 1050 mMD.

The AHe ages are younger (15-60 Ma) than the AFT central ages (136-169 Ma) for both samples R-12 and R-15. This suggest that the samples had a rather slow and protracted cooling through the partial helium retention zone (PHeRZ). The age dispersion is partly explained by both variation in radiation damage and grain size. Modelling grains with large differences in eU and S/V will help better constrain the various possible thermal histories for the well (FIGURE 62).

Effect of igneous intrusion(s)

The FT data revealed that some grains from R-12-14 and R-15 might have experienced high temperatures during the emplacement of igneous intrusions during the Paleogene. If this was the case, then some of the apatites in these samples might have lost all their helium at that time since helium in apatites is lost at lower temperatures than total annealing of fission tracks. The risk is higher for sample R-15 than for R-12-14. It is not possible to diagnose which grains might have been affected by a such thermal resetting event. Since all the reliable grains have ages < 60 Ma and some grains are much younger (down to 15 Ma), it means that other processes than igneous intrusions (probably

burial) have affected the grains, otherwise the grains would not be younger than c. 60 Ma. Consequently, the AHe data will be assumed to represent the effects of burial, although the effect of Paleogene volcanism cannot be excluded.

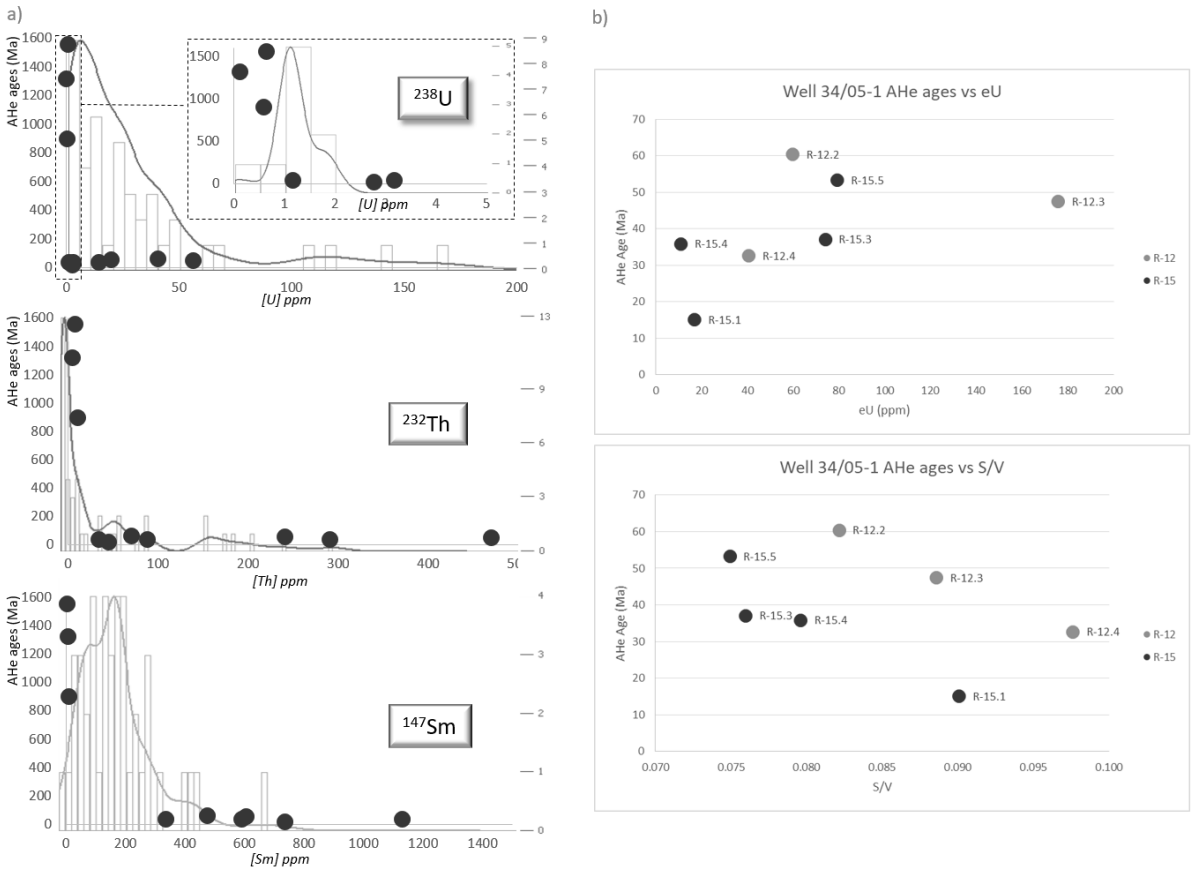

Figure 62: a) 34/05-1 Carboniferous samples AHe ages vs [U], [Th], [Sm] with AFT [U], [Th], [Sm] histograms and KDEs as background. The three grains with anomalously large AHe ages (>800 Ma) all have anomalously low uranium and samarium content in comparison to the 31 grains from the AFT population. b) AHe age dispersion plots: AHe ages vs eU and AHe ages vs S/V.

5.4.6 Thermal history modelling

5.4.6.1 Input data

AFT input data

Only samples R-12-14 and R-15 have enough fission track data to be used for inverse modelling purposes. Both fission track age and track lengths data are available for R-12-14, while only fission track age data are available for R-15 (not enough confined track lengths to be used as input data).

AHe input data

For sample R-12-14, all three grains with reliable ages (R-12.2, 3 and 4) are used in the model. They have S/V ratios varying from 0.082 (largest grain) to 0.098 (smallest grain) and eU varying from 41 to 176 ppm with AHe ages of respectively 60, 47 and 33 Ma. If the model can reproduce all three ages with a single thermal history, it would mean that radiation damage would be the main cause of age

dispersion in this sample. The small variation in grain size does not allow the influence of size (S/V) on age dispersion in this sample to be tested.

For sample R-15, AHe data from grains R-15.1, 3, 4 and 5 are used in the model. They have S/V ratios ranging from 0.075 to 0.09 and eU varying from 11 to 79 ppm with AHe ages of respectively 15, 37, 36 and 53 Ma. If the model can reproduce most ages with a single thermal history, it would mean that eU is probably the main cause of age dispersion between these grains. The small variation in grain size does not allow the influence of size (S/V) on age dispersion in this sample to be tested.

VR data

The VR samples that are not inferred to have been affected by igneous intrusions have been imported in QTQt (seven samples). The data is not used to constrain the model but is compared to predicted VR values for the same depths based on the various thermal histories.

5.4.6.2 Initial and final time-temperature constraints

Final conditions: Present-day temperature of sample

Using the estimated geothermal gradient of 28.3 ± 5.3°C.km^{-1}, sample R-12-14 has a present-day temperature of 30.9 ± 3.9°C, while sample R-15 has a temperature of 42.4 ± 6.1°C (FIGURE 63).

a) Prior information and MCMC chain parameters

Categories		Values
Prior information	Time Temperature	167.25 ± 167.25 Ma 80 ± 80 °C
	Max dT/dt Reheating Temperature offset Offset	1000 °C.My Yes 11.21 °C Constant
MCMC chain	Burn-in Post-burn-in Thinning	100,000 100,000 1
Proposed move	Time Temperature Offset Resample/Reject Reject complex	30 30 0.001 Resample Yes

b) Model names and characteristics

		Samples	Constraints	Gradient	tT points
Model 0		Both	None	Constant	Low (Simple)
Model 1	a	Both	Scenario 1	Constant	Low (Simple)
	b		Scenario 1 + VR	Constant	Low (Simple)
	c		Scenario 1 + VR	Constant	High (Complex)
Model 2	a	Both	Scenario 2 + VR	Constant	Low (Simple)
	b		Scenario 2 + VR	Constant	High (Complex)
	c		Scenario 2 + VR	Variable	Low (Simple)

c) Model constraints

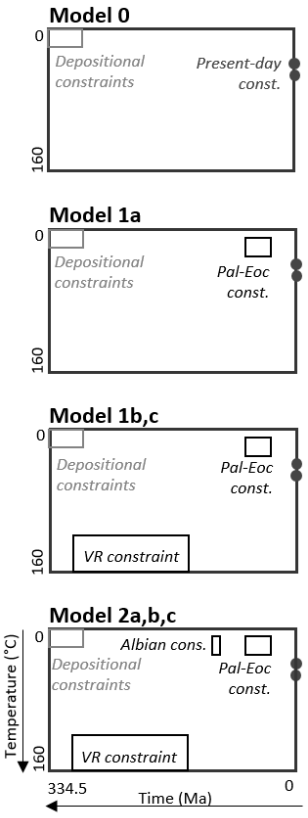

Figure 63: 34/05-1 QTQT modelling parameters. a) Prior information and MCMC chain parameters. b) Model names and characteristics. c) Visual retransitions of the different model constraints.

Initial conditions - Depositional age and temperatures

The depositional ages of sample R-12-14 and R-15 are respectively 311.4 ± 3.9 Ma and 316.6 ± 1.4 Ma. Since both samples are detrital and emplaced at the surface, their temperature at the time of emplacement (i.e. deposition) is defined as 10 ± 10°C (FIGURE 63).

5.4.6.3 Intermediate constraints

Time-temperature constraint boxes can be added to the model based on stratigraphy or external thermal indicators (e.g. VR). In QTQt, in the case of modelling a vertical profile, constraints only apply to the topmost sample (R-12-14 in this case).

Scenario 1: Paleocene-Eocene red clastics

In the first scenario, the red clastic unit is Paleocene-Eocene in age and there is only one unconformity in the well at 735 mMD. The basal clastics just above the unconformity were deposited at some point during the Paleocene-Eocene, so at 49.95 ± 16.05 Ma, which defines the x-axis of the constraint box. At the time of depositon of these basal clastics, sample R-12-14 was at a depth of 315 m. For simplification, no decompaction calculations have been undertaken. Using the present-day geothermal gradients, these depths translate as temperatures of respectively 18.9°C. The uncertainty of the surface temperature (±10°C) is higher than the uncertainty of the geothermal gradient, therefore it is the former which is propagated to these estimated sample paleo-temperatures. Therefore the y-axis of the constraint box is 18.9 ± 10°C for sample R-12-14 (FIGURE 63).

Scenario 2: Albian red clastics

In the second scenario, the red clastic unit is Albian in age and there are two unconformities at 735 mMD and 700 mMD. The deeper unconformity results in a constraint box defined by 106.75 ± 6.25 Ma (duration of the Albian) for the x-axis and 18.9 ± 10°C for the y-axis. The shallower unconformity results in a constraint box defined by 49.95 ± 16.05 Ma for the x-axis and 19.9 ± 10°C for the y-axis (FIGURE 63).

Intermediate constraint from VR data

The VR data analysed above can be used to create an additional constraint box (since the VR samples are not used as input data for the inverse modelling but only displayed at the end of the process for comparison). Sample R-12-14 starts at 870 mMD and terminates at 1230 mMD. The closest reliable VR samples yield values of 0.7 R_o% at 864 mMD and 0.85 at 1242.7 mMD. Using the Easy%Ro and Basin%Ro models, the maximum temperature reached by the sample can be estimated to be between 120°C and 160°C (FIGURE 64), *i.e.* 140 ± 20°C, which defines the constraint box y-axis for sample R-12-14 (FIGURE 63).

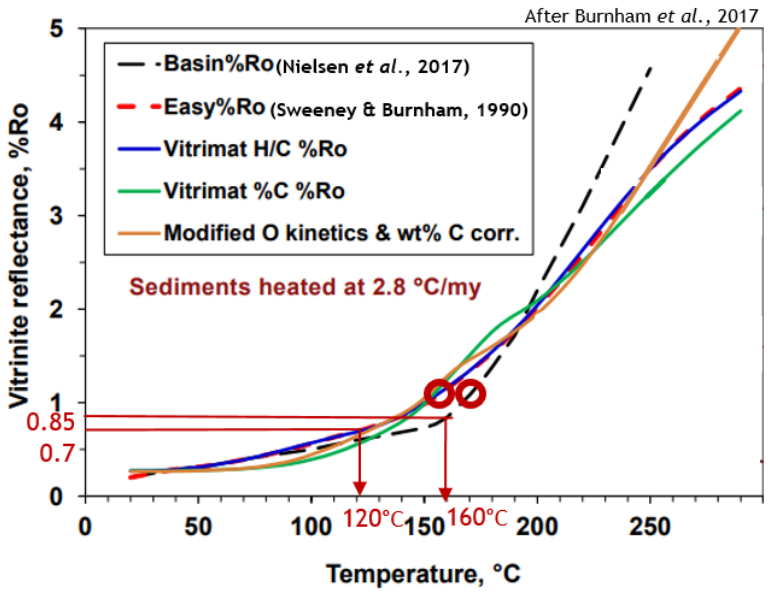

Figure 64: Maximum temperature reached by sample R-12-14 (34/05-1), estimated using the nearest VR samples (0.7 to 0.85%) converted to Tmax using the Basin&Ro and Easy%Ro models.

The maximum temperature must have been reached after deposition of the sample (*i.e.* post Westphalian D which means post 310 Ma for the most conservative case). As discussed earlier in SECTION 5.4.4, the VR of Carboniferous organic matter is assumed to be acquired before the Jurassic. The AFT central age of sample R-12-14 is 169 ± 7.8 Ma (Oxfordian-Toarcian) which means that the sample did not experience temperatures of 140 ± 20°C after this period. To err on the side of caution, the lower age limit will be fixed as top Jurassic (145 Ma), and hence the x-axis of the constraint box is defined as 145-310 Ma, or 227.5 ± 82.5 Ma (FIGURE 63).

5.4.6.4 Prior box and run parameters

For all models, the prior box is defined by 167.25 ± 167.25 Ma for the x-axis and 80 ± 80°C for the y-axis. Except when stated otherwise, the geothermal gradient of 28.3°C.km^{-1} is kept constant throughout the thermal history (*i.e.* the temperature gap between the two samples always remains the same and does not change with time) (FIGURE 63).

5.4.6.5 Modelling results

Stability of the log likelihood and log posterior chains

All the models yielded convergent log likelihood and posterior chains (*i.e.* no trend in post-burn-in models) (FIGURE 65).

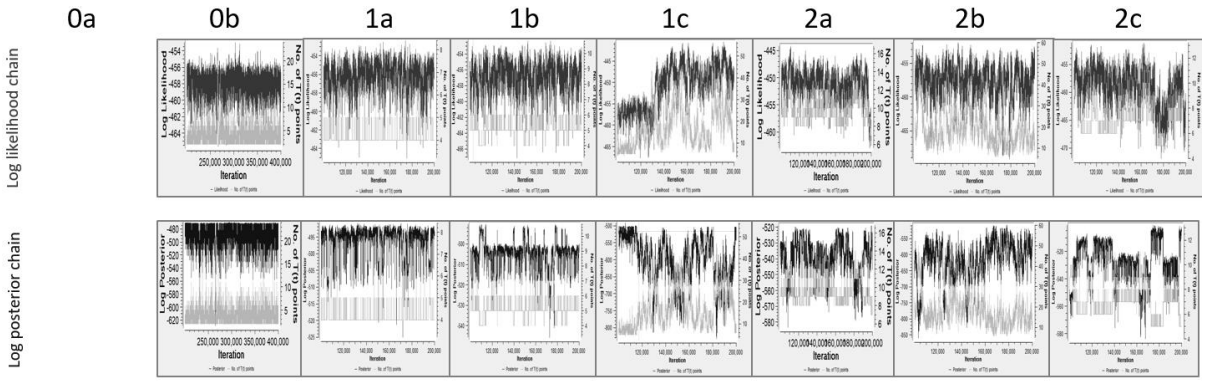

Figure 65: Log likelihood and log posterior chains for 34/05-1. Only models 1c and 2c have chains that are not stabilized.

The results and predictions of each scenario can be checked in Annex 2.

Scenario 0: No intermediate constraint

This scenariol is run to evaluate the information contained in the AFT and AHe data, independent of any geological assumptions on the temperature of the sample at any point in time.

The maximum posterior model shows a rapid increase in temperature during the first one hundred million years, followed by monotonic cooling to present-day temperatures. This simple thermal history produces a good match of the track length distribution and MTL but only a moderate match of the FT age (observed 167.2 Ma vs modelled 149.9 Ma) and a moderate match of the AHe ages. It also does not match the known stratigraphy of the well that should allow for the top sample to be near-surface temperatures at some time during the Paleocene-Eocene and some heating by burial during the Cenozoic.

Scenario 1a: Scenario 1, no VR constraint

This model is run with the unequivocal assumption that the top sample R-12-14 was near the surface during the Paleocene-Eocene as proven by the stratigraphy.

The first order thermal history for this model is similar to the last model except for a rapid cooling of c. 30°C at the end of the Eocene, from 40-60°C to 10-30°C (for the top sample, same in following paragraphs, unless stated otherwise), followed by heating to present-day temperatures after the Eocene (FIGURE 66, 1A.I).

The model with the maximum likelihood also shows a very rapid pulse of heating just before the Paleocene-Eocene cooling (FIGURE 66, 1A.III). This heating allows the resetting of one of the AHe grain that allows for a better match between modelled and measured age.

Model 1b: Scenario 1, with VR constraint

This model is run to evaluate the impact of adding a temperature constraint based on the VR data in the well.

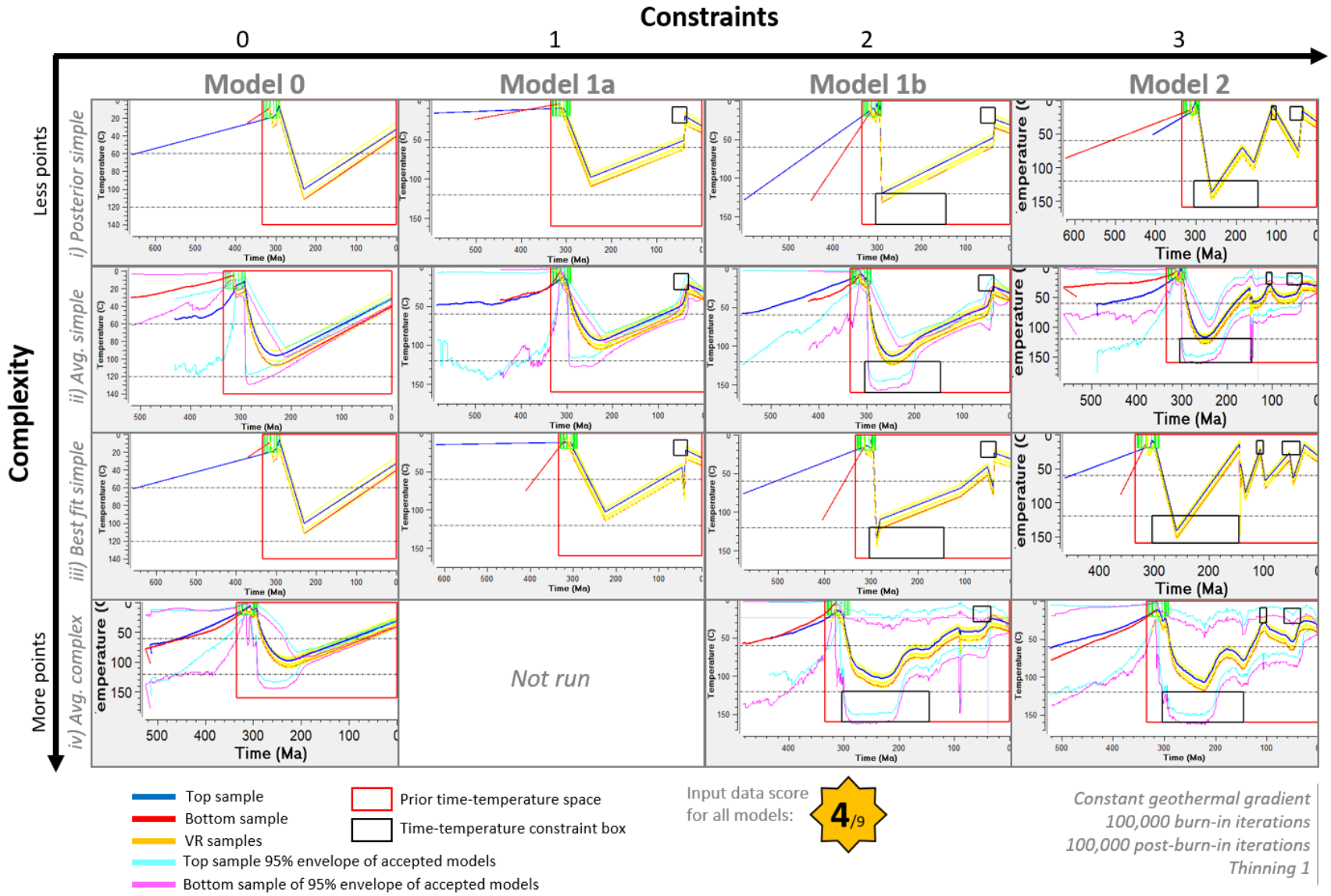

Figure 66: Summary of the various inverse modelling scenarios for borehole 34/05-1.

This model is identical to the previous one except that the rapid heating in the first one hundred million years reached slightly higher temperatures of c. 130°C (compared to c. 100°C in model 1a), caused by the time-temperature constraint box (FIGURE 66, 1B). This higher temperature allows for a very good match of the VR data.When allowing for more time-temperatures points, a heating spike at c. 95 Ma is visible in the maximum likelihood and expected models, but is absent in the maximum posterior model which is identical to the simple model. This means that the spike leads to a better overall fit of the observed and modelled data. When comparing the 'maximum likelihood' (with spike) and 'posterior' (without spike) models, it would seem that the improvement comes from one specific AHe grain. In the models without the spike, the modelled age of this AHe grain is consistently older than the measured age, while in the the models where the spike is present, the ages match.

Model 2: Scenario 2, with VR constraint

This model is run to evaluate the thermal history in the case that the red clastic unit is Albian in age as hypothesized by the operator.

Overall, the model for scenario 2 shows that the first-order cooling from c. 130°C to near-surface temperatures during the Albian is interrupted by a heating event during the middle and/or late Jurassic. After the Albian, rapid or slow heating to c. 60°C took place, followed by cooling to near-surface temperatures during the Paleocene-Eocene. The post Eocene history is similar to model 1.

Scenario 2 was also modelled with a variable geothermal gradient (28.34 ± 28.34°C.km^{-1}, since asymmetrical error, which would be more suitable to reflect plausible gradients, are not allowed in QTQt). This model did not yield any significant result.

5.4.6.6 Discussion

Paleocene-Eocene uplift

The models show that a rapid cooling pulse of c. 30°C, from c. 50°C to c. 20°C, occurred during the Paleocene-Eocene, with the highest probability being during the late Eocene. Such a cooling, at the present-day geothermal gradient, corresponds to an erosion of c. 1000 m of sediments (FIGURE 67A).

Using stratigraphic and depositional data from wells in the area, and comparing them to the expected subsidence due to post-rift thermal cooling, Jones et al. (2001b) estimated that an uplift of 300-600 m occurred at the Paleocene-Eocene boundary, followed by subsidence of 500-800 m from the Early Eocene to now (FIGURE 67B). Using a few isostatic assumptions, they also estimated that the Porcupine High was uplifted by an absolute minimum of 300 m at that time and was below seawater during the late Cretaceous and Paleocene (Jones et al., 2001b).

Therefore the exhumation derived from AFT/AHe data is two to three times greater than the minimum estimates from Jones et al. (2001b). The discrepancy can be accommodated by the possibility of a

higher geothermal gradient just before the uplift and/or higher temperatures before uplift caused by the thermal effect of igneous intrusions near the well.

The Paleocene-Eocene boundary uplift inferred by Jones et al. (2001b) is probably related to the latest Paleocene-earliest Eocene unconformity (PEBU) observed in other parts of the North-East Atlantic Margin (Smallwood and Gill (2002), Maclennan and Jones (2006), Champion et al. (2008b)). An erosional surface with a dendritic pattern, similar to the one observed in the Faroe-Shetland Basin (Smallwood and Gill, 2002) (FIGURE 67C AND D), is actually present in the northern part of the Porcupine Basin, although no study of this surface has been published so far. It is probable that the Paleocene-Eocene uplift and associated unconformity in QTQt models 1 and 2 is identical to the PEBU, and therefore dated at c. 56 ± 1 Ma.

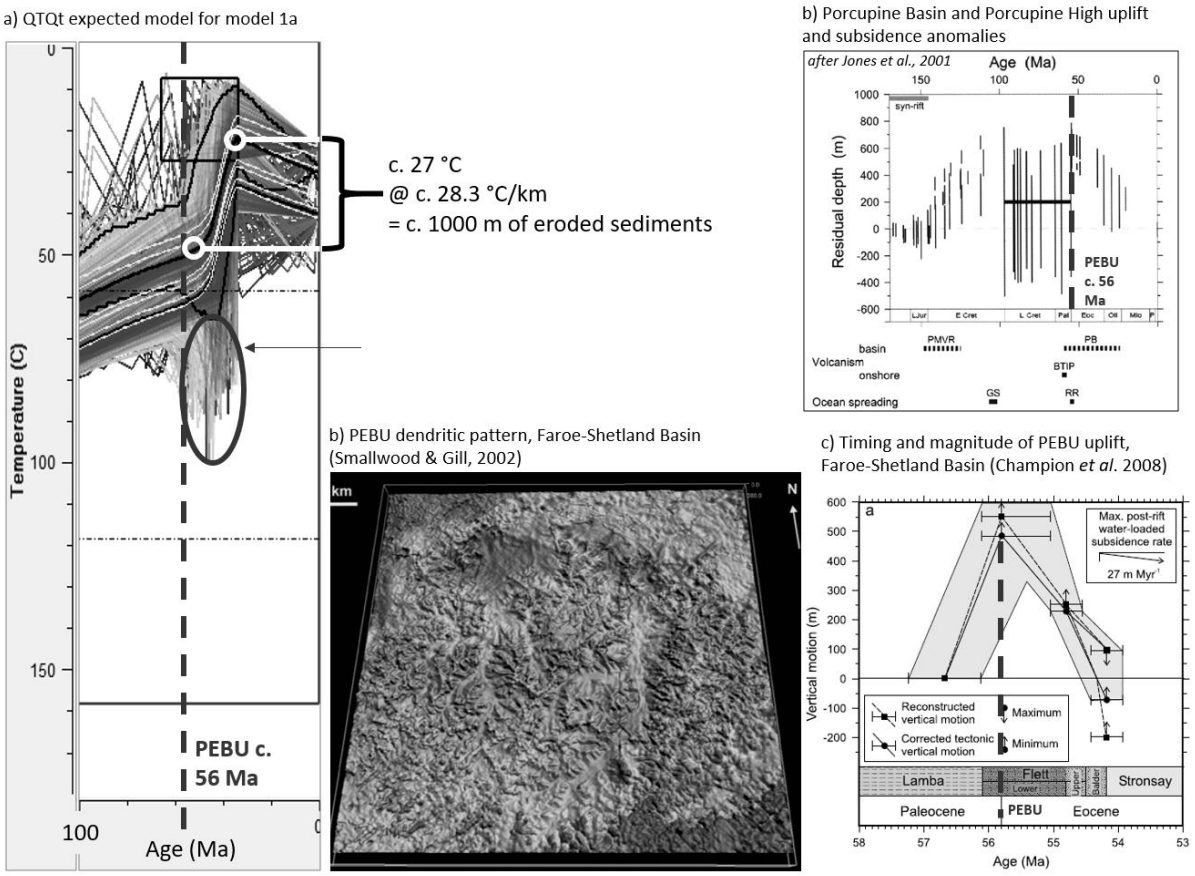

Figure 67: PEBU uplift, timing and magnitude in 34/05-1 and comparison to other locations in the Porcupine Basin and Faroe-Shetland Basin.Post-PEBU thermal history

The models show that after the Paleocene-Eocene uplift, a simple and continuous heating (burial) to present-day temperatures is sufficient to match the AFT and AHe data (FIGURE 68).

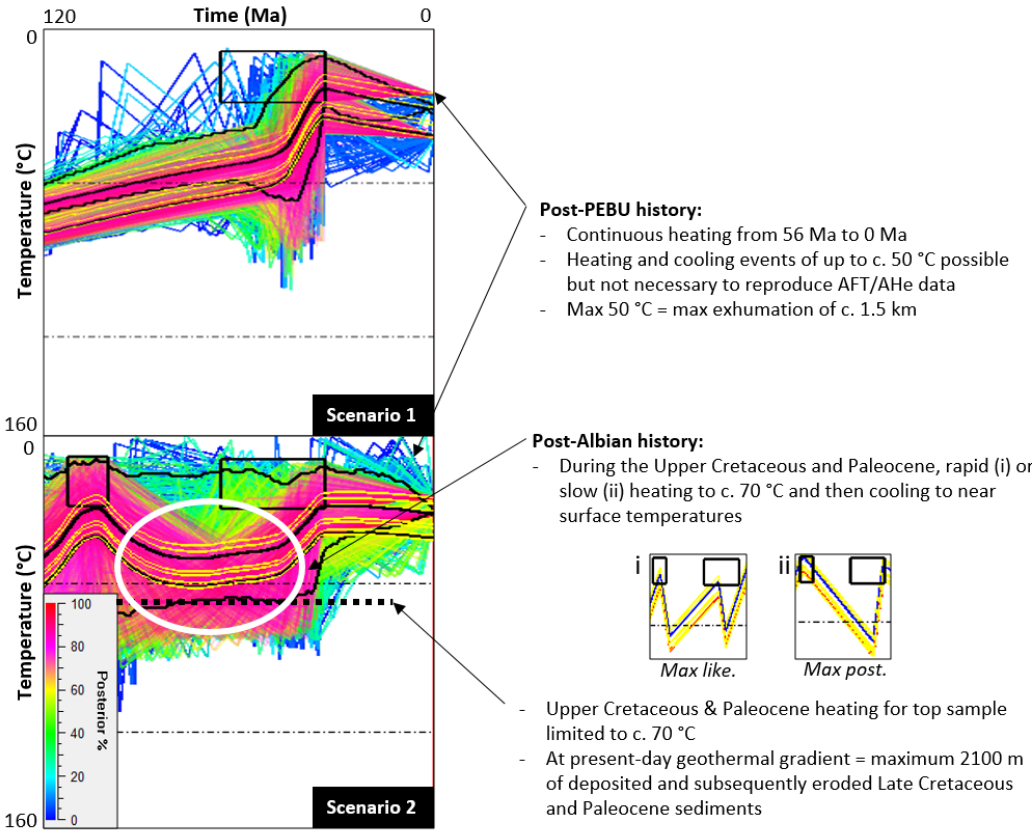

Figure 68: Post-Albian and post-PEBU thermal history for well 34/05-1.

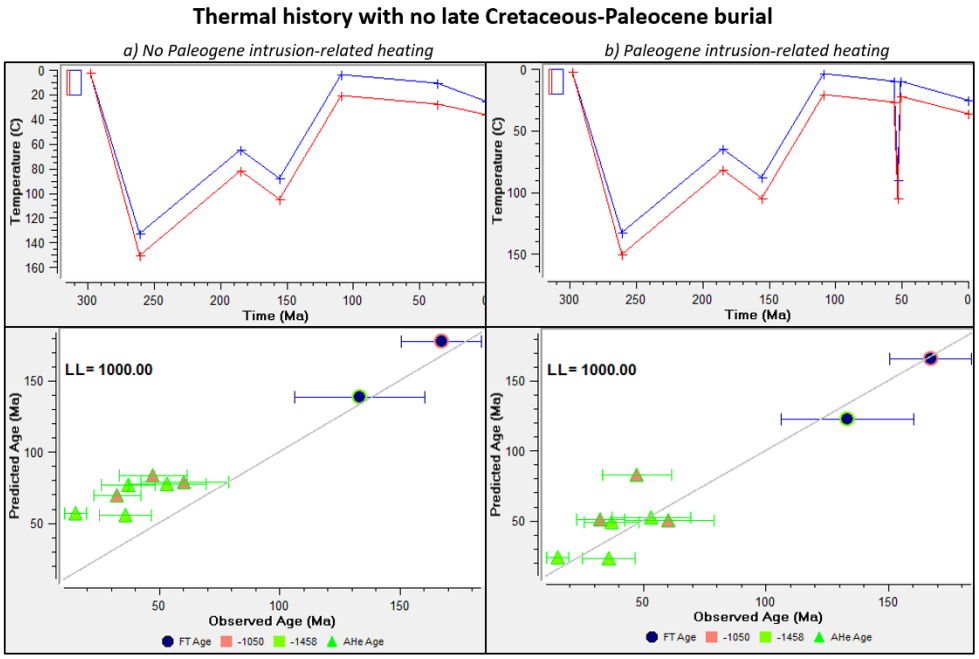

Figure 69: 34/05-1 forward modelling of AFT/AHe data with thermal histories without significant burial-related heating during the late Cretaceous-Paleocene. Left: No intrusion-related heating spike at 55 Ma. Note the good AFT ages match but poor AHe match. Right: Intrusion-related heating spike at 55 Ma. Note the better AHe ages match.

Eocene, Oligocene or Neogene uplift and erosion events are possible but not necessary given the available data. Such theoretical events would have a maximum cooling range of c. 50°C, since greater cooling ranges would require burial to temperatures that would yield lower AHe ages and higher MTLs (FIGURE 68). This maximum theoretical cooling translates to maximum exhumation of c. 1500 m. In reality any Eocene to Neogene exhumation would have probably been much smaller in magnitude. For comparison, the sonic velocity data yields an absolute maximum exhumation of 1110 m, with a minimum estimate of no erosion at all.

Post-Albian thermal history

When considering scenario 2 (the presence of Albian sands in the well), the modelling shows a period of rapid to slow heating to a maximum of c. 70°C (for the top sample), followed by a return to near-surface temperatures (FIGURE 68). The maximum temperature for the top sample corresponds to a burial under a maximum of 2100 m of Upper Cretaceous and Paleocene sediments.

In the Porcupine Basin, the wells with the greatest thicknesses of late Cretaceous to Paleocene sediments are in the northern central part of the basin, with a total thickness of c. 1000-1250 m in wells 35/06-1, 08-1, 08-2, 13-1 and 19-1 (FIGURE 33), composed of a combination of Cenomanian sands, Upper Cretaceous and Danian chalk and Paleocene clastics. Therefore, any late Cretaceous-Paleocene sedimentation on a basement high such as at 34/05-1 location is expected to be much less than the maximum thickness in the basin depocenter (*i.e.* <<1250 m, probably a few hundreds of meters at the maximum).

A forward model of a thermal history without burial during the late Cretaceous-Paleocene, based on the time-temperature path of the posterior model of model 2a, yields modelled AFT ages that match the observed AFT ages but all AHe ages are significantly older than the measured ages (FIGURE 69A). To obtain younger AHe ages, temperatures have to be greater than c. 40°C at some point during the late Cretaceous to Paleogene.

Such higher temperatures could be achieved by a higher paleogeothermal gradient. To reach temperatures of c. 60°C with for example 500 m of Upper Cretaceous-Paleocene sediments requires a geothermal gradient of 100°C.km^{-1}, which is highly unlikely for this time period.

Another hypothesis is that high temperatures were reached for a very short period of times due to the igneous intrusions. A very short-lived heating event could have reset the AHe system but not the AFT system. To test this hypothesis, a heating/cooling spike at 55 Ma was added to the previous forward model to mimic the effect of an igneous intrusion. This model still replicate the AFT ages but yield better AHe ages than the model without the thermal spike (FIGURE 69B).

In conclusion, if Albian sediments are actually present *in-situ* in this borehole, then the seemingly conflicting observation of thin Upper Cretaceous-Paleocene deposits on this basement high (a few hundreds of meters maximum based on regional geology) associated with Jurassic AFT central ages and Cenozoic AHe ages can best be resolved by a thermal history with no significant heating during the late Cretaceous-Paleocene but with a heat spike during the Paleogene caused by igneous intrusions.

Pre-Albian thermal history

The pre-Albian thermal history is poorly constrained. The simple models show a first-order monotonic cooling until the Albian or Paleocene-Eocene (FIGURE 70). However, the complex models suggest that the monotonic cooling might have been interrupted by a period of renewed heating from burial during the Jurassic. The cooling resumed at the Jurassic-Cretaceous boundary, probably associated with the BCU erosion (FIGURE 70).

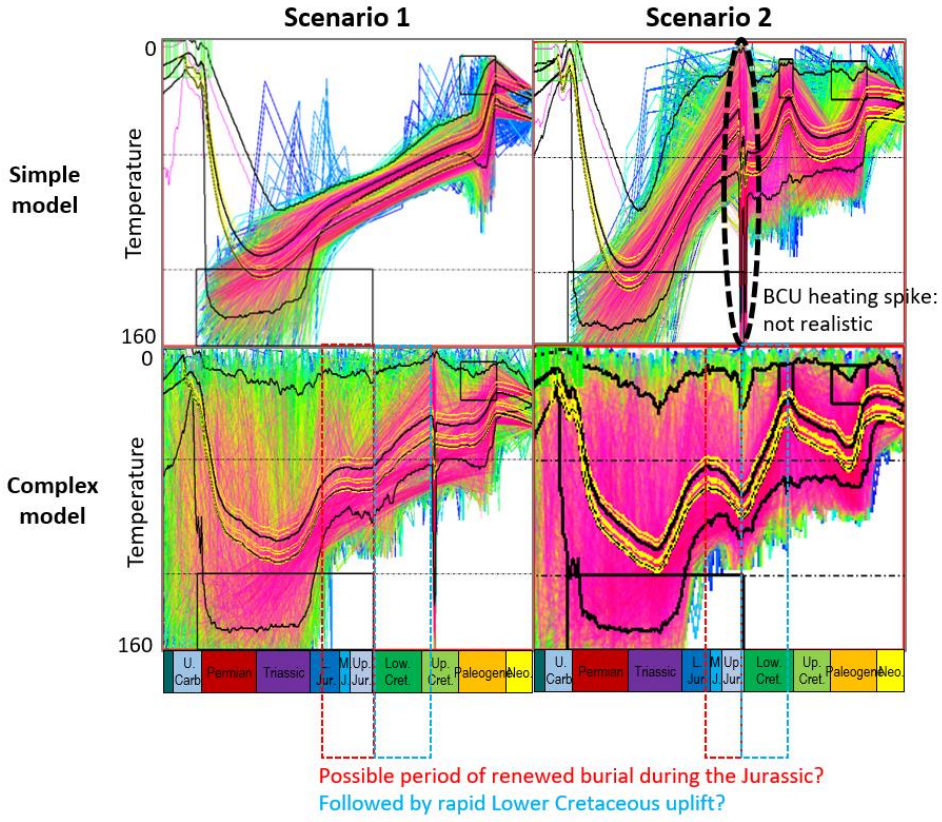

Figure 70: 34/05-1 pre-BCU thermal history analysis.

Timing of maximum temperature

All the models show that the top sample experienced its highest temperatures between 310-200 Ma (latest Carboniferous to base Jurassic) (FIGURE 71A). Regionally, the Carboniferous organic matter is believed to have acquired its highest maturity (and so VR) before the early Jurassic (Robeson et al., 1988) and probably during the Late Paleozoic (Corcoran and Clayton, 2001).

As expected, model 1a shows that a paleogeothermal gradient of c. 30°C and a maximum temperature of c. 130°C.km^{-1} for the top sample yield modelled VR that matches the observed VR.

Pre-Cenozoic exhumation estimates based on AFT/AHe alone

Model 1a shows a rapid heating of c. 100°C of the top sample during the late Carboniferous to Triassic times. Using a maximum geothermal gradient of 100°C.km^{-1}, this heating corresponds to burial of c. 1000 m of sediments during that period. Since there is still 315 m of late Carboniferous-early Permian sediments above the top sample, it means that c. 685 m of sediments were eroded above the TCU during subsequent exhumation (FIGURE 72).

If the maximum temperature was acquired at lower geothermal gradient, for example at present-day geothermal gradient of 28.34°C.km^{-1}, the amount of eroded sediments would be c. 3200 m (FIGURE 72); while an intermediary gradient of 60°C.km^{-1} (which could be associated to Mesozoic rifting) would correspond to 1350 m of eroded sediments (FIGURE 72).

All these estimates have to be seen as minimum since the thermochronology data allows for the top sample to reach higher temperatures than c. 130°C before the Jurassic (higher temperatures would lead to higher amount of eroded sediments). These estimates, which are independent of VR and sonic data, are quite close to the VR and sonic-derived estimates (FIGURE 72).

5.4.7 Conclusions

5.4.7.1 Exhumation history (thermochronology integrated with other constraints)

- Significant burial and heating occurred during the Late Carboniferous (with high geothermal gradients) and/or during the Permian and Triassic with lower geothermal gradients, leading to the highest temperatures experienced by the samples.
- Significant cooling occurred between the Permian and Lower Cretaceous, with possibly a poorly constrained phase of burial and heating during the middle and late Jurassic.
- The amount of material eroded before the Lower Cretaceous is estimated, using the sonic and VR data, at 2000 $\pm \frac{2000}{1000}$ m, which is in accordance with the absolute minimum estimate given by the thermochronological data modelling alone (independent of the sonic and VR data) at 685 m.
- During the late Cretaceous and Paleocene, the area experienced either 1) continuous uplift and erosion or 2) burial under a few hundreds of meters of chalk and clastic sediments that were removed but followed subsequent Paleocene-Eocene erosion. The two hypotheses rely on the absence or presence of Albian sands in the well, which is debatable.
- The area was probably affected by the regional latest Paleocene-earliest Eocene uplift and erosion which has affected large areas of the North-East Atlantic Margin, leading to maybe up to hundreds of meters of erosion at that time.
- From the Eocene to Recent no exhumation is required but erosion events of up to 1000 m during that period cannot be excluded based on the thermochronological data alone.

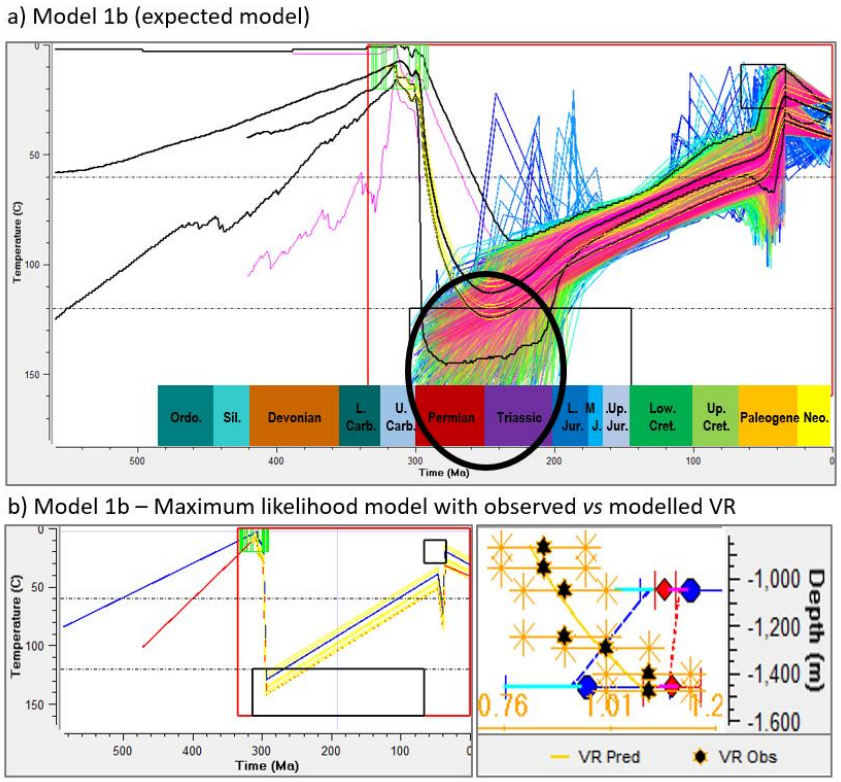

Figure 71: 34/05-1 thermal history inverse modelling. a) Model 1b, expected model with a random selection of accepted paths coloured by posterior percentage. Black ellipse showing that maximum temperatures for all paths are reached between 310 and 200 Ma. b) In the maximum likelihood model, the top sample reaches a maximum temperature of c. 130°C, which yields modelled VR matching observed VR.

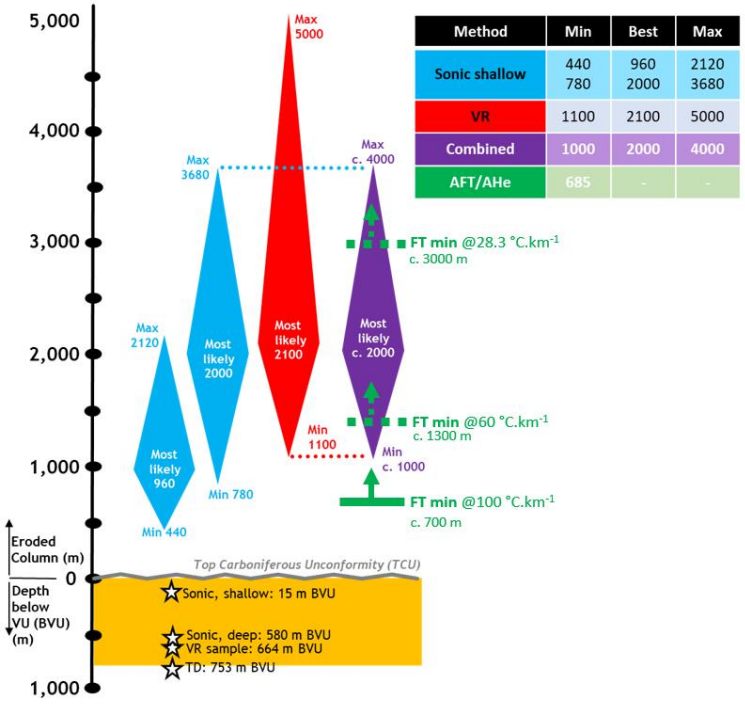

Figure 72: 34/05-1 pre-Cenozoic exhumation estimates from AFT/AHe alone, compared with estimates from sonic and VR data.

5.4.7.2 Upper Carboniferous igneous activity

Late Carboniferous apatites and zircons found in the Upper Carboniferous clastics indicates the likely presence of previously unrecognised tuffs in these units (such as the ones found in borehole 13/03-1 in the offshore Donegal Basin and in borehole 35/15-1 in the eastern margin of the Porcupine Basin).

5.4.7.3 Paleogene igneous activity

A new analysis of the well data revealed the probable presence of a doleritic intrusion between 1346 and 1364 mMD that has previously been misdiagnosed as a sandstone. This intrusion is probably Paleogene in age and associated with the North-East Atlantic Igneous Province but a younger or older Mesozoic age cannot be excluded. This intrusion extends the area proved to be affected by Paleogene intrusions a bit further to the west than presently mapped.

5.4.7.4 The impact of igneous activity on low-temperature thermochronological results

Sample R-15 demonstrates that some apatites have probably been affected by the Paleogene igneous activity in the area (through heating by thermal contact or hydrothermal fluids) resulting in the complete annealing of tracks at c. 60 Ma. However, the other grains might have been partially annealed but the extent is impossible to calculate. Similarly, the helium in some of the grains could have partially or totally leaked at that time while other grains not affected by the thermal activity would preserve their track length and helium contents. When these grains are used in thermal history modelling, there is an assumption that the data represents the result of burial and erosion and geothermal gradients variation only; which may not be the case. Offshore west of Ireland, the NEAM Paleogene igneous activity add significant uncertainties to the use and interpretation of confined fission track lengths and AHe data.

5.5 2006-2014 Porcupine High dredges

5.5.1 Sampling history

Between 2006 and 2014, three research campaigns were carried out to sample the basement that crops out on the north part of the Porcupine Bank (FIGURE 33 AND FIGURE 73).

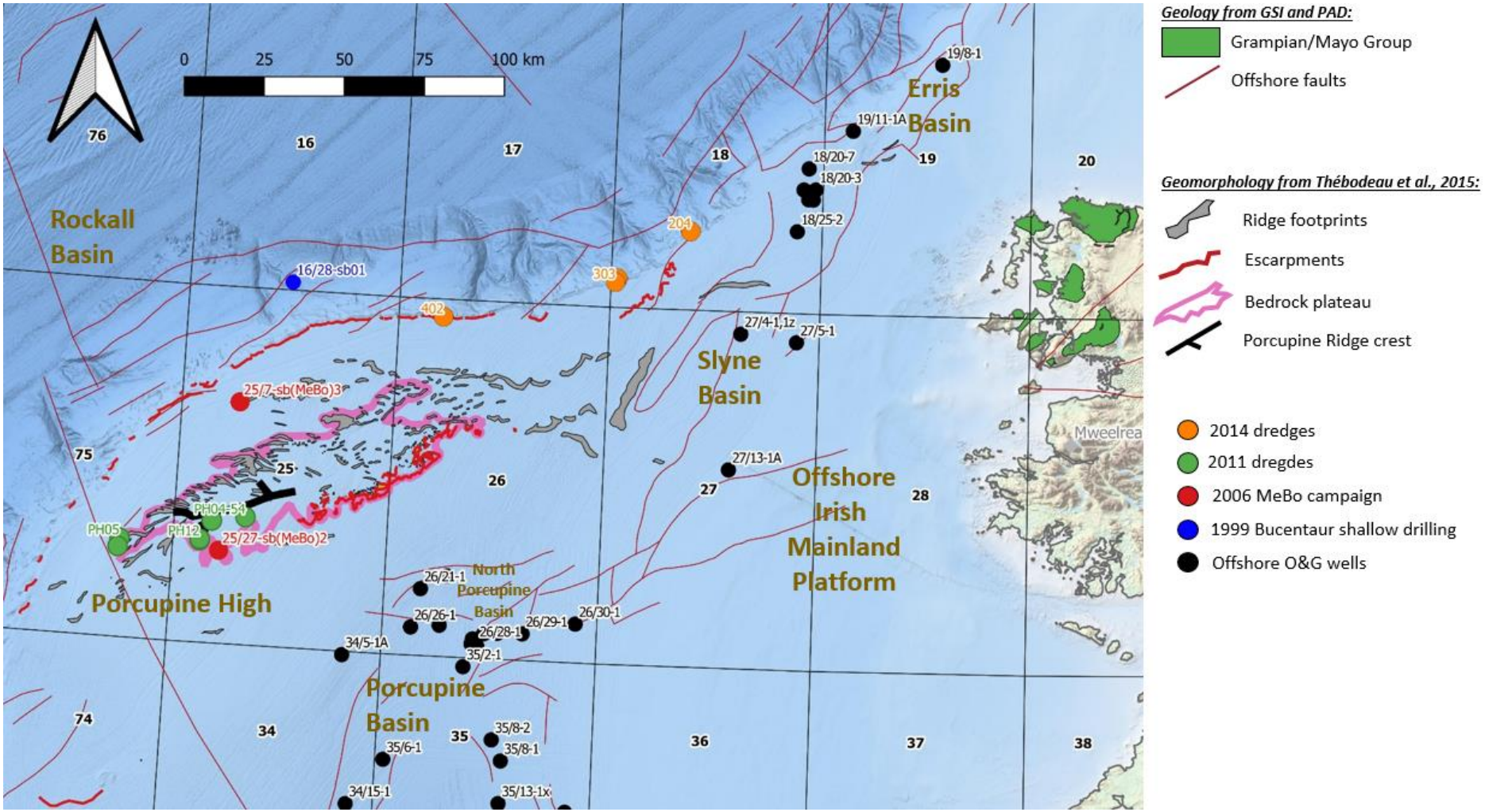

Figure 73: Location map of seabed samples from the 2006, 2011 and 2014 campaigns.

5.5.1.1 2006 campaign

In 2006, the Irish Shelf Petroleum Study Group (ISPSG) of the Petroleum Infrastructure Programme (PIP) and the Marine Institute (MI) jointly funded a shallow drilling campaign (campaign CE06-019, project IS06_04) undertaken by MARUM (the Center for Marine Environmental Sciences of the University of Bremen) and the Petroleum Affairs Division (PAD) (Murray and Freudenthal, 2006). The samples were drilled by the MeBo seafloor drill rig aboard the RV Celtic Explorer in quadrant 25 (FIGURE 73). Teams at UCD (ISPSG funded project IS06_10) and TCD subsequently undertook petrography, zircon and apatite U/Pb dating, zircon Hf isotopic analysis, K-feldspar Pb isotope analysis, AFT/AHe dating and thermal history modelling (Daly et al. (2008a), Cogné and Chew (2017), Chew et al. (2019)). Due to the gravelly nature of the seabed, rough weather and technical issues, only boreholes 25/7-sb(MeBo)3 and 25/27-sb(MeBo)2 successfully recovered samples that are believed to represent *in-situ* bedrock (Murray and Freudenthal, 2006).

5.5.1.2 2011 campaign

In 2011, the National Development Plan, the Geological Survey of Ireland (GSI) and the Marine Institute (MI) funded (through a Ship Time Grant in Aid awarded to Xavi Monteys, GSI) a dredging campaign (campaign CE11-017) undertaken by the GSI and MI. The dredges were carried out by the RV Celtic Explorer in quadrants 25 and 75 along an E-W transect (FIGURE 73). Teams at UCD and later NUIG (Informar funded project INF-11-02-TYR with Prof. Shane Tyrrell as PI) and TCD subsequently undertook SEM characterization, K-feldspar Pb isotope analysis, zircon and apatite U/Pb dating, AFT and AHe dating and thermal history modelling (Tyrrell (2013), Cogné and Chew (2017), Chew et al. (2019)).

5.5.1.3 2014 campaign

In 2014, another dredging campaign (CV014-021) was carried out as part of a successful Ship Time in Aid bid led by Adrian Patterson (NUIG). The samples were dredged at three main sites (sites 204, 302/303 and 402) by the RV Celtic Explorer in quadrants 18 and 26, on the north flank of the Porcupine High (FIGURE 73). Teams at NUIG, UCD and TCD(ISPSG/PIP funded project IS13-10, Prof. Shane Tyrrell as PI) undertook petrographic studies, apatite and zircon U/Pb dating, K-feldspar Pb isotope analysis and AFT dating on the basement samples (Chew and Cogné (2015), Barry et al. (2017), Chew et al. (2019)).

5.5.2 Geological summary

5.5.2.1 2006 campaign

25/7-sb(MeBo)3 recovered 0.8 m of *in-situ* orthogneiss (the North Porcupine High Orthogneiss, NPHO). The NPHO is weakly foliated with pink K-feldspar megacrysts floating in a dark matrix of quartz, feldspar, clinopyroxene, biotite, hornblende and opaque phases (Daly et al., 2008a).

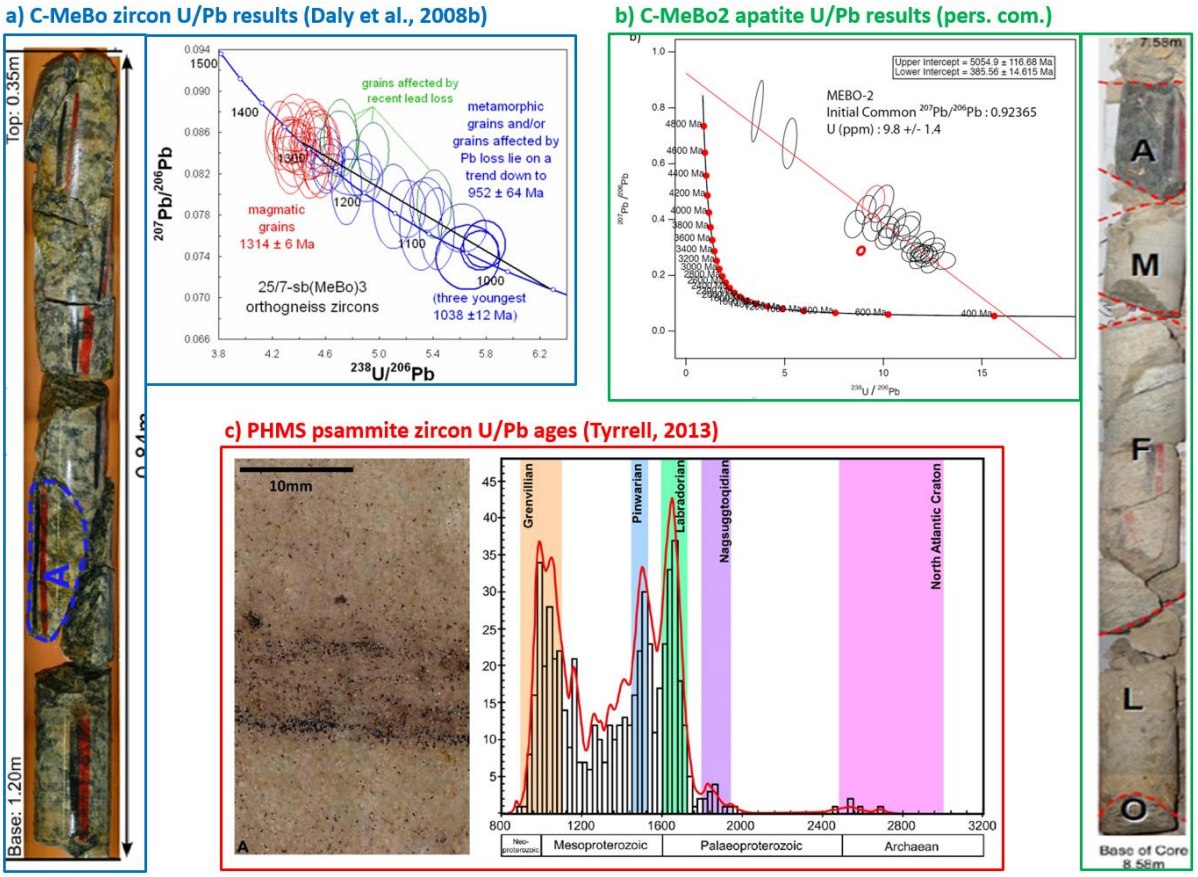

Figure 74: Legacy studies of the North Porcupine High seabed samples. a) Orthogneiss sample (C-MeBo) from shallow borehole 25/7-sb(MeBo)3: sample photo and zircon U/Pb data Tera-Wasserburg plot (Daly et al., 2008a); b) Deformed granite sample (C-MeBo2) from shallow borehole 25/27-sb(meBo)2: sample photo and apatite U/Pb Tera-Wasserburg plot (pers. com. D. Chew & N. Cogné); c) PHMS psammite sample (C-PH1-14) from seabed dredges PH1-14: sample photo and zircon U/Pb age density plot and KDE (Tyrrell, 2013).

The NPHO protolith is a K-feldspar megacrystic monzogranite that crystallised at c. 1310 Ma (FIGURE 74A) and was derived from c. 1.7-1.8 Ga Paleoproterozoic crust which has some affinity with the Rockall Bank and Rhinns Complex gneisses (but not with onshore Ireland or the Lewisian basement of NW Scotland). This 1.3 Ga granite was possibly part of a previously unknown phase of anorogenic magmatism associated with rifting. The granite was subsequently tectonically buried at c. 950 Ma, during the Grenville Orogeny, resulting in a gneissification and granulite-facies metamorphism (c. 12 kbar and c. 710°C) (Daly et al., 2008b) with apatite U/Pb ages of c. 880 Ma recording post-Grenville cooling (Chew et al., 2019).

Shallow core 25/27-sb(MeBo)2 recovered 2.92 m of Late Quaternary (< 300,000 years) conglomerate with boulders and cobbles of amphibolite, gabbroic anorthosite and foliated gneiss in a matrix of unconsolidated calcareous sand and *in-situ* limestone (Daly et al., 2008c). The foliated gneiss yielded a zircon U/Pb age of 490 Ma (possibly corresponding to arc magmatism immediately preceding the Grampian Orogeny) with a Late Caledonian apatite U/Pb age of 385 Ma from the same clast (Chew et al., 2019) (FIGURE 74B).

5.5.2.2 2011 campaign

The dredges from 10 sites along the E-W transect yielded a high proportion of red-green psammites (metamorphosed sandstones) believed to be derived from local *in-situ* bedrock. These low-grade quartzo-felspathic psammites contain abundant accessory minerals suggesting a granitic or gneissic source (titanite, epidote, zircon, tourmaline), while the K-feldspar Pb isotope data suggest that this source has an affinity with the Annagh Gneiss Complex (AGC) (Tyrrell, 2013). The zircon U/Pb ages indicate that the rocks have a Laurentian provenance and possibly belong to the lowermost part of the Dalradian Supergroup (FIGURE 74C) and are a lateral stratigraphic equivalent to the Grampian Group rocks of the Dalradian Supergroup in Co. Mayo (FIGURE 73). However, apatite U/Pb ages ranging from 0.9 to 1.8 Ga indicate that these rocks have not been severely affected by the Caledonian Orogeny unlike the Grampian Group rocks of Scotland or Ireland (Chew et al., 2019). This sequence of Late Neoproterozoic low-grade metamorphic rocks have been referred to as the Porcupine High Metasedimentary Sequence (PHMS) (Tyrrell, 2013).

5.5.2.3 2014 campaign

The dredges from the three sites recovered gneisses (42%) together with quartzite (21%), igneous rocks (15%), amphibolite (11%) and sedimentary rocks (<10%) (Barry et al., 2017). Most of the samples selected for analysis and isotope dating come from site 402.

A recent revision of the ages by Chew et al. (2019) based on the dataset of Barry et al. (2017) led to the classification of the samples into three broad groups of high-grade metamorphic rocks (herein termed HG1, HG2 and HG3) and two groups of low-grade metamorphic rocks (here termed LG1 and LG2):

- HG1: Gneisses with Archean U-Pb zircon ages (c. 2.75 Ga), 1.75 Ga apatite U-Pb ages and a Lewisian Pb-Kfsp signature
- HG2: Gneisses and amphibolites with Paleoproterozoic U-Pb zircon ages (1.83-1.94 Ga), 1.75 Ga apatite U-Pb ages and an AGC Pb-Kfsp signature
- HG3: Gneisses and amphibolites with Paleoproterozoic U-Pb zircon ages (1.55-2.02 Ga) and Grenville apatite U-Pb ages

- LG1 : Moine/Grampian metasediments (mica schists)
- LG2 : Upper Dalradian metasediments (greenschists)

All the gneiss samples are orthogneisses with a syenitic protolith and contain K-feldspar, quartz, biotite, epidote and muscovite but no garnet (Barry et al., 2017).

The final report from the 2014 dredge campaign (Barry et al., 2017) suggests that the samples are near-*in-situ* but does not provide any justification for other than i) the samples coming from an erosive surface (canyon heads); ii) the analyses were undertaken on cobbles or larger clasts only which are more likely to represent *in-situ* lithologies, and iii) that the preliminary thermochronological results indicate a shared thermal history (Barry et al., 2017). However, based on the diverse lithologies (gneiss, amphibolite, psammite, schist, igneous rocks, quartzite and sedimentary rocks), ages (Archean gneisses, Paleoproterozoic gneisses, Neoproterozoic psammites, Late Caledonian schists) and Pb isotope affinities (Lewisian, AGC, Rhinns Complex/Inishtrahull) seen both at each site and between the sites, it is more likely that the dredges represent seabed cobbles probably related to Quaternary glaciation with both *in-situ* rocks and glacial erratics (SEE DISCUSSION IN SECTION 5.5.3.1).

5.5.2.4 Discussion

Extent of the North Porcupine High Dalradian Basin

Offshore magnetic anomaly maps show a large negative anomaly covering most of the north Porcupine High (FIGURE 37A). This anomaly has previously been interpreted as Paleozoic (meta)sedimentary rocks with low magnetisation but with higher densities than Cenozoic or Mesozoic sedimentary rocks (Young and Bailey (1974), Riddihough and Max (1976), Kimbell et al. (2010)).

The dredged PHMS psammites at localities PH10 and PH14 and at the bottom of 26/26-1 are within or very close to this low magnetic anomaly (FIGURE 37A). This spatial correlation suggests that the magnetic anomaly is the footprint of a Neoproterozoic Dalradian basin (FIGURE 37B). A similar low magnetic anomaly is present onshore and offshore NW Mayo where Dalradian metasediments crop out (FIGURE 37A). The NPHO drilled by 25/7-sb(MeBo)3 is also located within the magnetic low, which would suggest that it is of small size (otherwise the older basement would probably result in a regional magnetic high). An analogue would be the Annagh Gneiss Complex in NW Co. Mayo, which has an areal extent of c. 60 km^2 but is not associated with a magnetic high (FIGURE 37A).

Samples PH1, 4 and 5 are located above a magnetic anomaly high interpreted as an igneous centre (Tate and Dobson, 1988). Therefore the presence of Dalradian metasediments above this anomaly would suggest that the igneous centre is probably still buried and does not crop out on the seabed.

Paleogene igneous centres

A gravity and magnetic anomaly high (c. 1090 km^2) is located below the summit of the Porcupine High (FIGURE 37A). Based on this gravity and magnetic anomaly high and the doming of the uppermost layers of rocks visible on seismic data, this anomaly has previously been interpreted as a possible igneous centre of undetermined age (Tate and Dobson, 1988). Most large igneous centres in the region are associated with the NAIP and therefore this anomaly is probably a Paleogene igneous centre such as the one that crops out on Skye and other parts of western Scotland.

However, an older age cannot be excluded, particularly since a pre-Late Cretaceous basalt has been encountered at the bottom of shallow borehole 16/28-sb01 (Haughton et al., 2005). Readman et al. (2003) suggest that another igneous centre might be present in the centre of quadrant 27, at the junction between the Porcupine High magnetic anomaly low and the NW Mayo magnetic anomaly low (FIGURE 37A). This igneous centre (probably Paleogene in age) might thus have intruded Dalradian metasediments associated with a magnetic anomaly low (FIGURE 37B). If the igneous centre was not present, there would probably be a continuous low magnetic anomaly from onshore NW Mayo to the NW margin of the North Porcupine High.

Location of the Fair Head – Clew Bay Line and the Skerd Rocks-Southern Upland Fault

The identification of Dalradian metasediments and an inlier of Paleoproterozoic gneiss in the North Porcupine High indicates that these rocks are part of the Grampian Terrane of Ireland (equivalent to the Central Highlands terrane of Scotland). The Grampian Terrane of Ireland and Scotland is broadly associated with a magnetic anomaly low (Riddihough and Max, 1976). In Co. Mayo, there is a sharp boundary between a low magnetic anomaly in the north and a high magnetic anomaly in the south. The boundary follows the inferred location of the Fair Head – Clew Bay Line (FHCBL) and separates weakly magnetic Neoproterozoic metasediments north of the Laurentian margin from highly magnetic volcanic arc and accretionary sediments of the Northwestern Terrane to the south (FIGURE 37B).

A similar sharp E-W trending magnetic boundary occurs on the Porcupine High just south of the bedrock plateau (FIGURE 37A). The highly magnetic basement south of the lineament has the same magnetic expression as the basement onshore and offshore west of Ireland south of the FHCBL and probably represents similar peri-Laurentia arc-related metamorphosed volcanic and sedimentary rocks (FIGURE 37B). Based on the onshore correspondence between the magnetic boundary and the FHCBL, it is possible that the boundary on the Porcupine High represents the continuation of the FHCBL. However, Kimbell et al. (2010) suggested that this magnetic boundary could be the offshore continuation of the Skerd Rocks-Southern Upland Fault. It is also possible that these two orogen-scale Caledonian faults have merged by the time they reach the Porcupine High.

Location of the Porcupine High Granite

As discussed above in section 5.5.2.1, the clast of deformed granite in the Late Quaternary conglomerate at 25/27-sb(MeBo)2 possibly comes from a granite associated with the early Grampian-Taconic volcanic arc resulting from the subduction of the Laurentian margin under the Iapetus ocean. Consequently, it is likely that this granite is located just south of the FHCBL as early Grampian (c. 490 Ma) volcanic arc intrusives are not found north of the FHCBL on the Irish or Scottish mainland. The site of 25/27-sb(MeBo)2 is located c. 10 km north of the inferred FHCBL (FIGURE 37A). It is possible that the outcrop of Grampian-Taconic arc-related granite is located just south of the inferred FHCBL (FIGURE 37B) and that clasts from this granite have been transported during the Late Quaternary to their present location.

Structural lineaments

Based on a geomorphological study, Thébaudeau et al. (2016) identified a series of ridges, escarpments and bedrock outcrops across the entire Porcupine Bank. The orientation and location of the ridge footprints and escarpments in the North Porcupine High allows the recognition of two main structural lineaments: 1) Caledonian NE-SW lineaments and 2) W-E lineaments (parallel to the Slyne Ridge which links the Porcupine High to the offshore Irish mainland platform) (FIGURE 37).

5.5.3 Legacy AFT and AHe results

AFT dating (analyst: Nathan Cogné, analyses done at the TCD FT Lab), AHe dating (analyst: David Chew, analyses done at Glasgow University) and thermal history modelling (Nathan Cogné) was undertaken on a number of samples from the three campaigns and are available in unpublished reports (Cogné and Chew (2017), Barry et al. (2017)). The legacy AFT/AHe results are described in ANNEX 1 SECTION 2.2.4 together with a qualitative interpretation and summarized in TABLE 14 and FIGURE 75 and FIGURE 76. New thermal history modelling was undertaken based on a selection of these samples.

5.5.3.1 Discussion: which samples are in-situ?

One of the key issues with dredge and ultra-shallow borehole samples is the uncertainty regarding the origin of the sample, as clearly only samples which are *in-situ* or near *in-situ* (originating from a nearby outcrop) can be used to determine the geological/thermal history of a region.

Table 14: Legacy AFT and AHe results for seabed samples from the North Porcupine High. Colour code: Red = Unsuitable for interpretation/modelling, Orange/light green/dark green: Suitable for interpretation/modelling poor/average/good data quality.

Well, Dredge, Dive	Sample	Depths		Temp.		Lithology	Age		n	Ns	$P(\chi^2)$	Central Age		Tracks	MTL	SD	SE	Cl	Dpar	U	n	Mean eU	Age cluster 2	Range of AHe ages (M	
		Seabed	Sample	Seabed	Sample		Age	±				Ma	±1σ Ma		μm	μm	μm	wg%	μm	ppm		ppm		Raw	F_T-correc
		m MSL	m BSB	°C	°C				-	-	-			-									-	Min-**Mean**-Max	Min-**Mean**-
27-sb(MeBo)2	C-MeBo2	192	0	10	10	Gneiss/granite clast	383.9	5.8	28	377	0.42	**144.1**	7.5	101	10.29	2.45	0.24	0.27	1.44		4	31	Yes 3/4	25-**34**-71	34-**47**-10
7-sb(MeBo)3	C-MeBo	254	0	10	10	Orthogneiss	1038.0	12.0	15	459	2.40229E-34	**157**	27	102	13.03	1.21	0.12	0.05	1.36		3	21	Yes 3/3	144-**148**-151	186-**192**-1
GSI PH1	C-PH1	234	0	10	10	Psammite	671	201	20	443	0.10	**142**	8	101	**9.69**	3.01	0.3	0.08	1.69	N/A	0	N/A	N/A	N/A	N/A
GSI PH4	C-PH4	218	0	10	10	Psammite	671	201	24	322	0.11	**184**	12	118	**9.86**	3.01	0.28	0.13	1.65	N/A	4	23	No	66-**93**-130	98-**132**-17
GSI PH5	C-PH5	364	0	10	10	Psammite	671	201	21	390	0.09	**194**	11	114	**9.79**	2.86	0.27	0.06	1.67	N/A	3	9	No	86-**107**-129	115-**135**-1
GSI PH10	C-PH10	364	0	10	10	Psammite	671	201	20	436	0.06	**193**	11	121	**9.76**	3.25	0.3	0.08	1.73	N/A	0	N/A	N/A	N/A	N/A
GSI PH12	C-PH12	249	0	10	10	Psammite	671	201	16	230	<0.01	**191**	20	92	**9.72**	3.08	0.32	0.06	1.49	N/A	0	N/A	N/A	N/A	N/A
V14-021 204	C-204-1	750	0	10	10	Micaschist	N/A	N/A	23	505	0.306641232	**180**	8	100	**12.46**	1.5	0.150350059	0.02	1.61	N/A	2	4	No	55-**76**-98	78-**101**-12
V14-021 302	C-302-1	600	0	10	10	Psammite	405.0	27.0	30	912	0.331124911	**143**	5	100	**12.61**	1.62	0.16	0.12	1.62	N/A	4	10	No	50-**73**-95	68-**103**-13
V14-021 303	C-303-1	600	0	10	10	Amphibolite	1750.0	20.0	25	1214	0.081701991	**283**	9	100	**12.65**	1.81	0.18	0.11	1.63	N/A	5	25	Yes 3/5	239-**351**-358	347-**459**-4
V14-021 402	C-402-1	500	0	10	10	Gneiss	1739.0	16.0	30	891	0.09594467	**425**	16	105	**12.05**	2.09	0.2	0.16	1.7	N/A	4/5	7	Yes 4/5	0-**0**-1	0-**1**-2
V14-021 402	C-402-3	500	0	10	10	Gneiss	1697.0	12.0	27	376	0.088445778	**289**	16	101	**12.03**	1.89	0.19	0.07	1.61	N/A	0	N/A	N/A	N/A	N/A
V14-021 402	C-402-4	500	0	10	10	Gneiss	967.0	6.0	29	513	0.513344638	**216**	10	103	**12.69**	1.45	0.14	0.08	1.69	N/A	0	N/A	N/A	N/A	N/A
V14-021 402	C-402-6	500	0	10	10	Greenschist	381.0	34.0	19	106	0.998835784	**190**	19	106	**12.49**	1.49	0.15	0.17	1.7	N/A	5	17	Yes 5/5	35-**44**-51	51-**64**-82
V14-021 402	C-402-8	500	0	10	10	Gneiss	1774.0	11.0	28	1288	0.091685405	**546**	18	100	**12.2**	1.8	0.18	0.33	1.67	N/A	3	62	Yes 3/3	276-**280**-285	351-**368**-3
V14-021 402	C-402-9	500	0	10	10	Gneiss	981.0	7.0	27	1246	0.065248456	**198**	7	61	**12.67**	1.83	0.23	0.06	1.55	N/A	5	34	No	246-**293**-343	313-**383**-4

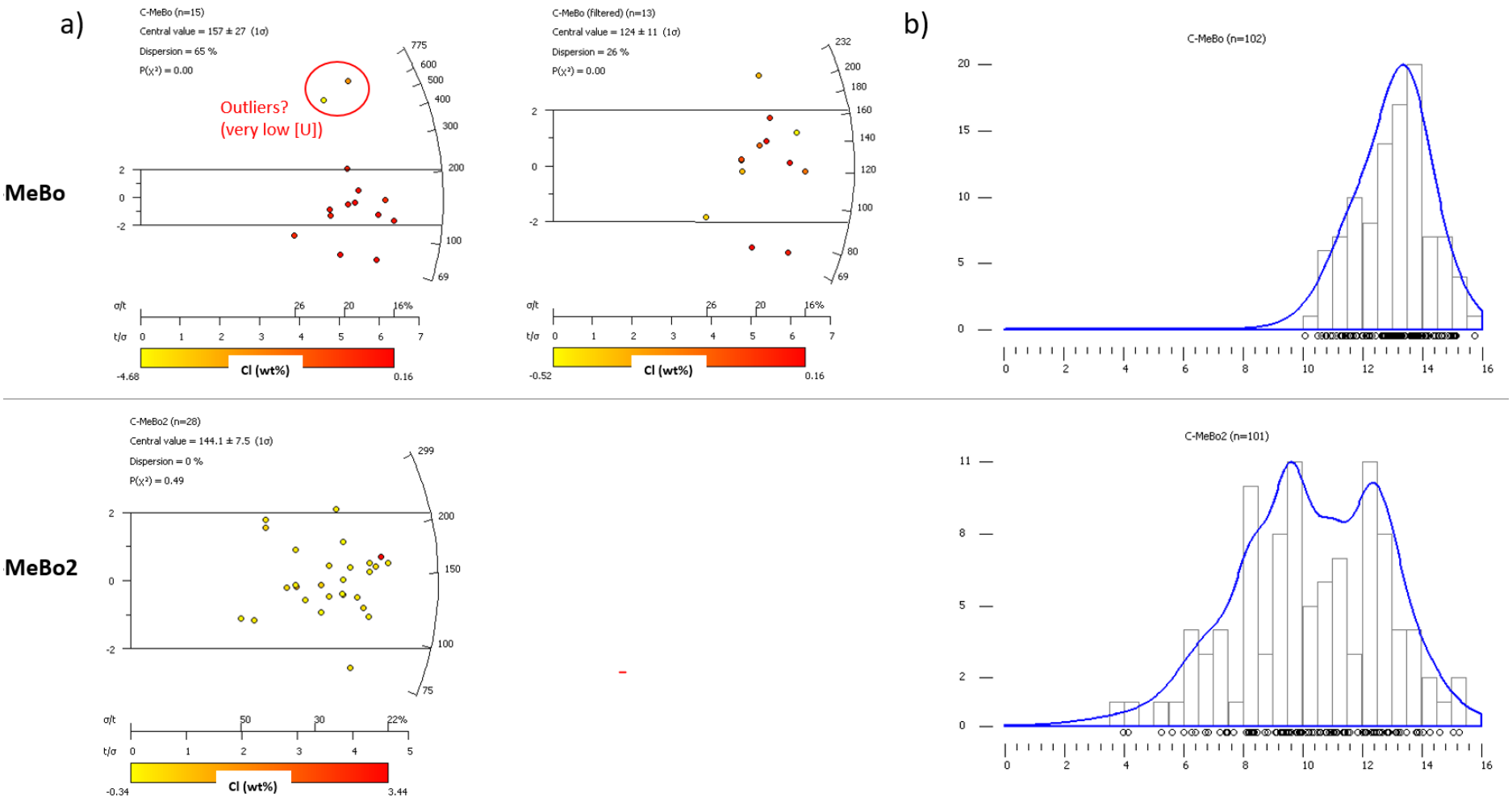

Figure 75: AFT results for sample C-MeBo (25/7-sb(MeBo)3) and C-MeBo2 (25/27-sb(MeBo)2). a) LAFT radial plots. b) Confined track lengths density plot and KDE function.

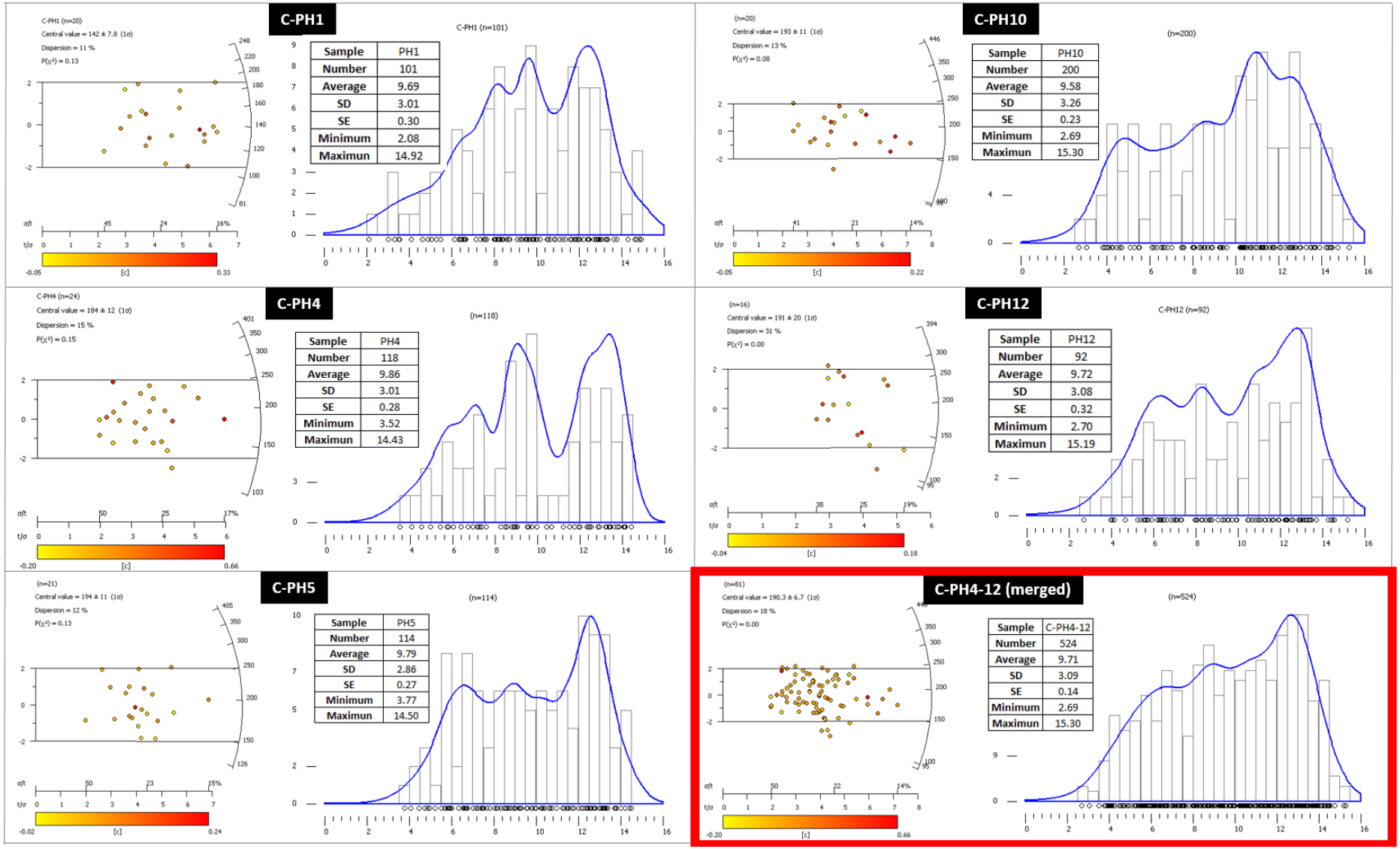

Figure 76: AFT results for samples C-PH1 to C-PH12 and merged sample C-PH4-12 (LAFT radial plots and confined track length density plots with KDE function).

Table 15: Geological information for all Porcupine High seabed samples, sorted out by AFT ages.

Sample	Lithology	Zircon U/Pb age	Apatite U/Pb age	Kfsp affinity	Basement group	Site	AFT age			AHe	MTL		In-situ?	(If not in-situ) Possible sources
							Ma	±	-	*Ma*	*Ma*	±		
C-PH1	Psammite	c. 0.8-1.8 Ga	c. 0.9-1.8 Ga	Mostly AGC	PHMS	PH	142	8	Base Cretaceous	n/a	9.69	3.01	Yes + hot fluids?	n/a
C-302-1	Psammite	c. 1-1.8 Ga	1-2.8 Ga?	?	PHMS? Other?	302/3	143	5		68-139	12.61	1.62	Possible	n/a
C-MeBo2	Gneiss clast	490 Ma	383 Ma	Caledonian	PHCG	MeBo2	144.1	7.5		51-57	10.29	2.45	Near + hot fluids?	OPWI?
C-MeBo	Gneiss	1.31 Ga	0.88 Ga	Rockall Rhinns	NPHO	MeBo3	157	27	Late Jurassic	186-197	13.03	1.21	Yes	n/a
C-402-11	Gneiss?	c. 2.75 Ga	c. 1.75 Ga	Lewisian	HG1	402	167	5	Middle Jurassic?	88-99	12.58	1.83	No	Probably Lewisian Complex in the Outer Hebrides
C-204-1	Micaschist	Detrital: Moine/ Grampian	Mostly Caledonian	?	LG1	204	180	8	Early Jurassic	78-123	12.46	1.5	Possible	Offshore Mayo, OPWI or Scotland?
C-402-6	Greenschist	Detrital: Upper Dalradian	Mostly Caledonian	?	LG2	402	190	19		51-82	12.49	1.49	Possible + hot fluids	n/a
C-PH4	Psammite	c. 0.8-1.8 Ga	c. 0.9-1.8 Ga	Mostly AGC	PHMS	PH	184	12		98-172	9.86	3.01	Yes	n/a
C-PH12	Psammite						191	20		n/a	9.72	3.08		
C-PH10	Psammite						193	11		n/a	9.76	3.25		
C-PH5	Psammite						194	11		115-162	9.79	2.86		
C-402-9	Gneiss	c. 1.55-2.02 Ga	c. post-Grenville	AGC?	HG3	402	198	7	Late Triassic	313-444	12.67	1.83	Possible	n/a
C-402-4	Gneiss						216	10		n-a	12.69	1.45		
C-402-13	Amphibolite						261	18	Ea.-Mid. Permian	95-99	12.57	1.71		
C-303-1	Amphibolite	c.1.83-1.94 Ga	c. 1.75 Ga	AGC	HG2	302/3	283	9		347-480	12.65	1.81	No	Probably from Central Highlands
C-402-3	Gneiss					402	289	16		n/a	12.03	1.89		
C-402-1	Gneiss	c. 2.75 Ga	c. 1.75 Ga	Lewisian	HG1		425	16	Late Caledonian	0-2	12.05	2.09		Probably Lewisian Complex in the Outer Hebrides, NW Scotland
C-402-8	Gneiss						546	18	Late Cadomian?	379-351	12.2	1.8		

HG1: High-grade metamorphic rock group 1
HG2: High-grade metamorphic rock group 2
HG3: High-grade metamorphic rock group 3
LG1: Low-grade metamorphic rock group 1
LG2: Low-grade metamorphic rock group 2
NPHO: North Porcupine High Orthogneiss
PHMS: Porcupine High Metasedimentary Sequence
PHCG: Porcupine High Caledonian Gneiss
Ap.: apatite
AGC: Annagh Gneiss Complex
Kfsp: K-feldspar
Zr.: zircon

In order to select samples which are likely in-*situ*, a detailed review of the lithological, geochronological and thermochronological data has been undertaken and can be found in ANNEX 1 SECTION 6. The conclusions of the analysis are (TABLE 15):

- The C-MeBo gneiss and C-PH1-14 psammites C-PH1-14 are *in-situ.*
- C-MeBo2 *is* probably *near in-situ* and might reflect the thermal history of the basement south of the FHCBL or the thermal history of the fault suture zone itself.
- The samples from the 2014 campaign contains both non-*in-situ* and *in-situ* samples. The large dispersion of AFT ages among the potential *in-situ* groups and the lack of meaningful trends from one site to another prevents the determination of one group as being more likely to be *in-situ* than another one. Due to the large variations in AFT/AHe ages and the difficulty in ascertaining the source of these dredge samples, they will not be used for quantitative modelling. The non-*in-situ* samples probably come from glacial deposits such as the Plio-Pleistocene Connemara Fan (McCarron et al., 2018) or the Donegal moraines (Ó Cofaigh et al., 2019).

5.5.4 Thermal history modelling

5.5.4.1 Input data

Based on their high likelihood to be *in-situ*, only samples C-MeBo, C-MeBo2 and merged sample C-PH4-12 will be quantitatively modelled since there is too much uncertainty on the provenance of the dredge samples from the 2014 campaign. All three samples have enough AFT ages, track lengths and AHe ages to be used as input data in the inverse models.

5.5.4.2 Initial and final time-temperature constraints

Final conditions: Present-day temperature of samples

All three samples come from the seabed with depths < 500 m and therefore have a present-day temperatures of 10 ± 1°C (SEE SECTION 2.1.3.1).

Initial conditions - Emplacement age and temperatures

The Lower Dalradian sample C-PH4-12 has a depositional age of c. 720-800 Ma (Dempster et al., 2002), *i.e.* 760 ± 40 Ma and a depositional temperature of 10 ± 10°C.

The C-MeBo2 apatites yield a U-Pb age of 384 ± 6 Ma which can be used as the starting age constraint. The closure temperature for apatite U/Pb ages is c. 375-600°C (Kirkland et al., 2018) but for the sake of simplification and to reduce the size of the prior time-temperature domain of the models, the temperature at the time of crystallisation is set at 140°C (*i.e*. high enough for complete annealing of any fission tracks).

The C-MeBo apatites have a crystallisation age of c. 880 Ma. However, preliminary modelling demonstrates that the thermal history is unconstrained before 200 Ma. For the sake of simplification and to reduce the size of the prior time-temperature domain of the models, the initial time-temperature constraint is set as 300 Ma and 140°C (allowing for an intermediate constraint at 250 ± 50 Ma, see next section).

5.5.4.3 Intermediate constraints

Since the samples do not come from a borehole no intermediate constraints based on stratigraphy can be inferred.

However, ZFT ages were acquired from an Upper Cretaceous sandstone in shallow borehole 16/28-sb01 (Green, 2001b). As discussed in SECTION 5.2.5.4, these ZFT zircon ages likely come from a Proterozoic gneiss complex on the NW flank of the North Porcupine High, similar to the NPHO. The ZFT ages likely reflect the thermal history of this Proterozoic gneiss complex rather than the post Late Cretaceous burial history in 16/28-sb01. Therefore, the ZFT ages can be used as an optional intermediate time-temperature for sample C-MeBo (the NPHO sample).

The modelling of the ZFT data indicated that the source area (*i.e.* the NPHO) was probably experiencing temperatures of c. 250-300°C at some point during the Permian-Triassic (see section 5.2.7.6). Therefore, the intermediate time-temperature constraint can be defined as 250 ± 50 Ma for the x-axis and 275 ± 25°C for the y-axis. This constraint will be used in one modelling scenario of C-MeBo.

Table 16: QTQt modelling parameters.

a) Prior information and MCMC chain parameters

Categories		C-MeBo	C-MeBo2	C-PH4-12
Prior information	Time Temperature	440 ± 440 Ma 70 ± 70°C	191.5 ± 19.5 Ma 70 ± 70 °C	400 ± 400 Ma 70 ± 70 °C
	Max dT/dt Reheating Temperature offset Offset	1000 °C.My Yes n/a n/a		
MCMC chain	Burn-in, Post-burn-in Thinning	10,000, 10,000 1		
Proposed move	Time, Temp, Offset Resample/Reject Reject complex	30, 28, n/a Resample Yes		
Initial conditions	Time Temperature	880 Ma 140 °C 400 °C	383 Ma 140 °C	760 ± 40 Ma 10 ± 10 °C
Final conditions	Time Temperature	0 Ma 10 ± 1 °C		

b) Model names and characteristics

	Sample	Scenario	Inputs	L_0	Constraints	tT points
Site 1	C-PH4-12	0 1 2a 2b	AFT+FTL AFT+AHe AFT+FTL+AHe AFT+FTL+AHe	Calculated Calculated Calculated Set at 16.3 µm	None None None None	Low (Simple) & high (Complex)
Site 2	C-MeBo	0 1 2 3	AFT+FTL AFT+Ahe AFT+FTL+Ahe AFT+FTL+AHe	Calculated Calculated Calculated Calculated	None None None 250 ± 50 Ma, 275 ± 25°C	Low & high Low & high Low & high High
Site 3	C-MeBo2	0a 0b 1a 1b 2 3a 3b	AFT+FTL+AHe AFT+FTL+AHe AFT+FTL AFT+FTL AFT+FTL AFT+FTL+AHe AFT+FTL+AHe	Calculated Calculated Calculated Calculated L0 = 16.3 µm L0 = 16.3 µm L0 = 16.3 µm	None None None None None None None	Low High Low High Low Low High

c) List of intermediate constraints

Sample	Time	Source
C-MeBo	250 ± 50 Ma 275 ± 25 °C	16/25-sb01 Late Cretaceous sand ZFT

5.5.4.4 Prior box and run parameters

The prior box for samples C-MeBo, C-MeBo2 and C-PH4-12 is defined respectively as 150 ± 150 Ma, 191.5 ± 191.5 Ma and 400 ± 400 Ma for the x-axis and 70 ± 70°C for the y-axis (except for one scenario for C-MeBo that uses a 200 ± 200°C y-axis to include the ZFT-based time-temperature constraint) (TABLE 16).

5.5.4.5 Modelling scenarios and results

Stability of the log likelihood and log posterior chains

All the models yielded convergent log likelihood and posterior chains (*i.e.* no trend in post-burn-in models) (FIGURE 77). The results of the modelling of each scenario are summarized in FIGURE 78.

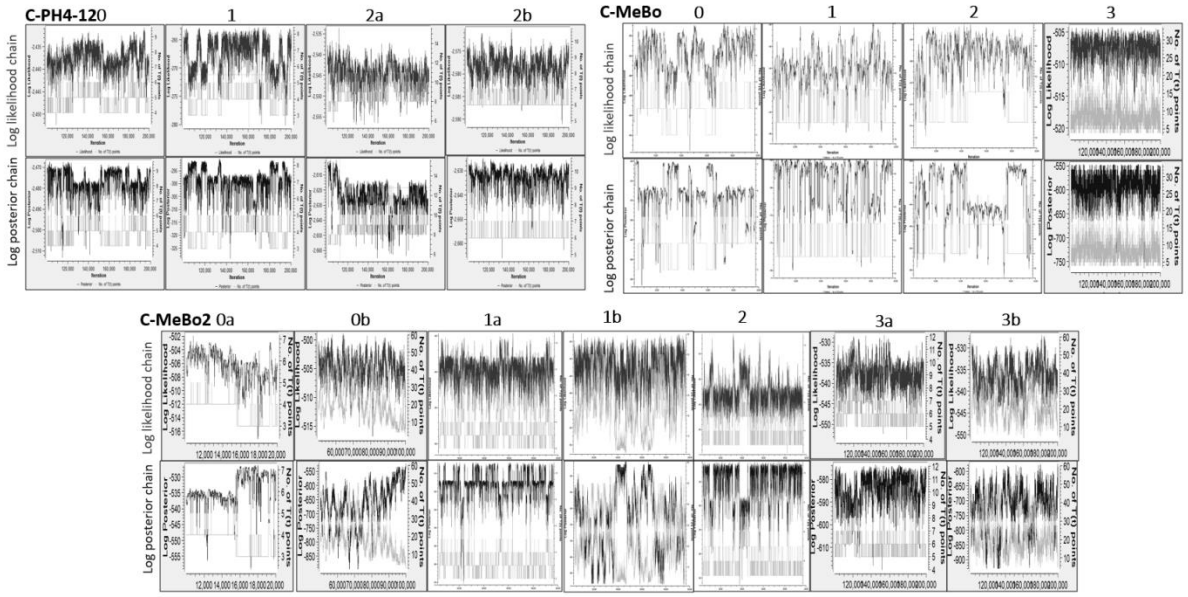

Figure 77: Log likelihood and log posterior chains for C-PH4-12, C-MeBo and C-MeBo2 models. All chains are stable.

Location 1 (summit of the PH) C-PH4-12

Scenario 0: AFT ages and track lengths only (no AHe ages)

This scenario is run to evaluate the information contained in the AFT and track length data alone, independent of the AHe ages.

The modelling shows that the sample might have spent a long time within the PAZ (as constrained by the wide range of track lengths) and only recently was exhumed and cooled down below 60°C (during the Paleogene). All models yield modelled AFT/AHe ages and track length distributions in good agreement with the AFT and AHe data (ANNEX 2).

Scenario 1: AFT and AHe only, no track lengths

This scenario is run to evaluate the information contained in the AFT and AHe ages only, independent of the information contained in the track lengths.

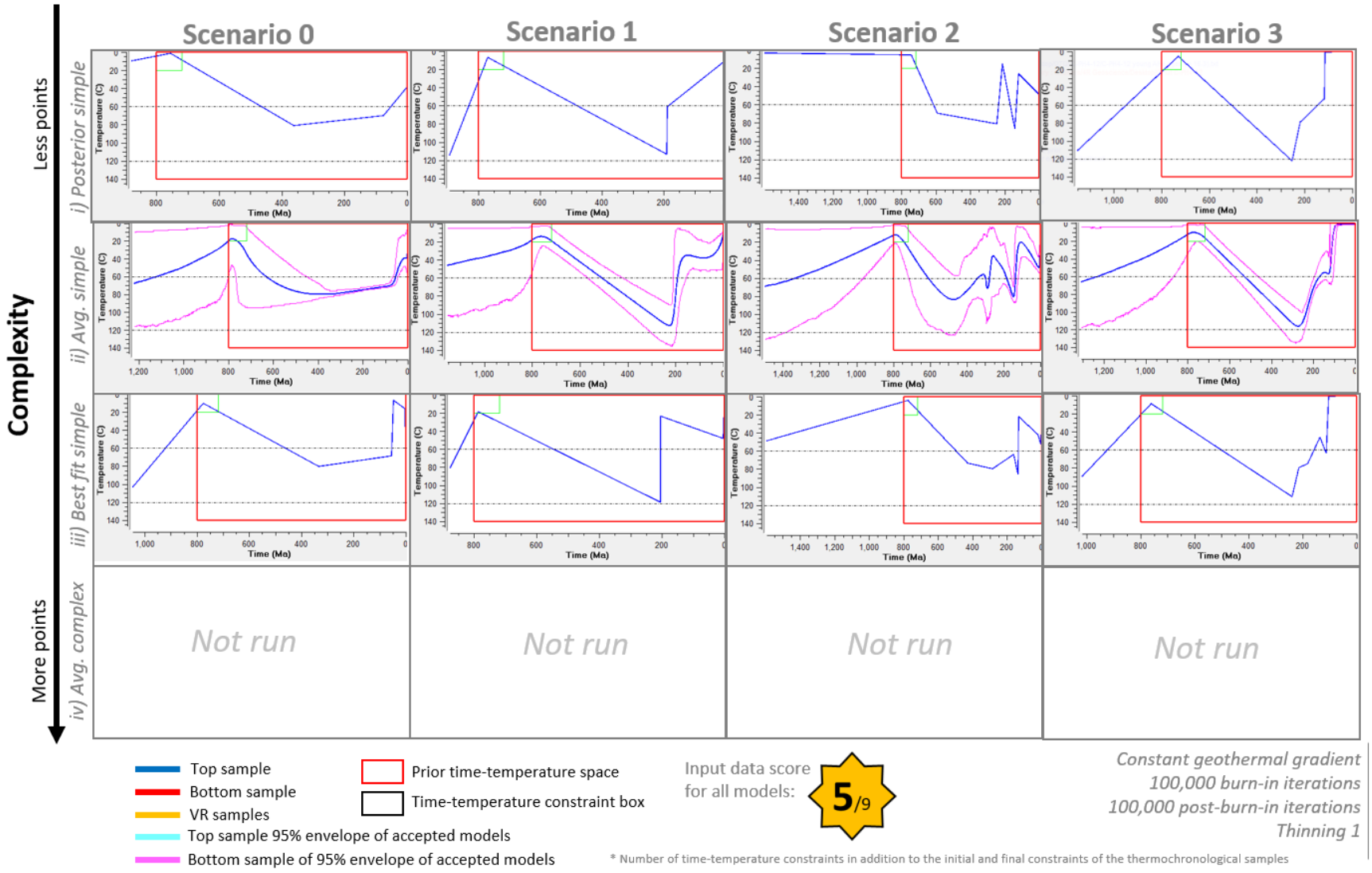

Figure 78: Results of thermal history modelling of sample C-PH4-12 (Norh Porcupine High).

The modelling shows a rapid cooling through the PAZ at c. 200 Ma (from temperatures closes to 120°C to temperatures below 40°C) followed by either a slow cooling to surface temperatures or rapid cooling and subsequent re-heating and cooling. All models yield modelled AFT/AHe ages and track length distributions in good agreement with the AFT and AHe data (ANNEX 2).

The modelling suggests that the sample have remained at temperatures below c. 60°C since the end of the Triassic.

Scenario 2a: all thermochronological data

This scenario is run to evaluate the information contained in the AFT, AHe ages and track lengths all together.

The modelling shows a complex thermal history with three or four main cooling periods at 500-300 Ma, 300-250 Ma, 150-100 Ma and 10-0 Ma. However, the predicted data do not match the observed ones: the AFT age is too old, the AHe ages are too young and the MTL peak is too high (ANNEX 2).

The poor match is probably due to the small number of track lengths greater than 15 µm while at the same time the AHe ages are old. To avoid having too many track lengths greater than 15 µm, the models tend to favour thermal histories with heating to 40-50°C during the late Cretaceous and Cenozoic. These heating episodes lead to helium diffusion and therefore AHe ages younger than the observed ones.

Several hypotheses can be invoked to explain the apparent contradictory thermal history information contained in the track length data and AHe ages:

1) The AHe ages are anomalously old because of (U-Th-Sm)-rich inclusions (which lead to excess He in comparison to dissolved and measured parent elements)
2) he He diffusion and track annealing algorithms used in the modelling are not suitable for this sample (Tamer and Ketcham, 2020).

1) The first hypothesis is unlikely because seven grains have been dated and they all yielded similar old AHe ages and therefore the chance of having a significant number of inclusions in all seven grains is very low.

2) It is possible that the default L_0-composition relationship used to calculate initial track lengths (L_0) is inadequate for these grains as the correlation coefficient for this relationship is known to be poor (Carlson et al., 1999). The following model tests this hypothesis.

Scenario 2b (all thermochronological data) - L_0 set at 15.3 and 16.3 and 16.7 µm

This model tests the hypothesis that the calculated L_0 was overestimated and should be smaller (*i.e.* removing the need to anneal the long track lengths by creating heating episodes in the last 100 Ma).

Three L_0 have been tested: 1) 15.3 µm which represents the longest measured track length in the sample; 2) 16.3 µm which represents the average L_0 measured by Green et al. (1986) for Durango and close to the average L_0 from the apatite dataset of Carlson et al. (1999) and is used as the default value in QTQt, and 3) 16.7 µm which is the longest measured L_0 in a compilation of L_0 datasets (Soares et al., 2013). Only 20,000 runs were used for these scenarios (both simple and complex models were run).

All three scenarios yield the exact same thermal history with a first cooling episode between c. 275 Ma and 145 Ma, followed by constant temperatures between c. 145 and 120 Ma, a second rapid cooling episode between 120 and 100 Ma and finally constant surface temperatures between 100 Ma and 0 Ma (FIGURE 79). The match between predicted and measured AFT/AHe ages and track length distributions is better than for the scenario with the L_0 calculated by QTQt.

First, the identical result for all three scenarios suggest that an initial track length value between 15.3 and 16.7 µm does not have an impact on the final thermal history.

However, the thermal history is different between the scenarios where L_0 is calculated automatically and the scenarios where it is user define. In the latter scenarios, the rapid cooling episode is slightly younger (c. 120-100 Ma = Aptian-Albian *vs* c. 120-145 Ma = Berriasian-Barremian), the pre-cooling maximum temperature at c. 300 Ma is higher (c. 120°C *vs* c. 80°C) and temperatures remain at c. 0°C during the 100-0 Ma period (*vs* reaching up to c. 40°C).

Despite the differences in thermal histories based on the type of L_0 used (calculated *vs* user set), several key characteristics common to both thermal histories are:

1) Protracted cooling between c. 300 Ma to c. 170 Ma (Permian to Lower Jurassic)
2) Stable temperatures or slight heating between 170-125 Ma (Late Jurassic and/or earliest Cretaceous)
3) Rapid cooling of c. 60°C during the Early Cretaceous (Berriasian-Barremian or Aptian-Albian)
4) Temperatures remain below 40°C between 100 Ma and now.

However, based on the better predicted results, the thermal history models based on a user defined L_0 (e.g. 16.3 µm) will be used for the discussions and further interpretation.

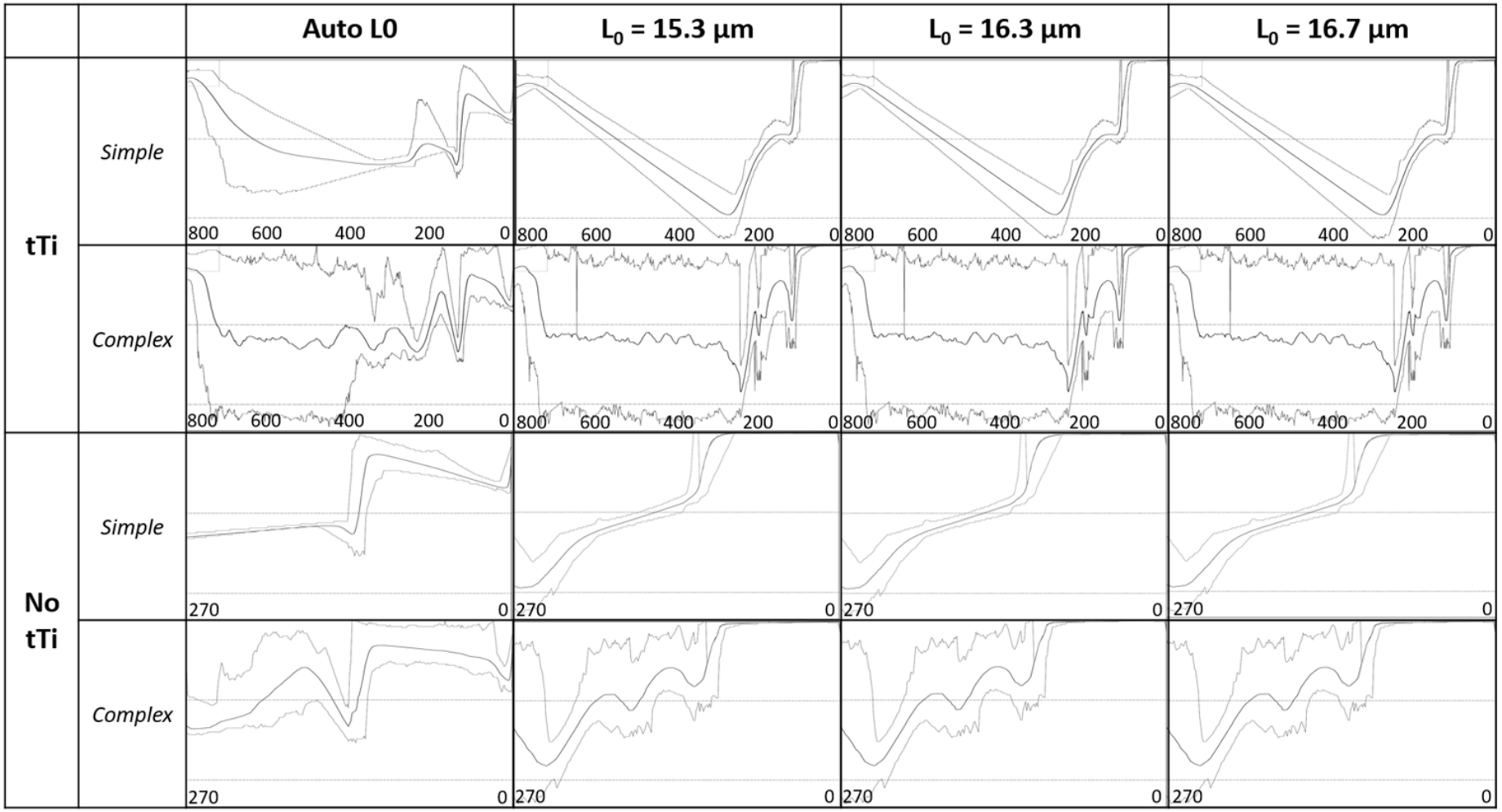

Figure 79: C-Ph4-12 modelling with automatic calculated L_0 or L_0 set up at 15.3, 16.3 and 16.7 µm (end-member cases). Models have been run with and without the initial time-temperature constraint and with simple and complex time-temperature paths.

Discussion

The modelling of the thermochronological data shows protracted cooling from c. 300 Ma to 100 Ma (early Permian to earliest Cretaceous, FIGURE 80) which is probably due to exhumation associated with the multi-phased protracted rifting of the NEAM that occurred during that time (Shannon, 1991).

The short period of heating (0-20°C maximum) between 145 and 125 Ma (Berriasian-Barremian) (FIGURE 80) is unlikely to be caused by burial. The central part of the Porcupine High is underlain by non-thinned continental crust with a thickness of 24-30 km (Licciardi et al., 2020), suggesting that it remained as a stable horst during that time, with its summit probably above sea water.

A possible cause of this heating pulse is the Early Cretaceous magmatism. Calvès et al. (2012) suggest that a magmatic province might have developed in the region during the Early Cretaceous as a consequence of the Late Jurassic main phase of rifting (comprising the Porcupine Median Volcanic Ridge in the Porcupine Basin, the Barra Volcanic Ridge System in the Rockall Basin and the J anomaly on the Newfoundland-Galicia margins). The delay between onset of rifting (during the Jurassic) and onset of magmatism (during the Early Cretaceous) could be the result of decompressional mantle melting associated with a short-lived (15-25 Ma long) rift (Calvès et al., 2012). This regional magmatism might have raised the regional or local geothermal gradients that could have resulted in partial annealing of the track lengths in sample C-PH4-12.

To the list of volcanic features that could belong to this Early Cretaceous volcanic province, the basalt at the base of shallow borehole 16/28-sb01 might also be added (FIGURE 73). Although it is not radiometrically dated, this basalt is overlain by a sandstone of possible Cenomanian age (and no younger than Late Cretaceous). Therefore, this basalt could well be Early Cretaceous in age and be an indicator of Early Cretaceous magmatism and a high heat flux on the North Porcupine High.

The Late Cretaceous and Cenozoic thermal history is characterized by near-surface temperatures with an absence of any significant heating or cooling events (FIGURE 80). This suggests that during the Late Cretaceous the summit of the PH was probably below sea level but did not experience high rates of subsidence and sedimentation. The expected Paleogene uplift event(s) might have temporarily raised the summit above sea level (Jones et al., 2001b) but any associated sub-aerial erosion was probably below a few hundreds of meters in thickness since no cooling is recorded by the thermochronological data.

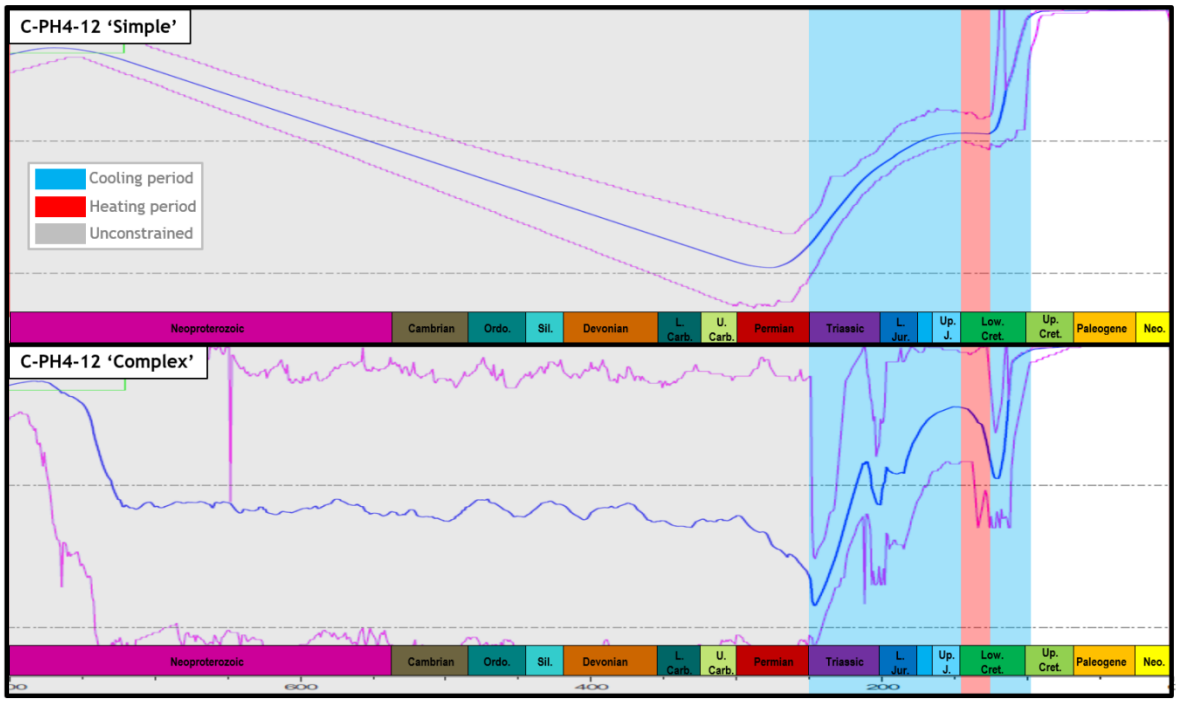

Figure 80: Thermal history modelling results for sample C-PH4-12.

Location 2 (NW side of the NPH) C-MeBo

Scenario 0: AFT ages and track lengths only (no AHe ages)

This scenario is run to evaluate the information contained in the AFT and track length data alone, independent of the AHe ages.

The complex expected model shows that the thermal history is unconstrained before c. 160 Ma. The simple expected model shows that the sample experienced rapid cooling from c. 120°C to below c. 50°C between c. 120-160 Ma (Late Jurassic-Early Cretaceous) and remained below 50-40°C since then (ANNEX 2).

However, while the track length distribution is perfectly matched by these models, the predicted AFT age is always younger (c. 130-140 Ma) than the measured age (QTQt central age of c. 197 Ma), albeit still within two standard deviations. The mismatch might indicate that the old AFT central age is not representative of the sample and should be younger. The rapid cooling between 120-160 Ma is probably constrained by the narrow distribution of long track lengths and the absence of shorter tracks.

Scenario 1: AFT ages and AHe ages (no track lengths)

This scenario is run to evaluate the information contained in the AFT and AHe data alone, independent of the track lengths.

Similarly to scenario 0, this scenario yields thermal histories with an even more rapid cooling pulse from c. 120°C to below c. 50°C between 145-170 Ma (Middle to Late Jurassic) and that the sample remained below c. 35°C since then (ANNEX 2).

Again, these models yield a younger AFT central age of c. 150 Ma, while the predicted AHe ages (110-130 Ma) are also younger than the measured ones (c. 145-150 Ma). The maximum posterior model yields a thermal history with instant cooling at c. 157 Ma to temperatures below 20°C with no subsequent heating. However, even this model yields AHe ages of 115-122 Ma and not c. 157 Ma as expected.

To conclude, the mismatch between predicted and modelled AFT central ages seems to be due to the AFT grain data alone and not due to the track length data or the AHe data. More AFT grains would probably be needed to improve the modelling results of this sample.

Scenario 2: All thermochronological data

This scenario is run to evaluate the information contained in all thermochronological data together.

This scenario yields thermal histories with a rapid cooling at c. 150-185 Ma (latest Early Jurassic to Late Jurassic, c. 6.5°C.Ma^{-1}). As in scenarios 0 and 1, the predicted AFT and AHe ages are younger than the measured ages, while the predicted track length distribution matches very well the measured track length distribution (ANNEX 2).

The modelling shows that the sample experienced rapid cooling throughout the Middle and Late Jurassic but remained at near-surface temperatures (< 40°C) since then. However, the small number of AFT grains (n = 15) and large AFT age dispersion (69 to 775 Ma) results in large uncertainties on the AFT central age and therefore on the thermal histories derived from it.

Scenario 3: All thermochronological data + ZFT constraint

This scenario is run to evaluate the effect of adding a time-temperature constraint based on the ZFT data from the shallow borehole 16/28-sb01 (Green, 2001b).

The modelling for this scenario shows that before rapid cooling during the Jurassic, the sample was probably buried deeper (ANNEX 2). Adding the ZFT data constrains the average cooling rate between 250-300°C and 120°C to a rate between c. 1°C.Ma^{-1} (if the sample cooled down below 250°C at 300 Ma) and c. 6.5°C.Ma^{-1} (if the sample cooled down below 250°C after c. 200 Ma).

Discussion

When compared to the thermal history derived from the samples at the summit of the PH (C-PH4-12), the NPHO seems to have experienced much more rapid exhumation during the Jurassic.

C-MeBo cooled down from c. 120°C to 20°C (*i.e.* 100°C) between 145-185 Ma. During that time, C-PH4-12 cooled down from only c. 65 to 55°C (*i.e.* 10°C). Subsequently, C-MeBo did not experience significant cooling during the Aptian-Albian while C-PH4-12 was being exhumed and cooled down by possibly up to 60°C.

Despite the uncertainties associated with the AFT data of C-MeBo, it seems that the two locations experienced very different thermal histories:

- The PHMS sample experienced protracted cooling from the Triassic to the end of the Early Cretaceous. Such cooling could be explained by continuous subaerial erosion of the summit of the Porcupine High that remained as a paleo-high throughout the various episodes of Mesozoic rifting, in accordance with the multi-proxy provenance studies done on boreholes in the North Porcupine and Slyne Basins (Tyrrell et al. (2007), Franklin et al. (2019)). The subaerial erosion (and cooling) stopped at the start of the Late Cretaceous after drowning of the summit due to thermal subsidence of the margins of the hyper-extended Rockall and Porcupine Basins (and later, due to rising sea levels).
- The NPHO sample experienced very rapid cooling during the Middle and Late Jurassic but not during the Early Cretaceous cooling episode. Such rapid cooling is better explained by tectonic uplift such as the tilting of a fault block during the acceleration of rifting activity during the Middle Jurassic which accelerated in the Late Jurassic. Therefore, it is probable that a major NE-SW fault occurs somewhere between the NPHO and PHMS outcrops: the block located to the NW of the fault would have been rotated during the Jurassic while the block to the SE of the fault would have been part of a more stable, unrifted basement block (FIGURE 81). The absence of Early Cretaceous cooling could have been due to being below sea level and/or burial under a thin layer of Early Cretaceous sediments that would have been subsequently eroded. The presence of perched Mesozoic basins on the north-west side of the Porcupine High (e.g. the Macdara and Fursa basins; Naylor and Shannon (2001)) supports the hypothesis of a tilted fault block (or at least a tectonically uplifted block) away from the more stable basement represented by the PHMS samples on the summit of the PH.

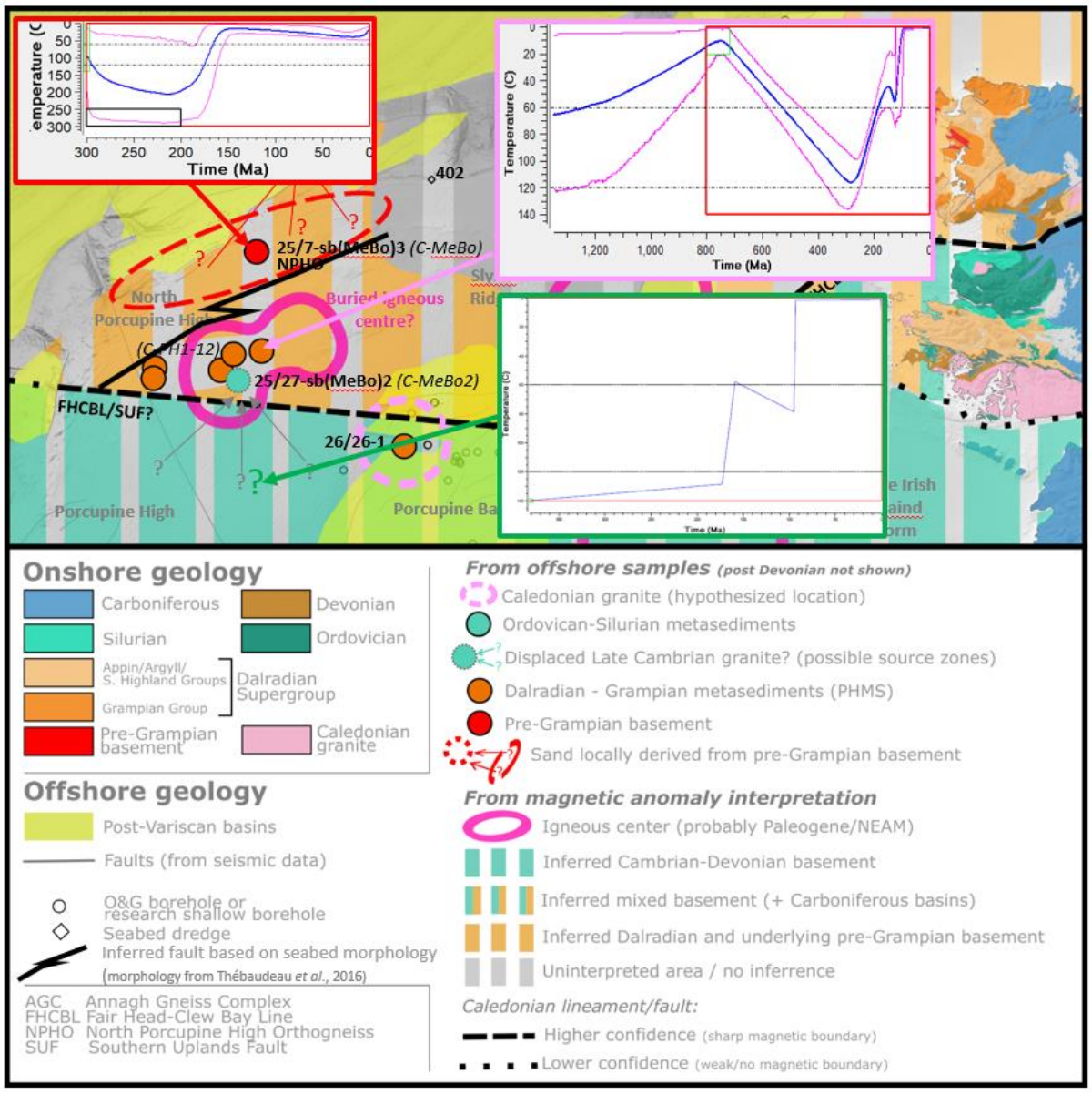

Figure 81: Plausible thermal histories of the three samples reflecting the exhumation of three different basement blocks separated by regional faults.

Location 3 (Summit of NPH) C-MeBo2

Scenario 0: All thermochronological data

The complex expected model shows that the thermal history is unconstrained before 200-250 Ma. The simple expected model shows that the sample likely cooled down slowly through the PAZ between 200-250 Ma and 50 Ma (c. 0.24°C.Ma^{-1}) with an acceleration in the cooling rate in the last 50 Ma (c. 1°C.Ma^{-1}). This model also shows that the sample had to have remained below c. 80-90°C between 250 and 50 Ma and below 60°C in the last 50 Ma. All models show a good match between the predicted and measured AFT/AHe ages and track length distributions (ANNEX 2).

Scenario 1: AFT ages and track lengths only (no AHe ages)

This scenario is run to evaluate the information contained in the AFT ages and track length data alone without the AHe ages.

The modelling shows a protracted cooling through the PAZ between 300 Ma and 10-20 Ma with rapid cooling from 60°C to 10°C in the last few millions of years (50°C or an exhumation or c. 1800 m of eroded sediments using the assumed present-day geothermal gradient of c. 28°C.km^{-1}). The modelling yields predicted AFT age and track length distributions that match the measured AFT data (ANNEX 2). However, this thermal history conflicts with the regional geology which does not allow for such large exhumation during the Neogene.

The unrealistic rapid Neogene-Quaternary exhumation seen in the modelling is essentially constrained by the track length data (not by the Mesozoic AFT age, nor the AHe ages which are absent in this scenario). In particular, this recent cooling must be constrained by the absence of very long track lengths. As discussed for sample C-PH4-12, it could be due to either an underestimation of the actual lengths or else an inadequate annealing model, possibly due to the calculated L_0. The former hypothesis cannot be tested but the latter can be by using a user set L_0 (see scenario 2 and 3 in next sections).

Scenario 2: AFT ages and track lengths only (no AHe ages), fixed L_0 = 16.3 µm

This model tests the hypothesis that the calculated L_0 was overestimated and should be smaller (*i.e.* removing the need to anneal the long track lengths by creating heating episodes in the last few millions of years). One scenario has been tested with a user set L_0 of 16.3 µm.

The simple likelihood model shows a thermal history characterized by rapid cooling through the PAZ from 170 to 160 Ma, followed by c. 20°C heating between 160-100 Ma and another phase of rapid cooling from 80 to 0°C around 95 Ma. Between 95 Ma and 0 Ma the temperatures remain at 0-10°C. This model yields predicted data that match the measured data (ANNEX 2).

On the other hand, the simple posterior and expected models converge on a thermal history with a protracted cooling phase from 120°C to 0-10°C between 190 and 50 Ma. These models also yield predicted data that match the measured data.

This scenario proves that the rapid Neogene - Quaternary cooling of scenario 0 and 1 is related to the modelling of track length annealing and might be caused by an unrealistic calculation of L_0. Employing a user-defined L_0 removes the need for temperatures higher than surface temperatures for at least the last 50 Ma. Employing a user-defined L_0 can therefore be tested in a scenario including the AHe ages as well (see next scenario).

Scenario 3: AFT ages and track lengths and AHe ages, fixed L_0 = 16.3 µm

The modelling of this scenario shows that the thermal history is unconstrained before 170 Ma (see the complex expected model, Annex 2).

All models show a first period of cooling from at least 120°C to c. 30°C from 170 Ma to 90-120 Ma, *i.e.* a cooling of c. 90°C from the Middle Jurassic until the Barremian or possibly until the end of the Cenomanian. This Mesozoic cooling period is followed by a period of heating to c. 70°C until c. 50 Ma, *i.e.* a 40°C heating that happened primarily during the Late Cretaceous and Paleocene. At c. 50 Ma, the models show a very rapid cooling of the sample to surface temperatures (c. 60°C) which remained at these low temperatures until the present-day.

Discussion

The rapid cooling (of c. 50°C) in the last 50 Ma in scenarios 0 and 1 would correspond to an exhumation of c. 1800 m of sediments assuming a geothermal gradient of 28°C.km^{-1} (as determined in the closest borehole, 26/26-1). This significant amount of exhumation is not in agreement with the regional geology and with the thermal history of nearby samples on the summit of the PH (C-PH4-12, C-MeBo) and on the margins (borehole 16/28-sb01, 26/26-1 and 34/05-1).

Scenario 2 demonstrated that this unrealistic Quaternary cooling might be partly caused by the L_0 parameter and that a default user set L_0 based on an average L_0 value from the literature yields more realistic thermal histories (without the large Neogene-Quaternary cooling).

Such a user-defined L_0, when used with the entire thermochronological dataset available for this sample, yields a thermal history dominated by the following phases:

1. 90°C cooling between 170 Ma and 120-90 Ma: this cooling can be linked with the main phase of Mesozoic rifting (Whiting et al., 2020) and corresponds to an exhumation of c. 3 km.
2. 40°C heating between 120-90 Ma and 50 Ma: this heating could be linked to the cessation of exhumation during the Late Cretaceous and Paleocene due to the high being under sea level and possibly some amount of burial due to carbonate sedimentation and/or an increase in geothermal gradient or surface temperatures.
3. 60°C cooling at 50 Ma: this cooling could be linked to the phase of transient Paleocene-Eocene boundary uplift observed in other parts of the NEAM (Champion et al., 2008a) and Ireland (Cogné et al., 2016). Such cooling would correspond to an exhumation of c. 2 km using the present-day geothermal gradient, but might have been less if the paleo-geothermal gradient was higher due to the widespread magmatic activity at the time (Wilkinson et al., 2017a).
4. Surface temperatures from 50 Ma to 0 Ma: the stable surface temperatures since 50 Ma can be interpreted as the Porcupine High being submerged again by the sea after the transient

Paleogene uplift and the cessation of subaerial erosion combined with an absence of significant subsidence and sedimentation on the summit of the high.

Since this thermal history is significantly different from C-PH4-12 it might reflect the thermal history of a different tectonic block. And since the sample might come from an outcrop located south of the FHCBL as discussed earlier, it is possible that the basement block to the south of the FHCBL had a significantly different tectono-thermal history than the Laurentian basement block to the north (which comprises the psammites of C-PH4-12).

Borehole 34/05-1 is also located south of the hypothesized FHCBL (**ERROR! REFERENCE SOURCE NOT FOUND.**B**ERROR! REFERENCE SOURCE NOT FOUND.**) and records a possible exhumation of up to 900 m during the Paleogene (SECTION 5.4.6.6). It is therefore possible that the basement block south of the FHCBL was uplifted and eroded significantly during the Paleogene, while the northern block (comprising the PHMS psammites, sample C-PH4-12) experienced a much smaller amount of uplift and erosion. While exhumation of 3 km is estimated for C-MeBo2 during this 50 Ma uplift event, it is possible that the actual erosion might have been 2 to 3 times smaller due to a higher paleogeothermal gradient (possibly produced by the inferred buried igneous centre under the Porcupine High summit) and intrinsic uncertainties associated with the thermochronological data and thermal history models.

However, it should be noted that this inferred difference in uplift and erosion between the northern and southern blocks at c. 50 Ma would most likely still be expressed in the present-day bathymetry, which is not the case (Thébaudeau et al., 2016).

During the Paleogene, the region was subject to significant magmatic activity linked to the opening of the NEAM. On the Porcupine High, Paleogene magmatism is expressed by the presence of igneous centres such as the one below the summit (Tate and Dobson, 1988), fluid inclusions from hot fluids (up to 200°C) in Eocene and Late Cretaceous sands in shallow boreholes on the western margin of the high (Green, 2001b) and igneous intrusions in boreholes on the eastern margin of the high (34/05-1). Magmatism can lead to the resetting of low-temperature thermochronometers due to either one or a combination of the following processes: 1) conductive heating associated with an igneous centre leading to a higher regional geothermal gradient (Murray et al., 2018); 2) conductive heating near slow-cooling igneous intrusions (Calk and Naeser, 1973); and 3) advective heating from hydrothermal hot fluids generated during the cooling of magma (Brown et al., 1994). The first mechanism leads to a semi-regional effect that affects all samples in the area, while the second and third mechanisms are discrete events that affect samples only locally (*i.e.* around an intrusion or within a fluid flow pathway)

Such magmatic overprinting of AFT ages has been invoked in Ireland for some Paleogene AFT ages in the east of Ireland (McCulloch, 1994) and for some offshore wells west of Ireland (e.g. 12/02-1, Green (2003)).

Rather than being due to differential tectonic history, the difference in AFT and AHe ages between the psammites samples and C-MeBo2 could possibly due to the effects of NAIP-related Paleogene magmatism in the area, and in particular hydrothermal fluids (since increased regional geothermal gradient would also affect the PHMS samples and contact heating by igneous intrusions are possible but spatially rarer than hydrothermal fluid flows). Hydrothermal fluids cannot circulate within tight basement rocks such as the PHMS psammites and other metamorphic rocks such as C-MeBo2. However, as discussed above, C-MeBo2 is possibly located within or near the FHCBL fault zone and also at the edge of the inferred igneous centre (FIGURE 81**ERROR! REFERENCE SOURCE NOT FOUND.**), and t herefore hydrothermal fluids associated with the igneous centre would have probably circulated preferentially within the FHCBL fault zone, resulting in thermal overprinting of the rocks within and near the fault zone.

However, while plausible, this hypothesis remains speculative since no evidence of fractured basement, fault zones or hydrothermal fluids have been proven on the summit of the North Porcupine High so far.

In conclusion, two end-member scenarios are hypothesized for this sample:

1. Two main phases of exhumation during the Middle Jurassic to Early Cretaceous (due to rifting) and at c. 50 Ma (transient uplift associated with the opening of the North-East Atlantic).
2. One main phase of exhumation during the Middle Jurassic to Early Cretaceous (due to rifting) and a reset of the AHe ages at c. 50 Ma due to NAIP magmatism (possibly related to hydrothermal fluids from an igneous centre circulating in FHCBL fault zone).

Based on the absence of indicators of hydrothermal fluids or heavily fractured basement in the area, the first hypothesis is favoured, despite the lack of present-day expression of differential exhumation on the seabed.

Provenance data from Paleocene-Eocene sandstones just to the east of the North Porcupine High could help discriminating between these two hypotheses. If the 50 Ma cooling is mostly due to exhumation, Early Eocene sandstones located in boreholes just to the east of the North Porcupine High should be derived mainly from the uplifted Caledonian peri-Laurentia sedimentary and volcanic rocks with little input from the Neoproterozoic PHMS basement. On the other hand, if the 50 Ma cooling is mostly due to localized magmatic activity, the sandstones should reflect a provenance from the Dalradian basement and from the peri-Laurentia rocks south of the inferred trace of the FHCBL.

5.5.5 Discussion

Non-uniform thermal histories

The three samples yielded three significantly different thermal histories (FIGURE 82). The PHMS composite sample (C-PH4-12) yielded a thermal history characterized by protracted cooling to surface temperatures throughout the Triassic, Jurassic and Early Cretaceous with no subsequent significant temperature changes. The NPHO sample (C-MeBo) yielded much more rapid cooling during the Middle and Late Jurassic. Finally, the PHG sample (C-MeBo2) yielded a thermal history also characterized by protracted cooling from at least the Middle Jurassic to the Early Cretaceous followed by another exhumation event at c. 50 Ma. Both samples C-MeBo and C-MeBo2 are associated with large uncertainties and additional data is required to better constrain and understand their thermal histories (e.g. better constraints on the autochthonous character of C-MeBo2, more AFT ages for C-MeBo, and alternative exhumation proxies from geological or geophysical datasets).

Presently, thermal histories derived from sample C-PH4-12 and to a lesser extent C-MeBo are judged robust enough to be used for correlation with other locations and for regional interpretation, although some uncertainties remain due to the discrepancy occurring depending on the type of L_0 used (calculated *vs* user defined, for C-PH4-12) and due to the low number of AFT ages (for C-MeBo).

Comparison with legacy modelling and interpretation

One of the reason that Barry et al. (2017) concluded that the samples from the 2014 campaign were *in-situ* is that the fission track data suggested that the samples experienced a "common uplift history". A review of the samples suggests otherwise. The samples present a wide range of AFT central ages varying from pre-Cambrian to Early Cretaceous and also varying AHe ages that precludes the sharing of a common thermal history. Cogné and Chew (2017) also pointed out the difference in exhumation behaviour between the PHMS basement (C-PH4-12) and the NPHO (C-MeBo), with a more rapid and older exhumation event in the the NPHO. The main difference in the modelling results is the lower temperatures reached by the psammite samples during the Permian-Triassic in comparison to the present-day model. C-MeBo2 was not modelled by Cogné and Chew (2017).

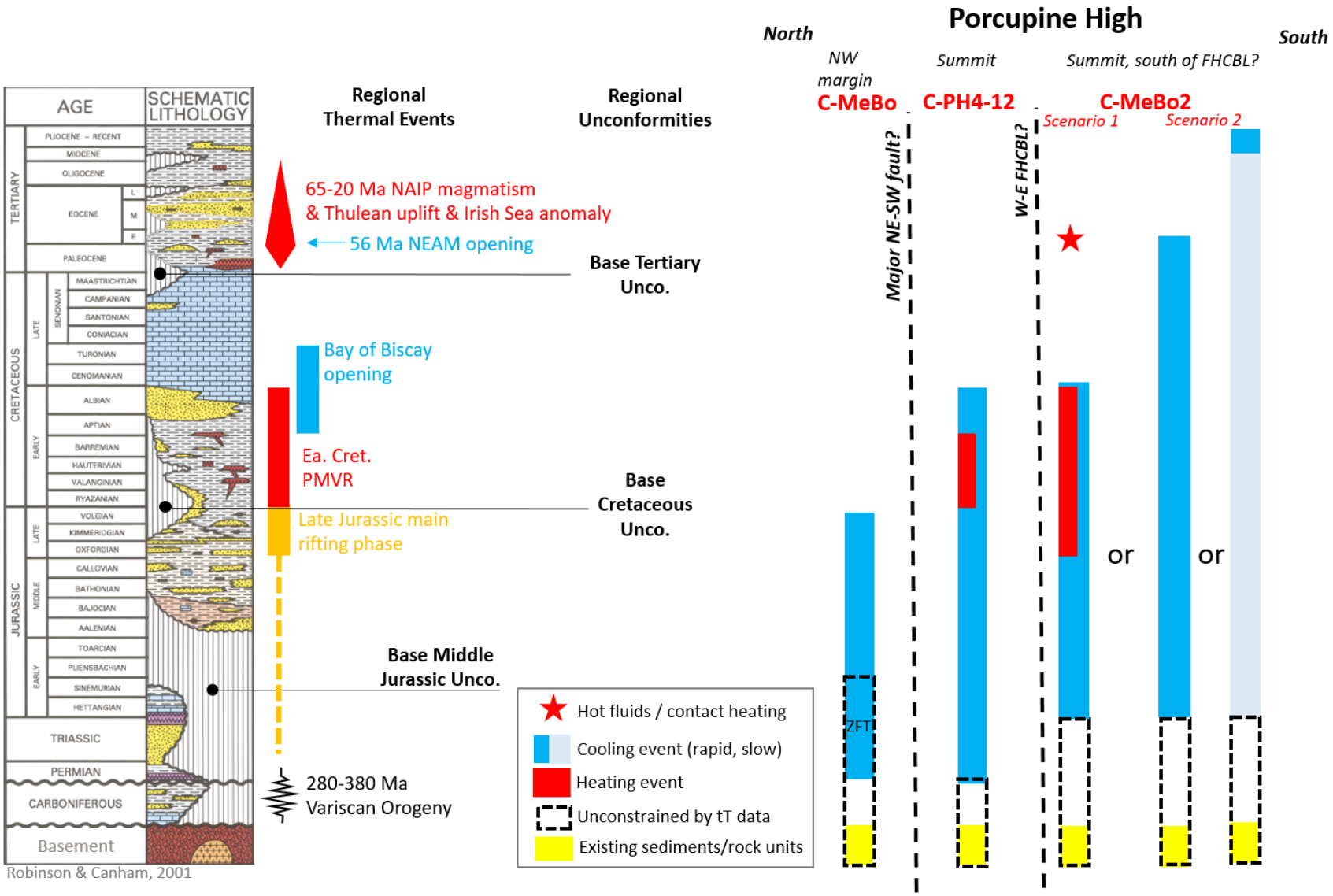

Figure 82: Possible thermal histories of the three samples compared with the main regional geological events.

5.6 Borehole 26/30-1

5.6.1 Exploration history and geological summary

26/30-1 is a dry exploration borehole drilled by Phillips (now ConocoPhillips) in 1982. The well targeted a normal fault trap with Middle Jurassic sandstone reservoirs located in the north-east margin of the Porcupine Basin (FIGURE 33 AND FIGURE 83). It was drilled to a total depth of 1722 mMD in 249 m of water.

The borehole encountered c. 166 m of post-Eocene sediments of uncertain age above c. 31 m of Eocene limestone, claystone and siltstone. The Eocene unit rests unconformably above c. 30 m of Campanian-Maastrichtian limestone, itself resting unconformably above c. 94 m of Aptian-Albian deltaic sands. An unconformity separates the Lower Cretaceous sands from a thick succession (c. 916 m) of Bathonian to Kimmeridgian (Middle-Upper Jurassic) claystones and sandstones with occasional thin dolomites and limestones. The Jurassic unit rests unconformably above 658 m of Westphalian C fluviatile sandstones, siltstones and shales with a basal sand described as a possible granite wash. The well terminated below the Carboniferous unit in 55 m of an undated granite (FIGURE 83 AND FIGURE 84).

5.6.2 Sonic velocity and VR-based exhumation estimates

The detailed analysis of the exhumation estimate using sonic and VR data is provided in ANNEX 1 SECTION 3.3. The VR data indicate that the Jurassic and Carboniferous sediments were in the past buried deeper than their present-day burial depths. The eroded sediments would most probably associated with the main unconformities in the borehole, *i.e.* the Base Aptian Unconformity (BAU) and/or the Base Eocene Unconformity (BEU). Eroded sediments associated with the BAU would be Kimmeridgian to Aptian in age, while eroded sediments associated with the BEU would be Maastrichtian to Eocene in age. 200 m to 1000 m of these sediments is estimated to have been eroded during the Early Cretaceous and/or during the Paleocene-Eocene. These estimates fall within the range of maximum thickness of eroded sediments derived from the sonic velocity data (1-2 km). The exhumation associated with the Jurassic-Carboniferous Unconformity cannot be quantified due to the overprinting associated with post-Jurassic burial.

Based on the VR data (and supporting sonic velocity data), it can be deduced that the AFT ages from the Jurassic and Carboniferous sediments have not been fully reset since deposition. However, apatites from samples deeper than c. 3000 ft (*i.e.* with Tmax greater than c. 60°C) probably resided in the PAZ for some time and experienced some amount of annealing.

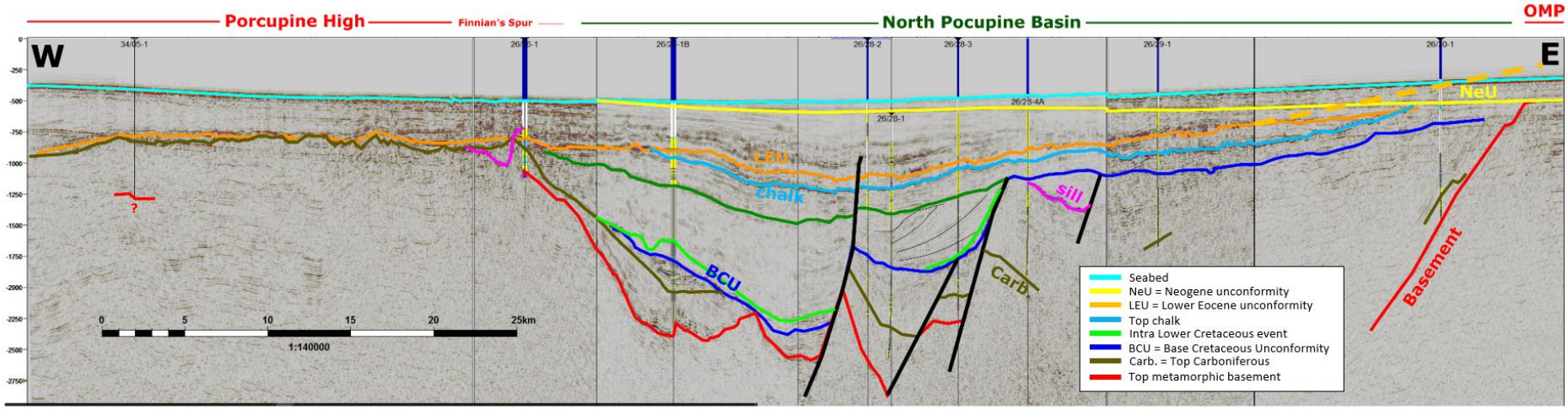

Figure 83: Regional seismic cross-section through 26/30-1.

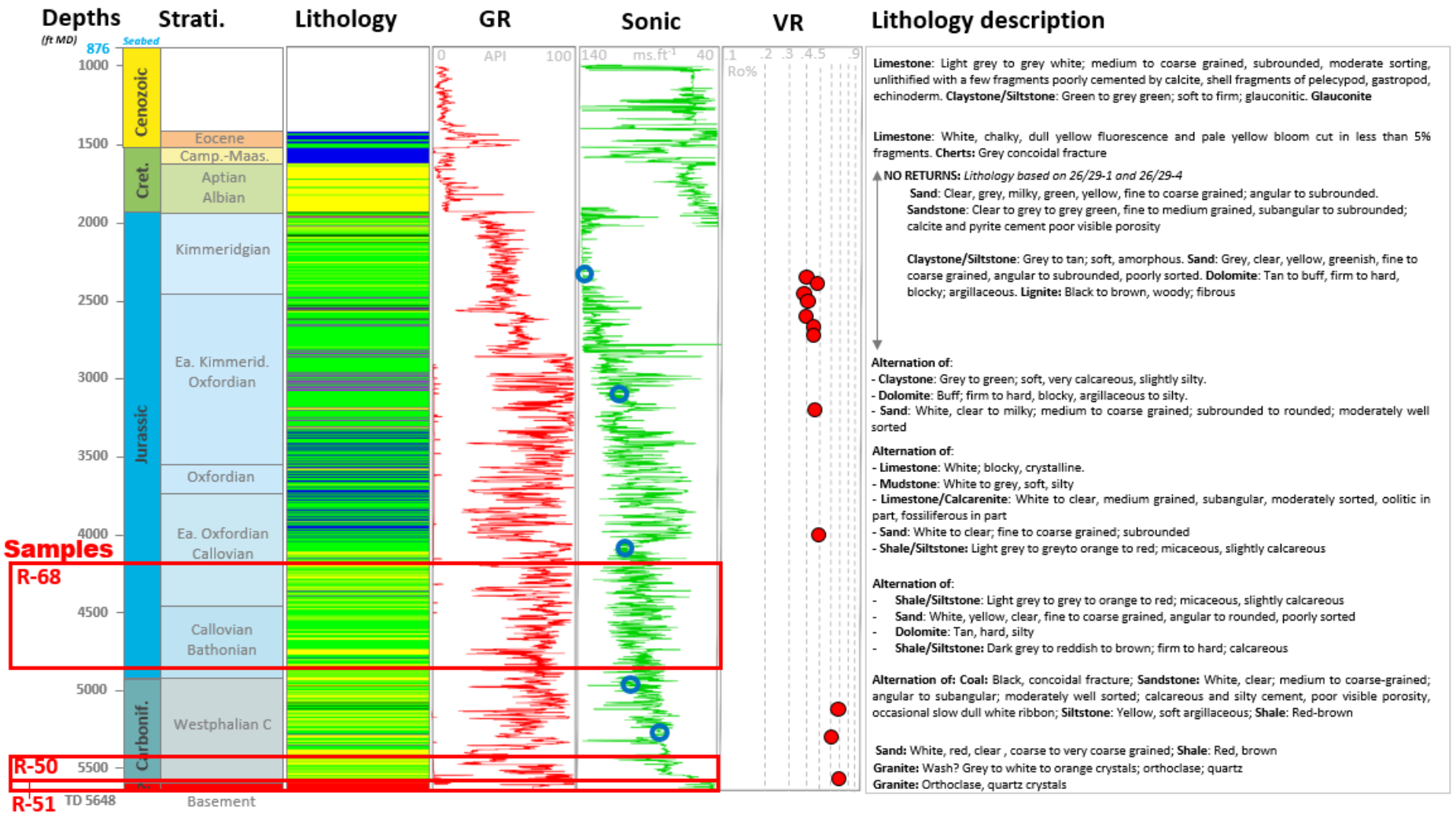

Figure 84: Well 26/30 1 stratigraphy, lithology, logs and sample depths (logs and lithology description from Armstrong (1982) and VR data from Doran et al. (1982)).

5.6.3 Samples

5.6.3.1 Sampling

Cuttings were sampled from the Bathonian to Early Oxfordian sands (sample R-68, 4184-4880 ft MD), the Westphalian C sands (sample R-50, 5430-5550 ft MD) and the basal granite wash and granite (sample R-51, 5560-5640 mMD).

5.6.3.2 Apatite and zircon yield

Sample R-68 (Bathonian to Early Oxfordian sands) yielded numerous apatite grains. 80 grains were analysed for AFT-U/Pb dating and an additional 80 grains were dated for U/Pb ages only. In addition, 182 zircons were analysed for U/Pb dating.

Sample R-50 (Westphalian C sands, raw weight of 50 grams due to limitations from PAD) yielded only four grains that could be dual-dated for AFT-U/Pb ages. An additional 17 grains were also analysed for U/Pb dating only. Zircons were picked for this sample but lost during polishing of the mount.

Sample R-51 (basal granite wash and granite, also with a raw weight of 50 grams) yielded 20 grains which were analysed for AFT-U/Pb ages while another 15 grains were dated for U/Pb only. 50 zircons were also analysed for U/Pb dating.

The Jurassic sands and basal granite yielded numerous apatites and zircons. The poor yield of apatites from the Westphalian C sandstone is unexpected since most Carboniferous sands offshore west of Ireland usually yield numerous apatites and zircons but could be due to the very low quantity of material that sampled for this detrital sample (50 grams) due to sampling volume constraints at the PAD core store.

5.6.4 U/Pb and trace element results

The detailed description of the U/Pb and trace element results is presented in ANNEX 1 (SECTION 1.3.3). Below is a summary and discussion of the results.

5.6.4.1 Oxfordian volcanic grains

Sample R-68 is dominated by a population of apatite grains dated at 159.8 ± 3.1 Ma (Oxfordian) with a trace element signature suggesting they are igneous grains derived from a primitive mafic to ultramafic magma, which is supported by the absence of Jurassic zircons in the sample (Figure 85). According to the biostratigraphic report (King et al., 1982), the sandstones are Bathonian to (Early) Oxfordian in age, *i.e.* they were deposited between 157.3-168.3 Ma, which overlaps with the U/Pb age of the igneous apatites (159.8 ± 3.1 Ma).

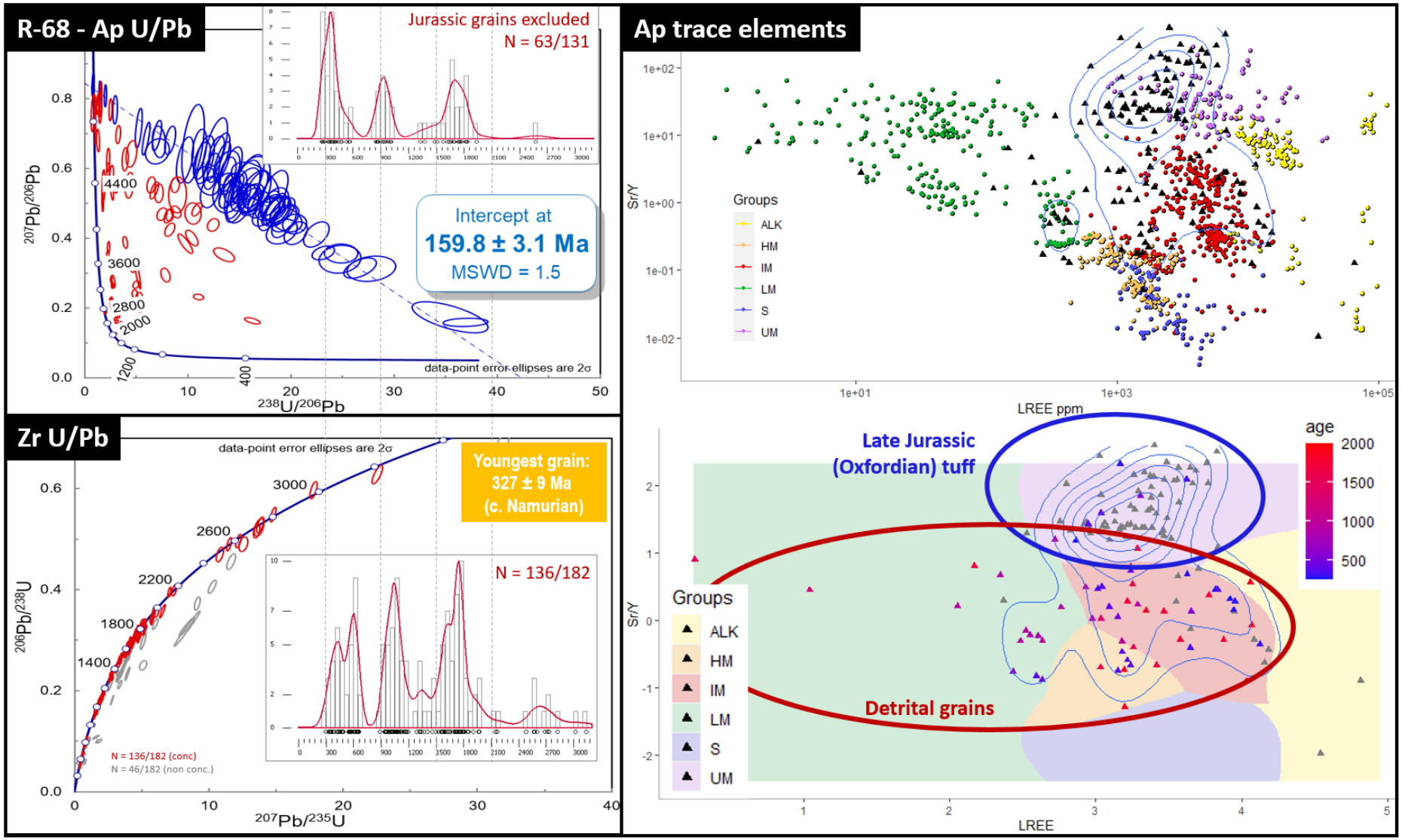

Figure 85: Sample R-68: Apatite and zircon U/Pb dating results and apatite trace element analysis.

This suggests that the magmatic activity associated with these igneous apatites was synchronous with the deposition of these sands (*i.e*. syn-sedimentary magmatism). The geological report describes the section between 4100-4935 ft as *'varicolored arkosic sands and sandstones, varicolored clays and beige limestone'* (Anonymous, 1982). The varicolored layers might represent syn-sedimentary volcanic tuffs from which the volcanic apatite come from.

In conclusion, the U/Pb dating and trace element characterisation of apatites in sample R-68 allowed the identification of an episode of Bathonian to Early Oxfordian mafic magmatism represented by syn-sedimentary tuffs in borehole 26/30-1. The significance of this Jurassic magmatism is further discussed in SECTION 7.2.2.

5.6.4.2 Age and nature of the basal granite

According to the well report, the basal sample (R-51) comprises a granite wash and an *in-situ* biotite granite below (Anonymous, 1982). The granite wash seems to correspond to a decrease in the sonic log from c. 75 $ms.ft^{-1}$ in the Carboniferous clastics to 55 $ms.ft^{-1}$ (i.e. implying a higher velocity), while there is another decrease to c. 40 $ms.ft^{-1}$ in the granite itself (Armstrong, 1982), which supports an interpretation of a basement lithology (FIGURE 84).

However, sample R-51 is dominated by Proterozoic zircon and apatite grains with a minor Early Paleozoic (Ordovician-Early Devonian) population. A component of the latter population likely represents the intrusion age if the sample is a Caledonian granite. Silurian apatite grains plot mostly within the high-grade metamorphic field with one grain in the low-grade metamorphic field and one in the ultramafic field. Both the zircon and apatite U-Pb age distributions and the apatite trace element data suggest that the high-velocity lithology found at the bottom of the well is actually not a granite. Instead, it is more likely that the basement rock has a metasedimentary protolith. The Jurassic apatite grains are likely cavings from the Jurassic sands above. If the next youngest grains (359.7 ± 9 and 381 ± 9 Ma) represent the crystallization age of the metasedimentary rock, then the basement unit is Late Devonian or Early Carboniferous in age, although no post-Caledonian high-grade metamorphic rocks are found on the Irish mainland or the offshore. Alternatively, the basement unit could be Silurian (i.e. Caledonian) in age and the younger Devonian grains would represent cavings from the overlying Carboniferous sands. In any case, the basement rock of 26/30-1 is re-interpreted here as a Silurian or Devonian meta-conglomerate and not as a granite. The significance of this new interpretation is discussed in SECTION 7.3.

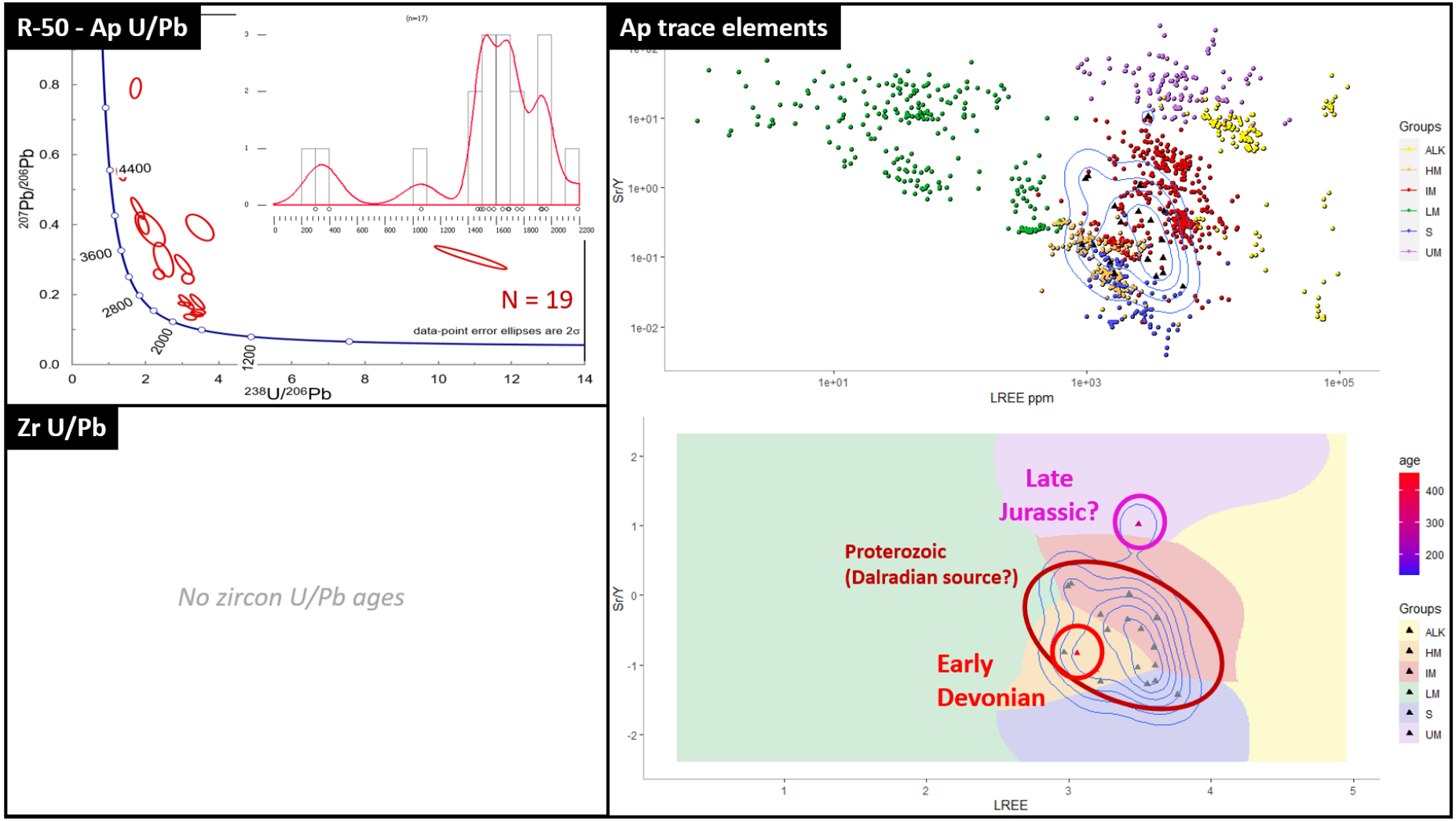

Figure 86: Sample R-50: Apatite and zircon U/Pb dating results and apatite trace element analysis.

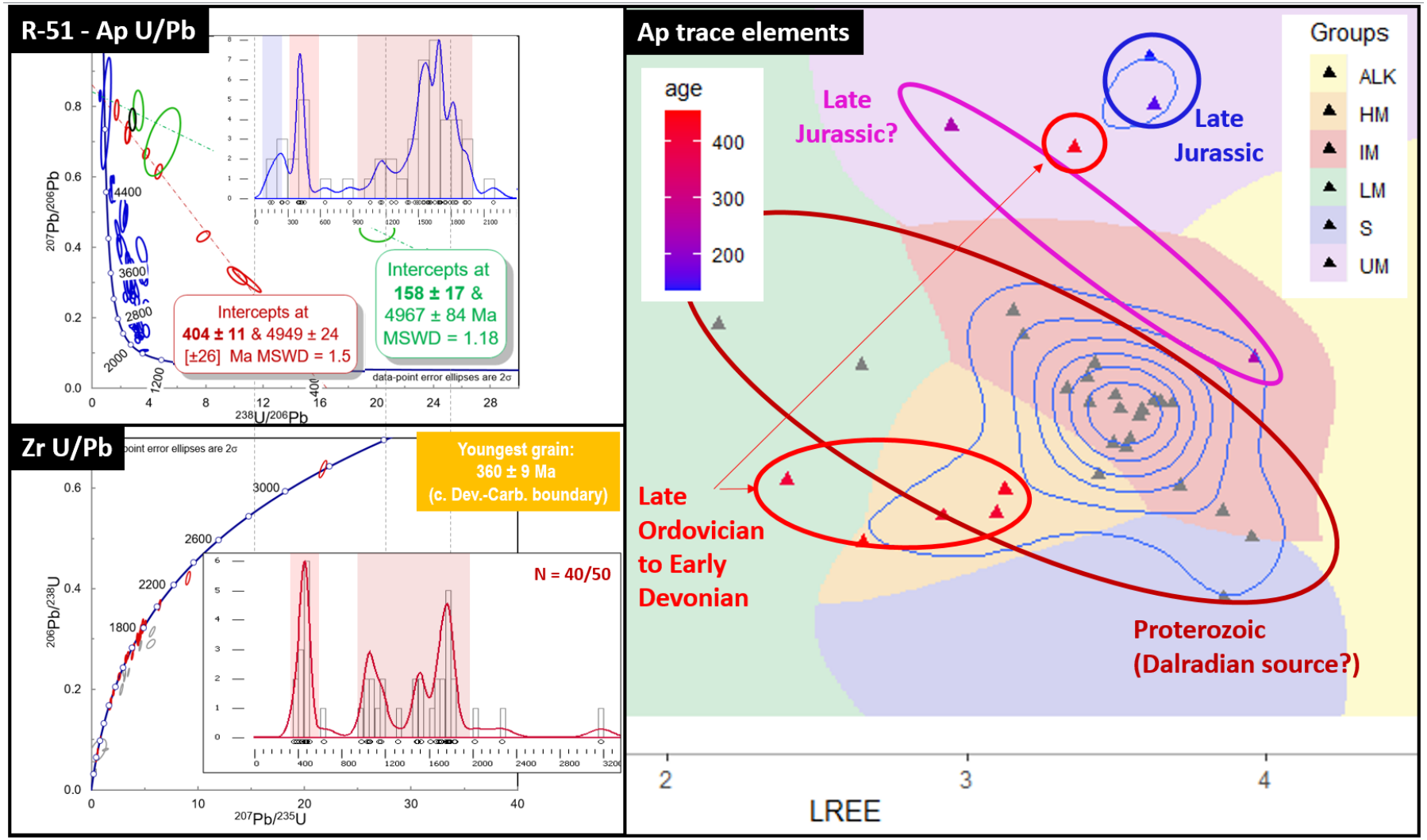

Figure 87: Sample R-51: Apatite and zircon U/Pb dating results and apatite trace element analysis.

5.6.5 Apatite AFT ages

The detailed description of the AFT results of sample R-68, 50 and 51 is presented in ANNEX 1 SECTION 2.3.3 together with a qualitative interpretation. Below is a summary and discussion of the results (TABLE 17).

Table 17: Sample information summary and AFT results. Sample R-50-51 is a composite sample (R-50 and R-51 combined).

Sample information								FTA					CTL				Kinetic		
Sample	Depths		Temp.		Lithology	Age		n	Ns	$P(\chi^2)$	Central Age		Tracks	MTL	SD	SE	Cl	Dpar	U
	Seabed	Sample	Seabed	Sample		Age	±												
	m MSL	*m BSB*	*°C*	*°C*				-	-	-	*Ma*	*±1σ Ma*	-	*µm*	*µm*	*µm*	*wg%*	*µm*	*ppm*
R68	249	1108	10	47	Sandstone	162.8	5.5	43	895	<0.01	**172**	10	28	10.63	2.89	0.55	0.232	1.6776	17.2
R-50	249	1400	10	56	Sandstone	313.1	1.9	2	27	0.7	**75.0**	**15.0**	0	-	-	-	0.135	1.6447	54.3
R-51	249	1434	10	57	Granite wash Granite	313.05 400-470	1.9 n-a	15	210	<0.01	**151**	**23**	11	11.28	1.64	0.49	0.101	1.936	13.5
R-50-51	249	1414	10	57	Sandstone	313.1	1.9	17	237	<0.01	**137.0**	**20.0**	11	11.28	1.64	0.49	0.105	1.8965	15.2

5.6.5.1 Sample R-68 (Bathonian-Early Oxfordian sands)

The detrital and volcanic (Jurassic) grains can be distinguished based on their trace element composition: the igneous grains have a higher U concentration, a higher Cl concentration and smaller Dpar (FIGURE 88A). In contrast to the igneous grains, the detrital grains experienced a pre-depositional thermal history, therefore it is better to consider them as two separate groups for thermochronological interpretation and modelling.

The AFT age of the volcanic grains (205 ± 16 Ma) is slightly older than the crystallisation age (160 ± 3 Ma), suggesting that the true AFT central age should be c. 160 Ma and that the grains have not been reset since crystallisation and deposition during the Bathonian-Oxfordian. The smaller number of track lengths is probably due to their younger age and lower [U] in comparison to the detrital grains.

The detrital grains have an AFT central age (173 ± 10 Ma) slightly older than the depositional age (162.8 ± 5.5 Ma) suggesting that the sample spent a certain amount of time within the PAZ but never experienced temperatures greater than c. 120 °C. This was expected based on the VR data. The bimodal track length distribution points toward a protracted episode of reburial from near-surface temperatures to temperatures within the PAZ, followed by exhumation to near-surface temperature again.

The very low number of track lengths for the volcanic grains preclude their use for thermal history inverse modelling. Only the population of detrital grains will be used as input data for the modelling.

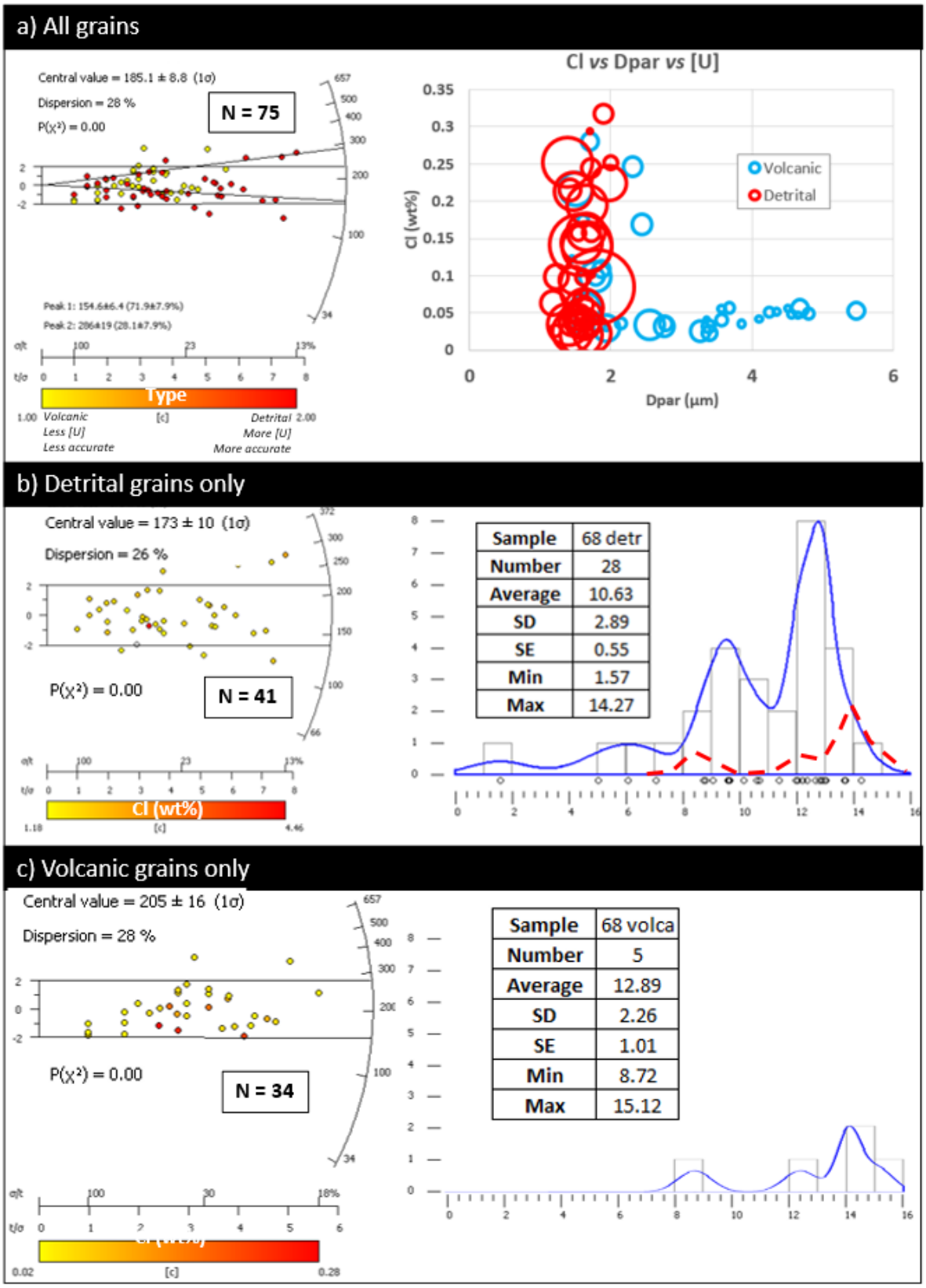

Figure 88: AFT data for sample R-68. a) Radial plot for all grains and Dpar (x-axis) vs Cl (y-axis) vs [U] (circle size) plot showing a difference in chemistry and therefore probably annealing behaviour between the volcanic (lower Cl, higher Dpar) and detrital grains (higher Cl, lower Dpar). B) Radial plot and track length distribution for the detrital grains only.

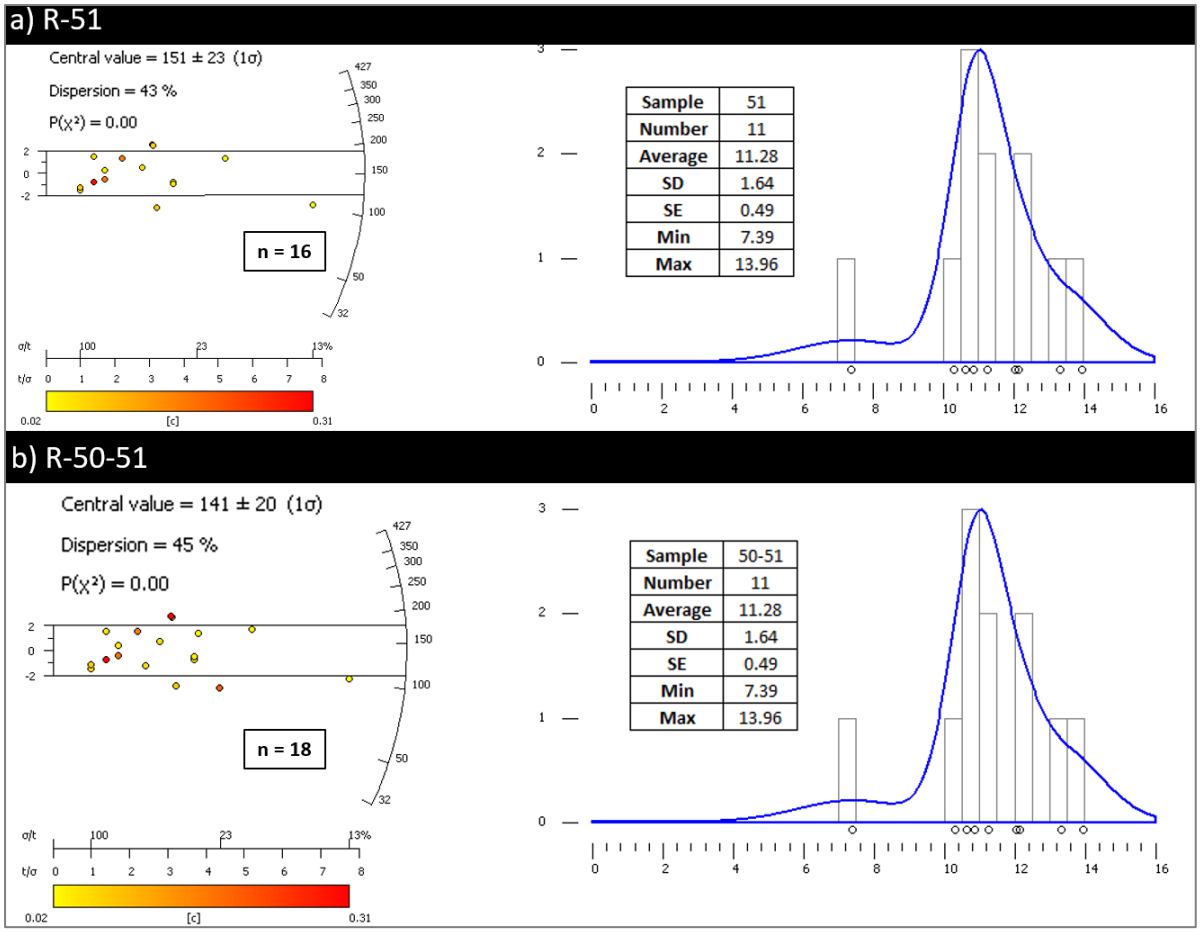

Figure 89: AFT results for a) sample R-51 and b) combined sample R-50-51.

5.6.5.2 Sample R-51 (Westphalian C? granite wash and in-situ Caledonian granite)

The AFT central age (151 Ma) is younger than the depositional age of the granite wash (older than c. 310 Ma), suggesting that the sample experienced temperatures greater than c. 120 °C after deposition. Despite the low number of track lengths, the apparent peak at 10.5 µm and low MTL of 11.28 µm suggest that the sample experienced a protracted cooling history through the PAZ (FIGURE 89A). Even though the sample comprises apatites from two lithologies with a different pre-Carboniferous thermal history (the *in-situ* basement and the Carboniferous wash above), the c. 150 Ma AFT age implies that any tracks inherited from these two different thermal histories were subsequently removed.

5.6.5.3 Combined sample R-50-51 (Westphalian C sands, granite wash and granite)

Since sample R-50 and R-51 are only c. 30 m apart in depth and have few AFT ages, it is possible to merge them as one combined sample to improve the size of the AFT age population (FIGURE 89B). This sample will be used for the thermal history modelling.

5.6.6 Thermal history modelling

5.6.6.1 Input data

The AFT ages and track lengths of sample R-68_detr (detrital grains only) and combined sample R50-51 are used for the thermal history inverse modelling.

5.6.6.2 Initial and final time-temperature constraints

There is no BHT data for this well. The gradient is defined as the average between two end-member gradients from two nearby wells: 26/28-1 with a gradient of c. 38°C.km^{-1} and 26/26-1 with a gradient of 28°C.km^{-1}, yielding an average gradient of 33°C.km^{-1}. Using this gradient, the two samples have present-day temperatures of 46.6°C (R-68_detr) and 56.7°C (R-50-51) (FIGURE 90).

a) Prior information and MCMC chain parameters

Categories		Values
Prior information	Time Temperature	174.04 ± 174.04 Ma 70 ± 70 °C
	Max dT/dt, Reheating Gradient/temp offset Offset	1000 °C.My, Yes 33 ± 33, 10.099 °C Constant
MCMC chain	Burn-in/Post-burn-in/Thinning	100,000 / 100,000/1
Proposed move	Time/Temp/Offset Resample/Reject, Reject complex	30/28/0.001 Resample, Yes

b) Scenario names and characteristics

Scenario	Samples	Constraints	Gradient	Max dt/dT	tT points
0a **0b**	Both	None	Constant	Default: 1000	Low (simple) High (complex)
1a **1b**	Both	VR	Constant	Default: 1000	Low (simple) High (complex)
2a **2b**	Both	5 constraints + VR	Constant	Default: 1000 20	Low (simple)
3	Both	5 constraints + VR	Variable	20	Low (simple)

c) Time-temperature constraints

Constraints	Time	Temperature
Initial R-50-51 Initial R-68	312.6 ± 2.6 Ma 162.8 ± 5.5 Ma	10 ± 10 °C 10 ± 10 °C
1	112.75 ± 12.25	15.70 ± 0.86
2	74.8 ± 8.8	17.74 ± 1.17
3	44.95 ± 11.05	18.76 ± 1.33
Final R-50-51 Final R-68	0 Ma	56.7 °C 46.6 °C

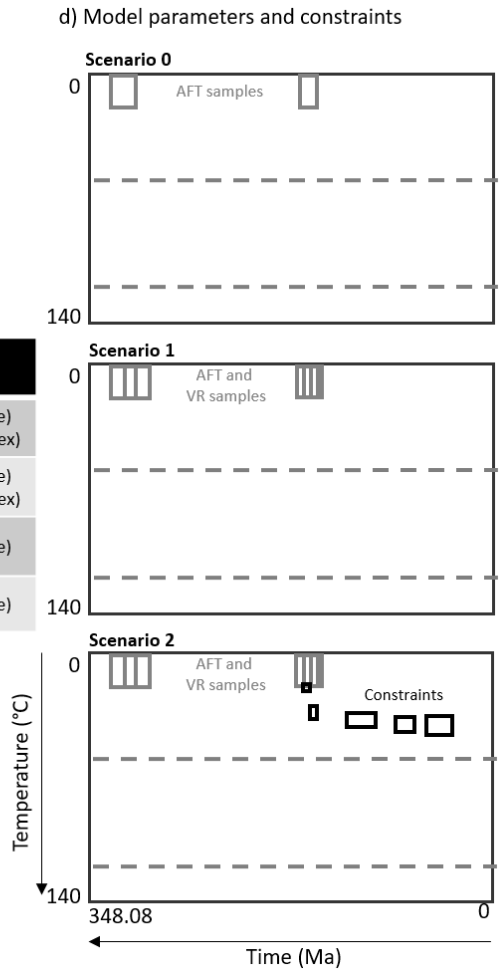

Figure 90: QTQt modelling parameters for borehole 26/30-1.

Sample R-68_detr is biostratigraphically dated as Bathonian to Early Oxfordian (King et al., 1982). Therefore, the deposition age for this sample is 162.8 ± 5.5 Ma (Bathonian-Oxfordian). Being a detrital sample, the temperature at time of emplacement is defined as 10 ± 10°C (Figure 90).

The AFT ages of sample R-50-51 are dominated by the detrital grains (13/17 non-Caledonian grains, 76%). Therefore, the depositional age of this combined sample can be approximated as Westphalian C, *i.e.* 312.6 ± 2.6 Ma. Being considered as a detrital sample, the temperature at the time of deposition is defined as 10 ± 10°C (FIGURE 90).

5.6.6.3 Intermediate constraints (from stratigraphy)

The shallowest VR (VR_0) sample is located at a depth range of 2342 ft (713.84 m). Above VR_0 there are three biostratigraphically dated units: Aptian-Albian (112.75 ± 12.25 Ma) at 1621-1930 ft (average depth of 1776 ft or 541 m), Campanian-Maastrichtian (74.8 ± 8.8 Ma) at 1523-1621 ft (average depth of 1572 ft or 479 m) and Eocene (44.95 ± 11.05 Ma) at 1420-1523 ft (average depth of 1472 ft or 449 m) (FIGURE 90).

At the time of deposition of these three units, the sample was located at a depth of respectively c. 172.7, 234.7 and 265.3 m. Using the geothermal gradient estimate (33 ± 5°C.km^{-1}), these paleodepths correspond to paleo-temperatures of 15.70 ± 0.86, 17.74 ± 1.17 and 18.76 ± 1.33 (FIGURE 90).

5.6.6.4 Modelling results

Stability of the log likelihood and log posterior chains

All the models yielded convergent log likelihood and posterior chains (*i.e.* no trend in post-burn-in models) (FIGURE 91).

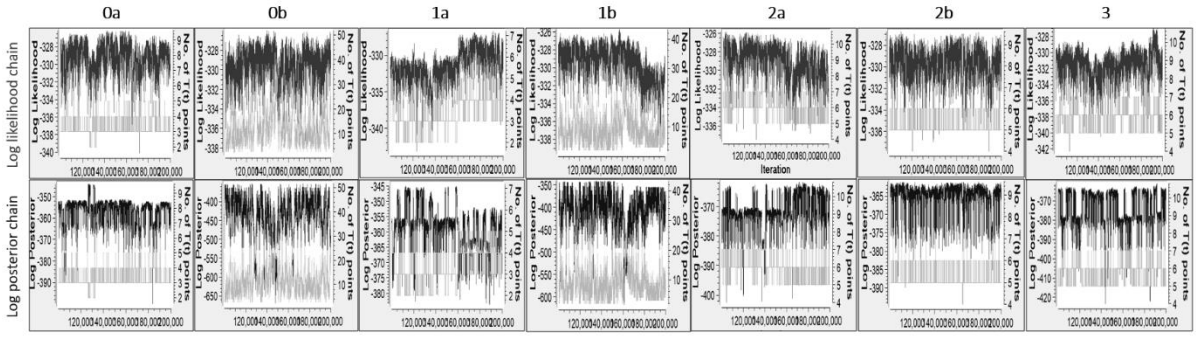

Figure 91: Log likelihood and log posterior chains for 26/30-1. All chains are stable.

Scenario 0: Two AFT samples, no constraints

This scenario is run to evaluate the thermal history information contained in the thermochronological data alone, without any intermediate constraints (FIGURE 90).

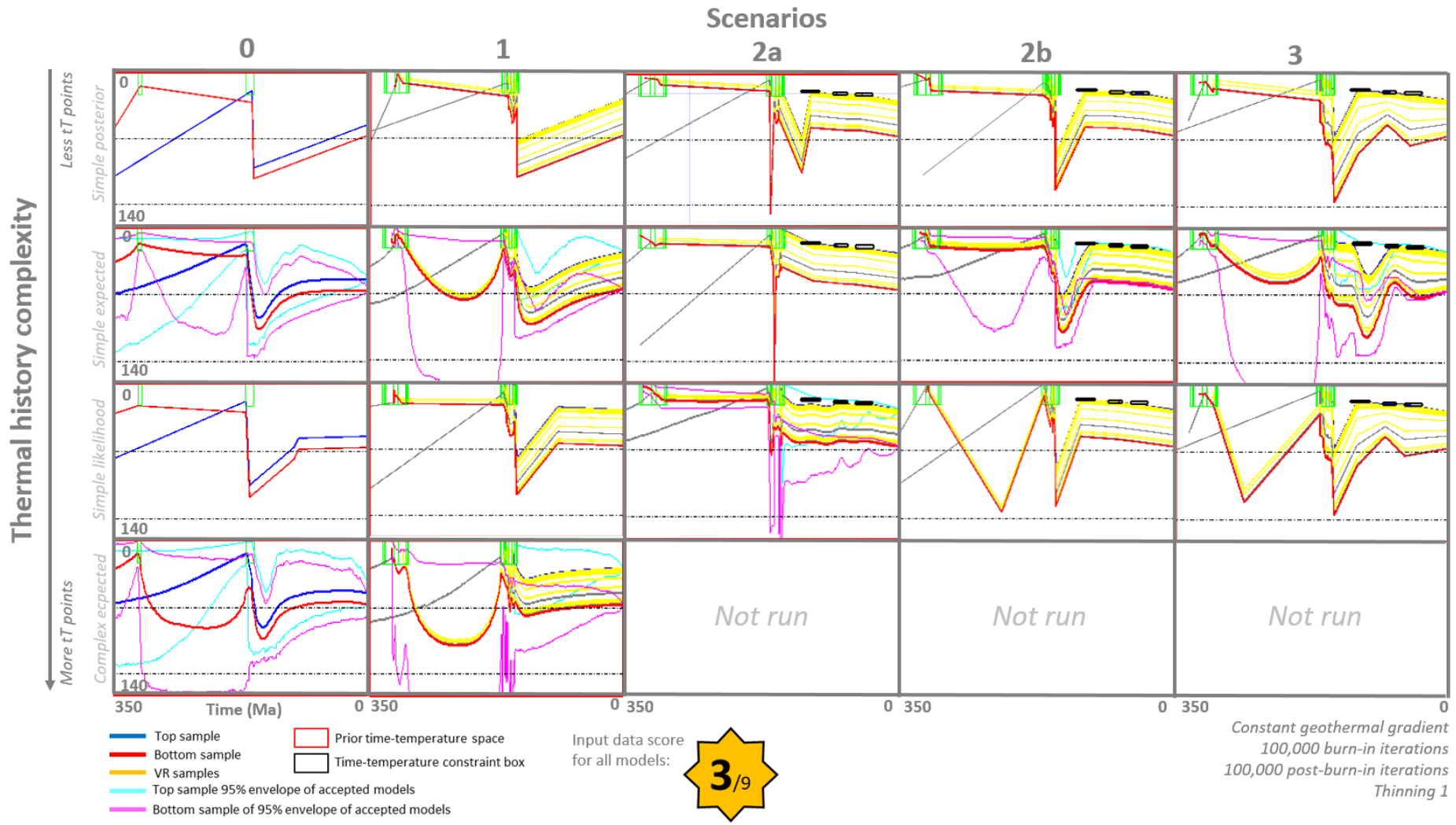

Figure 92: Results of the thermal history inverse modelling for borehole 26/30-1.

The complex expected model demonstrates that the thermal history in unconstrained before the deposition of sample R-68 (Bathonian-Oxfordian). All models show a very rapid heating of the samples from surface temperatures during the Bathonian-Oxfordian to c. 100°C within a few millions of years. This heating is followed by either 1) monotonic cooling to present-day temperatures (simple posterior model) or 2) rapid cooling to c. 60°C until 80-100 Ma (Cenomanian-Santonian) followed by a few degrees of cooling to present-day temperatures during the last 80-100 Ma (FIGURE 92 AND ANNEX 2) The match between the measured and modelled AFT and AHe data is good.

However, the modelled track length distribution shows a weak bimodality which does not exist in the projected measured track length distribution (but does exist in the non-projected track length distribution) (FIGURE 92 AND ANNEXES 2).

Scenario 1: Two AFT samples and VR samples

This scenario is run to evaluate the thermochronological information contained in the AFT and VR samples together (FIGURE 90).

The simple model yields the same results as the models of the previous scenario and the predicted VR values match perfectly the measured values. The complex posterior model shows constant temperatures < 60°C from the Carboniferous until the present-day with the exception of a very rapid heating and cooling spike at c. 155 Ma to temperatures > 120°C. This scenario also yields modelled AFT ages, VR values and track lengths which are in good agreement with the measured values. The complex likelihood model shows a different thermal history than the simple models for the segment older than 160 Ma. In this scenario, the bottom sample experiences high temperatures (>120°C) until c. 180 Ma, followed by a rapid cooling to surface temperatures between c. 180-160 Ma. Although this scenario yields matching AFT ages and track lengths, the modelled VR values of the Carboniferous samples are much higher than the measured ones. Therefore this thermal history is not plausible (FIGURE 92 AND ANNEX 2).

Scenario 2: Two AFT samples, VR samples and 5 time-temperature constraints

This scenario has the same input data as scenario 1 but with the five time-temperature constraints derived from the borehole stratigraphy.

The models for this scenario are characterized by a heating/cooling spike at c. 160 Ma. In addition to this spike, the likelihood model shows a heating episode to c. 90°C during the Late Jurassic, followed by cooling during the Early Cretaceous, while the posterior model shows a monotonic slow heating from the Jurassic until the present-day. The match between modelled and measured data is good, in particular for the track length distribution which is closer to the measured track length than in scenarios 0 and 1 (FIGURE 92 AND ANNEX 2).

The heating spike during the Middle-Late Jurassic cannot be explained by burial and erosion. It could either be a thermal event associated with the synchronous magmatism or else might not be associated with any real geological event.

A second scenario (scenario 2b) was run with a maximum cooling/heating rate (dt/dT) of 20°C.Ma^{-1} instead of the default value of 1000°C.Ma^{-1} (FIGURE 90). This allows testing if good models can be found without spikes such as the one described just above. As expected, the resulting models do not show any spikes. The models show thermal histories very similar to scenario 0 and 1 and the match between modelled and measured data is very good (FIGURE 92 AND ANNEX 2).

Scenario 3: Same as scenario 2 with variable geothermal gradient

This scenario aims at testing the possibility that there was significant different paleogeothermal gradients due to rifting during the Mesozoic or regional magmatism (during the Early Cretaceous and Paleogene). This is done by allowing the algorithm to modify the geothermal gradient (and therefore the temperature offset between samples) at any point during the thermal history ('Change offset' option is ticked and the offset parameter is set to 10). For this model, the maximum cooling/heating rate is also set as 20°C.Ma^{-1} to avoid heating/cooling spikes (FIGURE 90).

The models are very similar to scenario 0 and 1 with a rapid heating during the Late Jurassic and cooling from the Aptian-Albian to the present-day (for the shallowest samples). However, the deeper samples show more variations in temperatures with a prolonged period of cooling until the Campanian and another cooling period since the Eocene (FIGURE 92 AND ANNEX 2).

When looking at the entire population of models, the geothermal gradient is characterized by a four-phased history: 1) 160-110 Ma: High geothermal gradient (GG) averaging c. 55°C.km^{-1}; 2) 110-75 Ma: Decrease in the GG to c. 30°C.km^{-1}; 3) 75-45 Ma: Increase in the GG to c. 40-45°C.km^{-1}; 4)45-0 Ma: Decrease in the GG to c. 30°C.km^{-1}

This history of the GG potentially points toward a higher geothermal gradient during the Late Jurassic-Early Cretaceous and during the Eocene.

5.6.7 Discussions

5.6.7.1 Thermal history

Most models (see compilation in FIGURE 92), with or without intermediate time-temperature constraints, yield a similar thermal history characterized by: 1) *Rapid heating during the Middle-Late Jurassic*: This rapid heating is synchronous with the main period of rifting in the Porcupine Basin and therefore probably reflects syn-rift subsidence and burial, possibly accentuated by a higher geothermal gradient associated with the rifting and a magmatic pulse associated with the c. 160 Ma

effusive volcanism detected in the Bathonian-Early Oxfordian sediments; 2) *Rapid cooling during the Early Cretaceous (Berriasian-Barremian)*: This rapid cooling of all samples is interpreted as caused by uplift and erosion; 3) *Small monotonic heating from the Aptian until now*: This heating is interpreted as being caused by burial due to post-rift thermal subsidence.

The models that are believed to represent the truest thermal history are the simple posterior models of scenario 2b and 3 (FIGURE 92) since they include all possible input data (AFT, VR) and stratigraphic constraints, yield matching modelled and measured data and are not implausible based on the known regional geology.

5.6.7.2 Exhumation estimates

Using the assumed present-day geothermal gradient (33°C.km^{-1}), the Early Cretaceous cooling of c. 60°C would correspond to erosion of c. 2 km of sediments (ignoring compaction effects for the sake of simplification). Using a higher geothermal gradient of c. 55°C.km^{-1} (from results of scenario 3 modelling), the cooling would then be caused by the erosion of only 1.1 km of sediments.

The sonic velocities of the Jurassic and Carboniferous sediments indicate that they have been buried under a maximum of c. 1.1 km of material (otherwise they would have higher sonic velocities due to compaction). Therefore, it is likely that the geothermal gradient during the Early Cretaceous was close to c. 55°C.km^{-1} (rather than 33°C.km^{-1}). This elevated gradient is in accordance with a delayed thermal effect of the main phase of rifting as proposed by Calvès et al. (2012).

In conclusion, the Base Cretaceous Unconformity in borehole 26/30-1 is associated with the erosion of c. 1000 m of Latest Jurassic-Earliest Cretaceous sediments during the Berriasian-Barremian during a period of elevated geothermal gradient (c. 50-60°C.km^{-1}) caused by the delayed thermal effect of the main phase of rifting (Late Jurassic) in the Porcupine Basin.

5.6.7.3 Comparison with thermal histories from onshore West of Ireland

Cogné et al. (2014) derived several thermal histories from vertical profiles in the west of Ireland. The closest vertical profiles to 26/30-1 are Mweelrea in South Mayo and M^{t} Brandon in the Dingle Peninsula, Co. Kerry (both are c. 160 km away from 26/30-1, FIGURE 93).

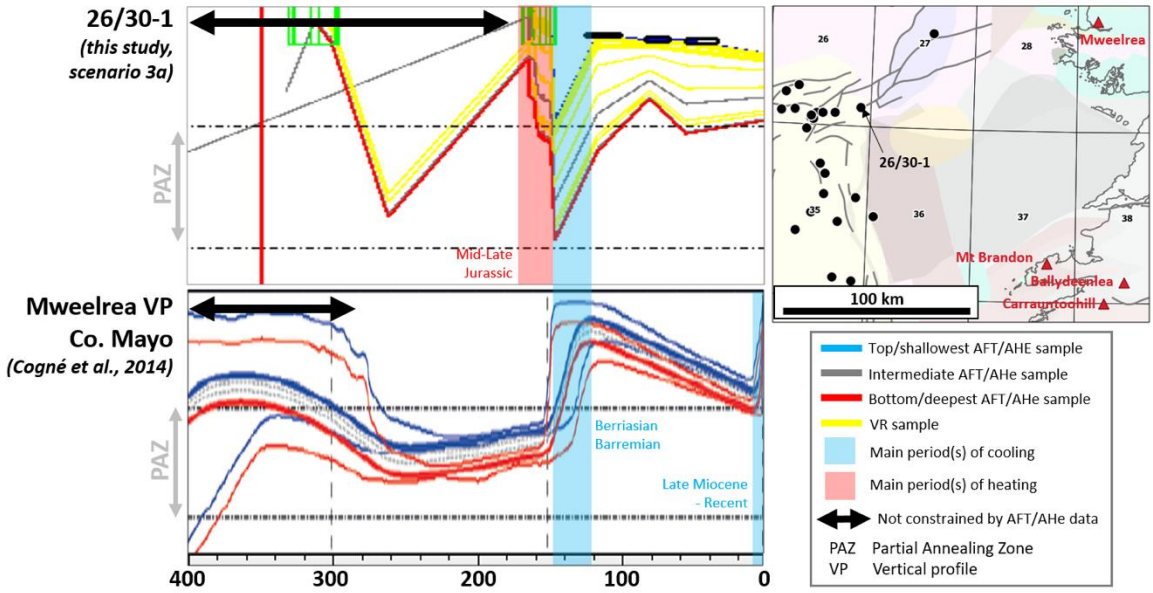

Figure 93: Comparison of thermal histories of borehole 26/30-1 and onshore Mweelrea vertical profile

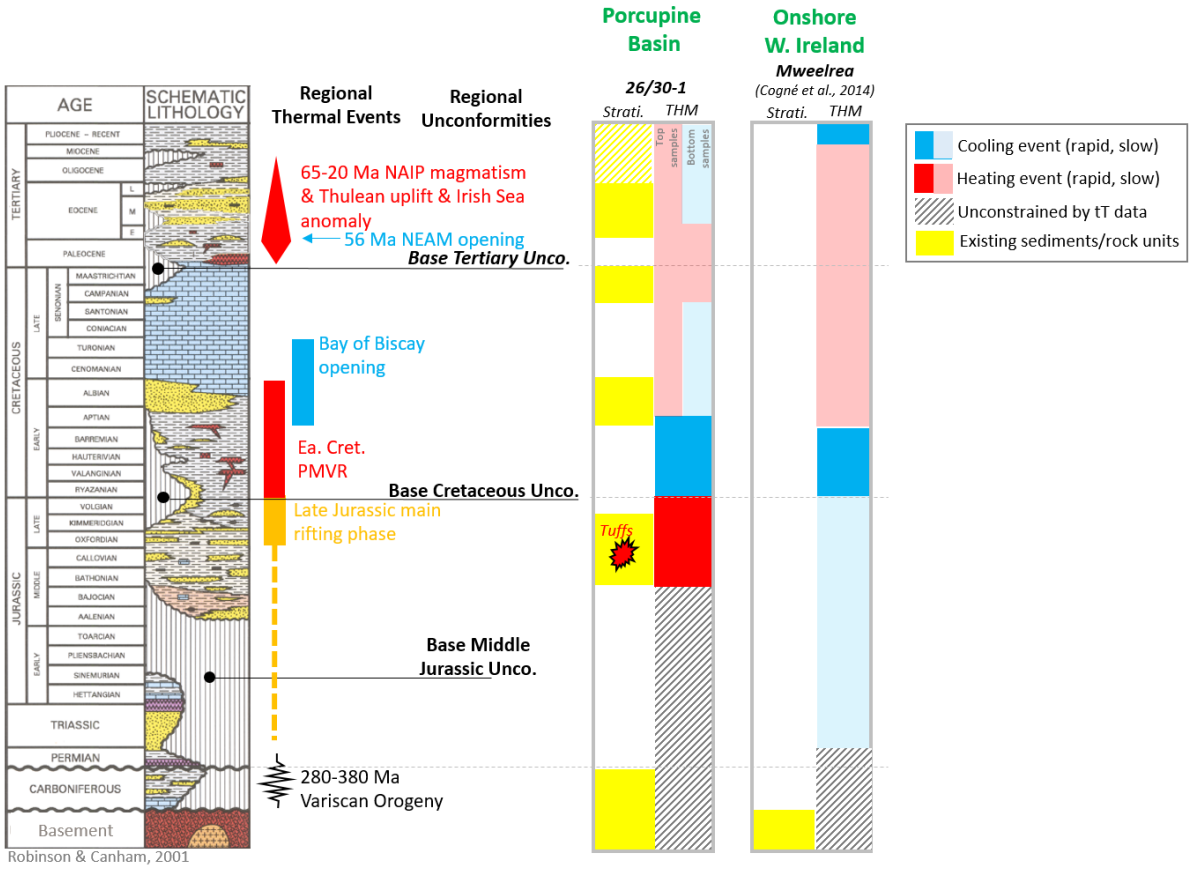

Figure 94: Summary of the thermal histories derived from thermochronological data from borehole 26/30-1 and the Mweelrea vertical profile (Cogné et al., 2014).

Both the Mweelrea and Mt Brandon profiles yield an identical rapid cooling event between 120 and 145 with a similar magnitude of c. 60°C, as in 26/30-1 (FIGURE 93 AND FIGURE 94). This suggests that the entire offshore platform between 26/30-1 and the west coast of Ireland was probably uplifted and eroded during this exhumation event.

5.6.8 Conclusions

5.6.8.1 Geochronology

- Discovery of a population of igneous apatite grains in the Bathonian-Oxfordian sands. The apatites are dated at 159.8 ± 3.1 Ma (Oxfordian) with a trace element signature suggesting they are igneous grains from a primitive mafic or ultramafic magma. The grains are interpreted as belonging to a previously unrecognized tuff in the Jurassic sands.
- The basal granite is probably Caledonian in age. However, the small size of the sample and the presence of detrital grains from the granite wash prevents further analysis.

5.6.8.2 Thermochronology

- Rapid heating during the Middle-Late Jurassic, synchronous with the main period of rifting in the Porcupine Basin therefore probably reflects syn-rift subsidence and burial, possibly accentuated by a higher geothermal gradient associated with rifting and a magmatic pulse associated with the c. 160 Ma effusive volcanism detected in the Bathonian-Early Oxfordian sediments.
- Rapid cooling during the Early Cretaceous (Berriasian-Barremian) probably caused by uplift and erosion.
- The Berriasian-Barremian cooling event is identical to the one observed on the west coast of Ireland at Mweelrea (Co. Maro) and Mt Brandon (Co. Kerry), suggesting that the entire offshore platform between 26/30-1 and the west coast of Ireland was uplifted and eroded at that time.
- A small amount of monotonic heating from the Aptian to the present day was probably caused by burial due to post-rift thermal subsidence.

5.7 Borehole 35/13-1

5.7.1 Exploration and geological summary

35/13-1 is a dry exploration borehole drilled in 1977 by Shell in the centre of the Porcupine Basin (FIGURE 33) to a final depth of 4405 mMD in 482.5 m of water. After drilling though c. 400 m of undetermined sediments, the well encountered almost 2km of Paleocene to Early Miocene clastics, resting on 465 m of Coniacian to Danian chalk and limestone. Below the chalk, the well encountered 1

km of Early Albian to Middle Cenomanian clastics intruded by three doleritic intrusions (155, 33 and 31 m thick) (Sussli and Hoogkmaer, 1977).

5.7.2 Nature and age of the igneous intrusions

The dolerite sills are tholeiitic and the rock-forming minerals are plagioclase (labradorite-bytownite, 40-50%), ophitic augite (30-40%) and altered olivine, amphibole, biotite and ilmenite (10-20%). K-Ar dating of the rocks yielded a minimum age of 25.8 ± 2.6 Ma (Late Oligocene) but the lack of extensive mineral alteration leading to potential argon loss led the authors to conclude that the true crystallisation age should not be much older than 25.8 Ma (Seemann et al., 1977).

5.7.3 Samples

5.7.3.1 Sampling strategy and results

The primary sampling target was the mafic intrusions (sample R-54, 3826-3981 mMD; sample R-55, 4023-4056 mMD). Sample R-54 yielded numerous apatites (100+ resulting in 40 AFT ages and 100 U/Pb ages) but no zircons. Sample R-55 unexpectedly yielded only one apatite and no zircons.

5.7.3.2 U/Pb, trace element and AFT results

The detailed description of the U/Pb and trace element results is presented in ANNEX 1 (SECTION 1.3.4 AND SECTION 2.3.4). Below is a summary and discussion of the results.

After elimination of grains with very large age errors (grey ellipses in FIGURE 95A), the sample yielded a weighted average ^{207}Pb-corrected U/Pb age of 61.6 ± 5.6 Ma (Danian-Selandian boundary), while the anchored discordia yielded a lower intercept age of 69.9 ± 4.8 Ma (latest Cretaceous-earliest Paleocene) (FIGURE 95A). The trace elements are in accordance with the mafic nature of the dolerite (they plot at the extremity of the mafic field (IM), which overlaps with the high-grade metamorphic field (HM, FIGURE 95B). The AFT central age is 66.8 ± 8.6 Ma but no confined track length was found due to low uranium content in the grains (average of 1.7 ppm) (FIGURE 40).

5.7.3.3 Discussion

Accounting for the U/Pb age uncertainty and predominance of Paleogene magmatic activity associated with the NAIP (rather than Late Cretaceous activity, which is rare, Wilkinson et al. (2017a)), the data indicates that the dolerite intrusion is Paleocene in age and not Late Cretaceous. The Paleocene age contradicts the legacy K-Ar Late Oligocene age which must have resulted from higher argon loss than expected by the analysts. Post-emplacement argon leakage is a phenomenon that has long been recognized as affecting most K-Ar dating of Irish Tertiary igneous rocks (Mitchell and Mohr, 1986).

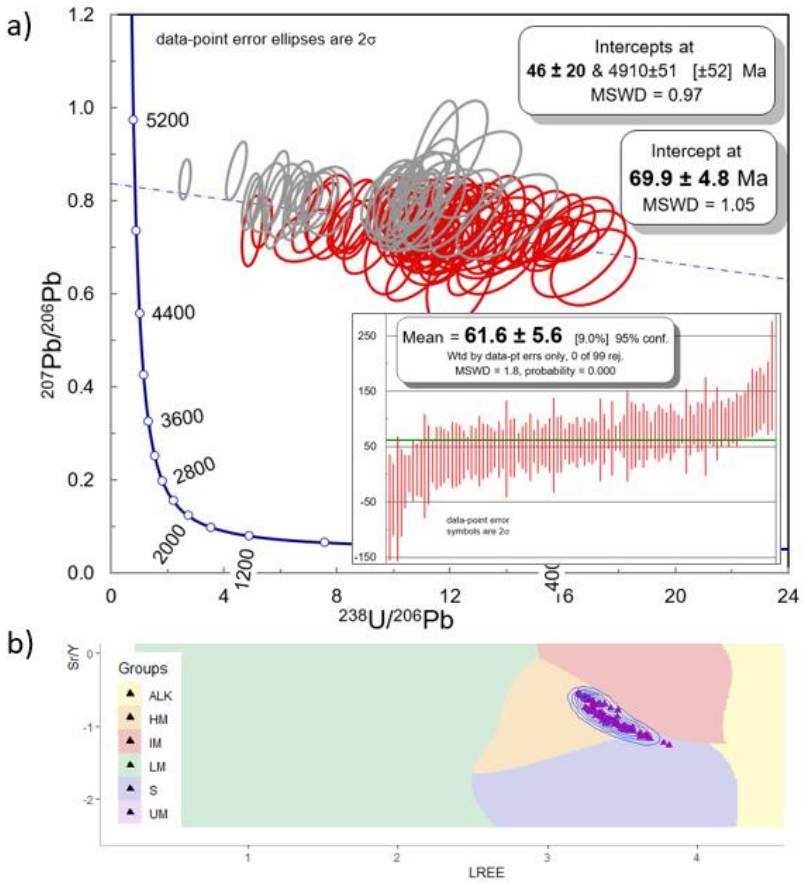

Figure 95: Apatite U/Pb and trace element results for sample R-54 (35/13-1).

The AFT age, which is identical to the crystallisation age (within error) indicates that the age has not been reset since emplacement during the Paleocene and that the present-day burial and temperature (109°C with a geothermal gradient of 29.2°C.km^{-1} based on 5 BHTs) is probably the maximum burial and temperature experienced by the sample. The AFT dataset for this borehole has not been modelled due to the young age of the intrusions (preventing any insights into the pre-Paleocene thermal history) and lack of AHe ages (limiting the detection of small-scale heating and cooling events during the Cenozoic.

5.8 Borehole 35/15-1

5.8.1 Exploration summary and geological summary

Borehole 35/15-1 is a dry hydrocarbon exploration well drilled in 1980 by Phillips to a final depth of 12,100 ft MD (3688 m). The well is located on the eastern margin of the Porcupine Basin, very close to one of the major N-S trending basin-bounding faults, in the hanging wall succession (FIGURE 33). It encountered a succession of Tertiary, Upper Cretaceous, Lower Cretaceous and Lower Carboniferous (to possibly Devonian) sediments.

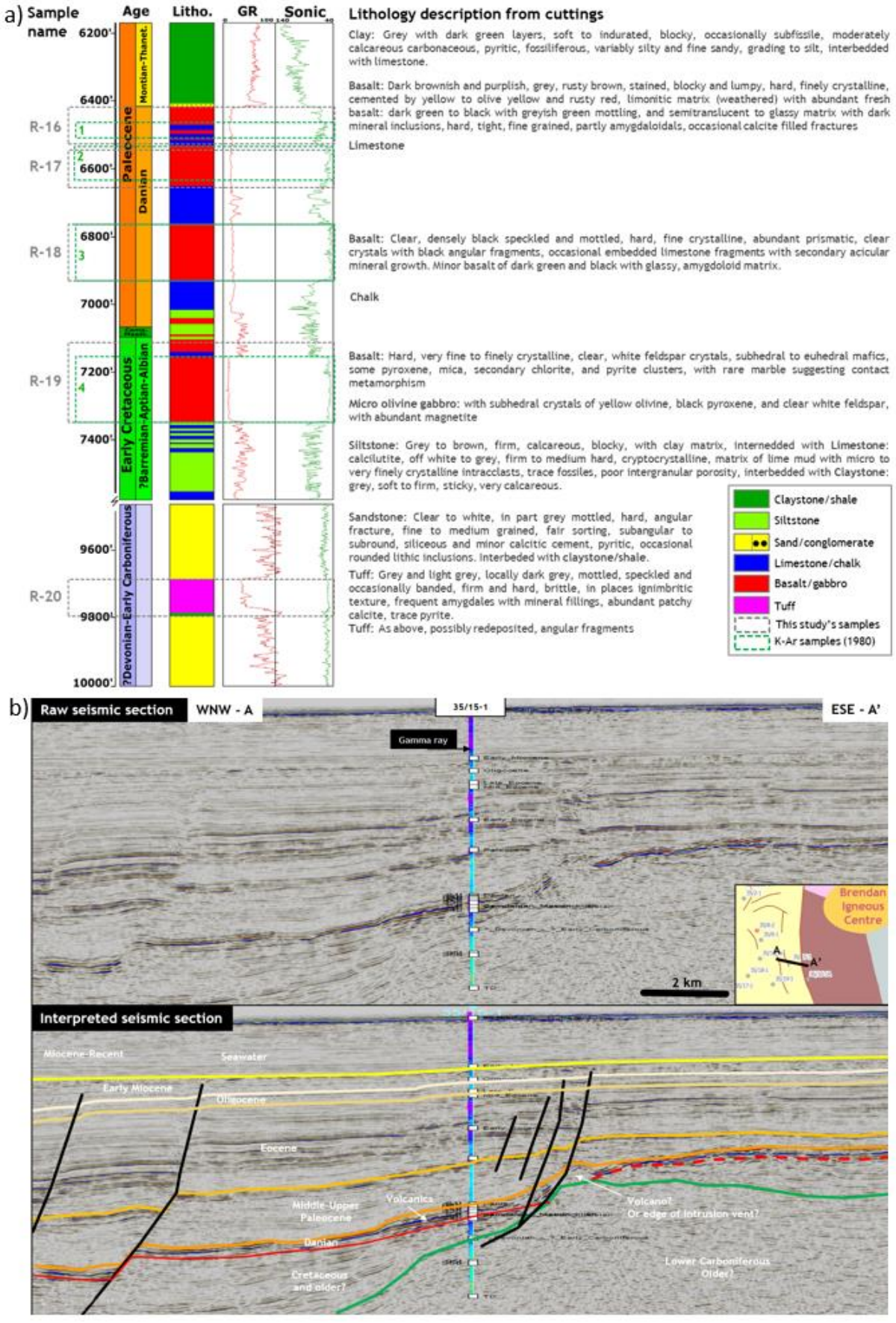

Figure 96: Borehole 35/15-1. a) Sample depths, age, log response, and lithology from composite log (Gerneck et al., 1980), b) raw and interpreted seismic section.

Several igneous units (basalts and micro-gabbro according to the composite log, Gerneck et al. (1980)) are present in the Danian, Upper and Lower Cretaceous sediments while a tuffaceous sand is present in the Paleozoic sediments (FIGURE 96A). Based on biostratigraphic interpretation and K-Ar dating undertaken by the operator, the basaltic lava flow and sills between 6400 and 7400 ft MD are either Late Danian or Thanetian in age and therefore are part of the early phase (pre-break-up) of magmatism of the North-East Atlantic Igneous Province (Wilkinson et al., 2017b). The magma was derived from the mantle (linked to the proto-Icelandic plume) and was emplaced in the Paleocene as a very hot and fluid magma on top of the paleo-seafloor (lava flow) as well as thin intrusions just underneath the seabed. The magma was probably emplaced as a single event or within a very short period of time and cooled very quickly, except for some slower-cooled flow cores and/or shallow intrusions (see a detailed discussion of the data underlying these conclusions in ANNEX 1 SECTION 4.

Samples

5.8.1.1 Sampling strategy

This well was targeted for its numerous igneous intrusions. Four samples were taken from cuttings at 6420-6520 ft (sample R-16, a basalt according to the composite log), 6540-6650 ft (R-17, basalt), 6760-6930 ft (R-18, basalt) and 7100-7350 ft (R-19, micro-gabbro) (FIGURE 96). An additional sample was taken at 9690-9800' in what was described in the composite log as a Lower Carboniferous grey tuff (R-20) (FIGURE 96). The aim of the sampling was to separate euhedral apatites from the volcanic units to obtain high quality AFT and AHe ages to constrain small exhumation events from the Carboniferous to the present day. This is the first thermochronological study undertaken for this borehole, so no legacy sample is available.

5.8.1.2 Apatite and zircon yield

Apatite and zircon yield

Sample R-16 yielded few apatites which were too small for AHe studies (probably because they come from a basalt) and yielding only four AFT ages were obtained for this sample and no AHe ages. Samples R-17 and R-18 yielded a good amount of large euhedral apatites. Five apatites were packed for AHe studies. After counting, polishin and laser ablation losses, only nine AFT ages could be measured for sample R-18. Sample R-19 was expected to have the best yield of large euhedral apatites since it was described as a micro-gabbro in the composite log (*i.e.* a larger grain size than the overlying units) and was the sample with the largest amount of cuttings (2916 g). However, this sample had only few apatites of poor quality and small in size. After counting and laser ablation losses, only three AFT ages were obtained. No apatites were found in the Lower Carboniferous tuff sample R-20. The lack of AFT

data for the bottom sample prevents the determination of the thermal history below the igneous units of sample R-16 to R-19 (the pre-Paleocene history).

Numerous zircons were picked from samples R-16, R-17 and R-18 (respectively, 180, 32, 80), but only two zircons were found in sample R-19.

5.8.2 Zircon and apatite U/Pb and trace elements results

The detailed description of the U/Pb and trace element results is presented in ANNEX 1 (SECTION 1.3.5). Below is a summary and discussion of the results.

5.8.2.1 Discussion

The majority of apatites (14/17) yielded Paleocene 207-corrected $^{238}U/^{206}Pb$ ages. A discordia age through these grains yield an age of 66 ± 7.5 Ma (FIGURE 97A) which supports the Paleocene dating of the operator but does not allow a refinement of this dating, Most of the Paleocene apatites plot in the UM field of the trace element biplot suggesting it is derived from a juvenile, relatively primitive mantle derived melt, while one grain plots at the outer edge of the IM field (similar to the apatites from the 35/13-1 dolerite).

The presence of numerous detrital zircons in the top three samples and of detrital apatites (older than Paleocene) in the top sample (FIGURE 97A AND B) suggest some amount of contamination by clastic beds. There is no sand within the sampled interval, however the lithology column of the composite log shows a conglomerate symbol for a thin three foot-thick unit just above the topmost lava flow (Gerneck et al., 1980). Although not described in the mud or composite log, this bed is the most likely source of the detrital grains of samples R-15-19.

Paleocene zircons

Thirteen Paleocene zircons were discovered in the samples that yielded a concordant age of 60.5 ± 0.6 Ma (FIGURE 97B). Zircons are not commonly found in basalts due to the low concentration of Zr in the igneous source (mantle) and the higher Zr saturation of mafic magmas compared to felsic ones (Shao et al., 2019). While zircon formation is possible in the late stage of crystallisation of a mafic pluton due to slow cooling, it is much less likely to occur in hyperabyssal (*i.e.* emplacement depth <2km) and extrusive rocks (Shao et al., 2019) such as the ones in borehole 35/15-1. No zircon has been described in the operator mineralogical study (Henderson, 1980). A trace element analysis by X-ray fluorescence was carried by the well operator on three samples and yielded low Zr concentration between 69 and 101 ppm, which is similar to typical MORB Zr concentrations of 73-74 ppm (Sun and McDonough, 1989). It is therefore unlikely that the zircons crystallized during the cooling of the mafic magma near the seabed.

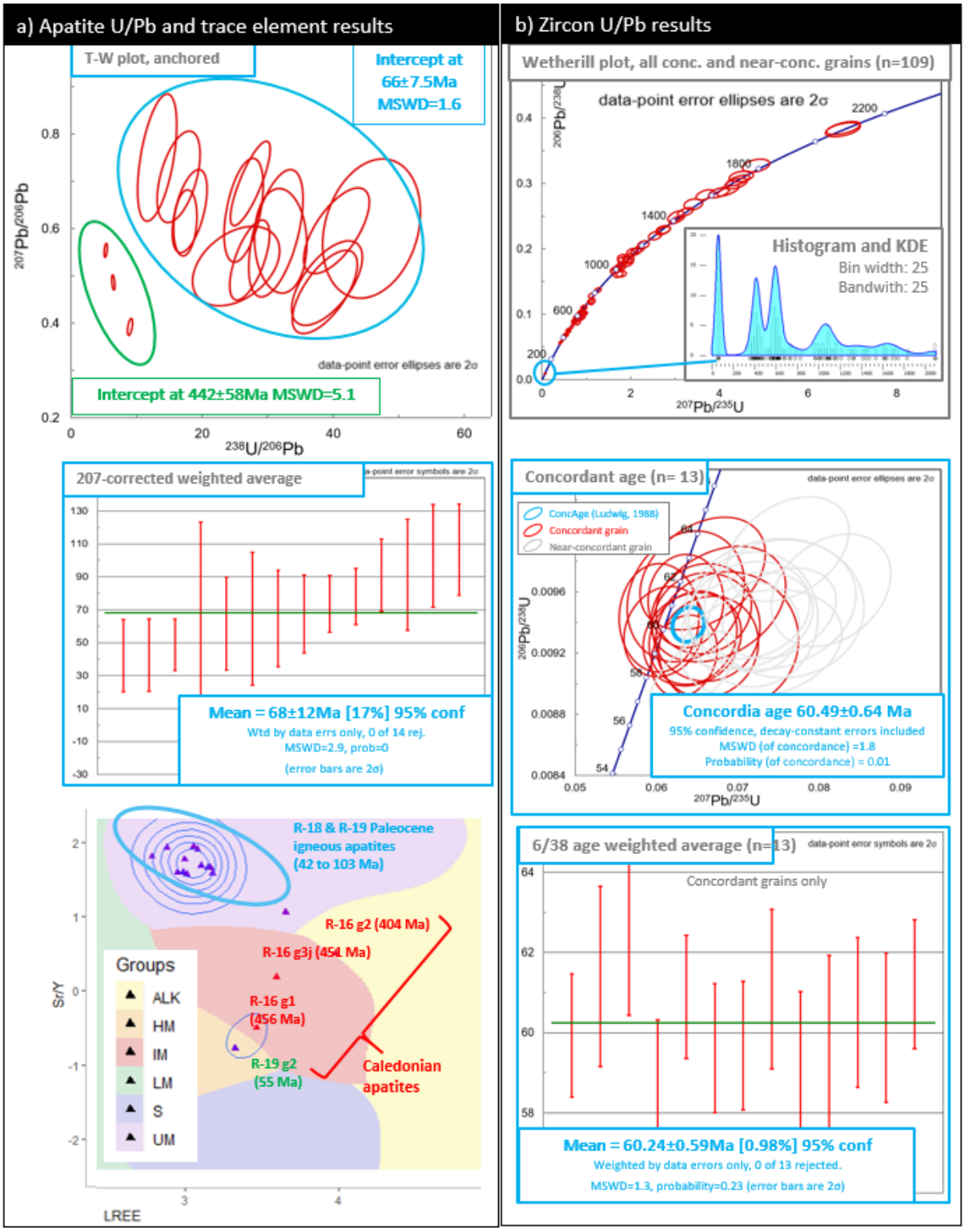

Figure 97: Zircon and apatite U/Pb ages and trace element results for combined sample R-16, R-18, R-19 (35/15-1).

However, crystallized zircons might have been transported with the magma from a deeper plutonic source as xenocrysts. Alternatively, the zircons might come from a volcanoclastic bed such as the inferred thin conglomerated just above the lava flow. The decreasing amount of Paleocene zircons

from the shallowest to deepest samples (R-16 = 14, R-17 = 3, R-18 = 3, R-19 = 0) supports the latter hypothesis.

Although not commonly dated, Paleocene zircons have been reported in various places of the British Tertiary Igneous Province (Wilkinson et al., 2017b) (TABLE 18). Hamilton et al. (1998) found 60.53 Ma zircons in an alkaline pegmatite from the Central Complex on Rum and 58.91 Ma zircons from a gabbro pegmatite of the Cuillin complex on Skye. Chambers et al. (2005) found 61.15 Ma zircons in the Muck tuff on the Isle of Muck. Finally, Ganerød et al. (2011) reported 61.32 Ma zircons from the Tardree rhyolite in Antrim. It is worthwhile to note that all the BIPIP zircon ages fall within a narrow range of 58.51-61.32 Ma (or basal Thanetian to Selandian) (TABLE 18). None of the few dated zircons in the BIPIP come from basalts.

Table 18: Paleocene zircons from the BIPIP.

Location	Lithology	Age	Reference
Skye, Cuillin complex	Gabbro pegmatite	58.91 Ma	Hamilton et al., 1998
Porcupine Basin	Basalt?	60.35 Ma	This study
Rum, Central Complex	Alkaline pegmatite	60.53 Ma	Hamilton et al., 1998
Muck Island	Tuffs	61.15 Ma	*Chambers et al., 2005*
Antrim, Tardree	Rhyolite	61.32 Ma	Ganerød et al., 2011

The mafic and shallow nature of the volcanism in borehole 35/15-1 is difficult to reconcile with the presence and depth distribution of detrital and Paleocene zircons and the depth distribution and geochemical signatures of apatites. The Paleocene zircon are therefore likely sourced from a Selandian (c. 60 Ma) tuffaceous microconglomerate that recorded a secondary phase of magmatism after the first phase of intrusive and extrusive mafic magmatism. Some of the Paleocene apatites might also come from this unit. The source of the tuff or eroded volcanic materials could be the nearby Brendan Igneous Centre (c. 40 km to the NW, FIGURE 33).

Age of magmatism

Due to uncertainties on the source rock of both the apatites and zircons and the large age uncertainty, the U/Pb data does not allow a refinement of the dating of the mafic volcanism in 35/15-1. The most conservative conclusion that can be derived is that it does not contradict its Paleocene age (FIGURE 98).

a)

Method	Event dated	Age estimates	Source
Stratigraphy	Mafic	Min/max 56-66 Ma Likely ~59-62 Ma Best ~62 Ma	Composite log Biostratigraphic report
K-Ar	Mafic and other? (+ host rock?)	Range 46-58.1 Ma Best 58.1 ± 1.8 Ma (possibly older)	Church et al., 1981
Apatite U/Pb	Mafic and other?	Free 62 ± 18 Ma Anchored 66 ± 7.5 Ma	This study
Zircon U/Pb	Mafic? Other?	ConcAge 60.37 ± 0.79 Ma	This study

b)

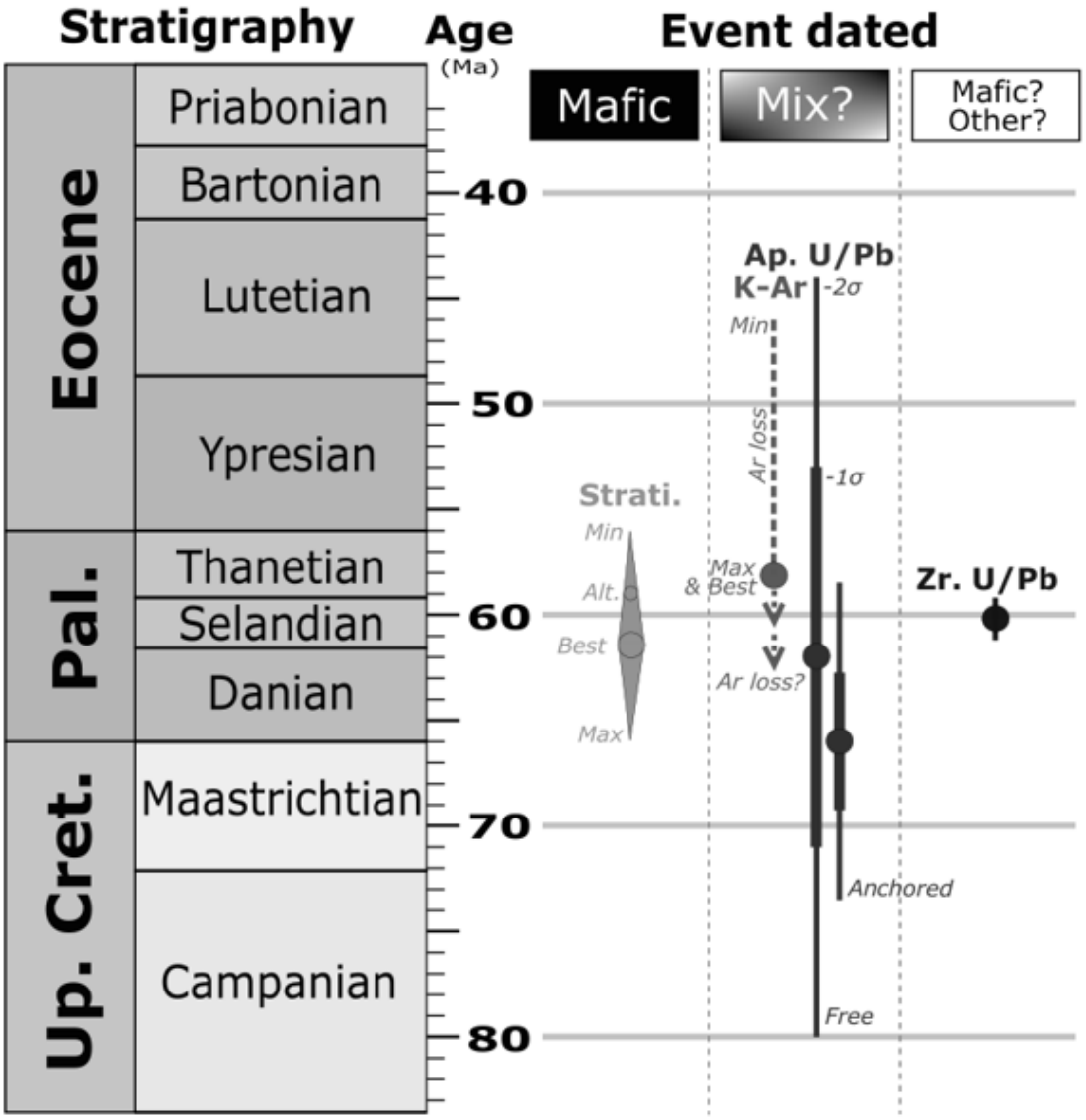

Figure 98: Summary of the various estimates of the age mafic igneous activity in borehole 35/15-1.

Based on stratigraphic data from the composite log, it is most likely upper Danian in age (c. 62 Ma), but a younger Selandian or basal Thanetian age cannot be excluded based on information from the biostratigraphic report (FIGURE 98).

The igneous zircons yield a precise age of 60.49 ± 0.64 Ma. However, due to uncertainties about their origin, it is not possible to assign that age to a particular event. It could either date the mafic volcanism itself (if we assume that the time between crystallisation in the deeper mafic pluton and being carried away to the surface is short, *i.e.* <1 Ma) or could date another volcanic event in the vicinity of the well (e.g. ash fall from a nearby volcanic centre such as the Brendan Centre) (FIGURE 98).

5.8.3 AFT and AHe Results

Table 19: Borehole 35/15-1 AFT results.

Sample	Depth	Seabed	Grains	Ns	Area	U/Ca*Ω	U/Ca	P(χ2)	Central Age	±1σ	Tracks	MTL	SD	SE
	m BSB	*m MSL*	n		*cm2*				*Ma*	*Ma*		*µm*	*µm*	*µm*
R-16	1632.2	310.9	4	75	7.06E-05	6.37E-06	9.03E-02	<0.01	115	36	6	11.54	0.55	0.22
R-17	1670.3	310.9	0	-	-	-		-	-	-	-	-	-	-
R-18	1746.5	310.9	9	33	2.60E-04	4.46E-06	1.72E-02	0.88	76	13	1	13.33	-	-
R-19	1862.3	310.9	3	11	1.07E-04	1.31E-06	1.22E-02	0.99	81	25	0	-	-	-
R-20	2630.4	310.9	0	-	-	-	-	-	-	-	-	-	-	-
R-16-19	1759	310.9	13	48	3.87E-04	6.15E-06	1.59E-02	0.98	79	11	N/A	N/A	N/A	N/A

The detailed description of the AFT results of sample R-68, 50 and 51 is presented in ANNEX 1 SECTION 2.3.5 together with a qualitative interpretation. Below is a summary and discussion of the results (TABLE 19, FIGURE 99, FIGURE 100).

5.8.3.1 AFT data discussion

The FT age (79 Ma) is 27% older than the crystallization age (c. 62 Ma), which is the theoretical maximum FT age for these igneous grains. This discrepancy is however explained by the small number of grains and their low concentration in uranium (c. 3.5 ppm). The low concentration of uranium and young ages led to a low number of spontaneous fission (N_s is only 48 for 13 grains), which explains the large uncertainty on the ages (on average ± 55% for each grain). There is no apparent correlation between AFT age and chlorine content for this sample (FIGURE 100B). The uranium content seems to be uniform with a range from 2.9 to 4.1 ppm and an average of 3.5 ppm (FIGURE 100C). The Dpar and chlorine values are quite uniform as well and no significant difference in annealing behaviour should be expected between the grains.

The older AFT age implies that the true AFT age is probably close to the crystallisation age and that the samples did not experience significant annealing and must have resided above the partial annealing

Sample	Grain	Shape in GFTC		Length	Diameter		S/V	R_{eq}*	Weight	Temp.	[^{238}U]	[^{232}Th]	[^{147}Sm]	eU	Th/U weight	[He]	Degassing	Raw Age	Error	F_T
		Geometry	GFT*	W	Max	Min														
				µm	µm	µm		µm	g	°C	ppm	ppm	ppm	ppm		nmol/g		Ma	Ma	
R-17	4	Hexagonal prism	2F	166	87	77	0.065	46.2	2.64E-06	68	1	3	4	2	3.2	0.2	Lack of heat	16	2	0.699
	2	Hexagonal prism	2F	235	94	83	0.057	52.2	4.36E-06	68	0	2	4	1	3.6	0.1	Ok	26	4	0.73
	3	Hexagonal prism	2F	227	84	71	0.064	46.6	3.26E-06	68	1	3	2	1	3.7	0.2	Ok	27	4	0.699
	1	Hexagonal prism	2F	329	86	75	0.060	50.1	5.04E-06	68	1	2	2	1	2.5	0.2	Small leak	33	5	0.718
	5	Hexagonal prism	2F	320	90	78	0.058	52.2	5.40E-06	68	0	1	1	1	3.8	0.2	Ok	38	6	0.729
R-18	2	Hexagonal prism	2F	167	96	84	0.060	50.2	3.24E-06	71	4	7	90	6	1.7	0.0	Lack of heat	0	0	0.721
	3	Hexagonal prism	1P1F	191	78	70	0.069	43.7	2.19E-06	71	4	4	57	5	1.1	0.0	Ok	0	0	0.679
	4	Hexagonal prism	1P1F	157	76	67	0.082	36.7	1.92E-06	71	4	6	68	6	1.3	0.0	Ok	0	0	0.664
	5	Hexagonal prism	1P1F	192	146	135	0.043	70.2	6.88E-06	71	4	4	58	5	1.0	0.3	Small leak	12	2	0.796
	1	Hexagonal prism	2F	219	163	143	0.037	80.2	1.22E-05	71	2	1	1	2	0.5	0.6	Ok	51	8	0.821
R-19	3	Hexagonal prism	2F	165	65	57	0.083	36.1	1.45E-06	75	6	9	134	9	1.6	0.0	Ok	0	0	0.62
	1	Hexagonal prism	2F	145	80	70	0.071	42.1	1.95E-06	75	2	11	914	9	5.1	0.1	Ok	1	0	0.672
	2	Hexagonal prism	2F	209	63	56	0.083	36.4	1.74E-06	75	2	12	987	10	5.4	0.8	Ok	11	2	0.621
	4	Hexagonal prism	2F	221	63	55	0.082	36.6	2.20E-05	75	0	0	0	0	-920.9	0.0	Ok	118	18	0.622

*F_T and R_{eq} from Alpha FT-ejection factor calculator (Gautheron *et al.*, 2012)

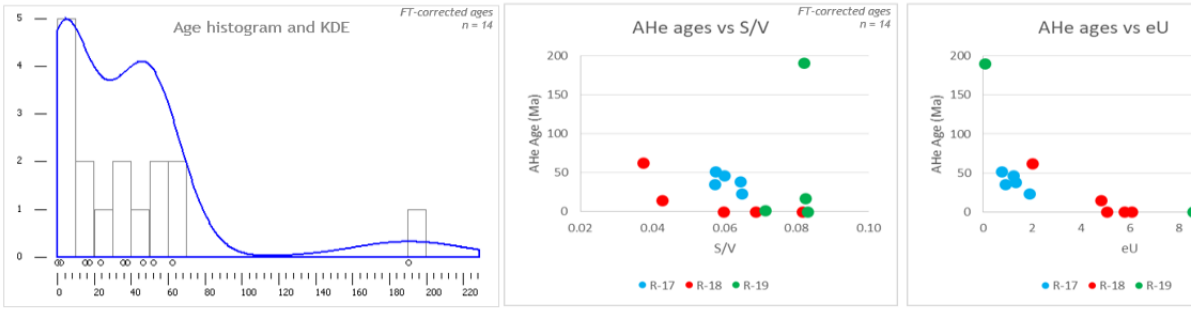

Figure 99: AHe results summary.

a)	Grains	Central age	[U]	Lengths
R-16	1?	100 ± 50 Ma	3.9 ppm	Not enough lengths (due to low U, young age)
R-17	Lost mount			
R-18	9	76 ± 13 Ma	3.5 ppm	
R-19	3	81 ± 25 Ma	2.6 ppm	
R-20	0	N/A	N/A	
R-18-19	11	77 ± 12 Ma	3.3 ppm	

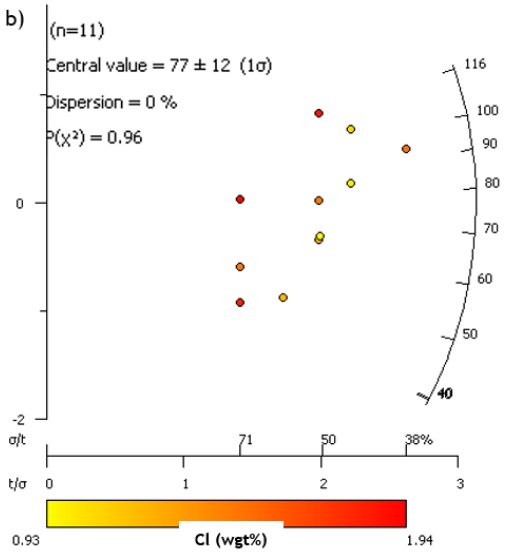

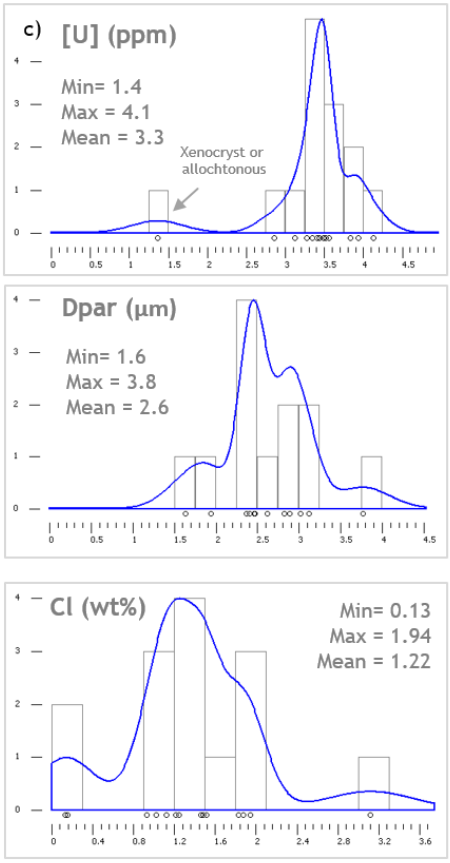

Figure 100: AFT results summary. a) Results per sample. b) Radial plot of combined sample R-16-19 with chlorine content for colour scale. c) Histograms and KDEs of [U], Dpar and Cl for all the grains in sample R16-19.

5.8.3.2 AHe Age dispersion

Taken as a whole, there is a large dispersion in F_T-corrected ages from 0 to 190 Ma with however a cluster of grains from samples R-18 and R-19 with an age of 0-1 Ma (5/14 grains) while the five grains from the shallowest sample (R-17) have all ages between 16 and 38 Ma (FIGURE 99).

The seven grains with AHe ages >15 Ma (called population 2) all have lower [U], [Th] and [Sm] than the remaining grains with ages <15 Ma (called population 1) (FIGURE 101). The concentrations measured on the apatites used for AFT dating are similar to the concentrations of the population grains 1 (most visible with [U], FIGURE 101A), suggesting that the concentrations of the population 2 grain are anomalous.

Based on the comparison with the AFT dataset, the first population is more likely to be *in-situ* grains from the basalts while the second population is either allochthonous (cavings) or have erroneous parent element concentration. To test this second hypothesos, it is possible to recalculate the AHe ages for these anomalous grains using the average ^{238}U, ^{232}Th and ^{147}Sm concentrations from the population 1 grains (FIGURE 102), since the igneous apatites have a narrow range of parent isotope concentrations. The corrected AHe ages range between 0.8 and 18.1 Ma (*vs* 16.5 to 118.5 Ma before the correction) (FIGURE 102A, C). The correction seems to have greatly reduced the age dispersion (FIGURE 102C). The correction yields ages in accordance with the good grains and suggests that all the grains from all three samples have very young AHe ages below 20 Ma and that most of them did not retain any radiogenic helium and have ages of c. 0 Ma. This test correction confirms that the seven oldest grains might have anomalous low parent isotopes concentrations.

Grain size effect: Ages vs S/V

When plotting the U-Th-Sm-corrected ages of sample R-17-18-19 *vs* S/V, the plot shows a weak negative correlation between ages and S/V (FIGURE 102D). It is possible that part of the remaining age dispersion could be explained by grain size variation. The hypothesis is tested below by inverse modelling of two grains (grains R-18.4 and R-18.5) with similar eU (respectively 5.8 and 4.8 ppm) but different S/V (respectively 8E-2 and 4E-2).

5.8.4 Thermal history modelling

Inverse modelling of the AFT and AHe data has been undertaken in order to 1) constrain the thermal history of the samples; 2) test the hypothesis of age dispersion caused by grain size; and 3) test the present-day geothermal gradient estimate. The data was inversed modelled using the HeFTy program (Ketcham, 2005).

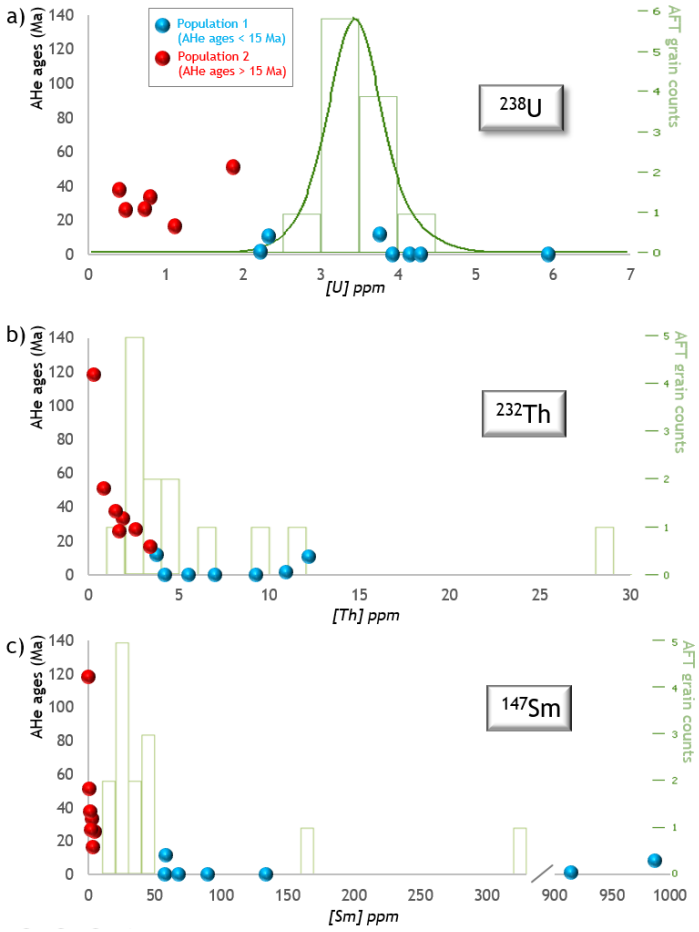

Figure 101: AHe ages vs [U], [Th] and [Sm] with AFT-derived [U], [Th] and [Sm] histogram as background.

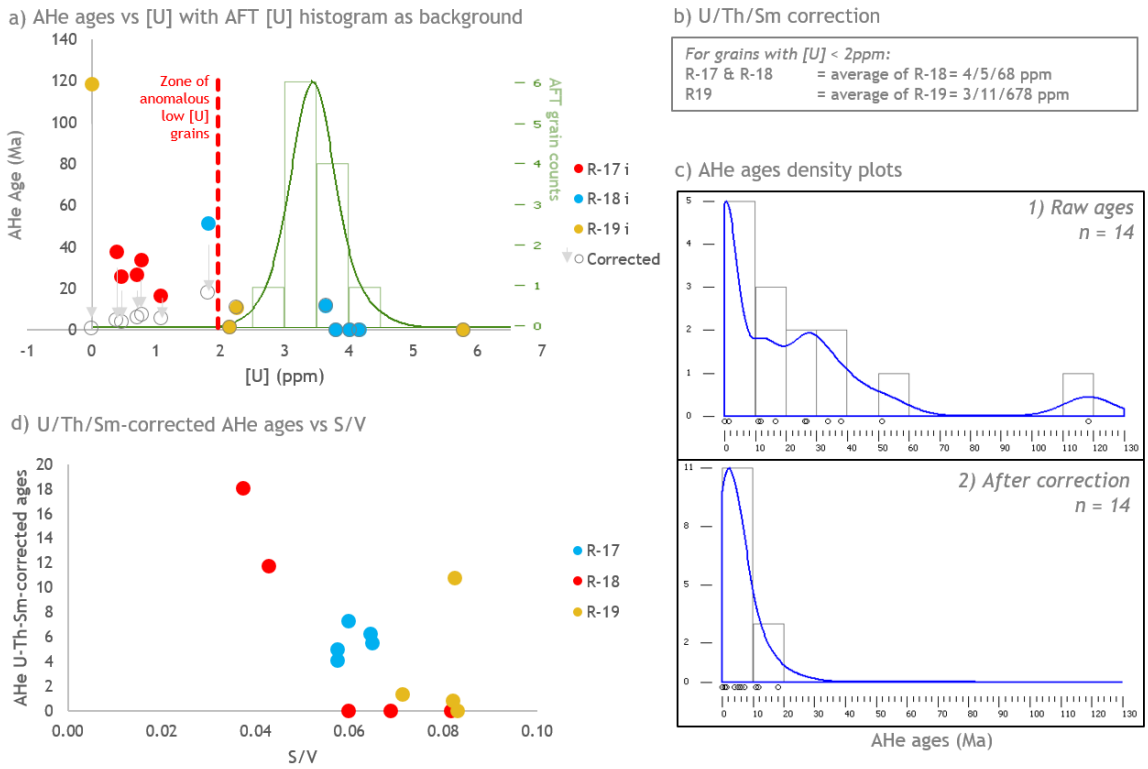

Figure 102: Possible causes of AHe age dispersion in sample R-17-19.

5.8.4.1 HeFTy input data

AFT input data

As discussed above, the 12 AFT ages yield a central age older than the crystallisation age, which is geologically impossible. For the modelling, it is better to input AFT data that represent an age close to the crystallisation age, otherwise the fit between modelled age (max. 62 Ma) and central age (79 Ma) will always be artificially poor. Therefore, the model employs the eight youngest grains out of the 13. In HeFTy, these eight grains have a central age of 61.9 ± 26.7 Ma. The mean age is very close to the assumed crystallisation age (c. 62 Ma), while the uncertainty allows for the model to test thermal histories where the actual AFT age is a bit younger. The eight grains all belong to samples R-18 and R-19.

AHe input data

As mentioned above, the AHe data of R-18.4 and R-18.5 are used to test the hypothesis that part of the remaining dispersion in AHe ages was due to grain size differences (S/V is a proxy for grain size). These two grains belong to the seven grains that did not need a U-Th-Sm-correction (population 1) and they have similar eU (4.8 and 5.8 ppm) but significantly different size (S/V = 0.082 and 0.04) (TABLE 20).

Table 20: Grains R-18.4 and R-18.5 information

Grain	eU	S/V	Raw AHe age
R-18.4	4.8 ppm	0.082 (small	0 Ma
R-18.5	5.8 ppm	0.04 (large)	11.8 Ma

Since the eight grains used for FT data and the two grains used for AHe data all belong to samples R-18 and R-19 (not to samples R-16 and R-17), the pseudo-sample used in HeFTy is renamed R-18-19.

Model constraints

Three models were run with different constraints: 1) Model 1: least constrained model, with only time-temperature of emplacement and present-day temperature; 2) Model 2: same as model 1, but with an addition of 6 intermediate time-temperature constraints derived from the stratigraphic data to simulate the burial history, and 3) Model 3: same as model 2, but with a theoretical burial and uplift/erosion during the Middle Eocene to demonstrate the range of possible undetected exhumation events.

Present-day geothermal gradient

The present-day geothermal gradient is derived from a bottom hole temperature (BHT) measurement of 163.4 °F (73°C) at 6906 ft. Assuming a seabed temperature of 10°C, the geothermal gradient is 35.7°C /km. The BHT temperature was probably not Horner-corrected. However, it was measured at the end of a long test and the gradient derived from it is quite elevated for the area. Consequently, no

correction has been attempted and 35.7°C /km is assumed to be the best-case estimate. Based on regional data, a variation of ± 10°C will be used as a minimum (25.7°C /km) and maximum estimates (45.7°C /km) (FIGURE 103A).

a)

	Min	Best	Max
Geothermal Gradient	25.7°C/km	35.7°C/km	45.7°C/km
Sample temperature	56.5°C	74.6°C	92.7°C
	74.6 ± 18.1°C		

b)

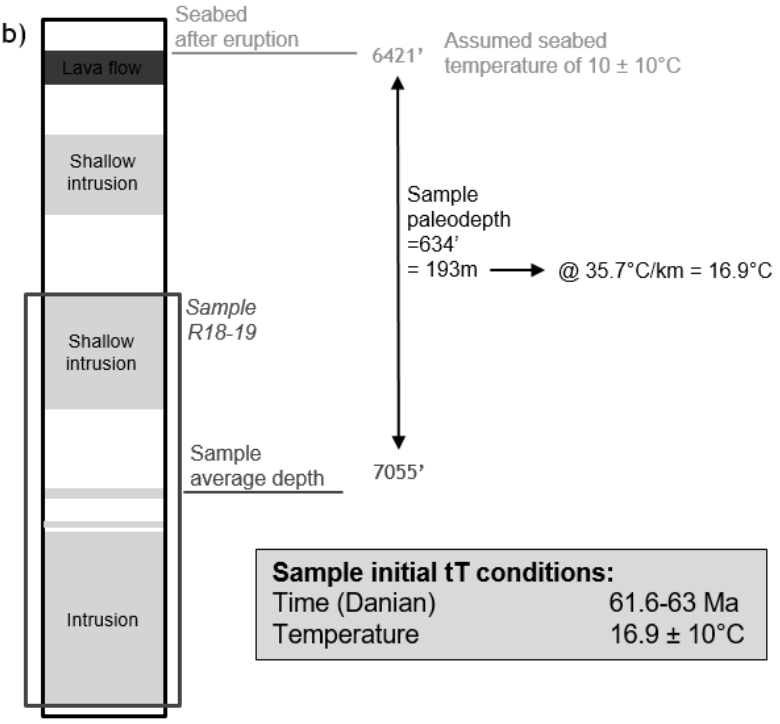

Figure 103: Estimates of present-day borehole geothermal gradient and sample temperatures at the time of emplacement. a) Minimum, best case and maximum estimates of borehole 35/15-1 geothermal gradient and sample present-day temperature. b) Sample temperature at the time of emplacement (c. 62 Ma).

Final conditions: Present-day temperature of sample

Using the best-case geothermal gradient, sample R-18-19 had a present-day temperature of 74.6°C. Using the minimum and maximum estimates of the gradient, the respective sample temperatures are 56.5°C and 92.7°C (FIGURE 103A).

This translates in HeFTy as a present-day temperature constraint of 74.6 ± 18.1°C. The large uncertainty on the present-day temperature is allowed to test if the AFT/AHe data contains information about the present-day sample temperature and therefore the present-day geothermal gradient.

Initial condition - Emplacement age

The emplacement age is defined as late Danian which is translated quantitatively in HeFTy as an age range of 61.6 to 63 Ma.

Initial condition - Emplacement temperature

A lava flow emplaced on the seabed and shallow intrusions like in 35/15-1 would have cooled down very quickly (within a few months or a few years, Worster et al. (1993), Polacci et al. (2018)). The temperature at time of emplacement can therefore be assumed to be the host rock temperature at the depth of emplacement.

The average depth of sample R-18-19 is 7055 ft MD. Assuming that the shallow intrusions were emplaced at the same time as the lava flows, then the paleo-seabed at time of emplacement would have been the top of this lava flow after eruption (now at 6421 ft MD). The shallow intrusions of sample R-18-19 would therefore have been emplaced at a paleo-depths of 634 ft or 193 m (not accounting for compaction) (FIGURE 103B). Using the present-day geothermal gradient, the sample would have had a temperature of 16.9°C. The uncertainty on this temperature is propagated from the default uncertainty on surface temperature, *i.e.* ± 10°C (FIGURE 103B).

Intermediate constraints

For the two models with intermediate conditions, a time-temperature constraint box has been added for each stratigraphic unit mentioned in the composite log. The six units are Thanetian, Early Eocene, Middle Eocene, Late Eocene, Oligocene and Early Miocene.

Forced uplift constraint

For model 3, the Middle Eocene constraint box has been divided in three constraints boxes in order to force a heating event followed by a cooling event to simulate an exhumation event and constrain the magnitude of undetectable uplift and erosion events. The Middle Eocene period was chosen arbitrarily as an illustration. A younger or older period could have been chosen to illustrate undetectable exhumation events. One constraint to respect when simulating an erosion-related cooling event in borehole 35/15-1 is that there is no apparent unconformities in the borehole. If there is a cooling event caused by the erosion of X meters of sediments at some point in time, then it is necessary that this cooling was preceded by the burial of these X meters of sediments (which are now eroded). Since there is no unconformity in the well, any erosion event removed at most the totality of the sediments during the stratigraphic unit in which the erosion occurs, plus some or most (but not all) of the sediments in the preceding stratigraphic unit. Otherwise, it would create an unconformity that would be visible in the stratigraphy of the well. For the modelling, a burial constraint box was defined as 40 to 45.5 Ma and 48 to 100°C, preceded by a constraint box between 47.8 and 45.5 Ma and 37 to 58°C and

succeeded by a constraint box between 40 and 36 Ma and 37 to 58°C (FIGURE 104C). These boxes simulate an early to middle Middle Eocene burial (heating) followed by a middle to late Middle Eocene uplift (cooling), followed by a short period of late Middle Eocene burial (heating).

Model 1

Model 1 shows that a wide range of continuous cooling histories can appropriately replicate the AFT/AHe data (magenta zone in FIGURE 104A). The model with the best fit yields an AFT age of 56.3 Ma, and AHe ages of 0.5 Ma and 11.7 Ma. All models defining the 'good' paths envelope (magenta zone) yield similar matching ages. This demonstrates that two AHe ages of 0 and 12 Ma can be derived with the same thermal history from two grains with the same eU but very different sizes. Consequently, the assumption that grain sizes causes part of the remaining age dispersion after U-Th-Sm correction is valid. The model also shows that the sample never experienced temperatures greater than c. 90°C and actually remained below 60°C through most of its history, except for the last c. 10 My.

Model 2

Model 2 shows that the burial history derived from the stratigraphic data (represented as a series of 6 time-temperature constraints) is sufficient to obtain a good fit of the AFT/AHe data (FIGURE 104B). This thermal history is also included within the 'good fit' envelope of model 1 (magenta area on FIGURE 104A). The best-fit history yielded and FT age of 60.8 and AHe ages of 0.6 and 12 Ma.

The path envelope of the 'good' paths (in magenta) seems to be located within the upper half of the four youngest time-temperature constraints (FIGURE 104B). Meanwhile, the lower third of these boxes are not even part of the green envelope of 'accepted' paths. This suggests that during the burial history (at least since c. 50 Ma), the geothermal gradient was probably a bit lower than now at c. 30°C.km^{-1} and definitely not greater than c. 35°C.km^{-1}.

The sampled present-day temperatures are above c. 64°C (corresponding to a geothermal gradient of 30°C.km^{-1}.) and up to the maximum temperature of 92.8°C (45.7°C.km^{-1}). The weighted mean thermal history has a present-day temperature of c. 75°C (36°C.km^{-1}), very close to the BHT-derived temperature of 74.6°C. The modelling suggests thus that the present-day gradient cannot be lower than 30°C and that the assumed gradient of 35.7°C /km is a valid assumption.

Overall, the modelling indicates that the borehole had a geothermal gradient of c. 30°C.km^{-1} throughout most of it history with possibly an increase to c. 35°C°C.km^{-1} that occurred in the last few million years.

Model 3

Model 3 yields a range of thermal histories with excellent fits, suggesting that uplift and erosion events might have happened but are not detectable.

However, the envelope of 'good paths' remains in the upper part of the pre-uplift burial constraint box (FIGURE 104C). Only the envelope of 'accepted' paths encompasses the entire box. This suggests that to best replicate the AFT/AHe data, any pre-rift burial would be limited to temperatures below c. 70°C. Any burial with associated higher temperatures would probably reset the AFT age to a much younger age than the measured age. This lower boundary, combined with the absence of unconformities in the Cenozoic section of the borehole, constrains any theoretical cooling event in the last 45 Ma to not be greater than c. 30°C, equivalent to a maximum exhumation per event of c. 800-1000 m.

Regional context

The closest published thermochornological dataset with both AFT and AHe data is the vertical profile of Mount Brandon in Dingle (Cogné et al., 2014). The inverse model of this dataset shows a significant Late Neogene cooling phase (40-50°C), interpreted as a true erosional event (FIGURE 105A). During the same period, 35/15-1 records an increase in burial during the last few millions of years, the opposite of the Mount Brandon model (FIGURE 105A).

Consequently it seems that these two locations probably had a decoupled thermal history for at least the last 25 My. While Mount Brandon was possibly actively being uplifted and eroded, 35/15-1 was being buried. Onshore west of Ireland might have therefore been a source of sediments for the subsiding Porcupine Basin at that time. The major basin bounding fault east of 35/15-1 might have separated the two blocks (or another lineament further east) (FIGURE 105B).

5.8.4.2 Conclusions

Inverse modelling of the available geo-thermochronological data for borehole 35/15-1 shows that a simple burial history alone is the simplest model that best fits the data. This simple burial history is in line with the lack of apparent stratigraphic discontinuity above the sample in the borehole.

The age dispersion in the grains from population 1 was hypothesized to be caused by grain size variations (AHe ages *vs* S/V positive correlation, FIGURE 102D). The modelled thermal history successfully predict the AHe ages of two grains with a large difference in size but with similar eU values. This successful modelling confirms that part of the dispersion in ages is caused by variations in grain sizes. Dispersion caused by variations in the amount of radiation damage could not be tested for this sample since all the grains had very similar eU values.

The modelling allows the identification of a narrow range of present-day temperatures and thermal histories that can yield the somewhat rare combination of a non-reset fission track system with fully reset helium system. The geothermal gradient was probably around 30°C.km^{-1} throughout the burial history of the sample and increased to c. 35°C.km^{-1} in the last few million years. The present-day gradient cannot be less than c. 30°C.km^{-1}

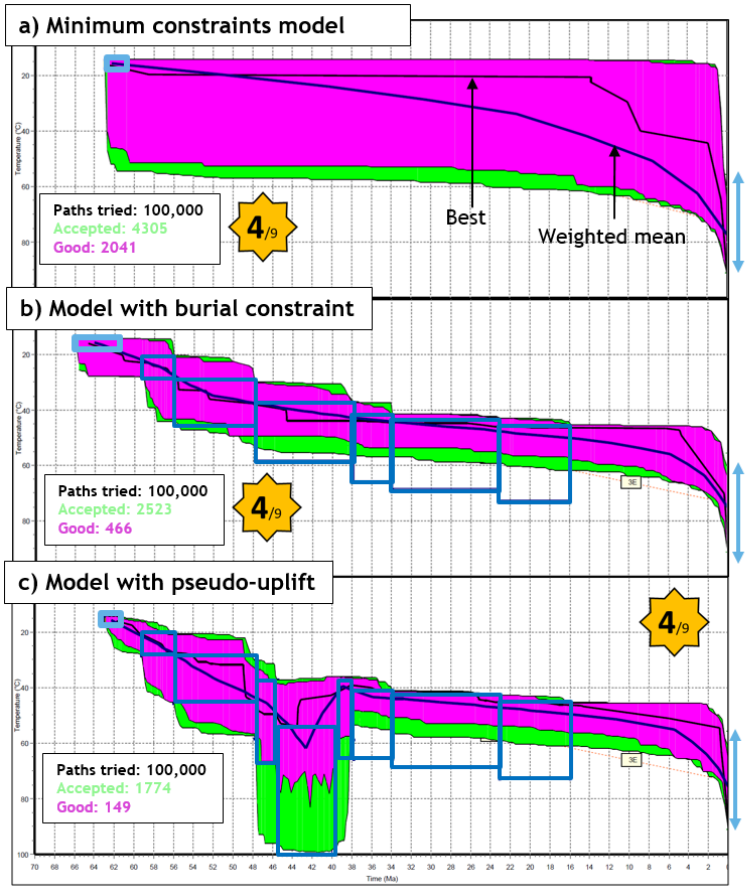

Initial t-T constraint
Present-day t-T constraint
Burial t-T constraints (from comp log)
'Good' paths envelope
'Accepted' paths envelope

d) HeFTy parameters

AFT: Annealing: Ketcham et al., 2007; Zeta mode: LA-ICPMS ratio, ζ: 19.449 ± 0.317; no lengths
AHe: Calibrations: Farley, 2000, stopping distances & alpha correction: Ketcham et al, 2011
Constraints: Deposition age: 61.6-63 Ma, temp.: 15.7 ± 1.6°C; present-day temp.: 73.4 ± 17.8°C
Segments: Path: monotonic consistent; Halve: 3 times; Randomizer style: episodic, no maximum dT/dt
Paths tried: 100,000

e) Modelling results

Sample		Measured age	Modelled age
AFT	*R-16-19*	59.2 ± 13 Ma*	a) 6.3 b) 60.8 c) 60.8
AHe	*R-18.4*	0.5 ± 0.5 Ma**	a) 0.51 b) 0.6 c) 0.63
	R-18.5	11.8 ± 1.8 Ma	a) 11.7 b) 12 c) 11.9

* AFT age modified to reflect emplacement age
** AHe age of 0 Ma, but used 0.5 ± 0.5 Ma in HeFTy to avoid a bug

Figure 104: Results of thermal history modelling of 35/5-1.

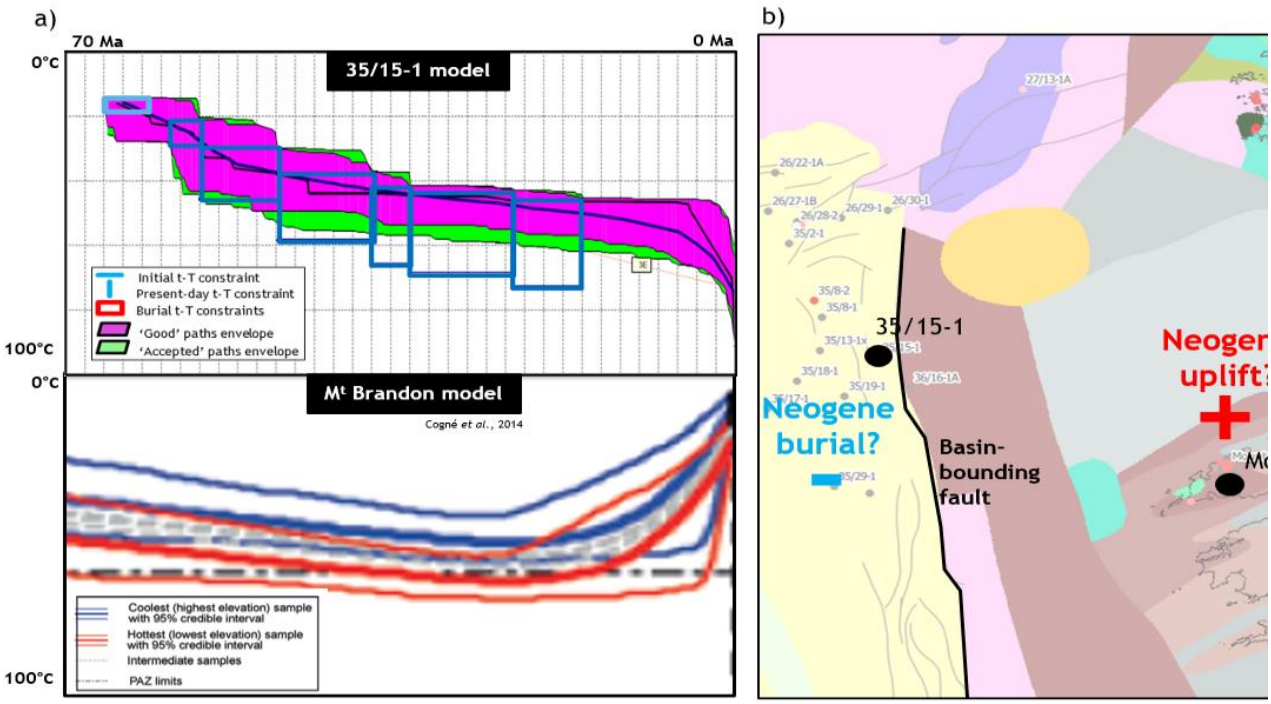

Figure 105: Thermal history comparison of borehole 35/15-1 and Mt Brandon vertical profile. a) Results from the thermal history modelling. b) Location of the two datasets and the main basin bounding fault possibly separating the two thermal history domains.

Undetected uplift and erosion events are possible. However, the associated cooling would have been maximum c. 30°C for the past 45 My, with higher values up to c. 50°C between 45-60 Ma. Such events would have required a significant increase in sedimentation rate before and/or after the uplift. These inferred cooling pulses translate to maximum erosion of c. 800-1000 m of sediments for events in the past 45 My, while the amount of uplift is unconstrained between 45-60 Ma.

The thermal history of the area in the vicinity of borehole 35/15-1 was decoupled from that of onshore west of Ireland for at least the last 25 My. While accelerated burial might have been dominant at the location of 35/15-1, exhumation was occurring at Mount Brandon. The major basin bounding fault just east of 35/15-1 may have separated these two tectonic domains. The uplift of SW Ireland at that time might have contributed sediments to the subsiding eastern part of the Porcupine Basin.

5.8.5 Conclusions

Despite samples from cuttings and a poor apatite yield and dispersed AHe ages, careful examination of the geo-thermochronological data, coupled with geological data from the borehole, allows several new insights about the well locality and the eastern margin of the Porcupine basin to be inferred:

1) Apatite and zircon U/Pb data confirms that an episode of Paleocene volcanism occurred in the area of borehole 35/15-1.
2) The apatite and zircon U/Pb data does not help to refine the age of the mafic volcanism. Based on conflicting stratigraphic data and zircon U/Pb results, it is probably either upper Danian in age (c. 62 Ma) or Selandian (c. 60 Ma).
3) Unexpected Paleocene igneous zircons were found in samples R-16, 17 and 18 with an age of 60.49 ± 0.64 Ma (Selandian). These igneous zircons could either be zircon xenocrysts (from a deeper part of the mafic plumbing system) or allochthonous grains from a suspected volcanoclastic deposit above sample R-16.
4) The c. 60 Ma igneous zircons are the first reported Paleocene zircons offshore Ireland.
5) The U/Pb dating of all AFT apatites allow the discrimination between *in-situ* Paleocene apatites belonging to the basalts from older apatites, likely incorporated from nearby sand beds (such as in sample R-16). This led to the identification of three AFT grains not belonging to the igneous units.
6) The combined sample (R-16-19) has an AFT central age of 79 ± 11 Ma and AHe F_T-corrected ages between 0 and 190 Ma.
7) Despite a poor yield of apatites suitable for fission track dating, the FT data show that the sample did not experience any significant amount of annealing, *i.e.* it resided at temperatures below c. 60°C.

8) The AHe age dispersion is primarily caused by the presence of an anomalous population of seven grains with older ages and low parent isotope concentration. This anomalous population has been ignored for thermal history interpretation and modelling.
9) The remaining dispersion in AHe ages is partly explained by grain size differences. Thermal modelling shows that plausible thermal histories can yield AHe ages between at least 0 and 11 Ma just due to grain size differences alone.
10) The inverse modelling demonstrates that only present-day temperatures between c. 64°C and c. 90°C can explain the data, with a preference for temperatures around 75°C, which is similar to the best estimate temperature derived from the BHT. It confirms that the geothermal gradient for borehole 35/15-1 has to be above 30°C /km and the best estimate is 35.7°C /km.
11) Inverse thermal modelling, with burial constraints derived from stratigraphic and geothermal gradient information, indicates that burial to present-day depths alone is enough to explain both the AFT and AHe data.
12) However, it is possible that small uplift, erosion and re-burial events occurred at any time during the burial history. The maximum amount of cooling possible (constrained by the continuous stratigraphic column and non-reset AFT ages) would be c. 30°C (c. 800-1000 m) since the Middle Eocene (the last 45 My).
13) In the last 25 My, an acceleration of burial might have been dominant at the location of 35/15-1 while exhumation occurred at Mount Brandon (Dingle Peninsula). The major basin bounding fault just east of 35/15-1 might have separated the two tectonic domains and the uplifted SW of onshore Ireland might have contributed sediments to the subsiding eastern part of the Porcupine Basin.
14) The study demonstrates the value of measuring U/Pb ages together with AFT ages for igneous samples from well cuttings (*i.e.* the identification of allochthonous grains to be discarded for AFT analysis). Such dual-dating is done routinely with the LAFT approach.
15) The study demonstrates that in certain cases, low-temperature thermochronological data and thermal history inverse modelling can help better constrain present-day sample temperatures and geothermal gradients.

6 Southern zone: Goban Spur, south Porcupine High

6.1 South Porcupine High

The southern part of the Porcupine High was sampled by the Ifremer Cyaporc campaign using the *Cyana* submersible (Auffret et al. (1987), Masson et al. (1989)). Several rocks were sampled as this segment of the IAM is poorly known and also represent a geodynamically interesting location, as it is an unstretched piece of continental crust located adjacent to a narrow band of possibly hyperextended crust, exhumed mantle and oceanic crust (Nirrengarten et al., 2018) (FIGURE 106).

Due to Ifremer sampling restrictions, only three samples could be retrieved: a metagabbro (R-21), a granite (R-22) and a gneiss (R-23). The metagabbro (R-21) yielded a U/Pb apatite age of 1395 ± 44 Ma and an AFT central age of 238 ± 9 Ma. The granite (R-22) yielded Late Caledonian zircon and apatite U/Pb ages of 424 ± 3 Ma and 421 ± 7 Ma respectively, an AFT central age of 222 ± 11 and AHe F_T-corrected ages ranging from 120 to 265 Ma. The gneiss (R-23) yielded a Mesoarchean zircon U/Pb age of 2870 ± 15 Ma and a Mesoarchean apatite U/Pb age of 2835 ± 45 Ma, an AFT central age of 391 ± 16 Ma and AHe ages ranging from 134-177 Ma.

However, uncertainties about whether the dive samples represent *in-situ* basement or glacial erratics (Masson et al., 1989) prevents their use as indicators of the basement geology and thermal history of this part of the South Porcupine High. The gneiss for example most likely represents ice-rafted debris as both its Archean U/Pb age and Devonian AFT age would be highly anomalous for this part of the IAM. A metagabbro was recently recovered by a Geological Society of Ireland dredge a few tens of kilometres further north and is believed to be *in-situ* (R. Strachan, pers. com.). This suggests that the metagabbro (R-21) might also be *in-situ* which would indicate that despite being located very close to the COB, this part of Porcupine High was not thermally affected by the opening of the Atlantic during the Early Cretaceous as it has a Triassic AFT age.

6.2 Goban Spur

6.2.1 Introduction

The Goban Spur (GS) forms the southernmost part of the Irish continental shelf and slope. It is located at the junction of the southern part of the Porcupine Basin, the south-western end of the Celtic Sea Basins and Cornubian Platform, and the north-western end of the Celtic and Armorican Shelf (FIGURE 106). The geology of the GS has been investigated by four DSDP boreholes drilled in 1985 (De Graciansky et al., 1985b), a series of seabed dredges and dives, notably the Ifremer campaigns SU01, CH58, CH66 and CH67 with the "R/V Le Suroît" and "R/V Jean Charcot" in 1975 and 1976 (Pautot et al. (1976), Didier et al. (1977a), Auffret et al. (1979a)) and the Cyaporc campaign in 1986 (dredge hauls

and dives with the *Cyana* submersible) (Auffret et al. (1987), Auzende et al. (1989) and Masson et al. (1989)), one exploration O&G borehole (62/07-1, Esso (1982)) (FIGURE 106). A number of seismic and gravity-magnetic studies have also helped constrain the geology (e.g. Scrutton (1979), Scrutton (1985), Peddy et al. (1989), Horsefield et al. (1994), Bullock and Minshull (2005), Yang et al. (2020)).

6.2.2 Geodynamical history

The Goban Spur is a starved, hyperextended, passive margin that formed during the opening of the Southern North Atlantic Ocean during the Mesozoic (Masson et al. (1984), Nirrengarten et al. (2018)). Before continental break-up, the Goban Spur was attached to the Galicia Bank, at the western tip of the North Iberian Margin, and to the Flemish Cap, offshore Newfoundland (FIGURE 107). Rifting started during the Permian-Triassic and lasted until the late Aptian, with the main phase of crustal thinning and hyperextension occurring during the Barremian to Aptian (De Graciansky and Poag, 1985; De Graciansky et al., 1985a; Yang et al., 2020). Lithospheric breakup occurred at c. 112 Ma resulting in a phase of mantle exhumation quickly followed by oceanic seafloor spreading that produced the first identifiable seabed magnetic anomaly, Chron C34 (Nirrengarten et al., 2018) (FIGURE 107).

The crustal architecture of the Goban Spur margin has been divided in four units by Yang et al. (2020), following the nomenclature of Peron-Pinvidic et al. (2013): a proximal domain with crust thickness >30 km, a necking domain with a thinned crust between c. 10-30 km, an hyperextended domain with crust c. < 10 km and an exhumed domain with serpentinized mantle peridodite. The Goban Spur plateau and slope corresponds for the most part to the proximal and necking domain, while two parallel thin bands of c. 70 km width along the edge of the continental slope corresponding to the hyperextended and exhumed domains (Yang et al., 2020) (FIGURE 108).

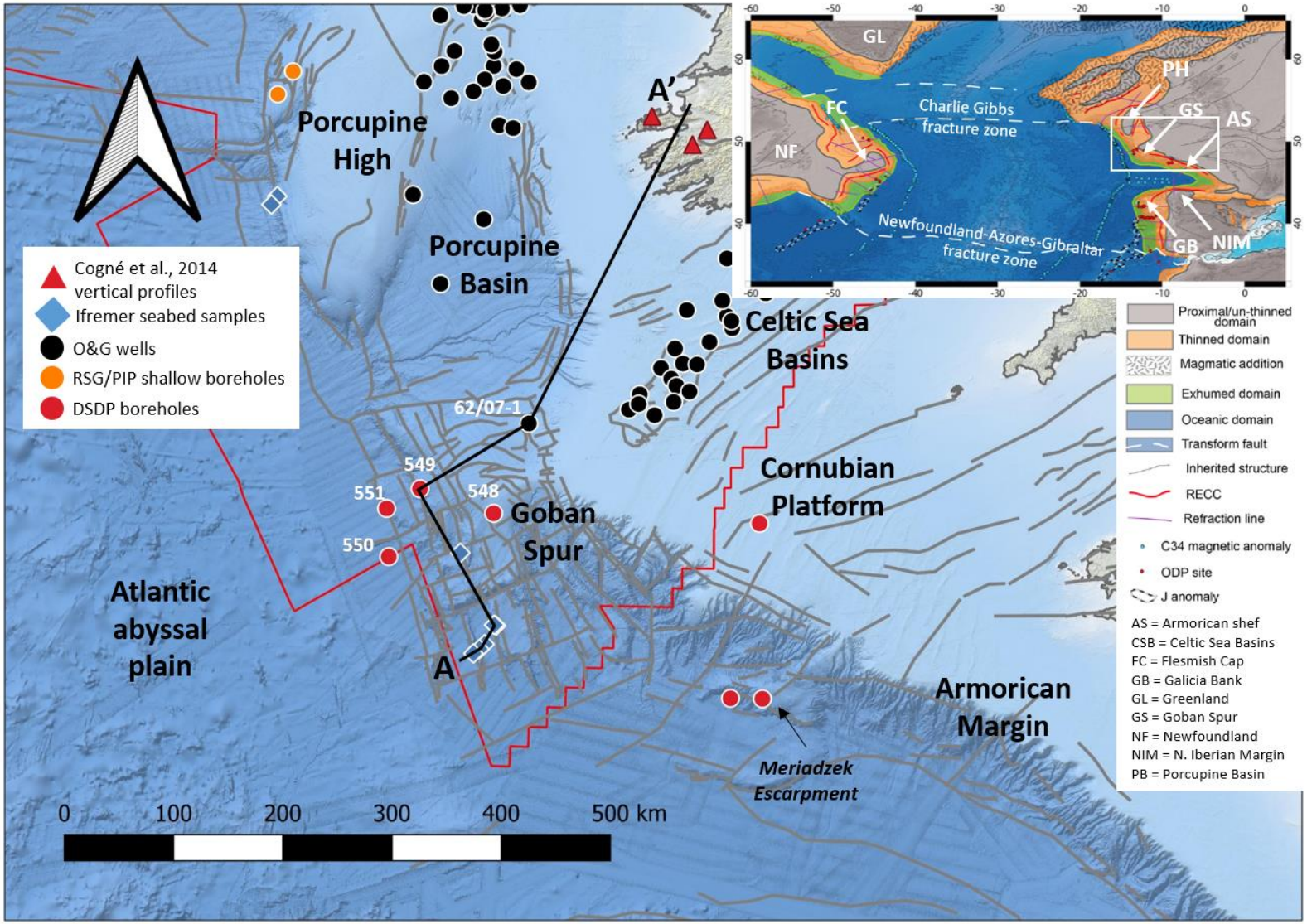

Figure 106: Location map of the Goban Spur seabed samples. The black line A-A' corresponds to the correlation in Figure 125. Insert: Bathymetric map of the North Atlantic superimposed with the rift domains (modified after Nirrengarten et al. (2018)).

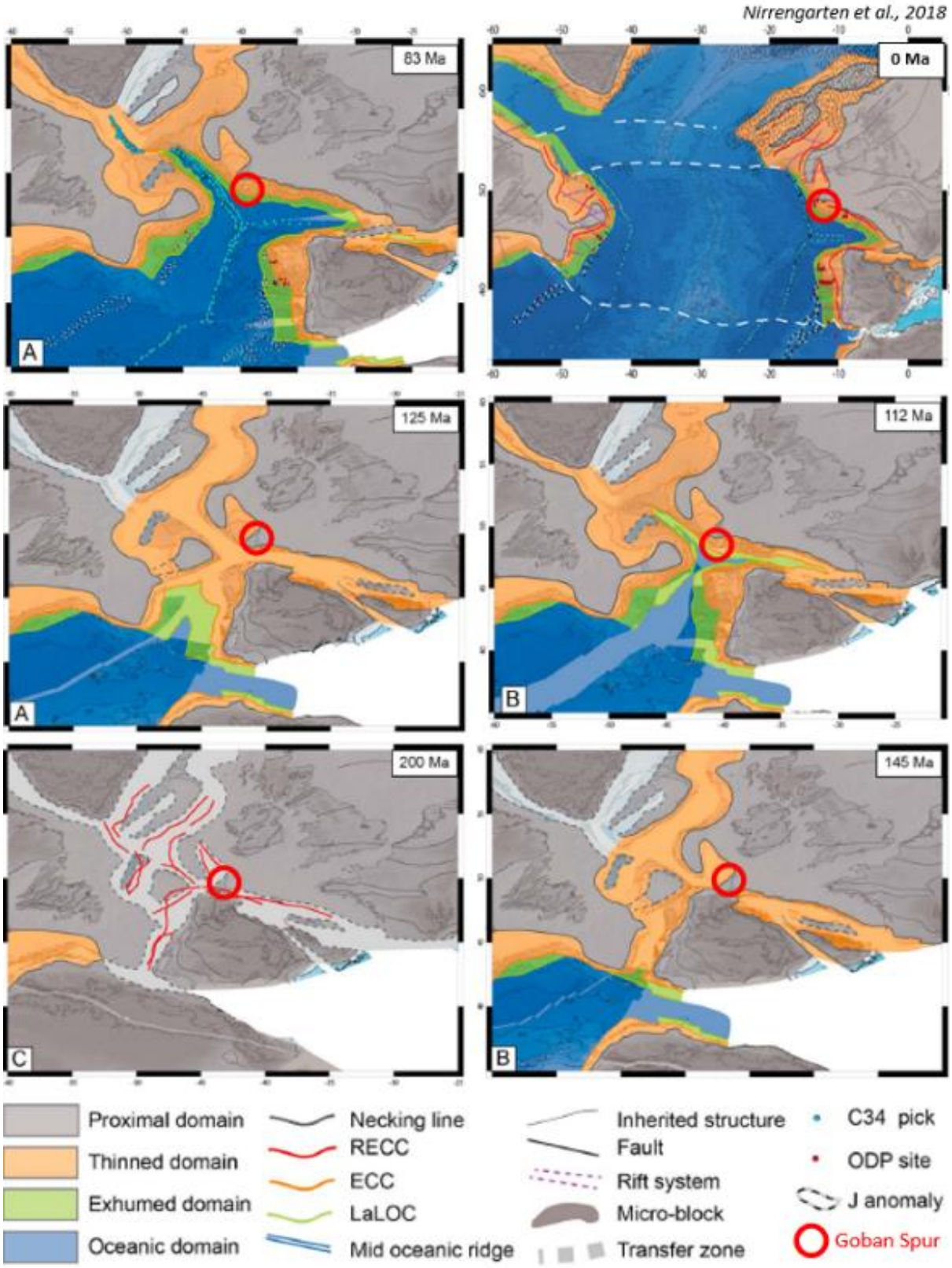

Figure 107: Restoration of the southern North Atlantic, with North America fixed atn present-day coordinates from 145 Ma to 0 Ma (modified after Nirrengarten et al. (2018)) with the location of the Goban Spur samples added.

In the southern part of the Goban Spur, the tips of rotated continental fault blocks are still apparent at the seabed where they form positive features oriented NW-SE, such as Granite Cliff 4000 (GC4) and Menez Bihan (see bathymetry expression and seismic cross-section on FIGURE 108).

6.2.3 Geological history

The pre-rift basement of the Goban Spur is constituted of Late Variscan granitoids at Menez Bihan and Granite Cliff 4000 (Auffret et al., 1979a), Paleozoic (Carboniferous, Devonian and older?) sediments and metasediments at King Arthur's Castle, Granite Cliff 4000 and the southern end of Pendragon Escarpement (Auffret et al., 1979a), non-deformed Paleozoic (probably Devonian) fine-grained sandstone at the northern tip of the Pendragon Escarpment (Masson et al., 1989) and folded, low-grade, Devonian sandstones and shales at DSDP Leg 548 and 549 (Auffret et al. (1979a), De Graciansky et al. (1985a)) (FIGURE 108).

Drilling results, dredges and seismic mapping demonstrated that the syn-rift succession is made of Barremian-Aptian marine mudstone, limestone and sandstone. Older Permian, Triassic, Jurassic sediments might be present in the deeper parts of some half-grabens but none have been recovered so far (De Graciansky et al., 1985a). The oldest post-rift sediments are Early to Late Albian siltstones and mudstones (DSDP sites 549 and 550). Just after the initiation of seafloor spreading, the Early Albian mudstones at site 549 (on the continental crust) were believed to be at near-sea level while the adjacent seafloor (the newly formed oceanic crust) was believed to be c. 1900 m below sea-level (De Graciansky et al., 1985a).

During the Late Cretaceous, the continental margin continued to subside and a condensed layer of chalk was deposited. Most of the relief created by the rotated fault blocks was filled by the end of the Santonian, resulting in more uniform and continuous post-Santonian lithologies throughout the area. During the Cenozoic, silica-rich chalks and oozes dominated, reflecting a deepening of the seafloor due to subsidence (De Graciansky et al., 1985a). However, the Late Paleocene-Early Eocene is characterized by brown chalks rich in terrigenous clay materials, volcanic debris and trace amount of iron and manganese. This terrigenous layer is coeval with the development of a deltaic platform in the north Porcupine Basin and unconformable fluviatile sediments in the Celtic Sea basins and they have been interpreted as being related to the uplift of the Irish landmass at that time (De Graciansky and Poag, 1985). Several unconformities are present within the post-rift succession: Late Cretaceous/Paleocene, Lower/Upper Paleocene, Lower/Middle Eocene, Lower/Upper Oligocene and Middle/Upper Miocene. These unconformities are believed to have been caused by changes in sea level, bottom-water circulation, carbonate compensation depth and water-mass boundaries (De Graciansky and Poag, 1985).

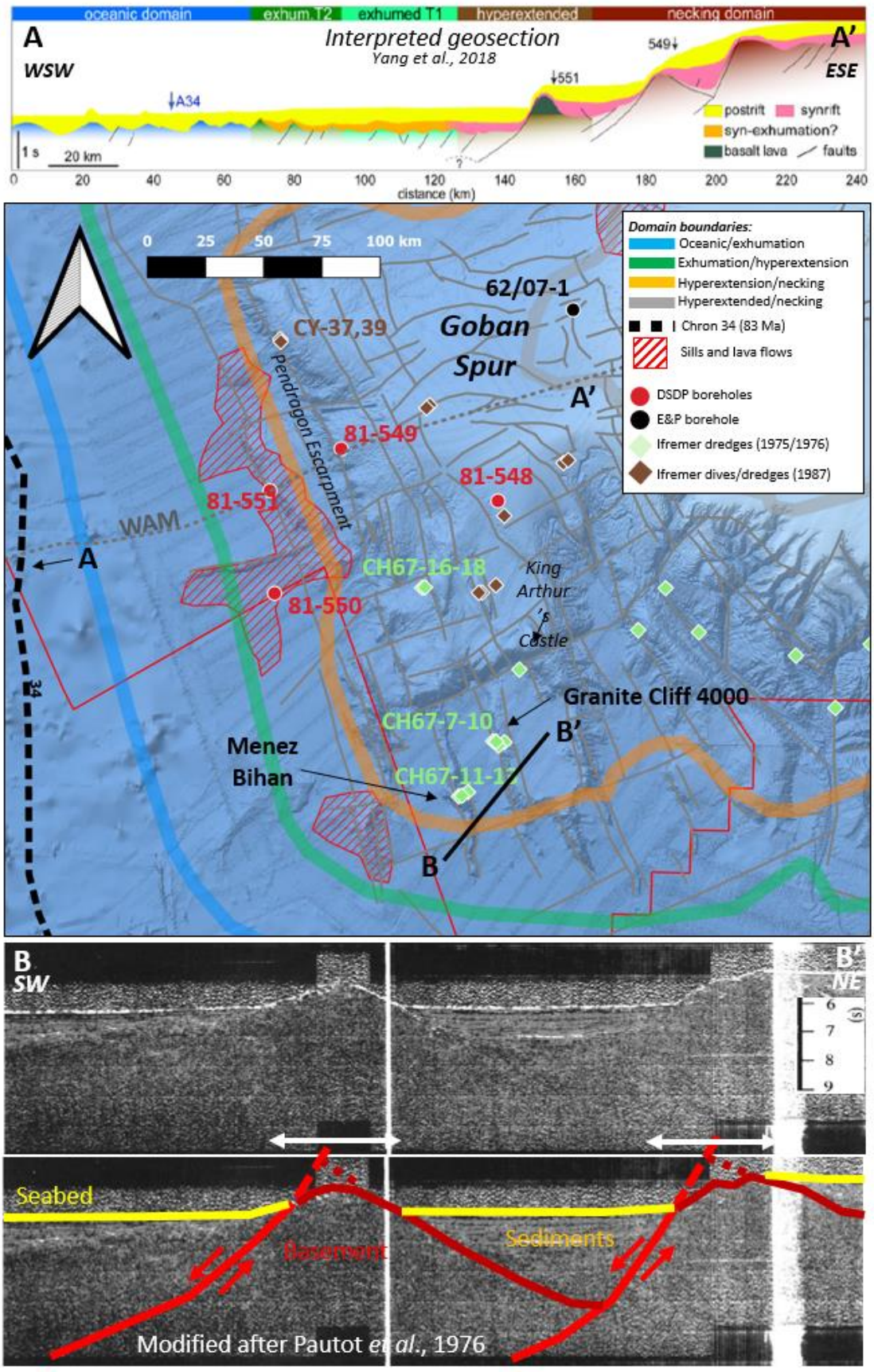

Figure 108: Goban Spur crustal domains, structural features WAM geosection and seismic section through Granite Cliff 4000 and Menez Bihan.

6.2.4 Magmatism

6.2.4.1 Early Cretaceous magmatism

While the Goban Spur is categorized as a non-volcanic margin (e.g. Louden and Chian (1999)), a small amount of magmatism occurred before lithospheric mantle break-up in the form of sills intruding the margin (Yang et al., 2020) (FIGURE 108). A lava flow of probably Valanginian age was also encountered in borehole 62/07-1 (Tate and Dobson, 1988) while clasts of undated volcanic rocks were found at the King Arthur Castle (FIGURE 108) in a breccia of Barremian-Cenomanian age (Auffret et al., 1979a). Further away, the Seabight Igneous Centre (Aptian-Albian, Tate and Dobson (1988)), Porcupine Median Volcanic Ridge in the Porcupine Basin, the Barra Volcanic Ridge System in the Rockall Basin and the J-anomaly on the Newfoundland-Galicia margins are all believed to belong to a single Early Cretaceous igneous province (Calvès et al. (2012), to which the Goban Spur magmatism would probably belong as well.

6.2.4.2 Paleogene magmatism

Late Paleocene to Late Eocene volcanic ash beds were found in DSDP boreholes 548, 549 and 550 (Knox, 1985). Further away, on the Meriadzek Escarpment, a tuffaceous microconglomerate with basalt clasts was found. The volcanic glass which composes 30% of this conglomerate was dated at 35 Ma (Auffret et al., 1979a), although the dating was probably undertaken using K-Ar dating which is subject to daughter argon loss and therefore the age should be considered as a minimum age. The basalt clasts have not been dated. No other Cenozoic igneous rocks were recovered in the other dredges by Ifremer on the Goban Spur and Armorican margin (Auffret et al., 1979a), suggesting that any igneous activity would probably have been minor and spatially restricted.

6.3 Samples

6.3.1 Sampling

6.3.1.1 Strategy

Sampling was undertaken on the rocks recovered by the Ifremer dredges and dives (campaigns SU01, CH67 and Cyaporc) which are now stored at the Ifremer core store in Brest, France. Sampling was limited by Ifremer to only large clasts and only a fraction of the clast to ensure that enough rock remained for future analyses (with a maximum of 500 grams for felsic crystalline rocks and a maximum of 750 grams for non-felsic crystalline rocks and sedimentary rocks).

The samples were selected to favour apatite-rich lithologies (e.g. felsic crystalline rocks) and clasts that were believed to be *in-situ* based on the published results (Auffret et al. (1979a), Masson et al. (1989)). The main candidates were the Late Variscan granitoids recovered at Granite Cliff 4000 (GC4) and

Menez Bihan (MB) (Auffret et al., 1979a). The content of these dredges at these locations were dominated by large granitic clasts with broken surfaces. This abundance of a single lithology, evidence of breakage surfaces from an outcrop together with elevated wire tension registered during dredging indicate that these clasts are in-situ and represent the basement that crops out at these locations (Auffret et al., 1979a). The granitic samples are R-24 and R-26 from the GC4 dredges and R-28 from the MB dredge. Two metamorphic clasts from these two locations also sampled (sample R-25 and R-27). A Paleozoic sandstone was also selected from dredge CH67-18 on the Goban Spur plateau.

A low-temperature thermochronology study of exploration borehole 62/07-1 has previously been attempted by a team at TCD, but the sampled cuttings failed to yield enough apatites to obtain interpretable results. Finally, a fission track study was done on a granulite clast from dredge CH67-12 at MB (Fügenschuh et al., 2003).

6.3.1.2 Samples

Sample R-24 (Ifremer sample CH67 DR08 D01, GC4) is a granodiorite dated at 275 ± 3 Ma by whole rock Rb/Sr and at 281 Ma by Rb/Sr on biotite (Auffret et al., 1979b). This granitoid was interpreted by Auffret et al. (1979a) as a Late Variscan intrusion, similar to the ones found in Cornwall and Spain.

Originally, sample R-25 intended to be an undated quartz diorite from dredge CH67 DR09 on GC4, which was reported in Auffret et al. (1979a) (their Table 3) as clast D4. However, due to the clast being too small, another clast from the same dredge was sampled, clast B14, which is a dark crystalline rock.

Sample R-26 (Ifremer sample CH67 DR10 D05, GC4) is described in the Ifremer catalogue as a granite. Other clasts in the same dredge are described by Auffret et al. (1979a) as a quartz diorite dated by whole rock Rb/Sr at 270 ± 3 Ma (clast D51), by K-Ar on biotite at 290 Ma (clast D54) and a quartz syenite (clast D52).

Sample R-27 come from clast 'B21' from dredge CH67 DR12 (MB). In their study of granulite samples from the Bay of Biscay, Fügenschuh et al. (2003) analysed a sample (here termed L-DR12-B21) that came from the same dredge and from a clast with the same name. Two clasts have this 'B21' number in the Ifremer catalogue, which probably indicate an identical lithology (in comparison to other clasts from the same dredge which other numbers). Therefore, sample R-27 is most probably from the same lithology as sample L-DR12-B21 which is descrbied by Fügenschuh et al. (2003) as a strongly foliated, medium-grained pyriclasite (*i.e.* a granulite) with plagioclase, orthopyroxene, clinopyroxene, hornblende, biotite, ilmenite, garnet and apatite.

Sample R-28 (Ifremer sample CH67 DR13, MB) is a granite. Other granite clasts in this dredge were dated by whole rock Rb/Sr at 251 ± 2 Ma and by K/Ar on biotite at 207 Ma (Auffret et al., 1979b).

Sample R-29 (Ifremer sample CH67 DR18, Goban Spur Plateau) is a fine-grained green sandstone. Similar clasts in this dredge have been described as possibly Paleozoic in age (Auffret et al., 1979b).

6.3.2 Apatite and zircon yield

All samples, except the sandstone, yielded numerous apatites which after counting and analyses provided 38 to 40 AFT ages per sample. The sandstone (sample R-29) only yielded eight apatites and AFT ages. Fügenschuh et al. (2003) calculated 16 AFT ages for their granulite sample L-DR12-B21. All samples yielded numerous zircons (> 50) expect for the granulite sample that yielded 17 zircons only.

Despite the small sample size allowed by Ifremer, the chosen lithologies yielded enough apatites and zircons grains both geo- and thermochronological analyses of all samples, except the green sandstone which does not have enough apatites to properly constrain the thermal history of this sample.

6.4 U/Pb and trace element results

The detailed description of the U/Pb and trace element results is presented in ANNEX 1 (SECTION 1.1). Below is a summary and discussion of the results.

6.4.1 Late Variscan granites and age of the underlying crust

The new apatite and zircon U/Pb ages of samples R-24, R-26 and R-28 (FIGURE 109) confirm the Late Variscan age of the GC4 granitic batholith (c. 297 Ma, FIGURE 110A) and MB batholith (c. 288 Ma) as identified by the campaign geologists (Auffret et al., 1979b). The presence of rare Cadomian zircon cores or grains in all three granite samples could suggest that the batholith intruded a crust with a Cadomian zircon age signature and would therefore probably belong to the Avalonian terrane or another peri-Gondwana terrane with Cadomian metamorphism (Fairey et al., 2018). The trace element biplot suggests that the batholiths are probably I-type granitoids (FIGURE 110B). I-type granitoid are often from hot magmas with high zircon saturation and a more mafic source resulting in fewer inherited zicons (as observed for these samples) than S-type granitoids which are often sourced from upper crustal rocks rich in zircons and colder magmas with lower zircon saturations resulting in numerous inherited zircons (Chew et al., 2020), such as the S-type granites of the Cornubian Batholith in Cornwall (Smith et al., 2019). The regional significance of the new data is discussed in SECTION 7.2.1.2.

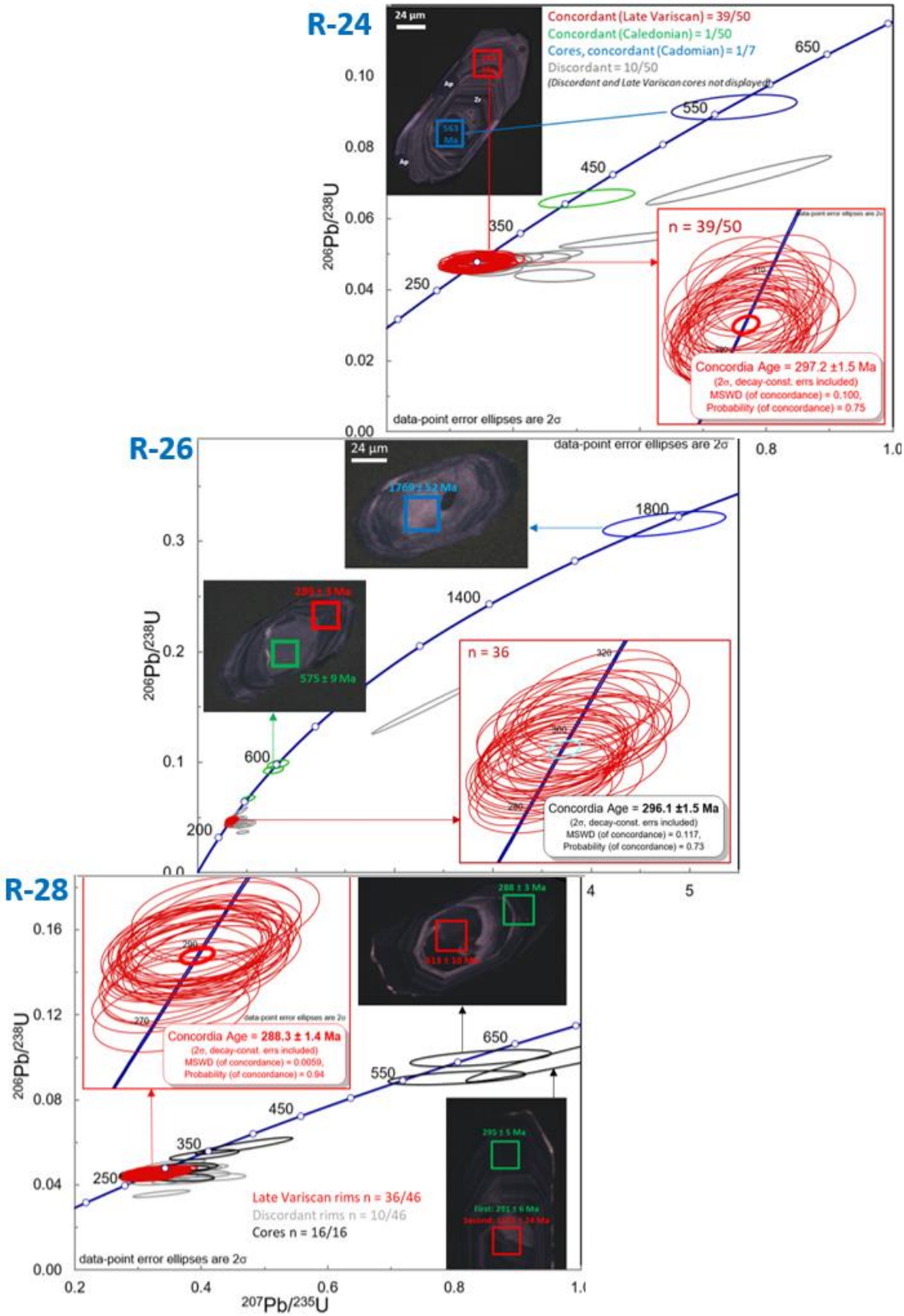

Figure 109: Zircon U/Pb ages from the Late Variscan granites (samples R-24, R-26, R-28).

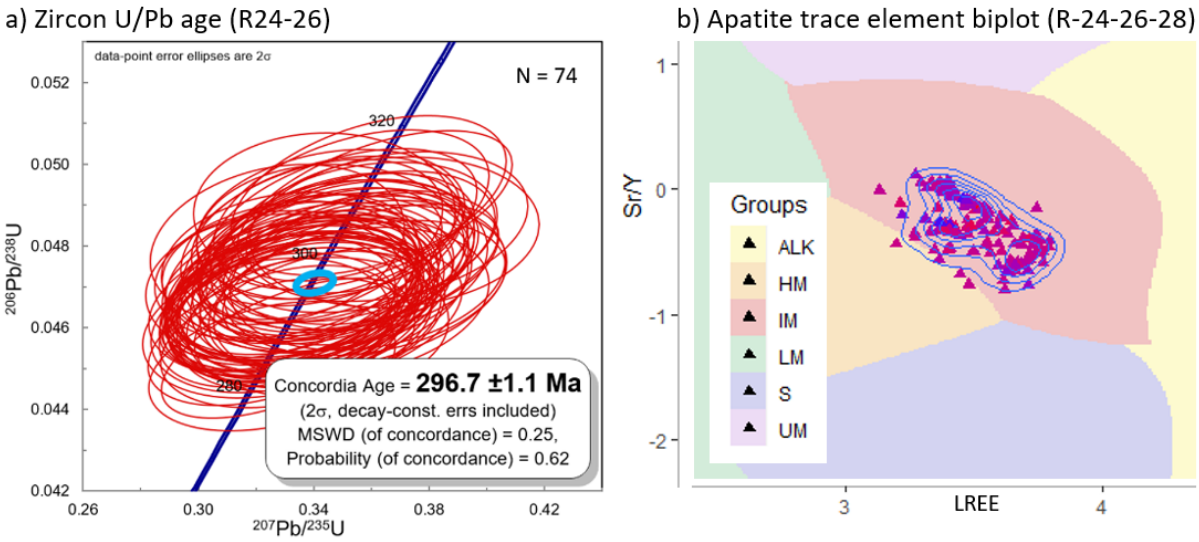

Figure 110: Zircon U/Pb ConcAge for samples R-24-26 and apatite trace element results for samples R-24-26-28.

6.4.2 Neoproterozoic basement

The granulite sample R-27 belongs to the Avalonian domain and was formed or metamorphosed during the Cadomian Orogeny (crystallisation of the matrix zircons at 571 Ma) and subsequently affected by the main phase of the Caledonian orogeny (crystallisation of the apatites at 446 Ma) (FIGURE 111). At c. 297 Ma, during the Late Variscan magmatic activity, zircon-bearing veins (FIGURE 111) were possibly formed from hydrothermal fluids or aplitic magmas linked to the emplacement of a granitic pluton at this location (*i.e.* sample R-28). The Cadomian granulite sample could well be *in-situ* since the Avalonian basement of the south of Ireland is expected to extend to the Goban Spur (Ady and Whittaker, 2019) and inherited zircons in the Late Variscan granites point toward such a basement age.

6.4.3 Neoarchean basement

A metamorphic rock at GC4 (R-25) yielded a zircon U/Pb age of 2764 ± 24 Ma and apatite U/Pb age of 1714 ± 16 Ma with trace elements indicating a possibly S-type or felsic I-type granitoid protolith (possibly at 2.8 Ga) subsequently affected by metamorphism leading to Pb and LREE loss in some of the grains (possibly at 1.7 Ga).

The zircon data is very similar (both in age and Pb loss pattern) to granulitic dredge clasts found on the Ortegal Plateau (OP), offshore NW Spain (clast dated at 2734 ± 2 Ma and 2761 ± 24 Ma, Guerrot et al. (1989)) (FIGURE 112). These Neoarchean granulites have a whole-rock Sm/Nd model age of 3 Ga, while other granulites on the OP yielded zircon U/Pb ages of c. 1.9 Ga with Sm/Nd model age of 2.3-2.6 Ga (Guerrot et al., 1989).

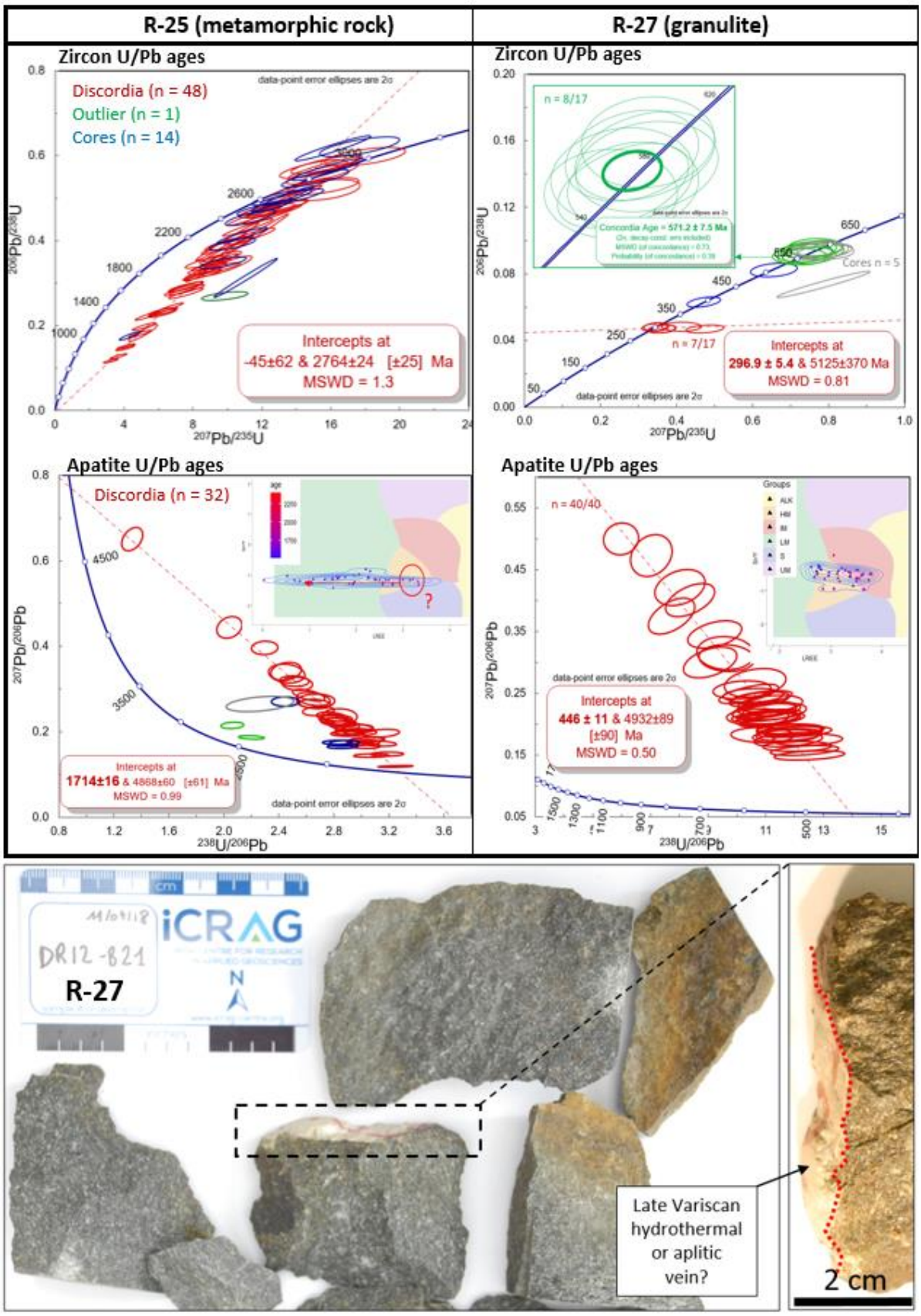

Figure 111: Zircon and apatite U/Pb ages and apatite trace elements for samples R-25 & R-27 and photos of sample R-27 with inferred Late Variscan vein.

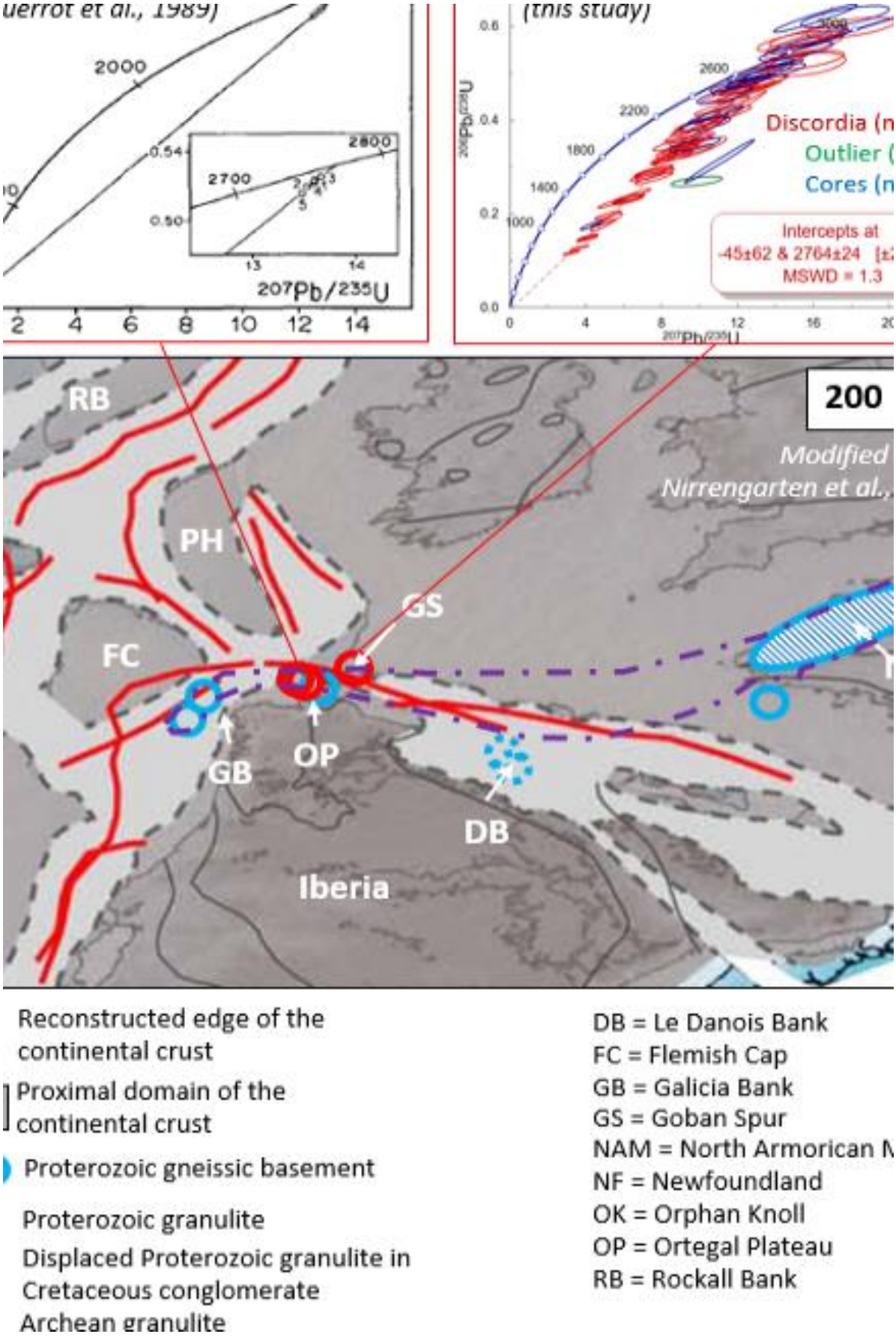

Figure 112: Location of the Proterozoic and Archean granulites of the Goban Spur and North Iberian Margin on a pre-break-up reconstruction of Western Europe (at 200 Ma).

Further to the west, on the Galician Bank (GB), Gardien et al. (2000) describe granulite dredge samples with amphibole Ar-Ar ages of c. 2-2.5 Ga and Ar-Ar K-feldspar ages of 1.5-1.6 Ga (cores) with recrystallized rims dated at 0.9 Ga (FIGURE 112). Granulitic metamorphism occurred at 7 ± 1 Kbar and 750 ± 50°C and was followed by rapid exhumation resulting in the granulitic basement being incorporated into the upper continental crust where it has resided for at least the last 900 Ma based on the K-feldspar Ar-Ar data (Gardien et al., 2000).

Both Archean and Paleoproterozoic granulites of the OP and GB have been related to the Paleoproterozoic Icartian relic basement of the North Armorican Massif (NAM) (Gardien et al. (2000); Guerrot et al. (1989)) which contains gneisses dated at 2-2.2 Ga (Calvez and Vidal, 1978) (FIGURE 112). The 2-2.2 Ga gneisses of Britanny, the 1.9 Ga zircon of the granulites of the OP and the 1.5-1.6 Ga K-feldspar cores of the granulites of the GB are interpreted as having formed in one tectonothermal event (the Icartian event) at 1.8-2-2 Ga and included plutonic magmatism as well as low and high-grade metamorphism (Guerrot et al. (1989), Gardien et al. (2000)). This 1.8-2.2 Ga Icartian event (GB, OP, NAM) and the 2.7-2.8 Ga high-grade metamorphic event on the OP are similar to two of the main tectonothermal events of the West African Craton (Guerrot et al., 1989), namely the 2.8-2.9 Liberian Orogeny and the 1.8-2.15 Ga Eburnean Orogeny (Markwitz et al., 2016), suggesting that the North Iberian Archean and Paleoproterozoic basement of the GB, OP and NAM are Gondwanian relics and that the West European plate was part of the West African Craton during at least the span of timesof these events (Gardien et al., 2000).

Some granulites were recovered from an Albian-Aptian conglomerate on Le Danois Bank (DB) (Capdevila et al., 1980) (FIGURE 112) and therefore they cannot be Pleistocene ice-rafted debris (Fügenschuh et al., 2003). However, their origin as in-situ basement or as allochthonous blocks and clasts is still unclear with two hypotheses being proposed: 1) they represent an in-situ relic basement that was once the continuation of the Icartian basement (Guerrot et al. (1989), Fügenschuh et al. (2003)); or 2) they are allochthonous blocks and clasts scattered during the initial opening of the Bay of Biscay and sourced from the Icartian basement that crops out in the NAM and probably on the Armorican shelf (Gardien et al., 2000) (FIGURE 112).

Some plate reconstruction models place the GS next to the OP before continental break-up and the formation of oceanic crust in the Bay of Biscay during the Early Cretaceous (Nirrengarten et al., 2018), juxtaposing the Archean basement blocks in both areas. This supports the presence of a continuous *in-situ* Archean basement extending across the blocks and the presence of a continuous Archean-Proterozoic relic basement extending from the NAM to the GB (FIGURE 112). If in-situ, this Archean granulitic basement would probably represent a piece of Gondwana and suggests that the Rheic Suture Zone (and the Avalonian crust) would probably be located to the N-NW of MB. It would place a new

constraint point on the location of the Rheic Suture Zone which is usually only constrained by onshore data from Spain, England and Brittany.

However, the presence of a Cadomian granulite at MB (R-27), to the south of GC4, seems to go against this hypothesis. If the Archean sample is not in-situ, it could be an ice-rafted debris (IRD). A zone of preferential deposition of IRD, fed by past gyratory currents from the British, Icelandic, Greenland and Laurentide (NE Canada) ice sheets, is known to extend from offshore Newfoundland to the foot of the Goban Spur margin (Peck et al., 2007) (FIGURE 113). Sample R-25 is located at the eastern edge of this zone and could therefore be an ice-rafted debris from the Archean basement of Scotland, Greenland or Canada.

Based on geochronological data alone, both hypotheses (*in-situ* Archean basement vs IRD from a Laurentian Archean basement) are equally possible.

6.4.4 Age and provenance of the green sandstone (R-29)

The age of the youngest zircon grain (280 Ma) indicates that the sandstone is late Early Permian or younger. This is younger than the expected Devonian age based on the dominance of Devonian sandstones from the dredges and boreholes (Lefort et al., 1984). However, the maximum age is based on only one grain and would need to be confirmed by dating additional samples. The dominant zircon age group is Late Caledonian in age. This peak could suggest the presence of a Late Caledonian intrusion that would crop out in the vicinity.

6.5 AFT and AHe results

The detailed description of the AFT and AHe results is presented in ANNEX 1 (SECTION 2.1). Below is a summary and discussion of the results (FIGURE 114).

6.5.1 Thermal history of the Late Variscan granites

Based on a qualitative interpretation of the AFT and AHe results, the granite sample from MB (AFT central age of 143 Ma and AHe ages of 90-100 Ma) was exhumed after (*i.e.* Late Jurassic-Early Cretaceous) the samples from the GC4 granite (*i.e.* Late Triassic-Early Jurassic; AFT central ages of 192-222 Ma and AHe ages of 50-130 Ma) (FIGURE 114). This could be due to the rotated fault block of Menez Bihan being closer to the continent-ocean boundary (COB) than the GC4 block (the two rotated fault block tip edges are separated by 22 km, FIGURE 108) and therefore being subject to more intensive rift-shoulder uplift before crustal and lithospheric break-up at c. 112 Ma (Pérez-Gussinyé, 2013), or due to the effect of syn-rift doming as observed at other paleo-triple junctions (White and Latin, 1993), or else due to the sampling of a different part of the rotated fault block tip and fault plane (*i.e*. different sections of exhumed PAZ).

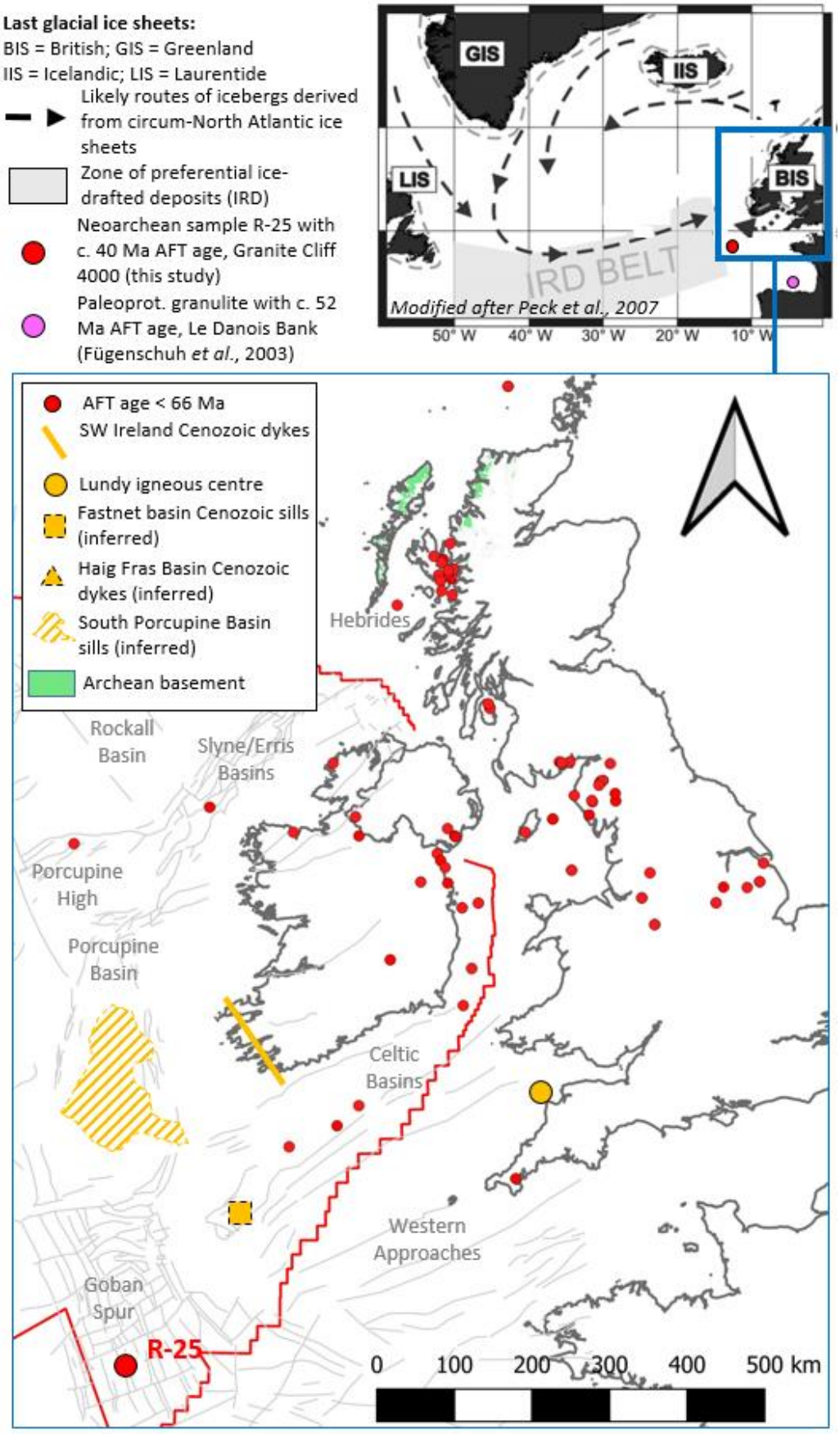

Figure 113: Maps of an Atlantic zone of preferential deposition of ice-rafted deposits (top) and of the British-Irish Isles with location of the Archean basement, the southern expression of the NAIP and the AFT samples ages younger than 66 Ma.

Sample	Age		FTA					CTL				Kinetic			AHe				
	Age	±	n	Ns	$P(\chi^2)$	Central Age		Tracks	MTL	SD	SE	Cl	Dpar	U	n	Mean eU	Age cluster?	Range of AHe ages (Ma)	
																		Raw	F_T-corrected
	Ma	*Ma*	-	-	-	*Ma*	*±1σ Ma*	-	*µm*	*µm*	*µm*	*wg%*	*µm*	*ppm*	-	*ppm*	-	*Min-**Mean**-Max*	*Min-**Mean**-Max*
R-24	297	2	39	2737	<0.01	**192**	9	291	**12.01**	2.81	0.16	0.26	1.95	45.3	5/5	103	Yes 3/5	59-**91**-173	87-**134**-136
R-25	1714	16	40	294	0.58	**42**	3	2	**13.14**	1.38	0.98	0.12	1.52	20.4	5/6	25	Yes 4/5	32-**41**-63	39-**49**-75
R-26	296	2	40	1181	<0.01	**222**	11	66	**12.86**	2.03	0.25	0.11	1.69	18.8	4/6	81	Yes 3/4	45-**84**-84	63-**109**-112
L-DR12-B21	n/a	n/a	16	1082	0.44	**212**	10	101	**12.98**	1.30	0.13	n/a	n/a	n/a	N/A	N/A	N/A	N/A	N/A
R-27	446	11	38	1709	0.01	**284**	9	152	**12.91**	1.78	0.14	0.20	2.02	20.9	0	N/A	N/A	N/A	N/A
R-28	288	1	40	1263	<0.01	**143**	6	97	**13.04**	1.67	0.17	0.08	1.74	25.3	5/6	121	Yes 4/5	10-**70**-76	14-**95**-101
R-29	n/a	n/a	8	211	0.20	**126**	10	13	**11.40**	2.18	0.60	0.11	1.66	31.0	0	N/A	N/A	N/A	N/A

Late Variscan granites

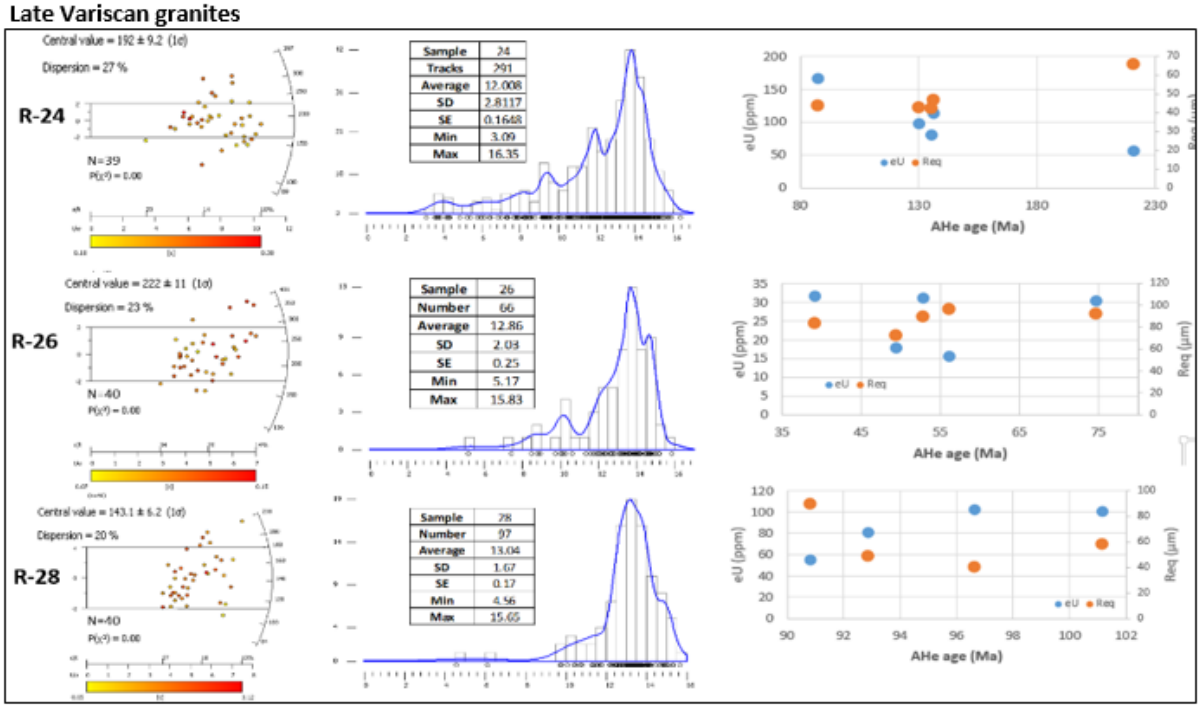

Metamorphic samples

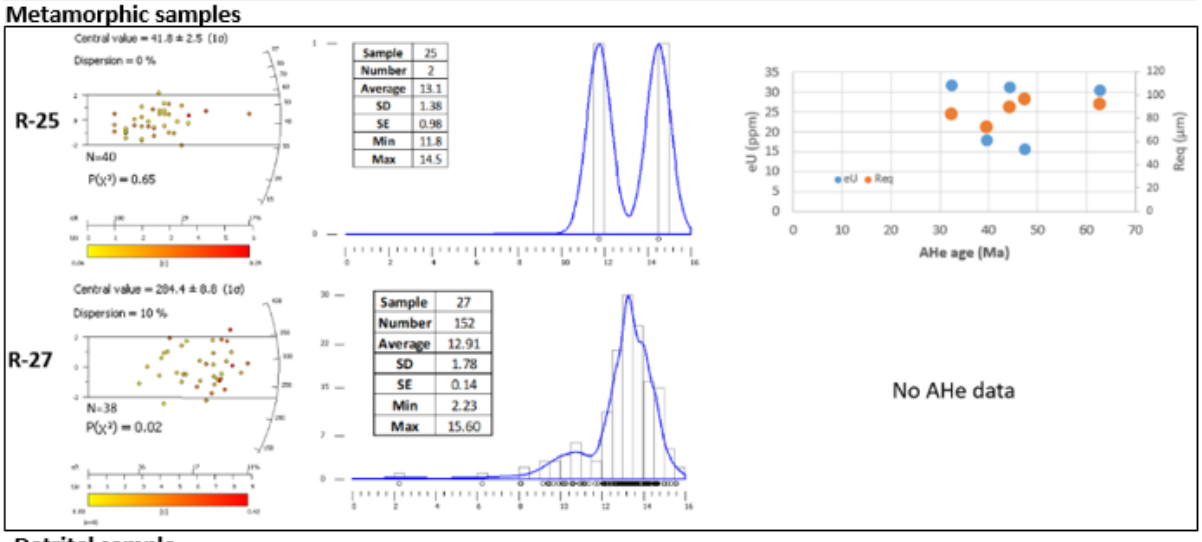

Detrital sample

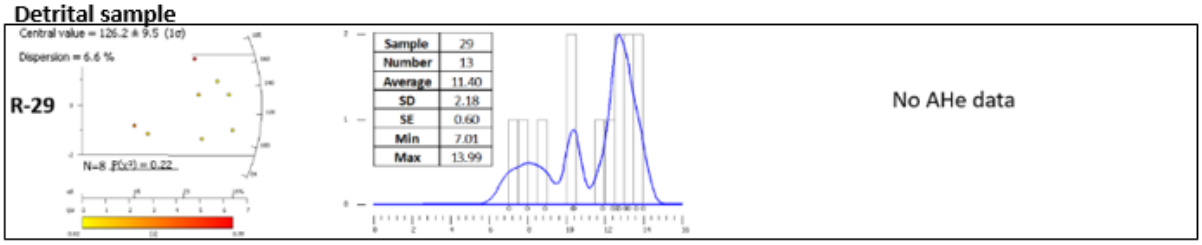

Figure 114: AFT and AHe results for the Goban Spur samples (R-24 to R-29).

6.5.2 Thermal history of the metamorphic samples

Both metamorphic samples (R-25 and R-27) have very different AFT ages than the granite samples nearby. At GC4, sample R-25 cooled down through the PAZ during the Eocene (FIGURE 114) while being very close (c. 1.5 km, FIGURE 108) to samples who cooled down through it during the Late Triassic-Early Jurassic (R-24 and R-26). At MB, sample R-27 cooled down during the Late Carboniferous-Early Permian (FIGURE 114) while being very close (largest theoretical distance between two samples is 5 km, FIGURE 108) to a sample that cooled down during the Late Jurassic-Early Cretaceous (R-28). Hypotheses that could explain this discrepancy are explored below in SECTION 6.6.5.

6.5.3 Thermal history of the detrital sample

For sample R-29, there are not enough AFT ages to derive reliable thermal history information from this sample because the individual FT age dispersion is large. The young AFT central age could either be the result of an old sandstone (e.g. Devonian) that was buried and then exhumed during the Mesozoic, possibly with partial annealing of tracks inherited from the source or else a younger sandstone (e.g Cretaceous or even Tertiary) that contain AFT ages inherited from the sources. The shape of the confined track length distribution could help discriminate between a detrital vs reset sample but for this sample there are only 13 confined track lengths which is not enough to be used for such purpose FIGURE 114).

6.6 Thermal history modelling

6.6.1 Input data

The samples will be modelled using the following input data:

- R-24: 39 AFT ages, 291 lengths and three AHe ages.
- R-25: 40 AFT ages, no lengths and five AHe ages
- R-26: 40 AFT ages, 66 lengths and three AHe ages
- R-27: 38 AFT ages, 152 lengths and no AHe ages
- R-28: 40 AFT ages,143 lengths and four AHe ages

R-29 will not be modelled since there are not enough AFT ages to obtain reliable thermal history information.

6.6.2 Initial and final time-temperature constraints

6.6.2.1 Final conditions: Present-day temperature of sample

All samples reside at water depths below 2500 m and therefore have a present-day temperature of 3 ± 1°C.

6.6.2.2 Initial conditions - Emplacement age and temperatures

Granitic samples R-24, R-26 and R-28

The crystallisation age of the GC4 granite is 296.7 ± 1.1 Ma (FIGURE 110) while for the MB granite it is 288.3 ± 1.4 Ma (FIGURE 109). The closure temperature for apatite U/Pb ages is c. 375-600°C (Kirkland et al., 2018) but for the sake of simplification and to reduce the size of the prior time-temperature domain of the models, the temperature at the time of crystallisation is set at 140°C (*i.e*. high enough for complete annealing of any fission tracks) (FIGURE 115).

Metamorphic samples R-25 and R-27

The apatite crystallisation age of sample R-25 is 1714 Ma (FIGURE 111), which is much older than the oldest AFT grain age in the sample (grain 29 at c. 97 Ma). Rather than using the crystallisation age (which would create a prior time-temperature box with unconstrained results between 1714 Ma and c. 100 Ma), it is preferable for this sample to let the initial time-temperature point be unconstrained. For the granulite sample R-27, the apatite crystallisation age is 446 ± 11 Ma (Late Ordovician) which can be used as the initial time constraint while the temperature is set at 140°C (for the same reason as the granitic samples) (FIGURE 116).

6.6.3 Intermediate constraints

Since the samples do not come from a borehole, no intermediate constraints based on stratigraphy can be inferred. However, Auffret et al. (1979a) mentions the presence of a Late Jurassic (Kimmeridgian-Tithonian) clast in dredge CH67-07 (on GC4), which is less than 1 km away from dredges 8 and 10. The clast is a pinkish white intrabiomicrite limestone with a microfacies indicating an intertidal/lagoonal depositional environment. This Late Jurassic limestone was interpreted as resting on top of the granitic basement and a part of a larger, Late Jurassic-Early Cretaceous, intertidal to upper bathyal, carbonate platform with a Thetyan affinity (with remnants now found all around the Bay of Biscay) (Auffret et al., 1979a).

A model could be run to test this hypothesis that the granitic basement was already cropping out during the Late Jurassic to form the basement of a carbonate platform. This hypothesis can be modelled using a time-temperature constraint defined as the time of deposition of the limestone, *i.e.* Kimmeridgian-Tithonian (151.15 ± 6.15 Ma), and as surface temperatures (10 ± 10°C). This constraint only applies to sample R-24 and R-26 (FIGURE 115).

a) Prior information and MCMC chain parameters

Categories		R-24	R-26	R-28
Prior info.	Time (± same, Ma)	197.1	224.43	144.85
	Temp. (°C)	70 ± 70		
	Max dT/dt, Reheating Gradient offset Offset	1000 °C.My, Yes n/a n/a		
MCMC chain	Burn-in Post-burn-in Thinning	100,000 100,000 1		
Prop. move	Time/Temp Offset Resample/Reject Reject complex	30 / 28 n/a Resample Yes		

b) Scenario names and characteristics

Sample	Scenario	Inputs	Constraints	tT points
R-24 R-26	0a 0b	All	None	Low (simple) High (complex)
	1a 1b	All	1	Low (simple) High (complex)
R-28	0a 0b	All	None	Low (simple) High (complex)

c) Time-temperature constraints

Constraints	R-24	R-26	R-28
Initial t Initial T	296.7.± 1.1 Ma 140 ± 0 °C		288.3.± 1.4 140 ± 0 °C
Interm t Interm T	151.15 ± 6.15 10 ± 10 °C		n/a
Final t Final T	0 Ma 3 ± 1 °C		

d) Model parameters and constraints

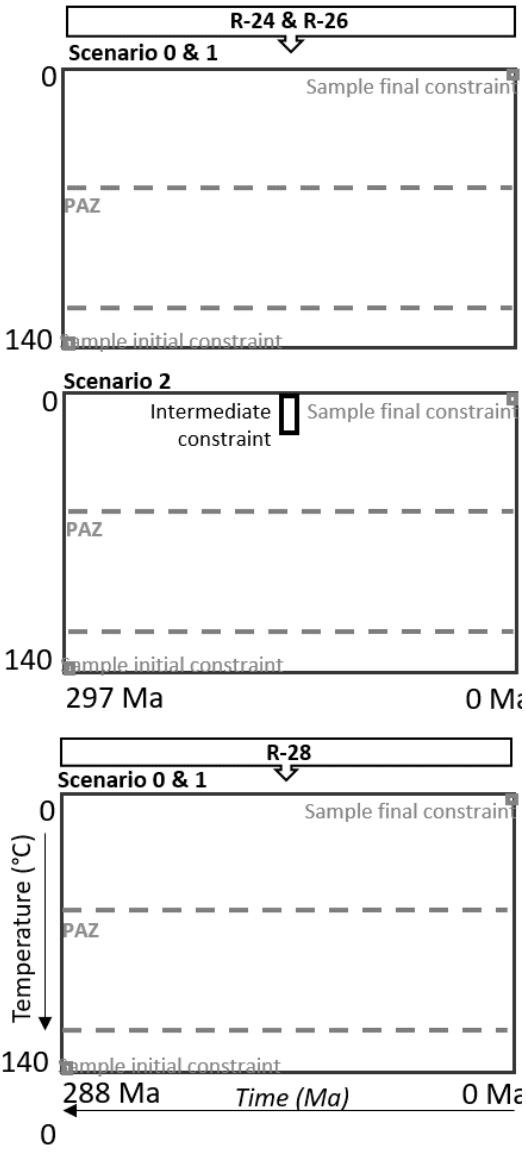

Figure 115: Thermal history modelling parameters for Late Variscan granite samples R-24, R-26 and R-28.

6.6.4 Prior box and run parameters

The time axis of all prior time-temperature boxes is defined by the initial time constraint (R-24, 26, 27, 28) or by the oldest AFT grain age for unconstrained samples (R-25). The temperature axis is defined as 70 ± 70°C for all samples. Unless stated otherwise, all run parameters are the default values and each model consist of 100,000 burn-in iterations and 100,000 post-burn-in iterations (FIGURE 115 AND FIGURE 116).

a) Prior information and MCMC chain parameters

Categories		R-25	R-27
Prior info	Time (± same, Ma) Temp. (± same °C)	47.4 70	282.4 70
	Max dT/dt Reheating Gradient offset Offset	1000 °C.My, Yes n/a n/a	
MCMC chain	Burn-in Post-burn-in Thinning	100,000 100,000 1	
Proposed move	Time/Temp/Offset Resample/Reject Reject complex	30 / 28 / n/a Resample Yes	

b) Scenario names and characteristics

Sample	Scenario	Inputs	Constraints	tT points
R-25	0	All	None	Low (simple)
R-27	0a 0b	All	None	Low (simple) High (complex)

c) Time-temperature constraints

Categories	R-25	R-27
Initial t Initial T	n/a n/a	446 ± 11 Ma 140 ± 0 °C
Final t Final T	0 Ma 3 ± 1 °C	

d) Model parameters and constraints

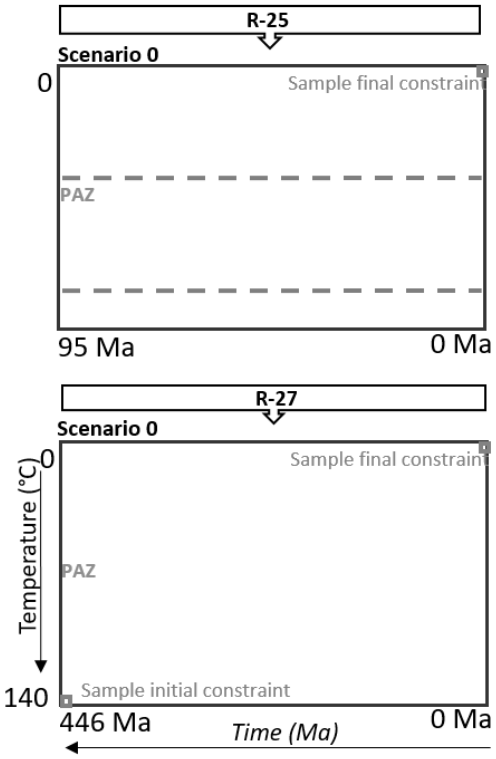

Figure 116: Thermal history modelling parameters for Late Variscan granite samples R-25 and R-27.

6.6.5 Modelling results

All thermal histories for each scenario, together with the main result plots can be consulted in ANNEX 1 SECTION 2.1.

6.6.5.1 Sample R-24 (Late Variscan granitoid, GC4)

Scenario 0: All input data

This scenario is run to evaluate the thermal history information contained in the thermochronological data alone, without the intermediate constraint. The complex expected model demonstrates that the thermal history is unconstrained before c. 220-250 Ma. The expected simple and complex models show a thermal history that can be summarized in four phases (FIGURE 117 AND FIGURE 118):

- 220-250 Ma to 155-170 Ma (c. Triassic to Mid-Late Jurassic): Moderate cooling from c. 90°C to 60°C
- 155-170 Ma to 135-140 Ma (c. Mid-Late Jurassic to Valanginian): Small heating a few degrees
- 135-140 Ma to 90-100 Ma (c. Valanginian to Albian-Cenomanian): Moderate cooling from c. 60°C to near-surface temperatures
- 90-100 Ma to 0 Ma (Late Cretaceous to now): The sample remained at near-surface temperatures (<30°C).

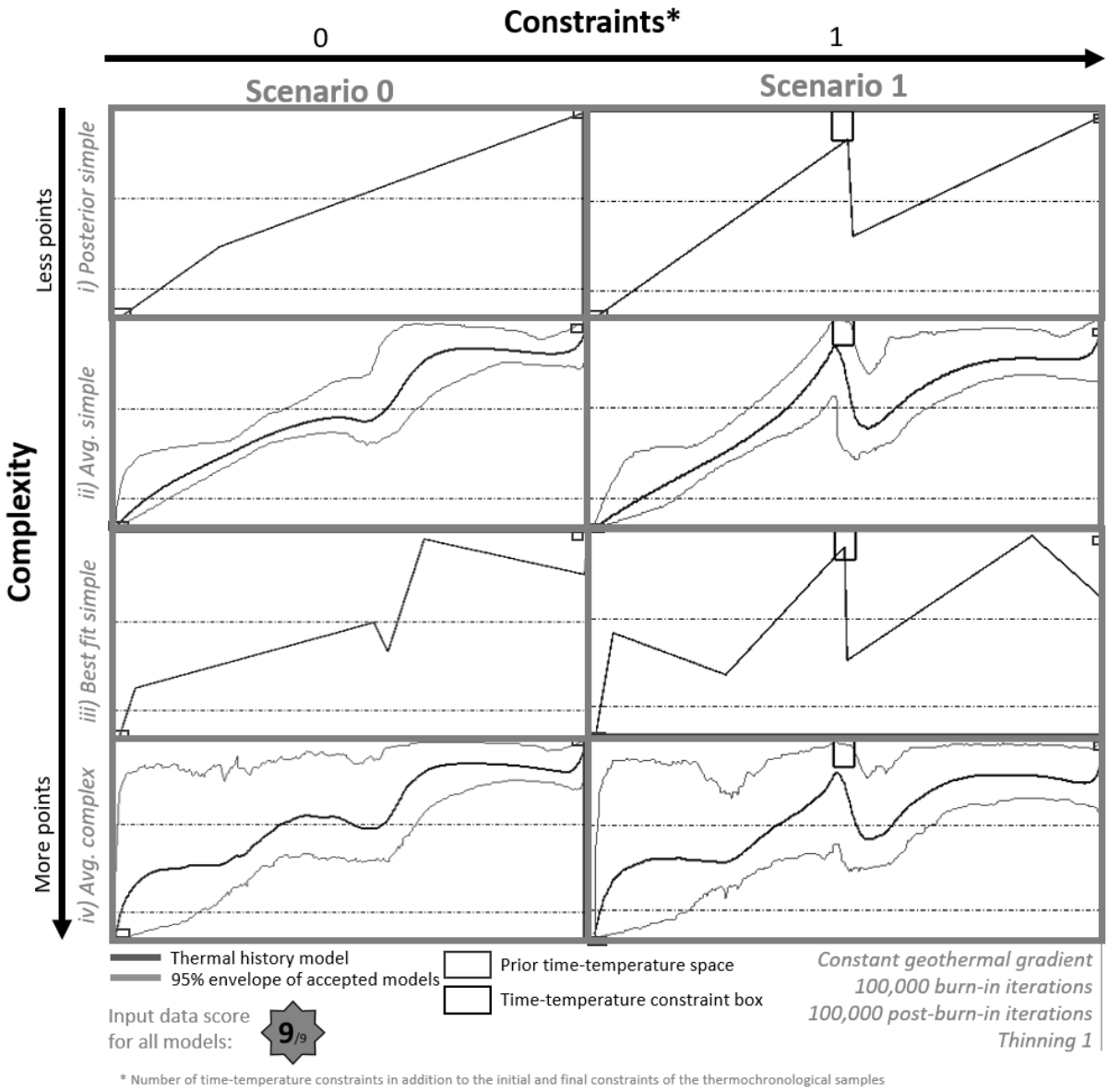

Figure 117: Thermal history modelling results for sample R-24 (model matrix).

These models yield modelled AFT ages and track length distributions that match well the measured data. However, they all yield modelled AHe ages younger than the measured one (c. 60 Ma instead of c. 90 Ma, FIGURE 118). The poor match between modelled *vs* measured AHe ages is probably caused by the track length distribution, since both of them influence the cooler part of the thermal history. The simple and complex posterior models also show that a simple monotonic cooling from c. 300 Ma to 0 Ma also yield modelled data in good agreement with the measured values.

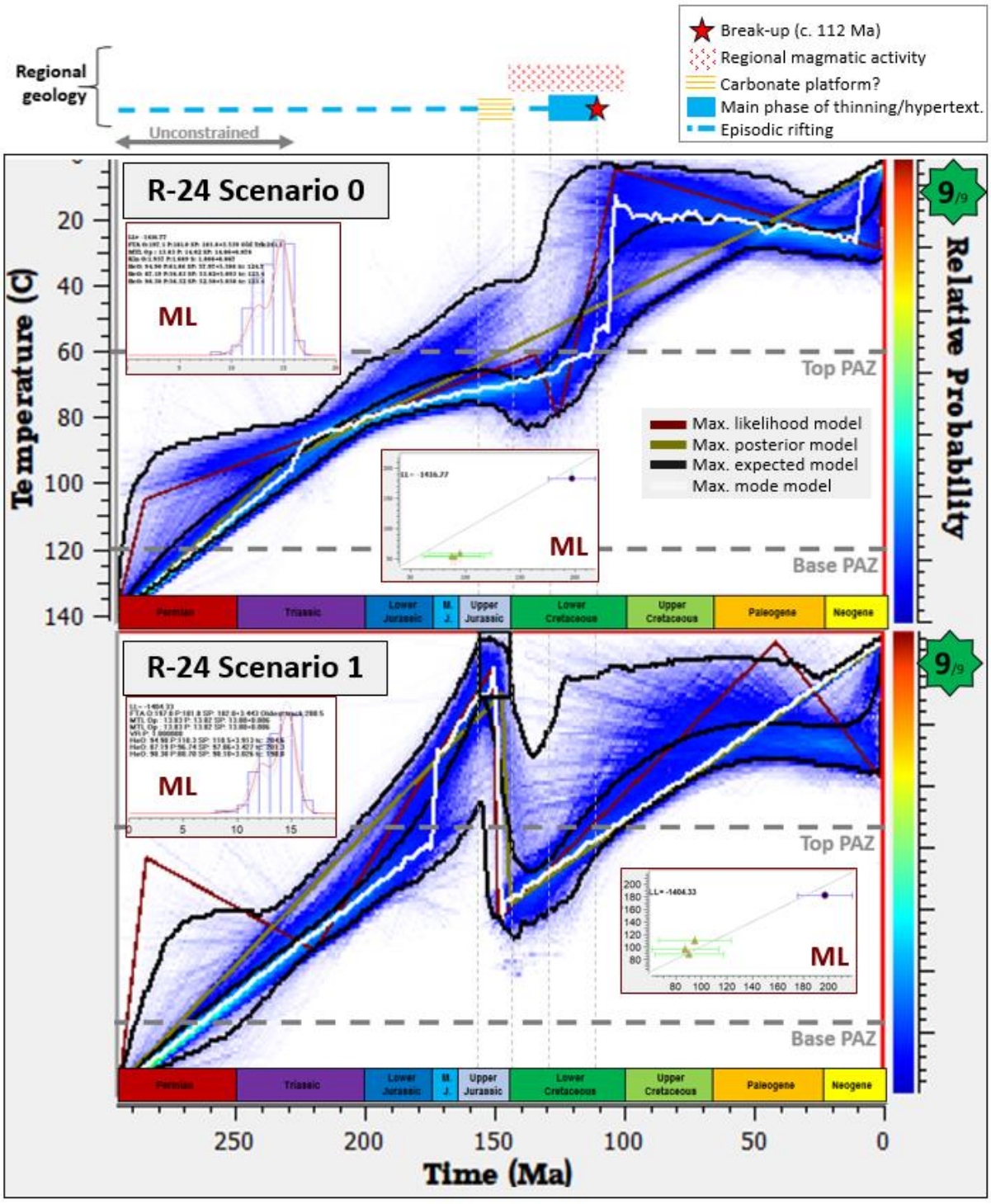

Figure 118: Thermal history modelling results (simple models for scenarios 0 and 1) for sample R-24 with regional geological context.

Scenario 1: All input data with the intermediate constraint

This scenario is run to evaluate the thermal history information contained in the thermochronological data together with the intermediate constraint derived from the Late Jurassic limestone clast. This scenario yields a very different thermal history with a monotonic cooling to surface temperature from c. 220 Ma to the Kimmeridgian (deposition of the Late Jurassic limestone), followed by a very rapid

heating to c. 90°C within 0-15 Ma. The sample then cools down to the present-day temperature with a decelerating rate of cooling until 0 Ma, except for the last c. 10 Ma when the cooling rate is much higher (FIGURE 118).

Discussion

The thermal history from scenario 0 fits well with the regional geological history. The cooling from c. 120°C to 0°C spans the Triassic to the end of the Early Cretaceous, which corresponds to the episodic rifting of the continental margin, while the main cooling episode (with the highest cooling rate of c. 3°C.Ma^{-1}) corresponds to the main phase of rifting and hyperextension (Barremian-Aptian) (FIGURE 118) and therefore must be primarily driven by rift-related exhumation processes. The period of heating between the Middle Jurassic and early Early Cretaceous could be due to either burial or an increase in paleogeothermal gradient or a combination of both. In this thermal history, any Jurassic or Early Cretaceous sediments deposited on top of GC4 would have been eroded in the subsequent Barremian-Aptian exhumation, suggesting that the clast of Upper Jurassic limestome is allochthonous. A higher geothermal gradient could be caused by the thinning of the lithosphere due to rifting which led to the phase of pre-break-up Early Cretaceous magmatism (FIGURE 118 AND DISCUSSION IN SECTION 7.2.2).

The thermal history from scenario 1 implies a very rapid heating of c. 80°C at c. 140-150 Ma followed by cooling during the rest of the Cretaceous. While not implausible, based on the known regional geology, this thermal history is less likely than the previous one. Consequently, it is hypothesized that the clast of Late Jurassic limestone is allochthonous and maybe come from a basement high which would have ceased its exhumation during the Jurassic before GC4, possibly because located further away from the continent-ocean boundary and therefore not being affected by the final exhumation just before lithospheric break-up.

To estimate the amount of exhumation associated with the Barremian-Aptian cooling episode of scenario 0, the paleogeothermal gradient has to be estimated. The present-day geothermal gradient at GC4 can be derived from measurements made in the DSDP boreholes. Gradients of 22.5, 27.2 and 54.9°C.km^{-1} were found in borehole 549, 548 and 550 (Foucher et al., 1985). From a crustal architecture point of view, site 550 is the best equivalent to GC4 (hyperextended crust, FIGURE 108), however, the high geothermal gradient at site 550 is considered anomalous (Foucher et al., 1985). However, at the time of hyperextension the geothermal gradient was probably higher than at the present-day. Using a compilation of geothermal gradient from the Red Sea and East African rift valley (Macgregor, 2018) as a proxy for the Early Cretaceous gradient at GC4, a minimum and maximum value of 20-80°C.km^{-1} can be estimated. At 20°C.km^{-1}, a cooling of c. 60°C corresponds to 3 km of erosion, while at 80°C.km^{-1} it

would correspond to only 750 m. Therefore, during the main phase of crustal thinning and hyperextension, an exhumation of 0.75-3 km occurred at GC4.

The research dredges sampled the stiff cliff on the SW side of the GC4 which represents the footwall of the major fault that separates the GC4 rotated fault block from the MB rotated fault block (see bathymetry and seismic section in FIGURE 108). Rather than representing subaerial erosion only, the Barremian-Aptian exhumation also probably represents the tectonic exhumation due to block tilting and exposure of the footwall (Stockli, 2005).

6.6.5.2 Sample R-25 (Archean granulite? GC4)

Scenario 0: All input data

This scenario is run to evaluate the thermal history information contained in all available thermochronological data. The modelling shows that the sample cooled down very quickly (a few millions of years maximum) from temperatures >120°C to near-surface temperatures at some point between 38-45 Ma (Lutetian-Bartonian or Middle Eocene) (FIGURE 119). The modelled and measured AFT age match, but only one predicted AHe age matches the measured AHe age, with the three other predicted AHe ages slightly younger than the measured ages.

Discussion

The difference in AFT/AHe ages and thermal histories between this sample and the granitic samples R-24 and R-26 can be explained by:

1. The sample being *in-situ* but coming from different elevations (= depths in marine sampling), resulting in sampling a different part of the exhumed PAZ/PHeRZ.
2. The sample being *in-situ* but having been affected by a localized thermal event (e.g. magmatism).
3. The sample not being *in-situ* and representing the thermal history of basement somewhere else on the continental margin. The reverse hypothesis (R-25 *in-situ* but not R-24 and R-26) cannot be made since the Late Variscan granitic clasts are the dominant lithology in the dredges (Auffret et al., 1979a), and very likely represent *in-situ* basement.

Hypothesis 1: Variable depths

Even a large difference in AFT ages such as between samples R-25 and R-24-26 can be explained by the first hypothesis. For example, the Sca Fell vertical profile in Northern England yielded AFT ages >300 Ma in the upper part of the profile and AFT ages as young as 58 Ma in the lower part of the profile (Green, 2002). The profile is less than 1 km in height and the AFT ages jump from 333 Ma to 65 Ma with only an altitude difference of c. 340 m. Łuszczak et al. (2017) demonstrated that such an age-elevation profile could be caused by the blanketing effect of sediments above high heat-generating plutons, resulting in localized high geothermal gradients without the need for an elevated basal heat flow.

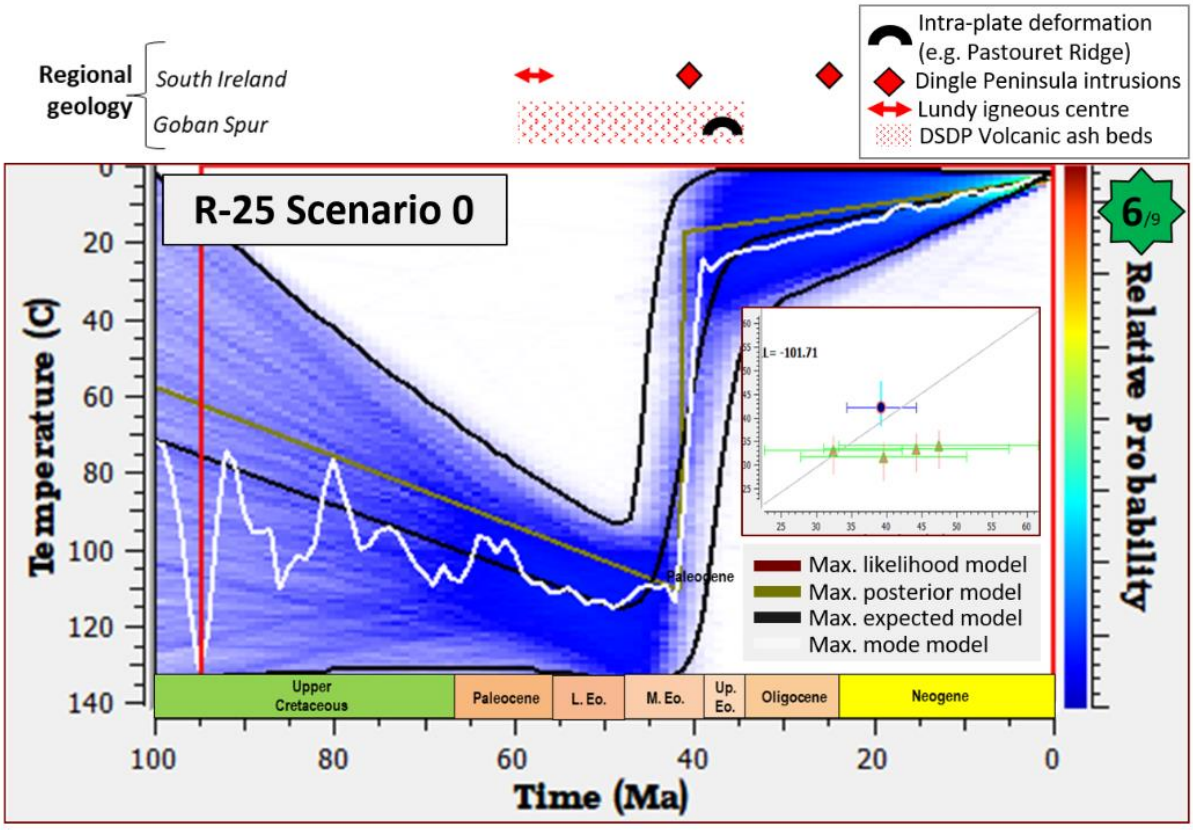

Figure 119: Thermal history modelling results for sample R-25 with regional geology context.

According to the PAD-GSI bathymetric data and the dredge location data from Auffret et al. (1979a), the dredges sampled seabed depths between 3200 and 4200 m, so a maximum depth difference of 1000 m. Based on the results from Northern England, such a depth difference could potentially result in the large AFT age difference seen in the samples. In this case, the metamorphic sample R-25 would have to come from the bottom of the cliff while the granite samples would have to come from the top part of it, and a Middle Eocene erosional event would have had to affect the sediments above the basement only (and not remove the basement itself) (FIGURE 120).

Intra-plate deformation occurred during the Late Cretaceous to Late Eocene due to the relative motion of the African and Eurasian plate, with the main phase occurring during the Eocene (Sibuet et al., 1984). In the Goban Spur, the Pastouret Ridge, SW of the Pendragon Escarpment, is interpreted as being caused by the compressional rejuvenation of an oceanic fracture zone (Sibuet et al., 1984). It is possible that such intra-plate compression might have caused a change in the seabed relief and bottom water circulation that could have led to the erosion of parts of the Goban Spur.

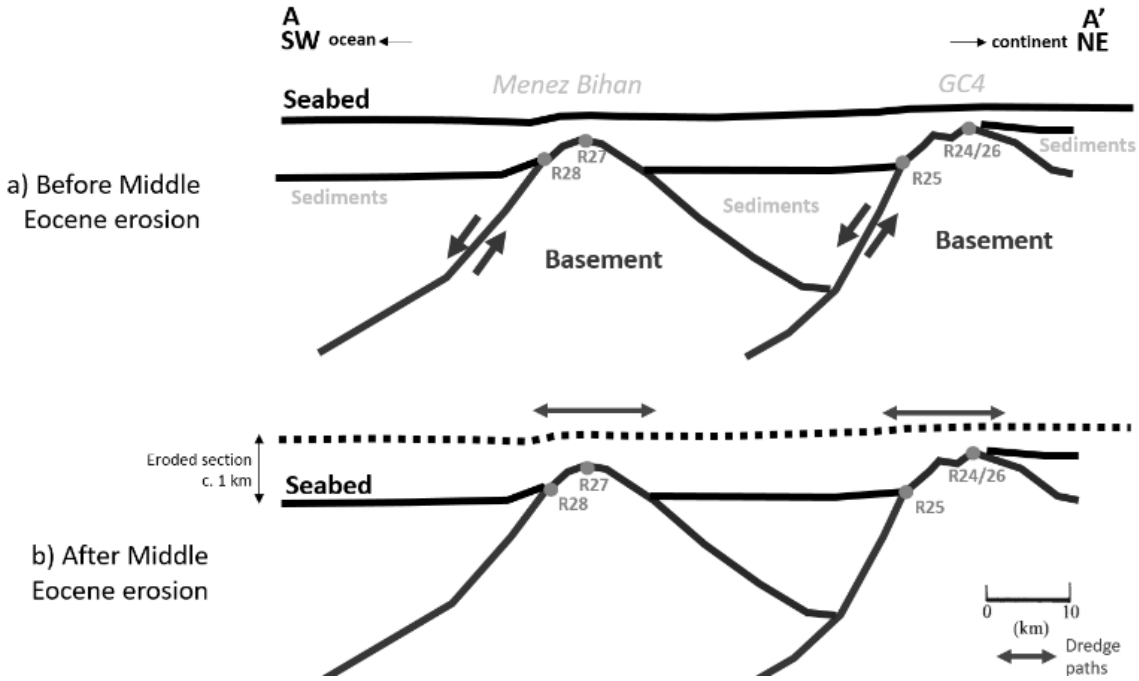

Figure 120: Middle Eocene erosion hypothesis.

Since sample R-24 could not have experienced temperatures greater than 40°C during the Middle Eocene (FIGURE 118) and since sample R-25 needs to have experienced temperatures greater than 120°C at the same time (FIGURE 119), a difference of minimum 80°C would have been required to reset sample R-25 but not sample R-24. With a depth difference of 1 km, this would have required a localized paleogeothermal gradient of 80°C.km^{-1}.

Such a high geothermal gradient could be produced by either a blanket effect over a heat-producing granite batholith (similar to the Lake District batholith, Łuszczak et al. (2017)) or else a localized heating due to magmatic activity, which is discussed in the next section.

Hypothesis 2: Localized magmatism

As discussed in section 6.2.4.2, the only evidence of magmatic activity in the Goban Spur area are ash beds of Late Paleoene to Late Eocene age, which could have originated from further away and do not necessarily indicate magmatic activity within the Goban Spur crust. The closest Cenozoic intrusive and extrusive igneous rocks are (see locations on FIGURE 113):

- inferred Paleogene sills in the Fastnet Basin (Caston et al., 1981),
- an inferred Cenozoic dyke system in the Haig Fras Basin (Tate and Dobson, 1988),
- inferred sills in the south Porcupine Basin (Horni et al. (2017), Gagnevin et al. (2017)),
- Cenozoic dykes in the SW of Co. Kerry and Co. Cork (Morris, 1974), including two of them dated at 25 and 42 Ma (Horne and MacIntyre, 1975),
- an igneous complex on Lundy Island (c. 57-60 Ma, Charles et al. (2017)).

Since the Paleogene North Atlantic Igneous Province seems to extend at least as far as the southern part of the Porcupine and Fastnet basins, it is not impossible that some minor magmatic activity

occurred in the Goban Spur. This could have led to localized heat flow that reset the AFT/AHe ages of sample R-25.

Hypothesis 3: Sample is not in-situ

The third hypothesis is that the sample is not *in-situ*. As discussed above (section 6.4.3), R-25 might be an ice-rafted debris associated with the zone of preferential deposition that extends from Newfoundland to the foot of the Goban Spur margin and which was sourced from the British, Icelandic, Greeland and NE Canadian ice sheets (Peck et al., 2007). In that case, the sample would have to come from an area with both Archean basement and Paleogene AFT/AHe ages. The closest location that matches both conditions is the Hebrides and NW coast of Scotland where the Archean Lewisian basement crops out and where some studies yielded Paleogene AFT/AHe ages due to contact with a Paleogene igneous centre heat aureole (Lewis et al., 1992b) (FIGURE 113), although Paleogene AFT ages are also known in the Archean basement on the eastern coast of Greenland (Hansen and Brooks, 2002) and could therefore also be a source.

Based on this new piece of information, the granulite with a 53 Ma AFT central age on Le Danois Bank from the study of Fügenschuh et al. (2003) could possibly also be an IRD rather than reflecting Pyrenean thrusting activity. More broadly, it raises questions about the autochthonous character of the Archean and Paleoproterozoic granulitic samples found around the Bay of Biscay and that have been interpreted as pieces of a relic basement once attached to the Icartian basement of the North Armorcian Domain in Brittany (France) (Guerrot et al. (1989), Gardien et al. (2000), Fügenschuh et al. (2003)).

Based on the low likelihood of both NAIP magmatism and *in-situ* Archean basement at GC4 and on the proximity of R-25 to a zone of IRDs partially sourced from zones with known Archean basement and Paleogene AFT ages, the third hypothesis is judged the most likely for now, although the first two hypotheses cannot be ruled out completely.

6.6.5.3 Sample R-26 (Late Variscan granite, GC4)

Scenario 0: All input data

This scenario is run to evaluate the thermal history information contained in the thermochronological data alone, without the intermediate constraint. The modelling solution is bimodal with two very different thermal histories (FIGURE 121 AND FIGURE 122):

1. The first thermal history is a near-monotonic cooling from c. 300 Ma to 0 Ma (e.g. the simple posterior model).
2. The second thermal history is a rapid cooling to near-surface temperatures from c. 300 Ma to 220-250 Ma, followed by a heating episode to 90-100°C from 220-250 Ma to 180-210 Ma, followed by a cooling episode to near-surface temperatures from 180-210 Ma to 130-170 Ma,

followed by a gentle heating until 10 Ma and concluded by a cooling to surface temperatures in the last 10 Ma (e.g. the simple likelihood model).

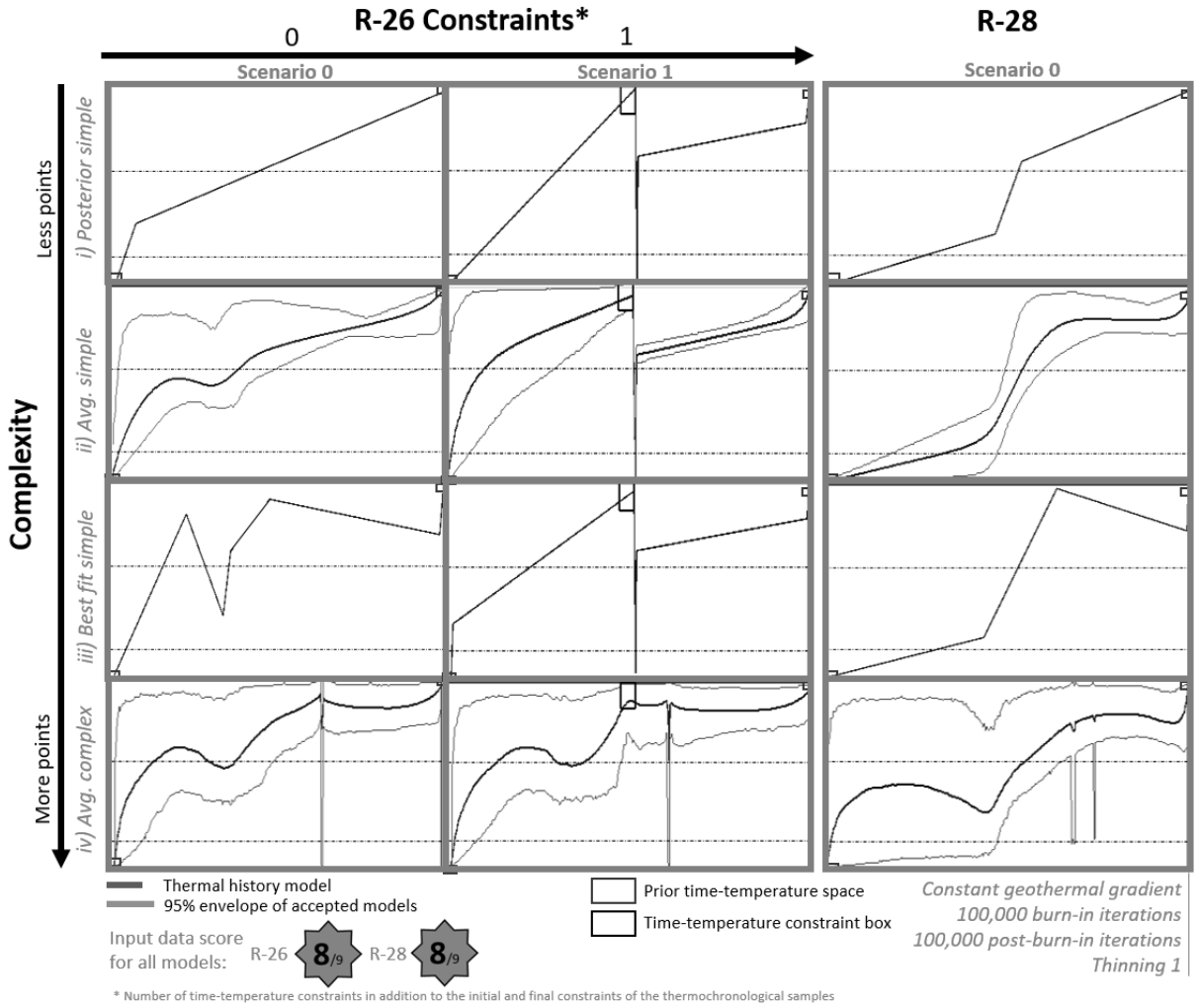

Figure 121: Thermal history models for samples R-26 and R-28 (model matrix).

Both histories yield predicted values that match the measured values. The complex model also has a heating 'spike' at c. 110 Ma which is likely caused by the cluster of AHe ages at that time. However, this spike does not improve the predicted values significantly.

Scenario 1: All input data with intermediate constraint

This scenario is run to evaluate the thermal history information contained in the thermochronological data together with the intermediate constraint derived from the Late Jurassic limestone clast. This scenario yields a simple model with a thermal history which is unrealistic while the complex model yields a thermal history similar to scenario 0.

The thermal history with a monotonic cooling history implies continuous erosion from the Permian to the present-day, which is not a plausible hypothesis for the tip of a Mesozoic rotated fault block that remained submerged under water since probably the Late Cretaceous (De Graciansky et al., 1985a).

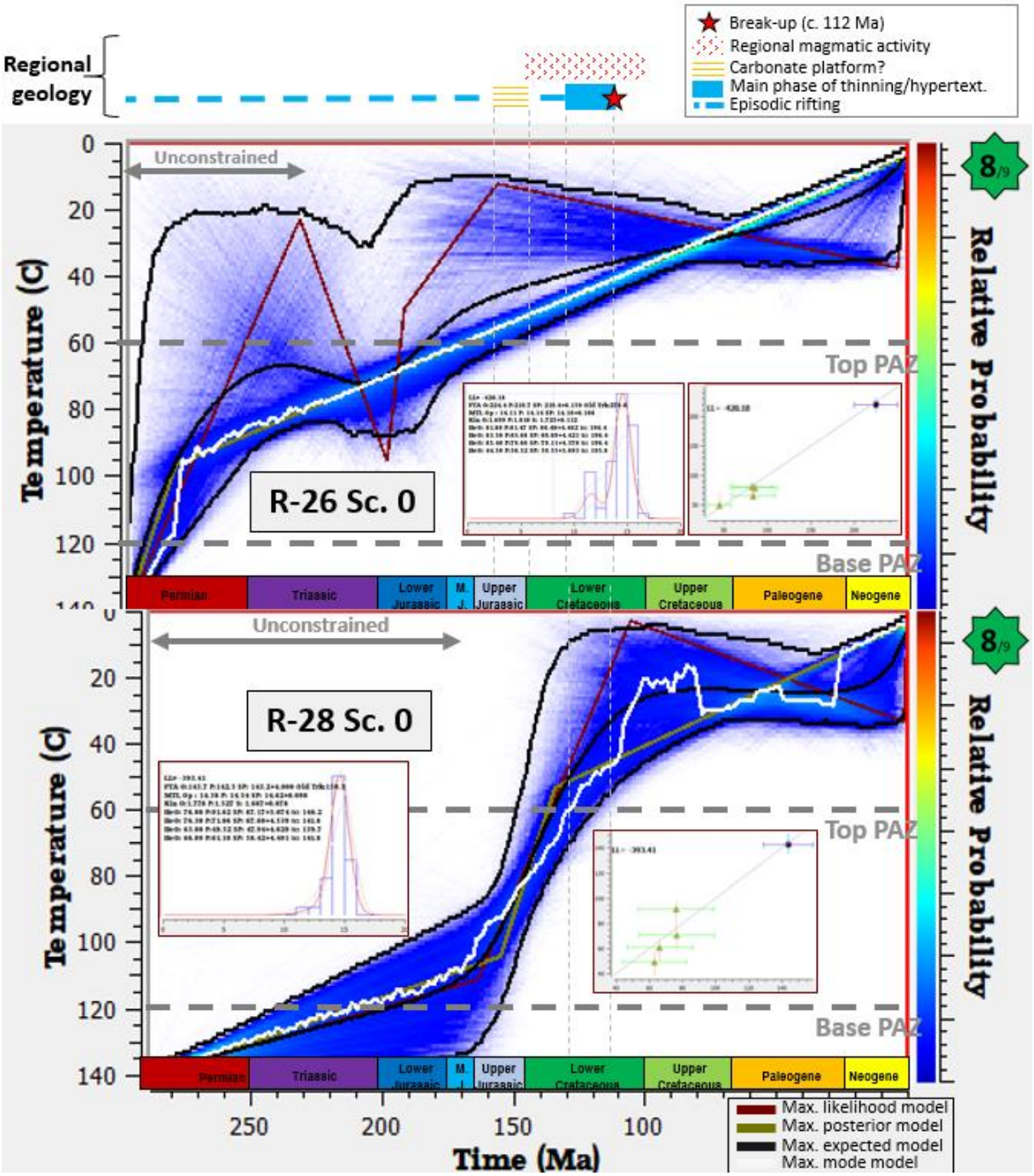

Figure 122: Thermal history results for Late Variscan granite sample R-26 (GC4) and R-28 (MB).

The thermal history with a Permian and Early-Middle Jurassic cooling and Triassic heating is also unlikely since it would imply that this sample was already near the surface during the Jurassic and did

not experience subsequent erosion during the Early Cretaceous main phase of rifting and hyperextension.

6.6.5.4 Sample R-27 (Granulite, MB)

Scenario 0: All input data

This scenario is run to evaluate the thermal history information contained in the thermochronological data alone, without the intermediate constraint. The complex expected model demonstrates that the thermal history is unconstrained before c. 320 Ma. The simple models yield a thermal history characterized by monotonic cooling until c. 100 Ma. The sample then remained at surface temperatures between 100 Ma and 0 Ma, with possible heating until 10 Ma followed by rapid cooling in the last 10 Ma (FIGURE 123).

Discussion

The thermal history reflects the protracted period of rifting from the Permian-Triassic until crustal and lithospheric break-up at the end of the Aptian. The lack of AHe data precludes obtaining a more refined thermal history. The episode of rapid cooling in the last 10 Ma must be constrained by the track length data, in particular a lack of long track lengths that would be expected if the Neogene cooling was not there (Vrolijk et al., 1992b). To reach temperatures of c. 40°C at 10 Ma as seen in the thermal history, the sample would have had to be buried under 1.2 to 1.9 km of sediments (assuming a seabed temperature of 3°C and a geothermal gradient of 20 to 30°C, see discussion in section 6.6.5.1). There is no evidence of such a large erosion in this area of the Goban Spur and therefore this Neogene cooling event is likely an artefact caused by the annealing model.

6.6.5.5 Sample R-28 (Late Variscan Granite)

Scenario 0: All input data

The complex expected model demonstrates that the thermal history is unconstrained before c. 170 Ma. All models show a unique thermal history characterized by a cooling from c. 120°C to surface temperatures from c. 170 Ma to c. 110 Ma (Middle Jurassic to end of Aptian). The sample then remains at surface temperatures (< 40°C) between 100 Ma and 0 Ma, with a possible small Neogene cooling event (FIGURE 121 AND FIGURE 122).

Discussion

The thermal history modelling indicates that sample R-26 was still deeply buried until the Middle Jurassic and experienced rapid exhumation (c. 2°C.Ma^{-1}) from the Middle Jurassic until the end of the Early Cretaceous. As for the previous samples, there is no evidence of a large Neogene erosion in this area of the Goban Spur and therefore the Neogene cooling event is likely an artefact caused by the

annealing model responding to a lack of long track tracks in the track length distribution by keeping the sample within the PAZ until very recently.

6.6.6 Discussion

6.6.6.1 Early Cretaceous rotation and exhumation of the Menez Bihan and GC4 fault blocks

Sample R-24 (GC4) and R-28 (Menez Bihan) show that the two rotated blocks might have shared a common exhumation history from the Early Cretaceous until the present-day but a different one before Early Cretaceous times (FIGURE 124 AND FIGURE 125).

The Early Cretaceous cooling of c. 60°C corresponds to exhumation of 750 to 3000 m of sediments (depending on the paleogeothermal gradient estimated at 20 to 80°C.km^{-1}, see section 6.6.5.1). The similar structural characteristics of the two rotated fault blocks (see cross section and bathymetric map in FIGURE 108) and the shared Early Cretaceous thermal history (FIGURE 124) points towards a synchronous rotation of the two blocks during the Early Cretaceous and probably during the main phase of rifting and hyperextension during the Barremian-Aptian. Consequently, the half-grabens created by the rotation of the fault blocks was likely filled by Early Cretaceous sediments, in particular Barremian-Aptian sediments.

The models seem to show the exhumation continuing until the end of the Albian, so possibly a few millions of years after lithospheric break-up and the start of post rift thermal subsidence. Although the resolution of the thermal history models is low, this might indicate that the crests of the rotated fault blocks might have remained above sea water for a few millions of years after the initiation of subsidence, resulting in continued subaerial erosion until they became drowned, probably at the start of the Late Cretaceous.

6.6.6.2 Different pre-Cretaceous thermal histories

Before the Early Cretaceous, the two blocks seem to have experienced a different thermal history. The MB block was exhumed during the Middle and Late Jurassic (possibly before but it is unconstrained by the thermochronological data) while the GC4 block experienced no exhumation and on the contrary possibly experienced a small amount of burial.

The different thermal histories might indicate a difference in tectonic settings during the Jurassic. For example, doming centred at the future location of the continent-ocean boundary (*i.e.* SW of MB) could have resulted in the uplift and erosion of MB while not affecting GC4 which is 30 km further to the NE, or MB might have acted as a horst during the Jurassic while the Granite Cliff 4000 might have acted as a graben.

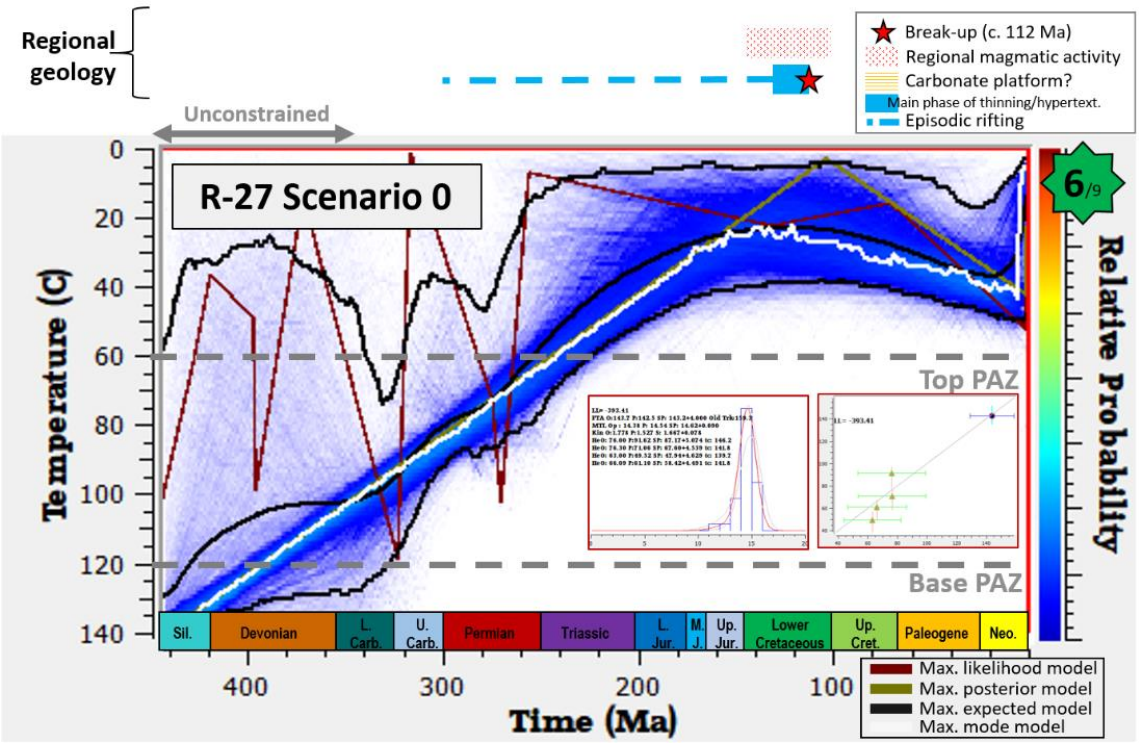

Figure 123: Thermal history modelling results for sample R-27 with regional geology context.

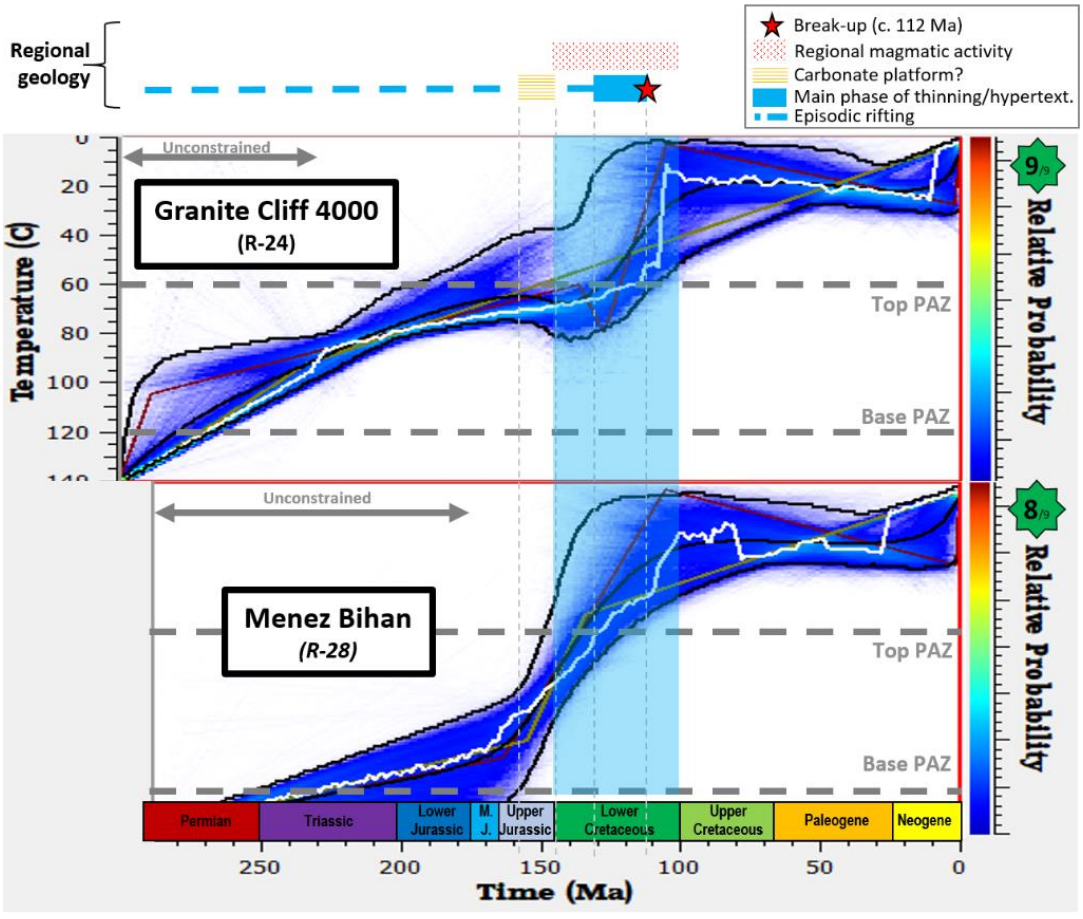

Figure 124: Comparison of the thermal histories of samples R-24 (Granite Cliff 4000) and R-26 (Menez Bihan).

However, the samples could also come from different depths on the two different dredge paths and therefore represent a different portion of the exhumed PAZ/PHeRZ, which could partly explain apparent differences in the thermal histories while still sharing a common exhumation history.

6.6.6.3 Enigmatic Eocene thermal event

The Archean metamorphic rock from Granite Cliff 4000 could either represent:

- an indicator of long distance ice-rafted debris coming from probably the Hebrides in Scotland
- the first indicator of localized elevated heat flow in the area during the Eocene, probably caused by the NAIP magmatism

6.6.6.4 Regional correlation

The results of the thermal history modelling are summarized in FIGURE 125 together with a summary of the stratigraphy of the DSDP borehole 549 on the Goban Spur 'Plateau' (De Graciansky et al., 1985a), borehole 62/07-1 in the Goban Graben (Colin et al., 1992) and the thermal histories of two vertical profiles in SW Ireland (Cogné et al., 2014).

The profiles in SW Ireland also show an important phase of cooling and exhumation during the Early Cretaceous, which suggests that the local exhumation due to fault block rotation at Menez Bihan and GC4 was also accompanied by regional uplift of the entire continental shelf from SW Ireland to the Goban Spur area. This regional Early Cretaceous uplift has been recognized in the Porcupine Basin (Jones et al., 2001a) and in the Fastnet and Celtic Basins (McMahon and Turner, 1998).

Prior to the Early Cretaceous, the SE of Ireland seemed to have experienced a period of tectonic quiescence with no significant exhumation taking place, although this apparent lack of cooling or heating events might simply be the result of an underconstrained thermal history. In contrast, the sites of MB and GC4 probably experienced episodic exhumation due to rifting processes.

The absence of any significant heating or cooling event from the Late Cretaceous until the present-day reflects rapid post-rift thermal subsidence and drowning of the tips of the fault blocks during the Late Cretaceous (Masson et al., 1984). The sedimentary succession in the half-grabens (DSDP 549, 62/07-1) reflects the exhumation history of the horsts, with a significant amount of continental syn-rift sediments of Early Cretaceous age followed by marine sediments of Late Cretaceous and Cenozoic age (FIGURE 125).

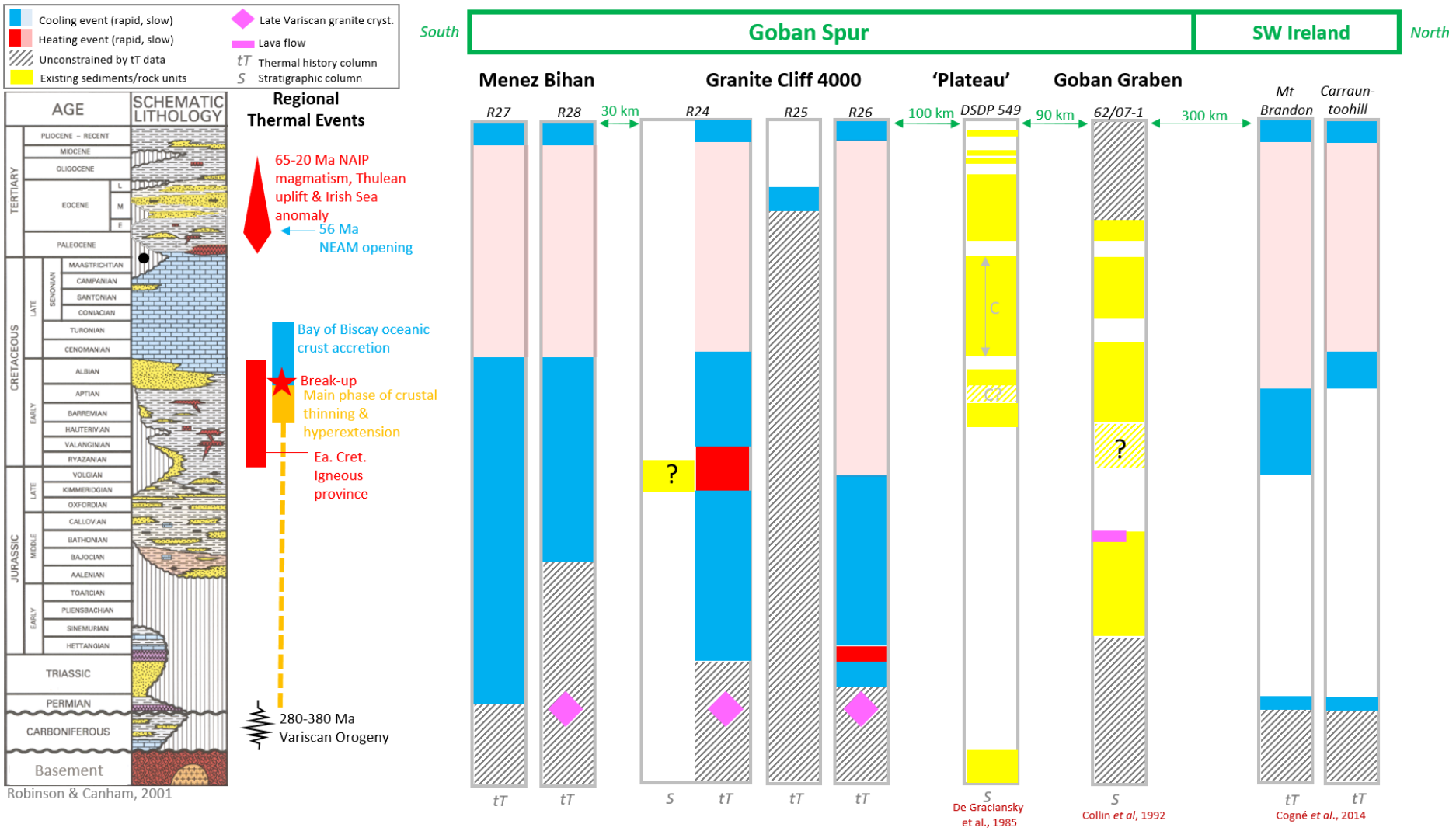

Figure 125: Episodes of cooling and heating (from thermal history modelling) and sedimentation (from boreholes) from a transect from the Goban Spur to SW Ireland. Location of transect is shown in Figure 106.

6.7 Conclusions

6.7.1 Geochronological results

The apatite and zircon U/Pb study led to the following conclusions:

- Confirmation of the Late Varsican age of the granites of Menez Bihan and Granite Cliff 4000 (R-24, R-26, R-28).
- The apatite trace element biplot suggests that the batholiths are I-type granitoids. Zircon inheritance was minimal consistent with an I-type affinity; Cadomian inherited grains and cores suggest that any crustal contamination might be from a Cadomian crust.
- A clast of an inferred granulite (R-27) at MB yielded a complex set of U/Pb ages with a few zircons dated at 571.2 ± 7.5 Ma (Cadomian) and 296.9 ± 5.4 Ma (Late Variscan) and a U-Pb apatite age of 446 ± 11 Ma (Late Ordovician-Early Silurian)
- This granulite was likely a metamorphic rock in the Avalonian domain that formed or was metamorphosed during the Cadomian Orogeny (crystallisation of the matrix zircons) and subsequently affected by the main phase of the Caledonian orogeny (crystallisation of the apatites). At c. 297 Ma, during the Late Variscan magmatic activity, new zircon growth was detected, and may be associated with hydrothermal fluids or aplitic magmas linked to the emplacement of the MB granitic pluton.
- One of the clasts (R-25) from GC4 is an Archean metamorphic rock yielding a zircon U/Pb age of 2764 ± 24 Ma and an apatite U/Pb age of 1714 ± 16 Ma.
- Similar ages have been found in granulites from the Ortegal Plateau, on the north Iberian margin. According to plate reconstruction models, before Mesozoic rifting, GC4 was located very close to the Ortegal Plateau, suggesting that the Neoarchean granulite could well be *in-situ* and represents a Neoarchean granulitic basement that extends from at least the southern tip of the Goban Spur to the northern tip of the Ortegal Plateau.
- However, the proximity of the sample to a zone of preferential deposition of IRD sourced from Archean basements that have been affected by the Paleogene NAIP magmatism (Lewisian of Scotland and the Archean North Atlantic Craton in southeast Greenland) points towards the sample being an IRD and not representative of in-situ basement geology nor the local thermal history. Therefore, other Archean and Proterozoic granulites found all around the Bay of Biscay and previously interpreted as representing local basement geology might actually also be IRDs.

6.7.2 Thermochronological results

The AFT and AHe study led to the following conclusions:

- Prior to the main phase of crustal thinning and hyperextension during the Early Cretaceous, the two rotated fault blocks of MB and GC4 probably experienced a different style and rate of exhumation with the MB showing rapid exhumation through the PAZ during the Middle-Late Jurassic while the GC4 sample shows a protracted cooling through the PAZ from the Permian to the Jurassic.
- Synchronous block rotation during the Early Cretaceous, with both tectonic and subaerial erosion exhumation (c. 750-3000 m of overburden removed), could explain the rapid c. 70°C cooling visible in samples at both MB and GC4. Temporally, it corresponds to the main phase of rifting and hyperextension (Barremian-Aptian) derived from stratigraphical information from the DSDP boreholes. The half-grabens in the region are therefore probably filled by Early Cretaceous sediments, in particular Barremian-Aptian sediments
- The crests of the rotated fault blocks might have remained above sea water for a few millions of years after break-up and initiation of thermal subsidence, resulting in continued subaerial erosion until they became drowned, probably at the start of the Late Cretaceous.
- Profiles in SW Ireland also show an important phase of cooling and exhumation during the Early Cretaceous, which suggests that the local exhumation due to fault block rotation at MB and GC4 was also accompanied by regional uplift of the entire continental shelf from SW Ireland to the Goban Spur area. This regional Early Cretaceous uplift has been recognized in the Porcupine Basin and in the Fastnet and Celtic Basins.
- The absence of any significant heating or cooling event from the Late Cretaceous until the present-day reflects rapid post-rift thermal subsidence and drowning of the tips of the fault blocks during the Late Cretaceous.

In conclusion, the thermochronological data from the southern tip of Goban Spur reflect the protracted Mesozoic rifting of the SW Ireland continental shelf that culminated in a phase of hyperextension during the Barremian-Aptian with fault block rotation and renewed exhumation due to probably a combination of fault movement denudation, rift shoulder uplift and regional uplift. The absence of significant magmatism and low post-rift sedimentation allowed the preservation of the thermochronological signature of the rifting history of a non-volcanic and hyperextended margin.

7 Syntheses

7.1 Exhumation and thermal history of the IAM

7.1.1 Introduction

The main objectives of the study were to apply a modern low-temperature thermochronological methodology to borehole and seabed samples from the IAM to constrain better the exhumation episodes of the margin since the Mesozoic, as has been successfully undertaken on onshore Ireland and Britain (Cogné et al. (2016), Döpke (2017), Łuszczak et al. (2017) and Łuszczak et al. (2018)). In particular, the study aimed at: 1) Improving understanding of the timing and magnitude of rift-related Mesozoic exhumation, and in particular test the hypothesis that the AFT ages and rift-related exhumation becomes younger from north to south (Cogné et al., 2014); 2) identifying a possible extension on the IAM of the Late Paleocene-Early Eocene exhumation that has affected the Central Irish Sea and NW England (as predicted by Jones et al. (2001b)); and 3) constraining potential Neogene exhumation events. Only half of the samples (21 out of 43) yielded suitable AFT and/or AHe data for thermal history inverse modelling (>10 AFT ages and/or >15 track lengths and/or AHe ages with reasonable age dispersion), which significantly limited the number of wells (and number of samples from each well) that could be investigated.

7.1.2 Mesozoic exhumation

7.1.2.1 Timing of exhumation

In the north, well 13/03-1 yielded Mesozoic thermal histories characterized by either rapid exhumation during the Late Jurassic or protracted exhumation since at least the Triassic and that culminated during the Early Jurassic. Further south, on the North Porcupine High, the remodelling of the PHMS psammite data yielded a protracted Mesozoic exhumation culminating with an accelerated phase during the Aptian-Albian, possibly interrupted by a phase of heating (syn-rift burial and/or an increased geothermal gradient) during the Berriasian-Barremian; while the Mesoproterozoic gneiss (C-MeBo) and the 26/26-1 and 34/05-1 boreholes show an exhumation event that culminates during the Late Jurassic. On the other side of the North Porcupine Basin, the new data from well 26/30-1 points towards a Barremian-Aptian main phase of exhumation that followed a phase of heating. Finally, much further south at the southern tip of the Goban Spur, the Late Variscan granites and Cadomian metamorphic basement yielded thermal histories characterized by protracted exhumation throughout the Mesozoic that accelerated during the Early Cretaceous (R-24) and ended at the end of the Albian (R-24, 27, 28), expect for sample R-26 which shows exhumation terminating in the middle of the Late Jurassic (FIGURE 126).

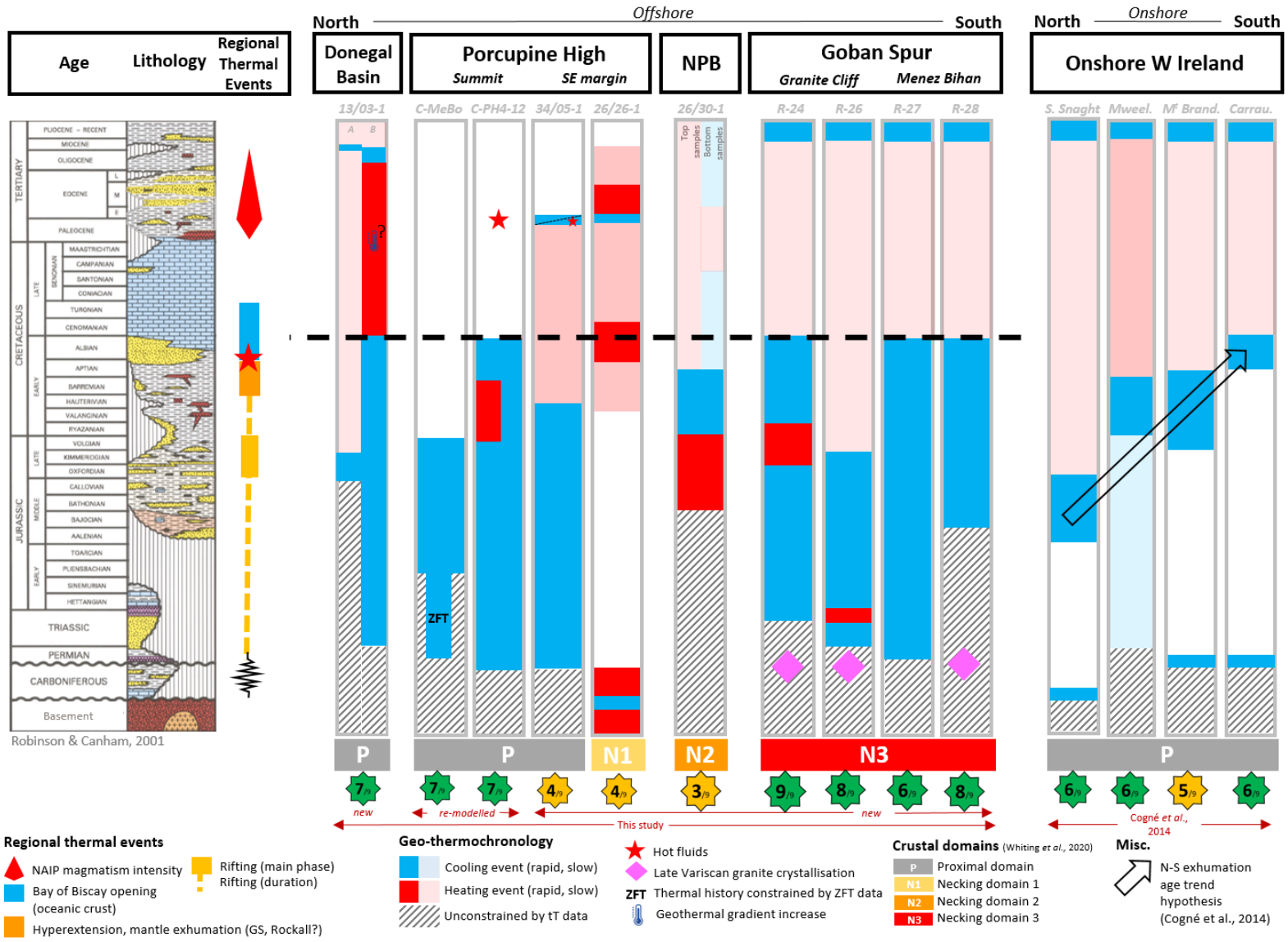

Figure 126: Summary of the thermal histories derived from the new offshore data and compared with the THM from onshore west of Ireland.

Several observations can be drawn from these thermal histories derived from the new AFT/AHe dataset. Firstly, there does not seem to be any exhumation/cooling age trend from north to south offshore west of Ireland as has been observed on the vertical profiles onshore west of Ireland (Cogné et al., 2014) (FIGURE 126). The Middle Jurassic cooling event observed in the Slieve Snaght vertical profile in NW Donegal is not seen in the offshore profiles that are dominated by Late Jurassic and Early Cretaceous cooling.

There is also no apparent correlation between the main phase of Mesozoic cooling/exhumation and the crustal domain from which the thermochronological are obtained. For example, a dominant phase of Early Cretaceous cooling is found in both a completely unstretched basement high (the psammites of the North Porcupine High, C-PH4-12) and in a necking class 3 domain (*i.e.* close to a hyperextended domain) such as the Late Variscan granites of Granite Cliff 4000 and Menez Bihan in the Goban Spur (FIGURE 126).

Using the compilation of legacy thermochronolgical data from Britain and Ireland (SEE SECTION 1.2), the AFT central age from surface or shallow boreholes from either crystalline samples or old clastic samples that have had their AFT ages reset can be used as a simplified proxy for the timing of Mesozoic exhumation. When the dataset is filtered to remove ages younger than 100 Ma (associated with the Greater Irish Sea anomaly or NAIP magmatism), the map shows a pattern of dominantly older ages in Britain and Northern Ireland (mostly 160-300 Ma) and younger ages in the rest of Ireland (mostly 120-200 Ma) (FIGURE 127). This pattern, which has not been recognized in the published literature so far, and cannot be explained by sample elevation alone, appears to support of the observation of diachronous rifting and exhumation of Cogné et al. (2014), but has to be reconciled with the lack of such an apparent diachronicity offshore west of Ireland.

The boundary between the younger AFT ages of Ireland and the older AFT ages of Northern Ireland and Britain (blue dashed and dotted line in FIGURE 127) coincides spatially with 1) the southern edge of the Northern Ireland and Scotland NAIP dyke swarm; 2) the southern edge of the inferred axis of igneous underplating extending from the Faroes to the Central Irish Sea (Al-Kindi et al., 2003); 3) the southern limit of a warm tongue of asthenosphere below western Scotland (Davis et al., 2012); and 4) is parallel and close to the NW-SE Anton Dohrn Transfer Zone (ADTZ) that extends from the northern tip of the Rockall High to the North Channel Basin (Doré et al., 1997). The transfer zone is believed to have been active during Mesozoic rifting (Doré et al., 1997) and is parallel to the axis of crustal break-up between the NE Canadian/Northern Iberian margins and the Celtic margin.

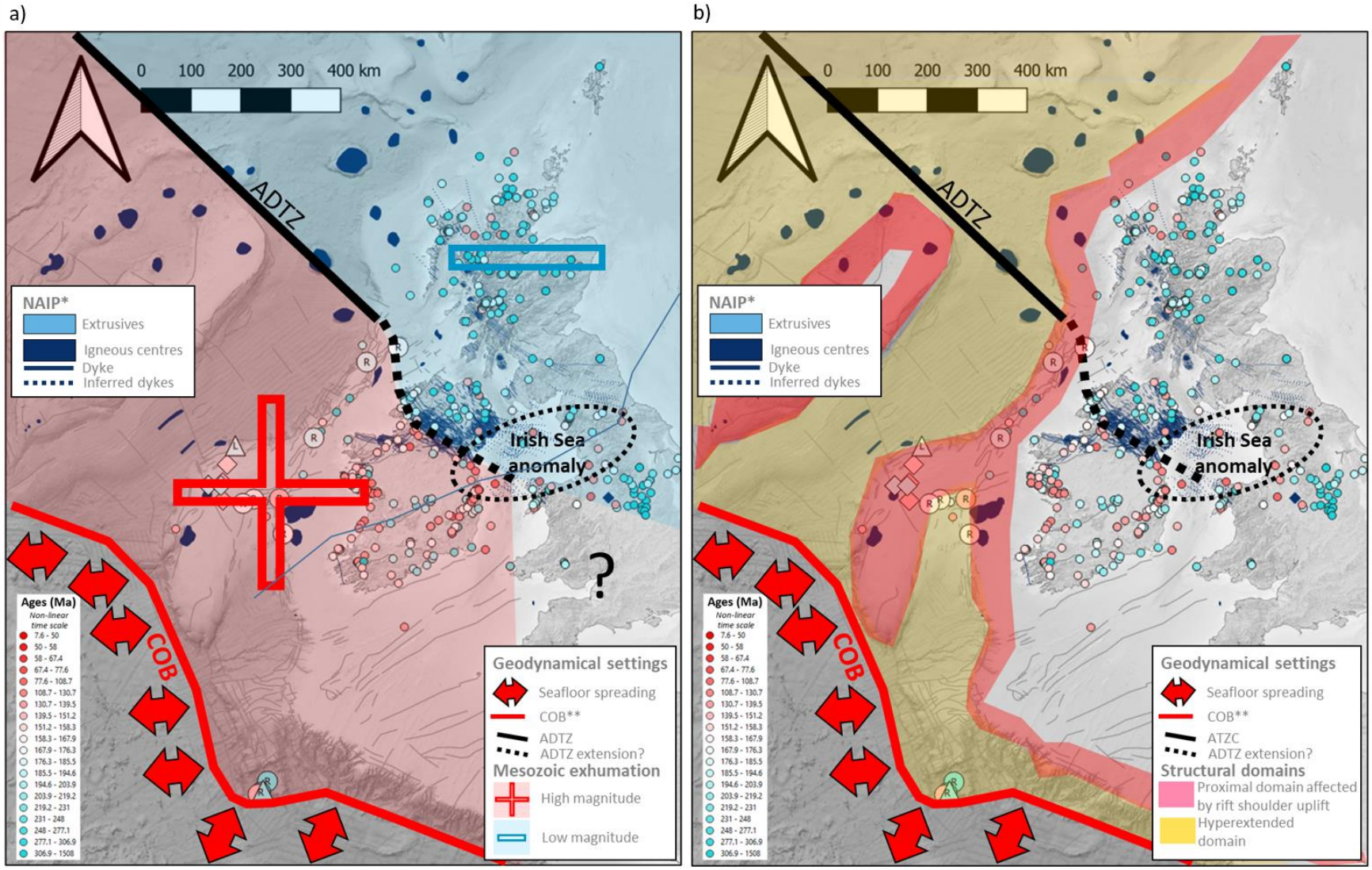

Figure 127: Thermochronological patterns linked to the Mesozoic exhumation of the British-Irish Isles. a) Inferred effects of the Anton-Dorhn Transfer Zone (ADTZ) on exhumation. b) Inferred effects of rift-should uplift on exhumation.

A hypothesis that can be put forward is that during the main phase of hyperextension, mantle exhumation and ultimately crustal breakup along the Celtic Margin, the entire lithosphere to the NE of the future break-up line was uplifted (resulting in exhumation that lasted until the end of the Early Cretaceous, area marked by the blue cross in FIGURE 127) but stopped at the NW-SE trending ADTZ that might have prevented the area to the NE (mostly Scotland and its offshore platform) being uplifted to the same magnitude (resulting in older AFT ages in Scotland). The lineament was later used as the preferential location for the NAIP dyke swarm and possibly igneous underplating and even the present-day asthenospheric 'warm tongue'. A likely secondary control on the Early Cretaceous exhumation and primary control for the Late Jurassic phase of rifting is rift-shoulder uplift. If a width of c. 70 km is used as a plausible extent of rift-shoulder uplift (Green et al., 2018) (area with the green crosses in FIGURE 127). This could explain the Late Jurassic to Early Cretaceous exhumation detected in borehole 13/03-1, which although it is located on the ADTZ, is close enough to the margin of the hyper-extended Rockall Basin to have possibly been affected by rift-shoulder uplift (FIGURE 127).

However, it has to be noted that despite the use of both AFT and AHe data and sometimes two samples within the same borehole, large uncertainties remain on the exact timing of the Mesozoic uplift as can be seen for example by the different thermal histories produced for samples R-24 and R-26 that come from the same granitic outcrop on Granite Cliff 4000, or by the seabed and borehole samples from the North Porcupine High (FIGURE 126). These variations in modelled thermal histories come from both uncertainties in the thermochronological data and modelling algorithms, and from differences in the true local thermal histories experienced by the samples caused for example by differential uplift within fault blocks or varying paleogeothermal gradients.

One such example of local influence can be observed in the database of legacy samples from Scotland, where the Northern Highlands block has younger AFT ages than the adjacent Hebrides and Central Highland blocks (FIGURE 128), suggesting that the Caledonian faults (the Moine Thrust Zone and Great Glen Fault) might have had an influence on the pattern of Mesozoic exhumation on the NEAM. The effect of Caledonian faults on exhumation may explain the different Mesozoic thermal histories observed in the North Porcupine High which is where the offshore extension of the onshore Fair-Head Clew Bay Line is interpreted to pass through (SECTION 5.5.5).

7.1.2.2 Magnitude of exhumation

The only locality where the magnitude of the Mesozoic exhumation could be estimated using different proxies were boreholes 26/26-1 and 34/05-a on the eastern edge of the North Porcupine High. The combination of three independent range estimates based on sonic velocity, VR and thermochronological data resulted in an estimated exhumation of c. 1-3 km of sediments with a best case estimate of c. 2 km. A similar range (0.75-3 km) was estimated based on thermal history modelling

alone (so hence a minimum estimate) of the Granite Cliff 4000 and Menez Bihan rotated fault blocks, although part of the exhumation there could also be due to tectonic, fault-related exhumation rather than surface uplift coupled with erosion.

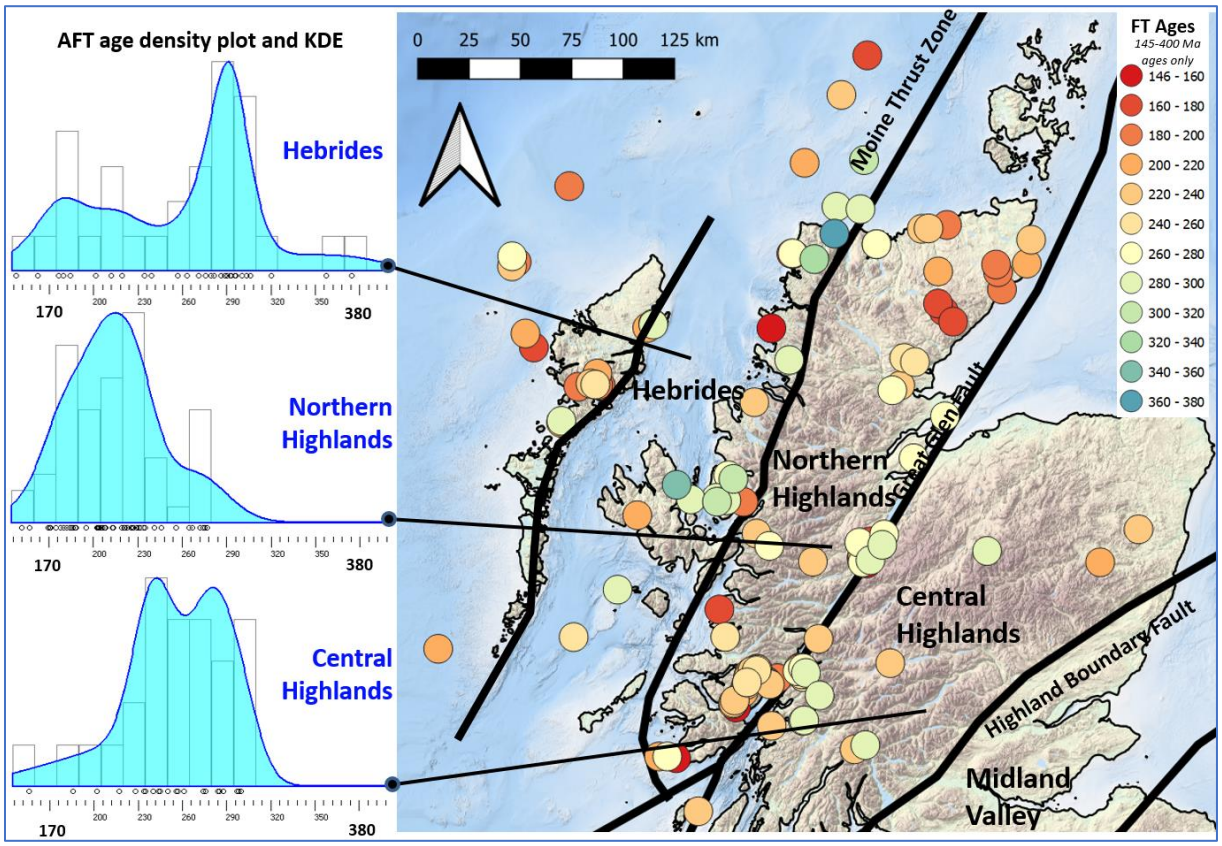

Figure 128: AFT ages and structural blocks in northern Scotland.

7.1.3 Paleogene Exhumation

In the north, the models from borehole 13/03-1 failed to detect any Paleogene exhumation despite being located above a thick c. 7 km thick high velocity body at the base of the crust that has been interpreted as representing igneous underplating (Al-Kindi et al., 2003) (FIGURE 129) and which to the SE has been linked to significant Paleogene exhumation in and around the central Irish Sea (see review in section 1.2.3). A small amount of Paleogene exhumation has probably occurred in this area and the Paleocene ages that dominate the AHe ages of the Carboniferous sample in the borehole may have been caused by this cooling episode. The lack of any significant Paleogene exhumation in this area associated with inferred igneous underplating shed some doubts on the relationship between underplating and exhumation at that time or else on the nature of the high velocity bodies themselves.

Further south, some of the thermal history end-members indicate a phase of exhumation close to the Paleocene-Eocene boundary, In particular, borehole 34/05-1 (on the eastern edge of the North Porcupine High) shows a likely rapid cooling pulse of c. 30°C corresponding to erosion of c. 1000 m of

sediments (FIGURE 129 AND FIGURE 130A), while some of the modelled thermal histories in the nearby well 26/26-1 (when ignoring the track length data, see discussion in section 5.3.6.6) show cooling of possibly 20°C or c. 650 m of exhumation (FIGURE 129 AND FIGURE 130A). Finally, the modelled thermal history of the granite sample C-MeBo2 on the summit of the NPH points towards 60°C cooling at that time, equivalent to c. 2 km of exhumation (FIGURE 129 AND FIGURE 130A). The higher and unrealistic exhumation magnitude at the location of C-MeBo2 might be a result of a higher geothermal gradient prior to exhumation, caused by the inferred igneous centre located below the NPH. Finally, remodelling of the legacy samples in shallow borehole 16/28-sb01 on the NW edge of the Porcupine High yielded a thermal history with two end-members, one of which implied c. 2km of exhumation possibly at the Paleocene-Eocene boundary (the other hypothesis involving hot fluids, see section 5.2.6.7).

This Early Eocene exhumation on the summit and NW and SE margins of the Porcupine High has been predicted by Jones et al. (2001b) using subsidence analysis of wells in the Porcupine Basin that record 300-600 m uplift at the Paleocene-Eocene boundary, as well as an estimate for a minimum of 300 m uplift of the Porupine High (FIGURE 129 AND FIGURE 130B). The discrepancy in magnitude can be accommodated by the possibility of a higher regional geothermal gradient immediately prior to uplift and/or higher temperatures prior to uplift caused by the thermal effect of igneous intrusions near the well. The Paleocene-Eocene boundary uplift inferred by Jones et al. (2001b) and detected by the new data and modelling on the Porcupine High is probably related to the latest Paleocene-earliest Eocene unconformity (PEBU) observed in other parts of the North-East Atlantic Margin such as in the Faroe-Shetland Basin where a pronounced erosional surface with a dendritic pattern is observed (Smallwood and Gill (2002), Maclennan and Jones (2006), Champion et al. (2008b)) (FIGURE 130C AND D) and in and around the Central Irish Sea (FIGURE 129) where a minimum of 300 m of exhumation at that time (out of a total of 1-2.4 km) is attributed to plume-related transient uplift (the remaining exhumation being caused by igneous underplating) (Łuszczak et al., 2018). There has been no attempt to map potential igneous underplating in this area using geophysical data, and therefore the correlation between underplating and exhumation cannot be tested here. The detection of possibly 1 km of exhumation of the NPH at the Paleocene-Eocene boundary could point towards this area being one of the main sources of sediments that fed the Early Eocene deltaic sequences in the northern part of the Porcupine Basin (Moore and Shannon (1992), Jones et al. (2001a)).

However, although several boreholes on the Porcupine High point towards kilometre-scale exhumation at the Paleocene-Eocene boundary, the absence of such an exhumation event in the psammite samples at the summit of the Porcupine High (C-PH4-12) or in the orthogneiss on the NW flank of the NPH (C-MeBo) (FIGURE 129) is difficult to explain. The sampling of different paleo-altitudes could be part of the reason as summits typically yield older thermochronological ages than samples

from valleys which have experienced the same thermal history. However, the likely presence of hot fluids that could have travelled in fractures raise some doubts on the origin of some of the young AHe ages in the samples. The small difference in timing between the regional Paleocene-Eocene exhumation and NAIP magmatism results in thermochronological data that are in some cases the product of one or both thermal events, and it can be at times difficult to deconvolve the influence of each mechanism in the thermal history models.

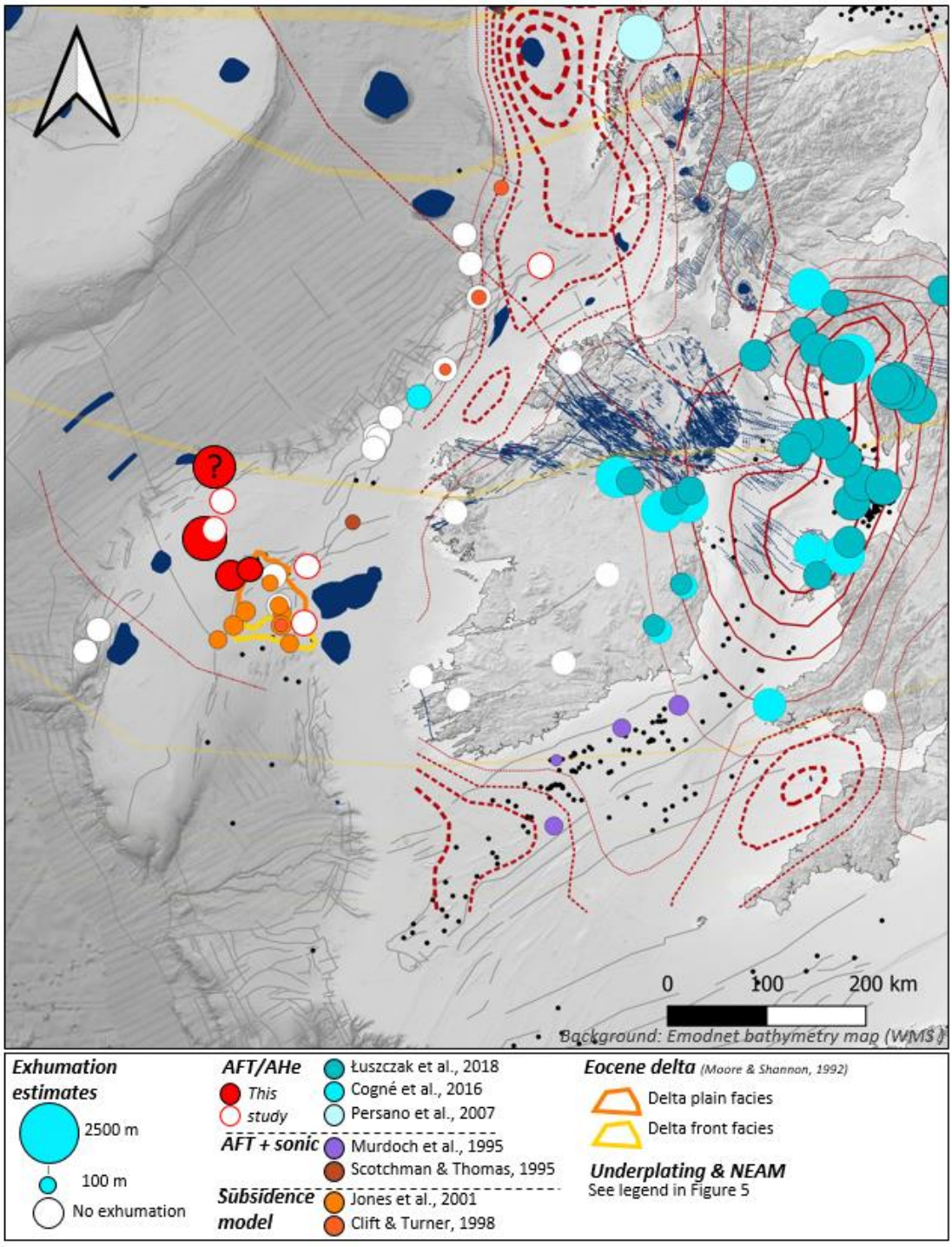

Figure 129: Paleogene exhumation of Ireland and Britain with new estimates for the AIM.

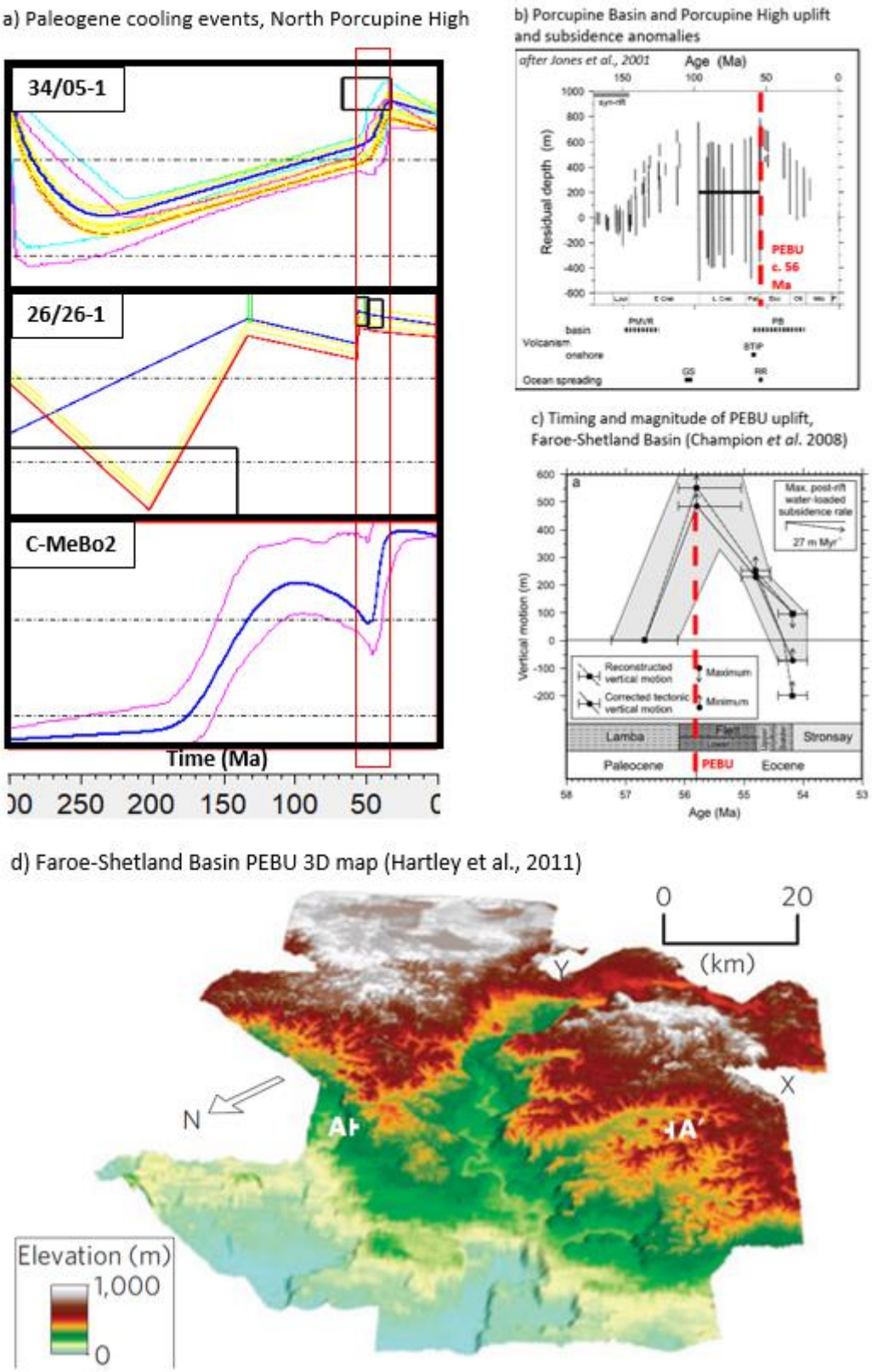

Figure 130: Paleogene transient uplift and exhumation of the Northern Porcupine High and Faroe-Shetland Basin.

No Paleogene exhumation was detected on the eastern side of the Northern Porcupine Basin in well 26/30-1, although the lack of AHe data in this borehole could prevent the detection of a small to medium-magnitude potential cooling event. Finally, no exhumation pulse was detected in the Goban Spur samples which was expected as the area is believed to be submerged under several thousands meters of water since the Late Cretaceous and has not experienced subaerial erosion since Early Cretaceous extension. The Archean sample R-25 with Middle Eocene (c. 40 Ma) AFT and AHe ages is believed to be represent ice-rafted debris and does not represent in-situ basement.

7.1.4 Neogene exhumation

The new data from borehole 13/03-1 in the Donegal Basin supports the interpretation from legacy studies of an Early to Middle Miocene (c. 10-20 Ma) exhumation event across the entire offshore NW Ireland shelf, with an estimated magnitude of c. 1 km of eroded sediments (FIGURE 131) that must have been reworked into both the Porcupine and Rockall basins. This late Oligocene to Miocene exhumation event was previously recognized by AFT, VR and stratigraphic studies in the NE Rockall basin well 5/22-1 (Jackson et al., 2020) and 12/02-1 (Green, 2003) and the Slyne Basin wells 18/20-1 (Green, 2004), 18/25-1 (Green, 2004) and 27/13-1A (Chapman et al., 1999) (FIGURE 131).

This event has been described in other part of the British Isles and the NEAM (Holford et al., 2009) and is believed to have been caused by the far-field transmission of compressional forces generated at the plate boundary such as, on the Atlantic side: 1) an increase in seafloor spreading rates in the earliest Miocene (Mosar et al., 2002), 2) the separation of Jan Mayen and Greenland in the late Early to Middle Miocene (Stoker et al., 2005), 3) the formation of the Iceland Plateau during the Middle Miocene caused by a major magma generation event and resulting in ridge push-like forces (Doré et al., 2008); and on the continental side: 4) a renewed compressional phase of the Alpine orogeny during the Miocene (Neoalpine) (Giorgio et al., 2003).

However, this event has not been detected in the various boreholes and seabed samples of the North Porcupine High (FIGURE 131), which suggests possible different Neogene exhumation behaviour between the Donegal-Slyne-Erris platform and the Porcupine High. One sample from the Porcupine High (C-PH4-12) shows a cooling event within the last 10 Ma. However because the thermal history model does not matching all the observed data, an alternative thermal history (using a user set L_0) does not display this Late Neogene cooling and thus suggests it might be a modelling artefact. Similarly, most samples from the Goban Spur also show a significant 20-40°C cooling phase within the last 10 Ma (FIGURE 131). While some of this cooling could be due to cooler waters during the Late Neogene, most of the cooling is believed to be a modelling artefact related to the track length distributions (Vrolijk et al. (1992b), Redfield (2010)). A significant Late Neogene cooling event has been recognized in the west

of Ireland (Cogné et al., 2014) while accelerated subsidence and sedimentation has been modelled in borehole 35/15-1, possibly l the Late Neogene exhumation onshore (FIGURE 131).

Despite the new data, the spatial distribution and magnitude of both Late Oligocene-Early-Middle Miocene and Late Neogene exhumation onshore and offshore west of Ireland and their respective causes are still poorly constrained.

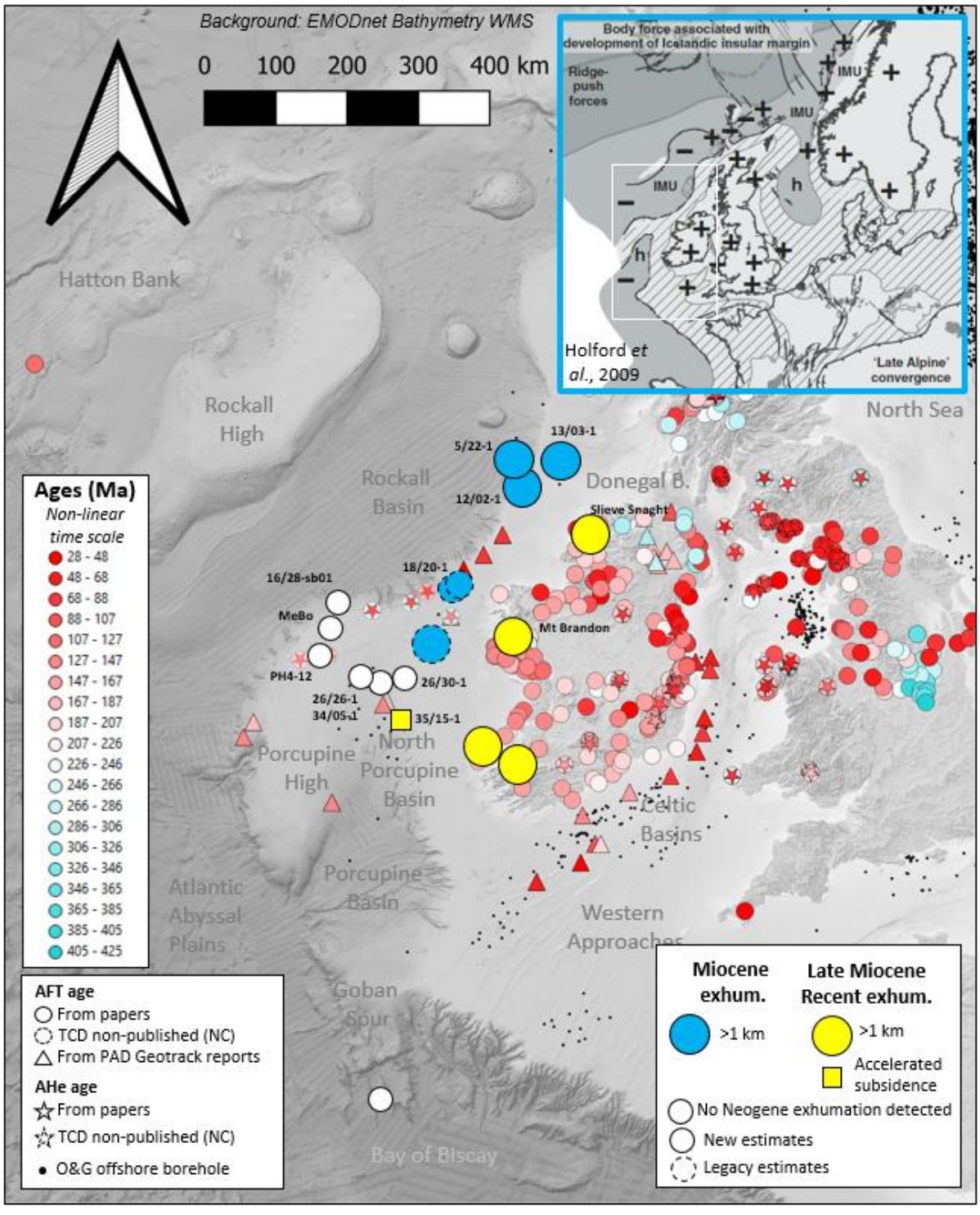

Figure 131: Neogene exhumation pattern on the IAM.

7.2 New geochronological constraints for Phaneorozoic magmatism on the offshore Irish Atlantic Margin

The new geo-thermochronological data from this study provide a wealth of new temporal and spatial information on the timing and nature of magmatism of this segment of the Irish Atlantic Margin. A regional compilation of magmatic activity in the offshore basins west of Ireland was provided by Tate and Dobson (1988), while more recent studies have focused on more localized igneous features (e.g. Magee et al. (2014), Gagnevin et al. (2017), Jackson et al. (2020)). A review of all igneous rocks in the offshore boreholes of the Irish Atlantic Margin is presented in FIGURE 132, together with the new information coming from this study.

7.2.1 Late Carboniferous-Early Permian magmatism (Variscan, SCLIP)

Location: 13/03-1, Granite Cliff 4000, Menez Bihan

7.2.1.1 13/03-1: Western extension of the British Late Carboniferous tholeiitic dyke swarm

The gabbro at the bottom of 13/03-1 has been dated at 297 ± 9 Ma by apatite U/Pb dating while its mineralogy suggests that the intrusion was derived from a tholeiitic magma (SECTION 4.4.5.2). Regionally, the Carboniferous-Permian magmatism in the British Isles is dominated by alkaline magmatism but one tholetiitic event is known to occur at the end of the Late Carboniferous (Upton et al., 2004). This event is often dated at 295-301 Ma (Upton et al., 2004), but Monaghan and Parrish (2006) and Monaghan and Browne (2010) propose a slightly older date for this event at around 308 Ma, while Torsvik et al. (2008) based on the age of volcanics from Northern Europe, argue for an age of 297 ± 4 Ma.

Despite the uncertainty on the age of emplacement and the duration of this tholeiitic phase, it fits well with the U/Pb age of the gabbro in 13/03-1. Therefore, both the radiometric age and the petrography of the intrusion point towards an affiliation with the Late Carboniferous (and possibly basal Permian) tholeiitic magmatism of Scotland and NW Europe.

The intrusion in borehole 13/03-1 is probably a tectonically-tilted dyke. The Late Carboniferous tholeiitic magmatism in Scotland is volumetrically dominated by a dyke swarm of W-E and NW-SE-orientated dykes extending from the North Sea to the Hebrides (Smythe et al., 1995), with only a few sills present in central Scotland and Northern England (Upton et al., 2004) (FIGURE 133). This supports the likelihood than the intrusion is dyke and not a sill. This swarm comprise dykes with an average width of 30 m and a maximum width of 75 m (Ritchey, 1939). Based on the arcuate nature of the dyke swarm, we would expect the dyke in 13/03-1 to be WNW-ESE-oriented and possibly thinner than the ones onshore Scotland since there seems to be a broad decrease in thickness from east to west (Smythe et al., 1995).

Borehole	Volcanic lithology	Stratigraphic unit	Radiometric dating	Event age	Source	Map category	Event
05/22-1	Tuffaceous claystone	Early Eocene	n/a	Early Eocene	Well reports	Tuffs - Possibly reworked	NAIP
	Tuff horizon	Early Eocene	n/a	Early Eocene	Well reports	Tuffs - In place	NAIP
	Volcaniclastic sandstone	Late Paleocene-Earliest Eocene	n/a	Late Paleocene-Earliest Eocene	Well reports	Volcaniclastics (transported)	NAIP
12/02-1	Tuffaceous claystone	Late Paleocene	n/a	Late Paleocene	Well reports	Tuffs - Possibly reworked	NAIP
	Dolerite sill	Late Paleocene	n/a	<= Late Paleocene	Well reports	Intrusion proven by wells	NAIP
	Volcaniclastic sandstone	Late Paleocene	n/a	Late Paleocene	Well reports	Volcaniclastics (transported)	NAIP
12/02-1Z	Basaltic lavas	Ea. Permian-Ea. Cretaceous	n/a	Ea. Permian-Ea. Cretaceous	Well reports	Lava flow	LCEP?
12/02-2	Volcaniclastic sandstone	Thanetian	n/a	Thanetian	Well reports	Volcaniclastics (transported)	NAIP
12/13-1A	Volcaniclastic sandstone	Permo-Triassic	n/a	Permo-Triassic	Well reports	Volcaniclastics (transported)	LCEP
			285 ± 11 Ma	Latest Carboniferous-Earliest Permian	This study	Volcaniclastics (transported)	
13/03-1	Tuffaceous claystone	Stephanian B-Westphalian D	n/a	Stephanian B-Westphalian D	Well reports	Tuffs - Possibly reworked	LCEP
	Gabbro	Westphalian B-C	n/a	<= Westphalian B-C	Well reports	Intrusion proven by wells	LCEP
			299.4 ± 8.5 Ma	Latest Carboniferous-Earliest Permian	This study	Intrusion proven by wells	
16/28-sb01	Basalt	Syn or pre-Late Cretaceous	n/a	Syn or pre-Late Cretaceous	Haughton et al., 2005	Lava flow	Ea. K?
18/20-1	Basalts, dolerite, tuffs (ROV samples)	Lower Tertiary	40-43 Ma	Lower Tertiary	Well reports, Dancer et al., 1999	Lava flow & tuffs - Possibly reworked	NAIP
	Volcaniclastic sandstone	Hettangian	n/a	Hettangian	Well reports	Volcaniclastics (transported)	Ea. J?
18/20-2, 2Z	Basalts, tuffs (ROV samples)	Paleocene	n/a	Paleocene	Well reports	Lava flow & tuffs - Possibly reworked	NAIP
18/20-3	Tuffs (ROV samples)	Paleocene	n/a	Paleocene	Well reports	Tuffs - Possibly reworked	NAIP
18/20-4	Basalt, tuffs (ROV samples)	Paleocene	n/a	Paleocene	Well reports	Lava flow & tuffs - Possibly reworked	NAIP
	Altered dark greenish-grey intrusive	Lower Toarcian	n/a	<= Toarcian (Early Jurassic)	Well reports	Intrusion proven by wells	NAIP?
18/20-5	Volcanics (logs + ROV samples?)	Teriary	n/a	Lower Tertiary	Well reports	Lava flow & tuffs - Possibly reworked	NAIP
18/25-1	Volcanics (logs + ROV samples?)	Lower Tertiary	n/a	Lower Tertiary	Well reports	Lava flow & tuffs - Possibly reworked	NAIP
	Altered light grey-green grey intrusive	Bajocian	n/a	<= Bajocian	Well reports	Intrusion proven by wells	Ea. K?
	Igneous sill	Bathonian	n/a	<= Bathonian	Well reports	Intrusion proven by wells	Ea. K?
18/25-2	Altered dark-greenish grey intrusion	Toarcian	n/a	<= Toarcian	Well reports	Intrusion proven by wells	Ea. K?
			c. 125-190 Ma	Mid Jurassic to Early Cretaceous	This study	Intrusion proven by wells	
18/25-3	Volcanics (logs + ROV samples?)	Paleocene	n/a	Paleocene	Well reports	Lava flow & tuffs - Possibly reworked	NAIP
	Altered basalt?	Early Triassic	n/a	Early Triassic	Well reports	Lava flow?	Ea. K?
19/08-1	Basalt, tuffs (ROV samples)	Tertiary	n/a	Tertiary	Well reports	Lava flow & tuffs - Possibly reworked	NAIP
19/11-1A	Basalt, tuffs (ROV samples)	Tertiary	n/a	Tertiary	Well reports	Lava flow & tuffs - Possibly reworked	NAIP
	Dolerite intrusions	Ea. Toarcian, Late Oxfordian, Kimmeridgian	n/a	<= Ea. Toarcian, Late Oxfordian, Kimmeridgian	Well reports	Intrusion proven by wells	NAIP?
26/21-1	Pyroclastics	Barremian-Aptian boundary	n/a	Barremian-Aptian boundary	Tate & Dobson, 1988	Tuffs - In place?	Ea. K?
26/22-1A	Palagonite tuff	Danian	n/a	Danian	Well reports	Tuffs - In place	NAIP
26/29-1	Tachylite	Paleocene-Maastrichtian	n/a	Paleocene-Maastrichtian	Well reports	Lava flow?	NAIP
26/30-1	Tuffs?	Bathonian-Ea. Oxfordian	159.8 ± 3.1 Ma	Middle-Late Jurassic (Oxfordian?)	This study	Tuffs - In place	Ea. K
27/05-1	Dolerite intrusion	Westphalian B	n/a	<= Westphalian B	Well reports	Intrusion proven by wells	NAIP?
34/05-1	Dolerite intrusion	Westphalian B	n/a	<= Westphalian B	This study	Intrusion proven by wells	NAIP?
35/02-1	Black submarine volcanic flow	Montian-Danian	n/a	Montian-Danian	Well reports	Lava flow	NAIP
	Dolerite intrusion	Kimmeridgian	n/a	<= Kimmeridgian	Well reports	Intrusion proven by wells	?
35/08-1	Volcanogenic sediments (water lain ash fall, fumice)	Aptian-Albian	n/a	Aptian-Albian	Well reports	Tuffs - In place	Ea. K
	Dolerite intrusion	Aptian-Albian	18 ± 6 Ma (K-Ar)	Lower Miocene	Well reports	Intrusion proven by wells	NAIP?
	Tuff, tuffaceous siltstone	Barremian	n/a	Hauterivian-Barremian	Well reports	Tuff - Possibly reworked	Ea. K
35/13-1	Volcanogenic sandstone	Up Paleocene Lowermost Eocene	n/a	Up Paleocene Lowermost Eocene	Well reports	Volcaniclastics (transported)	NAIP
	Pyroclastics	top Albian	n/a	top Albian	Tate & Dobson, 1988	Tuffs - In place?	Ea. K?
	Tholeiitic dolerite intrusive	Albian	25.8 ± 2.6 Ma (K-Ar)	Oligocene or older	Seamann, 1984	Intrusion proven by wells	NAIP
			65 ± 14 Ma (Ap U/Pb)	Paleogene	Well reports	Intrusion proven by wells	NAIP
35/15-1	Basalt lava flows & gabbro intrusion	Danian & Ea. Cretaceous	58.9 ± 1.8 Ma (K-Ar)	Paleocene	Well reports	Lava flow & Intrusion proven by wells	NAIP
			60-62 Ma (Ap U/Pb)	Selandian	This study	Lava flow & Intrusion proven by wells	NAIP
	Tuff	?Devonian-Ea. Carboniferous	n/a	?Devonian-Ea. Carboniferous	Well reports	Tuffs - In place	LDEC
35/13-1	Tholeiitic dolerite	Albian	K-Ar	<= Late Oligocene	Seamann, 1984	Intrusion proven by wells	NAIP
35/19-1	Basalt	Late Maastrichtian-Ea. Paleocene	n/a	Basal Paleocene	Well reports	Lava flow	NAIP
43/13-1	Basalt lava flow	?Early Paleocene	n/a	Basal Paleocene	Well reports	Lava flow	NAIP
62/07-1	Dark grey-black andesite	Callovian/Bathonian-Aptian/Berriasian	133.5 Ma (K-Ar)	Callovian/Bathonian-Aptian/Berriasian	Tate & Dobson, 1988	Lava flow	Ea. K
DSDP 81-549	Ash horizon (rhyolithic tuff)	Upper Eocene NP18	n/a	Upper Eocene NP18	Knox, 1985	Tuffs - In place	NAIP
	Ash horizon (rhyolithic tuff)	Upper Paleocene NP9	n/a	Upper Paleocene NP9	Knox, 1985	Tuffs - In place	NAIP
DSDP 81-550	Bentonite layers (altered basaltic/andesitic ash)	Basal Eocene NP10	n/a	Basal Eocene NP10	Knox, 1985	Tuffs - In place	NAIP
DSDP 48-401	Bentonite layers	Basal Eocene NP10	n/a	Basal Eocene NP10	Knox, 1985	Tuffs - In place	NAIP

Figure 132: Compilation of igneous rocks in offshore boreholes west of Ireland and the new radiometric data from this study.

Based on the observations above, it is suggested that the gabbro in 13/03-1 is a WNW-ESE-oriented tilted dyke belonging to the British Late Carboniferous theoliitic dyke swarm. Onshore the swarm is c. 250 km long, extending from the Hebrides on the West to Aberdeenshire and Northumberland to the east. Based on magnetic anomalies, Smythe (1994) suggested that the swarm extends at least another 200 km to the east under the North Sea, as far as the western margin of the Central Graben (FIGURE 133). The inferred dyke in 13/03-1 is 140 km away from the closest known dykes of the same age, located in the Hebrides and therefore significantly extends the areal footprint of the British Late Carboniferous tholeiitic dyke swarm towards the north-west. It is therefore expected that other similar dykes of the same age are present in the offshore Malin and Donegal basins and possibly further west in the northern part of the Erris Basin and below the eastern margin of the Rockall Basin (FIGURE 133).

Several theories have been advanced to explain the presence and geometry of this dyke swarm and the coeval Oslo Graben and Scania dyke swarms in Norway and Sweden. Smythe et al. (1995) proposed that the dyke swarms represented an incipient lithospheric rupture coeval with an assumed proto-Atlantic rift along the Rockall Basin and Norwegian-Greenland margin. An unrifted part of the proto-North Atlantic in the vicinity of what is now the Faroe Islands would have acted as a focused point for the extensional stresses, creating an arcuate stress field in NW Europe that could explain the direction of the British and Oslo Graben dyke swarms (Smythe et al., 1995). However, their model does not explain the trend of the Scania dykes, nor the lack of dykes closer to the Faroes Islands (e.g. in Northern Scotland). Alternatively, Ernst and Buchan (1997) proposed that the British, Oslo Graben and Scania swarms were radially extending from a mantle plume located below the Skagerrak Graben (FIGURE 133).

This hypothesis is supported by Torsvik et al. (2008) who demonstrated that at c. 300 Ma this mantle plume would have been located at the edge of the African Low Shear Velocity Province (LLSVP). The edge of such a LLSVP has been proposed to be the location for preferential rising of deep-rooted mantle plumes and explains the location of most of the large igneous provinces (LIP) since the Carboniferous (Burke and Torsvik (2004), Torsvik et al. (2008)). Torsvik et al. (2008) proposed that these dyke swarms together with the extrusive magmatism of that age in NW Europe could be categorized as a large igneous province termed the Skaggerak-Centered Large Igneous Province (SCLIP) (FIGURE 133).

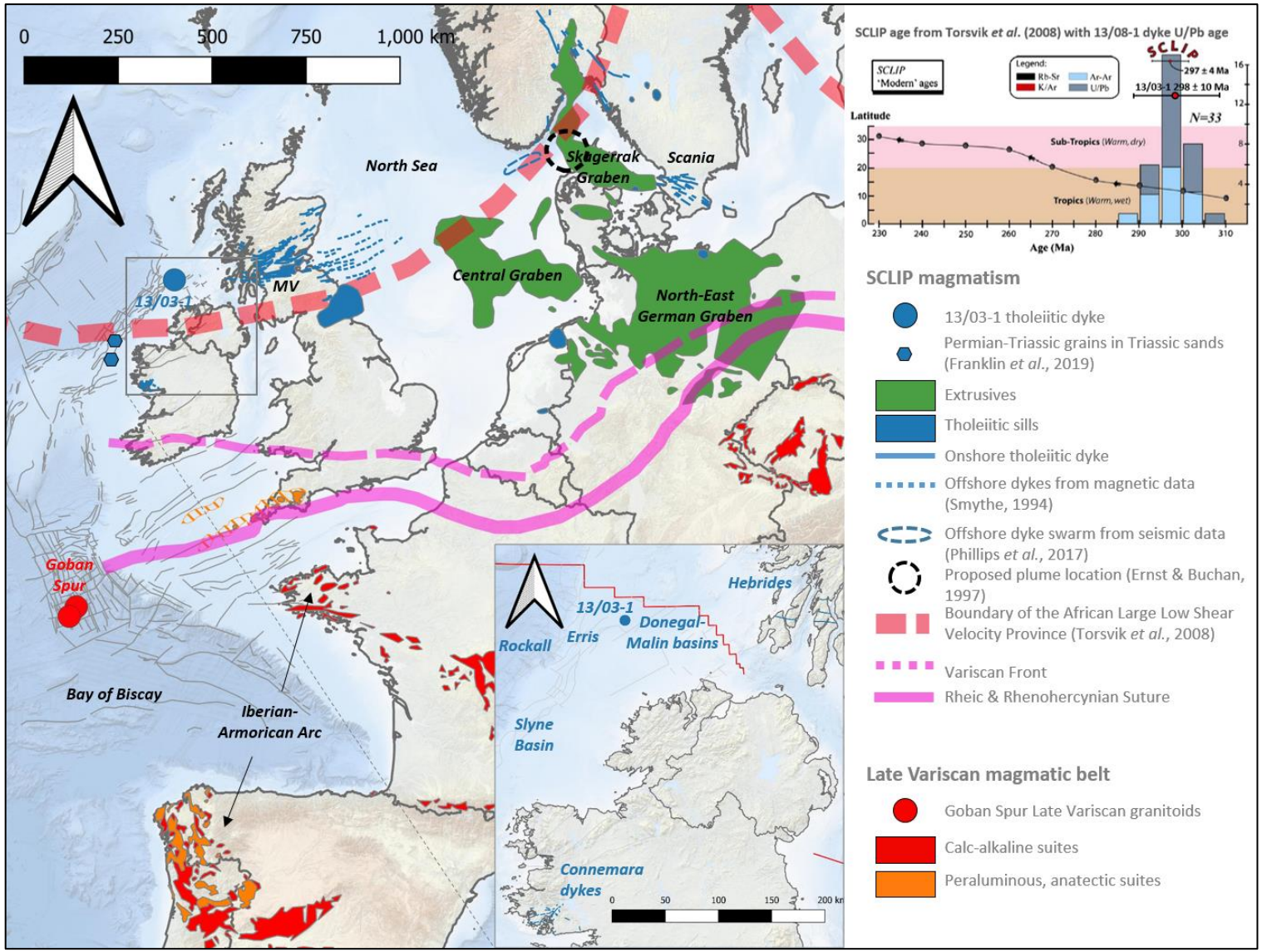

Figure 133: Map of the Late Carboniferous-Early Permian magmatism in NW Europe (the SCLIP and Late Variscan magmatic belt).

In both cases, the spatial distribution and geometry of the dyke swarms is one of the key arguments for the cause of the magmatism and its geodynamical significance. However, a large part of the region is offshore where there is much less data available to constrain the extent of these swarms. Smythe et al. (1995) used magnetic anomalies offshore east of Britain to identify wide dykes that might be the continuation of the British swarm. However these dykes were never drilled and their existence and age remains speculative. More recently, using seismic reflection data, Phillips et al. (2017) discovered a large tilted offshore dyke swarm in the Farsund Basin that they attributed to this c. 300 Ma tholeiitic magmatism based on cross-cutting relationship. This swarm is aligned with the expected direction based on Ernst and Buchan (1997)'s hypothesis (FIGURE 133). The 298 Ma offshore dyke in 13/03-1 is not constrained geometrically but is the first dyke to be dated in the Irish Atlantic offshore that clearly is part this magmatic province, thus providing a robust constraint point for any future mapping of the distribution of this SCLIP.

The presence of SCLIP magmatism offshore west of Ireland was inferred by Franklin et al. (2019) based on the discovery of a significant proportion of Permian-Triassic apatites and zircons in Triassic sandstones from boreholes in the Slyne Basin (Franklin et al., 2019). The dyke in 13/03-1 confirms that SCLIP-related extrusive igneous activity could have occurred in the Donegal-Malin Basin and would have provided a source of igneous material during the Triassic since the thermal history model of the area provided in this study suggests that exhumation started at the end of the Permian. Finally, it is worth noting that a series of Late Paleozoic dolerite dykes (the Logmór and Teach Dóite dykes) have been reported in West Connacht (Mohr, 2000) (FIGURE 133), but their origin and relationship to the regional Late Carboniferous magmatism is still unclear.

7.2.1.2 Goban Spur Late Variscan granites: the missing granites of the Ibero-Armorican Arc

The new apatite and zircon U/Pb ages of samples R-24, R-26 and R-28 (SECTION 6.4.1) confirm the Late Variscan age of the Granite Cliff 4000 granitic batholith (c. 296-297 Ma) and Menez Bihan batholith (c. 288 Ma) as identified by the campaign geologists (Auffret et al., 1979b).

The closest Late Variscan granites are the Cornubian Batholith in Cornwall (UK) and numerous granites in NW Spain and in Britanny, France (Pereira et al. (2014)) (FIGURE 133). The Cornubian Batholith and Goban Spur granites seem to be aligned on the same NE-SW structural lineament. However, their geochemical nature seems to be different with the Cornubian Batholith being a S-type granite (Smith et al., 2019), while the apatite trace elements from the Goban Spur granites point towards an I-type affinity, suggesting a difference in crustal nature along the lineament.

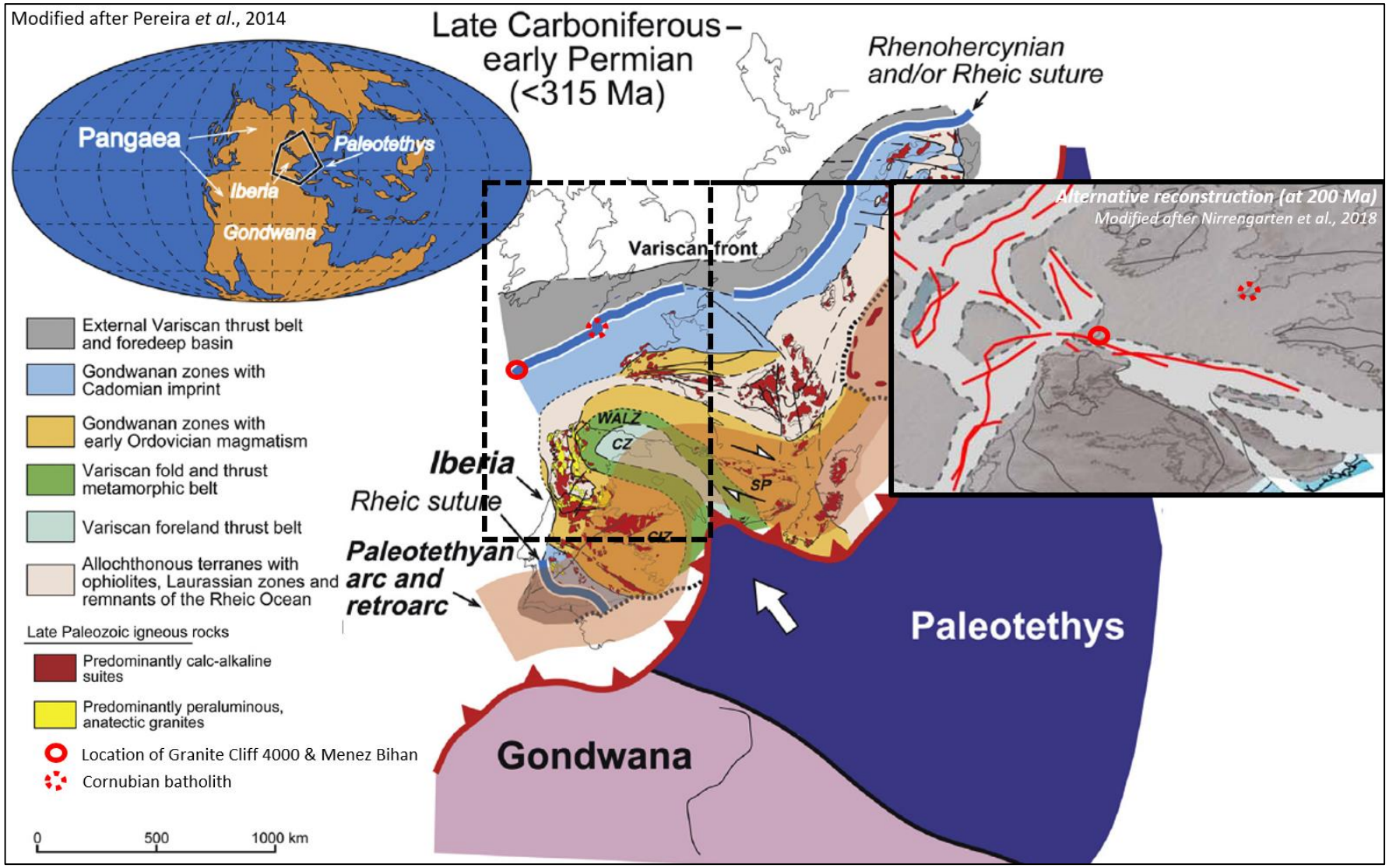

Figure 134: Location of Granite Cliff 4000 and Menez Bihan on a reconstruction of the Variscan Belt at c. 300 Ma (modified after Pereira et al. (2014).

When positioned on a pre-rifting plate reconstruction of west Europe (such as Nirrengarten et al. (2018), FIGURE 134), the Goban Spur Late Variscan granites sit on an arcuate trend between the Late Variscan granites from NW Spain and those of Cornwall and Britanny, France (the Ibero-Armorican Arc). However, in other reconstructions such as the one in Pereira et al. (2014), the Goban Spur and Cornwall granites are on the external outer edge of this arcuate trend FIGURE 134).

Although the presence and age of these Late Variscan granites have been proven since the late 1970s (Didier et al. (1977b), Auffret et al. (1979a)), they are rarely included in the regional compilations of Late Variscan magmatism (e.g. Pereira et al. (2015), Ballouard et al. (2017) see FIGURE 134). The origin of this Late Variscan magmatism is still poorly understood and the inclusion of the Goban Spur granites in future studies could help better understand this phase of magmatism.

7.2.2 Late Jurassic-Early Cretaceous magmatism (syn-rift)

New data points: 18/25-2, 26/30-1

The existence of a small Early Cretaceous magmatic province has been proposed by Calvès et al. (2012) who include the magmatic J anomaly along the Newfoundland-Galicia conjugate margins (Bronner et al., 2011), the Barra Volcanic Ridge System (BVRS, Scrutton and Bentley (1988)) and the Porcupine Margin Volcanic Ridge (PMVR, Calvès et al. (2012)) (FIGURE 135). To these features could be added the c. 133 Ma (Valanginian) lava flow in well 62/07-1 in the Goban Spur, Early Cretaceous sills along the Pendragon Escarpment in the Goban Spur as well as tholeiitic basalt at DSDP 80 site 551 (De Graciansky et al., 1985a; Yang et al., 2020), the Hauterivian-Barremian and Aptian-Albian ash bands in 35/08-1 and pyroclastics at the Barremian-Aptian boundary in 26/21-1 and at the top Albian in 35/13-1 in the Porcupine Basin (Tate and Dobson, 1988), although the pyroclastic in the last two boreholes are not described in the borehole composite logs (FIGURE 135). To this could also possibly be added the Porcupine Arch as an intrusive body (Gagnevin et al., 2017), the inferred Aptian-Albian Seabight Igneous Centre at the border between Goban Spur and the Porcupine Basin (Tate and Dobson, 1988), the lava flow at the bottom of 16/28-sb01 on the North Porcupine High (Haughton et al., 2005), clasts of undated volcanic rocks found in a breccia of Barremian-Cenomanian age at King Arthur Castle in the Goban Spur (Auffret et al., 1979a) and the lava flow in 12/02-1Z in the NE Rockall Basin that could be either Middle-Late Jurassic or Early Cretaceous in age (Serica, 2014), although this recent stratigraphic dating contradicts an older radiometric age of c. 250 Ma (Malcom Pringle pers. comm. as cited in Mecklenburgh (2003) (FIGURE 135).

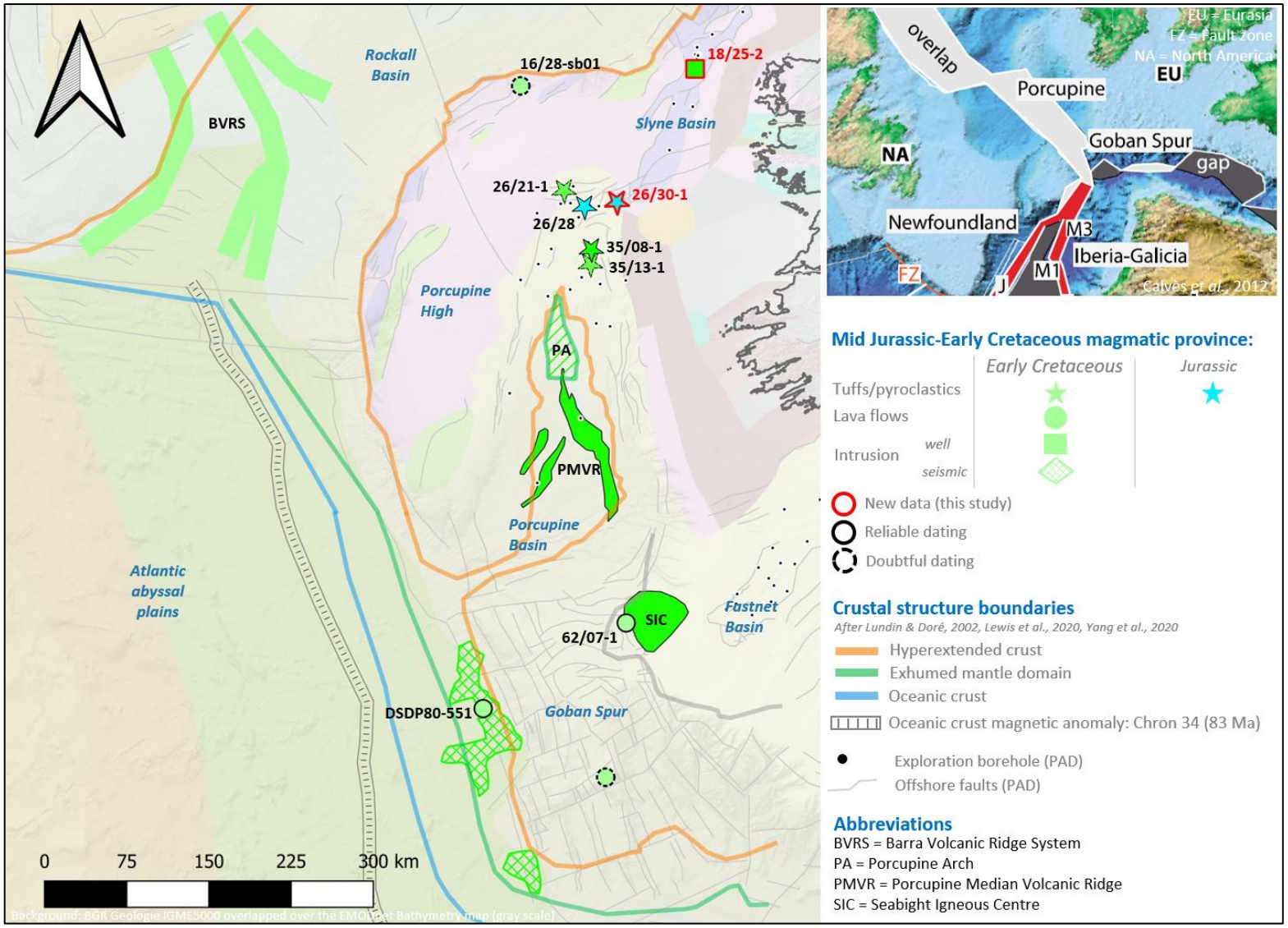

Figure 135: Map of the Middle Jurassic-Early Cretaceous magmatic province in the IAM.

The newly dated Late Jurassic-Early Cretaceous mafic intrusion in 18/25-2 (SECTION 4.6.2.2) extends the area of this magmatic province to the Slyne Basin (FIGURE 135) and provide the second radiometric age for this dataset which is otherwise dominated by correlation on seismic stratigraphy. The undated mafic intrusion in 18/25-1 (FIGURE 132), 11 km to the NNE, is therefore also probably Mesozoic in age (although a Paleogene age cannot be excluded completely).

The only proven occurrence of Jurassic magmatism in the Porcupine Basin are minor pyroclastic airfall tuffs found in Bajocian-Kimmeridgian sediments from boreholes in block 26/28 (MacDonald et al., 1987). The Middle-Late Jurassic (probably Oxfordian) apatites discovered in 26/30-1 (SECTION 5.6.4.1), 30 km to the east of block 26/28, most probably belong to the same tuffaceous horizons (FIGURE 135). An olivine-dolerite intrusion in the Fastnet Basin was dated, by biotite K-Ar, at 170 ± 4 Ma (Bajocian) (Caston et al., 1981). The Bajocian-Kimmeridgian tuffs from the Porcupine Basin and the Bajocian dolerite from the Fastnet Basin might belong to the same volcanic event. Another source for the tuffs could be the Jurassic volcanic province of the North Sea (e.g. the Rattray Volcanics (Ritchie et al. (1988), Quirie et al. (2019)).

7.2.3 Paleogene magmatism (NAIP)

New data point: 26/26-1, 34/05-1, 35/13-1, 35/15-1

A regional map of the North Atlantic Igneous Province has been compiled by Horni et al. (2017) while a compilation and analysis of the NAIP geochronological data was provided by Wilkinson et al. (2017a). Offshore Ireland, more than 20 boreholes have encountered NAIP-related rocks such as doleritic and gabbroic sills, basaltic lava flows, tuffaceous sandstones and claystones and ash beds (FIGURE 132), some of which have been presented and discussed by Seemann (1984) and Tate and Dobson (1988). Gravity, magnetic and seismic studies also contributed to the characterisation of the magmatic province offshore west of Ireland (Riddihough and Max (1976), Readman et al. (2003), Jackson et al. (2020)). The new geochronological data provide new insights into the Paleogene magmatism offshore west of Ireland.

7.2.3.1 34/05-1

An 18 m thick igneous intrusion, previously interpreted as a sandstone, has been identified in borehole 34/05-1 (1346-1364 mMD), along with with its thermal aureole which extends c. 20 m on either side. It is possible, but there is much less evidence, that other thinner intrusions are present at c. 970 mMD, 1050 mMD and at the base of the borehole (SECTION 5.4.2). A few apatites with Paleogene AFT ages are interpreted as having been reset by the magmatic activity associated with the igneous intrusions, either by conductive heating within the thermal aureole or by advective hydrothermal fluids.

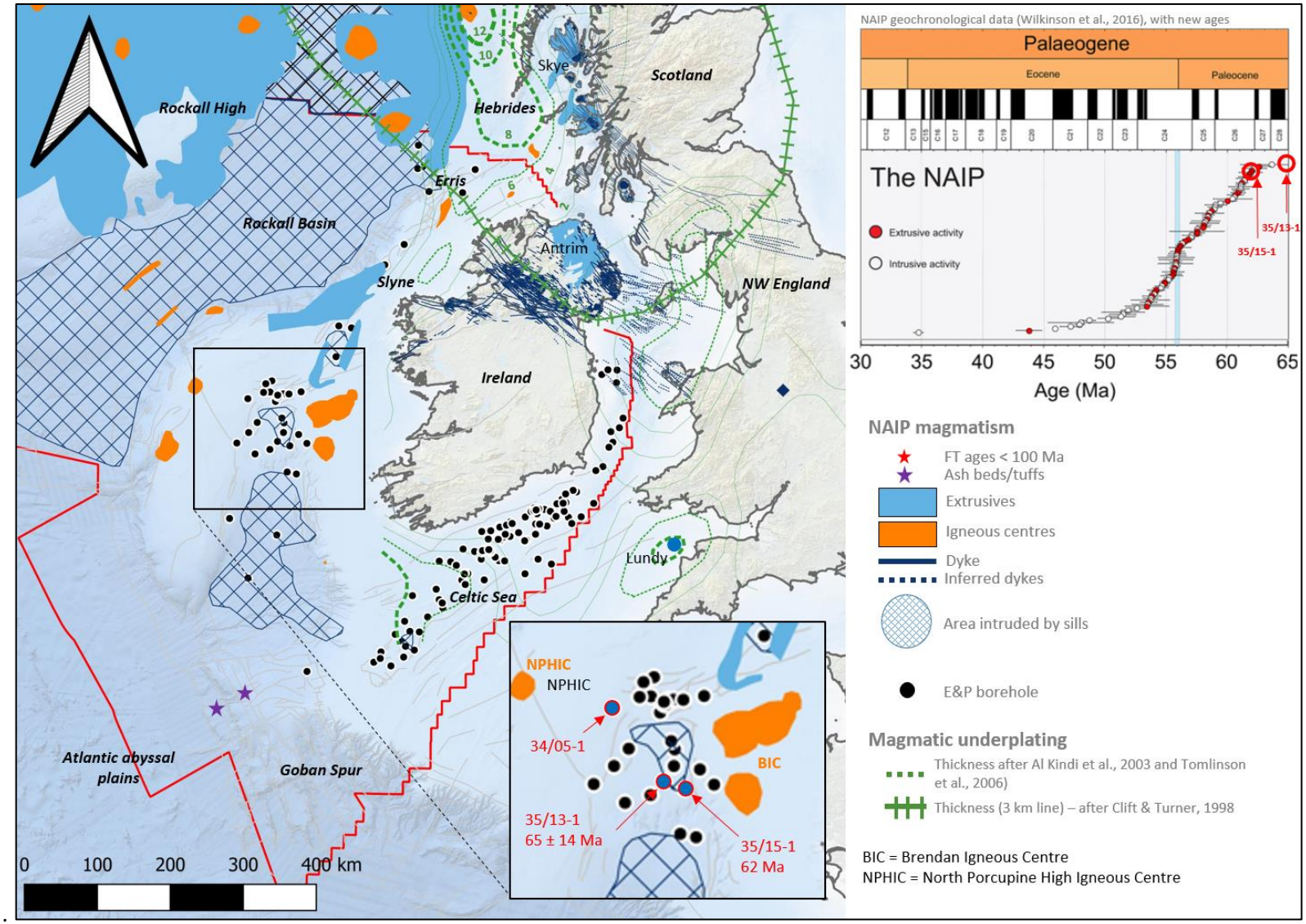

Figure 136: Map of the Irish section of the NAIP (compilation of published data and new results).

These Paleogene AFT grains, and the predominance of Paleogene mafic intrusions in the Porcupine Basin, point towards a Paleogene age for these sills. The presence of the intrusion in 34/05-1 extends the areal footprint of the Paleogene sills from the Porcupine Basin to the Porcupine High (FIGURE 136). The borehole is also located 50-70 km to the south-east of an inferred igneous centre of unknown age, the North Porcupine High Igneous Centre (NPHIC, FIGURE 136). If the NPHIC is Paleogene in age, then the intrusion(s) in 34/05-1 could also originate from this centre.

7.2.3.2 35/13-1

Three doleritic sills in 35/13-1 believed to be Late Oligocene in age (Seemann, 1984) have been dated at 61.6 ± 5.6 Ma and are therefore latest Cretaceous-Paleocene in age (probably Danian-Selandian) (SECTION 5.7.3.2).

Based on the Oligocene dating of the sills in 35/13-1 at the time, Seemann (1984) related these intrusions to dykes in the Dingle Peninsula (FIGURE 136) dated by K-Ar at 25 and 42 Ma (Horne and MacIntyre, 1975). Horne and MacIntyre (1975) interpreted these Middle Eocene and Oligocene dykes as representing a late phase of the NAIP magmatism that was spatially associated with a NW-SE-oriented fault zone and possibly originated as a dyke swarm from the Brendan Igneous Centre located c. 100 km to the north-west (Riddihough and Max, 1976) (FIGURE 136). The new dating of the sills in 35/13-1 raise doubts about the accuracy of the Oligocene K-Ar dating of the dyke onshore SW Ireland. Regionally, no other Oligocene magmatism is known on the Irish Atlantic Margin (a 18 Ma sill in 35/08-1 has been re-dated at 61 Ma, King et al. (2016)) and very few are known in the entire NAIP (Wilkinson et al., 2017a), while K-Ar dating is known to be susceptible to argon loss and consequently erroneously younger ages (Mitchell and Mohr (1986), Wilkinson et al. (2017a)).

In conclusion, although not precise, the new apatite U/Pb dating for the sills in 13/03-1 allow their re-assignment to the main pre-break-up, Paleocene phase of NAIP magmatism and point towards an erroneous dating of the dyke of SW Ireland previously dated at 20 Ma but more likely Paleocene-Eocene in age.

7.2.3.3 35/15-1

The mafic volcanism in 35/15-1 is most likely upper Danian in age (c. 62 Ma) based on its stratigraphic relationships, but could also be Selandian or basal Thanetian due to conflicting biostratigraphic data. The new apatite U/Pb data does not allow a refinement of the dating because of a large uncertainty on the discordia age (66 ± 7.5 Ma) and also because of uncertainties on the source of the apatites (probably the dolerite itself but possibly from a microconglomerate just above that in this case would be volcanoclastic in nature) (SECTION 5.8.2.1).

The presence of igneous zircons yielding a U/Pb age of 60.49 ± 0.64 Ma is interpreted as either dating the mafic magmatism itself (assuming a short period of time, <1Ma, between crystallisation in a deeper magmatic reservoir and their transport to the surface) or dating another volcanic event in the vicinity of the well (e.g. ash fall from a nearby volcanic centre such as the Brendan Centre, FIGURE 137)

The probable upper Danian age of the ultramafic volcanism is very similar to the mafic intrusions in the west of Ireland and Antrim lavas (Ganerød et al., 2010). This seems to confirm that the mafic Paleocene igneous activity might have progressed from south (West and North of Ireland, 61.97 ± 0.36 Ma and 62.6 ± 0.31 Ma) to north (West of Scotland, Faroes, 61.15 to 58.5 Ma) during the Paleocene as hypothesized by Ganerød et al. (2010) (FIGURE 137). However, the discovery of c. 60 Ma zircons in the borehole indicates a younger Selandian volcanic activity in the region which is in conflict to their hypothesis, unless this hypothesis is restricted to mafic volcanism only.

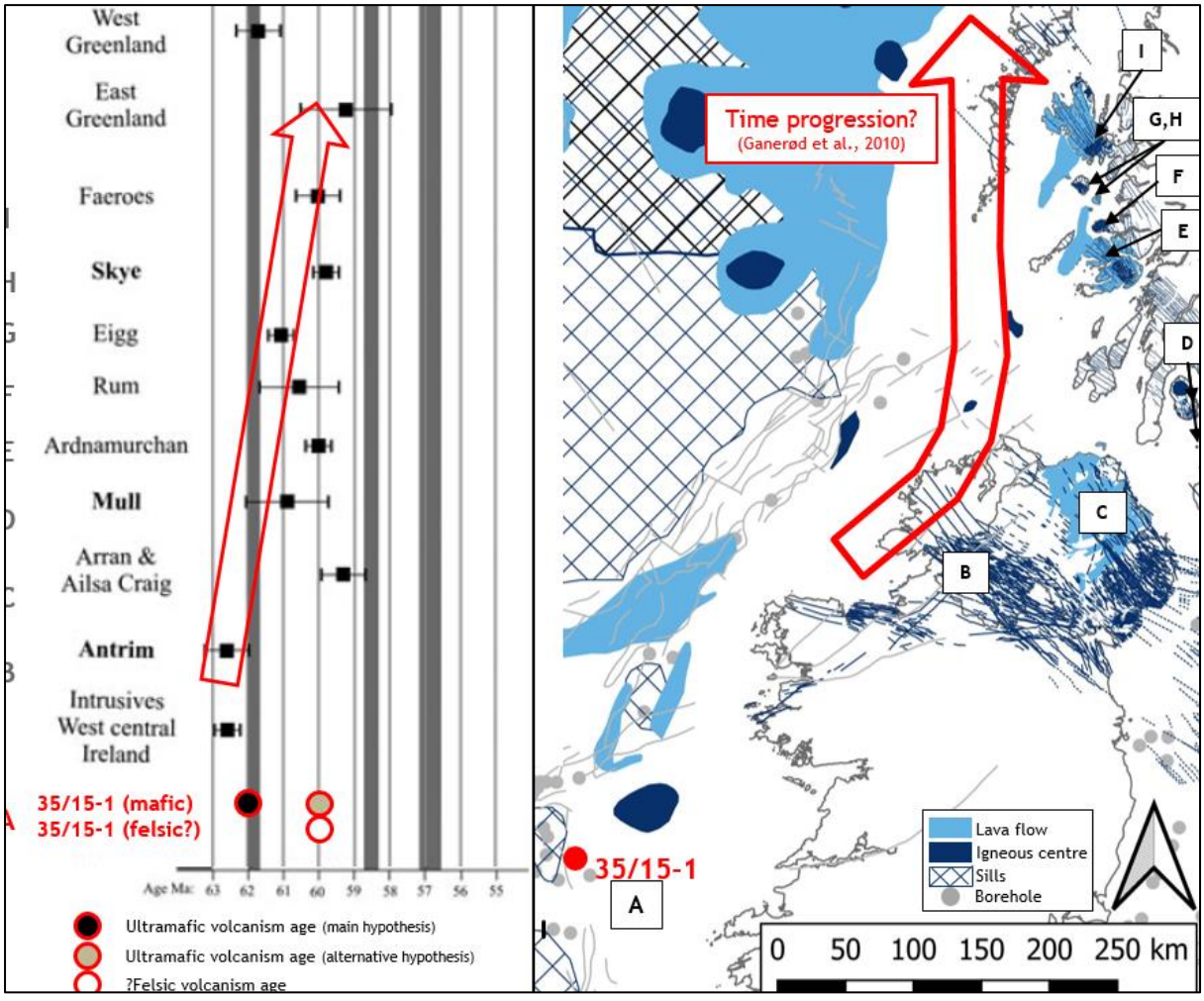

Figure 137: Well 35/15.1 volcanism in its regional context.

7.2.3.4 Magma geochemistry

Although close to each other (20 km), the doleritic sills in borehole 35/13-1 and 35/15-1 seem to have a different magma geochemistry. Most of the Paleocene apatites in borehole 35/15-1 plot (except

one) plot in the UM field of the trace element biplot while all the apatites of 35/13-1 plot within the edgeof the HM field which overlaps with the IM training points (FIGURE 138). The data suggests that the magma in 35/15-1 originated from a juvenile, relatively primitive mantle derived melt, while the magma in 35/13-1 is slightly more evolved. The Paleocene igneous zircons may also have been derived from a felsic magmatic episode indicating a bimodal magmatism which is well documented elsewhere in the NAIP of Britain and Ireland (Meade et al., 2014).

7.3 New geochronological constraints for the age and nature of the basement in the Irish Atlantic Margin

The new geochronological data provide new information on the age and nature of the basement of the North Porcupine High-North Porcupine Basin margins and at the SE tip of the Goban Spur.

7.3.1 North Porcupine High – North Porcupine Basin margins

A suite of in-situ low to high-grade metamorphic basement rocks at the bottom of well 26/26-1 (FIGURE 139) can be attributed with confidence to the Neoproterozoic Grampian Group (the lower part of the Dalradian Supergroup), based on its U/Pb detrital zircon signature (SECTION 5.3.4.1). The suite is probably an extension of the PHMS that crops out on the summit of the Porcupine High, 60 km to the northwest of 26/26-1 (Tyrrell, 2013) (FIGURE 139). The basement rocks were subjected to Late Caledonian metamorphism or contact metamorphism to temperatures >450°C that reset the U/Pb age of most the apatites (at 392 Ma). This data point provides a new robust (i.e. in-situ) constraint on the nature and age of the basement rocks in the area and on the location of the Iapetus Suture, and also most probably the Fair Head-Clew-Bay Line, which must both pass south of 26/26-1.

The new zircon U/Pb data for the Late Cretaceous sandstone in 16/28-sb01 (FIGURE 139) indicates that it is probably sourced from an outcrop of Proterozoic basement comprised of rocks with an age of c. 1.7 and 1.3 Ga (SECTION 5.2.5.4). A Proterozoic basement was already suggested by Tyrrell et al. (2007) for the North Porcupine High, based on *in-sit*u Pb isotopic analysis of detrital K-feldspar from the same Late Cretaceous sandstone. This outcrop is probably located on the NW flank of the where a c. 1.3 Ga gneiss (the NPHO) has previously been identified (Daly et al. (2008c), Chew et al. (2019)) and where a c. 1.5-2.02 Ga gneiss complex equivalent to the Annagh Gneiss Complex (AGC) is also suspected (Chew et al., 2019). The dominance of c. 1.7 Ga grains in this locally sourced Upper Cretaceous sandstone confirms that such an AGC equivalent is indeed likely present on the NW flank of the North Porcupine High (FIGURE 139). The absence of Cadomian, Archean and rarity of Caledonian grains indicate that at the time of deposition during the Late Cretaceous, the summit of the North Porcupine High was probably above sea level, maybe as an island providing the source of clastic materials being deposited in shallow waters on the margin of the high such as at the location of 16/28-sb01.

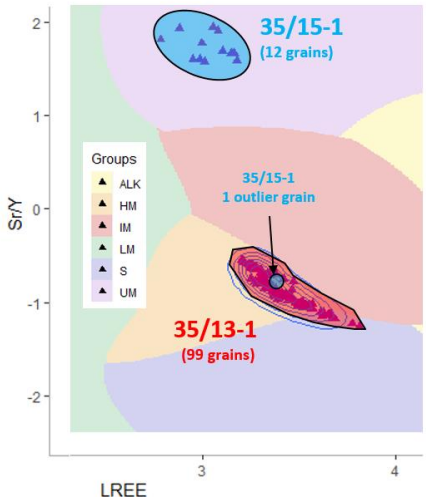

Figure 138: Comparison of the apatite trace element biplot for sills in 35/13-1 and 35/15-1.

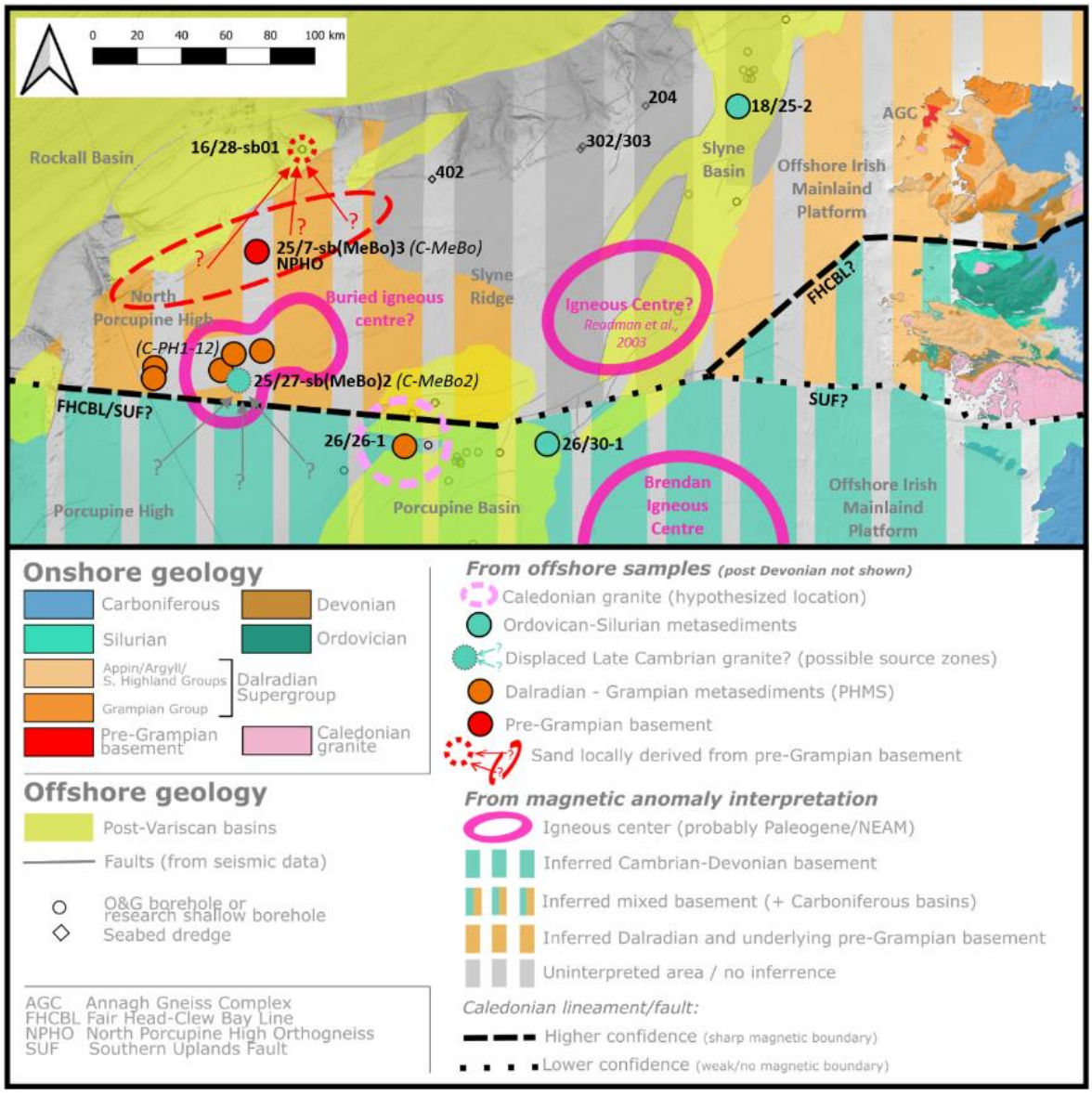

Figure 139: Geological map of the basement of the North Porcupine High and surrounding areas.

The high-velocity lithology at the bottom of 26/30-1 has been described as a granite by the well site geologist, however the new apatite and zircon U/Pb data points towards either a Silurian metamorphic conglomerate sourced from a Dalradian basement and reworked Orovician metasediments or a younger Devonian or Early Carboniferous compacted sandstone sourced from a Dalradian basement and Ordovician-Silurian metasediments (SECTION 5.6.4). Silurian claystones, siltstones and sandstones have been encountered at the bottom of borehole 18/25-2 and attributed to the Wenlock Formation (Geerlings, 2000), which is the only Silurian basement drilled offshore Ireland (Petroleum Infrastructure Program, 2020). . Silurian rocks crops out in on the coast Co. Mayo and Co. Galway, c. 150 km ENE of 26/30-1, at Clare Island, Louisburgh and Croagh Patrick (Holland, 2009). These rocks comprise conglomerates with clasts from the underlying Proterozoic basement as well as sandstones and tuffs (Holland, 2009), which could explain the mix of detrital metamorphic Proterozoic grains and syn-sedimentray igneous and metamorphic grains. The remnants of the onshore Ordovician-Silurian basins are located close and across the Fair Head-Clew Bay Line (FHCBL), a Caledonian lineament that represents the locus of collison of the Laurentian margin with a volcanic arc and the development of a forearc basin and orogenic and post-orogenic extensional basins during that time (Holland and Saunders, 2009). Since 26/30-1 is also located near the expected offshore extension of the FHCBL (FIGURE 139), the presence of Silurian basement at this location is not unlikely. Robeson et al. (1988) observed that the lack of high levels of maturity in the Carboniferous sediments of 26/30-1 indicated that the granite did not act as 'heat chimney' as observed in most cases onshore Ireland. The presence of a metasedimentary rather than granitic basement resolves this apparent discrepancy.

In conclusion, the new geochronological data acquired in this study allows to incrementally refine our understanding of the nature and age of the basement of the North Porcupine High and Slyne Ridge/North Porcupine Basin margins and of the location of the offshore extensions of the major Caledonian faults and lineaments.

7.3.2 Goban Spur (GS)

A clast of metamorphic rock at Menez Bihan (R-27) is interpreted as a granulite from a domain of *in-situ* Avalonian crust that formed or was metamorphosed during the Cadomian Orogeny (crystallisation of the matrix zircons at 571.2 ± 7.5 Ma) and subsequently affected by the main phase of the Caledonian orogeny (crystallisation of the apatites at 446 ± 11 Ma). At c. 297 Ma, during the Late Variscan magmatic activity, new zircon growth was detected, and may be associated with hydrothermal fluids or aplitic magmas linked to the emplacement of the MB granitic pluton. The inherited zircons found in the Late Variscan granites also support the presence of Avalonian basement in the area.

An Archean metamorphic rock yielded a zircon U/Pb age of 2764 ± 24 Ma and an apatite U/Pb age of 1714 ± 16 Ma. Although a fragment of relict Archean relict basement is plausible at this location based on plate reconstructions and the existence of a Proterozoic basement in the North Armorican domain, the Eocene AFT and AHe ages of the sample are difficult to explain at this location as either kilometre-scale erosion and/or Eocene magmatism would be required but are unlikely to be present on this part of the IAM. An alternative interpretation is that the Goban Spur sample is ice-rafted debris (IRD) from the Archean Lewisian basement of NW Scotland or the Archean basement of Greenland, where NAIP-related igneous centres caused resetting of AFT/AHe ages in the surrounding country rock. Indeed, a large zone of IRD deposition extends across the Atlantic from Newfoundland to the Goban Spur with debris originating from NE Canada, Greenland, Iceland and the British Isles (Peck et al., 2007). It is thus possible that the Archean and some of the Proterozoic granulites dredge samples from the North Iberian Margin may also represent ice-rafted debris which sheds some doubts on the tectonic reconstructions of crustal provinces undertaken in previous studies. For example, a 52 Ma AFT central age has been obtained for granulite sample from the Le Danois Bank and is interpreted as reheating during thrust stacking associated with the subduction of the Bay of Biscay oceanic crust under the Iberian Margin during the Late Cretaceous and Early Paleogene (Fügenschuh et al., 2003) but more likely represents IRD.

8 Conclusions and perspectives

The main objectives of the study were to constrain better the Mesozoic and Cenozoic exhumation events of the IAM, as has been successfully done onshore Ireland and the UK in recent years with the acquisition and modelling of both AFT/AHe datasets along vertical profiles.

A new dataset of modern low-temperature thermochronological data has been acquired on samples from boreholes and seabed dredges from the Irish Atlantic Margin (IAM). Igneous intrusions and basement rocks were primarily targeted but sandstones were also sampled in order to create vertical profiles within boreholes that allows the detection of small-scale magnitude exhumation events. While the sampling was a success thanks to the participation of PAD and the use of their core store, half of the samples did not yield enough apatite for thermal history modelling. The low number of suitable samples was however partially compensated by the compilation, reinterpretation and integration of legacy samples from a set of Geotrack reports provided by PAD and from published papers.

8.1 Thermochronology results

The new thermal histories for Mesozoic show that the Late Jurassic and Early Cretaceous are the two main phases of exhumation and cooling on the IAM. No north to south diachronous Mesozoic cooling and exhumation is observed as has been detected onshore west of Ireland. A compilation of legacy AFT/AHe data across Britain and Ireland and their offshore platforms shows for the first time an age pattern with older AFT ages in Scotland and Northern Ireland than in the rest of Ireland. This pattern is tentatively attributed to the influence of the Anton-Dohrn Transfer Zone (ADTZ) during an Early Cretaceous phase of plate-wide uplift that resulted in more exhumation to the SW of the transfer zone than to the NE. Early Cretaceous exhumation ages observed to the north of the ADTZ (e.g. 13/03-1, offshore NW Donegal) would have resulted from small-wavelength rift shoulder uplift that did not affect areas further away from the hyperextending basins (e.g. onshore Donegal). Caledonian faults might also create differential exhumation of the tectonic blocks between them, as is observed in the compilation of AFT data from northern Scotland and this could explain the dispersion in the timing of exhumation seen on the North Porcupine High.

The Paleogene exhumation visible in the Central Irish Sea and other parts of the NEAM has not been detected in the northern part of the IAM (well 13/03-1 in the Donegal Basin) despite the well being underlain by a high-velocity body at the base of the crust that has been interpreted as representing igneous underplating. However, c. 1 km exhumation has been detected on the North Porcupine High, which probably acted as one of the main source of sediments to the delta being formed at that time

in the northern part of the Porcupine Basin. However, detecting Paleogene exhumation offshore west of Ireland can be complicated by the possibility of hot fluids (from the coeval NAIP magmatism) having perturbed the AFT and AHe systems.

A significant Miocene exhumation (possibly greater than 1 km) has been detected in the northern part of the IAM (offshore NW Ireland), which is in agreement with previous AFT and seismostratigraphy studies undertaken in the NE Rockall, Erris and Slyne Basins, suggesting that the entire area was affected. However, the exhumation does not seem to extend to the North Porcupine High, nor the eastern platform of the Porcupine Basin. Finally, the Late Neogene exhumation event recognized in vertical profiles onshore west of Ireland has not been confirmed in any of the studied offshore samples. Some samples on the North Porupine High and Goban Spur yield such a Late Neogene cooling event but are believed to be modelling artefact due to biases in the track length distribution data. A zone with accelerated subsidence of Pliocene (or possibly even as old as Miocene) to recent age on the eastern margin of the Porcupine Basin (35/15-1) has been detected by thermal history modelling and might have been fed by detritus from the SW Irish onshore that was being uplifted at the time.

8.2 Geochronology results

FT-U/Pb dual-dating of apatites and U/Pb dating of zircons from basement and igneous rocks produced new additional constraints on the basement geology and spatial and temporal distribution of magmatism on the Irish Atlantic Margin.

On the North Porcupine High and margins of the North Porcupine Basin, the Dalradian basin has been proven to extend to the SE of the PHMS in an area (26/26-1, Finnian's Spur) that was affected by Caledonian metamorphism or magmatism, unlike the PHMS where Caledonian tectonomagmatic events did not reset detrital apatite U-Pb ages. A local detrital source for 1.7 Ga zircon has been confirmed on the NW flank of the North Porcupine High, which together with the previously documented 1.3 Ga orthogneiss form a Proterozoic gneissic basement. The age of this basement unit is similar to the age range of the oldest components of the Annagh Gneiss Complex of NW Mayo, comprising the Mullet Gneiss (1.753 ± 0.003 Ga), the Cross Point Gneiss (1.271 ± 0.006 Ga, 1.287 ± 0.038 Ga), the Doolough Granite (1.015 Ga) and some pegmatites (0.98-0.99 Ga) (DALY, 1996). They might therefore both belong to the same Proterozoic basement unit. Finally, a granite at the bottom of 26/30-1 has been re-interpreted as a Silurian meta-conglomerate (or a Devonian-Early Carboniferous compacted conglomerate) sourced from a Dalrdian basement and Ordovician metasediment basin, which might be affiliated and an offshore extension along the Fair-Head Clew Bay Line of the Silurian rocks of onshore Co. Mayo and Co. Galway.

In the Goban Spur, an Archean metamorphic clast with an Eocene AFT/AHe age is probably an ice-drifted clast originating from the Lewisian basement of NW Scotland or the Archean basement of SE Greenland (both of which have been affected by Paleogene NAIP magmatism that could explain the Eocene thermochronoligcal ages) and deposited at the eastern extremity of a zone of preferential deposition spanning the central North Atlantic between Newfoundland and the Goban Spur. Alternatively, but less likely, the clast might have been derived from a local relic basement that once formed a continuous Archean-Proterozoic basement extending from the North Armorican Domain (Icartian basement) to the Ortegal Plateau/southern Goban Spur and the Galicia Bank, before being fragmented by the opening of the Bay of Biscay during the Cretaceous. The high likelihood that the clast is ice-drifted, shed doubts on the origin of other Proterozoic and Archean clasts found along the North Iberian Margin and that have previously been interpreted as representing *in-situ* or near-*in-situ* basement.

The Goban Spur samples also confirm the presence of Late Variscan granitoids that belong to the Ibero-Armorican Arc but which are often ignored in the regional reconstructions of the Late Variscan magmatic belt of NW Europe. Finally, a Cadomian granulite at Menez Bihan might represent *in-situ* basement belonging to the Avalonian continent, which is supported by the rare Cadomian inherited zircons found in the Late Variscan granites.

An undated gabbro in a borehole located offshore NW Donegal (13/03-1) was dated at 297 Ma and is interpreted as a tilted gabbroic dyke that may represent the westernmost extension of the latest Carboniferous-earliest Permian tholeiitic Scottish dyke swarm. A sandstone from the eastern margin of the North Porcupine Basin (26/30-1) was revealed to be of tuffaceous origin and yielded Oxfordian volcanic apatite, while an undated dolerite from the Slyne Basin (18/25-2) was dated as Late Jurassic to Early Cretaceous. A sill of probably Paleogene age and previously interpreted as a sandstone was discovered in a borehole on the eastern margin of the North Porcupine High (34/05-1). The Late Oligocene age of three sills in a borehole from the Porcupine Basin (35/13-1) has been revised to Danian-Selandian, while the sills and lava flows from a nearby borehole (35/15-1) revealed a probable Danian age for the mafic magmatism but also Selandian zircons that are interpreted as sourced from a tuffaceous microconglomerate just above the basalts.

8.3 Perspectives

Improvements of the protocol

Dolerite and gabbros are useful targets for an offshore study as they provide igneous apatites that are best suited for thermochronological studies but which are rarely found in offshore borehole samples. However, these mafic igneous rocks have usually very low uranium content (a few ppm for the

intrusions in this study) and therefore do not yield enough confined track lengths for their use as input data in thermal history modelling. The use of ^{252}Cf irradiation for such samples would help increase the number of track lengths. The trace element concentrations routinely measured during the LAFT analysis could also be used to categorize the AFT grains into groups with different annealing characteristics.

Future studies

This geographically and temporally large-scale low-temperature geo-thermochronological study could be viewed as a reconnaissance study for more detailed and localized studies of the IAM. The detection of small magnitude events relies on the integration of many input data and geo-thermochronometers in order to reduce the number of possible thermal histories and would therefore be better suited to the study of multi-proxy datasets made of a few boreholes within a small area.

The Paleocene-Eocene exhumation event identified on the North Porcupine High is visible as a wavy unconformity in the seismic data of the North porcupine Basin. Although maybe not as marked as the one in the Faroe-Shetland Basin that led to the mapping of a paleo-dendritic drainage pattern interpreted as the result of transient uplift, the mapping of this surface in the 3D seismic cubes of the IAM could lead to a better understanding of the extent of this event in the IAM and its relationship to the coeval deposits in the deeper parts of the Porcupine Basin.

The absence of a detectable Paleogene exhumation event in 13/03-1 sheds some doubt on the usual interpretation of the high-velocity bodies at the base of crust as representing igneous underplating and/or on the assumption that igneous underplating is associated with exhumation. A thick (<10 km) high-velocity body is believed to be present under the Outer Hebrides and the neighbouring offshore (in particular St Kilda). Reinterpreting the legacy AFT/AHe data there and acquiring new vertical profiles in this area would better test the link between underplating and exhumation and which has been invoked to explain the Paleogene exhumation of the Irish Sea/NW England region.

Comparing the latest tectonostratigraphic information derived from seismic and borehole studies to the new exhumation data might help refine the geodynamical history of the area and better understand the sedimentary response to exhumation.

Basement rocks that have never been radiometrically dated are present in a few wells in the Porcupine and Slyne Basins. A geochronological (and possibly thermochronological) study of these basement rocks, combined with a study of the latest gravity and magnetic maps, might help better constrain the nature and age of the basement of the IAM and the offshore extensions of the main Caledonian lineaments and faults to better understand the evolution of the Caledonian Orogeny in Britain and Ireland.

9 References

Ady, B. E., and Whittaker, R. C., 2019, Examining the influence of tectonic inheritance on the evolution of the North Atlantic using a palinspastic deformable plate reconstruction, *in* Wilson, R. W., Houseman, G. A., McCaffrey, K. J. W., Doré, A. G., and Buiter, S. J. H., eds., Fifty Years of the Wilson Cycle Concept in Plate Tectonics, Volume 470, Geological Society of London, p. 0.

Al-Kindi, S., White, N., Sinha, M., England, R., and Tiley, R., 2003, Crustal trace of a hot convective sheet: Geology, v. 31, no. 3, p. 207-210.

Allen, P. A., Bennett, S. D., Cunningham, M. J. M., Carter, A., Gallagher, K., Lazzaretti, E., Galewsky, J., Densmore, A. L., Phillips, W. E. A., Naylor, D., and Hach, C. S., 2002, The post-Variscan thermal and denudational history of Ireland: Geological Society, London, Special Publications, v. 196, no. 1, p. 371-399.

Anell, I., Thybo, H., and Artemieva, I. M., 2009, Cenozoic uplift and subsidence in the North Atlantic region: Geological evidence revisited: Tectonophysics, v. 474, no. 1-2, p. 78-105.

Anonymous, P. P. C. I., 1982, 26/30-1 Final Well Report.

Antoine, C., Bruand, E., Guitreau, M., and Devidal, J.-L., 2020, Understanding Preservation of Primary Signatures in Apatite by Comparing Matrix and Zircon-Hosted Crystals From the Eoarchean Acasta Gneiss Complex (Canada): Geochemistry, Geophysics, Geosystems, v. 21, no. 7, p. e2020GC008923.

Armstrong, A. J., 1982, 26/30-1 Composite Llog: Phillips Petroleum Company.

Arrowsmith, S. J., Kendall, J. M., White, N., VanDecar, J. C., and Booth, D. C., 2005, Seismic imaging of a hot upwelling beneath the British Isles: Geology, v. 33, no. 5, p. 345-348.

Auffret, G., Auzende, J.-M., Cousin, M., Coutelle, A., Dobson, M., Geoghegan, M., Masson, D., Rolet, J., and Vaillant, P., 1987, Géologie des Escarpements de Porcupine et de Goban (N.E. Atlantique). Résultats de la campagne de plongée CYAPORC: Comptes Rendus de l'Academie des Sciences Serie II, v. 304, no. 16, p. 1003-1008.

Auffret, G., Pastouret, L., Cassat, G., de Charpal, O., Cravatte, J., and Guennoc, P., 1979a, Dredged Rocks from the Armorican and Celtic Margins: Initial Reports of the Deep Sea Drilling Project, v. 48, p. 473-491.

Auffret, G., Pastouret, L., Cassat, G., De Charpal, O., Cravatte, J., and Guennoc, P., 1979b, Dredged Rocks from the Armorican and Celtic Margins: Initial Reports of the Deep Sea Drilling Project (U. S. Government), 1979 , Vol. 68 , P. 473-491.

Ault, A. K., and Flowers, R. M., 2012, Is apatite U–Th zonation information necessary for accurate interpretation of apatite (U–Th)/He thermochronometry data?: Geochimica et Cosmochimica Acta, v. 79, p. 60-78.

Auzende, J. M., Cousin, M., Coutelle, A., Dobson, M., Geoghegan, M., Masson, D., Rolet, J., and Vaillant, P., 1989, Stratigraphie des escarpements encadrant la baie de Porcupine : résultats préliminaires de la campagne Cyaporc (juillet-août 1986): Oceanologica Acta, v. 12, no. 3, p. 117-131.

Ballouard, C., Poujol, M., Boulvais, P., and Zeh, A., 2017, Crustal recycling and juvenile addition during lithospheric wrenching: The Pontivy-Rostrenen magmatic complex, Armorican Massif (France), Variscan belt: Gondwana Research, v. 49, p. 222-247.

Barbarand, J., Hurford, T., and Carter, A., 2003, Variation in apatite fission-track length measurement: implications for thermal history modelling: Chemical Geology, v. 198, no. 1, p. 77-106.

Barnett-Moore, N., Hassan, R., Flament, N., and Müller, D., 2017, The deep Earth origin of the Iceland plume and its effects on regional surface uplift and subsidence: Solid Earth, v. 8, no. 1, p. 235-254.

Barry, A., Sun, K., and Tyrrell, S., 2017, IS13/10: Sourcelands, sand provenance and supply to North Atlantic margin basins: An integrated, multi-proxy approach: PIP.

Baxter, K., Buddin, T., Corcoran, D. V., and Smith, S., 2001, Structural modelling of the south Porcupine Basin, offshore Ireland: implications for the timing, magnitude and style of crustal extension: Geological Society, London, Special Publications, v. 188, no. 1, p. 275-290.

Biancotto, F., 2012, Estimating exhumation from seismic stacking velocity data : a case study from the Slyne Basin, offshore NW Ireland [PhD PhD]: TCD, 190 p.

Biancotto, F., Hardy, R. J. J., and Jones, S. M., Estimating The Magnitude Of Exhumation From 2D And 3D Seismic Velocity Datasets: A Case Study From Slyne Basin, Offshore Northwestern Ireland, *in* Proceedings SPE Offshore Europe Oil & Gas Conference & Exhibition2009/09/08/11 2009, Volume SPE 124191: Aberdeen, UK, SPE, p. 15.

Boschmann Käthler, W., 1986, Uran und Helium in Erzmineralien

und die Frage ihrer Datierbarkeit. Inaugural-Dissertation., Heidelberg, Universität Heidelberg, Heidelberg, Heidelberger Geowiss. Abh., 234 p.:

Bott, M. H. P., and Bott, J. D. J., 2004, The Cenozoic uplift and earthquake belt of mainland Britain as a response to an underlying hot, low-density upper mantle: Journal of the Geological Society, v. 161, no. 1, p. 19-29.

Boutoutaou, D., 2006, Geochemical evaluation of the Carboniferous in the 13/12-1 well, Ireland: Fugro Robertson Limited.

Brodie, J., and White, N., 1994, Sedimentary basin inversion caused by igneous underplating: Northwest European continental shelf: Geology, v. 22, no. 2, p. 147-150.

-, 1995, The link between sedimentary basin inversion and igneous underplating: Geological Society, London, Special Publications, v. 88, no. 1, p. 21-38.

Bronner, A., Sauter, D., Manatschal, G., Péron-Pinvidic, G., and Munschy, M., 2011, Magmatic breakup as an explanation for magnetic anomalies at magma-poor rifted margins: Nature Geoscience, v. 4, no. 8, p. 549-553.

Brown, R., Gallagher, K., and Duane, M., 1994, A quantitative assessment of the effects of magmatism on the thermal history of the Karoo sedimentary sequence: Journal of African Earth Sciences, v. 18, no. 3, p. 227-243.

Bullock, A. D., and Minshull, T. A., 2005, From continental extension to seafloor spreading: crustal structure of the Goban Spur rifted margin, southwest of the UK: Geophysical Journal International, v. 163, no. 2, p. 527-546.

Burke, K., and Torsvik, T. H., 2004, Derivation of Large Igneous Provinces of the past 200 million years from long-term heterogeneities in the deep mantle: Earth and Planetary Science Letters, v. 227, no. 3, p. 531-538.

Calk, L. C., and Naeser, C. W., 1973, The Thermal Effect of a Basalt Intrusion on Fission Tracks in Quartz Monzonite: The Journal of Geology, v. 81, no. 2, p. 189-198.

Calvès, G., Torvela, T., Huuse, M., and Dinkleman, M. G., 2012, New evidence for the origin of the Porcupine Median Volcanic Ridge: Early Cretaceous volcanism in the Porcupine Basin, Atlantic margin of Ireland: Geochemistry, Geophysics, Geosystems, v. 13, no. 6, p. n/a-n/a.

Calvez, J. Y., and Vidal, P., 1978, Two billion years old relicts in the Hercynian belt of Western Europe: Contributions to Mineralogy and Petrology, v. 65, no. 4, p. 395-399.

Capdevila, R., Boillot, G., Lepvrier, C., LMalod, J., and Mascle, G., 1980, Les formations cristallines du Banc Le

Danois (marge nord-ibérique). Comptes Rendus de l'Academie des Sciences Serie II, v. 291, p. 317-320.

Carlson, W. D., Donelick, R. A., and Ketcham, R. A., 1999, Variability of apatite fission-track annealing kinetics; I, Experimental results: American Mineralogist, v. 84, no. 9, p. 1213-1223.

Carminati, E., Cuffaro, M., and Doglioni, C., 2009, Cenozoic uplift of Europe: Tectonics, v. 28, no. 4.

Carter, A., 1990, The thermal history and annealing effects in zircons from the Ordovician of North Wales: International Journal of Radiation Applications and Instrumentation. Part D. Nuclear Tracks and Radiation Measurements, v. 17, no. 3, p. 309-313.

Carter, A., Bristow, C. S., and Hurford, A. J., 1995, The application of fission track analysis to the dating of barren sequences: examples from red beds in Scotland and Thailand: Geological Society, London, Special Publications, v. 89, no. 1, p. 57-68.

Caston, V., Dearnley, R., Harrison, R., Rundle, C., and Styles, M., 1981, Olivine-dolerite intrusionsin the Fastnet Basin: Journal of The Geological Society - J GEOL SOC, v. 138, p. 31-46.

Cawood, P. A., Nemchin, A. A., Smith, M., and Loewy, S., 2003, Source of the Dalradian Supergroup constrained by U–Pb dating of detrital zircon and implications for the East Laurentian margin: Journal of the Geological Society, v. 160, no. 2, p. 231-246.

Cawood, P. A., Nemchin, A. A., Strachan, R., Prave, T., and Krabbendam, M., 2007, Sedimentary basin and detrital zircon record along East Laurentia and Baltica during assembly and breakup of Rodinia: Journal of the Geological Society, v. 164, no. 2, p. 257-275.

Chamberlain, K. R., and Bowring, S. A., 2001, Apatite–feldspar U–Pb thermochronometer: a reliable, mid-range (~450°C), diffusion-controlled system: Chemical Geology, v. 172, no. 1, p. 173-200.

Chambers, L. M., Pringle, M. S., and Parrish, R. R., 2005, Rapid formation of the Small Isles Tertiary centre constrained by precise 40Ar/39Ar and U–Pb ages: Lithos, v. 79, no. 3, p. 367-384.

Champion, M. E. S., White, N. J., Jones, S. M., and Lovell, J. P. B., 2008a, Quantifying transient mantle convective uplift: An example from the Faroe-Shetland basin: Tectonics, v. 27, no. 1.

-, 2008b, Quantifying transient mantle convective uplift: An example from the Faroe-Shetland basin: Tectonics, v. 27, no. 1, p. TC1002.

Chapman, T. J., Broks, T. M., Corcoran, D. V., Duncan, L. A., and Dancer, P. N., 1999, The structural evolution of the Erris Trough, offshore northwest Ireland, and implications for hydrocarbon generation: Geological Society, London, Petroleum Geology Conference series, v. 5, p. 455-469.

Charles, J. H., Whitehouse, M., Andersen, J., Shail, R., and Searle, M., 2017, Age and petrogenesis of the Lundy granite: Paleocene intraplate peraluminous magmatism in the Bristol Channel, UK: Journal of the Geological Society, v. 175, p. jgs2017-2023.

Chen, Y., Zentilli, M. A., Clark, A. H., Farrar, E., Grist, A. M., and Willis-Richards, J., 1996, Geochronological evidence for post-Variscan cooling and uplift of the Carnmenellis granite, SW England: Journal of the Geological Society, v. 153, no. 2, p. 191-195.

Chew, D., and Cogné, N., 2015, No title (apatite U/Pb results summary): TCD.

Chew, D., and Donelick, R. A., 2012, Combined apatite fission track and U-Pb dating by LA-ICP-MS and its application in apatite provenance analysis, *in* Sylvester, P., ed., Quantitative Mineralogy and Microanalysis of Sediments and Sedimentary Rocks: St John's NL, Mineralogical Association of Canada, p. 219-247.

Chew, D., O'Sullivan, G., Caracciolo, L., Mark, C., and Tyrrell, S., 2020, Sourcing the sand: Accessory mineral fertility, analytical and other biases in detrital U-Pb provenance analysis: Earth-Science Reviews, v. 202, p. 103093.

Chew, D., Tyrrell, S., Daly, J. S., Cogné, N., Sun, K., and Badenszki, E., 2019, The basement geology of the Porcupine High - A key transatlantic link between the Caledonides and Appalachians, GSA 2019, Volume 51: Phoenix, Arizona, USA, GSA.

Chew, D. M., Donelick, R. A., Donelick, M. B., Kamber, B. S., and Stock, M. J., 2014a, Apatite Chlorine Concentration Measurements by LA-ICP-MS: Geostandards and Geoanalytical Research, v. 38, no. 1, p. 23-35.

Chew, D. M., Petrus, J. A., and Kamber, B. S., 2014b, U–Pb LA–ICPMS dating using accessory mineral standards with variable common Pb: Chemical Geology, v. 363, p. 185-199.

Clift, P. D., and Turner, J., 1998, Paleogene igneous underplating and subsidence anomalies in the rockall-Faeroe-Shetland area: Marine and Petroleum Geology, v. 15, no. 3, p. 223-243.

Cloetingh, S., Gradstein, F. M., Kooi, H., Grant, A. C., and Kaminski, M., 1990, Plate reorganization: a cause of rapid late Neogene subsidence and sedimentation around the North Atlantic?: Journal of the Geological Society, v. 147, no. 3, p. 495-506.

Cochrane, R., Spikings, R. A., Chew, D., Wotzlaw, J.-F., Chiaradia, M., Tyrrell, S., Schaltegger, U., and Van der Lelij, R., 2014, High temperature (>350°C) thermochronology and mechanisms of Pb loss in apatite: Geochimica et Cosmochimica Acta, v. 127, p. 39-56.

Cogné, N., and Chew, D., 2017, Porcupine High sample thermochornology results: PIP.

Cogné, N., Chew, D., and Stuart, F. M., 2014, The thermal history of the western Irish onshore: Journal of the Geological Society, v. 171, no. 6, p. 779-792.

Cogné, N., Chew, D. M., Donelick, R. A., and Ansberque, C., 2020, LA-ICP-MS apatite fission track dating: A practical zeta-based approach: Chemical Geology, v. 531, p. 119302.

Cogné, N., Doepke, D., Chew, D., Stuart, F. M., and Mark, C., 2016, Measuring plume-related exhumation of the British Isles in Early Cenozoic times: Earth and Planetary Science Letters, v. 456, p. 1-15.

Cohen, K. M., Finney, S. C., Gibbard, P. L., and Fan, J.-X., 2013 updated 2020, ISC International Stratigraphic Chart: Episodes, v. 36, p. 199-204.

Colin, J.-P., Ioannides, N. S., and Vining, B., 1992, Mesozoic stratigraphy of the Goban Spur, offshore south-west Ireland: Marine and Petroleum Geology, v. 9, no. 5, p. 527-541.

Cooper, B. S., Collins, A. G., and McEwan, J., 1978, Vitrinite reflectivity and Rock-Eval pyrolysis data on samples from the Texaco Ireland 13/3-1 well, offshore north-west Ireland: Robertson Research International Limited.

Corcoran, D. V., 2006, Exhumation in Irish sedimentary basins and implications for hydrocarbon exploration, offshore IrelandPhD]: Trinity College Dublin, 193 p.

Corcoran, D. V., and Clayton, G., 2001, Interpretation of vitrinite reflectance profiles in sedimentary basins, onshore and offshore Ireland: Geological Society, London, Special Publications, v. 188, no. 1, p. 61-90.

Corcoran, D. V., and Doré, A. G., 2005, A review of techniques for the estimation of magnitude and timing of exhumation in offshore basins: Earth-Science Reviews, v. 72, no. 3–4, p. 129-168.

Corcoran, D. V., and Mecklenburgh, R., 2005, Exhumation of the Corrib Gas Field, Slyne Basin, offshore Ireland: Petroleum Geoscience, v. 11, no. 3, p. 239-256.

Cox, K. G., Cox, K. G., McKenzie, D. P., and White, R. S., 1993, Continental magmatic underplating: Philosophical Transactions of the Royal Society of London. Series A: Physical and Engineering Sciences, v. 342, no. 1663, p. 155-166.

Cox, R., J., S., and Hodych, J., 2000, Apatite fission-track (FT) dating by LAM-ICP-MS analysis.: Goldschmidt 2000. Journal of Conference Abstracts, v. 5, p. 322.

Croisile, M., 1980, 34/05-1 composite log: Elf Aquitaine Ireland Ltd.

-, 1981, Geological report well 34/5-1.

Daly, J. S., 1996, Pre-Caledonian History of the Annagh Gneiss Complex North-Western Ireland, and Correlation with Laurentia-Baltica: Irish Journal of Earth Sciences, v. 15, p. 5-18.

Daly, J. S., Muir, R. J., and Cliff, R. A., 1991, A precise U-Pb zircon age for the Inishtrahull syenitic gneiss, County Donegal, Ireland: Journal of the Geological Society, v. 148, no. 4, p. 639-642.

Daly, J. S., Tyrrell, S., Badenszki, E., Haughton, P., and Shannon, P., 2008a, IS06/10: Petrographic and geochemical characterisation of the Porcupine High using recently recovered MeBo shallow cores.

Daly, J. S., Tyrrell, S., Badenszki, E., Horstwood, M., Lam, R., Haughton, P. D. W., Shannon, P., Whitehouse, M. J., and Sylvester, P., 2008b, Mesoproterozoic orthogneiss from the northern Porcupine High, offshore western Ireland (slides), p. 30.

Daly, S., Tyrrell, S., Haughton, P., Shannon, P., Badenszki, E., Toms, L., and Chew, D., 2008c, Characterisation of the Porcupine High using shallow cores (MeBo) - Project IS06/10 (slides): UCD, TCD.

Danišík, M., 2019, Integration of Fission-Track Thermochronology with Other Geochronologic Methods on Single Crystals, *in* Malusà, M. G., and Fitzgerald, P. G., eds., Fission-Track Thermochronology and its Application to Geology: Cham, Springer International Publishing, p. 93-108.

Davis, M. W., White, N. J., Priestley, K. F., Baptie, B. J., and Tilmann, F. J., 2012, Crustal structure of the British Isles and its epeirogenic consequences: British Isles crust: Geophysical Journal International, v. 190, no. 2, p. 705-725.

Davydov, V. I., Korn, D., Schmitz, M. D., Gradstein, F. M., and Hammer, O., 2012, The Carboniferous Period, *in* Gradstein, F., Ogg, J., Schmitz, M., and Ogg, G., eds., The Geologic Time Scale 2012, Volume 1, Elsevier, p. 603-651.

De Graciansky, P. C., and Poag, C. W., 1985, Geologic history of Goban Spur, Northwest Europe Continental Margin: US Government Printing Office.

De Graciansky, P. C., Poag, C. W., Cunningham, R., Loubere, P., Masson, D. G., Mazzullo, J. M., Montadert, L., Muller, C., Otsuka, K., Reynolds, L. A., Sigal, J., Snyder, S. W., Townsend, H. A., Vaos, S. P., and Waples, D., 1985a, The Goban Spur transect: Geologic evolution of a sediment-starved passive continental margin: Geological Society of America Bulletin, v. 96, no. 1, p. 58-76.

De Graciansky, P. C., Poag, C. W., and Foss, G., 1985b, Drilling on the Goban Spur: objectives, regional geological setting, and operational summary.

Dempster, T. J., Rogers, G., Tanner, P. W. G., Bluck, B. J., Muir, R. J., Redwood, S. D., Ireland, T. R., and Paterson, B. A., 2002, Timing of deposition, orogenesis and glaciation within the Dalradian rocks of Scotland: constraints from U–Pb zircon ages: Journal of the Geological Society, v. 159, no. 1, p. 83-94.

Didier, J., Guennoc, P., and Pautot, G., 1977a, Granodiorites, granulites et charnockites de l'éperon de Goban (marge armoricaine), au contact du domaine océanique: Comptes Rendus de l'Academie des Sciences Serie II, v. 284, p. 369-373.

Didier, J., Pautot, G., and Guennoc, P., 1977b, Granodiorites, granulites et charnockities de l'éperon de goban (marge armoricaine) au contact du domaine océanique: Comptes Rendus Hebdomadaires des Seances de l'Academie des Sciences (Académie des Sciences de Paris), 1977-02 , Vol. 284 , N. 9 , P. 713-716, v. 284.

Dobson, M. R., Garrett, P., Haynes, J. R., Jenkins, D. G., and Medani, A. H., 1976, Upper Cretaceous and Cenozoic carbonates from the margins of Rockall Trough, N. Atlantic: Journal of the Geological Society, v. 132, no. 6, p. 611-621.

Donelick, R. A., O'Sullivan, P. B., and Ketcham, R. A., 2005, Apatite Fission-Track Analysis: Reviews in Mineralogy and Geochemistry, v. 58, no. 1, p. 49-94.

Döpke, D., 2017, Modelling the thermal history of onshore Ireland, Britain and its offshore basins using low-temperature thermochronology [PhD PhD thesis]: Trinity College Dublin, 263 p.

Doran, T., Roveda, V. L., Lowe, S. P., and Whitbread, D. R., 1982, Geochemical evaluation of cuttings samples and sidewall cores from the Porcupine Basin well: 26/30-1, offshore Eire.

Doré, A. G., Cartwright, J., Stoker, M., Turner, J., and White, N., 2002, Exhumation of the North Atlantic Margin: Timing, Mechanisms and Implications for Petroleum ExplorationAbout this title, Geological Society, London, Geological Society, London, Special Publications, v. 1.

Doré, A. G., Lundin, E. R., Fichler, C., and Olesen, O., 1997, Patterns of basement structure and reactivation along the NE Atlantic margin: Journal of the Geological Society, v. 154, no. 1, p. 85-92.

Doré, A. G., Lundin, E. R., Jensen, L. N., Birkeland, Ø., Eliassen, P. E., and Fichler, C., 1999, Principal tectonic events in the evolution of the northwest European Atlantic margin: Geological Society, London, Petroleum Geology Conference series, v. 5, p. 41-61.

Doré, A. G., Lundin, E. R., Kusznir, N. J., and Pascal, C., 2008, Potential mechanisms for the genesis of Cenozoic domal structures on the NE Atlantic margin: pros, cons and some new ideas: Geological Society, London, Special Publications, v. 306, no. 1, p. 1-26.

Duddy, I. R., Gleadow, A. J. W., and Keene, J. B., 1983, Fission track dating of apatite and sphene from Paleogene sediments of deep sea drilling project leg 81, site 555, DSDP 81.

Ellis, D., and Stoker, M. S., 2014, The Faroe–Shetland Basin: a regional perspective from the Paleocene to the present day and its relationship to the opening of the North Atlantic Ocean: Geological Society, London, Special Publications, v. 397, no. 1, p. 11-31.

Ernst, R. E., and Buchan, K. L., 1997, Giant Radiating Dyke Swarms: Their Use in Identifying Pre-Mesozoic Large Igneous Provinces and Mantle Plumes, Large Igneous Provinces: Continental, Oceanic, and Planetary Flood Volcanism, p. 297-333.

Esso, 1982, Esso Exploration Ireland Inc 62/7-1 Well Completion Report: Esso Exploration Ireland Inc

Fairey, B. J., Kerrison, A., Meere, P. A., Mulchrone, K. F., Hofmann, M., Gärtner, A., Sonntag, B.-L., Linnemann, U., Kuiper, K. F., Ennis, M., Mark, C., Cogné, N., and Chew, D., 2018, The provenance of the Devonian Old Red Sandstone of the Dingle Peninsula, SW Ireland; the earliest record of Laurentian and peri-Gondwanan sediment mixing in Ireland: Journal of the Geological Society, v. 175, no. 3, p. 411-424.

Fame, M. L., Spotila, J. A., Owen, L. A., Dortch, J. M., and Shuster, D. L., 2018, Spatially heterogeneous post-Caledonian burial and exhumation across the Scottish Highlands: Lithosphere, v. 10, no. 3, p. 406-425.

Farley, K. A., 2000, Helium diffusion from apatite: General behavior as illustrated by Durango fluorapatite: Journal of Geophysical Research: Solid Earth, v. 105, no. B2, p. 2903-2914.

Farley, K. A., 2002, (U-Th)/He Dating: Techniques, Calibrations, and Applications: Reviews in Mineralogy and Geochemistry, v. 47, no. 1, p. 819-844.

Farley, K. A., Shuster, D. L., and Ketcham, R. A., 2011, U and Th zonation in apatite observed by laser ablation ICPMS, and implications for the (U–Th)/He system: Geochimica et Cosmochimica Acta, v. 75, no. 16, p. 4515-4530.

Farley, K. A., and Stockli, D. F., 2002, (U-Th)/He Dating of Phosphates: Apatite, Monazite, and Xenotime: Reviews in Mineralogy and Geochemistry, v. 48, no. 1, p. 559-577.

Farley, K. A., Wolf, R. A., and Silver, L. T., 1996, The effects of long alpha-stopping distances on (U・Th)/He ages: Geochimica et Cosmochimica Acta, v. 60, no. 21, p. 4223-4229.

Flowers, R. M., Ketcham, R. A., Shuster, D. L., and Farley, K. A., 2009, Apatite (U–Th)/He thermochronometry using a radiation damage accumulation and annealing model: Geochimica et Cosmochimica Acta, v. 73, no. 8, p. 2347-2365.

Foucher, J. P., Chenet, P. Y., and Roux, J. M., 1985, Geothermal measurements during deep sea drilling project leg 80.

Franklin, J., Tyrrell, S., Morton, A., Frei, D., and Mark, C., 2019, Triassic sand supply to the Slyne Basin, offshore western Ireland – new insights from a multi-proxy provenance approach: Journal of the Geological Society, v. 176, no. 6, p. 1120-1135.

Fügenschuh, B., Froitzheim, N., Capdevila, R., and Boillot, G., 2003, Offshore granulites from the Bay of Biscay margins: fission tracks constrain a Proterozoic to Tertiary thermal history: Terra Nova, v. 15, no. 5, p. 337-342.

Gagnevin, D., Haughton, P., Whiting, L., and Saqab, M., 2017, Geological and geophysical evidence for a mafic igneous origin of the Porcupine Arch, offshore Ireland: Journal of the Geological Society, v. 175, p. jgs2017-2041.

Gaida, K.-H., 1978, Petrography of the Terminal Core (4473-4483 ffet interval) of 13/3-1 well, off-Ireland: Deutsche Texaco Aktiengesellschaft.

Galbraith, R. F., and Green, P. F., 1990, Estimating the component ages in a finite mixture: International Journal of Radiation Applications and Instrumentation. Part D. Nuclear Tracks and Radiation Measurements, v. 17, no. 3, p. 197-206.

Gallagher, K., 2012, Transdimensional inverse thermal history modeling for quantitative thermochronology: Journal of Geophysical Research: Solid Earth, v. 117, no. B2, p. B02408.

-, 2017, QTQt v 5.6.0 User Guide: University of Rennes.

-, 2021, Comment on “Discussion: Extracting thermal history from low temperature thermochronology/A coment on the recent exchanges between Vermeesch and Tian and

Gallagher and Ketcham", by Paul Green and Ian Duddy, Earth Science Reviews, https://doi.org/10.1016/j.earscirev.2020.103197: Earth-Science Reviews, p. 103549.

Gallagher, K., Stephenson, J., Brown, R., Holmes, C., and Fitzgerald, P., 2005, Low temperature thermochronology and modeling strategies for multiple samples 1: Vertical profiles: Earth and Planetary Science Letters, v. 237, no. 1, p. 193-208.

Ganerød, M., Chew, D. M., Smethurst, M. A., Troll, V. R., Corfu, F., Meade, F., and Prestvik, T., 2011, Geochronology of the Tardree Rhyolite Complex, Northern Ireland: Implications for zircon fission track studies, the North Atlantic Igneous Province and the age of the Fish Canyon sanidine standard: Chemical Geology, v. 286, no. 3, p. 222-228.

Ganerød, M., Smethurst, M. A., Torsvik, T. H., Prestvik, T., Rousse, S., McKenna, C., Van Hinsbergen, D. J. J., and Hendriks, B. W. H., 2010, The North Atlantic Igneous Province reconstructed and its relation to the Plume Generation Zone: the Antrim Lava Group revisited: Geophysical Journal International, v. 182, no. 1, p. 183-202.

Gardien, V., Arnaud, N., and Desmurs, L., 2000, Petrology and Ar-Ar dating of granulites from the Galicia Bank (Spain): African craton relics in Western Europe: Geodinamica Acta, v. 13, no. 2, p. 103-117.

Gautheron, C., and Tassan-Got, L., 2010, A Monte Carlo approach to diffusion applied to noble gas/helium thermochronology: Chemical Geology, v. 273, no. 3, p. 212-224.

Gautheron, C., Tassan-Got, L., Barbarand, J., and Pagel, M., 2009, Effect of alpha-damage annealing on apatite (U–Th)/He thermochronology: Chemical Geology, v. 266, no. 3, p. 157-170.

Gautheron, C., Tassan-Got, L., Ketcham, R. A., and Dobson, K. J., 2012a, Accounting for long alpha-particle stopping distances in (U–Th–Sm)/He geochronology: 3D modeling of diffusion, zoning, implantation, and abrasion: Geochimica et Cosmochimica Acta, v. 96, no. Supplement C, p. 44-56.

Gautheron, C. E., and Tassan-Got, L., 2012, S/V Computation.

Gautheron, C. E., Tassan-Got, L., and Ketcham, R. A., 2012b, Alpha Ft-ejection Factor.

Geerlings, P., 2000, 18/25-2 composite well log: Enterprise Oil plc.

Gerneck, J. R., Saguiez, P., Brewster, J., McAdoo, R., and Luck, B. J., 1980, 35/15-1 composite log: Phillips Petroleum Company Ireland Limited.

Giorgio, V. D. P., Andrea, B., and and Matteo, M., 2003, Geological outline of the Alps: International Union of Geological Sciences, v. 26, no. 3, p. 175-180.

Gleadow, A. J. W., 1981, Fission-track dating methods: What are the real alternatives?: Nuclear Tracks, v. 5, no. 1, p. 3-14.

-, 2010, Fission Track Studio Software Manual.

Gleadow, A. J. W., Kohn, B., and Seiler, C., 2019, The future of fission-track thermochronology, *in* Malusà, M. G., and Fitzgerald, P. G., eds., Fission-track thermochronology and its application to geology, Springer International Publishing, p. 77-92.

Green, P., and Duddy, I., 2018, Apatite (U-Th-Sm)/He thermochronology on the wrong side of the tracks: Chemical Geology, v. 488, p. 21-33.

Green, P. F., 1986, On the thermo-tectonic evolution of Northern England: evidence from fission track analysis: Geological Magazine, v. 123, no. 5, p. 493-506.

Green, P. F., 1989, Thermal and tectonic history of the East Midlands shelf (onshore UK) and surrounding regions assessed by apatite fission track analysis: Journal of the Geological Society, v. 146, no. 5, p. 755-773.

-, 1993, Thermal history reconstruction in Erris Trough well 12/13-1A using apatite fission track analysis and vitrinite reflectance: Geotrack.

-, 2001a, Thermal history reconstruction in Errigal deepwater exploration well 5/22-1 using AFTA and vitrinite reflectance.

-, 2001b, Thermal history reconstruction in Irish Rockall trough boreholes 16/28-sb01, 83/20-sb01, 83/24-sb02 using AFTA, VR and fluid inclusion data GEOTRACK REPORT #777.

Green, P. F., 2002, Early Tertiary paleo-thermal effects in Northern England: reconciling results from apatite fission track analysis with geological evidence: Tectonophysics, v. 349, no. 1, p. 131-144.

Green, P. F., 2003, Thermal history reconstruction in offshore Ireland exploration well 12/2-1 using AFTA and vitrinite reflectance.

-, 2004, Thermal history reconstruction in the Slyne-Erris basins, offshore Ireland, based on AFT and VR data in wells 18/20-1, 18/25-1, 18/25-1, 19/5-1 and 19/11-1A.

Green, P. F., Duddy, I. R., and Bray, R. J., 1997, Variation in thermal history styles around the Irish Sea and adjacent areas: implications for hydrocarbon occurrence and tectonic evolution: Geological Society, London, Special Publications, v. 124, no. 1, p. 73-93.

Green, P. F., Duddy, I. R., Bray, R. J., and Lewis, C. L. E., 1993, Elevated palaeotemperatures prior to Early Tertiary cooling throughout the UK region: implications for hydrocarbon generation: Geological Society, London, Petroleum Geology Conference series, v. 4, no. 1, p. 1067-1074.

Green, P. F., Duddy, I. R., Gleadow, A. J. W., Tingate, P. R., and Laslett, G. M., 1986, Thermal annealing of fission tracks in apatite: 1. A qualitative description: Chemical Geology: Isotope Geoscience section, v. 59, no. Supplement C, p. 237-253.

Green, P. F., Duddy, I. R., and Hegarty, K. A., 2002, Quantifying exhumation from apatite fission-track analysis and vitrinite reflectance data: precision, accuracy and latest results from the Atlantic margin of NW Europe: Geological Society, London, Special Publications, v. 196, no. 1, p. 331-354.

Green, P. F., Duddy, I. R., Hegarty, K. A., Bray, R. J., Sevastopulo, G., Clayton, G., and Johnston, D., 2000, The post-Carboniferous evolution of Ireland: evidence from Thermal History Reconstruction: Proceedings of the Geologists' Association, v. 111, no. 4, p. 307-320.

Green, P. F., Japsen, P., Chalmers, J. A., Bonow, J. M., and Duddy, I. R., 2018, Post-breakup burial and exhumation of passive continental margins: Seven propositions to inform geodynamic models: Gondwana Research, v. 53, p. 58-81.

Guerrot, C., Peucat, J. J., Capdevila, R., and Dosso, L., 1989, Archean protoliths within Early Proterozoic granulitic crust of the west European Hercynian belt: Possible relics of the west African craton: Geology, v. 17, no. 3, p. 241-244.

Hall, B. D., and White, N., 1994, Origin of anomalous Tertiary subsidence adjacent to North Atlantic continental margins: Marine and Petroleum Geology, v. 11, no. 6, p. 702-714.

Hamilton, M. A., Pearson, D. G., Thompson, R. N., Kelley, S. P., and Emeleus, C. H., 1998, Rapid eruption of Skye lavas inferred from precise U–Pb and Ar–Ar dating of the Rum and Cuillin plutonic complexes: Nature, v. 394, no. 6690, p. 260-263.

Hansen, K., and Brooks, C. K., 2002, The evolution of the East Greenland margin as revealed from fission-track studies: Tectonophysics, v. 349, no. 1, p. 93-111.

Harrington, G. J., Higgs, K. T., and Zucchi, D., 2000, Biostratigraphic report on shallow borheole cores: 11/20-sb01, 16/28-sb01, 83/20-sb01, 83/24-sb01, 83/24-sb02.

Hartley, R. A., Roberts, G. G., White, N., and Richardson, C., 2011, Transient convective uplift of an ancient buried landscape: Nature Geoscience, v. 4, no. 8, p. 562-565.

Hasebe, N., Barbarand, J., Jarvis, K., Carter, A., and Hurford, A. J., 2004, Apatite fission-track chronometry using laser ablation ICP-MS: Chemical Geology, v. 207, no. 3, p. 135-145.

Hasebe, N., Carter, A., Hurford, A. J., and Arai, S., 2009, The effect of chemical etching on LA–ICP-MS analysis in determining uranium concentration for fission-track chronometry: Geological Society, London, Special Publications, v. 324, no. 1, p. 37-46.

Hasebe, N., Tamura, A., and Arai, S., 2013, Zeta equivalent fission-track dating using LA-ICP-MS and examples with simultaneous U–Pb dating: Island Arc, v. 22, no. 3, p. 280-291.

Haughton, P., Praeg, D., Shannon, P., Harrington, G., Higgs, K., Amy, L., Tyrrell, S., and Morrissey, T., 2005, First results from shallow stratigraphic boreholes on the eastern flank of the Rockall

Basin, offshore western Ireland: Geological Society, London, Petroleum Geology Conference series, v. 6, p. 1077-1094.

Hellstrom, J., Paton, C., Woodhead, J., and Hergt, J., 2008, Iolite: software for spatially resolved LA-(quad and MC) ICPMS analysis: Mineralogical Association of Canada short course series, v. 40, p. 343–348.

Henderson, P., 1980, The igneous rocks drilled from the Porcupine Basin.

Hetfeld, K., and Clayton, G., 2001, Thermal maturation report on shallow borehole cores: 16/28-sb01, 83/20-sb01 and 83/24-sb02: Trinity College Dublin.

Hillis, R. R., Holford, S. P., Green, P. F., Doré, A. G., Gatliff, R. W., Stoker, M. S., Thomson, K., Turner, J. P., Underhill, J. R., and Williams, G. A., 2008, Cenozoic exhumation of the southern British Isles: Geology, v. 36, no. 5, p. 371.

Hoggard, M. J., White, N., and Al-Attar, D., 2016, Global dynamic topography observations reveal limited influence of large-scale mantle flow: Nature Geoscience, v. 9, no. 6, p. 456-463.

Holford, S. P., Green, P. F., Duddy, I. R., Turner, J. P., Hillis, R. R., and Stoker, M. S., 2009, Regional intraplate exhumation episodes related to plate-boundary deformation: GSA Bulletin, v. 121, no. 11/12, p. 161-1628.

Holford, S. P., Green, P. F., Hillis, R. R., Underhill, J. R., Stoker, M. S., and Duddy, I. R., 2010, Multiple post-Caledonian exhumation episodes across NW Scotland revealed by apatite fission-track analysis: Journal of the Geological Society, v. 167, no. 4, p. 675-694.

Holford, S. P., Green, P. F., Turner, J. P., Williams, G. A., Hillis, R. R., Tappin, D. R., and Duddy, I. R., 2008, Evidence for kilometre-scale Neogene exhumation driven by compressional deformation in the Irish Sea basin system: Geological Society, London, Special Publications, v. 306, no. 1, p. 91-119.

Holland, C. H., 2009, Silurian, *in* Holland, C. H., and Sanders, I. S., eds., The geology of Ireland (second edition), Dunedin, p. 119-141.

Holland, C. H., and Saunders, I. S., 2009, Geology of Ireland, 2nd Edition, Dunedin Academic Press.

Holliday, D. W., 1993, Mesozoic cover over northern England: interpretation of apatite fission track data: Journal of the Geological Society, v. 150, no. 4, p. 657-660.

Horne, R. R., and MacIntyre, R. M., 1975, Apparent age and significance of Teriary dykes in the Dingle Peninsula: Scientific Proceedings of the Royal Dublin Society, v. 5, no. A, p. 293-299.

Horni, J. Á., Hopper, J. R., Blischke, A., Geisler, W. H., Stewart, M., McDermott, K., Judge, M., Erlendsson, Ö., Árting, U., Péron-Pinvidic, G., Hopper, J. R., Funck, T., Stoker, M. S., Gaina, C., Doornenbal, J. C., and Árting, U. E., 2017, Regional distribution of volcanism within the North Atlantic Igneous Province, The NE Atlantic Region. A Reappraisal of Crustal Structure, Tectonostratigraphy and Magmatic Evolution, Volume 447, Geological Society of London, p. 0.

Horsefield, S. J., Whitmarsh, K. R. B., White, R. S., and Sibuet, J.-C., 1994, Crustal structure of the Goban Spur rifted continental margin, Ne Atlantic: Geophysical Journal International, v. 119, no. 1, p. 1-19.

House, M. A., Farley, K. A., and Stockli, D., 2000, Helium chronometry of apatite and titanite using Nd-YAG laser heating: Earth and Planetary Science Letters, v. 183, no. 3, p. 365-368.

Hurford, A. J., 1977a, Fission track dates from two Galloway granites, Scotland: Geological Magazine, v. 114, no. 4, p. 299-304.

Hurford, A. J., 1977b, A preliminary fission track dating survey of Caledonian “newer and last granites” from the Highlands of Scotland: Scottish Journal of Geology, v. 13, no. 4, p. 271-284.

-, 1990a, International union of geological sciences subcommission on geochronology recommendation for the standardization of fission track dating calibration and data reporting: International Journal of Radiation Applications and Instrumentation. Part D. Nuclear Tracks and Radiation Measurements, v. 17, no. 3, p. 233-236.

-, 1990b, Standardization of fission track dating calibration: Recommendation by the Fission Track Working Group of the I.U.G.S. Subcommission on Geochronology: Chemical Geology: Isotope Geoscience section, v. 80, no. 2, p. 171-178.

Hurford, A. J., and Green, P. F., 1983, The zeta age calibration of fission-track dating: Chemical Geology, v. 41, p. 285-317.

Iyer, K., Rüpke, L., and Galerne, C. Y., 2013, Modeling fluid flow in sedimentary basins with sill intrusions: Implications for hydrothermal venting and climate change: Geochemistry, Geophysics, Geosystems, v. 14, no. 12, p. 5244-5262.

Jackson, C. A.-L., Magee, C., and Jacquemyn, C., 2020, Rift-related magmatism influences petroleum system development in the NE Irish Rockall Basin, offshore Ireland: Petroleum Geoscience, v. 26, no. 4, p. 511-524.

Jacovides, J., 2000, Biostratigraphic review of the Tertiary sequences from: UK Rockall Trough well 132/15-1, Erris Trough well 12/13-1, and the shallow boreholes 11/20-Sb01, 16/28-Sb01, 83/20-Sb01, 83/24-Sb01 and 83/24-Sb-02, Irish Rockall Trough: Millennia Ltd., Project No: 441/00.

Japsen, P., and Chalmers, J. A., 2000, Neogene uplift and tectonics around the North Atlantic: overview: Global and Planetary Change, v. 24, p. 165-173.

Jarvis, G. T., and McKenzie, D. P., 1980, Sedimentary basin formation with finite extension rates: Earth and Planetary Science Letters, v. 48, no. 1, p. 42-52.

Johnston, S., Doré, A. G., and Spencer, A. M., 2001, The Mesozoic evolution of the southern North Atlantic region and its relationship to basin development in the south Porcupine Basin, offshore Ireland: Geological Society, London, Special Publications, v. 188, no. 1, p. 237-263.

Johnstone, S., Hourigan, J., and Gallagher, C., 2013, LA-ICP-MS depth profile analysis of apatite: Protocol and implications for (U–Th)/He thermochronometry: Geochimica et Cosmochimica Acta, v. 109, p. 143-161.

Jolivet, M., 2007, Histoire de la dénudation dans le corridor du loch Ness (Écosse) : mouvements verticaux différentiels le long de la Great Glen Fault: Comptes Rendus Geoscience, v. 339, no. 2, p. 121-131.

Jones, D. W., and Underhill, J. R., 2011, Structural and stratigraphic evolution of the Connemara discovery, Northern Porcupine Basin: significance for basin development and petroleum prospectivity along the Irish Atlantic Margin: Petroleum Geoscience, v. 17, no. 4, p. 365-384.

Jones, S., White, N., and Lovell, B., 2001a, Cenozoic and Cretaceous transient uplift in the Porcupine Basin and its relationship to a mantle plume: Geological Society, London, Special Publications, v. 188, p. 345-360.

Jones, S. M., White, N., Clarke, B. J., Rowley, E., and Gallagher, K., 2002, Present and past influence of the Iceland Plume on sedimentation: Geological Society, London, Special Publications, v. 196, no. 1, p. 13-25.

Jones, S. M., White, N., and Lovell, B., 2001b, Cenozoic and Cretaceous transient uplift in the Porcupine Basin and its relationship to a mantle plume: Geological Society, London, Special Publications, v. 188, no. 1, p. 345-360.

Keeley, M. L., Lewis, C. L. E., Sevastopulo, G. D., Clayton, G., and Blackmore, R., 1993, Apatite fission track data from southeast Ireland: implications for post-Variscan burial history: Geological Magazine, v. 130, no. 02, p. 171.

Ketcham, R. A., 2005, Forward and Inverse Modeling of Low-Temperature Thermochronometry Data: Reviews in Mineralogy and Geochemistry, v. 58, no. 1, p. 275-314.

Ketcham, R. A., Carter, A., Donelick, R. A., Barbarand, J., and Hurford, A. J., 2007, Improved measurement of fission-track annealing in apatite using c-axis projection: American Mineralogist, v. 92, no. 5-6, p. 789-798.

Ketcham, R. A., Donelick, R. A., and Carlson, W. D., 1999, Variability of apatite fission-track annealing kinetics; III, Extrapolation to geological time scales: American Mineralogist, v. 84, no. 9, p. 1235-1255.

Ketcham, R. A., Gautheron, C., and Tassan-Got, L., 2011, Accounting for long alpha-particle stopping distances in (U–Th–Sm)/He geochronology: Refinement of the baseline case: Geochimica et Cosmochimica Acta, v. 75, no. 24, p. 7779-7791.

Ketcham, R. A., van der Beek, P., Barbarand, J., Bernet, M., and Gautheron, C., 2018, Reproducibility of Thermal History Reconstruction From Apatite Fission-Track and (U-Th)/He Data: Geochemistry, Geophysics, Geosystems, v. 19, no. 8, p. 2411-2436.

Kimbell, G. S., Ritchie, J. D., and Henderson, A. F., 2010, Three-dimensional gravity and magnetic modelling of the Irish sector of the NE Atlantic margin: Tectonophysics, v. 486, no. 1, p. 36-54.

King, A. D., Meyrick, R. W., and Gueinn, K. J., 1982, Well 26/30-1, Porcupine Basin, offshore Ireland. Stratigraphical/paleontological final report.

King, C., Gale, A. S., and Barry, T. L., 2016, A revised correlation of Tertiary rocks in the British Isles and adjacent areas of NW Europe, Geological Society of London.

Kirkland, C. L., Yakymchuk, C., Szilas, K., Evans, N., Hollis, J., McDonald, B., and Gardiner, N. J., 2018, Apatite: a U-Pb thermochronometer or geochronometer?: Lithos, v. 318-319, p. 143-157.

Knox, R. W. O. B., 1985, Stratigraphic Significance of Volcanic Ash in Paleocene and Eocene Sediments at Sites 549 and 550.

Knox, R. W. O. B., 1996, Tectonic controls on sequence development in the Palaeocene and earliest Eocene of southeast England: implications for North Sea stratigraphy: Geological Society, London, Special Publications, v. 103, no. 1, p. 209-230.

Laslett, G. M., Green, P. F., Duddy, I. R., and Gleadow, A. J. W., 1987, Thermal annealing of fission tracks in apatite 2. A quantitative analysis: Chemical Geology: Isotope Geoscience section, v. 65, no. 1, p. 1-13.

Lefort, J.-P., Hérissé, A., Peucat, J., and Deunff, J., 1984, The Goban Spur Paleozoic Basement.

Lewis, C., Carter, A., and Hurford, A., 1992a, Low-temperature effects of the Skye Tertiary intrusions on Mesozoic sediments in the Sea of Hebrides Basin: Geological Society London Special Publications, v. 62, p. 175-188.

Lewis, C. L. E., Carter, A., and Hurford, A. J., 1992b, Low-temperature effects of the Skye Tertiary intrusions on Mesozoic sediments in the Sea of Hebrides Basin: Geological Society of London Special Publications, v. 62, p. 175.

Lewis, C. L. E., Green, P. F., Carter, A., and Hurford, A. J., 1992c, Elevated K/T palaeotemperatures throughout Nortwest England: three kilometres of Tertiary erosion?: Earth and Planetary Science Letters, v. 112, no. 1, p. 131-145.

Li, W., Wang, L., Sun, K., Lang, M., Trautmann, C., and Ewing, R. C., 2010, Porous fission fragment tracks in fluorapatite: Physical Review B, v. 82, no. 14, p. 144109.

Licciardi, A., England, R. W., Piana Agostinetti, N., and Gallagher, K., 2020, Moho depth of the British Isles: a probabilistic perspective: Geophysical Journal International, v. 221, no. 2, p. 1384-1401.

Lippolt, H. J., Bähr, R., and Boschmann Käthler, W., 1989, ^{4}He diffusion from ore minerals, especially from hematite: Terra Abstr., v. 1, no. 1, p. 355.

Lippolt, H. J., Leitz, M., Wernicke, R. S., and Hagedorn, B., 1994, (Uranium + thorium)/helium dating of apatite: experience with samples from different geochemical environments: Chemical Geology, v. 112, no. 1, p. 179-191.

Lippolt, H. J., and Weigel, E., 1988, 4He diffusion in 40Ar-retentive minerals: Geochimica et Cosmochimica Acta, v. 52, no. 6, p. 1449-1458.

Lisker, F., Ventura, B., and Glasmacher, U. A., 2009, Apatite thermochronology in modern geology: Geological Society, London, Special Publications, v. 324, no. 1, p. 1-23.

Louden, K. E., and Chian, D., 1999, The deep structure of non–volcanic rifted continental margins: Philosophical Transactions of the Royal Society of London. Series A:
Mathematical, Physical and Engineering Sciences, v. 357, no. 1753, p. 767-804.

Ludwig, K. R., 1988, ISOPLOT for MS-DOS, a plotting and regression program for radiogenic-isotope data, for IBM-PC compatible computers, version 1.00, 88-557.

Lundin, E. R., and Doré, A. G., 2011, Hyperextension, serpentinization, and weakening: A new paradigm for rifted margin compressional deformation: Geology, v. 39, no. 4, p. 347-350.

Łuszczak, K., Persano, C., Braun, J., and Stuart, F. M., 2017, How local crustal thermal properties influence the amount of denudation derived from low-temperature thermochronometry: Geology, v. 45, no. 9, p. 779-782.

Łuszczak, K., Persano, C., and Stuart, F. M., 2018, Early Cenozoic Denudation of Central West Britain in Response to Transient and Permanent Uplift Above a Mantle Plume: Tectonics, v. 37, no. 3, p. 914-934.

MacDonald, H., Allan, P. M., and Lovell, J. P. B., Geology of oil accumulation in Block 26/28, Porcupine Basin, offshore Ireland, *in* Proceedings Petroleum geology of Northwest Europe, London, 1987, Volume 1, Graham & Trotman, p. 643-651.

Macgregor, D., 2018, A preliminary geothermal gradient map of the African Plate: PESGB Africa Conference 2017, p. 3.

Mackay, L. M., Turner, J., Jones, S. M., and White, N. J., 2005, Cenozoic vertical motions in the Moray Firth Basin associated with initiation of the Iceland Plume: Tectonics, v. 24, no. 5.

Mackay, L. M., and White, N. J., 2006, Accurate estimates of the spatial pattern of denudation by inversion of stacking velocity data: An example from the British Isles: Geochemistry, Geophysics, Geosystems, v. 7, no. 10, p. 34.

Maclennan, J., and Jones, S. M., 2006, Regional uplift, gas hydrate dissociation and the origins of the Paleocene–Eocene Thermal Maximum: Earth and Planetary Science Letters, v. 245, no. 1, p. 65-80.

Maclennan, J., and Lovell, B., 2002, Control of regional sea level by surface uplift and subsidence caused by magmatic underplating of Earth's crust: Geology, v. 30, no. 8, p. 675-678.

Magee, C., Jackson, C. A. L., and Schofield, N., 2014, Diachronous sub-volcanic intrusion along deep-water margins: insights from the Irish Rockall Basin: Basin Research, v. 26, no. 1, p. 85-105.

Malusa, M., and Fitzgerald, P. G., 2019, Fission-Track Thermochronology and its Application to Geology, Springer International Publishing.

Markwitz, V., Hein, K. A. A., Jessell, M. W., and Miller, J., 2016, Metallogenic portfolio of the West Africa craton: Ore Geology Reviews, v. 78, p. 558-563.

Masson, D. G., Dobson, M. R., Auzende, J. M., Cousin, M., Coutelle, A., Rolet, J., and Vaillant, P., 1989, Geology of Porcupine Bank and Goban Spur, Northeastern Atlantic — Preliminary results of the Cyaporc submersible cruise: Marine Geology, v. 87, no. 2, p. 105-119.

Masson, D. G., Montadert, L., and Scrutton, R. A., 1984, Regional geology of the Goban Spur continental margin.

McAteer, C. A., Daly, J. S., Flowerdew, M. J., Whitehouse, M. J., and Kirkland, C. L., 2010, A Laurentian provenance for the Dalradian rocks of north Mayo, Ireland, and evidence for an original basement–cover contact with the underlying Annagh Gneiss Complex: Journal of the Geological Society, v. 167, no. 5, p. 1033-1048.

McCarron, S., Praeg, D., Ó Cofaigh, C., Monteys, X., Thébaudeau, B., Craven, K., Saqab, M. M., and Cova, A., 2018, A Plio-Pleistocene sediment wedge on the continental shelf west of central Ireland: The Connemara Fan: Marine Geology, v. 399, p. 97-114.

McCulloch, A. A., 1993, Apatite fission track results from Ireland and the Porcupine basin and their significance for the evolution of the North Atlantic: Marine and Petroleum Geology, v. 10, no. 6, p. 572-590.

-, 1994, Low temperature thermal history of eastern Ireland: effects of fluid flow: Marine and Petroleum Geology, v. 11, no. 3, p. 389-399.

McDonnell, A., and Shannon, P. M., 2001, Comparative Tertiary stratigraphic evolution of the Porcupine and Rockall basins: Geological Society, London, Special Publications, v. 188, no. 1, p. 323-344.

McDowell, F. W., McIntosh, W. C., and Farley, K. A., 2005, A precise 40Ar–39Ar reference age for the Durango apatite (U–Th)/He and fission-track dating standard: Chemical Geology, v. 214, no. 3, p. 249-263.

McKenzie, D., 1978, Some remarks on the development of sedimentary basins: Earth and Planetary Science Letters, v. 40, no. 1, p. 25-32.

McMahon, N. A., and Turner, J., 1998, The documentation of a latest Jurassic-earliest Cretaceous uplift throughout southern England and adjacent offshore areas: Geological Society, London, Special Publications, v. 133, no. 1, p. 215-240.

Meade, F. C., Troll, V. R., Ellam, R. M., Freda, C., Font, L., Donaldson, C. H., and Klonowska, I., 2014, Bimodal magmatism produced by progressively inhibited crustal assimilation: Nature Communications, v. 5, no. 1, p. 4199.

Mecklenburgh, R., 2003, Well IRE 12/2-1Z "Dooish Deepwater Exploration" Final Well Report - Volume 1: Geological and Petrophysical Evaluation: Shell.

Meesters, A. G. C. A., and Dunai, T. J., 2005, A noniterative solution of the (U-Th)/He age equation: Geochemistry, Geophysics, Geosystems, v. 6, no. 4.

Min, K., Farley, K. A., Renne, P. R., and Marti, K., 2003, Single grain (U–Th)/He ages from phosphates in Acapulco meteorite and implications for thermal history: Earth and Planetary Science Letters, v. 209, no. 3, p. 323-336.

Mitchell, J. G., and Mohr, P., 1986, K–Ar systematics in Tertiary dolerites from West Connacht, Ireland: Scottish Journal of Geology, v. 22, no. 2, p. 225-240.

Mohr, P., 2000, Late Palaeozoic and Palaeocene magmatic intrusion levels in West Connacht and inferences for palaeotopography: Proceedings of the Geologists' Association, v. 111, no. 4, p. 337-343.

Monaghan, A. A., and Browne, M. A. E., 2010, Nine 40Ar/39Ar dates from Carboniferous igneous rocks of the Midland Valley of Scotland: British Geological Survey.

Monaghan, A. A., and Parrish, R. R., 2006, Geochronology of Carboniferous–Permian magmatism in the Midland Valley of Scotland: implications for regional tectonomagmatic evolution and the numerical time scale: Journal of the Geological Society, v. 163, no. 1, p. 15-28.

Moore, J. G., and Shannon, P. M., 1992, Palaeocene - Eocene deltaic sedimentation, Porcupine Basin, offshore Ireland - a sequence stratigraphic approach: First Break, v. 10, no. 12, p. 461-469.

Morris, P., 1974, A Tertiary Dyke System in South-West Ireland: Proceedings of the Royal Irish Academy. Section B: Biological, Geological, and Chemical Science, v. 74, p. 179-184.

Morton, A., Mundy, D., Bingham, G., Rasbury, E. T., Hemming, S. R., and Riggs, N. R., 2012, High-frequency fluctuations in heavy mineral assemblages from Upper Jurassic sandstones of the Piper Formation, UK North Sea: Relationships with sea-level change and floodplain residence, Mineralogical and Geochemical Approaches to Provenance, Volume 487, Geological Society of America, p. 0.

Mosar, J., Lewis, G., and Torsvik, T., 2002, North Atlantic sea-floor spreading rates: implications for the Tertiary development of inversion structures of the Norwegian–Greenland Sea: Journal of the Geological Society, v. 159, no. 5, p. 503-515.

Mudge, D. C., 2015, Regional controls on Lower Tertiary sandstone distribution in the North Sea and NE Atlantic margin basins: Geological Society, London, Special Publications, v. 403, no. 1, p. 17-42.

Muir, R. J., Fitches, W. R., and Maltman, A. J., 1994, The Rhinns Complex: Proterozoic basement on Islay and Colonsay, Inner Hebrides, Scotland, and on Inishtrahull, NW Ireland: Transactions of the Royal Society of Edinburgh: Earth Sciences, v. 85, no. 1, p. 77-90.

Murray, B., and Freudenthal, T., 2006, Report from cruise CE0619 with R/V Celtic Explorer on the Porcupine Bank: PAD.

Murray, K. E., Braun, J., and Reiners, P. W., 2018, Toward Robust Interpretation of Low-Temperature Thermochronometers in Magmatic Terranes: Geochemistry, Geophysics, Geosystems, v. 19, no. 10, p. 3739-3763.

Nasdala, L., Corfu, F., Schoene, B., Tapster, S. R., Wall, C. J., Schmitz, M. D., Ovtcharova, M., Schaltegger, U., Kennedy, A. K., Kronz, A., Reiners, P. W., Yang, Y.-H., Wu, F.-Y., Gain, S. E. M., Griffin, W. L., Szymanowski, D., Chanmuang N., C., Ende, M., Valley, J. W., Spicuzza, M. J., Wanthanachaisaeng, B., and Giester, G., 2018, GZ7 and GZ8 – Two Zircon Reference Materials for SIMS U-Pb Geochronology: Geostandards and Geoanalytical Research, v. 42, no. 4, p. 431-457.

Nauton-Fourteu, M., Tyrrell, S., Morton, A., Mark, C., O'Sullivan, G. J., and Chew, D. M., 2020, Constraining recycled detritus in quartz-rich sandstones: Insights from a multi-proxy provenance study of the Mid-Carboniferous, Clare Basin, western Ireland: Basin Research, v. n/a, no. n/a.

Naylor, D., and Shannon, P. M., 2001, Structural Nomenclature Porcupine Goban Region: Petroleum Infrastructure Programme, PSG Project P00/1.

Naylor, D., and Shannon, P. M., 2005, The structural framework of the Irish Atlantic Margin: Geological Society, London, Petroleum Geology Conference series, v. 6, p. 1009-1021.

-, 2009, Geology of offshore Ireland, The Geology of Ireland - Second Edition: Edinburgh, Dunedin Academic Press, p. 405-460.

Nielsen, S. B., Paulsen, G. E., Hansen, D. L., Gemmer, L., Clausen, O. R., Jacobsen, B. H., Balling, N., Huuse, M., and Gallagher, K., 2002, Paleocene initiation of Cenozoic uplift in Norway: Geological Society, London, Special Publications, v. 196, no. 1, p. 45-65.

Nirrengarten, M., Manatschal, G., Tugend, J., Kusznir, N., and Sauter, D., 2018, Kinematic Evolution of the Southern North Atlantic: Implications for the Formation of Hyperextended Rift Systems: Tectonics, v. 37, no. 1, p. 89-118.

NIST, 1992, Certificate of analysis, standard reference material 612, trace elements in a glass, National Institution of Standards and Technology, p. 4.

O'Connor, P. J., Long, C. B., and Evans, J. A., 1987, Rb-Sr whole-rock isochron studies of the Barnesmore and Fanad plutons, Donegal, Ireland: Geological Journal, v. 22, no. 1, p. 11-23.

O'Sullivan, G., Chew, D., Kenny, G., Henrichs, I., and Mulligan, D., 2020, The trace element composition of apatite and its application to detrital provenance studies: Earth-Science Reviews, v. 201, p. 103044.

Ó Cofaigh, C., Weilbach, K., Lloyd, J. M., Benetti, S., Callard, S. L., Purcell, C., Chiverrell, R. C., Dunlop, P., Saher, M., Livingstone, S. J., Van Landeghem, K. J. J., Moreton, S. G., Clark, C. D., and Fabel, D., 2019, Early deglaciation of the British-Irish Ice Sheet on the Atlantic shelf northwest of Ireland driven by glacioisostatic depression and high relative sea level: Quaternary Science Reviews, v. 208, p. 76-96.

Odell, R. T., and Walker, D., 1979, 12/13-1 and 12/13-1A completion report: Amoco ireland Exploration Company.

Oldroyd, D., 2002, Chapter 18 Tertiary uplift, Earth, Water, Ice and Fire: Two Hundred Years of Geological Research in the English Lake District, Geological Society of London, p. 243-254.

Ortelius, A., 1572, Europae.

Paton, C., Hellstrom, J., Paul, B., Woodhead, J., and Hergt, J., 2011, Iolite: Freeware for the visualisation and processing of mass spectrometric data: Journal of Analytical Atomic Spectrometry, v. 26, no. 12, p. 2508-2518.

Pautot, G. U. Y., Renard, V., Auffret, G., Pastouret, L. E. O., and De Charpal, O., 1976, A granite cliff deep in the North Atlantic: Nature, v. 263, no. 5579, p. 669-672.

Pay, M., and Geerlings, P., 2000, 18/25-2 geological completion report: Enterprise Oil.

Pearce, N. J. G., Perkins, W. T., Westgate, J. A., Gorton, M. P., Jackson, S. E., Neal, C. R., and Chenery, S. P., 1997, A Compilation of New and Published Major and Trace Element Data for NIST SRM 610 and NIST SRM 612 Glass Reference Materials: Geostandards Newsletter, v. 21, no. 1, p. 115-144.

Peck, V. L., Hall, I. R., Zahn, R., Grousset, F., Hemming, S. R., and Scourse, J. D., 2007, The relationship of Heinrich events and their European precursors over the past 60ka BP: a multi-proxy ice-

rafted debris provenance study in the North East Atlantic: Quaternary Science Reviews, v. 26, no. 7, p. 862-875.

Peddy, C., Pinet, B., Masson, D., Scrutton, R., Sibuet, J. C., Warner, M. R., Lefort, J. P., and Shroeder, I. J., 1989, Crustal structure of the Goban Spur continental margin, Northeast Atlantic, from deep seismic reflection profiling: Journal of the Geological Society, v. 146, no. 3, p. 427-437.

Pereira, M. F., Castro, A., and Fernandez, C., 2014, The inception of a Paleotethyan magmatic arc in Iberia: Geoscience Frontiers, v. 6.

Pereira, M. F., Castro, A., and Fernández, C., 2015, The inception of a Paleotethyan magmatic arc in Iberia: Geoscience Frontiers, v. 6, no. 2, p. 297-306.

Pérez-Gussinyé, M., 2013, A tectonic model for hyperextension at magma-poor rifted margins: an example from the West Iberia–Newfoundland conjugate margins: Geological Society, London, Special Publications, v. 369, no. 1, p. 403-427.

Peron-Pinvidic, G., Manatschal, G., and Osmundsen, P. T., 2013, Structural comparison of archetypal Atlantic rifted margins: A review of observations and concepts: Marine and Petroleum Geology, v. 43, p. 21-47.

Persano, C., Barfod, D. N., Stuart, F. M., and Bishop, P., 2007, Constraints on early Cenozoic underplating-driven uplift and denudation of western Scotland from low temperature thermochronometry: Earth and Planetary Science Letters, v. 263, no. 3, p. 404-419.

Petroleum Infrastructure Program, P., 2020, A new standard lithostratigraphic framework for offshore Ireland; regional chronostratigraphic summary chart: PIP.

Phillips, T. B., Magee, C., Jackson, C. A.-L., and Bell, R. E., 2017, Determining the three-dimensional geometry of a dike swarm and its impact on later rift geometry using seismic reflection data: Geology, v. 46, no. 2, p. 119-122.

Pointon, M. A., Cliff, R. A., and Chew, D. M., 2012, The provenance of Western Irish Namurian Basin sedimentary strata inferred using detrital zircon U–Pb LA-ICP-MS geochronology: Geological Journal, v. 47, no. 1, p. 77-98.

Polacci, M., Arzilli, F., La Spina, G., Le Gall, N., Cai, B., Hartley, M. E., Di Genova, D., Vo, N. T., Nonni, S., Atwood, R. C., Llewellin, E. W., Lee, P. D., and Burton, M. R., 2018, Crystallisation in basaltic magmas revealed via in situ 4D synchrotron X-ray microtomography: Scientific Reports, v. 8, no. 1, p. 8377.

Praeg, D., Stoker, M. S., Shannon, P. M., Ceramicola, S., Hjelstuen, B., Laberg, J. S., and Mathiesen, A., 2005, Episodic Cenozoic tectonism and the development of the NW European 'passive' continental margin: The STRATAGEM Project, v. 22, no. 9–10, p. 1007-1030.

Price, P. B., and Walker, R. M., 1963, Fossil tracks of charged particles in mica and the age of minerals: Journal of Geophysical Research (1896-1977), v. 68, no. 16, p. 4847-4862.

Quirie, A. K., Schofield, N., Hartley, A., Hole, M. J., Archer, S. G., Underhill, J. R., Watson, D., and Holford, S. P., 2019, The Rattray Volcanics: Mid-Jurassic fissure volcanism in the UK Central North Sea: Journal of the Geological Society, v. 176, no. 3, p. 462-481.

Readman, P. W., O'Reilly, B. M., Murphy, T., and Makris, J., 2003, A Gravity Anomaly Map of the Irish Western Seaboard: Irish Journal of Earth Sciences, v. 21, p. 133-142.

Redfield, T. F., 2010, On apatite fission track dating and the Tertiary evolution of West Greenland topography: Journal of the Geological Society, v. 167, no. 2, p. 261-271.

Reiners, P. W., and Farley, K. A., 1999, Helium diffusion and (U–Th)/He thermochronometry of titanite: Geochimica et Cosmochimica Acta, v. 63, no. 22, p. 3845-3859.

Riddihough, R. P., and Max, M. D., 1976, A geological framework for the continental margin to the west of Ireland: Geological Journal, v. 11, no. 2, p. 109-120.

Rider, M., 2002, Chapter 4 Temperature logging, The Geological Interpretation of Well Logs (Second Edition), Butterworth-Heinemann, p. 280.

Ritchey, J. E., 1939, The dykes of Scotland: Transactions of the Edinburgh Geological Society, v. 13, no. 4, p. 393-435.

Ritchie, J. D., Swallow, J. L., Mitchell, J. G., and Morton, A. C., 1988, Jurassic ages from intrusives and extrusives within the Forties igneous province: Scottish Journal of Geology, v. 24, no. 1, p. 81-88.

Roberts, D. G., Thompson, M., Mitchener, B., Hossack, J., Carmichael, S., and BjØRnseth, H. M., 1999, Palaeozoic to Tertiary rift and basin dynamics: mid-Norway to the Bay of Biscay – a new context for hydrocarbon prospectivity in the deep water frontier: Geological Society, London, Petroleum Geology Conference series, v. 5, p. 7-40.

Robeson, D., Burnett, R. D., and Clayton, G., 1988, The Upper Palaeozoic Geology of the Porcupine, Erris and Donegal Basins, Offshore Ireland: Irish Journal of Earth Sciences, v. 9, no. 2, p. 153-175.

Robinson, A. J., and Canham, A. C., 2001, Reservoir characteristics of the Upper Jurassic sequence in the 35/8-2 discovery, Porcupine Basin: Geological Society, London, Special Publications, v. 188, no. 1, p. 301-321.

Rohrman, M., and van der Beek, P., 1996, Cenozoic postrift domal uplift of North Atlantic margins: An asthenospheric diapirism model: Geology, v. 24, no. 10, p. 901-904.

Rowley, E., and White, N., 1998, Inverse modelling of extension and denudation in the East Irish Sea and surrounding areas: Earth and Planetary Science Letters, v. 161, no. 1, p. 57-71.

Rudge, J. F., Shaw Champion, M. E., White, N., McKenzie, D., and Lovell, B., 2008, A plume model of transient diachronous uplift at the Earth's surface: Earth and Planetary Science Letters, v. 267, no. 1, p. 146-160.

Schoene, B., and Bowring, S. A., 2006, U–Pb systematics of the McClure Mountain syenite: thermochronological constraints on the age of the 40Ar/39Ar standard MMhb: Contributions to Mineralogy and Petrology, v. 151, no. 5, p. 615.

Scotchman, I. C., and Thomas, J. R. W., 1995, Maturity and hydrocarbon generation in the Slyne Trough, northwest Ireland: Geological Society, London, Special Publications, v. 93, no. 1, p. 385-411.

Scrutton, R. A., 1979, Structure of the Crust and Upper Mantle at Goban Spur, Southwest of the British Isles – Some Implications for Margin Studies, *in* Keen, C. E., ed., Developments in Geotectonics, Volume 15, Elsevier, p. 201-215.

-, 1985, Modeling of magnetic and gravity anomalies at Goban Spur, Northeastern Atlantic.

Scrutton, R. A., and Bentley, P. A. D., 1988, Major Cretaceous volcanic province in southern Rockall Trough: Earth and Planetary Science Letters, v. 91, no. 1, p. 198-204.

Seemann, U., 1984, Tertiary intrusives on the Atlantic continental margin off southwest Ireland: Irish Journal of Earth Sciences, v. 6, no. 2, p. 229-235.

Seemann, U., Reijers, T. J. A., Engelhardt, E. D., and Reiman, K., 1977, Geological, geochemical and petrophysical analyses of rock samples from well 35/13-1: Shell.

Serica, Rockall & Slyne Basin Opportunities FEL 4/13, 1/09 and 1/06, *in* Proceedings Atlantic Ireland Conference, Dublin, 20th October 2014 2014, p. 16.

Shannon, P. M., 1991, The development of Irish offshore sedimentary basins: Journal of the Geological Society, v. 148, no. 1, p. 181-189.

Shannon, P. M., 1992, Early Tertiary submarine fan deposits in the Porcupine Basin, offshore Ireland: Geological Society, London, Special Publications, v. 62, no. 1, p. 351-373.

Shannon, P. M., Jacob, A. W. B., Makris, J., O'Reilly, B., Hauser, F., and Vogt, U., 1995, Basin development and petroleum prospectivity of the Rockall and Hatton region: Geological Society, London, Special Publications, v. 93, no. 1, p. 435-457.

Shao, T., Xia, Y., Ding, X., Cai, Y., and Song, M., 2019, Zircon saturation in terrestrial basaltic melts and its geological implications: Solid Earth Sciences, v. 4, no. 1, p. 27-42.

Shelford, P. H., 1967, The Namurian and Upper Viséan of the Limerick Volcanic Basin, Eire: Proceedings of the Geologists' Association, v. 78, no. 1, p. 121-IN128.

Shell, 1981, 26/26-1 Well completion log.

Shuster, D. L., and Farley, K. A., 2009, The influence of artificial radiation damage and thermal annealing on helium diffusion kinetics in apatite: Geochimica et Cosmochimica Acta, v. 73, no. 1, p. 183-196.

Shuster, D. L., Flowers, R. M., and Farley, K. A., 2006, The influence of natural radiation damage on helium diffusion kinetics in apatite: Earth and Planetary Science Letters, v. 249, no. 3, p. 148-161.

Sibuet, J.-C., Mathis, B., Pastouret, L., Auzende, J.-M., Foucher, J.-P., Hunter, P., Guennoc, P., Graciansky, P.-C., Montadert, L., and Masson, D., 1984, 56. MORPHOLOGY AND BASEMENT STRUCTURES OF THE GOBAN SPUR CONTINENTAL MARGIN (NORTHEASTERN ATLANTIC) AND THE ROLE OF THE PYRENEAN OROGENY1, p. 1153-1165.

Sláma, J., Košler, J., Condon, D. J., Crowley, J. L., Gerdes, A., Hanchar, J. M., Horstwood, M. S. A., Morris, G. A., Nasdala, L., Norberg, N., Schaltegger, U., Schoene, B., Tubrett, M. N., and Whitehouse, M. J., 2008, Plešovice zircon — A new natural reference material for U–Pb and Hf isotopic microanalysis: Chemical Geology, v. 249, no. 1, p. 1-35.

Smallwood, J. R., and Gill, C. E., 2002, The rise and fall of the Faroe–Shetland Basin: evidence from seismic mapping of the Balder Formation: Journal of the Geological Society, v. 159, no. 6, p. 627-630.

Smith, W. D., Darling, J. R., Bullen, D. S., Lasalle, S., Pereira, I., Moreira, H., Allen, C. J., and Tapster, S., 2019, Zircon perspectives on the age and origin of evolved S-type granites from the Cornubian Batholith, Southwest England: Lithos, v. 336-337, p. 14-26.

Smythe, D. K., 1994, Geophysical evidence for ultrawide dykes of the late Carboniferous quartz-dolerite swarm of northern Britain: Geophysical Journal International, v. 119, no. 1, p. 20-30.

Smythe, D. K., Russell, M. J., and Skuce, A. G., 1995, Intra-continental rifting inferred from the major late Carboniferous quartz-dolerite dyke swarm of NW Europe: Scottish Journal of Geology, v. 31, no. 2, p. 151-162.

Soares, C. J., Guedes, S., Hadler, J. C., Mertz-Kraus, R., Zack, T., and Iunes, P. J., 2014, Novel calibration for LA-ICP-MS-based fission-track thermochronology: Physics and Chemistry of Minerals, v. 41, no. 1, p. 65-73.

Soares, C. J., Guedes, S., Tello, C. A., Lixandrão Filho, A. L., Osório, A. M., Alencar, I., Dias, A. N. C., and Hadler, J., 2013, Further investigation of the initial fission-track length and geometry factor in apatite fission-track thermochronology†: American Mineralogist, v. 98, no. 8-9, p. 1381-1392.

Spencer, A. M., Birkeland, Ø., Knag, G. Ø., and Fredsted, R., 1999, Petroleum systems of the Atlantic margin of northwest Europe: Geological Society, London, Petroleum Geology Conference series, v. 5, p. 231-246.

Stockli, D. F., 2005, Application of Low-Temperature Thermochronometry to Extensional Tectonic Settings: Reviews in Mineralogy and Geochemistry, v. 58, no. 1, p. 411-448.

Stoker, M., 1999, Irish Rockall Shallow Drilling 1999 - Stratigraphic Summary, WB/99/22C.

Stoker, M. S., 1997, Mid- to late Cenozoic sedimentation on the continental margin off NW Britain: Journal of the Geological Society, v. 154, no. 3, p. 509-515.

Stoker, M. S., Holford, S. P., and Hillis, R. R., 2018, A rift-to-drift record of vertical crustal motions in the Faroe–Shetland Basin, NW European margin: establishing constraints on NE Atlantic evolution: Journal of the Geological Society, v. 175, no. 2, p. 263-274.

Stoker, M. S., Holford, S. P., Hillis, R. R., Green, P. F., and Duddy, I. R., 2010, Cenozoic post-rift sedimentation off northwest Britain: Recording the detritus of episodic uplift on a passive continental margin: Geology, v. 38, no. 7, p. 595-598.

Stoker, M. S., Praeg, D., Shannon, P. M., Hjestueln, B. O., Laberg, J. S., Nielsen, T., Van Weeringq, T. C. E., Sejrup, H. P., and Evans, D., 2005, Neogene evolution of the Atlantic continental margin of NW Europe (Lofoten Islands to SW Ireland): anything but passive: Geological Society, London, Petroleum Geology Conference series, v. 6, p. 1057-1076.

Stoker, M. S., Stewart, M. A., Shannon, P. M., Bjerager, M., Nielsen, T., Blischke, A., Hjelstuen, B. O., Gaina, C., McDermott, K., and Ólavsdóttir, J., 2016, An overview of the Upper Palaeozoic–

Mesozoic stratigraphy of the NE Atlantic region: Geological Society, London, Special Publications, v. 447.
Štolfová, K., and Shannon, P., 2009, Permo-Triassic development from Ireland to Norway: Basin architecture and regional controls: Geological Journal, v. 44, p. 652-676.
Stuart, F. M., and Persano, C., 1999, Laser melting of apatite for (U-Th)/He chronology progress to date, EOS, Volume 80.
Stuart, I. A., 1978a, 13/3-1 Final Geological Report: Texaco Ireland Ltd.
-, 1978b, 13/3-1 Final Geological Report: Texaco Ireland Ltd.
Stuart, I. A., Allan, M., and Butler, O. E., 1978, 13/3-1 Composite well log: Texaco Production Service Ltd.
Sun, S.-s., and McDonough, W. F., 1989, Chemical and isotopic systematics of oceanic basalts: implications for mantle composition and processes: Geological Society, London, Special Publications, v. 42, no. 1, p. 313-345.
Sussli, P. E., and Hoogkmaer, P. J. C., 1977, Well completion log 35/13-1: Shell.
Tamer, M., and Ketcham, R., 2020, Is Low-Temperature Fission-Track Annealing in Apatite a Thermally Controlled Process?: Geochemistry, Geophysics, Geosystems, v. 21, no. 3, p. e2019GC008877.
Tate, M. P., and Dobson, M. R., 1988, Syn- and post-rift igneous activity in the Porcupine Seabight Basin and adjacent continental margin W of Ireland: Geological Society, London, Special Publications, v. 39, no. 1, p. 309-334.
-, 1989, Pre-Mesozoic geology of the western and north-western Irish continental shelf: Journal of the Geological Society, v. 146, no. 2, p. 229-240.
Thébaudeau, B., Monteys, X., McCarron, S., O'Toole, R., and Caloca, S., 2016, Seabed geomorphology of the Porcupine Bank, West of Ireland: Journal of Maps, v. 12, no. 5, p. 947-958.
Thomson, K., Underhill, J. R., Green, P. F., Bray, R. J., and Gibson, H. J., 1999, Evidence from apatite fission track analysis for the post-Devonian burial and exhumation history of the northern Highlands, Scotland: Marine and Petroleum Geology, v. 16, no. 1, p. 27-39.
Thomson, S. N., Gehrels, G. E., Ruiz, J., and Buchwaldt, R., 2012, Routine low-damage apatite U-Pb dating using laser ablation–multicollector–ICPMS: Geochemistry, Geophysics, Geosystems, v. 13, no. 2.
Tiley, R., White, N., and Al-Kindi, S., 2004, Linking Paleogene denudation and magmatic underplating beneath the British Isles: Geological Magazine, v. 141, no. 3, p. 345-351.
Tomlinson, J. P., Denton, P., Maguire, P. K. H., and Booth, D. C., 2006, Analysis of the crustal velocity structure of the British Isles using teleseismic receiver functions: Geophysical Journal International, v. 167, no. 1, p. 223-237.
Torsvik, T. H., Smethurst, M. A., Burke, K., and Steinberger, B., 2008, Long term stability in deep mantle structure: Evidence from the ~300 Ma Skagerrak-Centered Large Igneous Province (the SCLIP): Earth and Planetary Science Letters, v. 267, no. 3, p. 444-452.
Tyrrell, S., 2013, Geochemical constraints on the age, affinity and history of the Porcupine High: Infomar.
Tyrrell, S., Haughton, P. D. W., and Daly, J. S., 2007, Drainage reorganization during breakup of Pangea revealed by in-situ Pb isotopic analysis of detrital K-feldspar: Geology, v. 35, no. 11, p. 971-974.
Underhill, J. R., 2001, Controls on the genesis and prospectivity of Paleogene palaeogeomorphic traps, East Shetland Platform, UK North Sea: Marine and Petroleum Geology, v. 18, no. 2, p. 259-281.
Upton, B. G. J., Stephenson, D., Smedley, P. M., Wallis, S. M., and Fitton, J. G., 2004, Carboniferous and Permian magmatism in Scotland: Geological Society, London, Special Publications, v. 223, no. 1, p. 195-218.
Vermeesch, P., 2009, RadialPlotter: A Java application for fission track, luminescence and other radial plots: Radiation Measurements - RADIAT MEAS, v. 44, p. 409-410.
-, 2012, On the visualisation of detrital age distributions: Chemical Geology, v. 312-313, p. 190-194.

Vermeesch, P., Sherlock, S. C., Roberts, N. M. W., and Carter, A., 2012, A simple method for in-situ U–Th–He dating: Geochimica et Cosmochimica Acta, v. 79, p. 140-147.

Vrolijk, P., Donelick, R., Queng, J., and Cloos, M., 1992a, Testing Models of Fission Track Annealing in Apatite in a Simple Thermal Setting: Site 800, Leg 129: Proc., scientific results, ODP, Leg 129, old Pacific crust, v. 129.

Vrolijk, P., Donelick, R. A., Queng, J., and Cloos, M., Testing models of fission track annealing in apatite in a simple thermal setting: site 800, leg 129, *in* Proceedings Proceedings of the Ocean Drilling Program, Scientific Results1992b, Volume 129, Citeseer, p. 169-176.

Warnock, A. C., Zeitler, P. K., Wolf, R. A., and Bergman, S. C., 1997, An evaluation of low-temperature apatite UTh/He thermochronometry: Geochimica et Cosmochimica Acta, v. 61, no. 24, p. 5371-5377.

White, N., and Latin, D., 1993, Subsidence analyses from the North Sea 'triple-junction': Journal of the Geological Society, v. 150, no. 3, p. 473-488.

White, N., and Lovell, B., 1997, Measuring the pulse of a plume with the sedimentary record: Nature, v. 387, no. 6636, p. 888-891.

White, R., and McKenzie, D., 1989, Magmatism at rift zones: The generation of volcanic continental margins and flood basalts: Journal of Geophysical Research: Solid Earth, v. 94, no. B6, p. 7685-7729.

Whiting, L., Haughton, P. D. W., and Shannon, P. M., 2020, From rifting to hyperextension: Upper Jurassic – Lower Cretaceous tectono-stratigraphy of the Porcupine Basin, Irish Atlantic Margin: Basin Research, v. n/a, no. n/a.

Wiedenbeck, M., Allé, P., Corfu, F., Griffin, W. L., Meier, M., Oberli, F., Quadt, A. V., Roddick, J. C., and Spiegel, W., 1995, Three natural zircon standards for U-Th-Pb, Lu-Hf, trace element and REE analyes: Geostandards Newsletter, v. 19, no. 1, p. 1-23.

Wiedenbeck, M., Hanchar, J. M., Peck, W. H., Sylvester, P., Valley, J., Whitehouse, M., Kronz, A., Morishita, Y., Nasdala, L., Fiebig, J., Franchi, I., Girard, J.-P., Greenwood, R. C., Hinton, R., Kita, N., Mason, P. R. D., Norman, M., Ogasawara, M., Piccoli, P. M., Rhede, D., Satoh, H., Schulz-Dobrick, B., Skår, O., Spicuzza, M., Terada, K., Tindle, A., Togashi, S., Vennemann, T., Xie, Q., and Zheng, Y.-F., 2004, Further Characterisation of the 91500 Zircon Crystal: Geostandards and Geoanalytical Research, v. 28, no. 1, p. 9-39.

Wilkinson, C. M., Ganerød, M., Hendriks, B. W. H., and Eide, E. A., 2017a, Compilation and appraisal of geochronological data from the North Atlantic Igneous Province (NAIP): Geological Society, London, Special Publications, v. 447, no. 1, p. 69-103.

Wilkinson, C. M., Ganerød, M., Hendriks, B. W. H., Eide, E. A., Péron-Pinvidic, G., Hopper, J. R., Funck, T., Stoker, M. S., Gaina, C., Doornenbal, J. C., and Árting, U. E., 2017b, Compilation and appraisal of geochronological data from the North Atlantic Igneous Province (NAIP), The NE Atlantic Region. A Reappraisal of Crustal Structure, Tectonostratigraphy and Magmatic Evolution, Volume 447, Geological Society of London, p. 0.

Wilkinson, M., 2016, Cenozoic erosion of the Scottish Highlands–Orkney–Shetland area: implications for uplift and previous sediment cover: Journal of the Geological Society.

Wolf, R. A., Farley, K. A., and Kass, D. M., 1998, Modeling of the temperature sensitivity of the apatite (U–Th)/He thermochronometer: Chemical Geology, v. 148, no. 1, p. 105-114.

Wolf, R. A., Farley, K. A., and Silver, L. T., 1996, Helium diffusion and low-temperature thermochronometry of apatite: Geochimica et Cosmochimica Acta, v. 60, no. 21, p. 4231-4240.

Worster, M. G., Huppert, H. E., and Sparks, R. S. J., 1993, The crystallization of lava lakes: Journal of Geophysical Research: Solid Earth, v. 98, no. B9, p. 15891-15901.

Yang, P., Welford, J. K., Peace, A. L., and Hobbs, R., 2020, Investigating the Goban Spur rifted continental margin, offshore Ireland, through integration of new seismic reflection and potential field data: Tectonophysics, v. 777, p. 228364.

Yoder, H. S., JR., and Tilley, C. E., 1962, Origin of Basalt Magmas: An Experimental Study of Natural and Synthetic Rock Systems: Journal of Petrology, v. 3, no. 3, p. 342-532.

Young, D. G. G., and Bailey, R. J., 1974, An interpretation of some magnetic data off the west coast of Ireland: Geological Journal, v. 9, no. 2, p. 137-146.

Zeitler, P. K., Enkelmann, E., Thomas, J. B., Watson, E. B., Ancuta, L. D., and Idleman, B. D., 2017, Solubility and trapping of helium in apatite: Geochimica et Cosmochimica Acta, v. 209, p. 1-8.

Zeitler, P. K., Herczeg, A. L., McDougall, I., and Honda, M., 1987, U-Th-He dating of apatite: A potential thermochronometer: Geochimica et Cosmochimica Acta, v. 51, no. 10, p. 2865-2868.

ZetaWare, 2003, BHT Correction, The Last Resort, Volume 2021, ZetaWare, Inc.

Ziegler, P. A., 1988, Evolution of the Arctic-North Atlantic and the Western Tethys, American Association of Petroleum Geologists.